Characterizing DNA Dynamics with Fluorescent Nucleobase Rotors

Ashkan Karimi

Department of Chemistry

McGill University, Montreal

May 2022

A thesis submitted to McGill University in partial fulfilment of the requirements of the degree of
Doctor of Philosophy

Dedicated to

whom inspired this, and understand this, without any knowledge of chemistry;

my parents, Afshan and Hossein

and to my godchild, Kani, on the occasion of stepping into the beautiful life

"Oh me! Oh life! of the questions of these recurring,

Of the endless trains of the faithless, […]

What good amid these, O me, O life?"

Answer:

"That you are here—that life exists and identity,

That the powerful play goes on, and you may contribute a verse"

Walt Whitman

Copyright Statement

Contributions

The intellectual guidance and funding for the projects in this thesis were provided by Prof. Nathan W. Luedtke. I would also like to thank all the collaborators (below), all of whom are leading researchers, highly diligent and have all contributed significantly to the work presented in this thesis.

Chapter 3: The dynamic fluorescence anisotropy and fluorescence lifetime data presented in Section 3.2 were performed and analyzed by Prof. Richard Börner (Table 3.1, Figures 3.3 and 3.4, Figures B1-3). Dr. William Copp conducted the deprotection and HPLC purification of ODN7'MG1-3 (Table B6) and we jointly collected the data presented in Figure 3.6, Section 3.1.1.

Chapter 4: Most of the experiments discussed in this chapter were jointly performed and analyzed with Kaixiang Wang, as part of his undergraduate research. Kaleena Basran synthesized nucleoside **15** and conducted photophysical experiments on it (Table 4.1 and Figure 4.4, Chapter 4). The fluorescence lifetime results reported in this chapter were measured and analyzed by Ehsan Hamzehpour (Table 4.3, Figure 4.9 and Figure C5).

Chapter 5: The NMR data reported in Section 5.4 and the CD spectra shown in Figure D9 were recorded and analyzed by Dr. Miguel Garavís Cabello.

I hereby confirm that all other contributions are the work of the author.

Abstract

Understanding the nature and function of DNA requires tools with high sensitivity and specificity. Over the past decades, fluorescent nucleobase analogs (FBAs) have emerged as a particularly powerful class of molecular probes. However, from the previously reported FBAs, some suffer from low brightness, some do not mimic the hydrogen bonding of natural nucleobases, and most have limited sensitivity towards single-stranded DNAs (*ss*-DNAs) and mismatched, well-matched or damaged duplex DNAs (*ds*-DNAs). To overcome these limitations, we need FBAs with high molar extinction coefficients and fluorescence quantum yields that depend on their microenvironment. Such FBAs would be of great interest in detecting and characterizing dynamic DNA secondary structures.

Our first foray into the world of nucleic acid structure probes involves the integration of a well-known and bright molecular rotor fluorophore, *trans*-stilbene, into thymidine. The resulting fluorescent nucleobase analog (^{ts}T) in *ds*-DNA is one of the brightest reported FBAs to date (Chapter 2). The ^{ts}T phosphoramidite was synthesized in 12 steps with an overall yield of 26% and incorporated into DNA oligonucleotides. This new thymidine mimic has a molar extinction coefficient (Ɛ) = 30’600 $M^{-1}cm^{-1}$ and an average fluorescence quantum yield (φ) = 0.143 when incorporated in *ds*-DNA. This value is 4.9-fold higher than the quantum yield of ^{ts}T in *ss*-DNA, 8.2-fold higher than in a *ds*-DNA with ^{ts}T:G mismatch and 28-fold higher than in a *ds*-DNA with ^{ts}T:T and ^{ts}T:C mismatches. Dynamic anisotropy measurements confirmed the relation between the fluorescence intensity of ^{ts}T molecular rotor with global dynamics of *ss*-DNA, and local dynamics of mismatched *ds*-DNA (Chapter 3). The exceptionally high fluorescence of ^{ts}T in *ds*-DNA stems from the rigid microenvironment of *ds*-DNA and the lack of photo-induced electron transfer (PET) quenching with natural nucleobases as suggested by our Density Functional Theory (DFT) calculations. In fact, ^{ts}T undergoes PET quenching selectively with 8-oxoguanine (OG) and can detect it at distances as far as 20 Å. In addition, Förster resonance energy transfer (FRET) between ^{ts}T and tC showed that this FRET pair has a small R_0 = 2.0 nm and thus can be applied as a spectroscopic ruler, and temperature-dependent measurements demonstrated that ^{ts}T can act as a molecular thermometer.

Inspired by ^{ts}T, we sought to probe *i*-motif structures, thus its cytosine analog, ^{ts}C, was synthesized to probe the pH-dependent folding of C-rich DNA into *i*-motif structures (Chapter 4). The

absorbance of ^{ts}C, like ^{ts}T, is red-shifted enough to not overlap with DNA natural bases absorbance, but it is blue-shifted enough to allow for energy transfer from unmodified DNA bases to the probe when it is positioned in an *i*-motif structure. ^{ts}C is the first light-up FBA for *i*-motif DNA that exhibits a bathochromic shift upon *i*-motif formation. These properties enable unprecedented sensitivity in detecting *i*-motif strand displacement reactions and temperature-dependent dynamics.

With a deeper understanding of the structure and dynamics of duplex, quadruplex, and single-stranded DNA, we proceeded to switch different duplex secondary structures and probe them using biophysical tools (Chapter 5). We designed a DNA sequence, containing a defined number and arrangement of C:T mismatches, capable of undergoing a global B-to-A-form helical transition upon adding one equivalent of Hg^{II} per mismatch, and possibly right-to-left-handed switching upon the addition of the second equivalent of Hg^{II}. In addition, we have found that by replacing C:T mismatches with T:T mismatches, the B-form DNA can switch to a Z-form-like duplex upon the addition of one equivalent of Hg^{II}. These processes are fast (<30 sec) and can be reversible when N-acetyl cysteine is added. This demonstrates that mismatch metallo bases have unique switching potential in DNA-based materials and devices.

Résumé

Comprendre la nature et la fonction de l'ADN nécessite des outils d'une sensibilité et d'une spécificité élevées. Au cours des dernières décennies, les analogues de bases azotés fluorescentes (BAF) ont émergé comme une classe particulièrement puissante de sondes moléculaires. Cependant, parmi les BAF précédemment reportés, certains souffrent d'une faible luminosité, ne parviennent pas à imiter la liaison hydrogènes des bases azotées naturelles, et la plupart ont une sensibilité limitée envers les simples brins d'ADN (ADNsb), les duplex mal appariés, bien appariés ou endommagés d'ADN (ADNdb) et les quadruplexes. Pour surmonter ces limitations, nous avons besoin de BAF avec des coefficients d'extinction molaire élevés dont le rendement quantique de fluorescence est dépendant de leur microenvironnement. De tels BAF seraient d'un grand intérêt pour détecter et caractériser les structures secondaires dynamiques de l'ADN.

Notre première incursion dans le monde des sondes de structure d'acide nucléique implique l'intégration d'un fluorophore à rotor moléculaire bien connu et brillant, le trans-stilbène, à la thymidine. L'analogue de base azotée fluorescente (^{ts}T) résultant dans l'ADN à double brin est l'un des BAF les plus brillants signalés à ce jour (chapitre 2). Le phosphoramidite ^{ts}T a été synthétisé en 12 étapes avec un rendement global de 26 % et incorporé comme nucléotides dans l'ADN. Ce nouveau mimétique de la thymidine a un coefficient d'extinction molaire (Ɛ) = 30'600 $M^{-1}cm^{-1}$ et un rendement quantique de fluorescence (φ) = 0,143 lorsqu'il est incorporé dans l'ADNdb. Ce dernier est 4,9 fois plus élevé que le rendement quantique de tsT dans l'ADNsb, 8,2 fois plus élevé que dans un ADNdb avec mésappariement ^{ts}T:G et même 28 fois plus élevé que dans un ADNdb avec des mésappariements ^{ts}T:T et ^{ts}T:C. Les mesures d'anisotropie dynamique ont confirmé la relation entre l'intensité de fluorescence du rotor moléculaire ^{ts}T avec la dynamique globale de l'ADNsb et de l'ADNdb bien apparié, et la dynamique locale de l'ADNdb non apparié (chapitre 3). La fluorescence exceptionnellement élevée de ^{ts}T dans l'ADNdb provient du microenvironnement rigide de l'ADNdb et de l'absence d'extinction par transfert d'électrons photo-induit (PET) avec des bases azotées naturelles, comme le suggèrent nos calculs de théorie fonctionnelle de la densité (DFT). Confirmé par des calculs théoriques, ^{ts}T subit une désactivation sélective du PET avec de la 8-oxoguanine (OG) et pourrait le détecter à des distances allant jusqu'à 20 Å. De plus, le transfert d'énergie de résonance Förster (FRET) entre ^{ts}T et tC a montré que cette paire de FRET a un petit R_0 = 2,0 nm et peut donc

être appliquée comme règle moléculaire et nos mesures dépendantes de la température ont démontré que ^{ts}T peut agir comme un thermomètre moléculaire.

Inspirés par ^{ts}T, nous avons cherché à sonder les structures i-motif, ainsi, son analogue de la cytosine, ^{ts}C, a été synthétisé pour sonder le repliement dépendant du pH de l'ADN riche en C dans les structures i-motif (Chapitre 4). L'absorbance de ^{ts}C, comme ^{ts}T, est suffisamment décalée vers le rouge pour ne pas chevaucher l'absorbance des bases naturelles de l'ADN, mais elle est également suffisamment décalée vers le bleu pour permettre le transfert d'énergie des bases de l'ADN à la sonde lorsqu'elle est positionnée dans une structure compacte i-motif. ^{ts}C est le premier BAF lumineux pour l'ADN i-motif et montre un décalage bathochrome. Ces propriétés permettent une sensibilité sans précédent dans la détection des réactions de déplacement de brin i-motif et de la dynamique dépendante de la température.

Avec une compréhension plus approfondie de la structure et de la dynamique de l'ADN duplex, quadruplex et à simple brin, nous avons procédé à la commutation de différentes structures duplex secondaires et à leur analyse à l'aide d'outils biophysiques (chapitre 5). Nous avons conçu une séquence d'ADN, contenant une certaine quantité de mésappariements C:T, capable de subir une transition hélicoïdale globale de forme B à A lors de l'ajout d'un équivalent de Hg^{II} par mésappariement, et commutation de droite à gauche lors de l'ajout du deuxième équivalent de Hg^{II}. De plus, nous avons découvert qu'en remplaçant les mésappariements C:T par des mésappariements T:T, l'ADN de forme B passe directement à l'ADN de type Z lors de l'ajout d'un équivalent de Hg^{II}. Ces processus sont rapides (<30 sec) et sont réversibles lorsque de la cystéine N-acétyle est ajoutée. Cela démontre que les métallobases mésappariées possèdent un potentiel de conversion unique dans les matériaux et dispositifs à base d'ADN.

Acknowledgments

The past five years of my PhD studies were the most remarkable years of my life. During this time, I experienced the joy of adventuring and exploring DNA wonderland, built the most amazing friendships I have ever had with some of my wonderful labmates, and practiced for my dream job in academia. The past enjoyable years were definitely not the easiest ones. Like any other PhD student, there were times I thought that my project was a dreadful endless jungle where there seems to be no way out! To that, a big lab transition was added when our group moved from Zurich to the other side of the ocean right before a pandemic hit us. During this time, what kept me motivated was the amazing and encouraging people I have had around me. Whom without their support, I could not deliver this thesis, and here I would like to express my special thanks and gratitude to them.

The first person I need to thank is my mentor Prof. Nathan Luedtke, who has shaped my scientific attitude and helped me to be a better researcher and a better human. I really appreciate his inspiring passion for science along with his enthusiasm to pass on his knowledge, his guidance along my way, his enormous support for my future, and his encouragement to not give up on my dreams. I will always cherish the chalk-talk in his office, which made me feel science has no borders. When in March 2017, I applied to join Nathan's lab, he took the risk to ignore my lack of experience in chemical biology and DNA chemistry and instead trusted my passion for learning. He was supportive enough to offer me a photophysical project after he figured out which direction my research interest lies on. When in February 2019, he officially announced that our lab was moving to McGill, I had reasons to stay, but the one reason that convinced me to move to Montreal was that I would continue learning under Nathan's mentorship. Nathan did everything he could to ease the transition for Morten and I including offering a room in his house for the early weeks in Montreal and generously supporting us. The most important thing I learned from him during the past few years was how to be a great mentor. Nathan taught me that having a friendly group atmosphere is the key and being a group leader is beyond merely supervising projects. When needed, Nathan could be as supportive and compassionate as a parent, and at the right time, I could enjoy our friendly chats and super funny moments at the group nights out. I will always be eternally grateful to him.

I am very grateful to Prof. Hanadi Sleiman, Prof. Gonzalo Cosa, and Prof. Michal Juríček, for serving on my committee and for their input and support of this work. Further, I would like to thank Prof. Matthew Harrington for accepting to serve as an internal examiner. I direct my further gratitude to Prof. Masad Damha for the great scientific advice he always gave me. My special thanks go to Prof. Richard Börner for his support and knowledge of photophysical studies, to Dr. Miguel Garavís for all his helpful discussions and conducting DNA NMR experiments. No one better than you can run a gel, Miguel! I also direct many thanks to Perepichka group, especially Ehsan Hamzehpoor for all his help with the fluorescence lifetime measurements and his incredible creativity in setting up the apparatus. The staff at the University of Zurich and McGill, without whom I would not of completed my work. Both Dr. Alex Wahba and Mr. Urs Stalder have provided me with mass spectra and guidance throughout my PhD. I sincerely acknowledge Dr. Thomas Fox and Dr. Robin Stein, for their help with NMR problems. I would also like to thank Ms. Chantal Marotte and Ms. Larissa Mostacciuolo for their advice and for answering all my questions about my PhD. I would like to thank the Swiss National Science Foundation, the University of Zurich, CMSZH, McGill University, NSERC, NRC, and Centre for Structural Biology for their generous financial support.

Luedtke's group members, past and present, have always been supportive and highly knowledgeable about research. It is so true that the real chemistry was the friends we made along the way. I cannot say enough about the great people I worked with over the past years at the University of Zurich and McGill. Banana, Bisi, Olli, and Pony have not been just my friends, but my "Schatzies" and like a family for me. I made the most amazing and beautiful friendship I have ever had with them, and the status of my work-life balance owes itself to them. Olli and Banana were the first to teach me DNA synthesis, fluorescence spectroscopy and gel electrophoresis. Pony taught me HPLC is not as painful as I initially thought. Banana was my "Schale" buddy who made my last year in Zurich as fun as possible. I will never forget our fondue and raclette nights at each other's places, "not gluten-free" hamburgers in Niederdorf, BBQ by the Zurich Lake, wine and cheese by Limmat river, "Nevado dance" at aperos, "Glue wine" at Irchel bar, "Perperla" games in crowded trains, hikes in Alpine, travels in Europe and lot of other great moments which made my memorable years in Zurich the most enjoyable part of my life. Nevertheless, the true friendship is beyond the geographical borders, and since I left Europe, we have stayed in close contact by video calls. Olli, who helped me a lot with my postdoc proposal, even two times came to Montreal for a visit – once with Bisi and her

lovely husband Rappi – and our relationship was unique enough that she asked Bisi and me to be the godparents of her baby, Kani, who was just born in April 2022!

I would like to thank Kaleeaanaa for being my Canadian “Schatzi”, who is always down for any adventure, travel, and hike, who always listened to my concerns in “sus” moments, who I can’t imagine how my time at McGill would be without her, and who always reminded me of the important departmental emails I never read! Jawad for our relaxing daily coffee time at 3 pm and Furby for our “really” funny chats. Masa Oppa, who taught me mass spectroscopy and suggested I eat ice cream to lose weight. I will never forget the “nasty” conversations I had with him! Aaron, who helped me work on my self-confidence when I was at the beginning of the PhD journey. Gosh, who always collects packaging airbags for me to burst them! Alessandra and Haily, who working close to their bench was fun. Gandalf, Govna, Kaifeng, and Scooby who have been fantastic additions to the lab, have been a lot of fun and kept me sane through many long nights. My sincere appreciation goes to Govna, Gosh, and Kaleeaanaa for proofreading my thesis. I would also like to thank all the undergraduates I had the honor of working with, Ron, Luca, Ilya, and Round. All of whom have had been incredibly smart, diligent, and fun. Round’s long and fruitful stay in the lab, his passion and hard work have significantly contributed to Chapter 4 of the thesis. I’m sure a bright future is waiting for this rising star.

Of the greatest fortunes I had, was having the Damha lab share their office and workspace with us at McGill. I will never forget Nardo and Miguelo, who with Kaleeaana and I formed “Core4” to embrace Montreal's freezing winter in the pandemic dark days by adventuring in the city with a tower waffle at Juliette and Chocolate, and Margaritha at 3 Amigos. Betto and Miguelo, both helped me with proofreading the Chapter 5 of the thesis. I thank Betto for being my shopping buddy and for his persistence in a “mission” in Vancouver, Cinéma Banque Scotia and eventually accomplishing it at Ada’s Friendsgiving party and changing my vision about the world! Morgane, for constant reminding of the hourly PhD salary! Cristina, for showing me the beautiful Montreal in Spring and post-pandemic days. Haley, for her enormous help with my postdoc proposal. Alicia, for translating my abstract into lovely French. Ada for the best hugs she gave me from time to time, and Adam, Dan, James, and Sunit for the great scientific and non-scientific talks.

Now that 24-years of being a student is almost coming to an end, I want to express my gratitude to all the mentors I got the opportunity to learn from them. I would really like to thank Prof.

Davar Boghaee, who encouraged me to follow my heart and let my love for chemistry guide me and in 2008 signed a card for me “To Ashkan, the future chemist”. He taught me chemistry and philosophy are inseparable. I would also like to thank Prof. Mohammad Bagher Teimouri, who showed me the beauty of organic chemistry and never got tired of constantly encouraging me. I would like to thank Prof. Hadi Behzadi, my first research supervisor, who taught me computational chemistry, and sadly is no longer with us to see how what I learnt from him has impacted many pages of this thesis. I would also like to thank Prof. Firouz Matloubi and Prof. Yvan Six, my MSc degree supervisors, for their advice, their support, and the opportunity to learn synthesis skills in their labs.

It must be unconventional, but I want to thank Zurich and Montreal for hosting me and being like a home for me. Probably more important than a PhD degree, is how living in these cities helped me to better know myself, accepting who I am, and trying to remove a painful mask that I covered myself behind it for years. Stepwise “coming out” to my friends, to my colleagues, to my family, and feeling comfortable to get out of the closet publicly, was a big step for me, which all happened during my stay in these cities. I’m deeply grateful to everyone who helped me in this stage of my life.

Last but not least, I consider myself incredibly lucky to have wonderful parents, Afshan and Hossein, who have been supportive of my ventures, even with being on the other side of the earth, who always have been passionate about my research and never got tired of me talking about every detail of my project, and whose wisdom I admire so much. My parents never wished to have a child with a PhD degree, they never expected me to be a distinguished student, and never pushed me for anything other than being a healthy and caring person enjoying life. However, besides their unconditional love, they have always had endless support and constant encouragement for my scientific ambitions and the academic path I have decided to step in and remain in. I would like to acknowledge my brother, Mahan, who has always been happy to make fun of me, yet always provides me with the support that I require. My lovely cat, Magi, who has been a member of our family since I started university 12 years ago, for being responsible for emotional supports. Special thanks I direct to my aunts: Afsoon, who is like a second mom for me; Fariba, who is always passionate to hear about my academic success; and Feri, who talking with her while having cheese and wine is always enjoyable. Finally, I think no one could be happier to see me graduating from PhD more than my grandma and nan, Maman Fereshteh and Ezzat Joon. I am very happy that they can see this moment.

Table of contents

List of abbreviations

^{o}C	Celsius degree
β	angle between the absorption and emission dipole
δ	chemical shift
ε	Extinction coefficient
θ	anisotropy decay
λ_{abs}	wavelength at the maximum absorbance
λ_{em}	wavelength at the maximum fluorescence emission
λ_{ex}	wavelength at the maximum excitation
μM	micromolar
τ	fluorescence lifetime
φ	fluorescence quantum yield
1D	one dimensional
2AP	2-aminopurine
2D	two dimensional
2PyG	8-(2-pyridyl)-2′-deoxyguanosine
4PVG	8-[2-(pyrid-4-yl)-ethenyl]-2′-deoxyguanosine
4QI	cyanine-indole-quinolinium
Å	Angstrom
A	adenine
ACN	acetonitrile
AO-R	acridine orange group
Adap	2-oxo-1,3-diazaphenoxazine
AnMBTZ	10-anthracene-10-yl-3-methylbenzothiazol-3-ium chloride
API	4-aminophthalimide

bp	base-pair
BSA	N,O-bis-(trimethylsilyl)-acetamide
Bz	benzoyl
C	cytosine
CD	circular dichroism
CRISPR	clustered regularly interspaced short palindromic repeats
CT	calf thymus
Cys	N-acetylcysteine
d	doublet
dA	deoxy adenosine
dan	6-(dimethylamino)-2-acylnaphthalene
DAPI	4’,6-diamidino-2-phenylindole
DBU	1,8-Diazabicyclo[5.4.0]undec-7-ene
dC	deoxy cytidine
DCM	dichloromethane
dd	doublet of doublets
ddd	doublet of doublet of doublets
DFT	density functional theory
dG	deoxy guanosine
DIPEA	N,N-diisopropylethylamine
DMABN	4-N,N-dimethylamino-benzonitrile
DMAP	4-dimethylaminopyridine
DMF	dimethylformamide
DMSO	dimethylsulfoxide
DMSO-d6	deuterated dimethylsulfoxide
DMT	4,4'-dimethoxytrityl

DNA	2'-deoxyribonucleic acid
DNG	deoxynucleic guanidine
Dns	Dansyl-nucleoside surrogate
dppf	1,1’-Bis(diphenylphosphino)ferrocene
Ds	7-(2-thienyl)imidazo[4,5-b]pyridine
ds-DNA	double-stranded DNA
dT	deoxy thymidine
DUP	duplex
EB	ethidium bromide
ESI	electrospray ionization
Et_3N	triethylamine
EtOAc	ethyl acetate
Em	fluorescence emission
Equiv	equivalent
Ex	Excitation
FANA	2’-fluoroarabinonucleic acids
FBA	fluorescent nucleobase analog
FBR	fluorescent nucleobase rotor
FCS	fluorescence correlation spectroscopy
FIT	forced intercalation
FLIM	fluorescence lifetime imaging
FMART	fluorescently modified adenine-release turn-on
FMR	fluorescent molecular rotors
FRAP	conducting fluorescence recovery after photobleaching
FRET	Förster resonance energy transfer
G	Guanine

GFP	green fluorescent protein
GNA	glycerol nucleic acids
h	hour (reaction time)
HBI	(4-hydroxybenzylidene)-2-methylimidazolin-3-one
HNA	hexose nucleic acid
HPLC	high performance liquid chromatography
HRMS	high-resolution mass spectra
HSQC	heteronuclear single quantum coherence
Hz	Hertz
i	*i*-motif
I	fluorescence intensity
iPr$_3$PhSO$_2$Cl	2,4,6-triisopropylbenzene-sulfonyl chloride
IR	Infra red
J	coupling constant
K_d	dissociation constant
LNA	locked nucleic acids
m	multiplet
MB	molecular beacon
min	minutes
MS	mass spectrometry
Neo	neomycin
NIS	N-iodosuccinimide
nM	nanomolar
NMR	nuclear magnetic resonance
NOE	nuclear overhauser effect
NOESY	nuclear overhauser effect spectroscopy

nt	nucleotide
ODN	oligonucleotide
OG	8-oxoguanine
ONA	oxepane nucleic acid
Pa	pyrrole-2-carbaldehyde
PBS	Phosphate buffered saline
Pc	pyrrolo-cytosines
PNA	peptide nucleic acid
PRODAN	6-propionyl-2-dimethylaminonaphthalene
*p*TolSH	*para*-toluenethiol
q	quartet
qPCR	quantitative Polymerase Chain Reaction
r	steady-state anisotropy
r.t.	room temperature
R_0	Förster radius
R_H	hydrodynamic radius
RMSD	root mean square deviation
s	singlet
S0	singlet ground state
S1	first excited state
SNA	serinol nucleic acids
SNP	single nucleotide polymorphism
ss-DNA	Single-stranded DNA
SSB	single-strand binding
StG	8-(2-phenylethenyl)-2’-deoxyguanosine
StyPy	pentafluorostyryl-aminopyrene

T	thymine
t	triplet
TBA	thrombin binding aptamer
TBAF	tetra-*n*-butylammoniumfluoride
TBS	*tert*-butyldimethylsilyl
TCSPC	time-correlated single-photon counting
TD-DFT	time-dependent density functional theory
TDS	Thermal difference spectra
TFO	triplex-forming oligonucleotide
TH	toehold
thA	thieno[3,4-d]-6-aminopyrimidine
THF	tetrahydrofuran
thT	thioflavin-T
TICT	twisted intramolecular charge transfer
TIPSCl	triisopropylsilyl chloride
TLC	thin layer chromatography
TMSOTf	trimethylsilyl trifluoromethanesulfonate
TO	thiazole orange
Tm	melting temperature at equilibrium
U	uracil
UBER	universal base excision reporter
UV	ultraviolet
WCF	Watson–Crick–Franklin
y	2-oxo(1H)pyridine
YO	oxazole yellow
z	imidazolin-2-one

Chapter 1 | Introduction

"Conclusion: Big helix in several chains, phosphates on outside." *Rosalind Franklin*

"A structure this pretty just had to exist." *James Watson*

1.1 Nucleic acids: Molecular basis of life

"Why is a raven like a writing desk?" This was Mad Hatter's riddle in *Alice's Adventures in Wonderland*. Alice could not answer this question because there was not an actual answer. However, science today has an answer for that: A raven and a tree's genomes consist of the same building blocks. These building blocks are nucleic acids, exquisite biopolymers that store all biological information essential for life which synergize structure and function like no other. Their unique chemical, biological and physical properties have captivated researchers for decades, which has resulted in the development of numerous applications, ranging from therapeutics and diagnosis to nanotechnology and computer science.

Despite the general belief, the discovery of 2'-deoxyribose nucleic acid (DNA) traces back to 80 years before the famous paper of *Watson* and *Crick*, when the Swiss scientist *Miescher* isolated and analyzed DNA. In 1869 *Miescher* developed his insightful theories explaining how biological molecules could encode genetic information.[1] By a fortunate historical coincidence, in the same decade *Darwin* had expounded the mechanism driving biological evolution and *Mendel* had described the basic laws of inheritance.[2] Finally, the importance of studying the structure and functions of DNA was revived when *Avery* proposed DNA rather than proteins as the carrier of genetic information.[3] This proposal was unambiguously proven in 1952 by *Hershey* and *Chase*.[4] In parallel with these discoveries, *Levene* showed nucleic acids are polynucleotide chains composed of four nucleotide units, including adenosine (dA), guanosine (dG), cytidine (dC) and thymidine (dT).[5] However, what truly acted as a cornerstone for unravelling the structure of the molecular basis of life was the discovery of the 1:1 ratio between A and T, and G and C nucleobases by *Chargaff*.[6] Shortly after this finding *Watson* and *Crick*, inspired by the unpublished X-ray diffraction data of *Franklin* and *Wilkins* suggesting the helical form of DNA,[7,8] proposed DNA's double helix structure.[9] The specific base-pairing of DNA nucleobases suggested a possible copying mechanism for the genetic material, where duplex DNA (*ds*-DNA), can be considered a "resting state" of genetic code, with information actively flowing into and out of single-stranded DNA (*ss*-DNA). Thus, after the discovery of DNA's double helix structure, *Watson* suggested that DNA acts as a template for self-replication, and genetic information transfers from DNA to RNA (transcription) and from RNA to protein (translation) in a unidirectional flow.[10]

Since *Crick*'s first formulation of the "central dogma of biology",[11] groundbreaking revelations of DNA's diverse and dynamic structures and their associated biological functions have been obtained. Synthetic nucleic acids now have applications in medicine,[12] gene editing (CRISPR-Cas9),[13] base editing,[14-21] and forensics.[22] In addition, today we know DNA is not merely a storage medium for genetic information; but it can also be used to construct various two- and three-dimensional nanostructures with novel properties,[23,24] molecular machines,[25,26] and media for digital data storage.[27] However, despite the wealth of information and progress, DNA nanostructures cannot replace natural systems, and patients with genetic diseases still suffer. This is because our understanding of DNA and RNA is far from complete. Thus, probing various structures and functions of DNA is of great importance and continues to fascinate those devoted to its study.

1.2 DNA structure and properties

DNA is a linear polymer consisting of 2'-deoxyribonucleotides composed of a cyclic five-carbon sugar (ß-D-2'-deoxyribose) with a phosphodiester linkage between 5' and 3' positions and a nitrogenous nucleobase at the C1' position (Figure 1.1A). The four main nucleobases are classed either as pyrimidines (T and C) or purines (A and G) due to the nature of the heterocyclic rings. The preferred conformation of the nucleotides is *anti,* where the hydrogen bonding face of each nucleobase is oriented away from the carbohydrate. The phosphate groups are deprotonated at neutral pH, rendering the DNA an anionic polymer. The negatively charged phosphate groups are located on the outside of the helical structure, and the nucleobases occupy the hydrophobic core of the helix, where each nucleobase interacts with adjacent nucleobases through π stacking and forms hydrogen bonds with the opposing nucleobase.[28] Thus, formation of G:C and A:T base-pairs between the two complementary polynucleotide strands stabilize the DNA double helix by hydrogen bonding and base stacking interactions (Fig 1.1B).

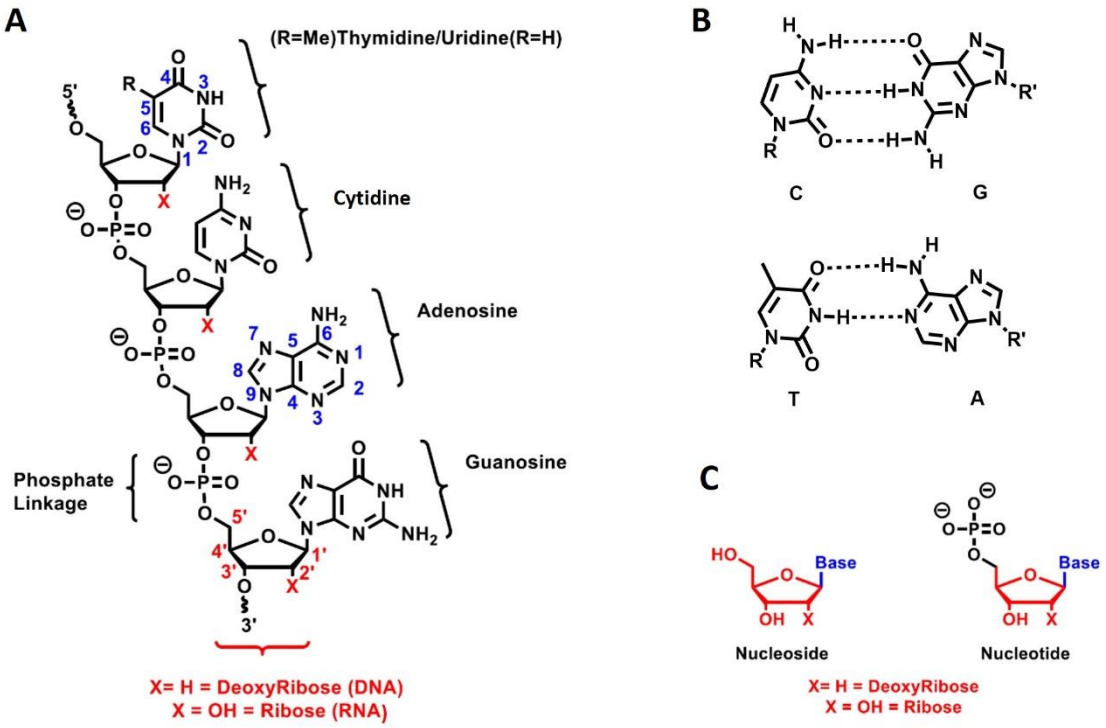

Figure 1.1. (A) Nucleic acid primary structure including nitrogenous heterocyclic nucleobases that are split into different classes: pyrimidines and purines. (B) *Watson-Crick-Franklin* base-pairs; G pairs with C *via* three hydrogen bonds and A pairs with T *via* two hydrogen bonds (R, R' = 2'-deoxyribose-phosphate backbone). (C) Nucleosides consist of a nucleobase attached, *via* a β-Glycosidic bond, to the 1' position of a 2'-deoxyribose (DNA) or ribose (RNA) sugar. A nucleotide is a nucleoside that contains a phosphate group.

1.3 Probing DNA by fluorescent probes

Biophysical techniques have been applied to nucleic acids, such as circular dichroism (CD),[29] thermal difference spectra (TDS),[30] X-ray crystallography,[31] cryo-electron microscopy,[32] and NMR[33] to provide structural information, probe their dynamics, and study their biological functions as well as binding interactions. While there is no doubt these methods have had significant success in the aforementioned applications, it is important to be aware of their limitations. For example, some of these techniques probe only global structures, some have low sensitivity and require samples with high purity, and some are incompatible with conformational analyses in living cells. Finally, the main drawback of these methods is they cannot be used for single-molecule studies in real-time. Fluorescence spectroscopy is a powerful tool for real-time probing of DNA molecules *in vitro* and *in vivo*.[34-37] It has high sensitivity and can be used for a variety of experiments such as dynamic

anisotropy and Förster resonance energy transfer (FRET) to probe local and global dynamics of nucleic acids.[38,39] In addition, since the natural DNA nucleobases are practically non-fluorescent, it is possible to conduct single-molecule fluorescent experiments without interfering background signals.[40] However, the success of fluorescence-based experiments largely depends on the selection of appropriate fluorescent probes.

In general, two different types of fluorescent probes have been developed for nucleic acids: covalent and non-covalent fluorescent probes (Figure 2). Non-covalent probes include groove binders and intercalating agents. Intercalating agents are molecules, normally contain aromatic ring(s) in their structure, that can bind to DNA through π-stacking and/or electrostatic interactions. Many polycyclic dyes with high fluorescence intensities and extinction coefficients can be used as DNA intercalators and stains, such as acridine orange and ethidium bromide dyes.[41] Usually, intercalators undergo fluorescence enhancement[42] and/or red-shifting in emission upon binding to DNA.[43] These changes in photophysical properties are due to the increased rigidity and shielding from water when intercalators are located between nucleotides in a DNA structure. In addition, the minor groove is the target of a large number of non-covalent binding agents, such as fluorescein-neomycin[44] and BODIPY-neomycin[45] conjugates. DNA binding with specific sequences, takes place by means of a combination of directed hydrogen bonding to base-pair edges, van der Waals interactions with the groove walls and electrostatic interactions.[46] Examples include pyrrole-imidazole polyamides.[47-49] Non-covalently attached fluorophores are mainly used for the visualization of nucleic acids in experimental biology procedures.[50-51] They can also be used to monitor folding and interactions of nucleic acids with their targets but are not able to provide site-specific data and present many other limitations, such as perturbation of DNA conformations in some cases.[52-53]

Covalent fluorescent probes, which provide labeling with high specificity, include two sub-categories: (1) external fluorescent probes, which can be attached to certain positions of DNA (nucleobase or backbone) *via* a non-nucleosidic linkage,[37,54-55] and (2) fluorescent base analogs (FBAs), in which a fluorophore substitutes one nucleobase within the DNA. External fluorescent probes are usually highly fluorescent dyes, such as rhodamine,[56] cyanine,[57] and fluorescein,[58] and normally cause minimal perturbation with DNA conformation. Thus, they are powerful markers for nucleic acids detection. However, apart from DNA visualization, they cannot sense DNA damage, helix structure, local dynamics and, in some cases, they perturb protein-enzyme interactions.[59-60] To be

able to detect different DNA conformations and DNA hybridization, external probes require at least one quencher[61] or one more fluorescent probe as a FRET pair;[62] which raises the risk of affecting the folding and thermal stability of the DNA.[63] An alternative for external probes are FBAs, which will be discussed in the Section 1.4, and can be categorized into four subsets: (1) chromophoric, in which a chromophore or a hydrocarbon is incorporated into DNA as C-nucleoside or as base surrogate;[55, 64-65] (2) extended, in which a fluorophore is attached to the nucleobase *via* a non-emissive linker; (3) isomorphic, which are nearly identical in structure to a natural nucleobase; and (4) expanded, which contain additional aromatic ring(s) fused to the purine or pyrimidine core (Figure 1.2).

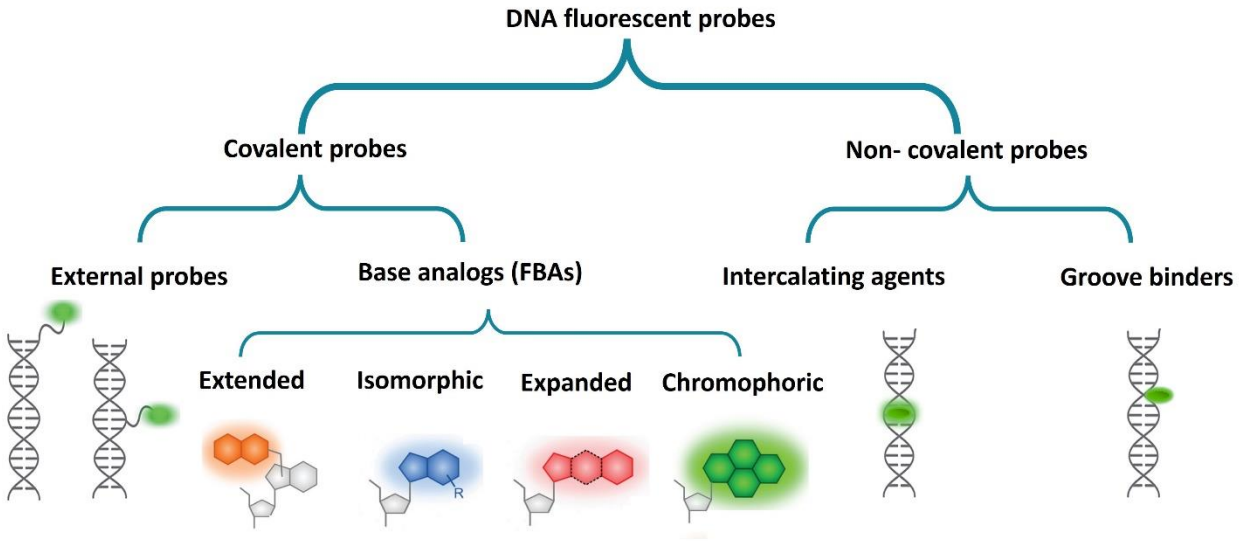

Figure 1.2. Fluorescence labeling strategies illustrated for the detection of DNA.

1.4 Fluorescent base analogs (FBAs)

FBAs are chemically modified DNA and RNA analogs that not only retain their chemical and biological functionalities, such as stacking, base-pairing and enzymatic incorporation, but also empower improved fluorescence properties for the analysis of nucleic acids. These molecules have emerged as extraordinarily useful tools for the molecular-level understanding of nucleic acid structures, activities, locations and interactions.[66] As the natural nucleobases are essentially non-fluorescent, significant modifications to nucleobase structure are required before they can be broadly useful as emissive tools. These modifications can either be made with an eye to preserving *Watson-Crick-Franklin* (WCF)-like pairing ability (that is, retaining 'canonical' pairing), or more dramatic

changes to the nucleobase architecture can be made, resulting in non-canonical designs. This relative lack of constraints allows the non-canonical nucleobases to have more widely varied emissive properties, but also can limit their ability to be recognized by enzymes. Some labeling and synthesis methods will be discussed in Chapter 2, Section 2.1. Below some of the most important reported FBAs are discussed and their structures are shown in Figure 1.3.

It is difficult to find among the many reviews dedicated to FBAs,[66-75] one that does not start with 2-aminopurine (2AP), formycin, and 2,6-diaminopurine (DAP) reported by *Stryer* in 1969.[76] Among these, 2AP emerged as a highly useful tool in nucleic acids research.[77] A few years later, *Leonard* discovered another bright fluorescent purine analog, ethenoadenine, which cannot form base-pairs due to addition of two carbons, forming a ring on the previous pairing edge.[78] In the 1990s, pyrimidine fluorescent analogs began to emerge, with notable examples including m^5K of *McLaughlin*[79] and the pteridines of *Hawkins*[80] such as 3MI[81] and 6MI.[82] C-glycosidic fluorescent nucleobases were synthesized around this time as well, as *Kool* reported the direct attachment of pyrene and other hydrocarbons to 2'-deoxyribose.[46] In 1998, *Moreau* expanded the pyrimidine structure by fusion with phenyl rings, reminiscent of *Leonard*'s earlier work, and reported BgQ as a larger-than-natural nucleobase.[83]

In the 2000s, work in this field began to expand rapidly. Notable advances include the development of base-discriminating FBAs such as BPP,[84] NPP,[85] ^{MD}I,[86] and ^{py}U[87] by *Saito* and *Okamoto*. *Wilhelmsson* synthesized a ring expanded cytidine analog (tC) at the same time,[88] and *Hocek* introduced extended fluorescent nucleobases as a facile way to modify the electronics of canonical nucleobases *via* conjugated linkers.[89] In addition, *Hirao* reported FBAs such as 2-amino-6-(2-thienyl)purine (s),[90] 7-(2-thienyl)imidazo[4,5-b]pyridine (Ds),[91] which could be enzymatically incorporated into pyrrole-2-carbaldehyde (Pa), 2-oxo(1H)pyridine (y), or imidazolin-2-one (z), and expanded the genetic alphabet.[92-97] In the late 2000s, *Sekine* designed pyrimidopyrimidine base analogs[98] while *Tor* significantly expanded the isomorphic fluorescent nucleobase pool by designing a series of thieno-appended analogs,[99-102] and *Wilhelmsson* reported the first fluorescent base analog FRET-pair.[103-104]

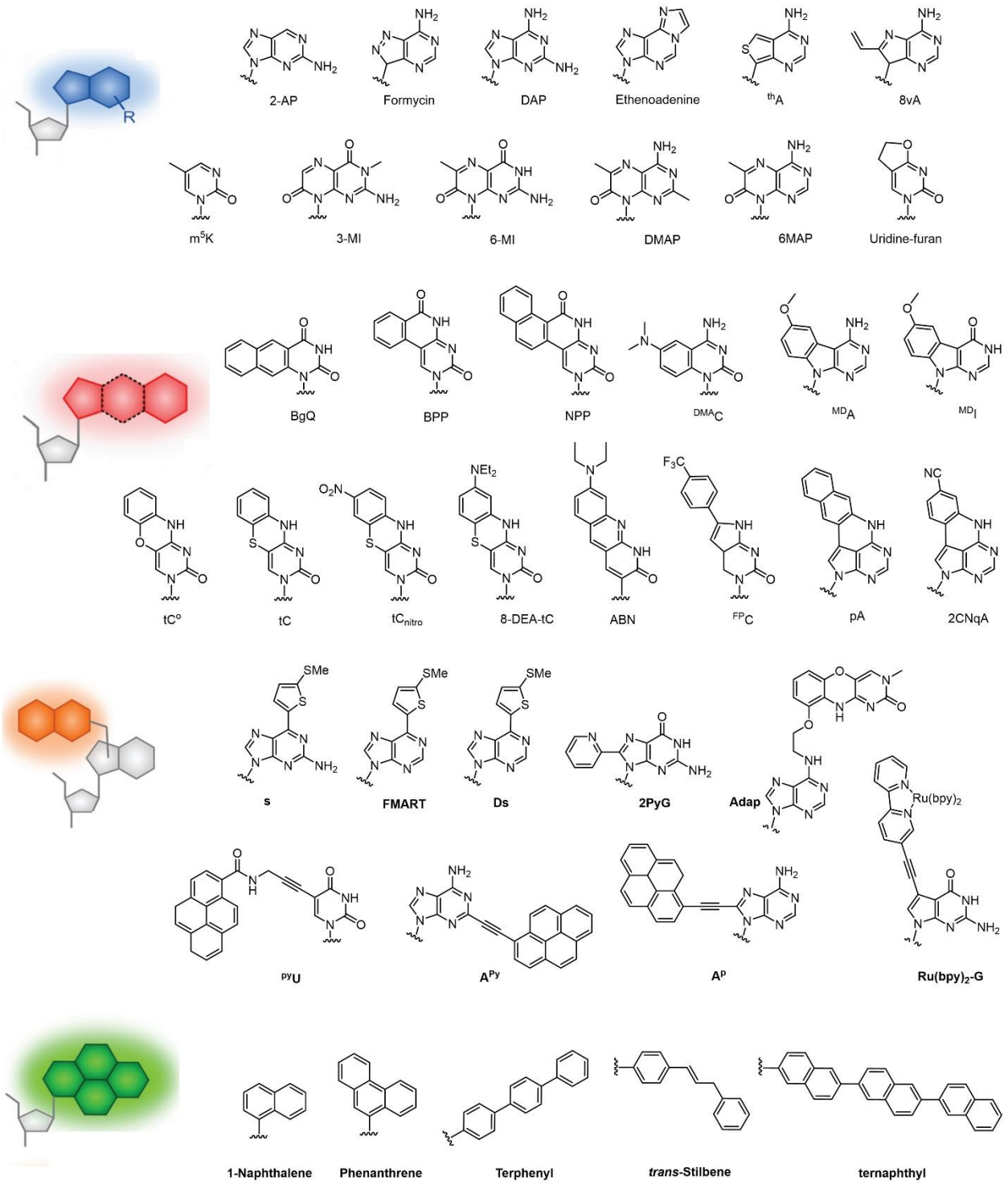

Figure 1.3. Some examples of the reported FBAs.

In the 2010s, the number of FBAs were dramatically increased, and start-ups and companies began to commercialize the FBA phosphoramidites (e.g tC,[88, 105] tC^{o},[106-108] tC$_{Nitro}$[104] as important members of tC family[109-110]) or oligonucleotides modified with an FBA (e.g 2AP). Thus, FBAs' applications began to expanded in many areas including single nucleotide polymorphism (SNP) detection,[111-113] microenvironment monitoring,[114-116] structural and morphological measurements,[117-119] polymerase activity testing,[120-122] and nanostructures stability investigations.[123] In the early 2010s, FBAs probing DNA secondary structures were introduced.[124] *Luedtke* reported 2PyG as a probe for G-quadruplex structures[125] and ^{DMA}C to probe *i*-motif formation[126] (these secondary structures will be discussed in Chapter 4, Section 4.1). *Tor* reported thieno[3,4-d]-6-aminopyrimidine (thA)[101] to monitor adenosine deaminase-catalyzed interconversion of this adenosine analog into inosine,[127] and *Beal* used RNA containing thA to evaluate the reactivity of ADAR2 enzyme.[128] Later, a furan-fused uracil analog was developed to conduct functional detection of human concentrative nucleoside transporters *in vivo*,[129] and adenosine derivative of 2-oxo-1,3-diazaphenoxazine (Adap) was reported, which could selectively detect 8-oxoguanine (OG)[130] and pair with it in primer extension.[131] In the late 2010s, research into FBAs as DNA repair probes increased[132-133] and *Kool* developed a series of FBAs for quantification of DNA damage and repair: FMART for real-time monitoring of MUTYH activity in OG repair,[134] a chromophoric pyrene as the electron donor to 1-methyladenine for measuring intracellular ALKBH3[135] and ALKBH2 activity,[54] or as an excimer clamp for measuring NTH1 activity in oxidized pyrimidines excision.[136]

Since 2008, the brightest reported FBA has been tC^{o} with a very modest brightness of only εφ = 2,000 $M^{-1}cm^{-1}$.[106] With the development of single-molecule fluorescence spectroscopy,[137] there was a growing need for bright FBAs. In 2020 to 2022 period, four extremely bright FBAs were reported: 2CNqA (εφ = 2,600 $M^{-1}cm^{-1}$) by *Wilhelmsson*,[138] which enabled "stealth" labeling of antisense oligonucleotide therapeutics;[139] ^{ts}T (εφ = 4,250 $M^{-1}cm^{-1}$) by *Luedtke,* which enabled probing both local and global dynamics of DNA (discussed in Chapters 2 and 3);[140] ^{RM}A$_{Qn}$ (εφ = 6,068 $M^{-1}cm^{-1}$) by *Seo,* a molecular rotor which was synthesized by direct arylation of DNA,[141] and finally ABN (εφ = 10,400 $M^{-1}cm^{-1}$) by *Purse,* the first FBA to offer single-molecule fluorescence detection capabilities.[142] During this time, tC^{o} triphosphates incorporated into an mRNA and live-cell visualization demonstrated the resulting transcript is translated into the correct protein,[143] *Sugiyama* reported a bifunctional trifluoromethylphenylpyrrolocytidine derivative (^{FP}dC) for both fluorescence and ^{19}F NMR

spectroscopic DNA analysis,[144] and *Jäschke* developed red-shifted and fluorogenic FBA photoswitches.[145] The choice of which fluorescent nucleobase is most appropriate for the given application depends on the context of the experiment. For example, in the design of reporters of enzymatic activity, fluorescent nucleobases might either interact with an enzyme substrate or serve as the substrate themselves; thus, on enzymatic reactions, their fluorescence signal changes can be detected in real-time.

1.5 Microenvironment-sensitive FBAs

Many fluorescent DNA probes predominantly offer qualitative information (e.g. detecting and visualizing DNA). However, in order to study nucleic acids' structural and conformational polymorphisms, interactions, and dynamics, quantitative information is needed. Such information, which usually targets the microenvironment around a probe, can be provided using two strategies: (1) diffusion-based experiments, such as fluorescence recovery after photobleaching (FRAP)[146-147] and fluorescence anisotropy;[148] and (2) microenvironment-sensitive probes. FRAP is governed by lateral diffusion of a fluorophore into a region where the dye has been destroyed by intense light. Fluorescence anisotropy is governed by the rotational diffusion of a dye that has been excited by polarized light, where rotational diffusion leads to depolarization of the emission light. Microenvironment sensitive probes include a variety of probes with high sensitivity to changes in polarity,[149-153] viscosity,[154] surrounding pH,[155-156] DNA mismatches,[87,157-158] hybridization,[109,159-160] structures,[155] and dynamics.[140] The main advantage of microenvironment-sensitive probes, compared with FRAP and fluorescence anisotropy methods, is their rapid and straightforward measurements which can provide higher sensitivity.[161] In addition, using microenvironment-sensitive probes in anisotropy measurements can provide more insights into DNA than a non-microenvironment-sensitive probe.[140] Table 1.1 outlines the discrimination power of some of the reported FBAs towards single-stranded, well-matched and mismatched DNA. In Section 3.1, Chapter 3, applications of microenvironment-sensitive probes as SNP reporters will be discussed in detail. Although it is not easy to classify all microenvironment-sensitive FBAs based on their structure-activity relationship, some classifications are presented below.

Table 1.1. Photophysical properties of some reported FBAs and their sensitivity towards DNA hybridization and mismatched pairs.[a]

Name	Ɛ (M^{-1} cm^{-1})	φ % (in *ds*-DNA)	Ɛ φ (in ds-DNA)	Mismatch sensitivity[b]	Hybridization sensitivity[c]	π (ns)[d]	θ (ns)[d]
2PyG[162]	20000	3	600	N.R	1.9	N.R	N.R
PA[163]	14000	10	1400	N.R	2	3.4	N.R
^{ts}T[140]	30600	13.9	4250	27	5	11	20
tC[164]	4000	19	760	1.2	1	6.9	N.R
tC^{o} [107]	9000	21	2000	N.R	1	5.5	N.R
3-MI[81,166]	5500[166]	29	1600	N.R	27	N.R	N.R
6-MI[82]	6800	25	1700	5.7[167]	1.1	5.5	3.27[168]
2-AP[76]	5600	1	50	N.R	6.0	N.R	N.R
BPP[84]	30000	0.2	60	20	23	3.3	N.R
NPP[85]	10200	0.7	71	14	7.4	N.R	N.R
^{MD}A[86]	2700	<0.1	2.4	100	10	N.R	N.R
^{MD}I[86]	7800	1.1	86	5.5	1	N.R	N.R
C^{hpp} [98]	6200	N.R	N.R	14	15	N.R	N.R
dFI[169]	N.R	1.3	N.R	4	19	N.R	N.R
7AQ[170]	N.R	N.R	N.R	2.4	N.R	N.R	N.R
^{Ph}pC[171]	N.R	N.R	N.R	6.7	2.9	N.R	N.R
boPhpC[172]	6650	25	1660	N.R	2.3	N.R	N.R
^{Mep}C[171]	N.R	N.R	N.R	2.0	2.7	N.R	N.R
thG[101]	4100	8[173]	310	2.9	1.4	N.R	N.R
^{ABOX}U[174]	21000	2.5	2250	7.7	2.5	N.R	N.R
^{BFU}U[174]	37000	6.8	220	5.6	3.4	N.R	N.R

[a] Extinction coefficient at the maximum absorbance wavelength (Ɛ), fluorescent quantum yield (φ) in *ds*-DNA, fluorescence lifetime (τ) and anisotropy decay (θ) are reported.

[b] Mismatch sensitivity was calculated as the ratio between the brightness of FBA in well-matched *vs.* mismatched *ds*-DNA.

[c] Hybridization sensitivity was calculated as the ratio between the brightness of FBA in *ds*-DNA *vs. ss*-DNA.

[d] Fluorescence lifetime and anisotropy decay are reported for duplex DNA.

Table 1.1 continue. Photophysical properties of some reported FBAs and their sensitivity towards DNA hybridization and mismatched pairs.[a]

Name	Ɛ (M^{-1} cm^{-1})	φ % (in *ds*-DNA)	Ɛ φ (in ds-DNA)	Mismatch sensitivity[b]	Hybridization sensitivity[c]	π (ns)[d]	θ (ns)[d]
P[175]	N.R	N.R	N.R	20	N.R	N.R	N.R
$^{RM}A_{Qn}$[141]	35700	17	6068	28.3	32.9	N.R	N.R
2CNqA[138]	9200	28	2600	N.R	1.1	9.0	N.R
$^{8\text{-DEA}}$-tC[176]	2700	5.6	150	2.6	5.25	N.R	N.R
$^{8Cl}tC^{o}$ [176]	5600	20	1120	2	2	N.R	N.R
C^{f} [177]	N.R	8.6	N.R	3.5	3	N.R	N.R
ABN[142]	20000	52	10400	1.4	1.1	N.R	N.R
dC^{TBdp} [178]	41900	N.R	N.R	2.1[c]	2.1[c]	1.5	N.R
dC^{bdp} [178, 116]	N.R	N.R	N.R	2.2[c]	1.6[c]	1.0	N.R
^{diox}T[179]	3600	20	622	3.8	2.2	1.9	N.R
^{b}T[180]	4500	0.4	18	N.R	2.8	N.R	N.R
qAN1[181]	8800	5.8	510	N.R	1.1	N.R	N.R
qAN4[182]	6300	4.4	275	N.R	1.7	0.7	N.R
^{DMA}T[183]	2900	20	580	2.2	2.2	N.R	N.R
Furan-dC[184]	N.R	N.R	N.R	2	N.R	N.R	N.R
$^{2\text{-Ant}}U$[185]	N.R	22	N.R	5.1	2.4	N.R	N.R
$^{9\text{-Ant}}U$[185]	N.R	3	N.R	3.1	2.8	N.R	N.R
^{3n7z}A[186]	N.R	14	N.R	2	7	N.R	N.R
U^{FL} [187]	N.R	N.R	N.R	8.3	2.2	N.R	N.R
C^{C} [188]	15200	2	301	N.R	4.3	N.R	N.R

[a] Extinction coefficient at the maximum absorbance wavelength (Ɛ), fluorescent quantum yield (φ) in *ds*-DNA, fluorescence lifetime (τ) and anisotropy decay (θ) are reported.

[b] Mismatch sensitivity was calculated as the ratio between the brightness of FBA in well-matched *vs.* mismatched *ds*-DNA.

[c] Hybridization sensitivity was calculated as the ratio between the brightness of FBA in *ds*-DNA *vs. ss*-DNA.

[d] Fluorescence lifetime and anisotropy decay are reported for duplex DNA.

Photo induced electron transfer (PET) probes: Upon PET quenching, FBAs can be either reduced or oxidized to form a charge-transfer complex with one of the surrounding nucleobases and further undergoing radiationless relaxation to the ground state. Electron-poor FBAs such as 2AP are reductively quenched by purines,[189] and electron-rich systems such as ^{MD}A (Figure 1.3) are oxidatively quenched by pyrimidines.[86] The degree of quenching can be estimated by comparing the redox potentials of the natural nucleobases with that of the FBA.[190-191] This determines whether an FBA is quenched by all four natural nucleobases or selectively by a few of them. For example, 2AP is quenched by all natural bases, with G being the most efficient quencher,[192] and upon incorporation into DNA its fluorescence is severely quenched by up to a 200-fold.[193] Thus, 2AP is not a sensitive probe in the context of well-folded nucleic acids. In contrast, FBAs that are selectively quenched by their complementary WCF pair, can discriminate between single-stranded and duplex DNAs and can be used to develop fluorogenic probes.[86] Beyond PET, other mechanisms have also been proposed to explain FBA quenching, such as the formation of dark non-emissive states *via* mixing and delocalizing of molecular orbitals of the fluorophore among neighboring nucleobases, as it has been proposed for 8-vinyladenosine (8vdA, Figure 1.3).[194]

pH-Sensitive probes: The energy level and electron density of HOMO and LUMO of FBAs can change at different pH values. Such probes demonstrate a pH-sensitive fluorescence and can be used to probe the folding and unfolding of DNA structures upon protonation and deprotonation. One example is ^{DMA}C which exhibits remarkable red-shifted absorption and emission maxima upon pH decrease and base (N3) protonation.[126] These properties were exploited to study the dynamics of folding and unfolding of *i*-motif and DNA duplexes of telomeric repeat sequences under real-time conditions.

Molecular rotors: The group of fluorophores known as fluorescent molecular rotors, have segmental mobility and their fluorescence intensity and/or wavelength is a function of mobility freedom. They are composed of rotary bond(s), and when bound to their target (e.g. duplex DNA, complementary DNA strand, aptamer, metal, or small molecules), their fluorescence changes. The remainder of this chapter focuses on molecular rotors and their applications in probing DNA.

1.6 Fluorescent molecular rotors (FMRs)

Over the past years the term “molecular rotors” have been extensively used in the contexts of biophysics,[195-196] photophysics,[197] synthetic biology,[198] nanoscience,[199-202] supramolecular chemistry[203-204] and even therapeutics[205] to describe molecules that consist of two parts that can easily rotate relative to each other. The rotation can be one-dimensional (which involves changes in a single angle) or two-dimensional (which involves changes in a dihedral angle). It is common to view the part with the larger moment of inertia as stationary (the stator) and the part with the smaller moment of inertia as the rotator. The rotator and the stator both turn around a common axis in the absence of molecular mounting. In the context of fluorescence spectroscopy (which is the focus of this chapter), the term molecular rotor is commonly used to describe a fluorescent molecule that can undergo an intramolecular twisting motion in the ground and/or excited state, in which the amount of rotation determines the fluorescence signal.

Typically, a fluorescent molecular rotor with a twisted excited state, consists of three subunits, an electron donor, an electron acceptor, and a “bridge” that is composed of a network of alternative single and double bonds. This network brings the donor and acceptor units in conjugation, thus facilitating electron movement between the pair, but it ensures minimum overlap of the electron donor and electron acceptor orbitals.[206] In this configuration, the molecule responds to photoexcitation with an intramolecular charge transfer from the donor to the acceptor unit and assumes the excited-state configuration D^{+}-π-A^{-}. The charge separation is associated with an increased dipole moment.[207] Polar solvent molecules orient themselves along the fluorophore dipole by aligning their electric fields. Upon relaxation, the solvent molecules return to the ground-state orientation. Consequently, the fluorophore exhibits a bathochromic shift that reflects the energy expended for the reorientation of the solvent molecules. The magnitude of this effect depends on the solvent polarity, that is, its dielectric constant.[208] Molecular rotors typically exhibit stronger solvatochromism in the twisted intramolecular charge transfer (TICT) state emission band than in the planar locally excited (LE) emission band. Furthermore, both the ground state and the excited state energy levels depend on the degree of intramolecular rotation.[209-211] The *Jabłonski* diagram of the energy states can be extended to include the TICT state energy levels (Figure 1.4). In the ground state, a planar conformation is energetically preferred, whereas the twisted conformation is the preferred conformation in the excited state due to the repulsive electrostatic forces.[212] Relaxation from the

TICT state occurs in one of the two ways: If the energy gap between the ground state (S0) and the energetically higher first excited state (S1) is large enough to allow photon emission (Figure 1.4A), such a molecule exhibits a distinct second emission band that is redshifted from the LE fluorescence.[213] Conversely, when the TICT energy gap is much smaller than the LE energy gap (Figure 1.4B), nonradiative relaxation occurs from the TICT conformation.[214] Fluorophores of this class exhibit only a single emission band.

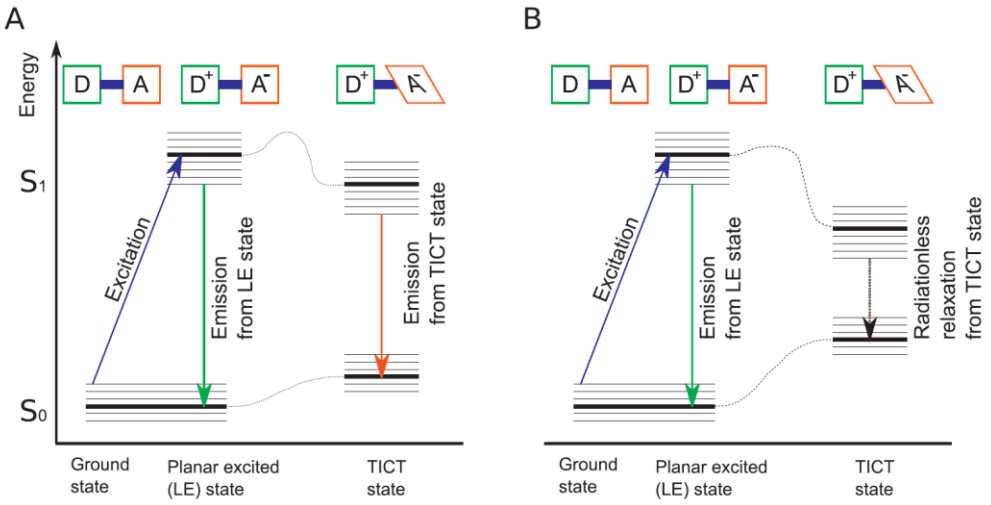

Figure 1.4. Extended *Jabłonski* diagram for molecular rotors. Different vibrational states (indicated by parallel lines) cause some energy loss, and emission from the LE state occurs at a longer wavelength than the excitation (*Stokes* shift). For molecular rotors, the excited state energy is lower in the TICT state, whereas the ground state energy is higher in the TICT state than in the LE state. Therefore, the S1 - S0 energy gap is lower in the TICT state with a correspondingly lower relaxation energy. In the case of molecular rotors with dual-band emission, the TICT energy gap is slightly smaller than the LE energy gap (A). If the TICT energy gap is much smaller than the LE energy gap, emission from the TICT state occurs without photon emission (B). This figure is adopted from REF[206], Springer Nature.

The most notable feature of molecular rotors is the dependency of the twisted state formation rate on the local microenvironment, predominantly the microviscosity of the solvent. In the case of molecular rotors that emit from the twisted state with a red-shifted emission band, steric hindrance of the twisted state formation in higher-viscosity solvents changes the emission in favor of the shorter-wavelength emission from the planar state.[215] In the case of molecular rotors that exhibit nonradiative relaxation from the twisted state, the fluorescent quantum yield increases in higher-viscosity solvents.[216] Due to their microenvironment and viscosity sensitivity, fluorescent molecular

rotors have found applications in cell biology,[217-218] as biosensors for both bulk and local microviscosity,[219-223] fluorogenic probes for a Halo tag,[224-225] detecting the formation of hydrophobic microdomains,[226] lipid–lipid packing,[227] peptide–protein interactions,[228] mapping microbubble viscosity,[229] selective protein detection in living cells,[230] and real-time monitoring of protein binding, aggregation and conformational changes.[206, 231-234] In the next section, applications of the fluorescent molecular rotor as DNA probes will be discussed.

1.7 FMRs as DNA probes

The inherent sensitivity of molecular rotors to the polarity and viscosity of their microenvironment allows simultaneous fluorescence readouts, making them highly attractive fluorescent probes. Rotational diffusion governs the propensity of a molecular rotor to form twisted states and therefore connects diffusivity to fluorescence quantum yield. In this respect, molecular rotors report diffusivity similar to anisotropy probes. However, the dominating factor in molecular rotor emission is the rotation of one segment relative to the other. The segment is generally very small and enjoys greater freedom of rotation than a typical anisotropy probe. The relationship between viscosity, rotational diffusivity, and intramolecular rotation makes molecular rotors attractive reporters of local dynamics in DNA.[235]

1.7.1 Non-covalent rotary DNA probes

Many DNA intercalators and groove binders have rotary properties and, while in the free form have a very low fluorescent quantum yield, are highly fluorescent when intercalated between DNA bases as their rotation is restricted.[236-238] One example is acridizinium molecular rotors (Figure 1.5), which upon intercalating with DNA, the intramolecular rotation of the molecule around the N-phenyl bond is restricted, leading to an increase in fluorescence signal.[239-240] *Ghadessy* and *Teo* reported a molecular rotor incorporating an acridine orange group (AO-R, Figure 1.5) that intercalates between DNA base-pairs, but upon displacement by p53, a DNA binding protein, its fluorescence turns off.[241]

Thioflavin-T (ThT, Figure 1.5), a benzothiazole based FMR with ultrafast non-radiative torsional motion around the central C–C bond in its excited state,[242] was used to study pre-melting of DNA and showed 220-fold higher fluorescence in the presence of calf thymus (CT) DNA.[243] The results obtained

with ThT have been compared with commonly used DNA stains, ethidium bromide (EB) and 4',6-diamidino-2-phenylindole (DAPI), which show only 15 and 27 times emission enhancement, respectively. In addition, ThT shows even a greater fluorescence enhancement when it binds to *ds*-DNAs containing cavity structures such as an abasic site, a gap site or a mismatch site.[244] The DNA cavities provide appropriate spaces to accommodate ThT and allow the occurrence of some specific interactions. ThT was also used to monitor the structural changes in natural CT DNA during pre-melting[243] and probe G-quadruplex formation.[245-246] It can tightly bind non-G-quadruplex DNAs with several GA motifs and dimerize them in a parallel double-stranded mode, accompanied by over 100-fold enhancement in the fluorescence emission of ThT.[247-248]

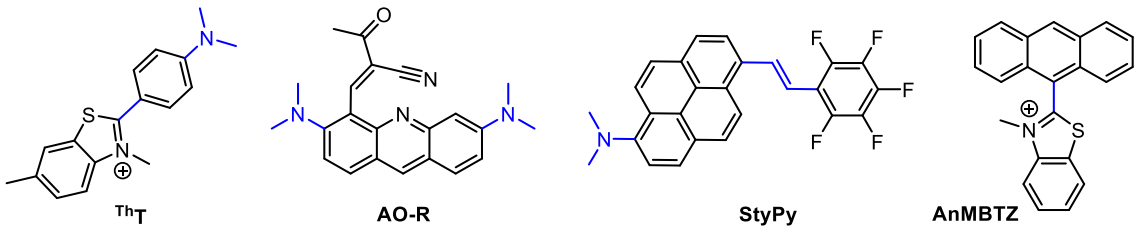

Figure 1.5. Some examples of non-covalent rotary probes for DNA. The relevant rotatable bonds are shown in blue color.

The *Walther* Group introduced pentafluorostyryl-aminopyrene (StyPy, Figure 1.5), a viscosity-sensitive probe, which has a push–pull structure with a TICT excited state that shows an enormous *Stokes* shift.[249] In another example, *Nath* and coworkers reported 10-anthracene-10-yl-3-methylbenzothiazol-3-ium chloride (AnMBTZ, Figure 1.5) as a turn-on intercalating probe and studied its interaction with DNA.[250]

1.7.2 External and linear rotary DNA probes

Inspired by the naturally occurring green fluorescent protein (GFP)[251], which contains a molecular rotor-type fluorophore having a (4-hydroxybenzylidene)imidazolin-3-one skeleton,[252] *Stafforst* and *Diederichsen* reported peptide nucleic acids (PNAs) incorporating a (4-hydroxybenzylidene)-2-methylimidazolin-3-one (HBI, Figure 1.6) residue and their fluorescence

enhancement by 2.2 times upon the formation of PNA–DNA duplexes.[253] *Seitz* and coworkers developed forced intercalation probes by controlling the conformation of the excited state of thiazole orange (TO, Figure 1.6) dyes upon intercalation between the base-pairs of the probe–target duplexes.[254-256] The concomitant viscosity increase restricts torsions around the methine bridge and prolongs the lifetime of the TO excited state.[257] For example, they used PNAs functionalized with TO as SNP sensors, where TO fluorescence increased up to 26-fold upon DNA-PNA hybridization and attenuated when forced to intercalate next to a mismatched base-pair.[258] The forced intercalation (FIT) probes were found to be useful for the detection of DNA in quantitative polymerase chain reaction (qPCR) and for wash-free detection of RNA in cells and tissues.[259-261] Later, to enhance both brightness and responsiveness, the highly responsive TO nucleoside was combined with the highly emissive oxazolopyridine analog JO in serinol (Figure 1.6).[261]

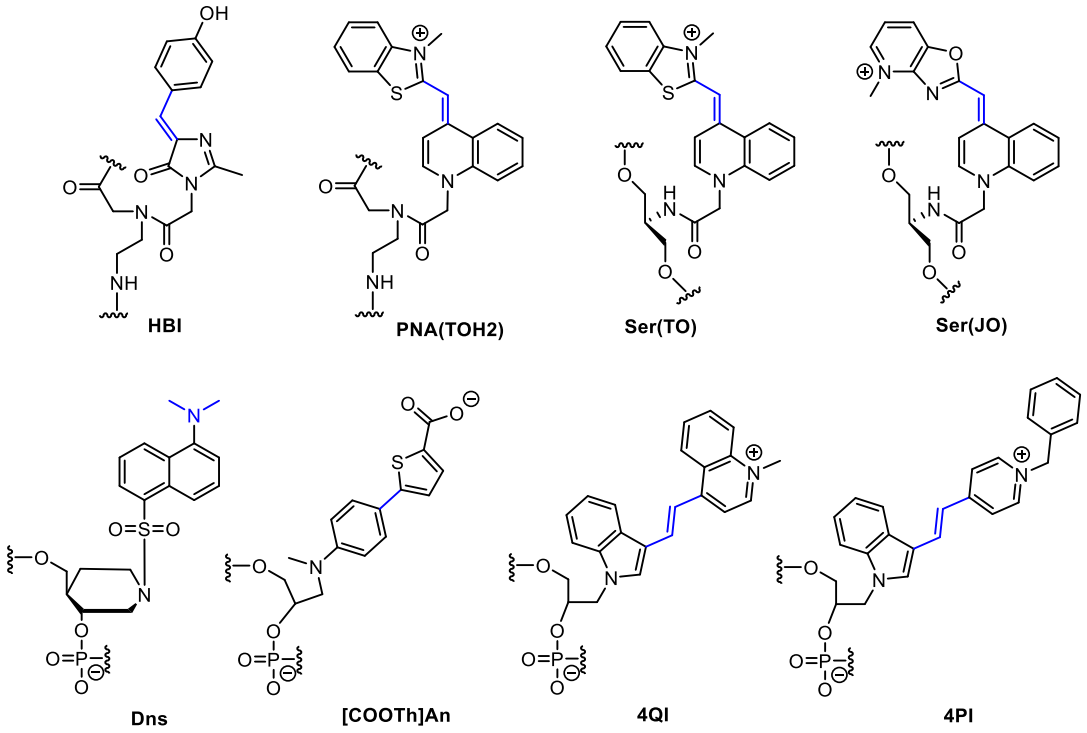

Figure 1.6. Some examples of linear rotary probes for DNA and PNA. The relevant rotatable bonds are shown in blue color.

Very recently, a solvatochromic Dansyl-nucleoside surrogate (Dns, Figure 1.6) based on (±)-*trans*-4-(hydroxymethyl) piperidin-3-ol was incorporated into DNA. The color-changing DNA probe could detect complementary oligonucleotides and distinguish mismatches in a Dansyl/nucleobase-

pair by the naked eye.[262] In another example, *Manderville* Group replaced a nucleoside with N-methyl-4-bromoaniline containing an acyclic N-glycol group and employed it in an on-strand *Suzuki–Miyaura* reaction. The synthesized donor–acceptor biaryl nucleobase surrogates demonstrated a 40-fold increase in emission intensity in single-stranded oligonucleotides.[263] Screening the best acceptor for turn-on fluorescence upon duplex formation afforded the carboxythiophene derivative [COOTh]An (Figure 1.6) exhibiting a 7.4-fold emission intensity increase upon formation of a single-bulged duplex with the surrogate occupying a pyrimidine-flanked bulge. Insertion of the [COOTh]An surrogate into the lateral TT loops produced by the antiparallel G-quadruplex of the thrombin binding aptamer (TBA) afforded a 4.1-fold increase in probe fluorescence that was accompanied by a 20 nm wavelength shift to the blue upon thrombin binding. In addition, *Manderville* and *Wetmore* presented cyanine-indole-quinolinium (4QI, Figure 1.6) hemicyanine dye tethered to an acyclic 1,2-propanediol linker and positioned it within the G-quadruplex loop in a TBA.[264] Thrombin binding to 4QI-TBA diminished π-stacking interactions between 4QI and the G-quadruplex, resulting in fluorescence quenching. Similarly, an indole−pyridinium (4PI, Figure 1.6) probe was synthesized and inserted into the loop residues of TBA to monitor G-quadruplex folding in the presence of Pb^{2+} versus K^{+}.[265]

Inspired by the FMRs targeted to hydrophobic protein pockets[224-225] and the similarities in hydrophobicity between these sites and abasic sites generated in DNA by base-excision repair, *Kool* introduced universal base excision reporter (UBER, Figure 1.7) probe which has TICT excited state.[266] Once the DNA glycosylases initiate base excision repair, the resulting hemiacetal abasic site, which is in equilibrium with its aldehyde form, provides a convenient handle targeted with reactive alpha nucleophiles. The molecular rotor design achieved a robust >250−500-fold increase in UBER fluorescence upon reaction with abasic sites in DNA.

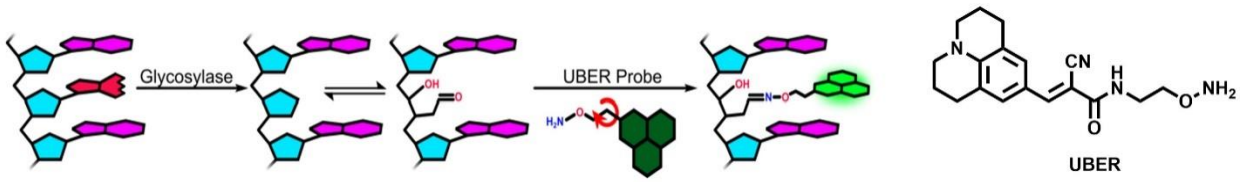

Figure 1.7. Light-up mechanism of the UBER probe design in measuring DNA glycosylase activity. The figure is adopted from REF[266].

1.8 Fluorescent nucleobase rotors (FBRs)

Numerous modified nucleobases have been extensively explored and utilized in recent years, containing a conjugated aromatic residue with a rotatable bond, which separates two aromatic entities and adds a new level of interplay between structure and photophysical properties.[153] The fluorescence of FBRs is a function of their rotary motions which depends on DNA stacking, conformation, dynamics, and hybridization. Thus, they have found great applications in probing SNPs, viscosity, molecular crowding and interactions. Despite the large number of reported FBRs, only a few of them were rationally designed to enhance microenvironment sensitivity by their rotary motions, and most of them were used in experiments that do not exploit the probes' rotary motions. On the other hand, the photophysical properties of FBRs cannot currently be predicted solely from their structures, despite significant research efforts dedicated to the further theoretical understanding of molecular rotors' properties. Therefore, a systematic review of the previously reported FBRs and more fundamental research on FBRs' structure-activity relationships are needed to expand their applications. In this section, FBRs are categorized based on their relevant rotatable bond(s) are categorized, and their applications are discussed.

1.8.1 FBRs based on dimethyl amino group

A classic and textbook example of compounds with a TICT excited state, is 4-*N,N*-dimethylamino-benzonitrile (DMABN). DMABN was one of the first molecules whose dual fluorescence in polar solvents was studied. DMABN is almost planar in the ground state, which corresponds to the maximum conjugation between the dimethyl amino and phenyl ring. According to the *Franck-Condon* principle, the LE state is still planar, but solvent relaxation occurs with a concomitant rotation of the dimethylamino group until it is twisted at nearly a right angle and the conjugation is lost. 6-Propionyl-2-dimethylaminonaphthalene (PRODAN) is another example of a well-known microenvironment-sensitive and strongly solvatochromic fluorophore.[267] However, it must be mentioned that the nature of the emitting state of PRODAN is still under debate. Some semiempirical calculations suggest emitting state of PRODAN is a TICT state involving rotation of the dimethylamino group and/or the propanoyl group,[268-270] while other studies conducted that the TICT state of PRODAN has an energy higher than its planar state.[271-272]

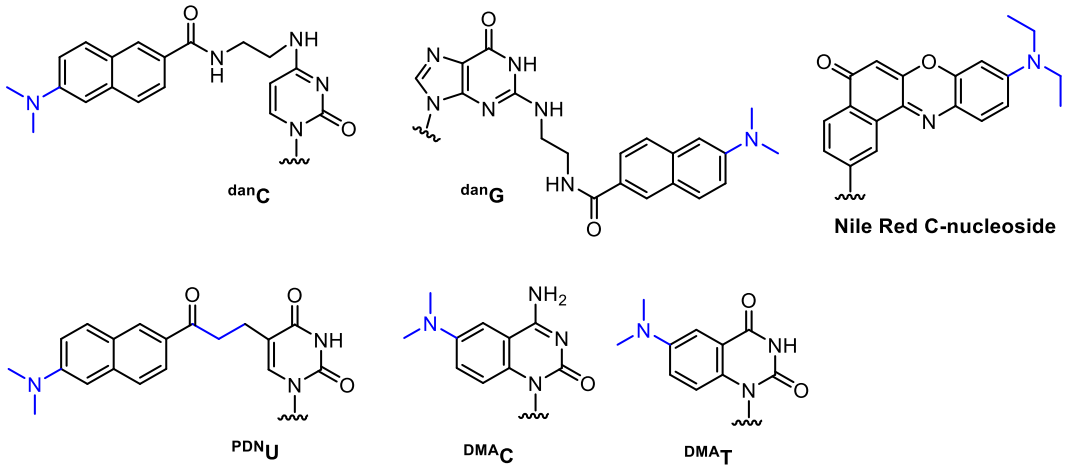

Figure 1.8. Some examples of reported FBRs containing a dimethyl (or diethyl) amino group. The relevant rotatable bonds are shown in blue color.

Saito and *Okamoto* synthesized DNAs containing ^{PDN}X (X = U, C, A, and G, Figure 1.8), to which a PRODAN fluorophore was attached at pyrimidine C5 or purine C8 positions.[273] The ^{PDN}X changed the *Stokes* shift values depending on the DNA structure. In particular, the excitation spectrum of the ^{PDN}X-containing *ds*-DNA shifted to a longer wavelength, and the fluorescence intensity was enhanced when ^{PDN}X could form a WCF base-pair with the opposing base. *Majima* described DNA oligonucleotides containing fluorophore dan (6-(dimethylamino)-2-acylnaphthalene) —modified cytidine and guanosine (^{dan}C and ^{dan}G, Figure 1.8) as novel microenvironment—sensitive fluorescent probes.[274] ^{dan}C and ^{dan}G could monitor the microenvironmental change in the major and minor grooves of DNA and could report RNA hybridization as well as B- to A-form and B- to Z-form DNA conformational transitions.[274-275] *Fujiwara* designed a Nile Red C-nucleoside (Figure 1.8) for examining the changes in the polarity of the microenvironment surrounding DNA.[150] Upon addition of β-cyclodextrin, the fluorescence intensity of the Nile Red nucleoside increased to 6.2 times the initial intensity due to prevention of the rotational freedom of the diethylamino group and the decrease in the polarity inside the cavity. *Luedtke* reported dimethylaniline fused to pyridines (^{DMA}C and ^{DMA}T, Figure 1.8) as probes for *i*-motif structures and DNA hybridization. ^{DMA}C is sensitive towards DNA folding, strand-displacement and *i*-motif formation.[75] ^{DMA}T showed a mismatch sensitivity, with up to 2.2-fold fluorescence enhancement when its dynamics was restricted in a well-matched duplex (^{DMA}T:A),[183] and could probe Hg^{II} binding to the T:T and C:T mismatches.[276-277]

1.8.2 FBRs with an aryl-aryl rotary bond

Aryl-aryl conjugated systems, are one of the most widely used molecular rotors.[278-279] The molecular structure of biphenyls has been the subject of many investigations; it is planar in the solid crystal[280] but is non-planar in the gas phase.[281] This non-planarity arises through rotation of the rings around the biphenyl bond, as a balance between hydrogen repulsion and favorable inter-ring π overlap. The relative rotation of the biphenyl rings with respect to each other can be tuned by substitution on one or both of the phenyl rings.[282-283] In unsubstituted biphenyl, the average angle is 44°.[284] Upon photoexcitation, the dihedral angle changes and biphenyl takes a planar geometry in S1. However, the biphenyl systems containing electron-donating and withdrawing group(s) act as push-pull TICT fluorophores and upon photoexcitation remain non-planar but still exhibit changes in their dihedral angle. Thus, in both cases, biphenyl systems demonstrate rotary motions and have inspired the design of many FBRs.

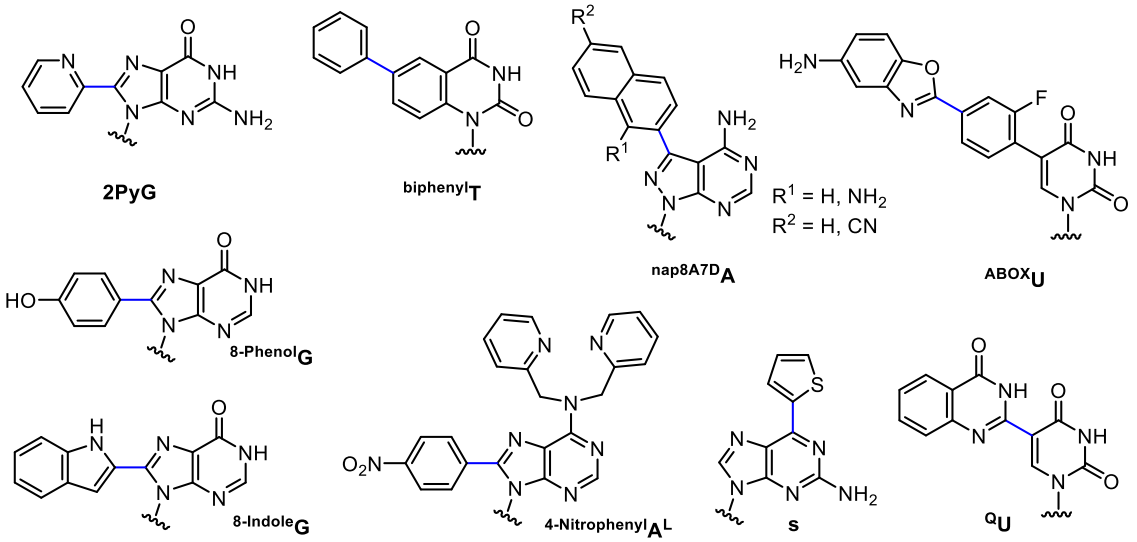

Figure 1.9. Fluorescent base derivatives bearing an aromatic group attached *via* aryl-aryl or aryl-vinyl bond to the base. The relevant rotatable bonds are shown in blue color.

Hocek attached fluorinated biaryl fluorescent labels to nucleoside triphosphates, such as ^{ABOX}U (Figure 1.9), and incorporated them into DNA using KOD XL polymerase.[174] These probes demonstrated large solvatochromic shifts (due to the differences in dipole moments of the ground and excited states). In addition, they were pH-sensitive, could recognize hairpin loops over *ds*-DNA, and detected mismatches by showing a higher fluorescence in the more rigid microenvironment.

Luedtke reported a series of biphenyl fused thymidine as solvatochromic probes,[149] and 8-(2-pyridyl)-2'-deoxyguanosine (2PyG, Figure 1.9) as a probe for G-quadruplex structures.[125] Due to its rotary behavior, 2-PyG was the first example of a fluorescent guanine mimic that exhibits higher quantum yield upon incorporation into folded oligonucleotides than that of the free nucleoside in water. Consistent with rotary motions and the more rigid microenvironment of G-quadruplex structures than *ds*-DNA, the quantum yield of 2PyG is two- to four-fold higher in the former. In contrast with the effect of local viscosity on fluorescence intensity, 2PyG showed a higher quantum yield in *ss*-DNA than *ds*-DNA due to the PET quenching in the duplex structure.[162] 2PyG was also used as a selective bidentate ligand for transition-metal ions and directed them to specific N7 sites in duplex and G-quadruplex structures.[285] *Saito* synthesized various 7-naphthylated 8-aza-7-deaza-2'-deoxyadenosine derivatives (^{nap8A7D}A, Figure 1.9), containing a cyano group at the 6-position of naphthalene ring to strengthen the push-pull system and attached an amino group to the sterically hindered 1-position of naphthalene to favor the twisted molecular geometry in the ground state.[286] ^{nap8A7D}A derivatives showed solvatochromic properties that could discriminate thymine bases in DNA duplexes by wavelength and intensity changes in fluorescence emissions. Another example of an FBR is 2-amino-6-(2-thienyl)purine (s, Figure 1.9), whose fluorescence intensity in RNA molecules changes according to the structural microenvironment.[287] Another approach to developing rotary fluorescent adenine analogs is to modify position 8 with aromatic groups.[288] 8-phenyl, 8-thienyl, and 8-furyladenine derivatives have been synthesized and some have dual emission bands due to the TICT excited state.[289] One such example is an 8-(4-nitrophenyl)adenine derivative bearing a chelating *N,N*-bis(2-pyridylmethyl)amine group at the C6 position ($^{4\text{-Nitrophenyl}}A^{L}$, Figure 1.9).[290] The electron density of the push-pull system was redistributed upon coordination to Pb^{2+}, thus, $^{4\text{-Nitrophenyl}}A^{L}$ was used as an "on–off"-type fluorescent sensor for Pd^{2+}. The *Hudson* group has recently synthesized biaryl quinazolinone-uracil nucleobase analogs (such as ^{Q}U, Figure 1.9), which responded to DNA-PNA hybridization by turning on fluorescence intensity.

1.8.3 FBRs with ethenyl rotor

Molecules with a double bond conjugating two aryl groups together undergo twisting around the double bond upon photoexcitation. Although sometimes this twisting can result in *trans* to *cis* photoisomerization (or *vice versa*), it can also lead to non-radiative decay to the same isomer. The main difference between FBRs containing aryl groups conjugated *via* an ethenyl linker with those

conjugated *via* an aryl-aryl single bond is that the former is planar in the ground state and thus, its excitation is more red-shifted than the biaryl systems.

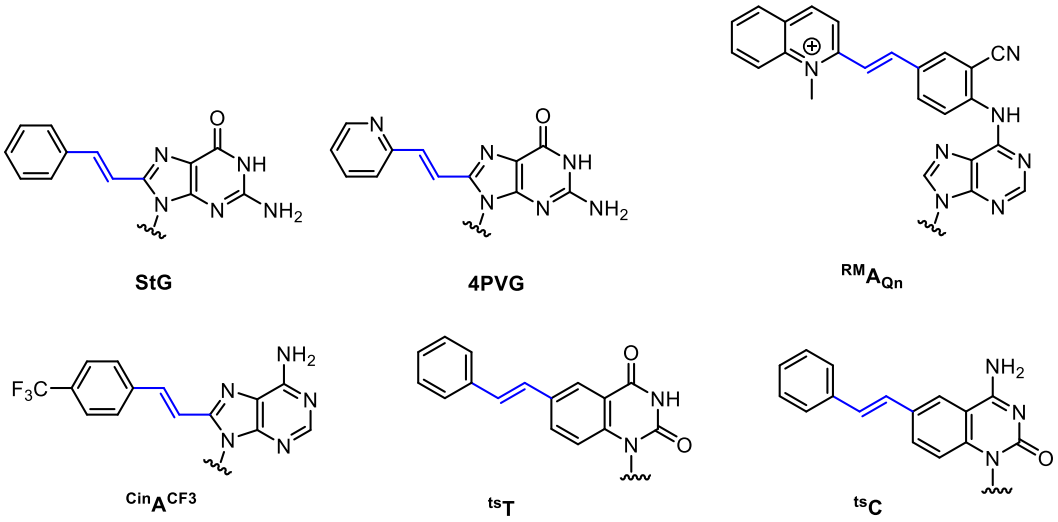

Figure 1.10. Some examples of reported FBRs with two aromatic rings conjugated *via* an ethylene linker. The relevant rotatable bonds are shown in blue color.

Luedtke reported 8-(2-phenylethenyl)-2′-deoxyguanosine (StG, Figure 1.10) and 8-[2-(pyrid-4-yl)-ethenyl]-2′-deoxyguanosine (4PVG, Figure 1.10) with enhanced fluorescence when DNA folded into G-quadruplexes compared with duplex structures.[291] ^{ts}T and ^{ts}C (Figure 1.10) are new FBRs reported in this thesis. ^{ts}T discriminates well-matched and mismatched nucleobases by up to 27.8-fold fluorescence enhancement in the more rigid, well-matched structure (this will be discussed in Chapters 2 and 3).[140] ^{ts}C is a light-up bathochromic probe that reports *i*-motif folding (Chapter 4). Another example is 8-(p-CF_3-cinnamyl)-modified adenosine ($^{Cin}A^{CF3}$, Figure 1.10),[289] which could recognize cyclin D1 mRNA marker by a 2-fold fluorescence increase.[292] Recently, *Seo* applied direct N6 arylation of adenosines located in natural oligonucleotides as a tool to incorporate quinolinium salts-attached vinyl aniline as a molecular rotor.[141] The resulting rotor ($^{RM}A_{Qn}$, Figure 1.10) revealed a 28.3 times higher fluorescence in a well-matched duplex than *ss*-DNA or mismatched *ds*-DNA.

1.8.4 FBRs with an ethynyl linker

Sonogashira coupling has been used to connect fluorophores to nucleobases *via* an ethynyl linker.[293,294] Most of the works have targeted the C5 position of pyrimidines,[295,296] such as U^{FL} (Figure

1.11), which discriminates between well- and mismatched base-pairings,[297] and C^{FL} (Figure 1.11), which was used as a fluorescent probe for DNA–protein (p53) or DNA–lipid interactions.[298]

The *Hocek* group functionalized adenosine with solvatochromic fluorophores 4-aminophthalimide (API) and 4-(dimethylamino)phthalimide (DAPI) *via* a propargyl linker.[299] API-labeled DNA was used for the detection of DNA-protein interactions with either the sequence-specific p53 protein or a non-specific single-strand binding (SSB) protein. Both proteins changed the polarity around the fluorophore and increased (2–3 fold) the intensity of API fluorescence. *Hocek* also attached a tryptophan-based fluorophore from cyan fluorescent protein and GFP-like fluorophores to C5 of cytosine *via* a propargyl tether.[300] The probe ^{Trp}C (Figure 1.11)[301] showed a 2.0-fold fluorescence increase in the presence of SSB protein, and *ds*-DNA containing C^{MBI} or C^{FBI} (Figure 1.11)[300] demonstrated 2.0−3.2 times higher fluorescence upon binding p53. In the absence of p53 protein, non-emissive energy dissipation was caused by bond rotation. Relaxation to the ground state by an emissive pathway requires planarity and was induced by constraining bond rotation, which was achieved by interactions of rotary C^{MBI} and C^{FBI} with the protein. C^{FBI} was also used in a time-resolved experiment monitoring incorporation of a single nucleotide by Vent(exo-) polymerase.[300] Other examples include C^{VDP} and C^{bdp} (Figure 1.11).[302-303] C^{VDP} is a viscosity-sensitive probe based on aminobenzylidenecyanoacetamide which showed a four-fold increase in fluorescence intensity upon DNA binding to the SSB protein.[302] C^{bdp} was used in time-correlated single-photon counting (TCSPC), fluorescence correlation spectroscopy (FCS), and fluorescence lifetime imaging (FLIM). C^{bdp} could respond to interactions with DNA-binding proteins and lipids by changes in the fluorescence lifetimes (from 0.8 to 2.1 ns) and revealed changes in the microenvironment of exogenous DNA in cells.[116] The applications of FBRs in detecting DNA structures was expanded by GFP-based uracil analogs, U^{HBI} and U^{FBI} which exhibited enhanced fluorescence upon triplex formation.[304]

Highly microenvironment-sensitive nucleosides (such as ^{3HC}U, Figure 1.11)[305] based on the 3-hydroxychromone fluorophore exhibiting a two-band ratiometric fluorescence response have been reported by *Burger* to probe DNA hybridization and DNA–protein interactions.[306-309] Near-IR emitting squaraine-modified nucleosides (such as U^{SQ}, Figure 1.11) have been reported, which exhibit >300-fold fluorescence enhancement in viscous conditions and thus, visualize highly viscous regions during various stages of cellular mitosis by fluorescence microscopy.[310] Recently *Seo* has reported two 2'-deoxyuridine triphosphates ($dU_{CN2}TP$, $dU_{PY}TP$, Figure 1.11) in which a *p*-vinylaniline-based

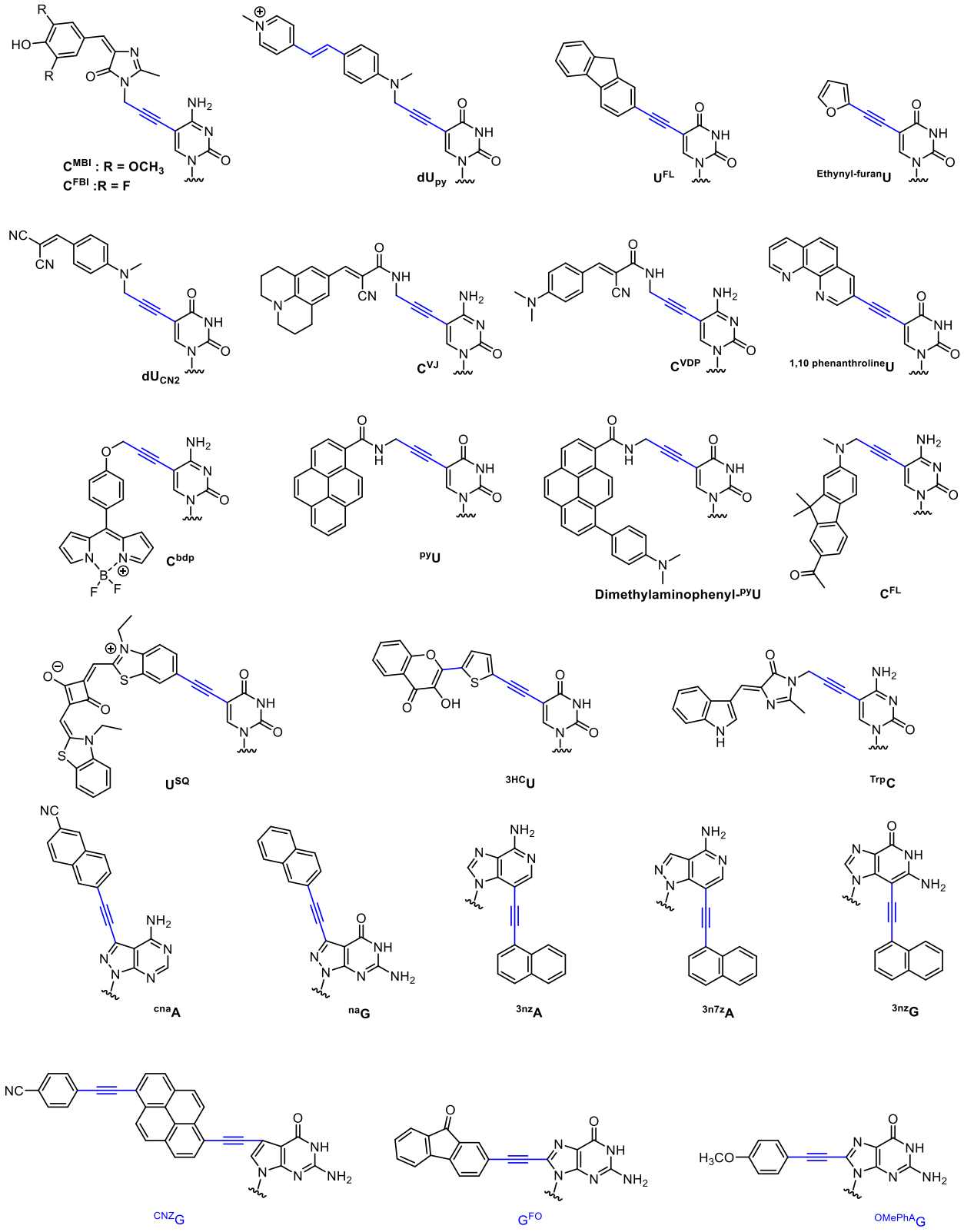

Figure 1.11. Some examples of FBAs with a conjugated ethynyl linker. The relevant rotatable bonds are shown in blue color.

fluorophore is linked through a propargyl unit at the C5 position.[311] The triphosphates were incorporated into DNA, and their fluorescence was strongly enhanced when the *c-myc* G-quadruplex was bound to nucleolin. This fluorescence increase originated from the restricted rotation of *p*-vinylaniline, which is a well-established rotor that displays high sensitivity toward environmental viscosity.[312-313]

Saito reported a wide variety of solvatochromic FBAs based on substituted purines and diverse aza- and/or deaza-analogs of purine bases with an ethynyl linker which formed a stable WCF base-pair and changed their emission wavelengths upon hybridization with target sequences.[314] As shown in Figure 1.11, some of these probes are naphthalene derivatives of 8-aza-7-deaza-2'-deoxyguanosine (^{na}G),[315] 8-aza-7-deaza-2'-deoxyadenosine (^{cna}A),[316] 7-deaza-2'-deoxyadenosine (^{CNZ}A), or 7-deaza-2'-deoxyguanosine (^{CNZ}G). The latter contains a 1,6-disubstituted pyrene chromophore.[317] Other probes of interest are 3-deaza-2'-deoxyguanosine (^{3nz}G)[318] and 3-deaza-2'-deoxyadenosine (^{3nz}A),[319] which exhibited dual fluorescence emission from a TICT state and an LE state. To tune the electron-donating/accepting ability of the ^{3nz}A nucleobase according to the design concept of charge-transfer, *Saito* reported ^{3n7z}A (Figure 1.11), comprising an 8-aza-3,7-dideazapurine (pyrazolo[4,3-c]pyridine) skeleton. This probe demonstrated much higher discrimination between well-matched T in the complementary strand by fluorescence enhancement and a distinct change in the emission wavelength.[186] Furthermore, modifications of adenine and guanine at position 8 with an aromatic group via an ethyne linker were explored by *Fischer* (e.g ^{OMePhA}G, Figure 1.11)[289] and *Hwang* (e.g G^{FO}, Figure 1.11)[320] which showed solvatochromic properties.

1.8.5 Rotors clamped between two nucleobases

Oligonucleotides incorporating stacking-sensitive nucleosides have been studied as dual rotors, which, based on the microenvironment, can rotate around both the glycosidic bond and the bond that links the nucleobase to the rotor. Pyrrolo-cytosines (pCs) are representative of this approach. Typically, the fluorophore is positioned opposite to an SNP site. Hybridization to a well-matched target causes the FBA to stack between the surrounding nucleobases, and locates the rotor partially out of the duplex. A fluorescence quenching is observed in this case (Figure 1.12). However, in the case of a mismatched target, the mismatch can flip out and provide enough space for the well-

stacked conformation of the rotor and a light-up response is observed (Figure 1.12). In comparison with ^{Me}pC, ^{Ph}pC (Figure 1.12) demonstrates two-fold higher sensitivity towards mismatches. This difference is due to the lack of TICT excited state in ^{Me}pC, where the conjugated phenyl is replaced with a methyl group.[171] In the case of ^{Ph}pC, its fluorescence intensity in *ss*-DNA is less than mismatched *ds*-DNA but higher than well-matched *ds*-DNA. This can be explained by the globular/hairpin structure of *ss*-DNA which results in the partial stacking of the rotor between the neighboring bases and causes a fluorescence enhancement as compared to the well-matched *ds*-DNA.[140]

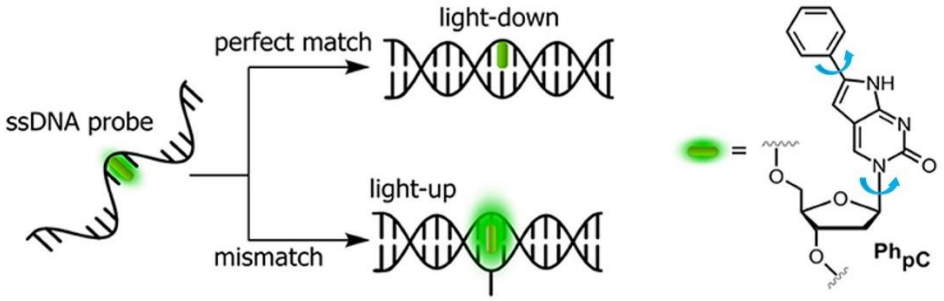

Figure 1.12. ^{Ph}pC is a dual FBR that, when the mismatched opposing base is flipped out, rotates around the glycosidic bond and places the rotary fluorophore between the DNA bases. The figure is adopted from REF[235] with minor changes.

Numerous molecular rotors showing mismatch detection responses due to rotation around the glycosidic bond have been described. The *Tor* group designed ^{furan}U, ^{thiophene}U, and ^{furan}C, as viscosity-sensitive fluorescent molecular probes (Figure 1.13).[154, 321] Viscous media impeded the free rotation of these heterocycles. This resulted in an increase in fluorescence intensity by reducing the contribution of the nonradiative decay pathway. When the oligonucleotide containing ^{furan}U was hybridized to a complimentary strand containing an abasic site on the opposite side, a significant emission enhancement was observed compared to that of the matched *ds*-DNA. Similar to the case with a mismatched-base flipping out, it is believed that the intrahelical vacant and confined space between the neighboring base-pairs effectively limited the free rotation of the furan-uracil single bond, resulting in an increase in fluorescence. ^{thiophene}U was found to be an efficient probe for the detection of G, OG, and its transverse mutation product T by providing significantly different emission intensities.[184] Numerous 6-azauracil derivatives have been synthesized containing furan,[322] thiofene,[322-323] or their corresponding benzoheterocycle[324] attached to the 5 position of uracil. With

more intensive push-pull interactions between electron-deficient uridine core and electron-rich, extended aromatic moieties, these extended 6-aza-uridines showed enhanced bathochromic shifts with remarkable sensitivity to polarity, pH or viscosity changes; however their rotary properties were not explored when incorporated into oligonucleotides.

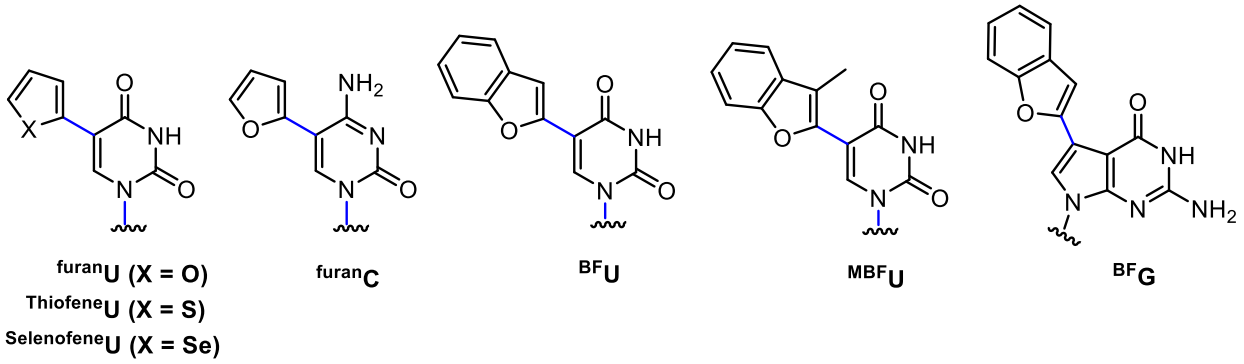

Figure 1.13. Some examples of FBRs that can be sandwiched between neighboring DNA bases. The relevant rotatable bonds are shown in blue color.

The *Srivatsan* Group synthesized $^{\text{Selenophene}}$U (Figure 1.13), which was incorporated into a bacterial ribosomal decoding site (A-site) and could effectively signal the binding of aminoglycoside antibiotics to the RNA construct.[325] *Srivatsan* also synthesized $^{\text{BF}}$U (Figure 1.13) and incorporated it into oligoribonucleotides using T7 RNA polymerase to produce fluorescent oligoribonucleotide constructs.[326] Abasic site-containing duplexes were constructed by hybridizing an RNA transcript to custom DNA and RNA oligonucleotides that contained an abasic-site surrogate. The RNA:DNA duplex containing an abasic site showed nearly a four-fold higher emission than the unmodified RNA:DNA duplex. An RNA:RNA duplex that possessed an abasic site opposite to the modified uracil showed slightly increased emission compared to that of the unmodified RNA:RNA duplex. In addition, they designed benzofuran-labeled 2'-deoxyuridine and demonstrated that it can distinguish an abasic site in a model depurinated sarcin/ricin RNA motif of a eukaryotic 28S rRNA.[327]

Linking a benzofuran to uracil inspired the *Seio* Group, and they made 5-(3-methylbenzofuran-2-yl)deoxyuridine ($^{\text{MBF}}$U, Figure 1.13), containing a methyl group that enforces a large twist between two aryl rings and thus showed better fluorescence enhancements than $^{\text{BF}}$U upon triplex formation.[328] The benzofuran moieties of $^{\text{BF}}$U and $^{\text{MBF}}$U, when located in the major groove can rotate when the DNA containing them forms a duplex with target nucleic acids (Figure 1.14A).

However, upon binding to triplex-forming oligonucleotides with a propylene linker (C3), the benzofuran ring becomes sandwiched between two bases (Figure 1.14B). These flanking bases make the benzofuran and uracil ring coplanar, thus enhancing the fluorescence of ^{BF}U and ^{MBF}U. This system was later used as an adenosine sensor which could detect the binding of adenosine to the abasic site next to ^{MBF}U.[329] In addition, *Seio* reported 7-(benzofuran-2-yl)-7-deazaguanine (^{BF}G, Figure 1.13),[330] which when incorporated into *ss*-DNA shows 91-fold fluorescence enhancement upon binding of SSB protein.[331]

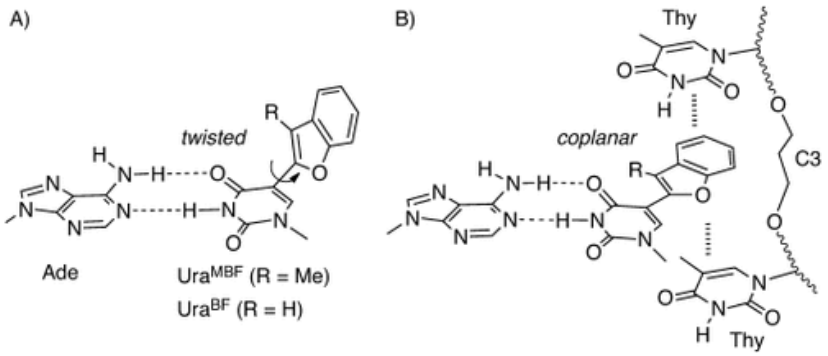

Figure 1.14. A benzofuran uracil analog (A) non-planar in *ds*-DNA and (B) forced to be planar in a triplex structure. The figure is adopted from REF[328].

1.9 Thesis objectives

This thesis aims to develop a novel fluorescent nucleobase rotor to probe the structure and dynamics of DNA in order to address fundamental biological questions about nucleic acids. Chapter 2 introduces the design and synthesis of a rotary base analog (^{ts}T) which overcomes the brightness and sensitivity limitations of the previously reported FBAs. Chapter 3 demonstrates that ^{ts}T possesses ideal molecular rotor properties for detecting local dynamic motions associated with base-pair mismatches. Its high brightness and rotary motions make ^{ts}T a microenvironment-sensitive thymine analog, exhibiting a 28-fold brighter fluorescence intensity when base-paired with A as compared to T or C. This type of tool could eventually be used in point-of-care clinal detection of single polymorphisms. In addition, ^{ts}T is the first FBA sensitive to long-range dynamic changes and can be used as a spectroscopic "ruler" for measuring distances to various types of DNA damage including oxidation and methylation. Chapter 4 builds on this by introducing the cytosine analog ^{ts}C for probing the folding and unfolding of C-rich sequences. Finally, in Chapter 5, we extend our structural studies

to the fast and reversible switching of DNA secondary structures by coordination of Hg^{II} to mismatches. We have designed and characterized a long *ds*-DNA containing numerous CT mismatches that is able to translate a series of local conformational changes into global helical transition upon the stochiometric addition of Hg^{II}. This unprecedented metal-base switching of DNA conformation may eventually be utilized as a switch for protein-binding interactions and/or future nanomechanical devices.

1.10 References

[1] Dahm, R., From discovering to understanding. Friedrich Miescher's attempts to uncover the function of DNA. *EMBO Rep* **2010,** *11* (3), 153-160.

[2] Richter, F. C., Remembering Johann Gregor Mendel: a human, a Catholic priest, an Augustinian monk, and abbot. *Molecular genetics & genomic medicine* **2015,** *3* (6), 483-485.

[3] Avery, O. T.; Macleod, C. M.; McCarty, M., Studies on the chemical nature of the substance inducing transformation of pneumococcal types: induction of transformation by a desoxyribonucleic acid fraction isolated from pneumococcus type III. *J. Exp. Med.* **1944,** *79* (2), 137-158.

[4] Hershey, A. D.; Chase, M., Independent functions of viral protein and nucleic acid in growth of bacteriophage. *J. Gen. Physiol.* **1952,** *36* (1), 39-56.

[5] Levene, P. A.; Jacobs, W. A., Über Inosinsäure. *Berichte der deutschen chemischen Gesellschaft* **1909,** *42* (1), 1198-1203.

[6] Elson, D.; Chargaff, E., On the desoxyribonucleic acid content of sea urchin gametes. *Experientia* **1952,** *8* (4), 143-145.

[7] Franklin, R. E.; Gosling, R. G., Molecular Configuration in Sodium Thymonucleate. *Nature* **1953,** *171* (4356), 740-741.

[8] Wilkins, M. H. F.; Stokes, A. R.; Wilson, H. R., Molecular structure of nucleic acids: molecular structure of deoxypentose nucleic acids. *Nature* **1953,** *171* (4356), 738-740.

[9] Watson, J. D.; Crick, F. H. C., Molecular structure of nucleic acids: a structure for deoxyribose nucleic acid. *Nature* **1953,** *171* (4356), 737-738.

[10] Watson, J. D., *Molecular Biology of the Gene*. Benjamin: W. A., New York, 1965.

[11] Crick, F., Central Dogma of Molecular Biology. *Nature* **1970,** *227* (5258), 561-563.

[12] Messikommer, A.; Seipel, K.; Byrne, S.; Valk, P. J. M.; Pabst, T.; Luedtke, N. W., RNA Targeting in Acute Myeloid Leukemia. *ACS Pharmacol. Transl. Sci.* **2020,** *3* (6), 1225-1232.

[13] Hsu, P. D.; Lander, E. S.; Zhang, F., Development and applications of CRISPR-Cas9 for genome engineering. *Cell* **2014,** *157* (6), 1262-1278.

[14] Huang, T. P.; Newby, G. A.; Liu, D. R., Precision genome editing using cytosine and adenine base editors in mammalian cells. *Nat. Protoc.* **2021,** *16* (2), 1089-1128.

[15] Musunuru, K.; Chadwick, A. C.; Mizoguchi, T.; Garcia, S. P.; DeNizio, J. E.; Reiss, C. W.; Wang, K.; Iyer, S.; Dutta, C.; Clendaniel, V.; Amaonye, M.; Beach, A.; Berth, K.; Biswas, S.; Braun, M. C.; Chen, H.-M.; Colace, T. V.; Ganey, J. D.; Gangopadhyay, S. A.; Garrity, R.; Kasiewicz, L. N.; Lavoie, J.; Madsen, J. A.; Matsumoto, Y.; Mazzola, A. M.; Nasrullah, Y. S.; Nneji, J.; Ren, H.; Sanjeev, A.; Shay, M.; Stahley, M. R.; Fan, S. H. Y.; Tam, Y. K.; Gaudelli, N. M.; Ciaramella, G.; Stolz, L. E.; Malyala, P.; Cheng, C. J.; Rajeev, K. G.; Rohde, E.; Bellinger, A. M.; Kathiresan, S., In vivo CRISPR base editing of PCSK9 durably lowers cholesterol in primates. *Nature* **2021,** *593* (7859), 429-434.

[16] Koblan, L. W.; Erdos, M. R.; Wilson, C.; Cabral, W. A.; Levy, J. M.; Xiong, Z.-M.; Tavarez, U. L.; Davison, L. M.; Gete, Y. G.; Mao, X.; Newby, G. A.; Doherty, S. P.; Narisu, N.; Sheng, Q.; Krilow, C.; Lin, C. Y.; Gordon, L. B.; Cao, K.; Collins, F. S.; Brown, J. D.; Liu, D. R., In vivo base editing rescues Hutchinson–Gilford progeria syndrome in mice. *Nature* **2021,** *589* (7843), 608-614.

[17] Porto, E. M.; Komor, A. C.; Slaymaker, I. M.; Yeo, G. W., Base editing: advances and therapeutic opportunities. *Nat. Rev. Drug Discov.* **2020,** *19* (12), 839-859.

[18] Lapinaite, A.; Knott, G. J.; Palumbo, C. M.; Lin-Shiao, E.; Richter, M. F.; Zhao, K. T.; Beal, P. A.; Liu, D. R.; Doudna, J. A., DNA capture by a CRISPR-Cas9–guided adenine base editor. *Science* **2020,** *369* (6503), 566.

[19] Rees, H. A.; Liu, D. R., Base editing: precision chemistry on the genome and transcriptome of living cells. *Nat. Rev. Genet.* **2018,** *19* (12), 770-788.

[20] Gaudelli, N. M.; Komor, A. C.; Rees, H. A.; Packer, M. S.; Badran, A. H.; Bryson, D. I.; Liu, D. R., Programmable base editing of A•T to G•C in genomic DNA without DNA cleavage. *Nature* **2017,** *551* (7681), 464-471.

[21] Komor, A. C.; Kim, Y. B.; Packer, M. S.; Zuris, J. A.; Liu, D. R., Programmable editing of a target base in genomic DNA without double-stranded DNA cleavage. *Nature* **2016,** *533* (7603), 420-424.

[22] Jordan, D.; Mills, D., Past, present, and future of DNA typing for analyzing human and non-human forensic samples. *Front. Ecol. Evol.* **2021,** *9*.

[23] Tikhomirov, G.; Petersen, P.; Qian, L., Fractal assembly of micrometre-scale DNA origami arrays with arbitrary patterns. *Nature* **2017,** *552* (7683), 67-71.

[24] Dey, S.; Fan, C.; Gothelf, K. V.; Li, J.; Lin, C.; Liu, L.; Liu, N.; Nijenhuis, M. A. D.; Saccà, B.; Simmel, F. C.; Yan, H.; Zhan, P., DNA origami. *Nat. Rev. Dis. Primers* **2021,** *1* (1), 13.

[25] Kopperger, E.; List, J.; Madhira, S.; Rothfischer, F.; Lamb, D. C.; Simmel, F. C., A self-assembled nanoscale robotic arm controlled by electric fields. *Science* **2018,** *359* (6373), 296.

[26] Ramezani, H.; Dietz, H., Building machines with DNA molecules. *Nat. Rev. Genet.* **2020,** *21* (1), 5-26.

[27] Ceze, L.; Nivala, J.; Strauss, K., Molecular digital data storage using DNA. *Nat. Rev. Genet.* **2019,** *20* (8), 456-466.

[28] Kool, E. T., Hydrogen bonding, base stacking, and steric effects in dna replication. *Annu. Rev. Biophys. Biomol. Struct* **2001,** *30*, 1-22.

[29] Kypr, J.; Kejnovská, I.; Renciuk, D.; Vorlícková, M., Circular dichroism and conformational polymorphism of DNA. *Nucleic Acids Res.* **2009,** *37* (6), 1713-1725.

[30] Mergny, J. L.; Li, J.; Lacroix, L.; Amrane, S.; Chaires, J. B., Thermal difference spectra: a specific signature for nucleic acid structures. *Nucleic Acids Res.* **2005,** *33* (16), e138.

[31] Chim, N.; Meza, R. A.; Trinh, A. M.; Yang, K.; Chaput, J. C., Following replicative DNA synthesis by time-resolved X-ray crystallography. *Nat. Commun.* **2021,** *12* (1), 2641.

[32] Wang, X.; Alnabati, E.; Aderinwale, T. W.; Maddhuri Venkata Subramaniya, S. R.; Terashi, G.; Kihara, D., Detecting protein and DNA/RNA structures in cryo-EM maps of intermediate resolution using deep learning. *Nat. Commun.* **2021,** *12* (1), 2302.

[33] Sakamoto, T.; Yamaoki, Y.; Nagata, T.; Katahira, M., Detection of parallel and antiparallel DNA triplex structures in living human cells using in-cell NMR. *Chem. Commun.* **2021,** *57* (52), 6364-6367.

[34] Lakowicz, J. R., *Principles of fluorescence spectroscopy*. 3rd ed.; Springer: New York, 2006.

[35] Triemer, T.; Messikommer, A.; Glasauer, S. M. K.; Alzeer, J.; Paulisch, M. H.; Luedtke, N. W., Superresolution imaging of individual replication forks reveals unexpected prodrug resistance mechanism. *Proc. Natl. Acad. Sci. U. S. A.* **2018,** *115* (7), E1366-e1373.

[36] Tera, M.; Luedtke, N. W., Chapter Nineteen - Cross-linking cellular nucleic acids via a target-directing double click reagent. In *Methods Enzymol.*, Chenoweth, D. M., Ed. Academic Press: 2020; Vol. 641, pp 433-457.

[37] Schreier, V. N.; Loehr, M. O.; Deng, T.; Lattmann, E.; Hajnal, A.; Neuhauss, S. C. F.; Luedtke, N. W., Fluorescent dATP for DNA synthesis in vivo. *ACS Chem. Biol.* **2020,** *15* (11), 2996-3003.

[38] Zhen, S. J.; Xiao, X.; Li, C. H.; Huang, C. Z., An Enzyme-Free DNA Circuit-Assisted Graphene Oxide Enhanced Fluorescence Anisotropy Assay for MicroRNA Detection with Improved Sensitivity and Selectivity. *Anal. Chem.* **2017,** *89* (17), 8766-8771.

[39] Zelger-Paulus, S.; Hadzic, M.; Sigel, R. K. O.; Börner, R., Encapsulation of Fluorescently Labeled RNAs into Surface-Tethered Vesicles for Single-Molecule FRET Studies in TIRF Microscopy. *Methods Mol. Biol.* **2020,** *2113*, 1-16.

[40] Platnich, C. M.; Rizzuto, F. J.; Cosa, G.; Sleiman, H. F., Single-molecule methods in structural DNA nanotechnology. *Chem. Soc. Rev.* **2020,** *49* (13), 4220-4233.

[41] Kapuscinski, J.; Darzynkiewicz, Z., Interactions of acridine orange with double stranded nucleic acids. Spectral and affinity studies. *J. Biomol. Struct. Dyn.* **1987,** *5* (1), 127-143.

[42] Cosa, G.; Focsaneanu, K. S.; McLean, J. R.; McNamee, J. P.; Scaiano, J. C., Photophysical properties of fluorescent DNA-dyes bound to single- and double-stranded DNA in aqueous buffered solution. *Photochem. Photobiol.* **2001,** *73* (6), 585-599.

[43] Kapuscinski, J., Interactions of nucleic acids with fluorescent dyes: spectral properties of condensed complexes. *J. Histochem. Cytochem.* **1990,** *38* (9), 1323-1329.

[44] Watkins, D.; Gong, C.; Kellish, P.; Arya, D. P., Probing A-form DNA: A fluorescent aminosugar probe and dual recognition by anthraquinone-neomycin conjugates. *Bioorg. Med. Chem.* **2017,** *25* (4), 1309-1319.

[45] Luedtke, N. W.; Carmichael, P.; Tor, Y., Cellular Uptake of Aminoglycosides, Guanidinoglycosides, and Poly-arginine. *J. Am. Chem. Soc.* **2003,** *125* (41), 12374-12375.

[46] Lauria, A.; Montalbano, A.; Barraja, P.; Dattolo, G.; Almerico, A. M., DNA minor groove binders: an overview on molecular modeling and QSAR approaches. *Curr. Med. Chem.* **2007,** *14* (20), 2136-2160.

[47] Kurmis, A. A.; Dervan, P. B., Sequence specific suppression of androgen receptor–DNA binding in vivo by a Py-Im polyamide. *Nucleic Acids Res.* **2019,** *47* (8), 3828-3835.

[48] Dervan, P. B.; Edelson, B. S., Recognition of the DNA minor groove by pyrrole-imidazole polyamides. *Curr. Opin. Struct. Biol.* **2003,** *13* (3), 284-299.

[49] Chenoweth, D. M.; Meier, J. L.; Dervan, P. B., Pyrrole-Imidazole Polyamides Distinguish Between Double-Helical DNA and RNA. *Angew. Chem. Int. Ed.* **2013,** *52* (1), 415-418.

[50] Kapuscinski, J., DAPI: a DNA-Specific Fluorescent Probe. *Biotech. Histochem.* **1995,** *70* (5), 220-233.

[51] Narayanaswamy, N.; Das, S.; Samanta, P. K.; Banu, K.; Sharma, G. P.; Mondal, N.; Dhar, S. K.; Pati, S. K.; Govindaraju, T., Sequence-specific recognition of DNA minor groove by an NIR-fluorescence switch-on probe and its potential applications. *Nucleic Acids Res.* **2015,** *43* (18), 8651-8663.

[52] Alzeer, J.; Luedtke, N. W., pH-Mediated fluorescence and G-quadruplex binding of amido phthalocyanines. *Biochemistry* **2010,** *49* (20), 4339-4348.

[53] Tatikolov, A. S., Polymethine dyes as spectral-fluorescent probes for biomacromolecules. *J. Photochem. Photobiol. C: Photochem. Rev.* **2012,** *13* (1), 55-90.

[54] Wilson, D. L.; Beharry, A. A.; Srivastava, A.; O'Connor, T. R.; Kool, E. T., Fluorescence probes for ALKBH2 allow the measurement of DNA alkylation repair and drug resistance responses. *Angew. Chem. Int. Ed.* **2018,** *57* (39), 12896-12900.

[55] Chan, K. M.; Xu, W.; Kwon, H.; Kietrys, A. M.; Kool, E. T., Luminescent carbon dot mimics assembled on DNA. *J. Am. Chem. Soc.* **2017,** *139* (37), 13147-13155.

[56] Rosenblum, B. B.; Lee, L. G.; Spurgeon, S. L.; Khan, S. H.; Menchen, S. M.; Heiner, C. R.; Chen, S. M., New dye-labeled terminators for improved DNA sequencing patterns. *Nucleic Acids Res.* **1997,** *25* (22), 4500-4504.

[57] Lacroix, A.; Vengut-Climent, E.; de Rochambeau, D.; Sleiman, H. F., Uptake and fate of fluorescently labeled DNA nanostructures in cellular environments: A cautionary tale. *ACS Central Science* **2019,** *5* (5), 882-891.

[58] Lopez, A.; Liu, B.; Huang, Z.; Zhang, F.; Liu, J., Fluorescein-stabilized i-motif DNA and its unfolding leading to a stronger adsorption affinity. *Langmuir* **2019,** *35* (36), 11932-11939.

[59] Fuller, C. W.; Middendorf, L. R.; Benner, S. A.; Church, G. M.; Harris, T.; Huang, X.; Jovanovich, S. B.; Nelson, J. R.; Schloss, J. A.; Schwartz, D. C.; Vezenov, D. V., The challenges of sequencing by synthesis. *Nat. Biotechnol.* **2009,** *27* (11), 1013-1023.

[60] Lacenere, C.; Garg, M. K.; Stoltz, B. M.; Quake, S. R., Effects of a modified dye-labeled nucleotide spacer arm on incorporation by thermophilic DNA polymerases. *Nucleosides Nucleotides Nucleic Acids* **2006,** *25* (1), 9-15.

[61] Kuhn, H.; Demidov, V. V.; Coull, J. M.; Fiandaca, M. J.; Gildea, B. D.; Frank-Kamenetskii, M. D., Hybridization of DNA and pna molecular beacons to single-stranded and double-stranded DNA targets. *J. Am. Chem. Soc.* **2002,** *124* (6), 1097-1103.

[62] Mergny, J. L.; Maurizot, J. C., Fluorescence resonance energy transfer as a probe for G-quartet formation by a telomeric repeat. *Chembiochem* **2001,** *2* (2), 124-132.

[63] Moreira, B. G.; You, Y.; Behlke, M. A.; Owczarzy, R., Effects of fluorescent dyes, quenchers, and dangling ends on DNA duplex stability. *Biochem. Biophys. Res. Commun.* **2005,** *327* (2), 473-484.

[64] Varghese, R.; Wagenknecht, H.-A., DNA as a supramolecular framework for the helical arrangements of chromophores: towards photoactive DNA-based nanomaterials. *Chem. Commun.* **2009,** (19), 2615-2624.

[65] Ren, R. X. F.; Chaudhuri, N. C.; Paris, P. L.; Rumney; Kool, E. T., Naphthalene, phenanthrene, and pyrene as DNA base analogues: Synthesis, structure, and fluorescence in DNA. *J. Am. Chem. Soc.* **1996,** *118* (33), 7671-7678.

[66] Xu, W.; Chan, K. M.; Kool, E. T., Fluorescent nucleobases as tools for studying DNA and RNA. *Nat. Chem.* **2017,** *9* (11), 1043-1055.

[67] Dziuba, D.; Didier, P.; Ciaco, S.; Barth, A.; Seidel, C. A. M.; Mély, Y., Fundamental photophysics of isomorphic and expanded fluorescent nucleoside analogues. *Chem. Soc. Rev.* **2021,** *50* (12), 7062-7107.

[68] Saito, Y.; Hudson, R. H. E., Base-modified fluorescent purine nucleosides and nucleotides for use in oligonucleotide probes. *J. Photochem. Photobiol. C: Photochem. Rev.* **2018,** *36*, 48-73.

[69] Srivatsan, S. G.; Sawant, A. A., Fluorescent ribonucleoside analogues as probes for investigating RNA structure and function. *Pure Appl. Chem.* **2010,** *83* (1), 213-232.

[70] Tanpure, A. A.; Pawar, M. G.; Srivatsan, S. G., Fluorescent nucleoside analogs: Probes for investigating nucleic acid structure and function. *Isr. J. Chem.* **2013,** *53* (6-7), 366-378.

[71] Manna, S.; Srivatsan, S. G., Fluorescence-based tools to probe G-quadruplexes in cell-free and cellular environments. *RSC Advances* **2018,** *8* (45), 25673-25694.

[72] Wilson, J. N.; Kool, E. T., Fluorescent DNA base replacements: reporters and sensors for biological systems. *Org. Biomol. Chem.* **2006,** *4* (23), 4265-4274.

[73] Sinkeldam, R. W.; Greco, N. J.; Tor, Y., Fluorescent analogs of biomolecular building blocks: Design, properties, and applications. *Chem. Rev.* **2010,** *110* (5), 2579-2619.

[74] Matarazzo, A.; Hudson, R. H. E., Fluorescent adenosine analogs: a comprehensive survey. *Tetrahedron* **2015,** *71* (11), 1627-1657.

[75] Wilhelmsson, L. M., Fluorescent nucleic acid base analogues. *Q. Rev. Biophys.* **2010,** *43* (2), 159-183.

[76] Ward, D. C.; Reich, E.; Stryer, L., Fluorescence studies of nucleotides and polynucleotides. I. Formycin, 2-aminopurine riboside, 2,6-diaminopurine riboside, and their derivatives. *J. Biol. Chem.* **1969,** *244* (5), 1228-1237.

[77] Lobsiger, S.; Blaser, S.; Sinha, R. K.; Frey, H. M.; Leutwyler, S., Switching on the fluorescence of 2-aminopurine by site-selective microhydration. *Nat. Chem.* **2014,** *6* (11), 989-993.

[78] Secrist, J. A., 3rd; Barrio, J. R.; Leonard, N. J., A fluorescent modification of adenosine triphosphate with activity in enzyme systems: 1,N 6 -ethenoadenosine triphosphate. *Science* **1972,** *175* (4022), 646-647.

[79] Wu, P. G.; Nordlund, T. M.; Gildea, B.; McLaughlin, L. W., Base stacking and unstacking as determined from a DNA decamer containing a fluorescent base. *Biochemistry* **1990,** *29* (27), 6508-6514.

[80] Hawkins, M. E.; Pfleiderer, W.; Mazumder, A.; Pommier, Y. G.; Balis, F. M., Incorporation of a fluorescent guanosine analog into oligonucleotides and its application to a real time assay for the HIV-1 integrase 3'-processing reaction. *Nucleic Acids Res.* **1995,** *23* (15), 2872-2880.

[81] Hawkins, M. E.; Balis, F. M., Use of pteridine nucleoside analogs as hybridization probes. *Nucleic Acids Res.* **2004,** *32* (7), e62.

[82] Hawkins, M. E.; Pfleiderer, W.; Balis, F. M.; Porter, D.; Knutson, J. R., Fluorescence properties of pteridine nucleoside analogs as monomers and incorporated into oligonucleotides. *Anal. Biochem.* **1997,** *244* (1), 86-95.

[83] Godde, F.; Toulmé, J.-J.; Moreau, S., Benzoquinazoline derivatives as substitutes for thymine in nucleic acid complexes. Use of fluorescence emission of benzo[g]quinazoline-2,4-(1H,3H)-dione in probing duplex and triplex formation. *Biochemistry* **1998,** *37* (39), 13765-13775.

[84] Okamoto, A.; Tainaka, K.; Saito, I., Clear distinction of purine bases on the complementary strand by a fluorescence change of a novel fluorescent nucleoside. *J. Am. Chem. Soc.* **2003,** *125* (17), 4972-4973.

[85] Okamoto, A.; Tainaka, K.; Saito, I., Synthesis and properties of a novel fluorescent nucleobase, naphthopyridopyrimidine. *Tetrahedron Lett.* **2003,** *44* (36), 6871-6874.

[86] Okamoto, A.; Tanaka, K.; Fukuta, T.; Saito, I., Design of base-discriminating fluorescent nucleoside and its application to t/c snp typing. *J. Am. Chem. Soc.* **2003,** *125* (31), 9296-9297.

[87] Okamoto, A.; Kanatani, K.; Saito, I., Pyrene-labeled base-discriminating fluorescent DNA probes for homogeneous SNP typing. *J. Am. Chem. Soc.* **2004,** *126* (15), 4820-4827.

[88] Wilhelmsson, L. M.; Sandin, P.; Holmén, A.; Albinsson, B.; Lincoln, P.; Nordén, B., Photophysical characterization of fluorescent DNA base analogue, tC. *J. Phys. Chem. B* **2003,** *107* (34), 9094-9101.

[89] Vrábel, M.; Horáková, P.; Pivonková, H.; Kalachova, L.; Cernocká, H.; Cahová, H.; Pohl, R.; Sebest, P.; Havran, L.; Hocek, M.; Fojta, M., Base-modified DNA labeled by [Ru(bpy)(3)](2+) and [Os(bpy)(3)](2+) complexes: construction by polymerase incorporation of modified nucleoside triphosphates, electrochemical and luminescent properties, and applications. *Chemistry (Easton)* **2009,** *15* (5), 1144-1154.

[90] Hirao, I.; Ohtsuki, T.; Fujiwara, T.; Mitsui, T.; Yokogawa, T.; Okuni, T.; Nakayama, H.; Takio, K.; Yabuki, T.; Kigawa, T.; Kodama, K.; Yokogawa, T.; Nishikawa, K.; Yokoyama, S., An unnatural base pair for incorporating amino acid analogs into proteins. *Nat. Biotechnol.* **2002,** *20* (2), 177-182.

[91] Hirao, I.; Kimoto, M.; Mitsui, T.; Fujiwara, T.; Kawai, R.; Sato, A.; Harada, Y.; Yokoyama, S., An unnatural hydrophobic base pair system: site-specific incorporation of nucleotide analogs into DNA and RNA. *Nat. Methods* **2006,** *3* (9), 729-735.

[92] Kimoto, M.; Hirao, I., Genetic alphabet expansion technology by creating unnatural base pairs. *Chem. Soc. Rev.* **2020,** *49* (21), 7602-7626.

[93] Feldman, A. W.; Romesberg, F. E., Expansion of the genetic alphabet: A chemist's approach to synthetic biology. *Acc. Chem. Res.* **2018,** *51* (2), 394-403.

[94] Malyshev, D. A.; Romesberg, F. E., The expanded genetic alphabet. *Angew. Chem. Int. Ed.* **2015,** *54* (41), 11930-11944.

[95] Kawai, R.; Kimoto, M.; Ikeda, S.; Mitsui, T.; Endo, M.; Yokoyama, S.; Hirao, I., Site-specific fluorescent labeling of RNA molecules by specific transcription using unnatural base pairs. *J. Am. Chem. Soc.* **2005,** *127* (49), 17286-17295.

[96] Hirao, I.; Harada, Y.; Kimoto, M.; Mitsui, T.; Fujiwara, T.; Yokoyama, S., A two-unnatural-base-pair system toward the expansion of the genetic code. *J. Am. Chem. Soc.* **2004,** *126* (41), 13298-13305.

[97] Kimoto, M.; Mitsui, T.; Yokoyama, S.; Hirao, I., A unique fluorescent base analogue for the expansion of the genetic alphabet. *J. Am. Chem. Soc.* **2010,** *132* (14), 4988-4989.

[98] Miyata, K.; Tamamushi, R.; Ohkubo, A.; Taguchi, H.; Seio, K.; Santa, T.; Sekine, M., Synthesis and properties of a new fluorescent bicyclic 4-N-carbamoyldeoxycytidine derivative. *Org. Lett.* **2006,** *8* (8), 1545-1548.

[99] Hurley, D. J.; Seaman, S. E.; Mazura, J. C.; Tor, Y., Fluorescent 1,10-phenanthroline-containing oligonucleotides distinguish between perfect and mismatched base pairing. *Org. Lett.* **2002,** *4* (14), 2305-2308.

[100] Noé, M. S.; Sinkeldam, R. W.; Tor, Y., Oligodeoxynucleotides containing multiple thiophene-modified isomorphic fluorescent nucleosides. *J. Org. Chem.* **2013,** *78* (16), 8123-8128.

[101] Shin, D.; Sinkeldam, R. W.; Tor, Y., Emissive RNA alphabet. *J. Am. Chem. Soc.* **2011,** *133* (38), 14912-14915.

[102] Srivatsan, S. G.; Greco, N. J.; Tor, Y., A highly emissive fluorescent nucleoside that signals the activity of toxic ribosome-inactivating proteins. *Angew. Chem. Int. Ed.* **2008,** *47* (35), 6661-6665.

[103] Börjesson, K.; Preus, S.; El-Sagheer, A. H.; Brown, T.; Albinsson, B.; Wilhelmsson, L. M., Nucleic acid base analog FRET-pair facilitating detailed structural measurements in nucleic acid containing systems. *J. Am. Chem. Soc.* **2009,** *131* (12), 4288-4293.

[104] Preus, S.; Börjesson, K.; Kilså, K.; Albinsson, B.; Wilhelmsson, L. M., Characterization of nucleobase analogue FRET acceptor tCnitro. *J. Phys. Chem. B* **2010,** *114* (2), 1050-1056.

[105] Stengel, G.; Urban, M.; Purse, B. W.; Kuchta, R. D., Incorporation of the fluorescent ribonucleotide analogue tCTP by T7 RNA polymerase. *Anal. Chem.* **2010,** *82* (3), 1082-1089.

[106] Stengel, G.; Urban, M.; Purse, B. W.; Kuchta, R. D., High density labeling of polymerase chain reaction products with the fluorescent base analogue tCo. *Anal. Chem.* **2009,** *81* (21), 9079-9085.

[107] Sandin, P.; Börjesson, K.; Li, H.; Mårtensson, J.; Brown, T.; Wilhelmsson, L. M.; Albinsson, B., Characterization and use of an unprecedentedly bright and structurally non-perturbing fluorescent DNA base analogue. *Nucleic Acids Res.* **2008,** *36* (1), 157-167.

[108] Börjesson, K.; Sandin, P.; Wilhelmsson, L. M., Nucleic acid structure and sequence probing using fluorescent base analogue tCO. *Biophys. Chem.* **2009,** *139* (1), 24-28.

[109] Burns, D. D.; Teppang, K. L.; Lee, R. W.; Lokensgard, M. E.; Purse, B. W., Fluorescence turn-on sensing of DNA duplex formation by a tricyclic cytidine analogue. *J. Am. Chem. Soc.* **2017,** *139* (4), 1372-1375.

[110] Rodgers, B. J.; Elsharif, N. A.; Vashisht, N.; Mingus, M. M.; Mulvahill, M. A.; Stengel, G.; Kuchta, R. D.; Purse, B. W., Functionalized tricyclic cytosine analogues provide nucleoside fluorophores with improved photophysical properties and a range of solvent sensitivities. *Chemistry (Easton)* **2014,** *20* (7), 2010-2015.

[111] Mizuta, M.; Seio, K.; Miyata, K.; Ohkubo, A.; Taguchi, H.; Sekine, M., A pyrimidopyrimidoindole nucleoside (dC PPI): photophysical properties and thermal stability of the modified DNA duplexes. *Nucleosides Nucleotides Nucleic Acids* **2007,** *26* (10-12), 1335-1338.

[112] Saito, Y.; Miyauchi, Y.; Okamoto, A.; Saito, I., Synthesis and properties of novel base-discriminating fluorescent (BDF) nucleosides: a highly polarity-sensitive fluorophore for SNP typing. *Tetrahedron Lett.* **2004,** *45* (42), 7827-7831.

[113] Hwang, G. T., Single-labeled oligonucleotides showing fluorescence changes upon hybridization with target nucleic acids. *Molecules* **2018,** *23* (1), 124.

[114] Brauns, E. B.; Madaras, M. L.; Coleman, R. S.; Murphy, C. J.; Berg, M. A., Measurement of local DNA reorganization on the picosecond and nanosecond time scales. *J. Am. Chem. Soc.* **1999,** *121* (50), 11644-11649.

[115] Jeong, H. S.; Kang, S.; Lee, J. Y.; Kim, B. H., Probing specific RNA bulge conformations by modified fluorescent nucleosides. *Org. Biomol. Chem.* **2009,** *7* (5), 921-925.

[116] Dziuba, D.; Jurkiewicz, P.; Cebecauer, M.; Hof, M.; Hocek, M., A rotational BODIPY nucleotide: An environment-sensitive fluorescence-lifetime probe for DNA interactions and applications in live-cell microscopy. *Angew. Chem. Int. Ed.* **2016,** *55* (1), 174-178.

[117] Godde, F.; Toulmé, J. J.; Moreau, S., 4-amino-1H-benzo[g]quinazoline-2-one: a fluorescent analog of cytosine to probe protonation sites in triplex forming oligonucleotides. *Nucleic Acids Res.* **2000,** *28* (15), 2977-2985.

[118] Hwang, G. T.; Seo, Y. J.; Kim, B. H., Pyrene-labeled deoxyuridine and deoxyadenosine: fluorescent discriminating phenomena in their oligonucleotides. *Tetrahedron Lett.* **2005,** *46* (9), 1475-1477.

[119] Martí, A. A.; Jockusch, S.; Li, Z.; Ju, J.; Turro, N. J., Molecular beacons with intrinsically fluorescent nucleotides. *Nucleic Acids Res.* **2006,** *34* (6), e50-e50.

[120] Kirk, S. R.; Luedtke, N. W.; Tor, Y., 2-Aminopurine as a real-time probe of enzymatic cleavage and inhibition of hammerhead ribozymes. *Bioorg. Med. Chem.* **2001,** *9* (9), 2295-2301.

[121] Raney, K. D.; Sowers, L. C.; Millar, D. P.; Benkovic, S. J., A fluorescence-based assay for monitoring helicase activity. *Proc. Natl. Acad. Sci. U. S. A.* **1994,** *91* (14), 6644-6648.

[122] Sandin, P.; Stengel, G.; Ljungdahl, T.; Börjesson, K.; Macao, B.; Wilhelmsson, L. M., Highly efficient incorporation of the fluorescent nucleotide analogs tC and tCO by Klenow fragment. *Nucleic Acids Res.* **2009,** *37* (12), 3924-3933.

[123] Sandin, P.; Tumpane, J.; Börjesson, K.; Wilhelmsson, L. M.; Brown, T.; Nordén, B.; Albinsson, B.; Lincoln, P., Thermodynamic aspects of DNA nanoconstruct stability and design. *J. Phys. Chem* **2009,** *113* (15), 5941-5946.

[124] Vummidi, B. R.; Alzeer, J.; Luedtke, N. W., Fluorescent probes for G-quadruplex structures. *Chembiochem* **2013,** *14* (5), 540-558.

[125] Dumas, A.; Luedtke, N. W., Cation-mediated energy transfer in G-quadruplexes revealed by an internal fluorescent probe. *J. Am. Chem. Soc.* **2010,** *132* (51), 18004-18007.

[126] Mata, G.; Luedtke, N. W., Fluorescent Probe for Proton-Coupled DNA Folding Revealing Slow Exchange of i-Motif and Duplex Structures. *Journal of the American Chemical Society* **2015,** *137* (2), 699-707.

[127] Sinkeldam, R. W.; McCoy, L. S.; Shin, D.; Tor, Y., Enzymatic interconversion of isomorphic fluorescent nucleosides: adenosine deaminase transforms an adenosine analogue into an inosine analogue. *Angew. Chem. Int. Ed.* **2013,** *52* (52), 14026-14030.

[128] Mizrahi, R. A.; Shin, D.; Sinkeldam, R. W.; Phelps, K. J.; Fin, A.; Tantillo, D. J.; Tor, Y.; Beal, P. A., A fluorescent adenosine analogue as a substrate for an A-to-I rna editing enzyme. *Angew. Chem. Int. Ed.* **2015,** *54* (30), 8713-8716.

[129] Claudio-Montero, A.; Pinilla-Macua, I.; Fernández-Calotti, P.; Sancho-Mateo, C.; Lostao, M. a. P.; Colomer, D.; Grandas, A.; Pastor-Anglada, M., Fluorescent nucleoside derivatives as a tool for the detection of concentrative nucleoside transporter activity using confocal microscopy and flow cytometry. *Mol. Pharm.* **2015,** *12* (6), 2158-2166.

[130] Taniguchi, Y.; Kawaguchi, R.; Sasaki, S., Adenosine-1,3-diazaphenoxazine derivative for selective base pair formation with 8-oxo-2′-deoxyguanosine in DNA. *J. Am. Chem. Soc.* **2011,** *133* (19), 7272-7275.

[131] Taniguchi, Y.; Kikukawa, Y.; Sasaki, S., Discrimination between 8-oxo-2′-deoxyguanosine and 2′-deoxyguanosine in DNA by the single nucleotide primer extension reaction with Adap triphosphate. *Angew. Chem. Int. Ed.* **2015,** *54* (17), 5147-5151.

[132] Wilson, D. L.; Kool, E. T., Fluorescent probes of DNA repair. *ACS Chem. Biol.* **2018,** *13* (7), 1721-1733.

[133] Ono, T.; Wang, S.; Koo, C.-K.; Engstrom, L.; David, S. S.; Kool, E. T., Direct fluorescence monitoring of DNA base excision repair. *Angew. Chem. Int. Ed.* **2012,** *51* (7), 1689-1692.

[134] Zhu, R.-Y.; Majumdar, C.; Khuu, C.; De Rosa, M.; Opresko, P. L.; David, S. S.; Kool, E. T., Designer fluorescent adenines enable real-time monitoring of MUTYH activity. *ACS Cent. Sci.* **2020,** *6* (10), 1735-1742.

[135] Beharry, A. A.; Lacoste, S.; O'Connor, T. R.; Kool, E. T., Fluorescence monitoring of the oxidative repair of DNA alkylation damage by ALKBH3, a prostate cancer marker. *J. Am. Chem. Soc.* **2016,** *138* (11), 3647-3650.

[136] Jun, Y. W.; Wilson, D. L.; Kietrys, A. M.; Lotsof, E. R.; Conlon, S. G.; David, S. S.; Kool, E. T., An excimer clamp for measuring damaged-base excision by the DNA repair enzyme NTH1. *Angew. Chem. Int. Ed.* **2020,** *59* (19), 7450-7455.

[137] Kondo, T.; Chen, W. J.; Schlau-Cohen, G. S., Single-molecule fluorescence spectroscopy of photosynthetic systems. *Chem. Rev.* **2017,** *117* (2), 860-898.

[138] Wypijewska del Nogal, A.; Füchtbauer, A. F.; Bood, M.; Nilsson, Jesper R.; Wranne, M. S.; Sarangamath, S.; Pfeiffer, P.; Rajan, V. S.; El-Sagheer, A. H.; Dahlén, A.; Brown, T.; Grøtli, M.; Wilhelmsson, L. M., Getting DNA and RNA out of the dark with 2CNqA: a bright adenine analogue and interbase FRET donor. *Nucleic Acids Res.* **2020,** *48* (14), 7640-7652.

[139] Nilsson, J. R.; Baladi, T.; Gallud, A.; Baždarević, D.; Lemurell, M.; Esbjörner, E. K.; Wilhelmsson, L. M.; Dahlén, A., Fluorescent base analogues in gapmers enable stealth labeling of antisense oligonucleotide therapeutics. *Sci. Rep.* **2021,** *11* (1), 11365.

[140] Karimi, A.; Börner, R.; Mata, G.; Luedtke, N. W., A highly fluorescent nucleobase molecular rotor. *J. Am. Chem. Soc.* **2020,** *142* (34), 14422-14426.

[141] Ravi Kumara, G. S.; Seo, Y. J., Directly arylated oligonucleotides as fluorescent molecular rotors for probing DNA single-nucleotide polymorphisms. *Biorg. Med. Chem.* **2022,** *56*, 116617.

[142] Samaan, G. N.; Wyllie, M. K.; Cizmic, J. M.; Needham, L.-M.; Nobis, D.; Ngo, K.; Andersen, S.; Magennis, S. W.; Lee, S. F.; Purse, B. W., Single-molecule fluorescence detection of a tricyclic nucleoside analogue. *Chem. Sci.* **2021,** *12* (7), 2623-2628.

[143] Baladi, T.; Nilsson, J. R.; Gallud, A.; Celauro, E.; Gasse, C.; Levi-Acobas, F.; Sarac, I.; Hollenstein, M. R.; Dahlén, A.; Esbjörner, E. K.; Wilhelmsson, L. M., Stealth fluorescence labeling for live microscopy imaging of mrna delivery. *J. Am. Chem. Soc.* **2021,** *143* (14), 5413-5424.

[144] Wee, W. A.; Yum, J. H.; Hirashima, S.; Sugiyama, H.; Park, S., Synthesis and application of a 19F-labeled fluorescent nucleoside as a dual-mode probe for i-motif DNAs. *RSC chem. biol.* **2021,** *2* (3), 876-882.

[145] Kolmar, T.; Becker, A.; Pfretzschner, R. A.; Lelke, A.; Jäschke, A., Development of red-shifted and fluorogenic nucleoside and oligonucleotide diarylethene photoswitches. *Chem. Eur. J.* **2021,** *27* (69), 17386-17394.

[146] Axelrod, D.; Koppel, D. E.; Schlessinger, J.; Elson, E.; Webb, W. W., Mobility measurement by analysis of fluorescence photobleaching recovery kinetics. *Biophys. J.* **1976,** *16* (9), 1055-1069.

[147] Govindaraj, K.; Hendriks, J.; Lidke, D. S.; Karperien, M.; Post, J. N., Changes in fluorescence recovery after photobleaching (FRAP) as an indicator of SOX9 transcription factor activity. *Biochim. Biophys. Acta - Gene Regul. Mech.* **2019,** *1862* (1), 107-117.

[148] Shinitzky, M.; Yuli, I., Lipid fluidity at the submacroscopic level: Determination by fluorescence polarization. *Chem. Phys. Lipids* **1982,** *30* (2), 261-282.

[149] Mata, G.; Luedtke, N. W., Synthesis and solvatochromic fluorescence of biaryl pyrimidine nucleosides. *Org. Lett.* **2013,** *15* (10), 2462-2465.

[150] Okamoto, A.; Tainaka, K.; Fujiwara, Y., Nile red nucleoside: Design of a solvatofluorochromic nucleoside as an indicator of micropolarity around DNA. *J. Org. Chem.* **2006,** *71* (9), 3592-3598.

[151] Ozaki, H.; Kawai, T.; Kuwahara, M., Synthesis and properties of microenvironment-sensitive oligonucleotides containing a small fluorophore, 3-aminobenzonitrile or 3-aminobenzoic acid. *Tetrahedron* **2017,** *73* (51), 7177-7184.

[152] Sinkeldam, R. W.; Greco, N. J.; Tor, Y., Polarity of major grooves explored by using an isosteric emissive nucleoside. *Chembiochem* **2008,** *9* (5), 706-709.

[153] Seio, K.; Kanamori, T.; Masaki, Y., Solvent- and environment-dependent fluorescence of modified nucleobases. *Tetrahedron Lett.* **2018,** *59* (21), 1977-1985.

[154] Sinkeldam, R. W.; Wheat, A. J.; Boyaci, H.; Tor, Y., Emissive nucleosides as molecular rotors. *Chemphyschem* **2011,** *12* (3), 567-570.

[155] Bielecka, P.; Dembska, A.; Juskowiak, B., Monitoring of pH using an i-motif-forming sequence containing a fluorescent cytosine analogue, tC. *Molecules* **2019,** *24* (5), 952.

[156] Lee, J. W.; Son, Y.-S.; Hwang, J. Y.; Park, Y.; Hwang, G. T., pH-Responsive quencher-free molecular beacon systems containing 2'-deoxyuridine units labeled with fluorene derivatives. *Org. Biomol. Chem.* **2017,** *15* (34), 7165-7172.

[157] Mishra, S.; Lahiri, H.; Banerjee, S.; Mukhopadhyay, R., Molecularly resolved label-free sensing of single nucleobase mismatches by interfacial LNA probes. *Nucleic Acids Res.* **2016,** *44* (8), 3739-3749.

[158] Okamoto, A.; Saito, Y.; Saito, I., Design of base-discriminating fluorescent nucleosides. *J. Photochem. Photobiol. C: Photochem. Rev.* **2005,** *6* (2), 108-122.

[159] Weinberger, M.; Berndt, F.; Mahrwald, R.; Ernsting, N. P.; Wagenknecht, H. A., Synthesis of 4-aminophthalimide and 2,4-diaminopyrimidine C-nucleosides as isosteric fluorescent DNA base substitutes. *J. Org. Chem.* **2013,** *78* (6), 2589-2599.

[160] Suzuki, A.; Kimura, K.; Ishioroshi, S.; Saito, I.; Nemoto, N.; Saito, Y., Synthesis of solvatofluorochromic 7-arylethynylated 7-deaza-2'-deoxyadenosine derivatives: application to the design of environmentally sensitive fluorescent probes forming stable DNA duplexes. *Tetrahedron Lett.* **2013,** *54* (19), 2348-2352.

[161] Su, X.; Xiao, X.; Zhang, C.; Zhao, M., Nucleic acid fluorescent probes for biological sensing. *Appl. Spectrosc.* **2012,** *66* (11), 1249-1261.

[162] Dumas, A.; Luedtke, N. W., Fluorescence properties of 8-(2-pyridyl)guanine "2PyG" as compared to 2-aminopurine in DNA. *Chembiochem* **2011,** *12* (13), 2044-2051.

[163] Bood, M.; Fuchtbauer, A. F.; Wranne, M. S.; Ro, J. J.; Sarangamath, S.; El-Sagheer, A. H.; Rupert, D. L. M.; Fisher, R. S.; Magennis, S. W.; Jones, A. C.; Hook, F.; Brown, T.; Kim, B. H.; Dahlen, A.; Wilhelmsson, L. M.; Grotli, M., Pentacyclic adenine: a versatile and exceptionally bright fluorescent DNA base analogue. *Chem. Sci.* **2018,** *9* (14), 3494-3502.

[164] Sandin, P.; Wilhelmsson, L. M.; Lincoln, P.; Powers, V. E. C.; Brown, T.; Albinsson, B., Fluorescent properties of DNA base analogue tC upon incorporation into DNA — negligible influence of neighbouring bases on fluorescence quantum yield. *Nucleic Acids Res.* **2005,** *33* (16), 5019-5025.

[165] Ward, D. C.; Reich, E.; Stryer, L., Fluorescence studies of nucleotides and polynucleotides. I. Formycin, 2-aminopurine riboside, 2,6-diaminopurine riboside, and their derivatives. *J. Biol. Chem.* **1969,** *244* (5), 1228-1237.

[166] Fasman, G. D., *CRC Handbook of Biochemistry and Molecular Biology: Proteins*. CRC press: 2018.

[167] Li, Y.; Lombardo, Z.; Joshi, M.; Hingorani, M. M.; Mukerji, I., Mismatch recognition by saccharomyces cerevisiae Msh2-Msh6: Role of structure and dynamics. *Int. J. Mol. Sci.* **2019,** *20* (17).

[168] Mariam, J.; Krishnamoorthy, G.; Anand, R., Use of 6-methylisoxanthopterin, a fluorescent guanine analog, to probe Fob1-mediated dynamics at the stalling fork barrier DNA sequences. *Chem. Asian J.* **2019,** *14* (24), 4760-4766.

[169] Dueymes, C.; Décout, J. L.; Peltié, P.; Fontecave, M., Fluorescent deazaflavin-oligonucleotide probes for selective detection of DNA. *Angew. Chem. Int. Ed.* **2002,** *41* (3), 486-489.

[170] Xie, Y.; Maxson, T.; Tor, Y., Fluorescent nucleoside analogue displays enhanced emission upon pairing with guanine. *Org. Biomol. Chem.* **2010,** *8* (22), 5053-5055.

[171] Hudson, R. H. E.; Ghorbani-Choghamarani, A., Selective fluorometric detection of guanosine-containing sequences by 6-phenylpyrrolocytidine in DNA. *Synlett* **2007,** *2007* (06), 870-873.

[172] Wojciechowski, F.; Hudson, R. H. E., Fluorescence and hybridization properties of peptide nucleic acid containing a substituted phenylpyrrolocytosine designed to engage guanine with an additional H-bond. *J. Am. Chem. Soc.* **2008,** *130* (38), 12574-12575.

[173] Kilin, V.; Gavvala, K.; Barthes, N. P. F.; Michel, B. Y.; Shin, D.; Boudier, C.; Mauffret, O.; Yashchuk, V.; Mousli, M.; Ruff, M.; Granger, F.; Eiler, S.; Bronner, C.; Tor, Y.; Burger, A.; Mély, Y., Dynamics of methylated cytosine flipping by UHRF1. *J. Am. Chem. Soc.* **2017,** *139* (6), 2520-2528.

[174] Riedl, J.; Pohl, R.; Rulíšek, L.; Hocek, M., Synthesis and photophysical properties of biaryl-substituted nucleos(t)ides. Polymerase synthesis of DNA probes bearing solvatochromic and pH-sensitive dual fluorescent and 19F NMR labels. *J. Org. Chem.* **2012,** *77* (2), 1026-1044.

[175] Furukawa, K.; Hattori, M.; Ohki, T.; Kitamura, Y.; Kitade, Y.; Ueno, Y., Nucleic acid probe containing fluorescent tricyclic base-linked acyclonucleoside for detection of single nucleotide polymorphisms. *Biorg. Med. Chem.* **2012,** *20* (1), 16-24.

[176] Teppang, K. L.; Lee, R. W.; Burns, D. D.; Turner, M. B.; Lokensgard, M. E.; Cooksy, A. L.; Purse, B. W., Electronic modifications of fluorescent cytidine analogues control photophysics and fluorescent responses to base stacking and pairing. *Chem. Eur. J.* **2019,** *25* (5), 1249-1259.

[177] Cekan, P.; Sigurdsson, S. T., Single base interrogation by a fluorescent nucleotide: each of the four DNA bases identified by fluorescence spectroscopy. *Chem. Comm.* **2008,** (29), 3393-3395.

[178] Güixens-Gallardo, P.; Humpolickova, J.; Miclea, S. P.; Pohl, R.; Kraus, T.; Jurkiewicz, P.; Hof, M.; Hocek, M., Thiophene-linked tetramethylbodipy-labeled nucleotide for viscosity-sensitive oligonucleotide probes of hybridization and protein–DNA interactions. *Org. Biomol. Chem.* **2020,** *18* (5), 912-919.

[179] Hirashima, S.; Han, J. H.; Tsuno, H.; Tanigaki, Y.; Park, S.; Sugiyama, H., New size-expanded fluorescent thymine analogue: Synthesis, characterization, and application. *Chem. Eur. J.* **2019,** *25* (42), 9913-9919.

[180] Lawson, C. P.; Fuchtbauer, A. F.; Wranne, M. S.; Giraud, T.; Floyd, T.; Dumat, B.; Andersen, N. K.; A, H. E.-S.; Brown, T.; Graden, H.; Wilhelmsson, L. M.; Grotli, M., Synthesis, oligonucleotide incorporation and fluorescence properties in DNA of a bicyclic thymine analogue. *Sci. Rep.* **2018,** *8* (1), 13970.

[181] Wranne, M. S.; Füchtbauer, A. F.; Dumat, B.; Bood, M.; El-Sagheer, A. H.; Brown, T.; Gradén, H.; Grøtli, M.; Wilhelmsson, L. M., Toward complete sequence flexibility of nucleic acid base analogue FRET. *J. Am. Chem. Soc.* **2017,** *139* (27), 9271-9280.

[182] Füchtbauer, A. F.; Wranne, M. S.; Sarangamath, S.; Bood, M.; El-Sagheer, A. H.; Brown, T.; Gradén, H.; Grøtli, M.; Wilhelmsson, L. M., Lighting up DNA with the environment-sensitive bright adenine analogue qAN4. *ChemPlusChem* **2020,** *85* (2), 319-326.

[183] Mata, G.; Schmidt, O. P.; Luedtke, N. W., A fluorescent surrogate of thymidine in duplex DNA. *Chem. Commun.* **2016,** *52* (25), 4718-4721.

[184] Greco, N. J.; Sinkeldam, R. W.; Tor, Y., An emissive C analog distinguishes between G, 8-oxoG, and T. *Org. Lett.* **2009,** *11* (5), 1115-1118.

[185] Saito, Y.; Motegi, K.; Bag, S. S.; Saito, I., Anthracene based base-discriminating fluorescent oligonucleotide probes for SNPs typing: Synthesis and photophysical properties. *Biorg. Med. Chem.* **2008,** *16* (1), 107-113.

[186] Suzuki, A.; Saito, M.; Katoh, R.; Saito, Y., Synthesis of 8-aza-3,7-dideaza-2′-deoxyadenosines possessing a new adenosine skeleton as an environmentally sensitive fluorescent nucleoside for monitoring the DNA minor groove. *Org. Biomol. Chem.* **2015,** *13* (27), 7459-7468.

[187] Ryu, J. H.; Seo, Y. J.; Hwang, G. T.; Lee, J. Y.; Kim, B. H., Triad base pairs containing fluorene unit for quencher-free SNP typing. *Tetrahedron* **2007,** *63* (17), 3538-3547.

[188] Johnson, A.; Karimi, A.; Luedtke, N. W., Enzymatic incorporation of a coumarin–guanine base pair. *Angew. Chem. Int. Ed.* **2019,** *58* (47), 16839-16843.

[189] Narayanan, M.; Kodali, G.; Xing, Y.; Stanley, R. J., Photoinduced electron transfer occurs between 2-aminopurine and the DNA nucleic acid monophosphates: Results from cyclic voltammetry and fluorescence quenching. *J. Phys. Chem. B* **2010,** *114* (32), 10573-10580.

[190] Seidel, C. A. M.; Schulz, A.; Sauer, M. H. M., Nucleobase-specific quenching of fluorescent dyes. 1. Nucleobase one-electron redox potentials and their correlation with static and dynamic quenching efficiencies. *J. Phys. Chem.* **1996,** *100* (13), 5541-5553.

[191] Psciuk, B. T.; Lord, R. L.; Munk, B. H.; Schlegel, H. B., Theoretical determination of one-electron oxidation potentials for nucleic acid bases. *J. Chem. Theory Comput.* **2012,** *8* (12), 5107-5123.

[192] Somsen, O. J. G.; Hoek, v. A.; Amerongen, v. H., Fluorescence quenching of 2-aminopurine in dinucleotides. *Chem. Phys. Lett.* **2005,** *402* (1), 61-65.

[193] Ward, D. C.; Reich, E.; Stryer, L., Fluorescence studies of nucleotides and polynucleotides: I. Formycin, 2-aminopurine riboside, 2,6-diaminopurine riboside, and their derivatives. *J. Biol. Chem.* **1969,** *244* (5), 1228-1237.

[194] Gaied, N. B.; Glasser, N.; Ramalanjaona, N.; Beltz, H.; Wolff, P.; Marquet, R.; Burger, A.; Mély, Y., 8-vinyl-deoxyadenosine, an alternative fluorescent nucleoside analog to 2′-deoxyribosyl-2-aminopurine with improved properties. *Nucleic Acids Res.* **2005,** *33* (3), 1031-1039.

[195] Doering, C.; Ermentrout, B.; Oster, G., Rotary DNA motors. *Biophys. J.* **1995,** *69* (6), 2256-2267.

[196] Sircar, R.; Greenswag, A. R.; Bilwes, A. M.; Gonzalez-Bonet, G.; Crane, B. R., Structure and activity of the flagellar rotor protein FliY: a member of the CheC phosphatase family. *J. Biol. Chem.* **2013,** *288* (19), 13493-13502.

[197] Chernick, E. T.; Abdollahi, M. F.; Tabasi, Z. A.; Junge, M. J.; Zhao, Y., Study of a carbazole–bromobenzothiadiazole derived fluorescent molecular rotor: crystal structure, redox activity, and solvatofluorochromic effects. *New J. Chem.* **2022,** *46* (2), 572-581.

[198] Baba, M.; Iwamoto, K.; Iino, R.; Ueno, H.; Hara, M.; Nakanishi, A.; Kishikawa, J.-i.; Noji, H.; Yokoyama, K., Rotation of artificial rotor axles in rotary molecular motors. *Proc. Natl. Acad. Sci. U.S.A.* **2016,** *113* (40), 11214.

[199] Bertosin, E.; Maffeo, C. M.; Drexler, T.; Honemann, M. N.; Aksimentiev, A.; Dietz, H., A nanoscale reciprocating rotary mechanism with coordinated mobility control. *Nat. Commun.* **2021,** *12* (1), 7138.

[200] Ketterer, P.; Willner Elena, M.; Dietz, H., Nanoscale rotary apparatus formed from tight-fitting 3D DNA components. *Sci. Adv.* **2016,** *2* (2), e1501209.

[201] Tomaru, T.; Suzuki, Y.; Kawamata, I.; Nomura, S.-i. M.; Murata, S., Stepping operation of a rotary DNA origami device. *Chem. Commun.* **2017,** *53* (55), 7716-7719.

[202] Rajendran, A.; Endo, M.; Hidaka, K.; Sugiyama, H., Direct and real-time observation of rotary movement of a DNA nanomechanical device. *J. Am. Chem. Soc.* **2013,** *135* (3), 1117-1123.

[203] Kay, E. R.; Leigh, D. A.; Zerbetto, F., Synthetic molecular motors and mechanical machines. *Angew. Chem. Int. Ed.* **2007,** *46* (1-2), 72-191.

[204] Kottas, G. S.; Clarke, L. I.; Horinek, D.; Michl, J., Artificial molecular rotors. *Chem. Rev.* **2005,** *105* (4), 1281-1376.

[205] Zhang, J.; Rakhimbekova, A.; Duan, X.; Yin, Q.; Foss, C. A.; Fan, Y.; Xu, Y.; Li, X.; Cai, X.; Kutil, Z.; Wang, P.; Yang, Z.; Zhang, N.; Pomper, M. G.; Wang, Y.; Bařinka, C.; Yang, X., A prostate-specific membrane antigen activated molecular rotor for real-time fluorescence imaging. *Nat. Commun.* **2021,** *12* (1), 5460.

[206] Haidekker, M. A.; Theodorakis, E. A., Environment-sensitive behavior of fluorescent molecular rotors. *J. Biol. Eng.* **2010,** *4* (1), 11.

[207] Schuddeboom, W.; Jonker, S. A.; Warman, J. M.; Leinhos, U.; Kuehnle, W.; Zachariasse, K. A., Excited-state dipole moments of dual fluorescent 4-(dialkylamino)benzonitriles: influence of alkyl chain length and effective solvent polarity. *J. Phys. Chem.* **1992,** *96* (26), 10809-10819.

[208] Ghoneim, N.; Suppan, P., Solvation of TICT states in solvent mixtures. *Pure Appl. Chem.* **1993,** *65* (8), 1739-1743.

[209] Grabowski, Z. R.; Dobkowski, J., Twisted intramolecular charge transfer (TICT) excited states: energy and molecular structure. *Pure Appl. Chem.* **1983,** *55* (2), 245-252.

[210] Grégoire, G.; Dimicoli, I.; Mons, M.; Dedonder-Lardeux, C.; Jouvet, C.; Martrenchard, S.; Solgadi, D., Femtosecond dynamics of "TICT" state formation in small clusters: The dimethylaminobenzomethyl ester−acetonitrile system. *J. Phys. Chem* **1998,** *102* (41), 7896-7902.

[211] Rullière, C.; Grabowski, Z. R.; Dobkowski, J., Picosecond absorption spectra of carbonyl derivatives of dimethylaniline: the nature of the tict excited states. *Chem. Phys. Lett.* **1987,** *137* (5), 408-413.

[212] Grabowski, Z. R.; Rotkiewicz, K.; Rettig, W., Structural changes accompanying intramolecular electron transfer: focus on twisted intramolecular charge-transfer states and structures. *Chem. Rev.* **2003,** *103* (10), 3899-4032.

[213] Atsbeha, T.; Mohammed, A. M.; Redi-Abshiro, M., Excitation wavelength dependence of dual fluorescence of DMABN in polar solvents. *J. Fluoresc.* **2010,** *20* (6), 1241-1248.

[214] Allen, B. D.; Benniston, A. C.; Harriman, A.; Rostron, S. A.; Yu, C., The photophysical properties of a julolidene-based molecular rotor. *Phys. Chem. Chem. Phys.* **2005,** *7* (16), 3035-3040.

[215] Rotkiewicz, K.; Grellmann, K. H.; Grabowski, Z. R., Reinterpretation of the anomalous fluorescense of p-n,n-dimethylamino-benzonitrile. *Chem. Phys. Lett.* **1973,** *19* (3), 315-318.

[216] Law, K. Y., Fluorescence probe for microenvironments: anomalous viscosity dependence of the fluorescence quantum yield of p-N,N-dialkylaminobenzylidenemalononitrile in 1-alkanols. *Chem. Phys. Lett.* **1980,** *75* (3), 545-549.

[217] Kuimova, M. K., Mapping viscosity in cells using molecular rotors. *Phys. Chem. Chem. Phys.* **2012,** *14* (37), 12671-12686.

[218] Levitt, J. A.; Kuimova, M. K.; Yahioglu, G.; Chung, P.-H.; Suhling, K.; Phillips, D., Membrane-bound molecular rotors measure viscosity in live cells via fluorescence lifetime imaging. *J. Phys. Chem.* **2009,** *113* (27), 11634-11642.

[219] Haidekker, M. A.; Theodorakis, E. A., Molecular rotors—fluorescent biosensors for viscosity and flow. *Org. Biomol. Chem.* **2007,** *5* (11), 1669-1678.

[220] Kuimova, M. K.; Yahioglu, G.; Levitt, J. A.; Suhling, K., Molecular rotor measures viscosity of live cells via fluorescence lifetime imaging. *J. Am. Chem. Soc.* **2008,** *130* (21), 6672-6673.

[221] Xiao, H.; Li, P.; Tang, B., Small molecular fluorescent probes for imaging of viscosity in living biosystems. *Chem. Eur. J.* **2021,** *27* (23), 6880-6898.

[222] Nipper, M. E.; Majd, S.; Mayer, M.; Lee, J. C. M.; Theodorakis, E. A.; Haidekker, M. A., Characterization of changes in the viscosity of lipid membranes with the molecular rotor FCVJ. *Biochim. Biophys. Acta - Biomembr.* **2008,** *1778* (4), 1148-1153.

[223] Sutharsan, J.; Lichlyter, D.; Wright, N. E.; Dakanali, M.; Haidekker, M. A.; Theodorakis, E. A., Molecular rotors: synthesis and evaluation as viscosity sensors. *Tetrahedron* **2010,** *66* (14), 2582-2588.

[224] Liu, Y.; Miao, K.; Dunham, N. P.; Liu, H.; Fares, M.; Boal, A. K.; Li, X.; Zhang, X., The cation−π interaction enables a halo-tag fluorogenic probe for fast no-wash live cell imaging and gel-free protein quantification. *Biochemistry* **2017,** *56* (11), 1585-1595.

[225] Clark, S. A.; Singh, V.; Vega Mendoza, D.; Margolin, W.; Kool, E. T., Light-up “channel dyes” for haloalkane-based protein labeling in vitro and in bacterial cells. *Bioconjugate Chem.* **2016,** *27* (12), 2839-2843.

[226] Viriot, M. L.; Carré, M. C.; Geoffroy-Chapotot, C.; Brembilla, A.; Muller, S.; Stoltz, J. F., Molecular rotors as fluorescent probes for biological studies. *Clin. Hemorheol. Microcirc.* **1998,** *19* (2), 151-160.

[227] Olšinová, M.; Jurkiewicz, P.; Pozník, M.; Šachl, R.; Prausová, T.; Hof, M.; Kozmík, V.; Teplý, F.; Svoboda, J.; Cebecauer, M., Di- and tri-oxalkyl derivatives of a boron dipyrromethene (BODIPY) rotor dye in lipid bilayers. *Phys. Chem. Chem. Phys.* **2014,** *16* (22), 10688-10697.

[228] Goh, W. L.; Lee, M. Y.; Joseph, T. L.; Quah, S. T.; Brown, C. J.; Verma, C.; Brenner, S.; Ghadessy, F. J.; Teo, Y. N., Molecular rotors as conditionally fluorescent labels for rapid detection of biomolecular interactions. *J. Am. Chem. Soc.* **2014,** *136* (17), 6159-6162.

[229] Hosny Neveen, A.; Mohamedi, G.; Rademeyer, P.; Owen, J.; Wu, Y.; Tang, M.-X.; Eckersley Robert, J.; Stride, E.; Kuimova Marina, K., Mapping microbubble viscosity using fluorescence lifetime imaging of molecular rotors. *Proc. Natl. Acad. Sci. U.S.A.* **2013,** *110* (23), 9225-9230.

[230] Yu, W.-T.; Wu, T.-W.; Huang, C.-L.; Chen, I. C.; Tan, K.-T., Protein sensing in living cells by molecular rotor-based fluorescence-switchable chemical probes. *Chem. Sci.* **2016,** *7* (1), 301-307.

[231] Hawe, A.; Filipe, V.; Jiskoot, W., Fluorescent molecular rotors as dyes to characterize polysorbate-containing IgG formulations. *Pharm. Res.* **2010,** *27* (2), 314-326.

[232] Kung, C. E.; Reed, J. K., Fluorescent molecular rotors: a new class of probes for tubulin structure and assembly. *Biochemistry* **1989,** *28* (16), 6678-6686.

[233] Sawada, S.; Iio, T.; Hayashi, Y.; Takahashi, S., Fluorescent rotors and their applications to the study of G-F transformation of actin. *Anal. Biochem.* **1992,** *204* (1), 110-117.

[234] Lindgren, M.; Sörgjerd, K.; Hammarström, P., Detection and characterization of aggregates, prefibrillar amyloidogenic oligomers, and protofibrils using fluorescence spectroscopy. *Biophys. J.* **2005,** *88* (6), 4200-4212.

[235] Michel, B. Y.; Dziuba, D.; Benhida, R.; Demchenko, A. P.; Burger, A., Probing of nucleic acid structures, dynamics, and interactions with environment-sensitive fluorescent labels. *Front. Chem.* **2020,** *8*, 112.

[236] Kalel, R.; Mora, A. K.; Ghosh, R.; Dhavale, D. D.; Palit, D. K.; Nath, S., Interaction of a julolidine-based neutral ultrafast molecular rotor with natural DNA: Spectroscopic and molecular docking studies. *J. Phys. Chem. B* **2016,** *120* (37), 9843-9853.

[237] Dragan, A. I.; Casas-Finet, J. R.; Bishop, E. S.; Strouse, R. J.; Schenerman, M. A.; Geddes, C. D., Characterization of PicoGreen interaction with dsDNA and the origin of its fluorescence enhancement upon binding. *Biophys. J.* **2010,** *99* (9), 3010-3019.

[238] Xu, H.; Geng, F.; Wang, Y.; Xu, M.; Lai, X.; Qu, P.; Zhang, Y.; Liu, B., A label-free fluorescent molecular switch for a DNA hybridization assay utilizing a G-quadruplex-selective auramine O. *Chem. Commun.* **2015,** *51* (41), 8622-8625.

[239] Ihmels, H.; Engels, B.; Faulhaber, K.; Lennartz, C., New dyes based on amino-substituted acridizinium salts-synthesis and exceptional photochemical properties. *Chem. Eur. J.* **2000,** *6* (15), 2854-2864.

[240] Ihmels, H.; Faulhaber, K.; Sturm, C.; Bringmann, G.; Messer, K.; Gabellini, N.; Vedaldi, D.; Viola, G., Acridizinium salts as a novel class of DNA-binding and site-selective DNA-photodamaging chromophores. *Photochem. Photobiol.* **2001,** *74* (4), 505-511.

[241] Goh, W. L.; Lee, M. Y.; Lim, T. X.; Chua, J. S.; Brenner, S.; Ghadessy, F. J.; Teo, Y. N., A novel molecular rotor facilitates detection of p53-DNA interactions using the Fluorescent Intercalator Displacement Assay. *Sci. Rep.* **2018,** *8* (1), 12946.

[242] Singh, P. K.; Kumbhakar, M.; Pal, H.; Nath, S., Ultrafast torsional dynamics of protein binding dye thioflavin-t in nanoconfined water pool. *J. Phys. Chem. B* **2009,** *113* (25), 8532-8538.

[243] Murudkar, S.; Mora, A. K.; Singh, P. K.; Nath, S., Ultrafast molecular rotor: an efficient sensor for premelting of natural DNA. *Chem. Commun.* **2012,** *48* (43), 5301-5303.

[244] Liu, L.; Shao, Y.; Peng, J.; Liu, H.; Zhang, L., Selective recognition of ds-DNA cavities by a molecular rotor: switched fluorescence of thioflavin T. *Mol. Biosyst.* **2013,** *9* (10), 2512-2519.

[245] Liu, L.; Shao, Y.; Peng, J.; Huang, C.; Liu, H.; Zhang, L., Molecular rotor-based fluorescent probe for selective recognition of hybrid g-quadruplex and as a k+ sensor. *Anal. Chem.* **2014,** *86* (3), 1622-1631.

[246] Renaud de la Faverie, A.; Guédin, A.; Bedrat, A.; Yatsunyk, L. A.; Mergny, J.-L., Thioflavin T as a fluorescence light-up probe for G4 formation. *Nucleic Acids Res.* **2014,** *42* (8), e65-e65.

[247] Liu, S.; Peng, P.; Wang, H.; Shi, L.; Li, T., Thioflavin T binds dimeric parallel-stranded GA-containing non-G-quadruplex DNAs: a general approach to lighting up double-stranded scaffolds. *Nucleic Acids Res.* **2017,** *45* (21), 12080-12089.

[248] Zhu, J.; Yan, Z.; Zhou, W.; Liu, C.; Wang, J.; Wang, E., Lighting up the thioflavin t by parallel-stranded tg(ga)n DNA homoduplexes. *ACS Sens.* **2018,** *3* (6), 1118-1125.

[249] Ludwanowski, S.; Samanta, A.; Loescher, S.; Barner-Kowollik, C.; Walther, A., A modular fluorescent probe for viscosity and polarity sensing in DNA hybrid mesostructures. *Adv. Sci.* **2021,** *8* (5), 2003740.

[250] Kumar, B.; Ghosh, R.; Mora, A. K.; Nath, S., Anthryl benzothiazolium molecular rotor-based turn-on DNA probe: Detailed mechanistic studies. *J. Phys. Chem. B* **2019,** *123* (35), 7518-7527.

[251] Shimomura, O., Structure of the chromophore of Aequorea green fluorescent protein. *FEBS Lett.* **1979,** *104* (2), 220-222.

[252] Paige, J. S.; Wu, K. Y.; Jaffrey, S. R., RNA mimics of green fluorescent protein. *Science* **2011,** *333* (6042), 642-646.

[253] Stafforst, T.; Diederichsen, U., Synthesis of alaninyl and N-(2-aminoethyl)glycinyl amino acid derivatives containing the green fluorescent protein chromophore in their side chains for incorporation into peptides and peptide nucleic acids. *Eur. J. Org* **2007,** *2007* (6), 899-911.

[254] Seitz, O.; Bergmann, F.; Heindl, D., A convergent strategy for the modification of peptide nucleic acids: Novel mismatch-specific pna-hybridization probes. *Angew. Chem. Int. Ed.* **1999,** *38* (15), 2203-2206.

[255] Socher, E.; Bethge, L.; Knoll, A.; Jungnick, N.; Herrmann, A.; Seitz, O., Low-noise stemless PNA beacons for sensitive DNA and RNA detection. *Angew. Chem. Int. Ed.* **2008,** *47* (49), 9555-9559.

[256] Kummer, S.; Knoll, A.; Socher, E.; Bethge, L.; Herrmann, A.; Seitz, O., Fluorescence imaging of influenza H1N1 mRNA in living infected cells using single-chromophore FIT-PNA. *Angew. Chem. Int. Ed.* **2011,** *50* (8), 1931-1934.

[257] Karunakaran, V.; Pérez Lustres, J. L.; Zhao, L.; Ernsting, N. P.; Seitz, O., Large dynamic stokes shift of DNA intercalation dye thiazole orange has contribution from a high-frequency mode. *J. Am. Chem. Soc.* **2006,** *128* (9), 2954-2962.

[258] Köhler, O.; Jarikote, D. V.; Seitz, O., Forced intercalation probes (FIT Probes): thiazole orange as a fluorescent base in peptide nucleic acids for homogeneous single-nucleotide-polymorphism detection. *Chembiochem* **2005,** *6* (1), 69-77.

[259] Hövelmann, F.; Bethge, L.; Seitz, O., Single Labeled DNA FIT Probes for Avoiding False-Positive Signaling in the Detection of DNA/RNA in qPCR or Cell Media. *Chembiochem* **2012,** *13* (14), 2072-2081.

[260] Kummer, S.; Knoll, A.; Socher, E.; Bethge, L.; Herrmann, A.; Seitz, O., Fluorescence imaging of influenza H1N1 mRNA in living infected cells using single-chromophore FIT-PNA. *Angew. Chem. Int. Ed.* **2011,** *50* (8), 1931-1934.

[261] Hövelmann, F.; Gaspar, I.; Ephrussi, A.; Seitz, O., Brightness enhanced DNA FIT-probes for wash-free RNA imaging in tissue. *J. Am. Chem. Soc.* **2013,** *135* (50), 19025-19032.

[262] Cui, H.; Fang, J.; Sun, M.; Liu, Z.; Li, Z.; Liu, K.; Liu, M., Color-changing fluorescent DNA probe containing solvatochromic Dansyl-nucleoside surrogate for sensing local variation of DNA duplex. *Bioorg. Med. Chem. Lett.* **2022,** *59*, 128551.

[263] Manning, T. W.; Van Riesen, A. J.; Manderville, R. A., Screening internal donor–acceptor biaryl nucleobase surrogates for turn-on fluorescence affords an aniline–carboxythiophene probe for protein detection by G-quadruplex DNA. *Bioconjugate Chem.* **2021,** *32* (8), 1791-1801.

[264] Gray, M. D.; Deore, P. S.; Chung, A. J.; Van Riesen, A. J.; Manderville, R. A.; Prabhakar, P. S.; Wetmore, S. D., Lighting up the thrombin-binding aptamer G-quadruplex with an internal cyanine-indole-quinolinium nucleobase surrogate. Direct fluorescent intensity readout for thrombin binding without topology switching. *Bioconjugate Chem.* **2020,** *31* (11), 2596-2606.

[265] Johnson, R. E.; Van Riesen, A. J.; Manderville, R. A., On-strand Knoevenagel insertion of a hemicyanine molecular rotor loop residue for turn-on fluorescence detection of Pb-induced G-quadruplex rigidity. *Bioconjugate Chem.* **2021,** *32* (10), 2224-2232.

[266] Wilson, D. L.; Kool, E. T., Ultrafast oxime formation enables efficient fluorescence light-up measurement of DNA base excision. *J. Am. Chem. Soc.* **2019,** *141* (49), 19379-19388.

[267] Weber, G.; Farris, F. J., Synthesis and spectral properties of a hydrophobic fluorescent probe: 6-propionyl-2-(dimethylamino)naphthalene. *Biochemistry* **1979,** *18* (14), 3075-3078.

[268] Nowak, W.; Adamczak, P.; Balter, A.; Sygula, A., On the possibility of fluorescence from twisted intramolecular charge transfer states of 2-dimethylamino-6-acylnaphthalenes. A quantum-chemical study *J. Mol. Struc. Theochem* **1986,** *139*, 13-23.

[269] Parusel, A. B. J.; Schneider, F. W.; Köhler, G., An ab initio study on excited and ground state properties of the organic fluorescence probe PRODAN. *J. Mol. Struc. Theochem* **1997**, 341-346.

[270] Parusel, A., Semiempirical studies of solvent effects on the intramolecular charge transfer of the fluorescence probe PRODAN. *J. Chem. Soc., Faraday Trans.* **1998,** *94* (19), 2923-2927.

[271] Ilich, P.; Prendergast, F. G., Singlet adiabatic states of solvated PRODAN: a semiempirical molecular orbital study. *J. Phys. Chem.* **1989,** *93* (11), 4441-4447.

[272] Samanta, A.; Fessenden, R. W., Excited state dipole moment of PRODAN as determined from transient dielectric loss measurements. *J. Phys. Chem* **2000,** *104* (39), 8972-8975.

[273] Tainaka, K.; Tanaka, K.; Ikeda, S.; Nishiza, K.-i.; Unzai, T.; Fujiwara, Y.; Saito, I.; Okamoto, A., PRODAN-conjugated DNA: Synthesis and photochemical properties. *J. Am. Chem. Soc.* **2007,** *129* (15), 4776-4784.

[274] Kimura, T.; Kawai, K.; Majima, T., Monitoring of microenvironmental changes in the major and minor grooves of DNA by dan-modified oligonucleotides. *Org. Lett.* **2005,** *7* (26), 5829-5832.

[275] Kimura, T.; Kawai, K.; Majima, T., Probing the microenvironments in the grooves of Z-DNA using dan-modified oligonucleotides. *Chem. Commun.* **2006,** (14), 1542-1544.

[276] Schmidt, O. P.; Mata, G.; Luedtke, N. W., Fluorescent base analogue reveals T-HgII-T base pairs have high kinetic stabilities that perturb DNA metabolism. *J. Am. Chem. Soc.* **2016,** *138* (44), 14733-14739.

[277] Schmidt, O. P.; Benz, A. S.; Mata, G.; Luedtke, N. W., HgII binds to C–T mismatches with high affinity. *Nucleic Acids Res.* **2018,** *46* (13), 6470-6479.

[278] Michoff, M. E. Z.; Castillo, M. E.; Leiva, E. P. M., A reversible molecular switch based on the biphenyl structure. *J. Phys. Chem* **2013,** *117* (48), 25724-25732.

[279] Oesch, D.; Luedtke, N. W., Fluorescent chemosensors of carbohydrate triols exhibiting TICT emissions. *Chem. Commun.* **2015,** *51* (63), 12641-12644.

[280] Charbonneau, G.-P.; Delugeard, Y., Structural transition in polyphenyls. III. Crystal structure of biphenyl at 110 K. *Acta Crystallogr. B: Struct. Sci. Cryst. Eng. Mater.* **1976,** *32* (5), 1420-1423.

[281] Almenningen, A.; Bastiansen, O.; Fernholt, L.; Cyvin, B. N.; Cyvin, S. J.; Samdal, S., Structure and barrier of internal rotation of biphenyl derivatives in the gaseous state: Part 1. The molecular structure and normal coordinate analysis of normal biphenyl and pedeuterated biphenyl. *J. Mol. Struct.* **1985,** *128* (1), 59-76.

[282] Barclay, M.; Bjornsson, R.; Cipriani, M.; Terfort, A.; Fairbrother, D. H.; Ingólfsson, O., The role of the dihedral angle and excited cation states in ionization and dissociation of mono-halogenated biphenyls; a combined experimental and theoretical coupled cluster study. *Phys. Chem. Chem. Phys.* **2019,** *21* (8), 4556-4567.

[283] Grein, F., Twist Angles and Rotational Energy Barriers of Biphenyl and Substituted Biphenyls. *J. Phys. Chem. A .* **2002,** *106* (15), 3823-3827.

[284] Im, H. S.; Bernstein, E. R., Geometry and torsional motion of biphenyl in the ground and first excited singlet state. *J. Chem. Phys.* **1988,** *88* (12), 7337-7347.

[285] Dumas, A.; Luedtke, N. W., Site-specific control of N7–metal coordination in DNA by a fluorescent purine derivative. *Chem. Eur. J.* **2012,** *18* (1), 245-254.

[286] Saito, Y.; Suzuki, A.; Yamauchi, T.; Saito, I., Design and synthesis of 7-naphthyl-8-aza-7-deaza-2'-deoxyadenosines as environmentally sensitive fluorescent nucleosides. *Tetrahedron Lett.* **2015,** *56* (23), 3034-3038.

[287] Kimoto, M.; Mitsui, T.; Harada, Y.; Sato, A.; Yokoyama, S.; Hirao, I., Fluorescent probing for RNA molecules by an unnatural base-pair system. *Nucleic Acids Res.* **2007,** *35* (16), 5360-5369.

[288] Ingale, S. A.; Seela, F., 7-Deaza-2'-deoxyguanosine: Selective nucleobase halogenation, positional impact of space-occupying substituents, and stability of DNA with parallel and antiparallel strand orientation. *J. Org. Chem.* **2016,** *81* (18), 8331-8342.

[289] Zilbershtein, L.; Silberman, A.; Fischer, B., 8-(p-CF3-cinnamyl)-modified purine nucleosides as promising fluorescent probes. *Org. Biomol. Chem.* **2011,** *9* (22), 7763-7773.

[290] Li, J.-P.; Wang, H.-X.; Wang, H.-X.; Xie, M.-S.; Qu, G.-R.; Niu, H.-Y.; Guo, H.-M., Push–pull-type purine nucleoside-based fluorescent sensors for the selective detection of Pd2+ in aqueous buffer. *Eur. J. Org* **2014,** *2014* (11), 2225-2230.

[291] Dumas, A.; Luedtke, N. W., Highly fluorescent guanosine mimics for folding and energy transfer studies. *Nucleic Acids Res.* **2011,** *39* (15), 6825-6834.

[292] Zilbershtein-Shklanovsky, L.; Kafri, P.; Shav-Tal, Y.; Yavin, E.; Fischer, B., Development of fluorescent double-strand probes labeled with 8-(p-CF3-cinnamyl)-adenosine for the detection of cyclin D1 breast cancer marker. *Eur. J. Med. Chem.* **2014,** *79*, 77-88.

[293] Greco, N. J.; Tor, Y., Furan decorated nucleoside analogues as fluorescent probes: Synthesis, photophysical evaluation and site-specific incorporation. *Tetrahedron* **2007,** *63* (17), 3515-3527.

[294] Grünewald, C.; Kwon, T.; Piton, N.; Förster, U.; Wachtveitl, J.; Engels, J. W., RNA as scaffold for pyrene excited complexes. *Biorg. Med. Chem.* **2008,** *16* (1), 19-26.

[295] Skorobogatyi, M. V.; Malakhov, A. D.; Pchelintseva, A. A.; Turban, A. A.; Bondarev, S. L.; Korshun, V. A., Fluorescent 5-alkynyl-2'-deoxyuridines: High emission efficiency of a conjugated perylene nucleoside in a DNA duplex. *Chembiochem* **2006,** *7* (5), 810-816.

[296] Rist, M.; Amann, N.; Wagenknecht, H.-A., Preparation of 1-ethynylpyrene-modified DNA via Sonogashira-type solid-phase couplings and characterization of the fluorescence properties for electron-transfer studies. *Eur. J. Org* **2003,** *2003* (13), 2498-2504.

[297] Hwang, G. T.; Seo, Y. J.; Kim, B. H., A highly discriminating quencher-free molecular beacon for probing DNA. *J. Am. Chem. Soc.* **2004,** *126* (21), 6528-6529.

[298] Dziuba, D.; Pospíšil, P.; Matyašovský, J.; Brynda, J.; Nachtigallová, D.; Rulíšek, L.; Pohl, R.; Hof, M.; Hocek, M., Solvatochromic fluorene-linked nucleoside and DNA as color-changing fluorescent probes for sensing interactions. *Chem. Sci.* **2016,** *7* (9), 5775-5785.

[299] Riedl, J.; Pohl, R.; Ernsting, N. P.; Orság, P.; Fojta, M.; Hocek, M., Labelling of nucleosides and oligonucleotides by solvatochromic 4-aminophthalimide fluorophore for studying DNA–protein interactions. *Chem. Sci.* **2012,** *3* (9), 2797-2806.

[300] Riedl, J.; Ménová, P.; Pohl, R.; Orság, P.; Fojta, M.; Hocek, M., GFP-like fluorophores as DNA labels for studying DNA–protein interactions. *J. Org. Chem.* **2012,** *77* (18), 8287-8293.

[301] Kuba, M.; Pohl, R.; Hocek, M., Synthesis of 2'-deoxycytidine and its triphosphate bearing tryptophan-based imidazolinone fluorophore for environment sensitive fluorescent labelling of DNA. *Tetrahedron* **2018,** *74* (46), 6621-6629.

[302] Dziuba, D.; Pohl, R.; Hocek, M., Polymerase synthesis of DNA labelled with benzylidene cyanoacetamide-based fluorescent molecular rotors: fluorescent light-up probes for DNA-binding proteins. *Chem. Commun.* **2015,** *51* (23), 4880-4882.

[303] Dziuba, D.; Pohl, R.; Hocek, M., Bodipy-labeled nucleoside triphosphates for polymerase synthesis of fluorescent DNA. *Bioconjugate Chem.* **2014,** *25* (11), 1984-1995.

[304] Kanamori, T.; Takamura, A.; Tago, N.; Masaki, Y.; Ohkubo, A.; Sekine, M.; Seio, K., Fluorescence enhancement of oligodeoxynucleotides modified with green fluorescent protein chromophore mimics upon triplex formation. *Org. Biomol. Chem.* **2017,** *15* (5), 1190-1197.

[305] Barthes, N. P. F.; Gavvala, K.; Dziuba, D.; Bonhomme, D.; Karpenko, J.; Dabert-Gay, A. S.; Debayle, D.; Demchenko, A. P.; Benhida, R.; Michel, B. Y.; Mély, Y.; Burger, A., Dual emissive analogue of deoxyuridine as a sensitive hydration-reporting probe for discriminating mismatched from matched DNA and DNA/DNA from DNA/RNA duplexes. *J. Mater. Chem. C* . **2016,** *4* (14), 3010-3017.

[306] Barthes, N. P. F.; Karpenko, J.; Dziuba, D.; Spadafora, M.; Auffret, J.; Demchenko, A. P.; Mély, Y.; Benhida, R.; Michel, B. Y.; Burger, A., Development of environmentally sensitive fluorescent and dual emissive deoxyuridine analogues. *RSC Advances* **2015,** *5* (42), 33536-33545.

[307] Dziuba, D.; Karpenko, I. A.; Barthes, N. P. F.; Michel, B. Y.; Klymchenko, A. S.; Benhida, R.; Demchenko, A. P.; Mély, Y.; Burger, A., Rational design of a solvatochromic fluorescent uracil analogue with a dual-band ratiometric response based on 3-hydroxychromone. *Chem. Eur. J.* **2014,** *20* (7), 1998-2009.

[308] Dziuba, D.; Postupalenko, V. Y.; Spadafora, M.; Klymchenko, A. S.; Guérineau, V.; Mély, Y.; Benhida, R.; Burger, A., A universal nucleoside with strong two-band switchable fluorescence and sensitivity to the environment for investigating DNA interactions. *J. Am. Chem. Soc.* **2012,** *134* (24), 10209-10213.

[309] Kuznetsova, A. A.; Kuznetsov, N. A.; Vorobjev, Y. N.; Barthes, N. P.; Michel, B. Y.; Burger, A.; Fedorova, O. S., New environment-sensitive multichannel DNA fluorescent label for investigation of the protein-DNA interactions. *PLoS One* **2014,** *9* (6), e100007.

[310] Zhang, Y.; Yue, X.; Kim, B.; Yao, S.; Belfield, K. D., Deoxyribonucleoside-modified squaraines as near-IR viscosity sensors. *Chem. Eur. J.* **2014,** *20* (24), 7249-7253.

[311] Ravi Kumara, G. S.; Seo, Y. J., Polymerase-mediated synthesis of p-vinylaniline-coupled fluorescent DNA for the sensing of nucleolin protein–c-myc G-quadruplex interactions. *Org. Biomol. Chem.* **2021,** *19* (26), 5788-5793.

[312] Kumbhar, H. S.; Deshpande, S. S.; Shankarling, G. S., Aggregation induced emission (AIE) active carbazole styryl fluorescent molecular rotor as viscosity sensor. *ChemistrySelect* **2016,** *1* (9), 2058-2064.

[313] Hou, M.-X.; Liu, L.-Y.; Wang, K.-N.; Chao, X.-J.; Liu, R.-X.; Mao, Z.-W., A molecular rotor sensor for detecting mitochondrial viscosity in apoptotic cells by two-photon fluorescence lifetime imaging. *New J. Chem.* **2020,** *44* (26), 11342-11348.

[314] Shinohara, Y.; Matsumoto, K.; Kugenuma, K.; Morii, T.; Saito, Y.; Saito, I., Design of environmentally sensitive fluorescent 2′-deoxyguanosine containing arylethynyl moieties: Distinction of thymine base by base-discriminating fluorescent (BDF) probe. *Bioorg. Med. Chem. Lett.* **2010,** *20* (9), 2817-2820.

[315] Saito, Y.; Suzuki, A.; Okada, Y.; Yamasaka, Y.; Nemoto, N.; Saito, I., An environmentally sensitive fluorescent purine nucleoside that changes emission wavelength upon hybridization. *Chem. Commun.* **2013,** *49* (50), 5684-5686.

[316] Suzuki, A.; Nemoto, N.; Saito, I.; Saito, Y., Design of an environmentally sensitive fluorescent 8-aza-7-deaza-2′-deoxyadenosine derivative with dual fluorescence for the specific detection of thymine. *Org. Biomol. Chem.* **2014,** *12* (4), 660-666.

[317] Saito, Y.; Suzuki, A.; Ishioroshi, S.; Saito, I., Synthesis and photophysical properties of novel push–pull-type solvatochromic 7-deaza-2′-deoxypurine nucleosides. *Tetrahedron Lett.* **2011,** *52* (37), 4726-4729.

[318] Suzuki, A.; Yanagi, M.; Takeda, T.; Hudson, R. H. E.; Saito, Y., The fluorescently responsive 3-(naphthalen-1-ylethynyl)-3-deaza-2′-deoxyguanosine discriminates cytidine via the DNA minor groove. *Org. Biomol. Chem.* **2017,** *15* (37), 7853-7859.

[319] Suzuki, A.; Yanaba, T.; Saito, I.; Saito, Y., Molecular design of an environmentally sensitive fluorescent nucleoside, 3-deaza-2′-deoxyadenosine derivative: Distinguishing thymine by probing the DNA minor groove. *Chembiochem* **2014,** *15* (11), 1638-1644.

[320] Kim, M. J.; Seo, Y.; Hwang, G. T., Synthesis and photophysical properties of 2′-deoxyguanosine derivatives labeled with fluorene and fluorenone units: toward excimer probes. *RSC Advances* **2014,** *4* (23), 12012-12017.

[321] Greco, N. J.; Tor, Y., Simple fluorescent pyrimidine analogues detect the presence of DNA abasic sites. *J. Am. Chem. Soc.* **2005,** *127* (31), 10784-10785.

[322] Sinkeldam, R. W.; Hopkins, P. A.; Tor, Y., Modified 6-aza uridines: Highly emissive pH-sensitive fluorescent nucleosides. *Chemphyschem* **2012,** *13* (14), 3350-3356.

[323] Hopkins, P. A.; McCoy, L. S.; Tor, Y., Enzymatic incorporation and utilization of an emissive 6-azauridine. *Org. Biomol. Chem.* **2017,** *15* (3), 684-690.

[324] Zheng, C.; Zhai, W.; Hong, J.; Zhang, X.; Zhu, Z.; Wang, L., Synthesis of two 6-aza-uridines modified by benzoheterocycle as environmentally sensitive fluorescent nucleosides. *Tetrahedron Lett.* **2017,** *58* (31), 3008-3013.

[325] Pawar, M. G.; Nuthanakanti, A.; Srivatsan, S. G., Heavy atom containing fluorescent ribonucleoside analog probe for the fluorescence detection of RNA-ligand binding. *Bioconjugate Chem.* **2013,** *24* (8), 1367-1377.

[326] Tanpure, A. A.; Srivatsan, S. G., A microenvironment-sensitive fluorescent pyrimidine ribonucleoside analogue: synthesis, enzymatic incorporation, and fluorescence detection of a DNA abasic site. *Chem. Eur. J.* **2011,** *17* (45), 12820-12827.

[327] Tanpure, A. A.; Srivatsan, S. G., Synthesis and photophysical characterisation of a fluorescent nucleoside analogue that signals the presence of an abasic site in RNA. *Chembiochem* **2012,** *13* (16), 2392-2399.

[328] Kanamori, T.; Ohzeki, H.; Masaki, Y.; Ohkubo, A.; Takahashi, M.; Tsuda, K.; Ito, T.; Shirouzu, M.; Kuwasako, K.; Muto, Y.; Sekine, M.; Seio, K., Controlling the fluorescence of benzofuran-modified uracil residues in oligonucleotides by triple-helix formation. *Chembiochem* **2015,** *16* (1), 167-176.

[329] Kanamori, T.; Masaki, Y.; Oda, Y.; Ohzeki, H.; Ohkubo, A.; Sekine, M.; Seio, K., DNA triplex-based fluorescence turn-on sensors for adenosine using a fluorescent molecular rotor 5-(3-methylbenzofuran-2-yl) deoxyuridine. *Org. Biomol. Chem.* **2019,** *17* (8), 2077-2080.

[330] Tokugawa, M.; Kaneko, K.; Saito, M.; Kanamori, T.; Masaki, Y.; Ohkubo, A.; Sekine, M.; Seio, K., Synthesis of responsive fluorescent nucleobases 7-(benzofuran-2-yl)-7-deazahypoxanthine and 7-(benzofuran-2-yl)-7-deazaguanine using cross-coupling reaction. *Chem. Lett.* **2014,** *44* (1), 64-66.

[331] Tokugawa, M.; Masaki, Y.; Canggadibrata, J. C.; Kaneko, K.; Shiozawa, T.; Kanamori, T.; Grøtli, M.; Wilhelmsson, L. M.; Sekine, M.; Seio, K., 7-(Benzofuran-2-yl)-7-deazadeoxyguanosine as a fluorescence turn-ON probe for single-strand DNA binding protein. *Chem. Commun.* **2016,** *52* (19), 3809-3812.

Chapter 2 | ^{ts}T is a highly fluorescent nucleobase molecular rotor

"Faces come and faces go in circular ***rotation***. But something yearns within to grow beyond infatuation."

Don McLean

2.1 Introduction: DNA modifications and synthesis

Canonical nucleotides can undergo natural modifications.[1] For example, there are predominant modifications in tRNAs that tune various functions such as increasing the stability of local structures or mediating the rate of translation.[2] Inspired by nature's efforts, a myriad of synthetic analogs of nucleosides and oligonucleotides have been prepared to improve targeted delivery,[3] nuclease resistance,[4] or other physicochemical and biological properties.[5] As highlighted in Figure 2.1, almost any site of the sugar moiety, phosphodiester backbone, nucleobase or combinations thereof is amenable to introducing chemical modifications.

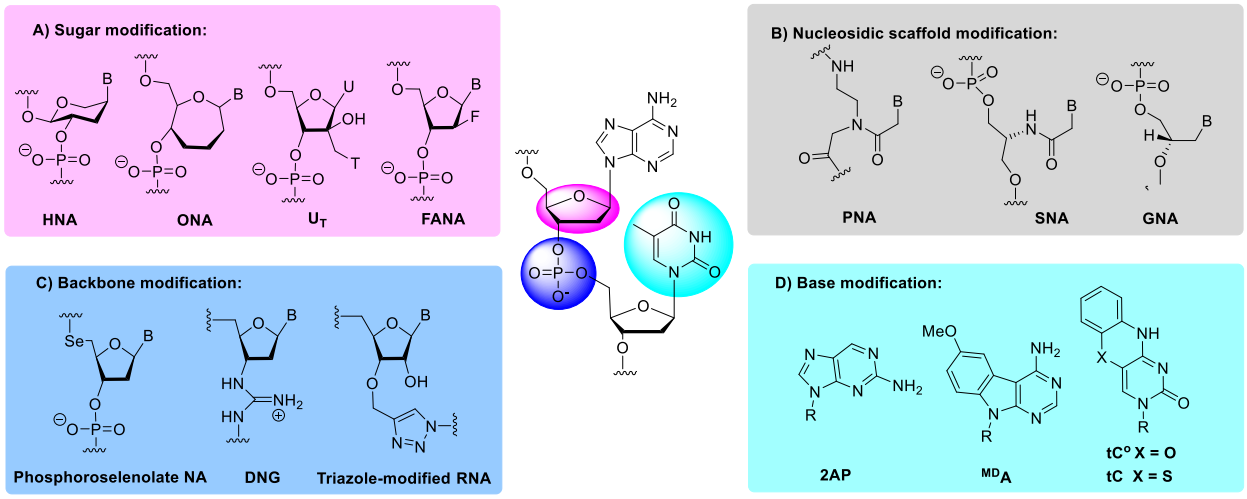

Figure 2.1. Chemical modifications introduced in nucleic acids includes sugar-modified nucleic acids, backbone-modified nucleic acids, nucleobase modifications and nucleic acid analogs bearing modifications at multiple sites.

2.1.1 DNA modifications

In the context of sugar modifications, both 6-membered[6] and 7-membered[7] ring nucleic acids have been explored, including hexose nucleic acids (HNAs) and oxepane nucleic acids (ONAs) which are among the most notable (Figure 2.1A).[8,9] Another interesting modification of the sugar unit results by linking a second nucleobase at C2 of the sugar *via* a methylene group.[10] One of the first examples of "double-headed" nucleotides was an uridine linked to a thymine base (U_T), which pairs with two adenine bases on the complementary strand.[11] 2′-fluoroarabinonucleic acids (FANA)[12] and locked

nucleic acids (LNAs)[13] are among the sugar modifications that alter nucleic acid stability and biological properties. In peptide nucleic acids (PNAs, Figure 2.1B), the entire sugar-phosphate backbone is substituted with a neutral polyamide-based scaffold, reminiscent of the chemical architecture found in proteins. This DNA mimic forms highly stable duplex and triplex structures with PNA, DNA, or RNA oligonucleotides. Related to PNAs are glycerol nucleic acids (GNAs)[14] and serinol nucleic acids (SNAs),[15] the chiral DNA mimics in which the entire sugar-phosphate scaffold of DNA is replaced by acyclic backbones (Figure 2.1B). Examples of phosphate backbone modifications include triazole linkages[16] and substitution of the non-bridging oxygens with another chalcogen[17] or borane (Figure 2.1C).[18] In addition, there have been reports of replacing the phosphodiester linkage with a positively charged guanidinium group to synthesize deoxynucleic guanidine (DNG, Figure 2.1B) with improved cellular uptake.[19]

2.1.2 Base modifications

Another class of DNA modifications are modified nucleobases which can increase the thermal stability of duplexes[20] or quadruplexes,[21] enhance gene silencing activities,[22] enable the introduction of fluorescent[23] or redox labels,[24] convey additional reactivity,[25] assemble quantum dots,[26] or expand the genetic alphabet.[27] Modifications at the N4 and C5 positions of pyrimidine, the C8 position of adenine, and the N7 (or S7[28]) and C8 (or N8 in 8-AzaG[29]) positions of guanine are known to cause minimal disruption of WCF base-pairing, as introduced bulky groups sit comfortably in the major groove.[30] At these positions, base modifications can be compatible with polymerases,[31-32] and do not disrupt the genetic information carried by the DNA or RNA sequences.[33] Therefore, nucleobases are interesting sites to introduce fluorescent labels (Figure 2.1D). FBAs have the advantage of exact positioning within RNA and DNA structures compared to conjugated fluorophores and intercalating dyes.[34] Consequently, their fluorescence may be sensitive towards single *versus* double-stranded DNA,[35] secondary structures,[23] dynamic motions[36] and nucleobase damages.[37] In addition, base modifications can be used for labeling and visualization of nucleic acids within cells or even living organisms without interfering with biological processes.[38]

2.1.3 Synthesis of modified bases

Numerous synthetic pathways have been devised to introduce modifications at the level of the nucleobase. These methods mainly involve formation of a glycosidic bond between an altered

nucleobase and an activated sugar unit (Figure 2.2A-C) or alternatively, making modifications of suitable synthetic nucleoside precursors (Figure 2.2D). Direct glycosylation reactions of activated sugar moieties are commonly used since they grant access to a wide variety of base-modified nucleoside analogs.[39] The *Vorbrüggen* nucleosidation reaction is the most commonly used method for synthesizing modified nucleosides and involves the nucleophilic attack of persilylated nucleobases on acylated sugar residues in the presence of a *Lewis* acid (Fig. 2.2A).[40] Despite the immense success of this method, it is often impaired by moderate N7/N9 regioselectivity and/or poor α/β stereoselectivity as well as compatibility issues of relatively strong *Lewis* acid conditions with specific functional groups. Stereoselectivity for the desired β-anomer can be achieved by using 1-*O*-acetylribofuranosyl derivatives that mediate a C2-*O*-ester neighboring group effect. High stereoselectivity and good yields can be obtained using this approach, but subsequent 2'-deoxygenation procedures must be performed to obtain the desired 2'-deoxyribonucleosides. These additional synthetic steps result in low to moderate overall yields.[28, 41-43] Milder variants of the *Vorbrüggen* reaction include the N-iodosuccinimide (NIS)-mediated addition of persilylated nucleobases on glycals which has been successfully applied to constrained nucleic acids[44] or the use of *Brønsted* acid catalysts such as pyridinium triflate salts.[45]

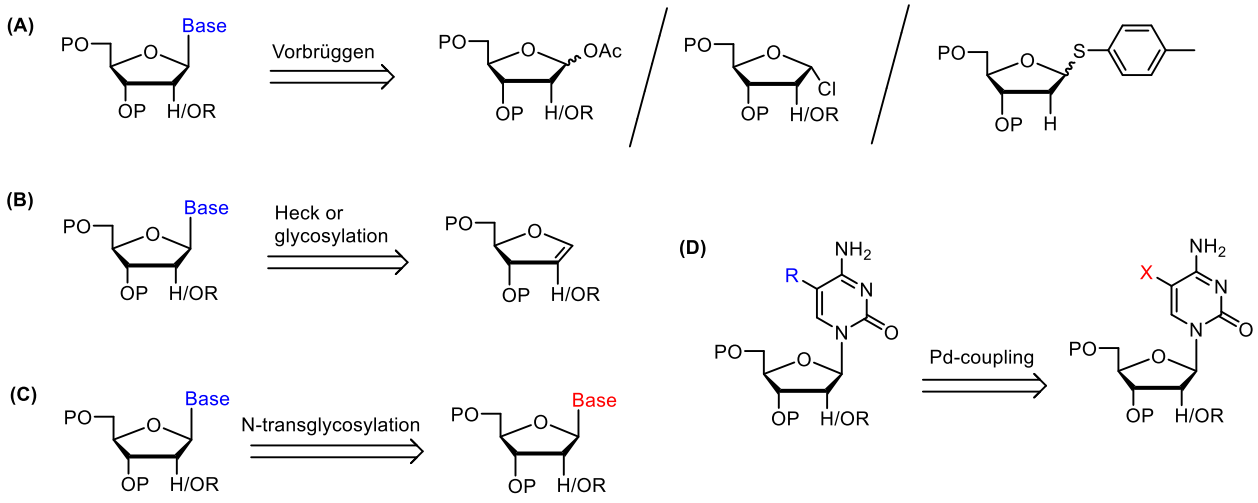

Figure 2.2. Main synthetic pathways to nucleobase-modified purine and pyrimidine nucleoside analogs: (A) the Vorbrüggen nucleosidation reaction involving *Lewis* acid activated nucleophilic attack, (B) the Pd-catalyzed *Heck* reaction;[46-47] (C) chemoenzymatic transglycosylation methods; (D) Pd-assisted cross-coupling reactions with pyrimidine (or purine) precursors.[48]

To further develop β-selective N-glycosylation reactions, the *Luedtke* Group has established a protocol using 2'-deoxythioribosides which can undergo *Vorbrüggen*-type N-2'-deoxyribosilation by ring-expanded nucleobase analogs that exhibit limited solubility and poor nucleophilicity.[49] Thioglycosides provide a highly attractive alternative to the commonly used α-glycoside chloride for the stereoselective synthesis of β-nucleosides (Figure 2.2A). Thioglycosides can be activated in the presence of an *in situ* silylated nucleobase using NIS/HOTf as promoters. By tuning the protecting groups at the C3 and C5 hydroxyls, a β/α ratio of 4:1 can be achieved.[49] Compared to other more commonly used methodologies, this approach can provide enhanced yields, higher β-selectivity, shorter reaction times, and a broader scope of nucleobase substrates.

2.1.4 DNA synthesis

Nature uses DNA polymerases for enzymatic DNA synthesis. Inspired by nature, the enzymatic incorporation of modified nucleoside triphosphates has emerged as a powerful tool for synthesizing functionalized oligonucleotides.[50] However, fortunately for life and unfortunately for modified oligonucleotide synthesis, the natural polymerases can be selective for canonical nucleoside triphosphates.[51] As an alternative, other enzymes such as ligases can be used to construct modified oligonucleotides. This can be achieved either by templated ligation of two fully modified oligonucleotide precursors or by the ligase-mediated polymerization of tri- or penta-nucleotide fragments.[5] Nevertheless, the current access to a vast array of oligonucleotide chemical modifications is largely provided by automated solid-phase synthesis.[52] This technology is based on the stepwise addition of activated nucleoside building blocks by P–O bond formation relying on a P^{III} center.[53] The

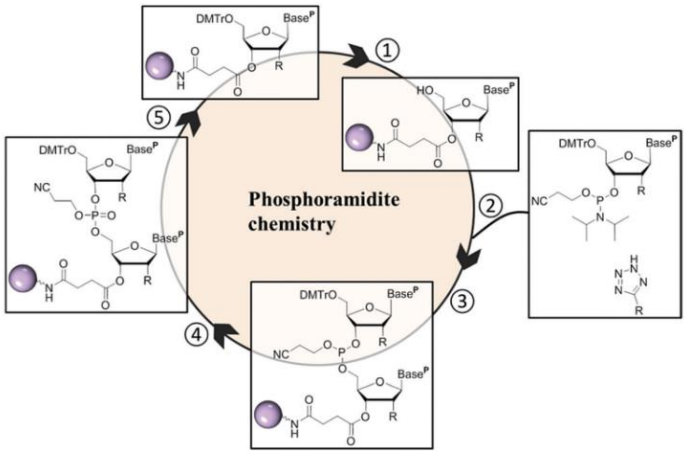

Figure 2.3. Schematic representation of the solid-support syntheses of oligonucleotides. The synthetic cycle with phosphoramidite chemistry includes (1) deprotection of the DMT groups (deblock step); (2) condensation of the incoming phosphoramidite building block with a tetrazole activation step (coupling step); (3) capping of the unreacted hydroxyl groups; (4) oxidation to P^V; and (5) either the cycle is repeated, or the sequence is subjected to a global deprotection protocol.

most common building blocks used in solid-phase synthesis of oligonucleotides are nucleoside 3′-phosphoramidites[54] and 3′-H-phosphonates.[55] A schematic representation of the use of 3′-phosphoramidites in solid-phase synthesis is described in Figure 2.3. In addition, recently, mechanochemistry has been introduced as an exciting tool for synthesizing DNA dimers and trimers under near solvent-free conditions.[56] Another strategy to incorporate the modified nucleosides into DNA is the post-synthesis approach, which uses copper-free biorthogonal reactions such as strain-promoted alkyne–azide cycloaddition,[57] photoclick alkene–tetrazole cycloaddition,[58] Diels–Alder reactions,[59] and sulfo-click reactions.[60] The main advantage of this method is its compatibility with functional groups such as azides, aldehydes, thiols, and tetrazines that cannot easily tolerate solid-phase synthesis conditions.[5]

2.2 Probe design

Most FBAs suffer from fluorescence quenching by neighboring residues *via* photo-induced electron transfer (PET) and thus, have limited applications in single-molecule studies.[61-64] On the other hand, the few FBAs such as tC^o and related analogs that are highly fluorescent,[65-67] exhibit little-to-no environmental sensitivity and therefore have limited utility as reporters of DNA hybridization,[68] nucleobase damages,[69] base-pair mismatches,[70-71] and DNA dynamics.[36] Given the growing clinical interest in point-of-care detection of SNPs,[72] there have been numerous efforts towards the development of SNP sensors based on FBA-mismatch detection.[70-71] However, these attempts have thus far resulted in either bright FBAs with low sensitivity towards SNPs, [66, 68, 73-75] or highly sensitive FBAs with low brightness.[76-79]

To better understand the relationship between the fluorescent quantum yield and the energy level of probe's molecular orbitals, Density Functional Theory (DFT) calculations were conducted on selected previously reported FBAs (Table A1, Appendix A). The data shown in Figure 2.4 demonstrate that electron-poor systems such as 2AP are reductively quenched by purines,[80] and electron-rich systems such as ^{MD}A are oxidatively quenched by pyrimidines.[78] The brightest, previously reported fluorescent nucleobase analogs, such as tC^o ($\varepsilon \times \varphi \approx 2{,}000$ cm^{-1} M^{-1}),[65, 81] avoid PET quenching by having HOMO-LUMO energy levels that are intermediate between the HOMO of guanine and the LUMO of thymidine.

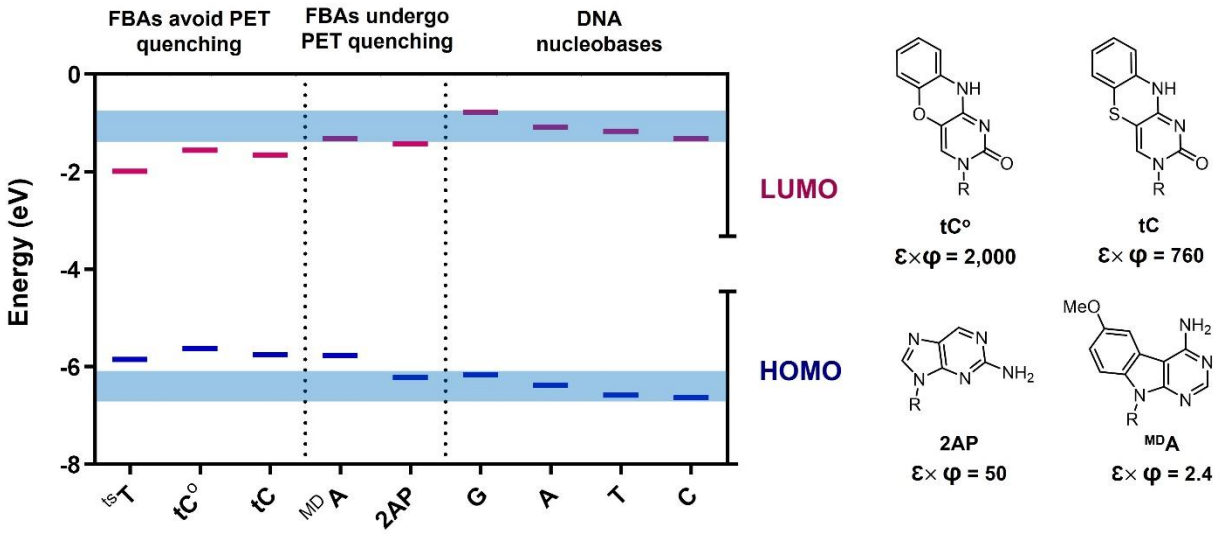

Figure 2.4. Structures and brightness of FBAs in duplex DNA ($cm^{-1}M^{-1}$) and their calculated HOMO/LUMO energy levels (eV). DFT calculations (where R = Me) were performed using B3LYP/6-31++G(d) in water (see Section 2.9.1 for details). The blue area demonstrates the range of the unmodified DNA nucleobases HOMO and LUMO energy levels, in which the most easily reduced nucleobase (T) has the lowest LUMO, and the most easily oxidized base, G, has the highest HOMO.[82]

trans-Stilbene is known to be a bright probe due to its high extinction coefficient (44,000 $M^{-1}cm^{-1}$ in methanol) and modest quantum yield (2.2% in methanol). As DFT calculations suggest, the *trans*-stilbene analog of thymidine (^{ts}T, Figure 2.5) has a HOMO and LUMO which avoid PET with natural DNA bases (Figure 2.4) and, thus, could have a high fluorescence quantum yield. The design of ^{ts}T was also inspired by the excellent base-pairing specificities of 6-substituted quinazolines.[83-86] Time-dependent DFT (TD-DFT) calculations suggested that ^{ts}T can preserve the *trans*-stilbene photophysical properties because the pyrimidine ring has a minimal effect on the HOMO-LUMO of ^{ts}T (Figure 2.5). Nevertheless, what makes ^{ts}T a unique FBA is *trans*-stilbene viscosity sensitivity and rotary properties.[87-88] In fact, when photoexcited, *trans*-stilbene twists around the central ethylenic bond, and the rotation causes fluorescence quenching of the probe due to the decrease in the π-conjugation and increase in the intersystem crossing. Thereby, the fluorescence signal of *trans*-stilbene is directly related to the degree of free rotation around the ethylenic bond which depends on the environment's rigidity or viscosity.[88] Thus, it was hypothesized that ^{ts}T could be a bright probe with high sensitivity towards DNA dynamics, binding interactions, and base-pairings.[89,90]

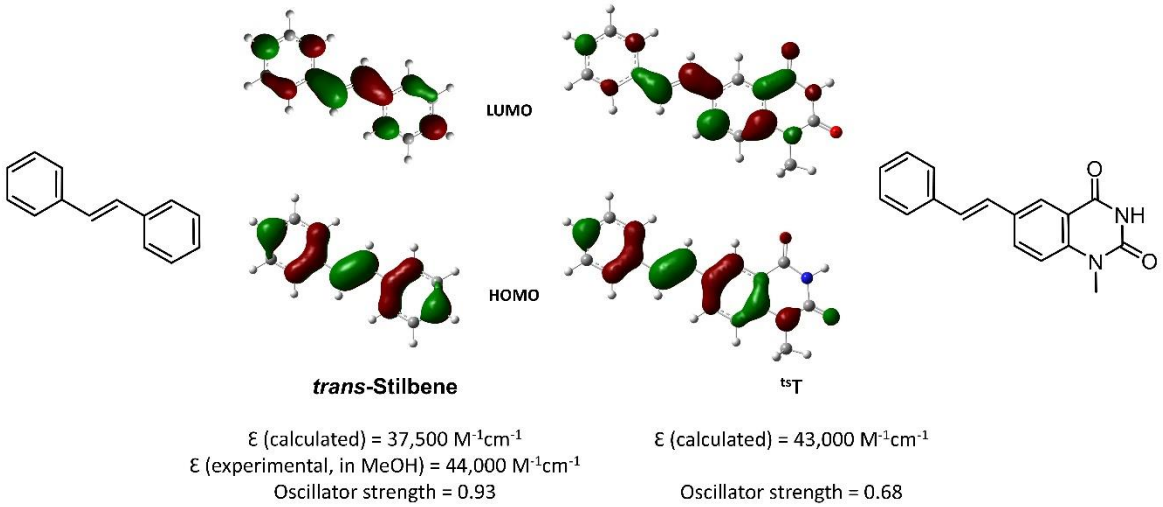

Figure 2.5. Structure, optimized geometry, and some photophysical properties of *trans*-stilbene and ^{ts}T, calculated by TD-DFT [CAM-b3lyp/6-31++G(d,p)].

2.3. Synthesis of ^{ts}T nucleoside

Inspired by the theoretical calculations, we commenced the synthesis of ^{ts}T nucleoside with the preparation of 2'-deoxythioriboside **5** according to a previously established protocol.[49,91] Commercially available 1,3,5-tri-*O*-acetyl-2-deoxy-*D*-ribose **1** as an anomeric mixture was treated with *para*-toluenethiol (*p*TolSH) and $BF_3{\cdot}Et_2O$ at −78 °C to afford thioglycoside **2** (Scheme 2.1). The resulting 2'-deoxythioriboside was used without purification for the next step. Deacetylation of **2** was then conducted using K_2CO_3 in a mixture of MeOH/CH_2Cl_2 to give diol **3**. Regioselective silylation of the primary alcohol with triisopropylsilyl chloride (TIPSCl) afforded compound **4**, followed by acetylation of the remaining alcohol to generate 2'-deoxythioriboside **5**. The crude mixture was filtered through silica gel to get 45 g pure thiosugar **5** with an overall yield of 87% over 4 steps reactions (Scheme 2.1). In the next step, 2'-deoxythioriboside **5** was N-glycosylated with 6-bromo-quinazoline-2,4-(1H,3H)-dione using the combination of N,O-bis-(trimethylsilyl)-acetamide (BSA), NIS, and trimethylsilyl trifluoromethanesulfonate (TMSOTf) to afford **6** in 55% yield (α/β = 1.0:1.8, >10 g scale, Scheme 2.1). The diastereoisomers could be isolated using flash column chromatography.

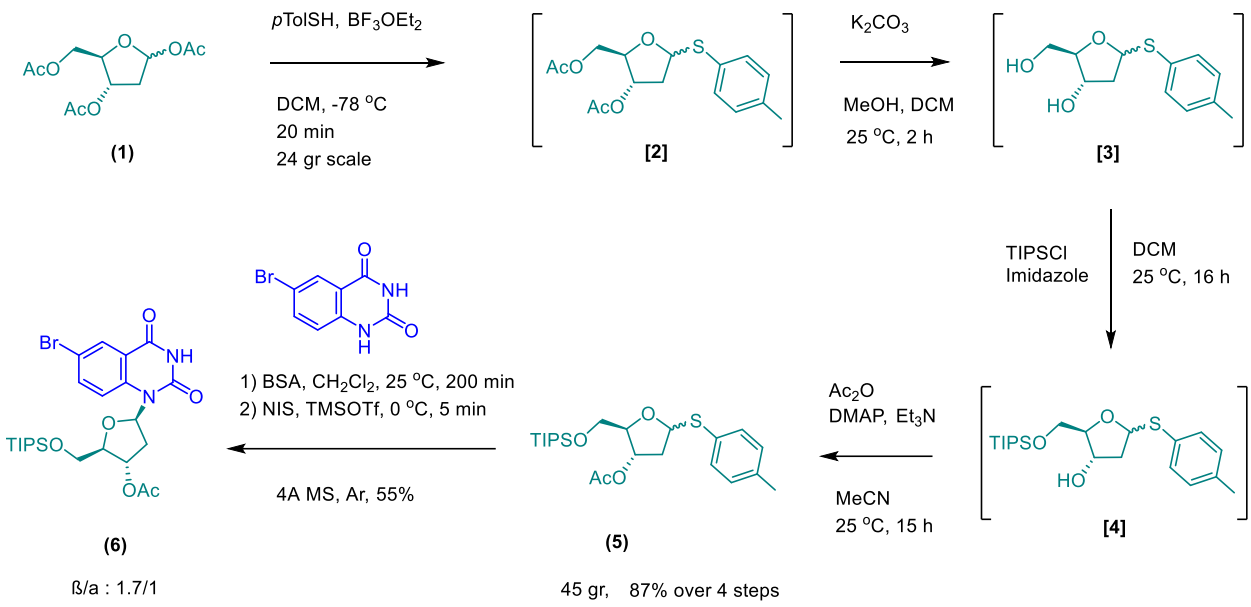

Scheme 2.1. Generating the N-2'-deoxythioriboside quinazoline **6**. *p*TolSH = para toluene sulfonic acid, DCM = dichloromethane, TIPS = triisopropylsilyl, and DMAP = 4-dimethylaminopyridine, BSA = bis(trimethylsilyl)acetamide, NIS = N-iodosuccinimide, TMSOTf = trimethylsilyl trifluoromethanesulfonate.

Conducting the *Suzuki-Miyaura* coupling on acetylated nucleoside **6β** to synthesize the *trans*-stilbene scaffold was unsuccessful, possibly due to the poisoning of the reaction's catalyst by the acetate group.[91] To facilitate the cross-coupling reaction, the C3-*O*-acetate of **6β** was converted into a C3-*O*-silyl ether to give **7** in 95% yield over two steps (Scheme 2.2).

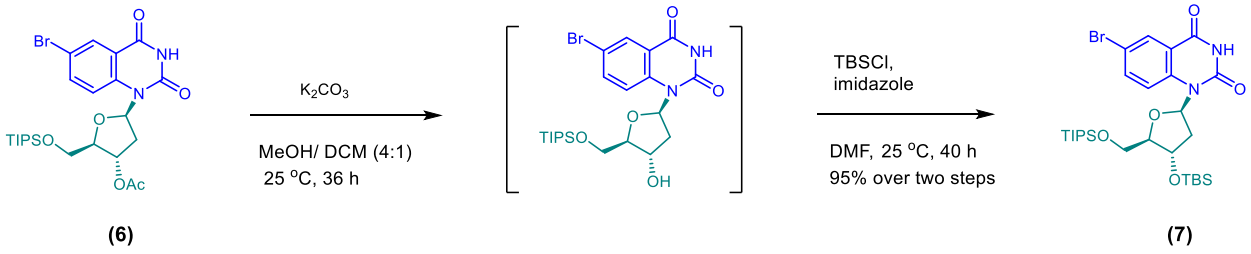

Scheme 2.2. Synthesis of the silyl-protected nucleoside **7**. TBS = *tert*-butyldimethylsilyl, and DMF = dimethylformamide.

The silyl-protected nucleoside **7** underwent an efficient *Suzuki-Miyaura* coupling reaction with *trans*-2-phenylvinyl boronic acid pinacol ester. After a brief optimization (Table A2, Appendix A),

1,4-dioxane, Cs_2CO_3, and Pd(dppf)Cl_2 were selected as the optimum solvent, base, and catalyst, respectively. Under these conditions, **8a** was isolated in 98% yield (Scheme 2.3). The scope of this reaction was explored using electron-withdrawing (**8b**), electron-donating (**8c**), and extended conjugated systems (**8d**). The isolated yields are reported in Table 2.1.

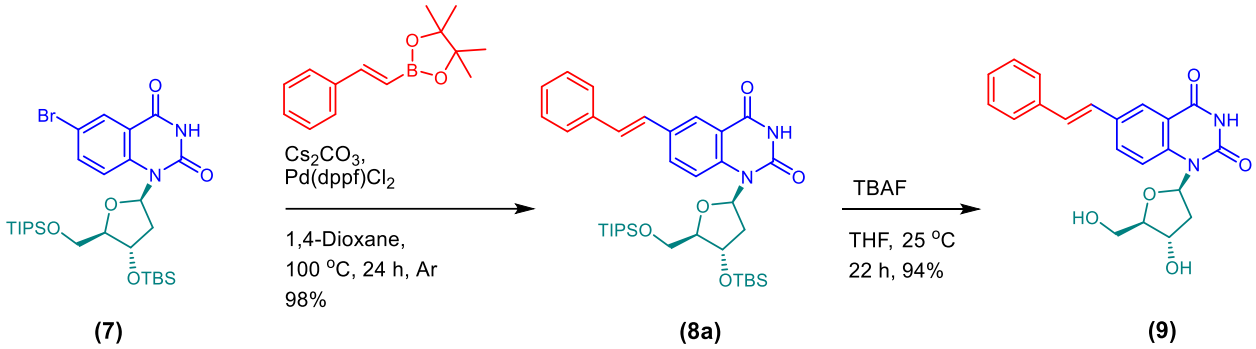

(7) **(8a)** **(9)**

Scheme 2.3. Synthesis of the ^{ts}T nucleoside **9**. dppf = 1,1′-Bis(diphenylphosphino)ferrocene, TBAF = tetra-*n*-butylammoniumfluoride, and THF = tetrahydrofuran.

Table 2.1. *Suzuki-Miyaura* coupling of different boronic pinacol esters on nucleoside **7**.[a]

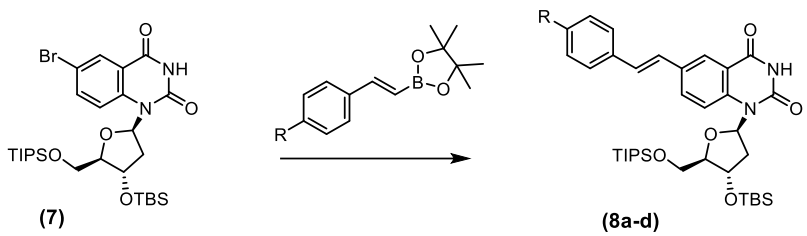

(7) **(8a-d)**

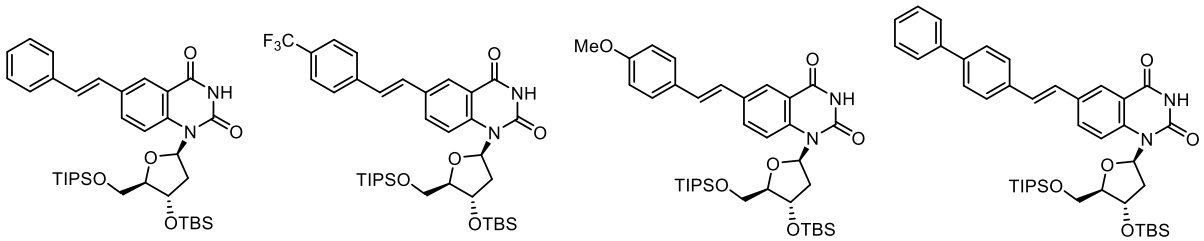

(8a): 98% **(8b)**: 73% **(8c)**: 18% **(8d)**: 50%

[a]Reaction conditions: 1 mmol *trans*-2-phenylvinyl boronic acid pinacol ester (2.0 equiv.), 1.5 mmol Cs_2CO_3 (3.0 equiv.), 0.1 mmol Pd(dppf)Cl_2 (10 mol%), 1.0 mL 1,4-dioxane, Ar, 24 h.

Silyl deprotection of ^{ts}T nucleoside **8a** was achieved using TBAF in THF (Scheme 2.3). For purification, we first tried quenching the reaction mixture by NH_4Cl, followed by workup and column

chromatography (DCM/MeOH).[91] However, this method could not remove tetrabutylammonium hydroxide. Treating the reaction mixture with DOWEX and $CaCO_3$ in methanol[92] was also unsuccessful. Surprisingly, directly loading the reaction mixture (without quenching and workup) to the column and running it with 100% MeCN resulted in a good separation.

2.4. Photophysical properties of ^{ts}T nucleoside

The photophysical properties of **8a**–**d** are summarized in Table 2.2. All reported derivatives exhibited large extinction coefficient values (ε_{max} = 9,700 – 48,000 cm^{-1} M^{-1}). The quantum yields of these compounds are variable in methanol (φ = 0.01 – 0.48). The *Stokes* shift values suggest the presence of a push-pull system, where the pyrimidine group acts as an electron acceptor in the excited state.[93] The magnitude of this push-pull effect is augmented by electron-donating groups in **8c** but diminished by the electron-withdrawing group in **8b**. Indeed, the calculated HOMO-LUMO gaps (MeO-^{ts}T < ^{ts}T < CF_3-^{ts}T) were inversely correlated with the Stokes shifts of these compounds in methanol. As compared to *trans*-stilbene itself (ε_{310nm} = 44,000 cm^{-1} M^{-1}, φ = 0.02), the ^{ts}T nucleoside **8a** exhibits a similar extinction coefficient (ε_{310nm} = 48,000 cm^{-1}), yet much larger quantum yield (φ = 0.31) in methanol. This suggests that although the pyrimidine ring causes a push-pull electron system, ^{ts}T preserves the *trans*-stilbene photophysical properties. Taken together, our data demonstrate that the unsubstituted ^{ts}T nucleoside **8a** is brighter than other synthesized derivatives and the most similar to *trans*-stilbene. Thus, **8a** was the nucleoside of choice for further synthesis steps.

Table 2.2. Photophysical properties of ^{ts}T nucleosides **8a**–**d** and *trans*-stilbene in methanol[a]

Substituent	ε_{max} (cm^{-1} M^{-1})	λ_{abs} max (nm)	λ_{em} max (nm)	Stokes shift (10^3 cm^{-1})	φ	ε_{max} φ
8a (^{ts}T)	48,000	310	430	9.0	0.31	14,784
8b (CF_3-^{ts}T)	4,900	315	415	7.6	0.48	2,347
8c (MeO-^{ts}T)	17,000	320	465	9.7	0.01	187
8d (Ph-^{ts}T)	9,700	325	440	8.0	0.05	475
***trans*-Stilbene[b]**	44,000	295	350	5.3	0.02	1,056

[a] All data were collected at 22 °C, and the concentration of ^{ts}T nucleoside was fixed at 3.0 µM.
[b] *trans*-Stilbene exhibits an ε = 29,100 $cm^{-1}M^{-1}$ and φ = 0.04 in hexane,[94 95] and an ε = 44,000 $cm^{-1}M^{1}$ and φ = 0.02 measured in methanol (determined here).

Absorbance and fluorescence of ^{ts}T nucleoside **9** were measured in different solvents (Table 2.3) and decreasing quantum yields and increasing *Stokes* shifts of ^{ts}T were observed with increasing solvent polarity (Figure 2.6). The solvatochromic fluorescence of **9** and the fluorescence properties of **8a**–**d** are consistent with the presence of a TICT excited state, leading to non-radiative decay.[96, 97] In polar media, the solvent stabilizes electron transfer from the donor to the acceptor. The subsequent transition from the TICT excited state to the ground state results in a low fluorescence quantum yield.[98] Having a planar structure in the ground state, the absorption maxima of **9** was found to be similar in different solvents. This is in agreement with previous studies on donor-acceptor biphenyls, which showed the excitation to the first excited state is independent of the twist angle and the solvent, whereas the emissive state is highly sensitive to solvent polarity.[99-100]

Table 2.3. Photophysical properties of ^{ts}T nucleoside **9** in various solvents[a]

Solvent	ε_{max} (cm^{-1} M^{-1})	λ_{abs} max (nm)	λ_{em} max (nm)	Stokes shift (10^3 cm^{-1})	φ	E_T^{30} (kcal mol^{-1})[101]
Toluene	39,600	315	405	7.1	0.75	33.9
Dioxane	32,300	310	405	7.6	0.74	36
DCM	33,600	310	415	8.2	0.57	40.7
DMF	42,800	310	415	8.2	0.69	43.2
MeCN	44,400	310	415	8.2	0.51	45.6
MeOH	32,700	310	435	9.3	0.30	55.4
Water	38,000	310	455	10.3	0.11	63.1
aq. PBS	28,500	310	455	10.3	0.12	-

[a] All data were collected at 22 ^{o}C, and the concentration of ^{ts}T nucleoside was fixed at 3.0 μM. In order to maximize the solubility, all samples had a final DMSO content of 0.04%.

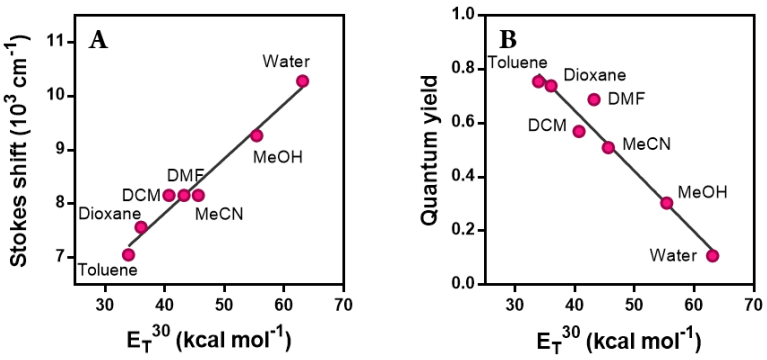

Figure 2.6. (A) Plot between *Stokes* shift of ^{ts}T nucleoside **9** and E_T^{30} values of various solvents (R^2 = 0.97). (B) Plot between quantum yield of ^{ts}T nucleoside **9** and E_T^{30} values of various solvents (R^2 = 0.95).

To further evaluate the potential of ^{ts}T as a fluorescent molecular rotor with microenvironment sensitivity, the absorption and fluorescence emission of nucleoside **9** was measured in various mixtures of methanol and glycerol. These solvents have very similar polarities yet drastically different viscosities. The quantum yield of ^{ts}T increased with increasing viscosity (Figure 2.7), consistent with rotation-induced fluorescent quenching.

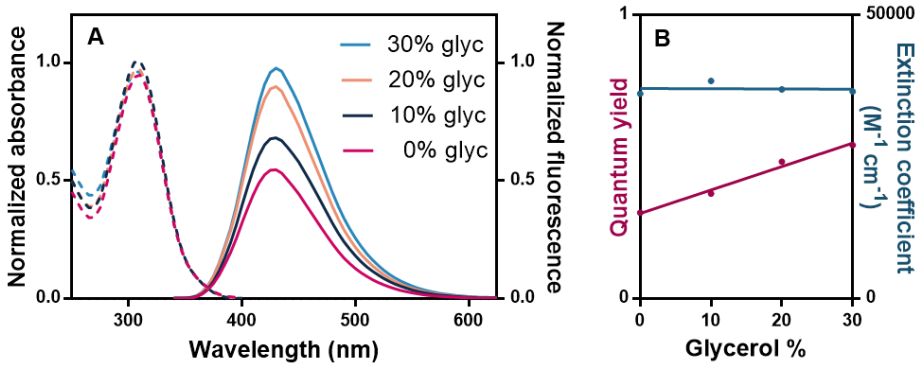

Figure 2.7. (A) Absorption (dashed lines) and fluorescence (solid lines) of ^{ts}T nucleoside **9** in a mixture of methanol and glycerol. (B) Quantum yield and extinction coefficient of ^{ts}T nucleoside **9** versus glycerol content. Extinction coefficients were calculated at 310 nm and emission spectra were collected using Ex = 310 nm.

2.5. Synthesis of ^{ts}T-modified DNA

Encouraged by the photophysical properties of ^{ts}T nucleoside, we next prepared the ^{ts}T phosphoramidite for incorporation into DNA. The nucleoside **9** was treated with DMTCl and

subsequently chlorophosphoramidite to obtain >500 mg of pure tsT phosphoramidite **11** (Scheme 2.4). The entire 12-step sequence required only seven chromatographic separations and provided **11** in a 26% overall isolated yield.

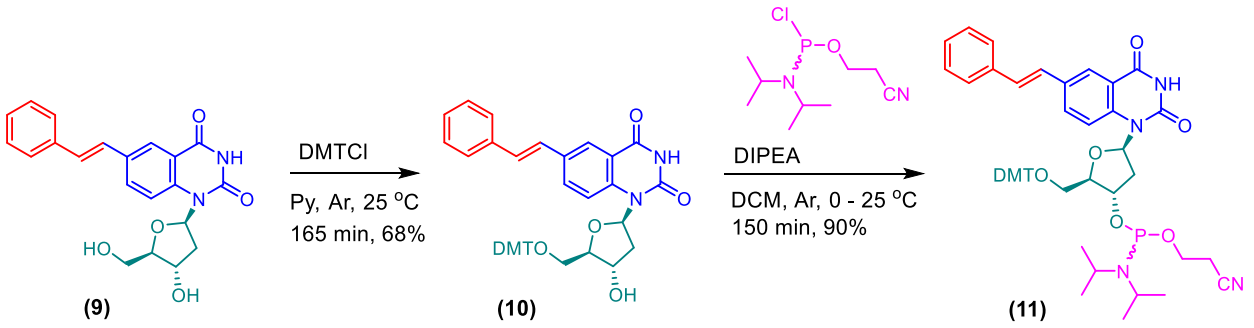

Scheme 2.4. Synthesis of the tsT phosphoramidite. DMTCl = 4,4'-dimethoxytriphenylmethyl chloride, DIPEA = *N,N*-diisopropylethylamine.

Using standard solid-phase supported synthesis,[102] tsT was incorporated into different DNA oligonucleotides (ODN1–7). Following their HPLC purification and mass confirmation (Table A3 and Figure A1, Appendix A) and annealing to complementary strands, canonical B-form secondary structures were observed using circular dichroism (Figure A2, Appendix A). Thermal denaturation experiments revealed that tsT exhibits similar base-pairing specificity as thymidine,[103] with the temperature of ODN1 duplex melting (T_m) being tsT:C/T < tsT:G < tsT:A (Table 2.4 and Figure A3, Appendix A). The maximum absorbance of tsT remains very strong in DNA (ε_{310nm} =30,600 ± 700 cm^{-1} M^{-1}) and sufficiently red-shifted to have no overlap with the natural bases (Figure 2.8).

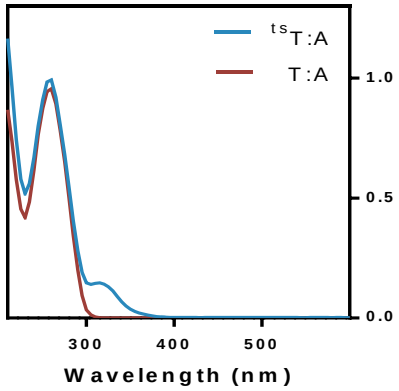

Figure 2.8. Normalized absorbance spectra of tsT-modified and unmodified ODN1. The ratio of absorbance at 260 nm and 310 nm was used to calculate an extinction coefficient of tsT in DNA = 30,600 ± 700 cm^{-1} M^{-1}. Data were recorded at 22 °C in PBS buffer (pH = 7.4). DNA concentrations were kept at 2.0 µM.

Table 2.4. Biophysical properties of DNA containing ^{ts}T[a, b]

Sequences (5′ → 3′)	Oligonucleotides		ε_{260} (cm^{-1} M^{-1})	λ_{abs} (nm)	T_m(°C)	ΔT_m(°C) [c]
GCGTA ^{ts}T CGTATACAC	ODN1	^{ts}T:A	257,000	310	55.0	+5.7
		^{ts}T:G	255,000	310	53.0	-
		^{ts}T:C	251,000	310	51.0	-
		^{ts}T:T	253,000	310	50.8	-
		ss-^{ts}T	155,000	315	-	-
GCGTA ^{ts}T GCGTATACAC	ODN2	^{ts}T:A	273,000	310	60.2	+3.9
		^{ts}T:T	269,000	310	56.1	-
		ss-^{ts}T	164,000	315	-	-
GCGTA ^{ts}T ATGTATACAC	ODN3	^{ts}T:A	271,000	310	54.1	+4.4
		ss-^{ts}T	169,000	310	-	-
GCGA ^{ts}T ATATATATAGCG	ODN4	^{ts}T:A	286,000	310	48.0	-0.3
		ss-^{ts}T	186,000	310	-	-
GCGA ^{ts}T CGATATATAGCG	ODN5	^{ts}T:A	289,000	310	51.6	+2.1
		ss-^{ts}T	181,000	310	-	-
GCGA ^{ts}T ATAGATATAGCG	ODN6	^{ts}T:A	288,000	310	52.3	-3.1
		ss-^{ts}T	187,000	310	-	-
GCGA ^{ts}T CGCGCGCTAGCG	ODN7	^{ts}T:A	291,000	310	64.1	+5.5
		ss-^{ts}T	163,000	310	-	-

[a] The average extinction coefficient (ε) of ^{ts}T in DNA at 310 nm is 30,600 ± 700 cm^{-1} M^{-1}. [b] All data were collected at 22 °C, PBS buffer and pH = 7.4. [c] ΔT_m = T_m (^{ts}T-modified DNA) - T_m (corresponding unmodified DNA).

2.6. Fluorescence properties of ^{ts}T in DNA

The seven duplexes containing ^{ts}T:A all exhibited brighter fluorescence (ε × φ = 3,000 – 5,260 cm^{-1} M^{-1}) than the free nucleoside in water (1,570 cm^{-1} M^{-1}), as well as the single-stranded oligonucleotides (ε × φ = 610 – 3,730 cm^{-1} M^{-1}). These results confirm a lack of fluorescence quenching *via* PET as predicted by DFT calculations. They also suggest that ^{ts}T can be applied as a DNA hybridization probe since it has a 4.9-fold higher fluorescence quantum yield in the more rigid environment of *ds*-DNA. The brightness of ^{ts}T was exceptionally sensitive to base-pairing stability, with ε × φ values ranging from 150 – 4,250 cm^{-1}M^{-1}, with ^{ts}T:A >> ^{ts}T:G > ^{ts}T:C/T (Table 2.5, Figure 2.9)

which demonstrated the same trending as melting temperatures. This same trend was also reported for the relative broadness of thymidine imino proton resonances in ^{1}H NMR spectra of unmodified T:A, T:G, and T:T base-pairs in *ds*-DNA,[104] thereby suggesting dynamic quenching of ^{ts}T by wild-type molecular motions. The effect of dynamic motions on ^{ts}T fluorescence will be discussed in more details in Chapter 3.

Table 2.5. Biophysical properties of DNA containing ^{ts}T[a, b]

Oligonucleotides		λ_{em} max (nm)	φ	Eφ ($cm^{-1}M^{-1}$)
ODN1	^{ts}T:A	440	0.139	4,250
	^{ts}T:G	445	0.017	520
	^{ts}T:C	440	0.005	150
	^{ts}T:T	440	0.005	150
	ss-^{ts}T	445	0.028	860
ODN2	^{ts}T:A	440	0.098	3,000
	^{ts}T:T	440	0.012	370
	ss-^{ts}T	440	0.020	610
ODN3	^{ts}T:A	440	0.134	4,100
	ss-^{ts}T	445	0.026	800
ODN4	^{ts}T:A	440	0.135	4,130
	ss-^{ts}T	440	0.028	860
ODN5	^{ts}T:A	440	0.154	4,710
	ss-^{ts}T	445	0.030	920
ODN6	^{ts}T:A	440	0.167	5,110
	ss-^{ts}T	440	0.035	1,070
ODN7	^{ts}T:A	440	0.172	5,260
	^{ts}T:G	445	0.024	740
	ss-^{ts}T	445	0.122	3,730

[a] The average extinction coefficient (Ɛ) of ^{ts}T in DNA at 310 nm is 30,600 $\pm$ 700 cm^{-1} M^{-1}.

[b] All measurements were performed at 22 ^{o}C in PBS buffer (pH = 7.4), with DNA concentrations = 2.0 μM.

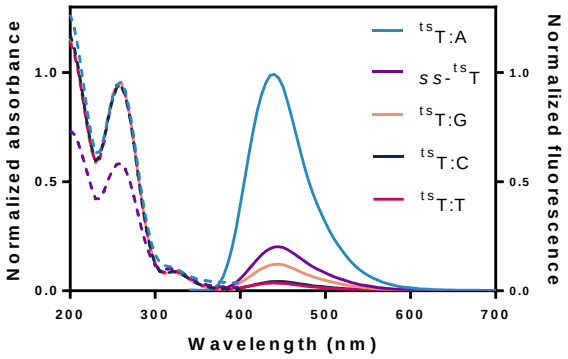

Figure 2.9. Absorption (dashed line) and fluorescence (solid line) of single-stranded and duplex ODN1 containing ^{ts}T. Data were recorded at 22 ^{o}C in PBS buffer (pH = 7.4). DNA concentrations were kept at 2.0 μM.

2.7. Conclusion

We reported an efficient synthesis of *trans*-stilbene analog of thymidine (^{ts}T) as a microenvironment sensitive probe with the molecular rotor properties. The design of ^{ts}T was inspired by the excellent base-pairing specificities of 6-substituted quinazolines together with the desirable photophysical properties of *trans*-stilbene that include viscosity-sensitive emissions. DFT calculations predicted that ^{ts}T should not undergo fluorescence quenching *via* PET. We–therefore–commenced the synthesis of ^{ts}T by preparing 6-bromo-quinazoline-2,4-(3H)-dione nucleoside **7** as a single diastereoisomer on a multi-gram scale in a 46% overall yield (7 steps). *Suzuki-Miyaura* coupling, followed by silyl deprotection, furnished ^{ts}T nucleoside **9** in a 92% isolated yield over two steps. Decreasing quantum yields and increasing *Stokes* shifts of nucleoside **9** were observed with increasing solvent polarity, consisted with the formation of a TICT excited state leading to non-radiative decay. The quantum yield of ^{ts}T **9** increased with increasing viscosity in mixtures of methanol and glycerol, confirming the potential of ^{ts}T as a fluorescent molecular rotor. ^{ts}T phosphoramidite **11** was synthesized (total yield of 26% over 12 steps) and incorporated into DNA. CD and melting temperature experiments revealed that ^{ts}T has little-to-no impact on the global structure of DNA. The average brightness of ^{ts}T in *ds*-DNA was measured as 4,370 cm^{-1} $M^{-1,}$ making it one of the brightest reported FBAs reported to date.

2.8. Experimental

2.8.1 Theoretical computations

The molecular geometries and thermal corrections were optimized with B3LYP DFT functional theory[105] paired with the 6-31++G(d) basis set.[106] Calculations were performed in the water phase (C-PCM algorithm)[107] at 298.15 K. The first frequency was utilized to assess whether structures were in their true optimized form. Conformers distributions were executed using Spartan,[108] and Gaussian 16[109] was used to calculate orbital energies. In order to simplify calculations, deoxyribose (dR) was replaced with a methyl group.

2.8.2 Synthesis and characterization of nucleosides

All reagents were obtained from commercial sources and used without further purification. NMR data were collected on either a Bruker AVIII-400 or 500 MHz. Chemical shifts (δ) are given in parts per million (ppm) and are reported relative to residual solvent peaks: $CDCl_3$ (δH 7.26, δC 77.16 ppm), DMSO-d_6 (δH 2.50, δC 39.52 ppm), acetone-d_6 (δH 2.05, δC 29.84 ppm). Coupling constants (*J*) are given in Hertz (Hz). ^{13}C-spectra were recorded broadband proton decoupled. Mass spectra were recorded on an Advion expression CMS and High-resolution mass spectra were obtained on a Bruker MaXis high-resolution QTOF or a Thermo QExactive high-resolution Orbitrap. Masses are given as m/z.

2.8.3 Biophysical experiments

Fluorescence spectroscopy: DMSO stock solutions of the ^{ts}T nucleoside **8a**—**d** and **9** were prepared and stored at -20°C, and later thawed and diluted to an *OD* = 0.10 ± 0.01 at the most red-shifted absorbance maxima. All measurements were collected on a Molecular Devices SpectraMax M5 in a 1 cm path-length quartz cuvette. Quantum yields were calculated using the most red-shifted absorbance maxima of samples. Quinine hemisulfate (φ_R = 0.546) in 0.5 M H_2SO_4 (n_R = 1.346) was used as a fluorescent standard. Quantum yields were calculated using the equation shown below[93]:

$$\Phi = \Phi_{\mathrm{R}} \frac{F}{F_{\mathrm{R}}} \frac{A_{\mathrm{R}}}{A} \frac{n^2}{{n_{\mathrm{R}}}^2}$$

where φ_R is the quantum yield of the fluorescent standard, F and F_R are the integrated emissions of the sample and reference, respectively. A and A_R are the optical densities of the sample and reference respectively (both set to 0.10 ± 0.01). n and n_R are the refractive indexes of the sample and reference respectively. The refractive indexes of solvents used in this work are: n_{PBS} = 1.335, n_{water} = 1.333, $n_{methanol}$ = 1.328, $n_{dioxane}$ = 1.422, n_{DMF} = 1.431, n_{DCM} = 1.424, n_{ACN} = 1.344, and $n_{toluene}$ = 1.497.

Oligonucleotide stock solutions were diluted into PBS buffer (pH = 7.4, Na^+ concentration of ≈137 mM) to a final concentration of 2.0 µM using their extinction coefficient at 260 nm. All measurements were collected on a Molecular Devices SpectraMax M5 in a 1 cm path-length quartz cuvette. Quantum yields were calculated using the most red-shifted absorbance maxima of samples. Quinine hemisulfate (φ_R = 0.546) in 0.5 M H_2SO_4 (n_R = 1.346) was used as the fluorescent standard, and quantum yields were calculated using the above equation.

CD Spectroscopy: Circular dichroism spectra of annealed duplex DNA (2.0 µM) were measured from 220 nm to 350 nm at 22 °C with a 2 nm bandwidth with 0.1 nm steps at a scanning rate of 20 nm min^{-1} in 1 cm path length thermo-controlled strain-free quartz cuvette on a JASCO J-715 spectrometer.

Melting Temperature Analysis (T_m): UV thermal denaturation data were obtained by measuring the absorbance at 260 nm as a function of temperature in a 1 cm path length thermo-controlled strain-free quartz cuvette on a Varian CARY 100 UV-visible spectrophotometer equipped with a Peltier temperature controller. Solutions of pre-folded duplex DNA (0.2 µM) in aqueous buffer (PBS buffer, pH = 7.4) were equilibrated at 20 °C for a minimum of 10 min and slowly ramped to 90 °C with 0.2 °C steps at a rate of 12 °C h^{-1}. The melting temperatures were determined from the maximal slope of the curve (maximal first derivative). T_m values were calculated as the average from the heating and cooling curves that showed little or no hysteresis.

2.8.4 Oligomer synthesis, purification and folding

Synthesis: Unmodified oligonucleotides were purchased from Sigma-Aldrich as HPLC-purified products. Standard DNA phosphoramidites, solid supports, and all necessary reagents were purchased from LinkTech and Sigma-Aldrich. Modified oligonucleotides were synthesized on a 1.0 µmol scale using a Bioautomation Co. Mermade 4 DNA synthesizer according to the Trityl-on

procedure. Three coupling reactions were performed for the site-specific introduction of the modified nucleoside into oligonucleotides. The freshly made phosphoramidite **11** was dissolved in dry acetonitrile (0.1 M) immediately prior to use. The synthesis of the oligonucleotides was monitored by DMT deprotection. Upon completion of the sequences, the oligonucleotides were cleaved from the solid support and deprotected by treatment with 1.0 mL of 33 % aqueous ammonium hydroxide at 55 ^{o}C overnight in a 1.5 mL screw-top cap tube. The resulting products were lyophilized and filtered through Glen-Pak DNA purification cartridges to remove incomplete synthesis products and to deprotect the 5'–DMT during elution.

Purification: The obtained solutions were lyophilized to dryness and purified by HPLC column chromatography using a semi-prep C-18 reverse-phase column (YMCbasic B-22-10P 150 x 10 mm) using a Varian 140 Pro Star HPLC system. The gradient conditions were typically acetonitrile: 0.1 M triethylammonium acetate (TEAA, pH 7.4), 2:98 to 10:90 over 35 minutes, and with the rate of 3.00 mL/min. Elution was monitored by UV absorption at 260 and 310 nm. Peaks were collected and twice lyophilized to dryness from water. The purities of ^{ts}T-containing oligonucleotides ODN1–7 were found to be >90% (260 nm) according to analytical, reverse-phase chromatography using a Waters XBridge C8, 5 µm 4.6 x 150 mm. A gradient of 5–40% of acetonitrile in 0.1 M triethylammonium acetate (TEAA, pH 7.4), was applied over 35 minutes at 0.4 mL/min. ODN1–7 were analyzed by LC-MS using a Dionex Ultimate 3000 UHPLC coupled to a Bruker Maxis Impact QTOF in negative ESI mode. Samples were run through a Phenomenex Luna C18(2)-HST column (2.5 µM 120A 2.1 x 100 mm) using a gradient of 90% mobile phase A (100 mM HFIP and 5 mM TEA in H_2O) and 10% mobile phase B (MeOH) to 40% mobile phase A and 60% mobile phase B in 20 minutes. The data was processed and spectra deconvoluted using the Bruker DataAnalysis software version 4.2.

Folding: Oligonucleotide stock solutions were prepared in deionized water, and their concentrations were determined by absorbance at 260 nm using the molar extinction coefficient calculated using a nearest-neighbor model.[110] The molar extinction coefficient of ^{ts}T nucleotide at 260 nm was determined 15,400 $cm^{-1}M^{-1}$ using the absorbance of ^{ts}T nucleoside **9** at 260 nm. For calculated extinction coefficients of ^{ts}T-modified oligonucleotides see Table 2.4. Double-stranded oligonucleotides were prepared by diluting the complementary sequences (1.0 : 1.2 equiv. ratio) in the PBS buffer (pH = 7.4, Na^+ concentration of ≈137 mM) and heating to 95 °C for 5 min, followed by slow cooling to room temperature over 4 h.

2.9 Appendixe A

2.9.1 Tables

Table A1. Calculated [b3lyp/6-31++G(d)] HOMO and LUMO energy values (eV) in water.

	^{ts}T	tC^{o}	tC	^{MD}A	2AP	G	A	C	T
LUMO	-1.99	-1.56	-1.65	-1.32	-1.43	-0.78	-1.08	-1.17	-1.33
HOMO	-5.85	-5.63	-5.76	-5.77	-6.22	-6.16	-6.38	-6.58	-6.63

Table A2. Optimization of the *Suzuki-Miyaura* reaction condition on nucleoside **7**.[a]

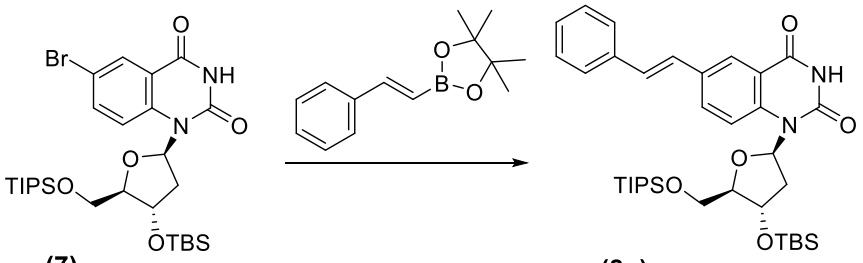

(7) **(8a)**

Entry	Base	Solvent	Catalyst	Temperature (°C)	Yield (%)[b]
1	KOAc	1,4-dioxane	$Pd(OAc)_2$	90	40%
2	KOAc	1,4-dioxane	$Pd(dppf)Cl_2$	90	52%
3	KOAc	toluene	$Pd(dppf)Cl_2$	90	44%
4	KOtBu	1,4-dioxane	$Pd(dppf)Cl_2$	90	58%
5	Cs_2CO_3	1,4-dioxane	$Pd(dppf)Cl_2$	90	86%
6	Cs_2CO_3	1,4-dioxane	$Pd(dppf)Cl_2$	100	93%
7	Cs_2CO_3	1,4-dioxane	$Pd(dppf)Cl_2$	105	80%

[a] Reaction conditions: 1 mmol *trans*-2-phenylvinyl boronic acid pinacol ester (2.0 equiv.), 1.5 mmol base (3.0 equiv.), 0.1 mmol Catalyst (10 mol%), 1.0 mL solvent, Ar, 12 h.
[b] isolated yield.

Table A3. Synthesized oligomers with calculated and observed masses.

Oligonucleotides	Sequences (5' → 3')	Calc. (m/z)	Found (m/z)	δ (ppm)
ODN1	GCGTA ^{ts}T CGTATACAC	4687.8488	4687.9219	15.6
ODN2	GCGTA ^{ts}T GCGTATACAC	5016.9014	5016.9844	16.6
ODN3	GCGTA ^{ts}T ATGTATACAC	5015.9061	5016.0078	20.3
ODN4	GCGA ^{ts}T ATATATATAGCG	5368.9643	5368.9375	5.0
ODN5	GCGA ^{ts}T CGATATATAGCG	5369.9594	5369.9688	1.8
ODN6	GCGA ^{ts}T ATAGATATAGCG	5393.9702	5393.9688	0.3
ODN7	GCGA ^{ts}T CGCGCGCTAGCG	5347.9382	5347.9375	0.1

2.9.2 Figures

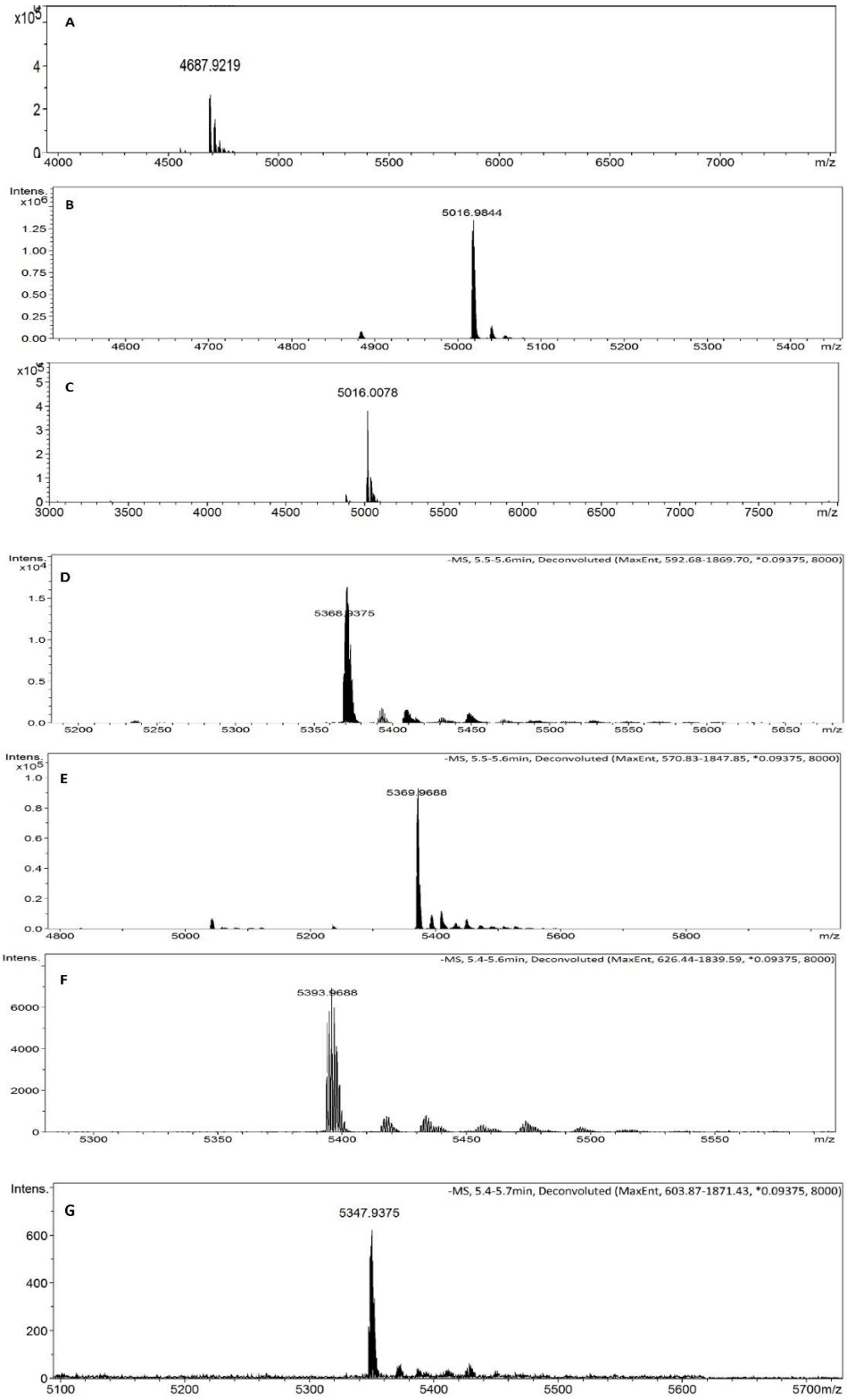

Figure A1. ESI-MS analysis of (A) ODN1, (B) ODN2, (C) ODN3, (D) ODN4, (E) ODN5, (F) ODN6, and (G) ODN7.

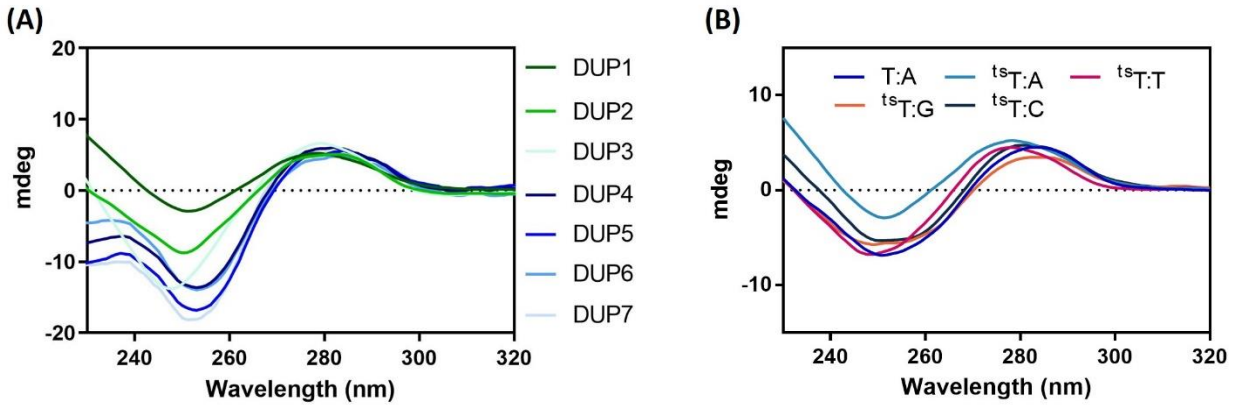

Figure A2. CD spectra of (A) DUP1–7 prepared from OND1–7. (B) Matched, mismatched and unmodified duplexes of DUP1/ODN1.

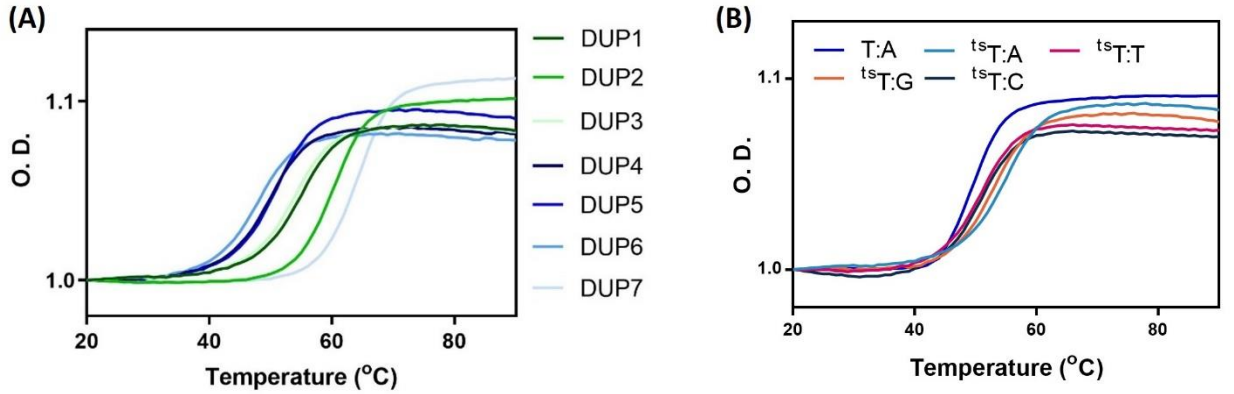

Figure A3. Normalized thermal melting data of (A) DUP1–7 containing ODN1–7 duplexes. (B) Well-matched, mismatched and unmodified duplexes of ODN1 and the corresponding unmodified well-matched duplex.

2.9.3 Synthesis and characterization

***p*-Tolyl-3,5-di-*O*-acetyl-1-thio-2-deoxy-α,β-D-ribofuranoside [2]**

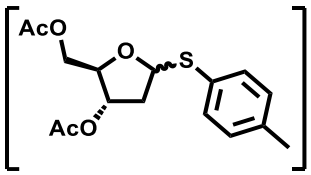

Procedure: To a stirring solution of 1,3,5-tri-*O*acetyl-2-deoxy-α,β-D-ribose **1** (24.0 g, 92.3 mmol, 1.0 equiv.) at -78 ^{o}C in CH_2Cl_2 (310 mL) was added *p*-TolSH (14.7 g, 119 mmol, 1.3 equiv.). After 5 min, $BF_3{\cdot}OEt_2$ (43.0 mL, 349 mmol, 3.8 equiv.) was added dropwise. The reaction mixture was stirred for 20 min and then quenched with aq. sat. $NaHCO_3$. The resulting solution was extracted with CH_2Cl_2 and combined organic layer was washed with sat. sol. NaCl, dried over $MgSO_4$, filtered, and evaporated *in vacuo*. The yellow crude product was used directly for the next reaction without purification.

Characterization: R*f* = (Hexane/EtOAc, 7:3): 0.36, **MS** (ESI) = 346.87 ([M+Na]$^+$ calculated 347.09). R*f* and ESI MS data are consistent with those previously reported.[49]

***p*-Tolyl-1-thio-2-deoxy-α,β-D-ribofuranoside [3]**

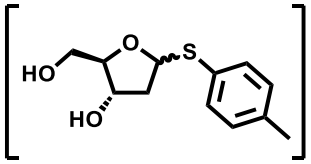

Procedure: To a stirring solution of unpurified di-acetate thioglycoside **2** (29.9 g) in a mixture of MeOH/CH_2Cl_2 (340 mL, 4:1) was added K_2CO_3 (31.5 g, 228 mmoles). The reaction mixture was stirred at room temperature for 2h and then quenched with a solution of HCl (500 mL, 1.00M). The mixture was three times extracted with $CHCl_3$, dried, filtered, and evaporated *in vacuo*. TLC showed full conversion of **2** to **3**. The crude **3** was used for the next reaction without purification.

Characterization: R*f* = (CH_2Cl_2:MeOH, 94:6): 0.25, **MS** (ESI) = 262.98 ([M+Na]$^+$ calculated 263.07). R*f* and ESI MS data are consistent with those previously reported.[49]

***p*-Tolyl-1-thio-5-*O*-triisopropylsilyl-2-deoxy- α,β -D-ribofuranoside [4]**

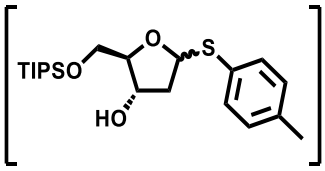

Procedure: To a stirring solution of unpurified diol thioglycoside **3** (26.4 g) in CH_2Cl_2 (400 mL) were added TIPSCl (21.2 g, 110 mmoles) and imidazole (7.49 g, 110 mmoles). The reaction mixture was stirred at room temperature for 16h and then quenched with H_2O. The resulting solution was extracted with CH_2Cl_2 and the combined organic layer was dried, filtered, and evaporated *in vacuo*. TLC showed a full conversion of **3** to **4**. The crude product **4** was used for the next reaction without purification.

Characterization: R*f* = (CH_2Cl_2:MeOH, 94:6): 0.48, **MS** (ESI) = 419.07 ($[M+Na]^+$ calculated 419.20). R*f* and ESI MS data are consistent with those previously reported.[49]

***p*-Tolyl-3-*O*-acetyl-1-thio-5-*O*-triisopropylsilyl-2-deoxy-α,β-D-ribofuranoside (5)**

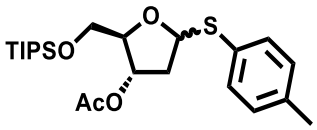

Procedure: To a stirring solution of unpurified thioglycosides **4** (47.6 g) in MeCN (400 mL), were added Et_3N (24.0 mL, 172 mmoles), Ac_2O (17.0 mL, 180 mmoles) and DMAP (1.60 g, 13.1 mmoles). The reaction mixture was stirred at room temperature for 15 h. The reaction color after 30 min stirring changed from yellowish to brownish. The reaction quenched with sat. sol. NaCl and the resulting solution was extracted with CH_2Cl_2. The combined organic layer was dried by $MgSO_4$, filtered, and evaporated under the reduced pressure. The crude product **5** (49.0 g) was filtered three times through silica (height= 4-5 cm) in a large Büchner funnel with EtOAc/hexane gradient from 0 % to 20 %. After three times filtration, pure thioglycoside **7** (α/β: 1.0:2.1, 35.9 g, 81.8 mmol, 89 % over 4 steps) was obtained.

Characterization: R*f* = (hexane:EtOAc, 9:1): 0.38, **^{1}H NMR** (400 MHz, $CDCl_3$) δ **α:** 7.41 (dd, *J* = 8.2, 2.0 Hz, 2H), 7.10 (dd, *J* = 7.9, 4.5 Hz, 2H), 5.47 (dd, *J* = 9.3, 5.8 Hz, 1H), 5.29 (dt, *J* = 5.7, 1.8 Hz, 1H), 4.33 (dt, *J* = 5.7, 1.8 Hz, 1H), 4.08 (dd, *J* = 4.4, 1.5 Hz, 1H), 3.81 (dt, *J* = 10.5, 3.9 Hz, 1H), 3.57 (dd, *J* = 10.5, 6.6 Hz, 1H), 2.32 (s, 3H), 2.26 (dd, *J* = 9.2, 5.6 Hz, 1H), 2.09 (s, 3H), 1.10 – 1.03 (m, 21H) **β:** 7.41 (dd, *J* = 8.2, 2.0 Hz, 2H), 7.10 (dd, *J* = 7.9, 4.5 Hz, 2H), 5.68 (dd, *J* = 7.7, 3.1 Hz, 1H), 5.23 (dt, *J* = 7.4, 2.8 Hz, 1H), 4.33 (q, *J* = 3.4 Hz, 1H), 3.94 (dd, *J* = 10.8, 3.4 Hz, 1H), 3.84 (dd, *J* = 7.6, 3.2 Hz, 1H), 2.79 (dt, *J* = 14.9, 7.6 Hz, 1H), 2.32 (s, 3H), 2.13 (t, *J* = 2.8 Hz, 1H), 2.09 (s, 3H), 1.28 – 1.24 (m, 21H). **MS** (ESI) = 460.86 ($[M+Na]^+$ calculated 461.22). The spectroscopic data are consistent with those previously reported.[49]

1′-(3′-*O*-acetyl-5′-*O*-triisopropylsilyl-2′-deoxy-β-D-ribofuranoside)-6-bromo-quinazoline-2,4-(3H)-dione (6β)

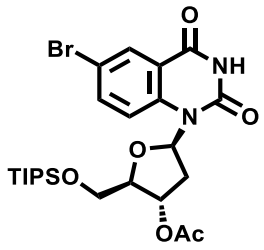

Procedure: To a suspension of 6-bromo-quinazoline-2, 4-(1*H*, 3*H*)-dione (5.70 g, 23.7 mmol, 1.25 equiv.) in dry CH_2Cl_2 (300 mL) with activated molecular sieves (MS 4Å, 30.0 g), BSA (12.0 mL, 49.3 mmol, 2.6 equiv.) was added dropwise over 5 min under Ar atmosphere. The solution was stirred at room temperature for 180 min. This solution was then cooled to 0 ^oC and the solution of thioglycoside **5** (α/β = 1.0:2.5, 8.31 g, 19.0 mmol, 1.0 equiv.) was added to the reaction mixture. After 20 min, NIS (4.70 g, 20.9 mmol, 1.1 equiv.) and TMSOTf (2.10 mL, 11.6 mmol, and 0.61 equiv.) were added and the reaction mixture color changed from light brown to a red. The reaction mixture was stirred for 5 min at 0 ^oC, then quenched with aq. sat. $Na_2S_2O_3$ and diluted with CH_2Cl_2. To this green color solution, aq. sat. $NaHCO_3$ was added and the organic phase was washed for three times. The aqueous phase was also washed with CH_2Cl_2 for three times. The combined organic phase was dried over $MgSO_4$, filtered, and concentrated under reduced pressure to result crude **6** as yellow oil. The crude product was subjected to the flash column chromatography on silica gel EtOAc/hexane, gradient from 0 % to

40 %, to isolate **β** isomer (5.82 g, 10.5 mmol, 55 %) and **α** isomer (3.42 g, 6.16 mmol, 33 %) as white foams.

Characterization: R*f* (hexane/EtOAc, 6:4): 0.85; **^{1}H NMR** (400 MHz, $CDCl_3$) δ: 8.52 (br, 1H), 8.32 (d, *J* = 2.5 Hz, 1H), 7.87 (d, *J* = 9.1 Hz, 1H), 7.64 (dd, *J* = 9.1, *2.5* Hz, 1H), 6.79 (dd, *J* = 9.6 *, 6.2* Hz, 1H), 5.52 (dt, *J* = 8.0, 2.9 Hz, 1H), 4.09-4.00 (m, 3H), 2.88-2.80 (m, 1H), 2.15 (dd, *J* = 6.3, 2.1 Hz, 1H), 2.11 (s, 3H), 1.29-1.24 (m, 21H). The spectroscopic data are consistent with those previously reported.[49]

1′-(3′-*O*-tertbutyldimethylsilyl-5′-*O*-triisopropylsilyl-2′-deoxy-β-D ribofuranoside)-6-bromoquinazoline- 2,4-(3*H*)-dione (7)

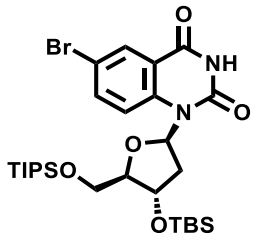

Procedure: To a stirred solution of β nucleoside **6** (1.70 g, 3.06 mmol, 1.0 equiv.) in a mixture of MeOH/CH_2Cl_2 (80.0 mL, 4:1), was added K_2CO_3 (710 mg, 5.14 mmoles, 1.7 equiv.). The reaction mixture was stirred at room temperature for 36 h and then concentrated under the reduced pressure. The crude material was taken up in EtOAc and washed with sat. sol. NaCl. The aqueous phase was back extracted with EtOAc and the combined organic layer was dried, filtered, and evaporated to give unprotected nucleoside as an off-white foam. The product was used in the next step without further purification. To a stirred solution of unprotected nucleoside in DMF (65.0 mL), TBDMSCl (730 mg, 4.84 mmoles, 1.6 equiv.) and imidazole (340 mg, 4.99 mmoles, 1.6 equiv.) were added. The reaction mixture was stirred at room temperature for 40 h and then quenched with sat. sol. NaCl. The resulting solution was extracted with EtOAc and the combined organic layer was dried, filtered, and concentrated under reduced pressure. The crude product (1.88 g) was subjected to flash column chromatography on silica gel EtOAc/hexane, gradient from 0 % to 40 %, to give protected nucleoside **7** (1.78 g, 2.90 mmoles, 95 % over two steps) as a white foam.

Characterization: R*f* (hexane/EtOAc, 9:1): 0.35; **^{1}H NMR** (400 MHz, $CDCl_3$) δ: 8.97 (br, 1H), 8.32 (d, *J* = 2.4 Hz, 1H), 7.69 (d, *J* = 9.2 Hz, 1H), 7.63 (dd, *J* = 8.9, 2.4 Hz, 1H), 6.73 (t, *J* = 7.7 Hz, 1H), 4.73 (dt, *J* = 8.7, 4.4 Hz, 1H), 4.04 (dd, *J* = 11.5, 2.8 Hz, 1H), 3.92 (dd, *J* = 11.5, 3.2 Hz, 1H), 3.84 (dt, *J* = 5.7, 2.9 Hz, 1H), 2.72 (dt, *J* = 13.3, 8.1 Hz, 1H), 2.08-2.02 (m, 1H), 1.16-1.08 (m, 21H), 0.90 (d, *J* = 1.1 Hz, 9H), 0.10 (d, *J* = 1.0 Hz, 3H), 0.08 (d, *J* = 1.0 Hz, 3H). The spectroscopic data are consistent with those previously reported.[91]

1′-(3′-*O*-tertbutyldimethylsilyl-5′-*O*-triisopropylsilyl-2′-deoxy-β-D ribofuranoside)-6-styryl-quinazoline- 2,4-(3*H*)-dione (8a)

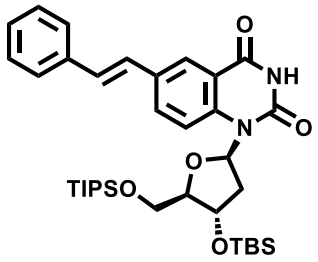

Procedure: Cs_2CO_3 (1.90 g, 5.83 mmol, 3.2 equiv.) was added to a dry round flask contained nucleoside **7** (1.14 g, 1.85 mmol, 1.0 equiv.). Then, *trans*-styryl boronic acid pinacol ester (894 mg, 3.89 mmol, 2.1 equiv.), Pd(dppf)Cl_2 (213 mg, 0.291 mmol, 0.16 equiv.) and freshly degassed dry 1,4-dioxane (15 mL, 0.12M) were added to the mixture. The reaction was stirred at 100 ^{o}C for 24 h under an Ar atmosphere. Then, the reaction was quenched with sat. sol. NaCl, extracted with EtOAc, dried over $MgSO_4$ and filtered through a pad of celite. The crude product was subjected to flash column chromatography on silica gel EtOAc/Hexane, gradient from 0 % to 40 %, to give protected ^{ts}T nucleoside **8a** (1.17 g, 1.80 mmol, 98 %) as a white foam.

Characterization: R*f* (hexane/EtOAc, 8:2): 0.42; **^{1}H NMR** (400 MHz, $CDCl_3$) δ: 8.32 (d, *J* = 2.1 Hz, 1H), 8.18 (br, 1H), 7.76 (d, *J* = 8.7 Hz, 1H), 7.70 (dd, *J* = 9.0, 1.9 Hz, 1H), 7.53 (d, *J* = 7.7 Hz, 2H), 7.38 (t, *J* = 7.5 Hz, 2H), 7.29 (t, *J* = 7.5 Hz, 1H), 7.19 – 7.05 (m, 2H), 6.74 (t, *J* = 7.6 Hz, 1H), 4.76 (dt, *J* = 8.7, 4.5 Hz, 1H), 4.06 (dd, *J* = 11.2, 3.0 Hz, 1H), 3.94 (dd, *J* = 11.3, 3.5 Hz, 1H), 3.87 – 3.85 (m, 1H), 2.81 (dt, *J* = 13.2, 8.0 Hz, 1H), 2.07 (ddd, *J* = 12.5, 7.6, 3.8 Hz, 1H), 1.20 – 1.05 (m, 21H), 0.91 (9H, s), 0.11 (s, 3H), 0.10 (s, 3H). **^{13}C NMR** (126 MHz, $CDCl_3$) δ 162.2, 150.1, 138.9, 136.8, 133.1, 132.6, 129.8, 128.8,

128.0, 126.6, 126.3, 125.9, 117.2, 117.1, 86.5, 84.0, 70.2, 61.1, 37.1, 25.8, 18.1, 18.0, 12.0, -4.5, -4.8. **HRMS** (ESI): *m/z* 651.36445 ($[M+H]^+$ $C_{36}H_{55}O_5N_2Si_2^+$ requires 651.36440).

1′-(3′-*O*-tertbutyldimethylsilyl-5′-*O*-triisopropylsilyl-2′-deoxy-β-D ribofuranoside)-6-(4-trifluoromethyl)-styryl-quinazoline- 2,4-(3*H*)-dione (8b)

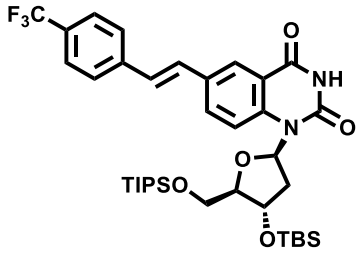

Procedure: Cs_2CO_3 (520 mg, 1.60 mmol, 3.1 equiv.) was added to a dry round flask contained nucleoside **7** (316 mg, 0.52 mmol, 1.0 equiv.). Then, *trans*-2-[4-(trifluoromethyl)phenyl] boronic acid (266 mg, 1.16 mmol, 2.5 equiv.), $Pd(dppf)Cl_2$ (75 mg, 0.09 mmol, 0.18 equiv.) and freshly degassed dry 1,4-dioxane (4.0 mL) were added to the mixture. The reaction was stirred at 100 ^{o}C for 30 h under an Ar atmosphere. Then, the reaction was quenched with sat. sol. NaCl, extracted with EtOAc, dried over $MgSO_4$ and filtered through a pad of celite. The crude product was subjected to flash column chromatography on silica gel EtOAc/Hexane, gradient from 0 % to 40 %, to give protected ^{ts}T nucleoside **8b** (270 mg, 0.38 mmol, 73 %) as a white foam.

Characterization: R*f* (hexane/EtOAc, 9:1): 0.24; **^{1}H NMR** (500 MHz, $CDCl_3$) δ: 10.16 (s, 1H), 8.39 (d, *J* = 2.2 Hz, 1H), 7.78 (d, *J* = 8.8 Hz, 1H), 7.69 (dd, *J* = 8.9, 2.3 Hz, 1H), 7.59 (s, 4H), 7.15 (s, 2H), 6.80 (t, *J* = 7.7 Hz, 1H), 4.77 (ddd, *J* = 8.7, 5.4, 3.9 Hz, 1H), 4.07 (dd, *J* = 11.3, 2.9 Hz, 1H), 3.96 (dd, *J* = 11.3, 3.5 Hz, 1H), 3.87 (dd, *J* = 5.5, 3.0 Hz, 1H), 2.82 (dt, *J* = 13.3, 8.0 Hz, 1H), 2.10 (ddd, *J* = 13.3, 7.6, 3.9 Hz, 1H), 1.18 – 1.07 (m, 21H), 0.92 (s, 9H), 0.12 (s, 3H), 0.10 (s, 3H). **^{13}C NMR** (126 MHz, $CDCl_3$) δ 162.2, 150.0, 140.3, 139.5, 133.0, 132.4, 129.8, 129.5, 128.9, 128.2, 126.8, 126.3, 125.7 (q, *J* = 3.9 Hz), 125.3, 123.1, 117.4, 117.2, 86.6, 84.1, 70.3, 60.5, 25.9, 18.2, 18.1, 18.0, 12.1, -4.5, -4.8. **HRMS** (ESI): *m/z* 741.33323 ($[M+Na]^+$ $C_{37}H_{53}F_3O_5N_2Si_2Na^+$ requires 741.3337).

1′-(3′-*O*-tertbutyldimethylsilyl-5′-*O*-triisopropylsilyl-2′-deoxy-β-D ribofuranoside)-6-(4-methoxy)-styryl-quinazoline- 2,4-(3*H*)-dione (8c)

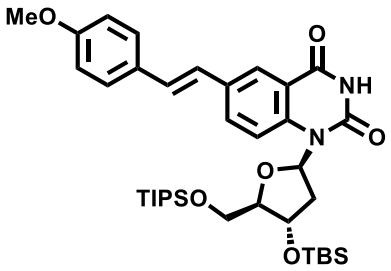

Procedure: Cs_2CO_3 (574 mg, 1.76 mmol, 3.5 equiv.) was added to a dry round flask contained nucleoside **7** (308 mg, 0.50 mmol, 1.0 equiv.). Then, 4-methoxy *trans*-styryl boronic acid (231mg, 1.30 mmol, 2.6 equiv.), Pd(dppf)Cl_2 (70 mg, 0.09 mmol, 0.17 equiv.) and freshly degassed dry 1,4-dioxane (5.0 mL) were added to the mixture. The reaction was stirred at 90 ^{o}C for 30 h under an Ar atmosphere. Then, the reaction was quenched with sat. sol. NaCl, extracted with EtOAc, dried over $MgSO_4$ and filtered through a pad of celite. The crude product was subjected to flash column chromatography on silica gel EtOAc/Hexane, gradient from 0 % to 40 %, to give protected ^{ts}T nucleoside **8c** (60 mg, 0.09 mmol, 18 %) as a white foam.

Characterization: R*f* (hexane/EtOAc, 8:2): 0.35; **^{1}H NMR** (400 MHz, $CDCl_3$) δ: 9.33 (s, 1H), 8.33 (s, 1H), 7.71 (s, 2H), 7.48-7.42 (m, 2H), 7.13 (d, *J* = 16.3 Hz, 1H), 7.06 (t, *J* = 7.8 Hz, 1H), 6.98 – 6.88 (m, 3H), 5.56 (ddd, *J* = 8.6, 4.1, 2.4 Hz, 1H), 4.44 (d, *J* = 2.6 Hz, 1H), 4.03 (dd, *J* = 10.8, 2.4 Hz, 1H), 3.98 (dd, *J* = 10.7, 2.8 Hz, 1H), 3.83 (s, 3H), 2.86 (dt, *J* = 14.4, 8.3 Hz, 1H), 2.55 (ddd, *J* = 14.4, 7.7, 4.1 Hz, 1H), 1.20 – 1.06 (m, 21H), 0.92 (s, 9H), 0.12 (s 3H), 0.10 (s, 3H). **HRMS** (ESI): *m/z* 703.35685 ($[M+Na]^+$ $C_{36}H_{55}O_5N_2Si_2^+$ requires 703.35691).

1′-(3′-*O*-tertbutyldimethylsilyl-5′-*O*-triisopropylsilyl-2′-deoxy-β-D ribofuranoside)-6-(4-phenyl)-styryl-quinazoline- 2,4-(3*H*)-dione (8d)

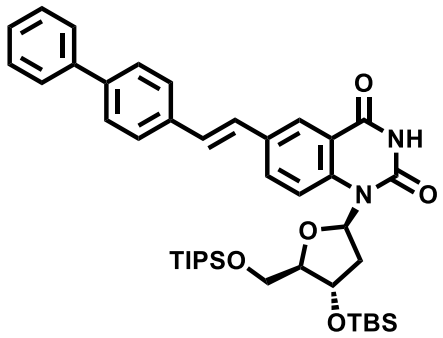

Procedure: Cs_2CO_3 (587 mg, 1.80 mmol, 3.7 equiv.) was added to a dry round flask contained nucleoside **7** (301 mg, 0.49 mmol, 1.0 equiv.). Then, *trans*-2-(4-biphenyl)vinyl boronic acid (280 mg, 1.25 mmol, 2.6 equiv.), Pd(dppf)Cl_2 (64 mg, 0.08 mmol, 0.16 equiv.) and freshly degassed dry 1,4-dioxane (7 mL) were added to the mixture. The reaction was stirred at 100 ^{o}C for 30 h under an Ar atmosphere. Then, the reaction was quenched with sat. sol. NaCl, extracted with EtOAc, dried over $MgSO_4$ and filtered through a pad of celite. The crude product was subjected to flash column chromatography on silica gel EtOAc/Hexane, gradient from 0 % to 20 %, to give protected ^{ts}T nucleoside **8d** (178 mg, 0.25 mmol, 50%) as a white foam.

Characterization: R*f* (hexane/EtOAc, 8:2): 0.23; **^{1}H NMR** (400 MHz, $CDCl_3$) δ: 8.64 (s, 1H), 8.36 (br, 1H), 7.77 (d, *J* = 8.8 Hz, 1H), 7.72 (d, *J* = 8.9 Hz, 1H), 7.65—7.59 (m, 6H), 7.48—7.34 (m, 4H), 7.23—7.11 (m, 2H), 6.77 (t, *J* = 7.7 Hz, 1H), 4.77 (dt, *J* = 9.0, 4.3 Hz, 1H), 4.10—4.03 (m, 1H), 3.99—3.92 (m, 1H), 3.87 (d, *J* = 4.8 Hz, 1H), 2.82 (dt, *J* = 15.0, 8.0 Hz, 1H), 2.09 (td, *J* = 9.1, 4.7 Hz, 1H), 1.27 – 1.09 (m, 21H), 0.92 (9H, s), 0.12 (s, 3H), 0.11 (s, 3H). **^{13}C NMR** (126 MHz, $CDCl_3$) δ 162.0, 150.0, 140.9, 140.7, 139.0, 135.9, 133.3, 132.9, 129.5, 129.0, 127.6, 127.2, 127.0, 126.4, 126.0, 117.5, 117.1, 86.6, 84.1, 70.3, 62.0, 37.2, 25.9, 18.2, 18.1, 12.1, -4.4, -4.7. **HRMS** (ESI): *m/z* 769.37765 ($[M+Na]^+$ $C_{42}H_{58}NaO_5N_2Si_2^+$ requires 769.37765).

1′-(2′-deoxy-β-D ribofuranoside)-6-styryl-quinazoline- 2,4-(3*H*)-dione (2)

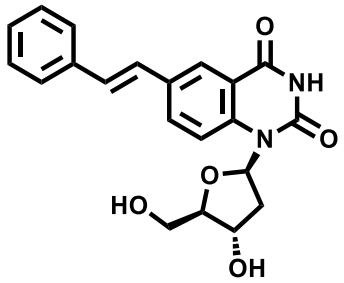

Procedure: To a stirred solution of nucleoside **9** (870 mg, 1.34 mmol, 1.0 equiv.) in THF (15 mL), was added TBAF (1M solution in THF, 6.62 mL, 4.9 equiv.). The mixture was stirred at room temperature for 22 h and then directly loaded onto a silica gel column chromatography. Purification using 100 % MeCN as eluent afforded pure deprotected nucleoside **2** (480 mg, 1.26 mmol, 94 %) as a white solid.

Characterization: R*f* (CH_2Cl_2/MeOH, 95:5): 0.15; **^{1}H NMR** (500 MHz, DMSO-d_6) δ 11.67 (br, 1H), 8.18 (d, *J* = 2.1 Hz, 1H), 7.93 (dd, *J* = 9.0, 2.2 Hz, 1H), 7.89 (d, *J* = 8.9 Hz, 1H), 7.64 (d, *J* = 7.3 Hz, 2H), 7.39 (t, *J* = 7.7 Hz, 2H), 7.33 (d, *J* = 6.7 Hz, 1H), 7.30 – 7.27 (m, 2H), 6.69 (t, *J* = 7.8 Hz, 1H), 5.28 (d, *J* = 5.1 Hz, 1H), 5.00 (t, *J* = 5.2 Hz, 1H), 4.42 (dq, *J* = 8.6, 4.4 Hz, 1H), 3.74 – 3.63 (m, 3H), 2.65 (dt, *J* = 13.3, 8.2 Hz, 1H), 1.95 (ddd, *J* = 13.5, 7.4, 3.6 Hz, 1H). **^{13}C NMR** (101 MHz, acetone-d_6) δ 162.4, 151.0, 140.2, 138.1, 133.5, 132.9, 130.0, 129.6, 128.6, 127.5, 127.5, 126.3, 118.5, 118.1, 87.9, 85.3, 71.2, 62.3, 37.6. **HRMS** (ESI): *m/z* 379.13001 ($[M-H]^-$ $C_{21}H_{19}O_5N_2^-$ requires 379.12995).

1′-[5′-*O*-(4,4-dimethoxytrityl)-2′-deoxy-β-d-ribofuranoside]-6-styryl-quinazoline- 2,4-(3*H*)-dione (10)

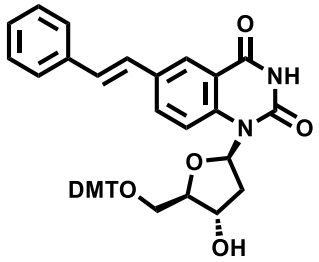

Procedure: Nucleoside **2** (548 mg, 1.44 mmol, 1.0 equiv.) was co-evaporated with pyridine (3 x 3.00 mL) and then suspended in pyridine (5.00 mL). To the stirring solution was added dropwise DMTCl (690 mg, 2.03 mmol, 1.4 equiv.) dissolved in 3.00 mL pyridine. A clear red reaction mixture was observed which was stirred at room temperature for 165 min. The reaction was then quenched with a sat. sol. $NaHCO_3$. The resulting mixture was extracted with CH_2Cl_2 and the combined organic layer was dried over $MgSO_4$, filtered, and co-evaporated *in vacuo* with pyridine. The crude product was purified by column chromatography on silica gel (CH_2Cl_2/MeOH/Et_3N, 99.5:0:0.5 → 89.5:10:0.5) to obtain nucleoside **10** (666 mg, 0.980 mmol, 68 %) as a white foam.

Characterization: R*f* (CH_2Cl_2/MeOH, 94:6): 0.25; **^{1}H NMR** (400 MHz, $CDCl_3$) δ 8.18 (s, 1H), 8.06 (d, *J* = 8.9 Hz, 1H), 7.46 (ddt, *J* = 7.5, 5.9, 3.0 Hz, 4H), 7.39 – 7.21 (m, 10H), 6.95 – 6.78 (m, 8H), 5.53 (d, *J* = 5.1 Hz, 1H), 4.89 – 4.92 (m, 1H), 4.05 (s, 1H), 3.73 (s, 6H), 2.96 – 2.89 (m, 2H), 2.27 – 2.22 (m, 1H). **^{13}C NMR** (126 MHz, $CDCl_3$) δ 162.7, 158.6, 150.9, 144.5, 138.6, 136.9, 135.8, 135.6, 132.6, 132.1, 130.4, 130.3, 129.2, 128.7, 128.6, 127.9, 127.8, 127.0, 126.5, 126.4, 126.1, 118.0, 117.2, 113.2, 113.1, 86.5, 85.2, 83.9, 70.2, 62.3, 55.1, 37.1. **HRMS** (ESI): *m/z* 705.25641 ($[M+Na]^+$ $C_{42}H_{38}O_7N_2Na^+$ requires 705.25712).

1′-[3′-*O*-[2-cyanoethoxy-(*N*,*N*-diisopropylamino)-phosphino]-(5′-*O*-(4,4-dimethoxytrityl)-2′-deoxy-β-d-ribofuranoside]-6-styryl-quinazoline- 2,4-(3*H*)-dione (3)

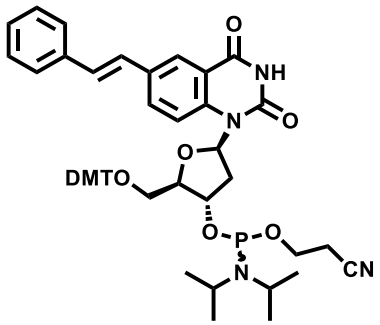

Procedure: To a stirred solution of nucleoside **10** (474 mg, 0.694 mmol, 1.0 equiv.) in CH_2Cl_2 (10.0 mL) at 0 ^{o}C, was added freshly distilled diisopropylethylamine (DIPEA, 607 µL, 3.49 mmol, 5.0 equiv.) and the reaction was stirred 10 min at 0 ^{o}C under an atmosphere of Ar. To this solution was added 2-cyanoethyl *N*,*N*-diisopropylchlorophosphoramidite (607 µL, 2.72 mmol, 4.0 equiv) and the reaction was stirred at 22 ^{o}C for 150 min while it was monitored by TLC every 30 min. The reaction mixture was then loaded directly to a silica gel column, without any quenching or workup steps. The residue was purified by flash column chromatography (elution time of 10 min) on silica gel (hexane/EtOAc/Et_3N, 60:40:0.5 → 40:60:0.5) to obtain nucleoside **3** (552 mg, 0.625 mmol, 90 %, diastereomeric mixture) as a white foam. It is worth noting that chromatography solvents were distillated prior to use.

Characterization: R*f* (hexane/EtOAc, 4:6): 0.45 and 0.55; **^{1}H NMR** (400 MHz, $CDCl_3$) δ 8.20 (s, 2H), 8.09 (d, *J* = 2.7 Hz, 1H), 8.07 (d, *J* = 2.8 Hz, 1H), 7.49 – 7.44 (m, 8H), 7.40 – 7.28 (m, 20H), 6.93 – 6.80 (m, 16H), 5.07 – 4.96 (m, 2H), 4.22 – 4.09 (m, 8H), 3.77 – 3.76 (m, 12H), 2.93 (dd, *J* = 13.8, 8.9 Hz, 2H), 2.76 (td, *J* = 6.2, 2.0 Hz, 4H), 2.60 (t, *J* = 6.3 Hz, 2H), 2.38 (t, *J* = 6.5 Hz, 2H), 1.29 – 1.26 (m, 24H), 1.02 (d, *J* = 6.7 Hz, 6H). **^{31}P NMR** (162 MHz, $CDCl_3$) δ 150.4, 149.9. **HRMS** (ESI): *m*/*z* 905.36436 ($[M+Na]^+$ $C_{51}H_{55}O_8N_4NaP^+$ requires 905.36497).

2.9.4 NMR spectra

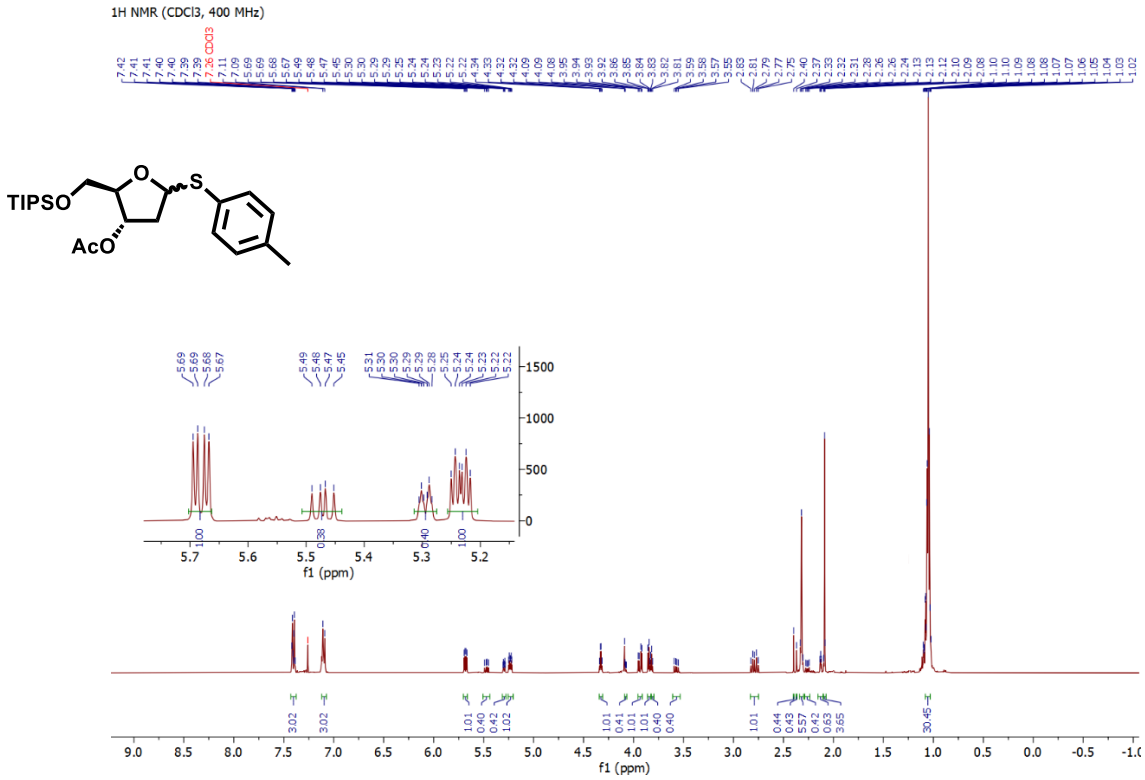

^{1}H NMR spectrum of **5**.

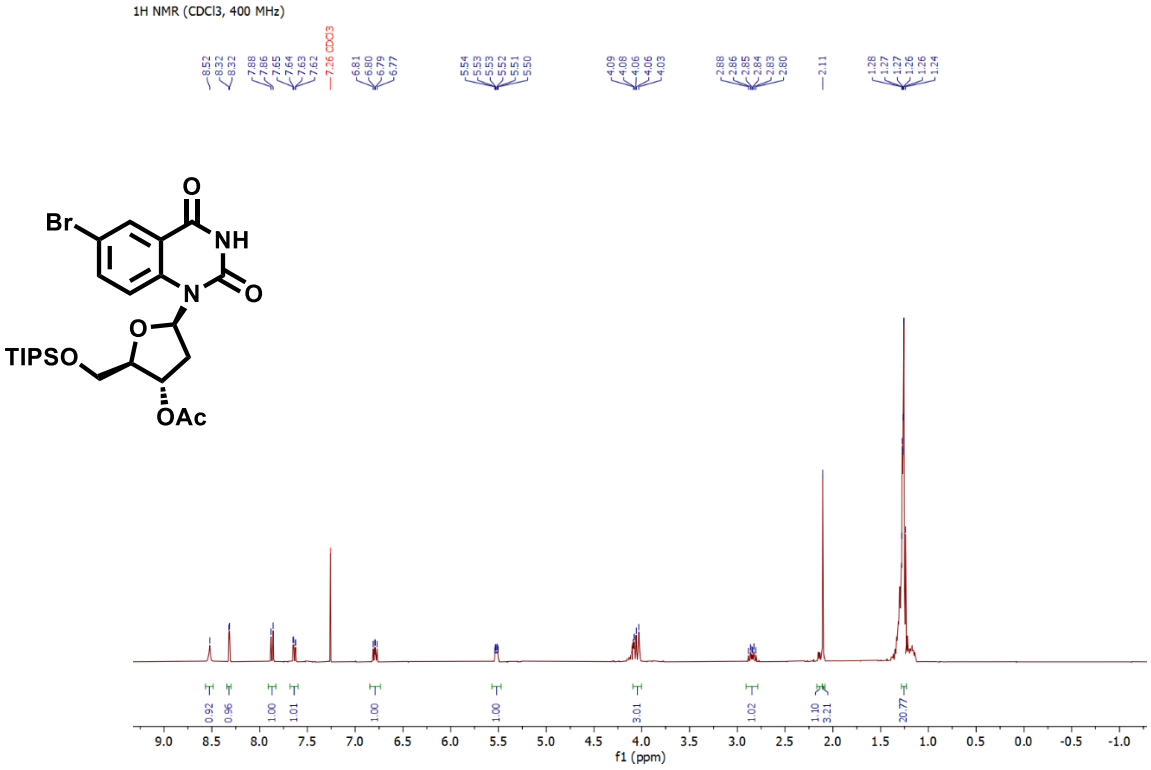

^{1}H NMR spectrum of **6β**.

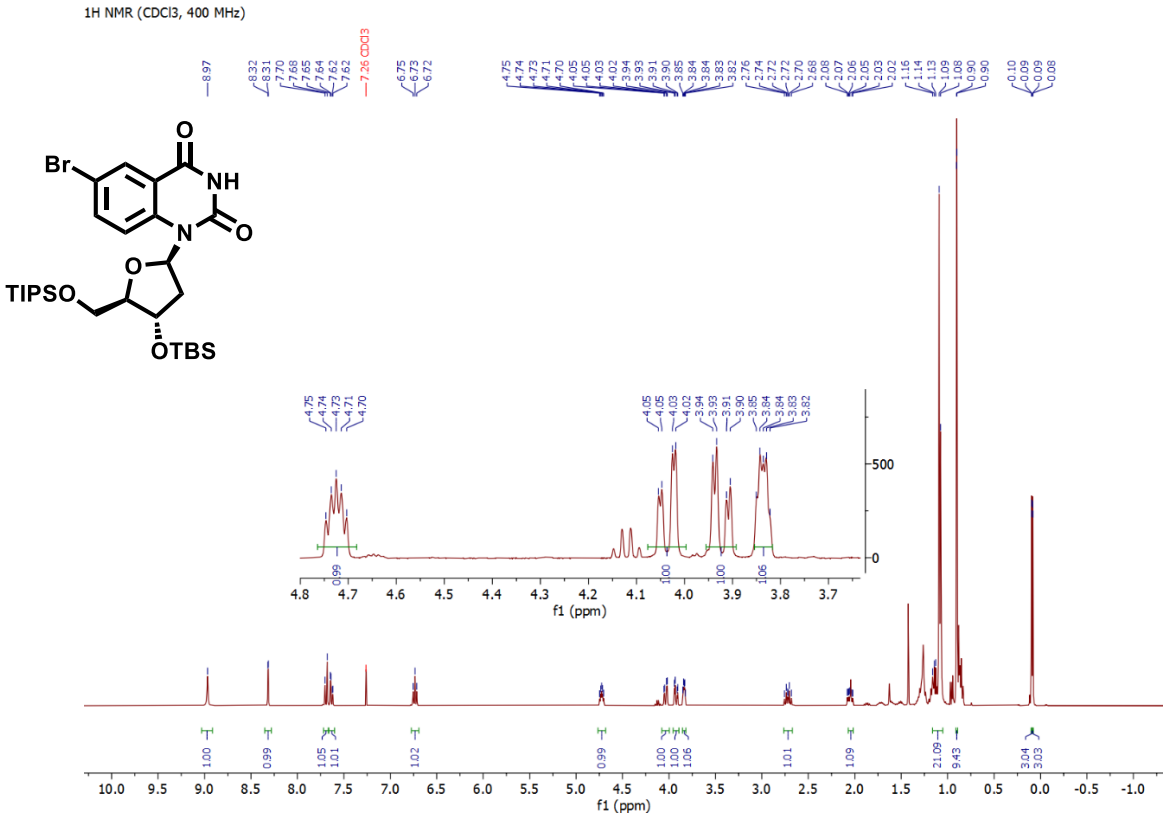

^{1}H NMR spectrum of **7**.

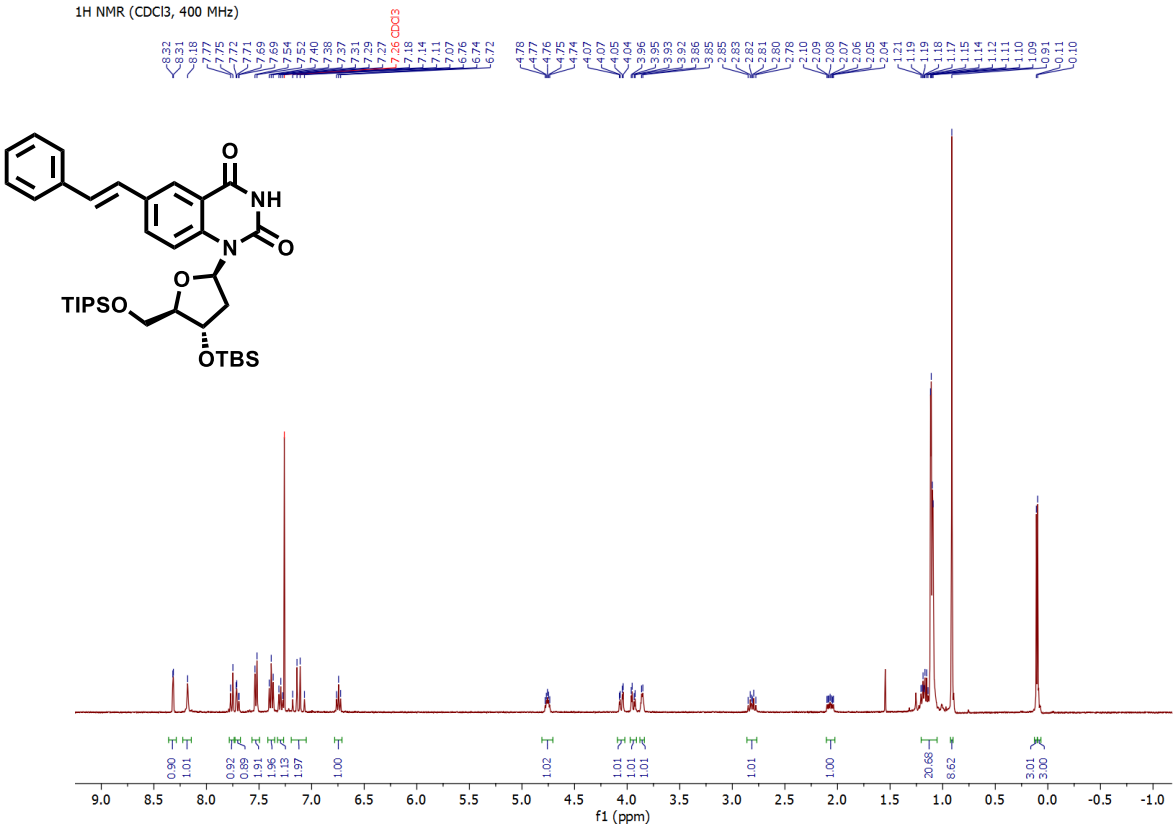

^{1}H NMR spectrum of **8a**.

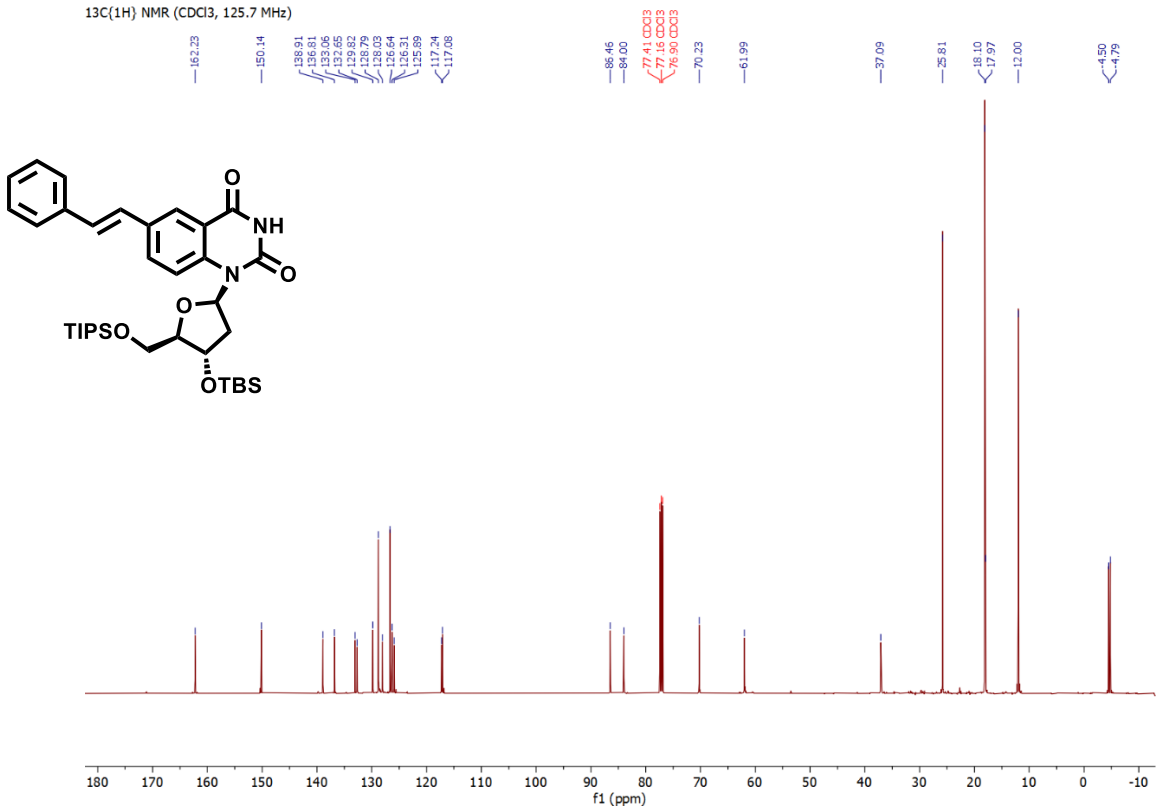

^{13}C NMR spectrum of **8a**.

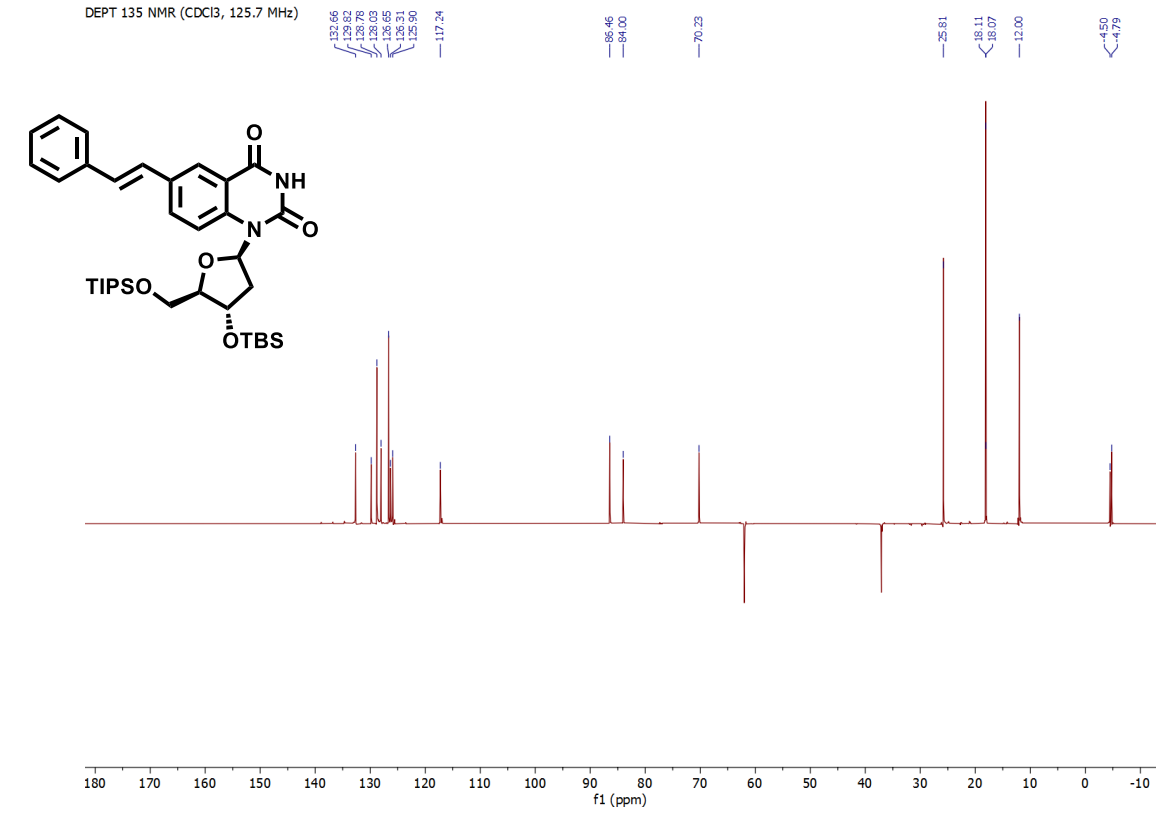

DEPT 135 spectrum of **8a**.

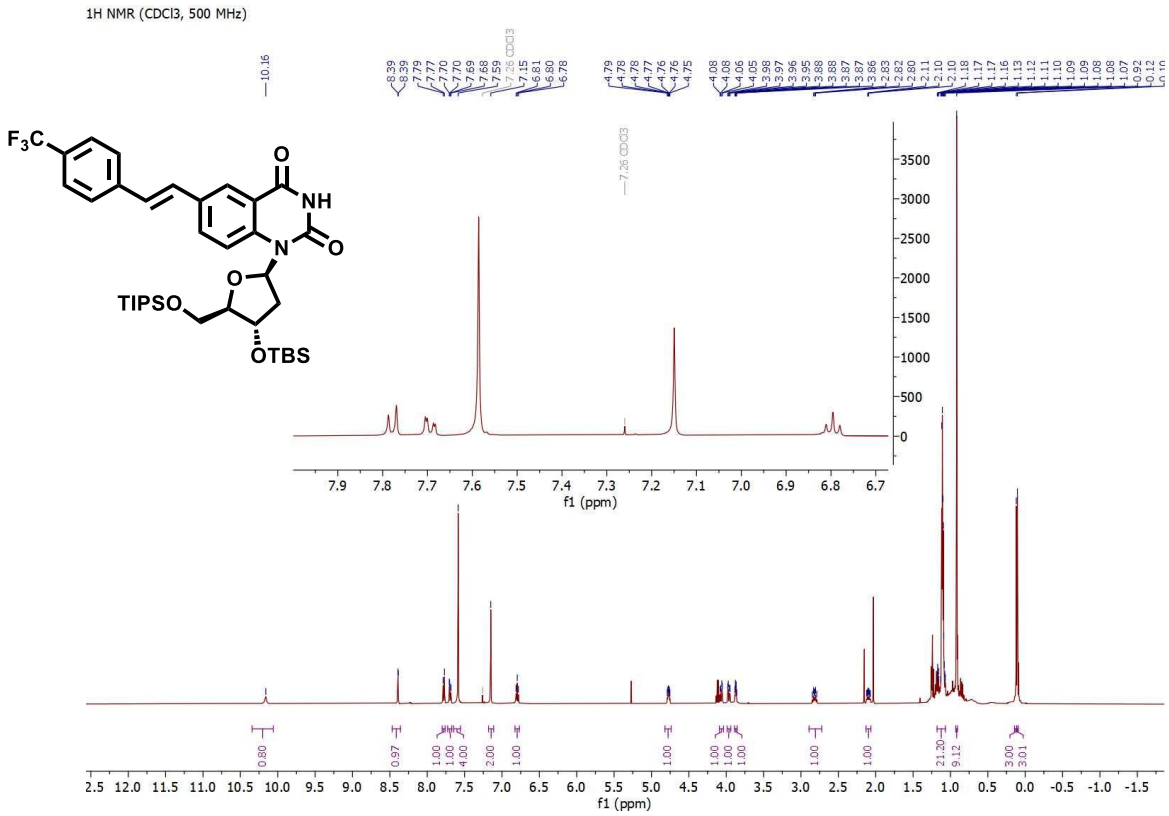

^{1}H NMR spectrum of **8b**.

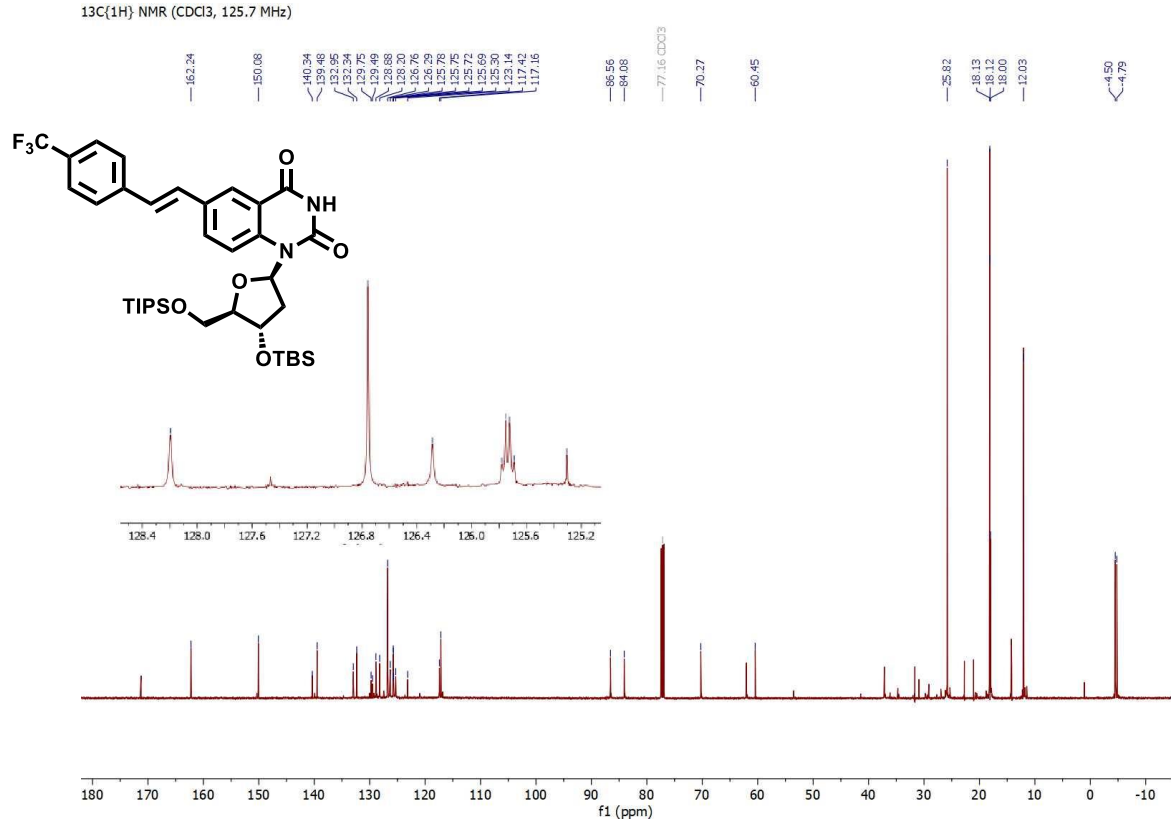

^{13}C NMR spectrum of **8b**.

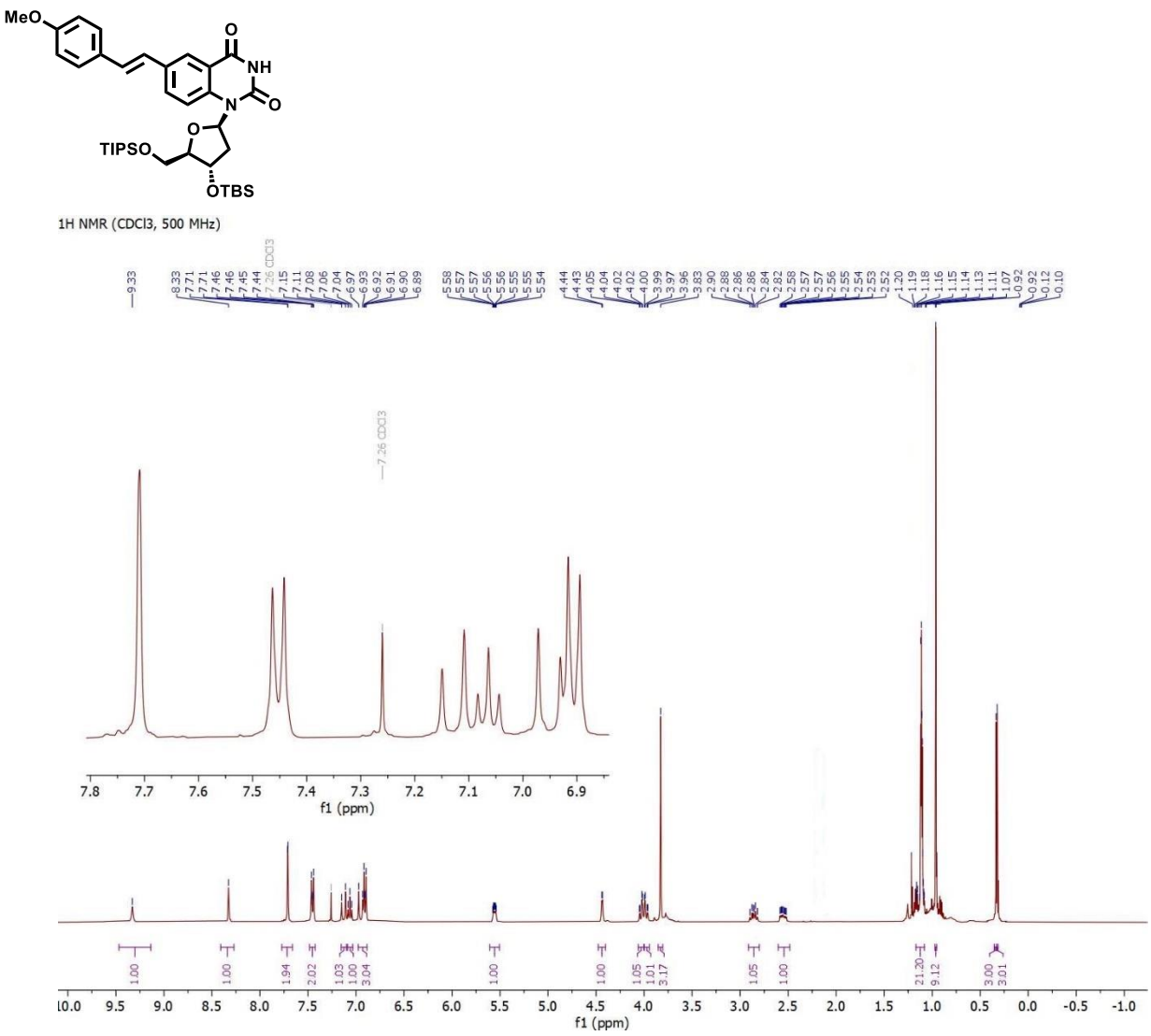

^{1}H NMR spectrum of **8c**.

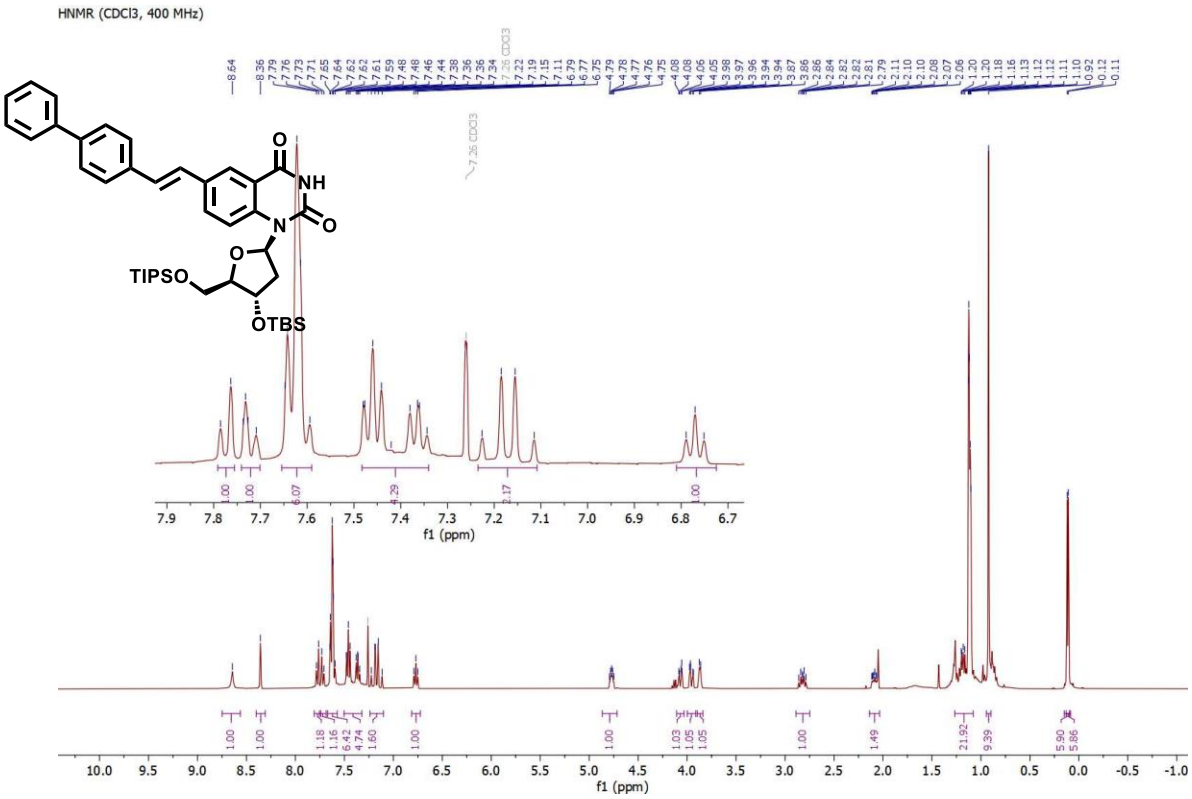

^{1}H NMR spectrum of **8d**.

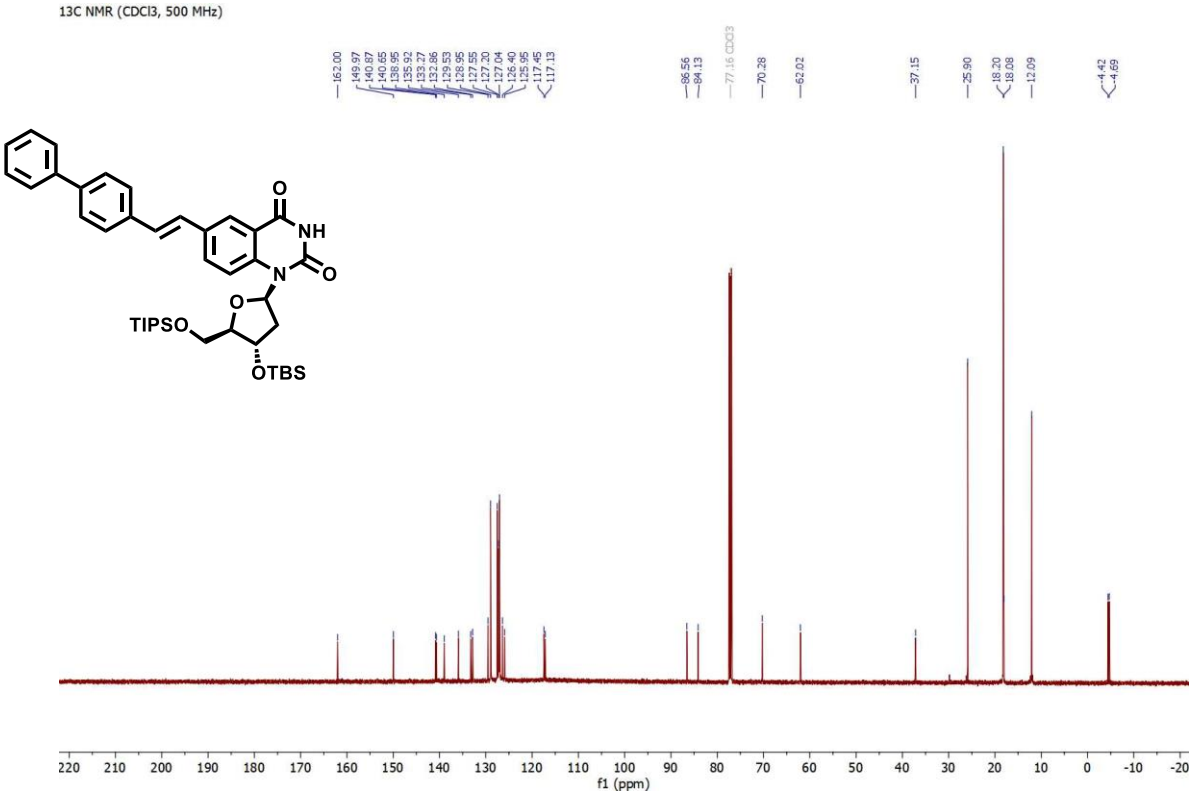

^{13}C NMR spectrum of **8d**.

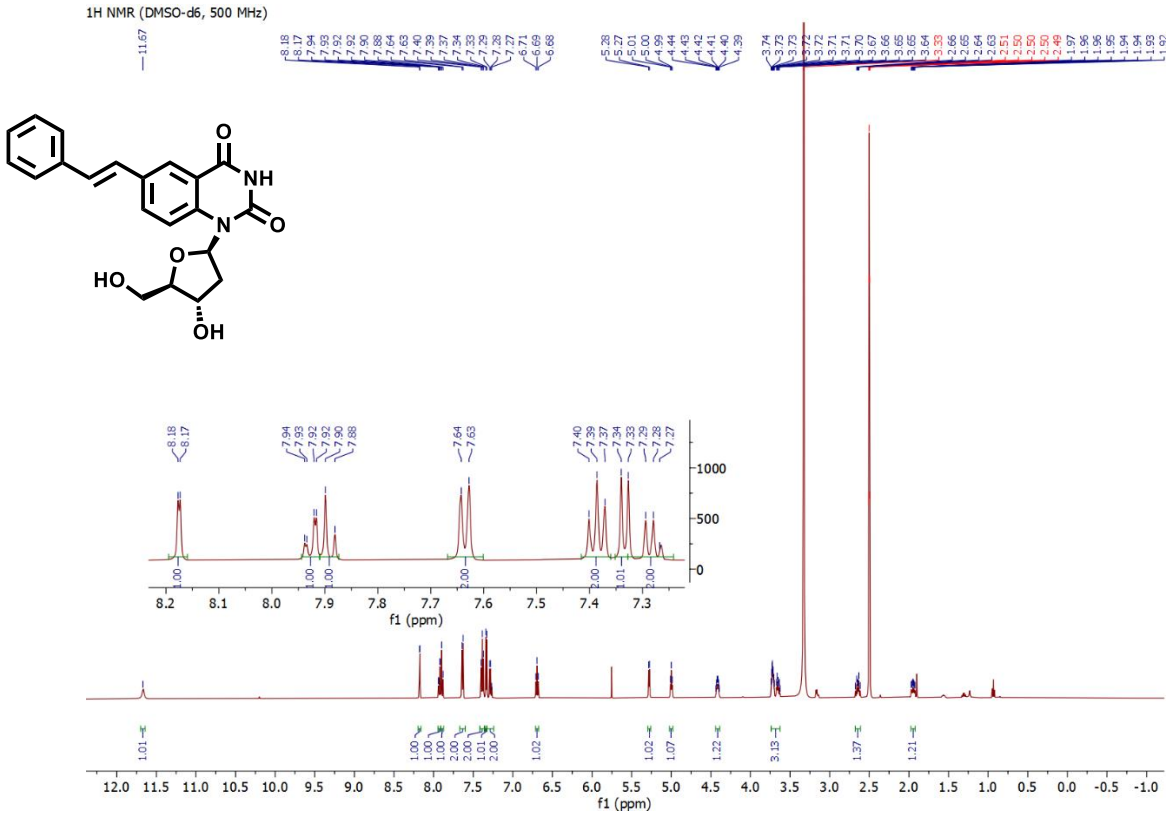

^{1}H NMR spectrum of **9**.

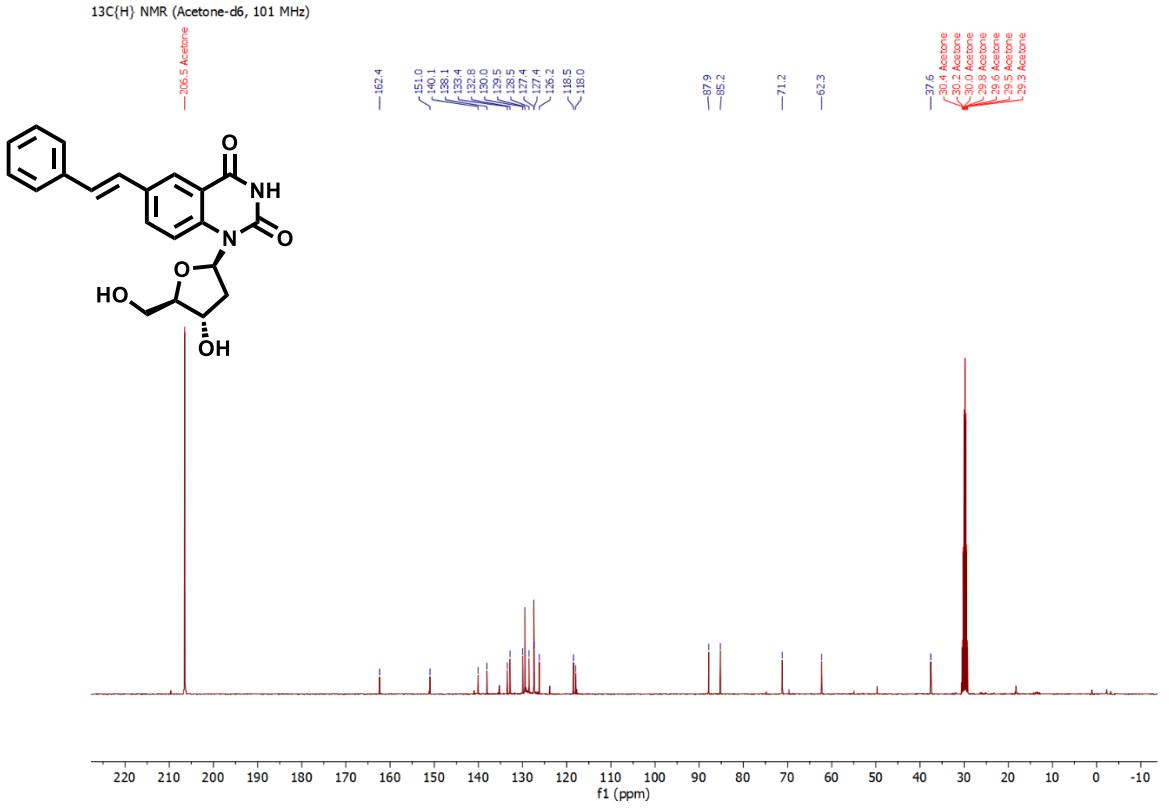

^{13}C NMR spectrum of **9**.

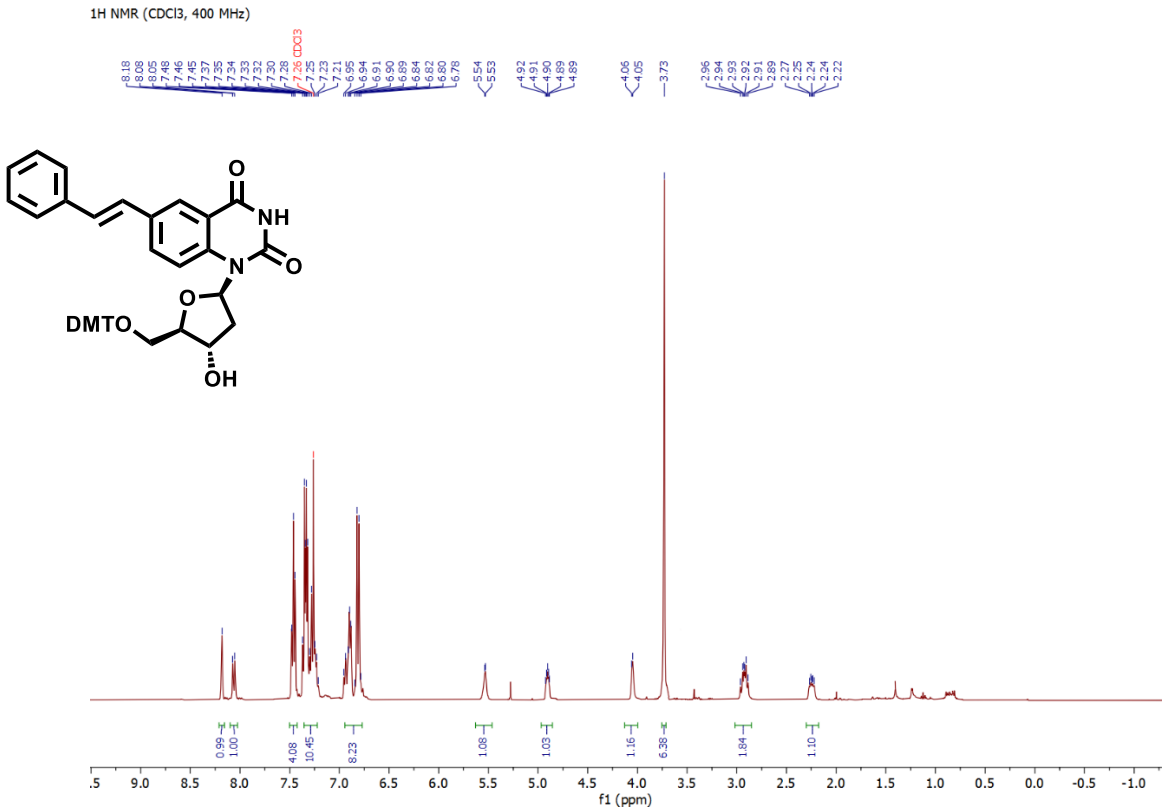

^{1}H NMR spectrum of **10**.

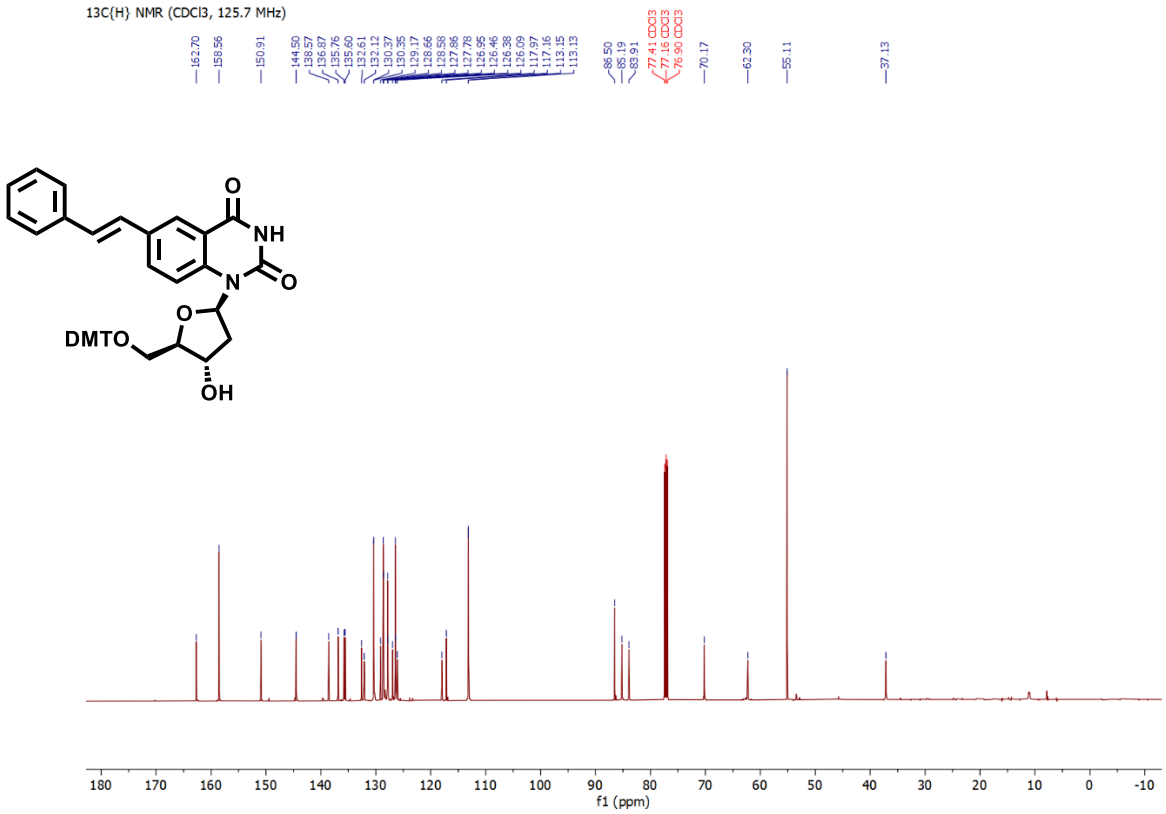

^{13}C NMR spectrum of **10**.

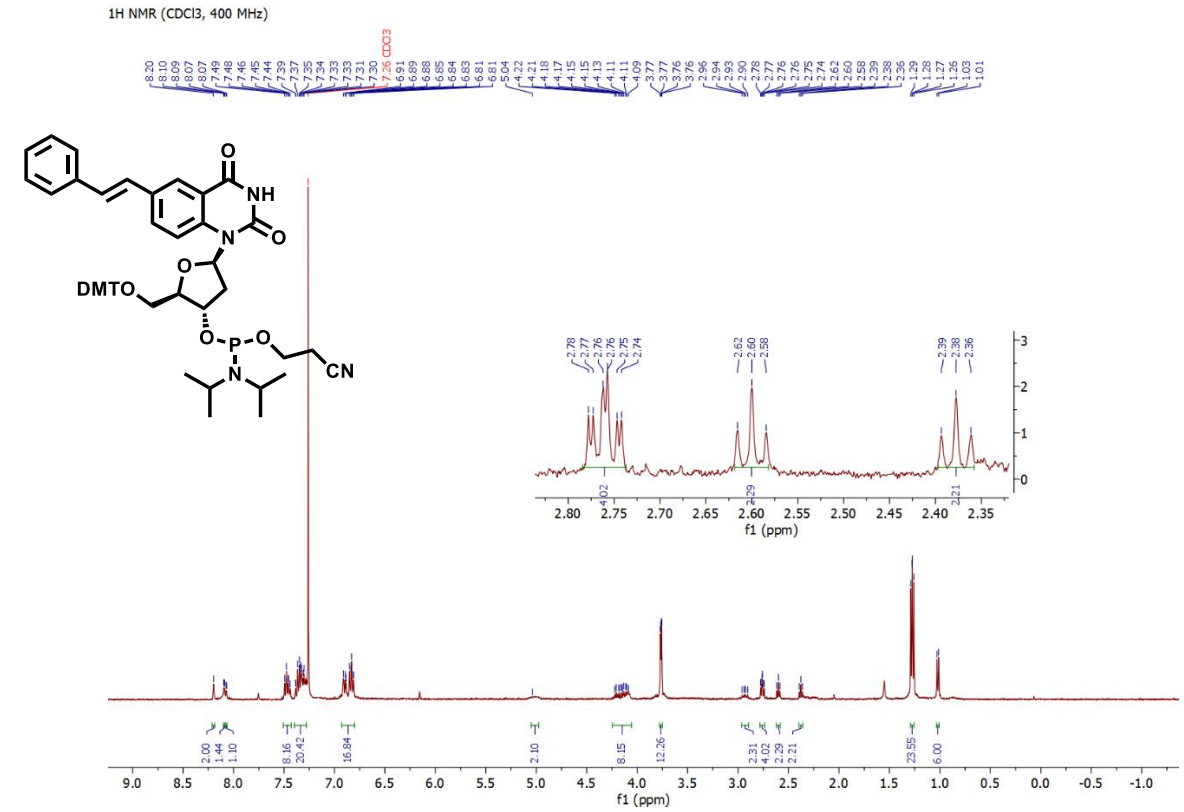

^{1}H NMR spectrum of **11**.

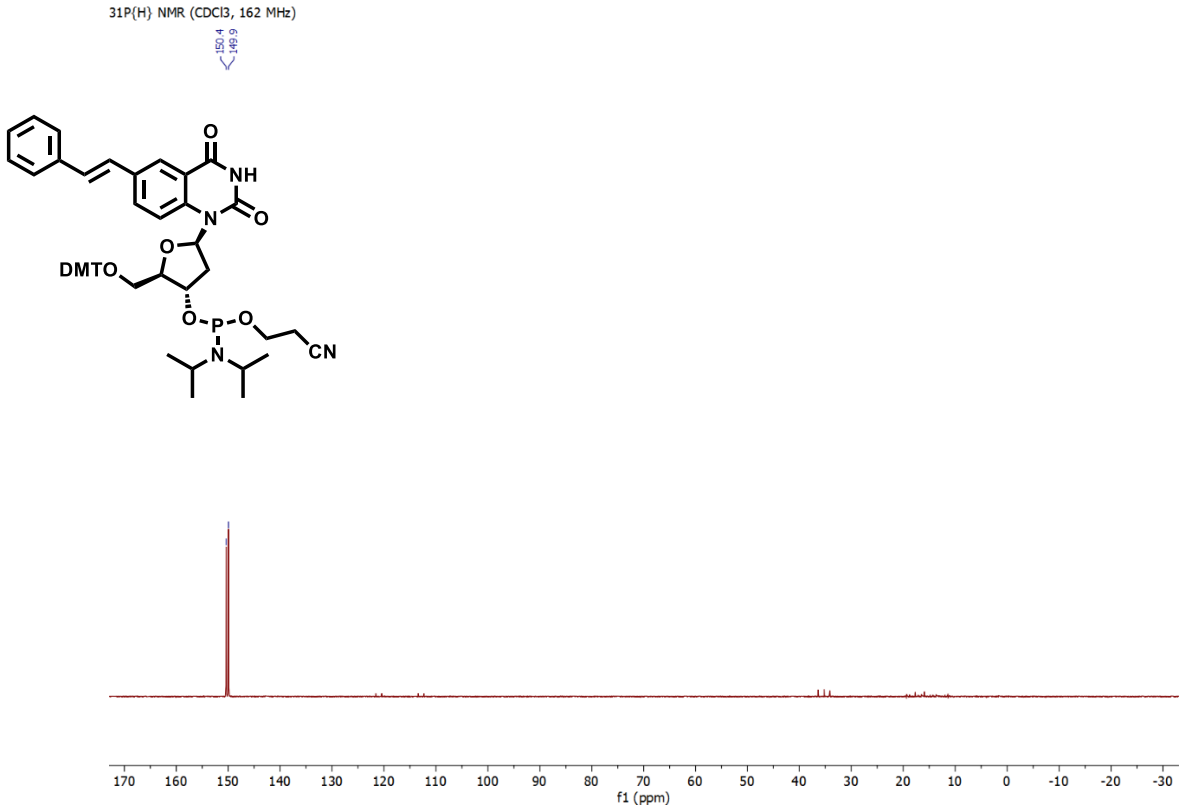

^{31}P NMR spectrum of **11**

2.10 References

[1] Harcourt, E. M.; Kietrys, A. M.; Kool, E. T., Chemical and structural effects of base modifications in messenger RNA. *Nature* **2017,** *541* (7637), 339-346.

[2] Pan, T., Modifications and functional genomics of human transfer RNA. *Cell Res.* **2018,** *28* (4), 395-404.

[3] Adams, D.; Gonzalez-Duarte, A.; O'Riordan, W. D.; Yang, C. C.; Ueda, M.; Kristen, A. V.; Tournev, I.; Schmidt, H. H.; Coelho, T.; Berk, J. L.; Lin, K. P.; Vita, G.; Attarian, S.; Planté-Bordeneuve, V.; Mezei, M. M.; Campistol, J. M.; Buades, J.; Brannagan, T. H., 3rd; Kim, B. J.; Oh, J.; Parman, Y.; Sekijima, Y.; Hawkins, P. N.; Solomon, S. D.; Polydefkis, M.; Dyck, P. J.; Gandhi, P. J.; Goyal, S.; Chen, J.; Strahs, A. L.; Nochur, S. V.; Sweetser, M. T.; Garg, P. P.; Vaishnaw, A. K.; Gollob, J. A.; Suhr, O. B., Patisiran, an RNAi therapeutic, for hereditary transthyretin amyloidosis. *N. Engl. J. Med.* **2018,** *379* (1), 11-21.

[4] Bennett, C. F.; Baker, B. F.; Pham, N.; Swayze, E.; Geary, R. S., Pharmacology of antisense drugs. *Annu. Rev. Pharmacol. Toxicol.* **2017,** *57* (1), 81-105.

[5] McKenzie, L. K.; El-Khoury, R.; Thorpe, J. D.; Damha, M. J.; Hollenstein, M., Recent progress in non-native nucleic acid modifications. *Chem. Soc. Rev.* **2021,** *50* (8), 5126-5164.

[6] Herdewijn, P., Nucleic acids with a six-membered 'carbohydrate' mimic in the backbone. *Chem. Biodivers.* **2010,** *7* (1), 1-59.

[7] Habibian, M.; Martínez-Montero, S.; Portella, G.; Chua, Z.; Bohle, D. S.; Orozco, M.; Damha, M. J., Seven-membered ring nucleoside analogues: Stereoselective synthesis and studies on their conformational properties. *Org. Lett.* **2015,** *17* (21), 5416-5419.

[8] Augustyns, K.; Vandendriessche, F.; Van Aerschot, A.; Busson, R.; Urbanke, C.; Herdewijn, P., Incorporation of hexose nucleoside analogues into oligonucleotides: synthesis, base-pairing properties and enzymatic stability. *Nucleic Acids Res.* **1992,** *20* (18), 4711-4716.

[9] Sabatino, D.; Damha, M. J., Oxepane nucleic acids: Synthesis, characterization, and properties of oligonucleotides bearing a seven-membered carbohydrate ring. *J. Am. Chem. Soc.* **2007,** *129* (26), 8259-8270.

[10] Madsen, C. S.; Witzke, S.; Kumar, P.; Negi, K.; Sharma, P. K.; Petersen, M.; Nielsen, P., Additional base-pair formation in DNA duplexes by a double-headed nucleotide. *Chem. Eur. J.* **2012,** *18* (24), 7434-7442.

[11] Hornum, M.; Stendevad, J.; Sharma, P. K.; Kumar, P.; Nielsen, R. B.; Petersen, M.; Nielsen, P., Base-pairing properties of double-headed nucleotides. *Chem. Eur. J.* **2019,** *25* (30), 7387-7395.

[12] Peng, C. G.; Damha, M. J., Polymerase-directed synthesis of 2'-deoxy-2'-fluoro-β-d-arabinonucleic acids. *J. Am. Chem. Soc.* **2007,** *129* (17), 5310-5311.

[13] Veedu, R. N.; Vester, B.; Wengel, J., Enzymatic incorporation of LNA nucleotides into DNA strands. *Chembiochem* **2007,** *8* (5), 490-492.

[14] Zhang, L.; Peritz, A.; Meggers, E., A simple glycol nucleic acid. *J. Am. Chem. Soc.* **2005,** *127* (12), 4174-4175.

[15] Kashida, H.; Murayama, K.; Toda, T.; Asanuma, H., Control of the chirality and helicity of oligomers of serinol nucleic acid (SNA) by sequence design. *Angew. Chem. Int. Ed.* **2011,** *50* (6), 1285-1288.

[16] Shelbourne, M.; Brown, T.; El-Sagheer, A. H.; Brown, T., Fast and efficient DNA crosslinking and multiple orthogonal labelling by copper-free click chemistry. *Chemical Communications* **2012,** *48* (91), 11184-11186.

[17] Conlon, P. F.; Eguaogie, O.; Wilson, J. J.; Sweet, J. S. T.; Steinhoegl, J.; Englert, K.; Hancox, O. G. A.; Law, C. J.; Allman, S. A.; Tucker, J. H. R.; Hall, J. P.; Vyle, J. S., Solid-phase synthesis and structural characterisation of phosphoroselenolate-modified DNA: a backbone analogue which does not impose conformational bias and facilitates SAD X-ray crystallography. *Chem. Sci.* **2019,** *10* (47), 10948-10957.

[18] Sergueev, D. S.; Shaw, B. R., H-phosphonate approach for solid-phase synthesis of oligodeoxyribonucleoside boranophosphates and their characterization. *J. Am. Chem. Soc.* **1998,** *120* (37), 9417-9427.

[19] Skakuj, K.; Bujold, K. E.; Mirkin, C. A., Mercury-free automated synthesis of guanidinium backbone oligonucleotides. *J. Am. Chem. Soc.* **2019,** *141* (51), 20171-20176.

[20] Rausch, C.; Zhang, P.; Casas-Delucchi, C. S.; Daiß, J. L.; Engel, C.; Coster, G.; Hastert, F. D.; Weber, P.; Cardoso, M C., Cytosine base modifications regulate DNA duplex stability and metabolism. *Nucleic Acids Res.* **2021,** *49* (22), 12870-12894.

[21] Tsvetkov, V. B.; Zatsepin, T. S.; Belyaev, E. S.; Kostyukevich, Y. I.; Shpakovski, G. V.; Podgorsky, V. V.; Pozmogova, G. E.; Varizhuk, A. M.; Aralov, A. V., i-Clamp phenoxazine for the fine tuning of DNA i-motif stability. *Nucleic Acids Res.* **2018,** *46* (6), 2751-2764.

[22] Le, B. T.; Hornum, M.; Sharma, P. K.; Nielsen, P.; Veedu, R. N., Nucleobase-modified antisense oligonucleotides containing 5-(phenyltriazol)-2'-deoxyuridine nucleotides induce exon-skipping in vitro. *RSC Advances* **2017,** *7* (86), 54542-54545.

[23] Vummidi, B. R.; Alzeer, J.; Luedtke, N. W., Fluorescent probes for G-quadruplex structures. *Chembiochem* **2013,** *14* (5), 540-558.

[24] Kodr, D.; Yenice, C. P.; Simonova, A.; Saftić, D. P.; Pohl, R.; Sýkorová, V.; Ortiz, M.; Havran, L.; Fojta, M.; Lesnikowski, Z. J.; O'Sullivan, C. K.; Hocek, M., Carborane- or metallacarborane-linked nucleotides for redox labeling. Orthogonal multipotential coding of all four DNA bases for electrochemical analysis and sequencing. *J. Am. Chem. Soc.* **2021,** *143* (18), 7124-7134.

[25] Vaníková, Z.; Janoušková, M.; Kambová, M.; Krásný, L.; Hocek, M., Switching transcription with bacterial RNA polymerase through photocaging, photorelease and phosphorylation reactions in the major groove of DNA. *Chem. Sci.* **2019,** *10* (14), 3937-3942.

[26] Chan, K. M.; Xu, W.; Kwon, H.; Kietrys, A. M.; Kool, E. T., Luminescent carbon dot mimics assembled on DNA. *J. Am. Chem. Soc.* **2017,** *139* (37), 13147-13155.

[27] Malyshev, D. A.; Romesberg, F. E., The expanded genetic alphabet. *Angew. Chem. Int. Ed.* **2015,** *54* (41), 11930-11944.

[28] Tor, Y.; Valle, S. D.; Jaramillo, D.; Srivatsan, S. G.; Rios, A. C.; Weizman, H., Designing new isomorphic fluorescent nucleobase analogues: the thieno[3,2-d]pyrimidine core. *Tetrahedron* **2007,** *63*, 3608-3614.

[29] Wierzchowski, J.; Wielgus-Kutrowska, B.; Shugar, D., Fluorescence emission properties of 8-azapurines and their nucleosides, and application to the kinetics of the reverse synthetic reaction of purine nucleoside phosphorylase. *Biochim. Biophys. Acta* **1996,** *1290* (1), 9-17.

[30] Obeid, S.; Baccaro, A.; Welte, W.; Diederichs, K.; Marx, A., Structural basis for the synthesis of nucleobase modified DNA by Thermus aquaticus DNA polymerase. *Proc. Natl. Acad. Sci. U.S.A.* **2010,** *107* (50), 21327.

[31] Cahová, H.; Panattoni, A.; Kielkowski, P.; Fanfrlík, J.; Hocek, M., 5-substituted pyrimidine and 7-substituted 7-deazapurine dntps as substrates for DNA polymerases in competitive primer extension in the presence of natural dNTPs. *ACS Chem. Biol.* **2016,** *11* (11), 3165-3171.

[32] Ehrenschwender, T.; Wanninger-Weiß, C.; Wagenknecht, H.-A., BODIPY-modified uridines as potential fluorescent probes for nucleic acids that are recognized by DNA-polymerases. *Nucleic Acids Symp. Ser.* **2008,** *52* (1), 349-350.

[33] Carell, T.; Brandmayr, C.; Hienzsch, A.; Müller, M.; Pearson, D.; Reiter, V.; Thoma, I.; Thumbs, P.; Wagner, M., Structure and function of noncanonical nucleobases. *Angew. Chem. Int. Ed.* **2012,** *51* (29), 7110-7131.

[34] Xu, W.; Chan, K. M.; Kool, E. T., Fluorescent nucleobases as tools for studying DNA and RNA. *Nat. Chem.* **2017,** *9* (11), 1043-1055.

[35] Tanpure, A. A.; Srivatsan, S. G., A microenvironment-sensitive fluorescent pyrimidine ribonucleoside analogue: synthesis, enzymatic incorporation, and fluorescence detection of a DNA abasic site. *Chem. Eur. J.* **2011,** *17* (45), 12820-12827.

[36] Mariam, J.; Krishnamoorthy, G.; Anand, R., Use of 6-methylisoxanthopterin, a fluorescent guanine analog, to probe Fob1-mediated dynamics at the stalling fork barrier DNA sequences. *Chem. Asian J.* **2019,** *14* (24), 4760-4766.

[37] Zhu, R.-Y.; Majumdar, C.; Khuu, C.; De Rosa, M.; Opresko, P. L.; David, S. S.; Kool, E. T., Designer fluorescent adenines enable real-time monitoring of MUTYH activity. *ACS Cent. Sci.* **2020,** *6* (10), 1735-1742.

[38] Schreier, V. N.; Loehr, M. O.; Deng, T.; Lattmann, E.; Hajnal, A.; Neuhauss, S. C. F.; Luedtke, N. W., Fluorescent dATP for DNA synthesis in vivo. *ACS Chem. Biol.* **2020,** *15* (11), 2996-3003.

[39] Roy, B.; Depaix, A.; Périgaud, C.; Peyrottes, S., Recent trends in nucleotide synthesis. *Chem. Rev.* **2016,** *116* (14), 7854-7897.

[40] Hoffer, M.; Duschinsky, R.; Fox, J. J.; Yung, N., Simple syntheses of pyrimidine-2'-deoxy-ribonucleosides. *J. Am. Chem. Soc.* **1959,** *81* (15), 4112-4113.

[41] Chien, T.-C.; Chen, C.-S.; Chern, J.-W., Nucleosides XIII. Facile synthesis of 4-amino-1-(2-deoxy-β-d-ribofuranosyl)quinazolin-2-one as a 2'-deoxycytidine analog for oligonucleotide synthesis. *J. Chin. Chem. Soc.* **2005,** *52* (6), 1237-1244.

[42] Fossey, C.; Landelle, H.; Laduree, D.; Robba, M., Synthesis of N-1β-D-arabinofuranosyl and N-1-2'-deoxy-β-D-erythro-pentofuranosyl thieno [3,2-d] pyrimidine nucleosides. *Nucleosides Nucleotides* **1994,** *13* (4), 925-937.

[43] Liu, H.; Gao, J.; Kool, E. T., Size-expanded analogues of dG and dC: Synthesis and pairing properties in DNA. *J. Org. Chem.* **2005,** *70* (2), 639-647.

[44] Lietard, J.; Leumann, C. J., Synthesis, pairing, and cellular uptake properties of C(6')-functionalized tricyclo-DNA. *J. Org. Chem.* **2012,** *77* (10), 4566-4577.

[45] Sniady, A.; Bedore, M. W.; Jamison, T. F., One-flow, multistep synthesis of nucleosides by brønsted acid-catalyzed glycosylation. *Angew. Chem. Int. Ed.* **2011,** *50* (9), 2155-2158.

[46] Daves, G. D., C-glycoside synthesis by palladium-mediated glycal-aglycon coupling reactions. *Acc. Chem. Res.* **1990,** *23* (6), 201-206.

[47] Wellington, K. W.; Benner, S. A., A review: Synthesis of aryl C-glycosides via the heck coupling reaction. *Nucleosides Nucleotides Nucleic Acids* **2006,** *25* (12), 1309-1333.

[48] Agrofoglio, L. A.; Gillaizeau, I.; Saito, Y., Palladium-assisted routes to nucleosides. *Chem. Rev.* **2003,** *103* (5), 1875-1916.

[49] Mata, G.; Luedtke, N. W., Stereoselective N-glycosylation of 2-deoxythioribosides for fluorescent nucleoside synthesis. *J. Org. Chem.* **2012,** *77* (20), 9006-9017.

[50] Borsenberger, V.; Kukwikila, M.; Howorka, S., Synthesis and enzymatic incorporation of modified deoxyuridine triphosphates. *Org. Biomol. Chem.* **2009,** *7* (18), 3826-3835.

[51] Coulther, T. A.; Stern, H. R.; Beuning, P. J., Engineering polymerases for new functions. *Trends Biotechnol.* **2019,** *37* (10), 1091-1103.

[52] Roy, S.; Caruthers, M., Synthesis of DNA/RNA and their analogs via phosphoramidite and H-phosphonate chemistries. *Molecules* **2013,** *18* (11).

[53] Letsinger, R. L.; Lunsford, W. B., Synthesis of thymidine oligonucleotides by phosphite triester intermediates. *J. Am. Chem. Soc.* **1976,** *98* (12), 3655-3661.

[54] Beaucage, S. L.; Caruthers, M. H., Deoxynucleoside phosphoramidites—A new class of key intermediates for deoxypolynucleotide synthesis. *Tetrahedron Lett.* **1981,** *22* (20), 1859-1862.

[55] Vlaho, D.; Damha, M. J., Synthesis of chimeric oligonucleotides having modified internucleotide linkages via an automated H-phosphonate/phosphoramidite approach. *Curr. Protoc. Nucleic Acid Chem.* **2018,** *73* (1), e53.

[56] Thorpe, J. D.; O'Reilly, D.; Friščić, T.; Damha, M. J., Mechanochemical synthesis of short DNA fragments. *Chem. Eur. J.* **2020,** *26* (41), 8857-8861.

[57] Tera, M.; Luedtke, N. W., Chapter Nineteen - Cross-linking cellular nucleic acids via a target-directing double click reagent. In *Methods Enzymol.*, Chenoweth, D. M., Ed. Academic Press: 2020; Vol. 641, pp 433-457.

[58] Nikić, I.; Estrada Girona, G.; Kang, J. H.; Paci, G.; Mikhaleva, S.; Koehler, C.; Shymanska, N. V.; Ventura Santos, C.; Spitz, D.; Lemke, E. A., Debugging eukaryotic genetic code expansion for site-specific click-PAINT super-resolution microscopy. *Angew. Chem. Int. Ed.* **2016,** *55* (52), 16172-16176.

[59] Naik, A.; Alzeer, J.; Triemer, T.; Bujalska, A.; Luedtke, N. W., Chemoselective modification of vinyl DNA by triazolinediones. *Angew. Chem. Int. Ed.* **2017,** *56* (36), 10850-10853.

[60] Clavé, G.; Dursun, E.; Vasseur, J.-J.; Smietana, M., An entry of the chemoselective sulfo-click reaction into the sphere of nucleic acids. *Org. Lett.* **2020,** *22* (5), 1914-1918.

[61] Johnson, A.; Karimi, A.; Luedtke, N. W., Enzymatic incorporation of a coumarin–guanine base pair. *Angew. Chem. Int. Ed.* **2019,** *58* (47), 16839-16843.

[62] Hawkins, M. E.; Balis, F. M., Use of pteridine nucleoside analogs as hybridization probes. *Nucleic Acids Res.* **2004,** *32* (7), e62.

[63] Wojciechowski, F.; Hudson, R. H. E., Fluorescence and hybridization properties of peptide nucleic acid containing a substituted phenylpyrrolocytosine designed to engage guanine with an additional H-bond. *J. Am. Chem. Soc.* **2008,** *130* (38), 12574-12575.

[64] Hudson, R. H. E.; Ghorbani-Choghamarani, A., Selective fluorometric detection of guanosine-containing sequences by 6-phenylpyrrolocytidine in DNA. *Synlett* **2007,** *2007* (06), 870-873.

[65] Sandin, P.; Börjesson, K.; Li, H.; Mårtensson, J.; Brown, T.; Wilhelmsson, L. M.; Albinsson, B., Characterization and use of an unprecedentedly bright and structurally non-perturbing fluorescent DNA base analogue. *Nucleic Acids Res.* **2008,** *36* (1), 157-167.

[66] Teppang, K. L.; Lee, R. W.; Burns, D. D.; Turner, M. B.; Lokensgard, M. E.; Cooksy, A. L.; Purse, B. W., Electronic modifications of fluorescent cytidine analogues control photophysics and fluorescent responses to base stacking and pairing. *Chem. Eur. J.* **2019,** *25* (5), 1249-1259.

[67] Turner, M. B.; Anderson, B. A.; Samaan, G. N.; Coste, M.; Burns, D. D.; Purse, B. W., Synthesis of fluorescence turn-on DNA hybridization probe using the (DEA) tC 2'-deoxycytidine analog. *Curr. Protoc. Nucleic Acid Chem.* **2018,** *75* (1), e59-e59.

[68] Sandin, P.; Wilhelmsson, L. M.; Lincoln, P.; Powers, V. E. C.; Brown, T.; Albinsson, B., Fluorescent properties of DNA base analogue tC upon incorporation into DNA — negligible influence of neighbouring bases on fluorescence quantum yield. *Nucleic Acids Res.* **2005,** *33* (16), 5019-5025.

[69] Wilson, D. L.; Kool, E. T., Fluorescent probes of DNA repair. *ACS Chem. Biol.* **2018,** *13* (7), 1721-1733.

[70] Jean, J. M.; Hall, K. B., 2-Aminopurine fluorescence quenching and lifetimes: Role of base stacking. *Proc. Natl. Acad. Sci. U.S.A.* **2001,** *98* (1), 37.

[71] Dueymes, C.; Décout, J. L.; Peltié, P.; Fontecave, M., Fluorescent deazaflavin–oligonucleotide probes for selective detection of DNA. *Angew. Chem. Int. Ed.* **2002,** *41* (3), 486-489.

[72] Kandoth, C.; McLellan, M. D.; Vandin, F.; Ye, K.; Niu, B.; Lu, C.; Xie, M.; Zhang, Q.; McMichael, J. F.; Wyczalkowski, M. A.; Leiserson, M. D. M.; Miller, C. A.; Welch, J. S.; Walter, M. J.; Wendl, M. C.; Ley, T. J.; Wilson, R. K.; Raphael, B. J.; Ding, L., Mutational landscape and significance across 12 major cancer types. *Nature* **2013,** *502* (7471), 333-339.

[73] Burns, D. D.; Teppang, K. L.; Lee, R. W.; Lokensgard, M. E.; Purse, B. W., Fluorescence turn-on sensing of DNA duplex formation by a tricyclic cytidine analogue. *J. Am. Chem. Soc.* **2017,** *139* (4), 1372-1375.

[74] Gardarsson, H.; Kale, A. S.; Sigurdsson, S. T., Structure–function relationships of phenoxazine nucleosides for identification of mismatches in duplex DNA by fluorescence spectroscopy. *Chembiochem* **2011,** *12* (4), 567-575.

[75] Mata, G.; Schmidt, O. P.; Luedtke, N. W., A fluorescent surrogate of thymidine in duplex DNA. *Chem. Commun.* **2016,** *52* (25), 4718-4721.

[76] Okamoto, A.; Tainaka, K.; Saito, I., Clear distinction of purine bases on the complementary strand by a fluorescence change of a novel fluorescent nucleoside. *J. Am. Chem. Soc.* **2003,** *125* (17), 4972-4973.

[77] Okamoto, A.; Tainaka, K.; Saito, I., Synthesis and properties of a novel fluorescent nucleobase, naphthopyridopyrimidine. *Tetrahedron Lett.* **2003,** *44* (36), 6871-6874.

[78] Okamoto, A.; Tanaka, K.; Fukuta, T.; Saito, I., Design of base-discriminating fluorescent nucleoside and its application to t/c snp typing. *J. Am. Chem. Soc.* **2003,** *125* (31), 9296-9297.

[79] Miyata, K.; Tamamushi, R.; Ohkubo, A.; Taguchi, H.; Seio, K.; Santa, T.; Sekine, M., Synthesis and properties of a new fluorescent bicyclic 4-N-carbamoyldeoxycytidine derivative. *Org. Lett.* **2006,** *8* (8), 1545-1548.

[80] Narayanan, M.; Kodali, G.; Xing, Y.; Stanley, R. J., Photoinduced electron transfer occurs between 2-aminopurine and the DNA nucleic acid monophosphates: Results from cyclic voltammetry and fluorescence quenching. *J. Phys. Chem. B* **2010,** *114* (32), 10573-10580.

[81] Bood, M.; Fuchtbauer, A. F.; Wranne, M. S.; Ro, J. J.; Sarangamath, S.; El-Sagheer, A. H.; Rupert, D. L. M.; Fisher, R. S.; Magennis, S. W.; Jones, A. C.; Hook, F.; Brown, T.; Kim, B. H.; Dahlen, A.; Wilhelmsson, L. M.; Grotli, M., Pentacyclic adenine: a versatile and exceptionally bright fluorescent DNA base analogue. *Chem. Sci.* **2018,** *9* (14), 3494-3502.

[82] Seidel, C. A. M.; Schulz, A.; Sauer, M. H. M., Nucleobase-specific quenching of fluorescent dyes. 1. Nucleobase one-electron redox potentials and their correlation with static and dynamic quenching efficiencies. *J. Phys. Chem.* **1996,** *100* (13), 5541-5553.

[83] Godde, F.; Toulmé, J.-J.; Moreau, S., Benzoquinazoline derivatives as substitutes for thymine in nucleic acid complexes. Use of fluorescence emission of benzo[g]quinazoline-2,4-(1H,3H)-dione in probing duplex and triplex formation. *Biochemistry* **1998,** *37* (39), 13765-13775.

[84] Krueger, A. T.; Lu, H.; Lee, A. H. F.; Kool, E. T., Synthesis and properties of size-expanded DNAs: Toward designed, functional genetic systems. *Acc. Chem. Res.* **2007,** *40* (2), 141-150.

[85] Xie, Y.; Maxson, T.; Tor, Y., Fluorescent nucleoside analogue displays enhanced emission upon pairing with guanine. *Org. Biomol. Chem.* **2010,** *8* (22), 5053-5055.

[86] Hirashima, S.; Han, J. H.; Tsuno, H.; Tanigaki, Y.; Park, S.; Sugiyama, H., New size-expanded fluorescent thymine analogue: Synthesis, characterization, and application. *Chem. Eur. J.* **2019,** *25* (42), 9913-9919.

[87] Saltiel, J.; D'Agostino, J. T., Separation of viscosity and temperature effects on the singlet pathway to stilbene photoisomerization. *J. Am. Chem. Soc.* **1972,** *94* (18), 6445-6456.

[88] Wilhelm Hans, E.; Gebert, H.; Regenstein, W., Effect of substituents on the viscosity dependence of fluorescence and on the S1 - T1 energy gap of donor-acceptor substituted trans-stilbenes. *Z. Naturforsch., A: Phys. Sci.* **1997,** *52* (12), 837.

[89] Greco, N. J.; Sinkeldam, R. W.; Tor, Y., An emissive C analog distinguishes between G, 8-oxoG, and T. *Org. Lett.* **2009,** *11* (5), 1115-1118.

[90] Goh, W. L.; Lee, M. Y.; Joseph, T. L.; Quah, S. T.; Brown, C. J.; Verma, C.; Brenner, S.; Ghadessy, F. J.; Teo, Y. N., Molecular rotors as conditionally fluorescent labels for rapid detection of biomolecular interactions. *J. Am. Chem. Soc.* **2014,** *136* (17), 6159-6162.

[91] Mata, G.; Luedtke, N. W., Synthesis and solvatochromic fluorescence of biaryl pyrimidine nucleosides. *Org. Lett.* **2013,** *15* (10), 2462-2465.

[92] Kaburagi, Y.; Kishi, Y., Operationally simple and efficient workup procedure for TBAF-mediated desilylation: application to halichondrin synthesis. *Org. lett.* **2007,** *9* (4), 723-726.

[93] Lakowicz, J. R., *Principles of fluorescence spectroscopy*. 3rd ed.; Springer: New York, 2006.

[94] Beale, R. N.; Roe, E. M. F., Ultra-violet absorption spectra of trans- and cis-stilbenes and their derivatives. Part I. trans- and cis-Stilbenes. *J. Chem. Soc.* **1953,** (0), 2755-2763.

[95] Taniguchi, M.; Lindsey, J. S., Database of absorption and fluorescence spectra of >300 common compounds for use in photochemCAD. *Photochem. Photobiol.* **2018,** *94* (2), 290-327.

[96] Waldeck, D. H., Photoisomerization dynamics of stilbenes. *Chem. Rev.* **1991,** *91* (3), 415-436.

[97] Steffen, F. D.; Sigel, R. K. O.; Börner, R., An atomistic view on carbocyanine photophysics in the realm of RNA. *Phys. Chem. Chem. Phys.* **2016,** *18* (42), 29045-29055.

[98] Rettig, W., Charge separation in excited states of decoupled systems tict compounds and implications regarding the development of new laser dyes and the primary process of vision and photosynthesis. *Angew. Chem. Int. Ed.* **1986,** *25*, 971-988.

[99] Maus, M.; Rettig, W., Electronic relaxations in donor–acceptor biphenyls. *Chem. Phys. Lett.* **2000,** *324* (1), 57-63.

[100] Maus, M.; Rettig, W.; Jonusauskas, G.; Lapouyade, R.; Rullière, C., Subpicosecond transient absorption of donor−acceptor biphenyls. Intramolecular control of the excited state charge transfer processes by a weak electronic coupling. *J. Phys. Chem. A* **1998,** *102* (38), 7393-7405.

[101] Reichardt, C., Solvatochromic dyes as solvent polarity indicators. *Chem. Rev.* **1994,** *94* (8), 2319-2358.

[102] Abramova, T., Frontiers and approaches to chemical synthesis of oligodeoxyribonucleotides. *Molecules* **2013,** *18* (1), 1063-1075.

[103] Aboul-ela, F.; Koh, D.; Tinoco, I., Jr.; Martin, F. H., Base-base mismatches. Thermodynamics of double helix formation for dCA3XA3G + dCT3YT3G (X, Y = A,C,G,D. *Nucleic Acids Res.* **1985,** *13* (13), 4811-4824.

[104] Schmidt, O. P.; Jurt, S.; Johannsen, S.; Karimi, A.; Sigel, R. K. O.; Luedtke, N. W., Concerted dynamics of metallo-base pairs in an A/B-form helical transition. *Nat. Commun.* **2019,** *10* (1), 4818.

[105] Zhao, Y.; Schultz, N. E.; Truhlar, D. G., Exchange-correlation functional with broad accuracy for metallic and nonmetallic compounds, kinetics, and noncovalent interactions. *J Chem Phys* **2005,** *123* (16), 161103.

[106] Hariharan, P. C.; Pople, J. A., The influence of polarization functions on molecular orbital hydrogenation energies. *Theor. Chim. Acta* **1973,** *28* (3), 213-222.

[107] Cossi, M.; Barone, V., Time-dependent density functional theory for molecules in liquid solutions. *J. Chem. Phys.* **2001,** *115* (10), 4708-4717.

[108] W. Hehre, J. Y., P. Klunzinger, L. Lou, Wavefunction Inc. *Irvine, CA* **2008**.

[109] Frisch, M. J., Gaussian, Inc. *Wallingford, CT* **2010**.

[110] Cantor, C. R.; Warshaw, M. M.; Shapiro, H., Oligonucleotide interactions. 3. Circular dichroism studies of the conformation of deoxyoligonucleotides. *Biopolymers* **1970,** *9* (9), 1059-1077.

Chapter 3 | Probing DNA local and global structure

"…is about questioning, studying, ***probing*** nature. You probe, and, if you're lucky, you get strange clues."

Lene Hau

3.1 Introduction: Detection of DNA hybridization, damage, and mutations

DNA encodes all of our genetic information. Consequently, any error within a DNA sequence may initiate disease-states and impact the health of an individual. These errors can occur naturally when DNA is exposed to light or chemical reagents (DNA damage) or during DNA replication, mitosis, or meiosis (DNA mutation). The main difference between these two types of errors is that DNA damage changes the chemical structure of a nucleobase while a mutation simply alters the sequence. Therefore, the biological consequences of DNA damage and DNA mutation can be different. Preserving genomic sequence information in living organisms is essential for the perpetuation of life. At the same time, mutagenesis plays an indispensable part in its maintenance of evolution, while also contributing to cancer, certain human diseases, and aging. It is known that DNA, the basic unit of inheritance, is an intrinsically reactive molecule and is highly susceptible to chemical modifications by endogenous and exogenous agents. Furthermore, the DNA polymerases make some mistakes, thereby burdening cells with potentially disadvantageous mutations. However, cells are equipped with intricate and sophisticated systems—DNA repair, damage tolerance, and cell death pathways—that collectively function to reduce the deleterious consequences of DNA damage.

Several methods have been developed to measure the activity of DNA repair enzymes and detect single-nucleotide polymorphisms (SNPs) which involve a variation of a single nucleotide at a specific location in the genome.[1-5] Among these methods, molecular beacon (MB) probes have been widely used for the detection of SNPs, real-time detection of nucleic acids, quantification of polymerase chain reactions (PCRs), isothermal amplification, as DNA microarray–immobilized probes, and as antisense probes for detecting RNA *in vivo*.[6-9] An MB probe is an oligonucleotide that forms a hairpin-like stem-loop structure tagged with a fluorophore and a quencher at 5′ and 3′ terminus (Figure 3.1A). The hairpin loop consists of approximately 15–25 nucleotides that are complementary to the target DNA, and the terminal stems are composed of 5–7 nucleotides that are complementary to each other.[10-12] When the MB probe exists in the form of a hairpin structure, the fluorescence disappears because the quencher is positioned close to the fluorophore. When the MB probe meets its target DNA, the hairpin structure opens, and fluorescence is restored due to the separation of the fluorophore and quencher units. The advantage of MB probes over single-dye probes (linear probes) is that they provide high signal-to-noise ratios and high degrees of mismatch discrimination. Despite these attractive features, MB probes have a disadvantage in that they require a specific target

sequence of 15–25 nucleotides to separate the fluorophore and quencher upon dimerization with the target. In addition, because the hairpin must be opened, the rate of hybridization is slower than that of a corresponding linear probe. Finally, both the fluorophore and quencher units are required, adding to the cost of preparation.

If fluorescent oligonucleotides could be made to function in a similar manner to that of MB probes, but without the need for quencher units, such probes would be simpler and cheaper to produce. Furthermore, quencher-free DNA probes could be prepared with the fluorophore positioned anywhere along the sequence, not only at the end of the stem. Examples of fluorescence-based sequence detection, discrimination of alleles, and DNA quantification using oligonucleotides containing only a single fluorophore unit include: guanine-quenching probes, cyanine-containing probes, FBAs, and microenvironment-sensitive probes.

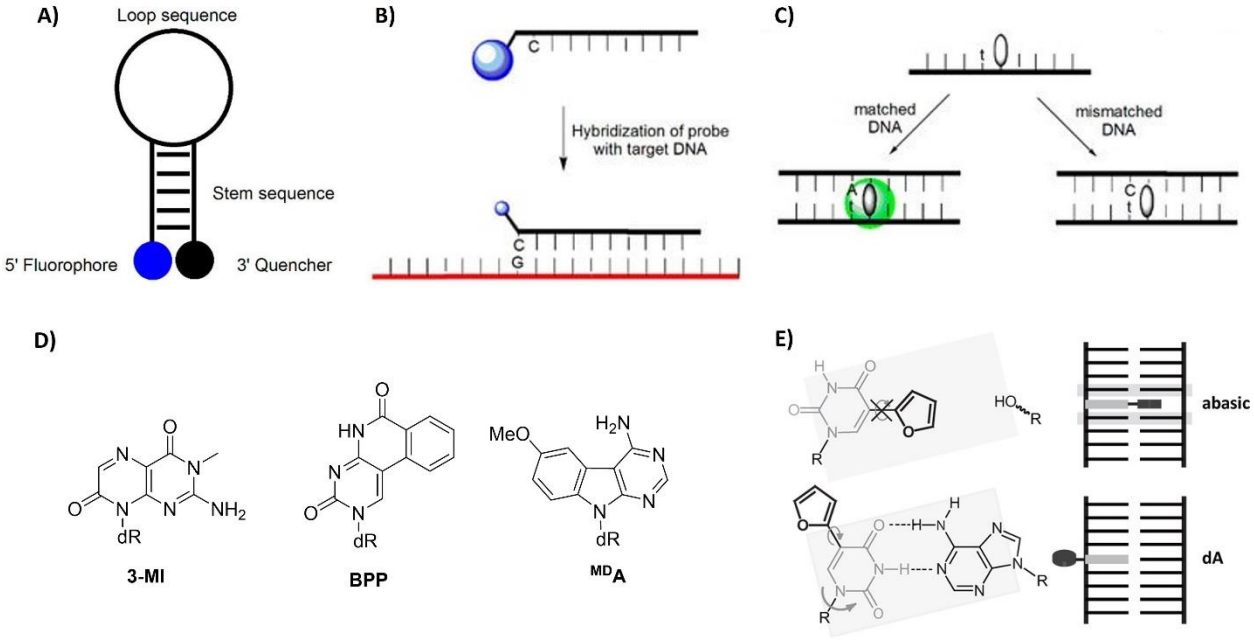

Figure 3.1. Principle of (A) MB probes, (B) guanine-quenching probes, (C) forced intercalation probes, (D) some FBAs, and (E) molecular rotor probes. Figure A, B, and C are adopted from REF[13] and figure E is adopted from REF[14].

Guanine-quenching probes: Two types of probes have been designed based on the guanine bases' function as energy acceptors.[15-16] In the first type, hybridization causes PET quenching when fluorophores are placed adjacent to cytosine residues (Figure 3.1B).[17-19] In the second type,

dequenching occurs when a DNA strand containing a fluorophore adjacent to guanine residues hybridizes to the complementary strand.[20] The main drawback of these systems is that they have low sensitivity and are limited to specific sequences.

Cyanine-containing probes: Some cyanines such as thiazole orange (TO) and oxazole yellow (YO) have been inserted at an internal position of oligonucleotides.[21-24] When these probes hybridize to the complementary DNA target, forced intercalation and fluorescence enhancement were observed (Figure 3.1C).[25] The fluorescence of these covalently linked intercalators is sensitive to structural disturbances caused by an adjacent base mismatch. However, these probes are relatively bulky modifications and can disturb the secondary structure of DNA.

Fluorescent base analogs (FBAs): The classical FBA, 2-aminopurine (2AP), maintains complementarity to thymine but also wobble pairs with cytosine. It shows reduced fluorescence upon base-pairing with T or C.[26] Thus, fluorescent base analogs that are structurally similar to native nucleobases, have been widely developed with the goal of achieving increased fluorescence intensities upon highly specific base-pairing with a single residue.[13, 27-28] Some FBAs with the highest SNP discrimination are 3-MI,[29] BPP,[30] and ^{MD}A (Figure 3.1D).[31] 3-MI forms a bulge following the formation of a matched duplex, leading to an increase of up to 27-fold in fluorescence intensity. The bulge-formation strategy has been used to detect PCR products of an HIV-1 detection system.[29] However, the major problem with these probes is that their fluorescence is fully quenched in the off mode, rendering detection of the nucleobase in different hybridization states impossible.

Microenvironment-sensitive probes: As previously discussed in Section 1.5, Chapter 1, fluorescent nucleosides have been employed as microenvironment-sensitive probes,[32] utilizing their high sensitivity to detect changes in local polarity,[33] viscosity,[14] and pH.[34] For example, oligonucleotides containing furan-modified dU have been used to detect abasic sites (Section 1.8.5, Chapter 1).[35-36] When the functionalized strand was hybridized and the abasic site was located across from it, a significant emission enhancement was observed as compared to that of the matched duplex.[14] It is believed that the vacant space provided by the confined abasic site limited the rotation of the furan-uracil single bond, resulting in an increase of fluorescence (Figure 3.1E). Such fluorescent nucleobase rotors have also been used to detect DNA hybridization,[37] mismatches and oxidatively damaged bases.[38-39] However the previously reported probes suffer from low brightness,[40] and are

usually sensitive enough for abasic sites but not mismatches and transverse mutation products.[38] In addition, pH-sensitive probes have been used as hybridization probes. The *Asanuma* Group used 7-hydroxycoumarin (pK_a = 8.8 in *ss*-DNA and pK_a > 10 in *ds*-DNA), which was quenched upon protonation in the absence of the target strand.[41] Even though the pH-responsive probes have also been used for SNP identification of mutant/wild-type bases,[42] their applications are mostly limited to DNA hybridization, where the complementary strand assists deprotonation.

Here we will discuss how the rotary behavior of ^{ts}T makes it the most mismatch-sensitive probe to date that can detect both local and global dynamics of DNA. Even though ^{ts}T discriminates between matched and mis-matched bases, thanks to its exceptionally high brightness, its fluorescence even in the off-mode remained high enough to be detected by dynamic anisotropy measurements. Thus, we used ^{ts}T to probe the dynamics of mismatched and well-matched duplexes, as well as single-stranded DNA. The results generated from time-correlated single-photon counting (TCSPC) provided insights into the fundamental dynamic behavior of DNA. In addition, we conducted distance-dependence studies and applied ^{ts}T as a spectroscopic ruler, where it could selectively detect (1) an A:A mismatch or an abasic site by short-range dynamic induction; (2) an O6-methylguanine (MG) or 8-oxoguanine (OG) damage by the means of electron transfer; and (3) a FRET acceptor *via* energy transfer.

3.2 ^{ts}T discriminates between mismatches

Oligonucleotides containing ^{ts}T exhibited a 4.9-fold fluorescence enhancement upon hybridization with a fully complementary sequence (Figure 3.2). This observation was in agreement with our DFT calculations and solvent-dependent photophysical experiments which suggested ^{ts}T is microenvironment-sensitive and, in contrast with most of the FBAs,[29, 43-45] does not undergo PET quenching in duplex DNA. Taken together, the fluorescence enhancement of ^{ts}T during hybridization with the fully complementary strand is explainable by formation of the rigid duplex DNA which inhibits ^{ts}T from rotation around the ethylenic bond. Comparing the well-matched DNA (^{ts}T:A) with mismatched DNAs (^{ts}T: G, C, T) revealed the ability of ^{ts}T to discriminate a single nucleotide with $\varepsilon \times \varphi$ values ranging from 150 – 4,250 $cm^{-1}\,M^{-1}$ (Figure 3.2 and Table B1, Appendix B). This fluorescence diminution is a result of the higher flexibility of mismatched bases. The greatest fluorescence change was observed for ^{ts}T:C and ^{ts}T:T mismatches. The ^{ts}T:G wobble base-pair, due to its stronger pairing

interactions as compared to the other mismatched bases, showed less fluorescence quenching. Similar trends were also observed in the thermal melting (T_m) of ^{ts}T:A > ^{ts}T:G > ^{ts}T:C/T, consistent with the relative broadness of thymidine imino proton resonances in ^{1}H NMR spectra of T:G and T:T base pairs in duplex DNA.[46] Together these results suggested that fluorescence quenching of ^{ts}T is related to increased molecular motions of mismatched ^{ts}T:C/T base pairs over both ^{ts}T:G (wobble) and ^{ts}T:A base pairs.

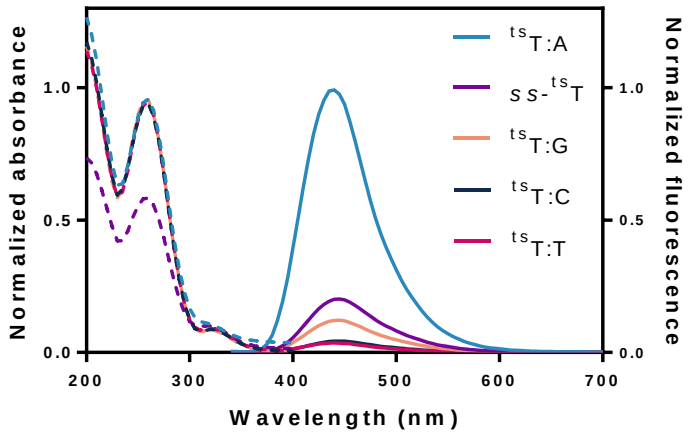

Figure 3.2. Absorption (dashed line) and fluorescence (solid line) of single-stranded and duplex ODN1 containing ^{ts}T. Data were recorded at 22 ^{o}C in PBS buffer (pH = 7.4). DNA concentrations were kept at 2.0 µM. ODN1 sequence: 5'–GCGTA**^{ts}T**CGTATACAC–3'

To gain insight into the relationships between ^{ts}T dynamic motions and brightness in DNA, TCSPC experiments were conducted using *ds*-^{ts}T:A, *ds*-^{ts}T:T and *ss*-^{ts}T samples of ODN1 (Table 3.1, Figure B1, Appendix B). All time-resolved data fit to single-exponential decay models (R^2 = 0.98 – 0.99,). At 25 ^{o}C, the fluorescence lifetime values (τ) of ^{ts}T in DNA were *ds*-^{ts}T:A (11 ns), *ss*-^{ts}T (5.4 ns), and *ds*-^{ts}T:T (4.5 ns), reflecting the same trends as their steady-state brightness. Upon heating each sample over a "pre-melting" temperature range of 25 ^{o}C → 45 ^{o}C where no significant global melting of the duplexes was observed (at 45 ^{o}C, only 12% of *ds*-^{ts}T:A and 17% of *ds*-^{ts}T:T were melted), the τ values of ^{ts}T decreased in a linear fashion for both *ds*-^{ts}T:A (-0.11 ns per ^{o}C, Figure 3.3) and *ss*-^{ts}T (-0.05 ns per ^{o}C, Figure 3.3). These results are consistent with increased "breathing" motions of nucleobases with increasing temperatures.[47] Surprisingly, the τ values of *ds*-^{ts}T:T increased over this same temperature range (+0.03 ns per ^{o}C), suggesting increasing rigidity of the mismatch with increasing temperature. This result is consistent with the higher affinity and positive entropy change

exhibited by T:T mismatches for Hg^{II} binding over these temperatures.[48-49] Previously, it was suggested that water is released from the T:T base pairs with increasing temperature, making T:T mismatch bases bind stronger to Hg^{II} at higher temperatures.[46, 49] However, this fluorescence lifetime enhancement stops after the duplex begins to melt. At 55 °C, where 57% of *ds*-^{ts}T:A and 85% of *ds*-^{ts}T:T were melted, the τ values for all three samples neared convergence due to thermal melting of the duplexes (Figure 3.3).

Table 3.1. Fluorescence lifetime (τ), anisotropy decay (θ), steady-state anisotropy (<r>), angle between excitation and emission dipole (β) and hydrodynamic radius (R_H) of ^{ts}T in ODN1.[a]

	T (°C)	τ (ns)	θ (ns)	<r>	β (°)[b]	R_H (nm)[c]
	25	11.1 ± 0.1	20 ± 4.2	0.07 ± 0.01	44 ± 2	2.70 ± 0.18
***ds*-^{ts}T:A**	35	10.0 ± 0.1	19 ± 3.8	0.08 ± 0.01	43 ± 2	2.68 ± 0.18
	55	6.6 ± 0.1	8.5 ± 2.8	0.06 ± 0.02	45 ± 3	2.09 ± 0.22
***ss*-^{ts}T**	25	4.5 ± 0.1	7.9 ± 1.7	0.04 ± 0.01	47 ± 2	1.98 ± 0.14
***ds*-^{ts}T:T**	25	5.4 ± 0.1	5.3 ± 1.6	0.02 ± 0.02	51 ± 2	1.74 ± 0.17[d]

[a]All measurements were performed at 22 °C, PBS buffer and pH = 7.4. DNA concentrations = 2.0 μM.
[b]Calculated from fundamental anisotropy, r_o (Eq. B5).
[c]Calculated from θ (Eq. B4). In figure B2, Appendix B, the fundamental anisotropy is plotted against β.
[d]Value reflects local dynamics, not R_H.

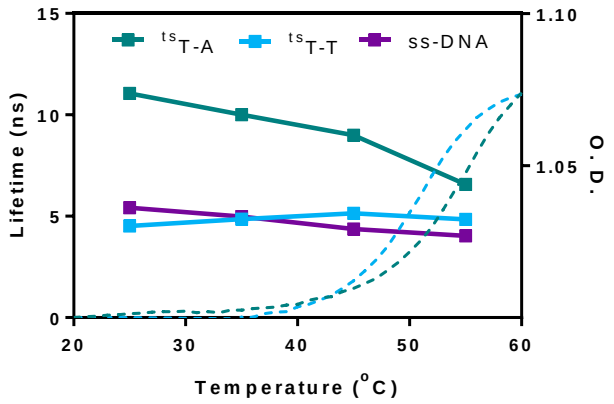

Figure 3.3. Temperature-dependent fluorescence lifetime values (averaged values of three measurements with standard errors) as compared to global thermal melting according to absorbance changes (O.D., dashed lines) at 260 nm.

To evaluate local and global dynamic motions, TCSPC experiments were used to measure time-resolved fluorescence anisotropy decay (θ, Figure 3.4, Table 3.1). At 25 °C, the θ values of ^{ts}T in DNA followed the same trends as steady-state quantum yields and fluorescence lifetime measurements, where *ds*-^{ts}T:A (θ = 20 ns) >> *ss*-^{ts}T (θ = 7.9 ns) > *ds*-^{ts}T:T (θ = 5.3 ns). The θ values of *ds*-^{ts}T:A at 25 °C and 35 °C were essentially identical (θ = 19 – 20 ns, Table 3.1 and Figure 3.4B), suggesting that the θ values are reflecting global motions of the duplex at these temperatures. We therefore used the θ value at 25 °C to calculate the hydrodynamic radius of the duplex (R_H, Eq. B4, Appendix), giving R_H = 2.70 ± 0.18 nm (Table 3.1). This value is in agreement with the previously reported R_H values of duplex DNA measured by fluorescence anisotropy, sedimentation velocity and Monte Carlo simulations.[50-54] Comparing our results with the time-resolved fluorescence anisotropy data of 6-MI,[55] we noticed the duplex containing 6-MI has a smaller anisotropy decay time than duplex containing ^{ts}T (3.2 ns vs 20.0 ns) and consequently a smaller hydrodynamic radius per base. This reinforces skepticism on considering 6-MI as a "real" mimic of guanosine, which was already under argument considering thermal destabilization of duplexes containing 6-MI.[56-58]

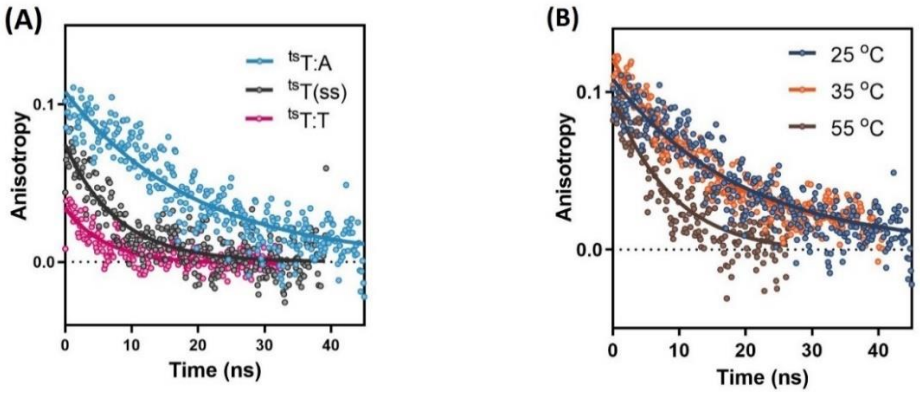

Figure 3.4. Time-resolved fluorescence anisotropy of (A) ODN1 *ss*-^{ts}T, *ds*-^{ts}T:T and *ds*-^{ts}T:A at 25 °C, (B) ODN1 *ds*-^{ts}T:A at 25, 35, and 55 °C. All measurements were conducted in PBS buffer (pH = 7.4).

At 55 °C the θ of *ds*-^{ts}T:A (8.5 ns) approached that of *ss*-^{ts}T at 25 °C (7.9 ns). These values are consistent with the conversion of a "rod-like" duplex (R_H = 2.70 nm) into a "worm-like" chain of *ss*-DNA (R_H = 2.09 nm, Table 3.1).[59-60] The close agreements between our results obtained from photophysical properties of ^{ts}T, with the global physical properties of *ss*-DNA,[61-62] suggest that *ss*-DNA contains partially-ordered nucleobases with correlation times dominated by concerted, global motions of the entire molecule. In contrast, the θ for mismatched, duplex *ds*-^{ts}T:T (5.3 ns) primarily

reflects rapid, local dynamics, since this value is much lower than that of *ds*-^{ts}T:A (20 ns), and it is even lower than *ss*-^{ts}T at 25 ^{o}C (7.9 ns). These results are consistent with previous NMR measurements and molecular dynamics simulations suggesting the presence of rapid, local motions of base-pair mismatches in otherwise canonical duplexes.[63] To our knowledge, this is the first time an FBA has been used to determine the hydrodynamic radii of *ss*-DNA. Our results suggest that the dynamic motions of a base-pair mismatch in *ds*-DNA are even greater than those present in *ss*-DNA.

3.3 Distance-dependent duplex perturbation

Previous studies have focused on using FBAs to detect mismatches and/or DNA lesions in the opposing or adjacent nucleobase. Given the high sensitivity of ^{ts}T to DNA local dynamics, we decided to evaluate how far away ^{ts}T can sense a DNA error or damage. For this purpose, different oligonucleotides were synthesized using solid-phase DNA synthesis, and then hybridized with different complementary strands forming duplexes containing a mismatch, an abasic (AP) site, or a damage at different distances from the probe.

3.3.1 Distance-dependent detection of an A:A mismatch and an AP site

An AT-rich sequence containing ^{ts}T, ODN4 (5'–GCGA**^{ts}T**ATATATATAGCG–3'), was hybridized with different complementary strands forming duplexes containing an A:A mismatch one to five base-pairs (bps) away from the ^{ts}T:A pair (*ds*-^{ts}T/AA$_n$, where n = 1, 3, and 5 represents how many bps the mismatch is away from ^{ts}T, Table 3.2). As shown in Figure 3.5A, the fluorescence of ^{ts}T is quenched by 16% when an A:A mismatch is one bp away from the ^{ts}T:A pair. However, the fluorescence of ^{ts}T is almost insensitive towards the presence of an A:A mismatch more than three bps away (<5% quenching). In addition, ODN4 was hybridized with complementary strands containing an AP site one to five bps away from ^{ts}T:A pair (*ds*-^{ts}T/AP$_n$, where n = 1, 3, and 5 represents the position of AP site, Table 3.2). The fluorescence experiments with DNA containing an AP site (Figure 3.5B) demonstrated similar results as DNA containing an A:A mismatch, with 24% quenching the fluorescence of ^{ts}T when the AP site is one bp away from the ^{ts}T:A pair and <6% quenching when the AP site is more than three

bps away. Taken together, these results suggest that mispaired bases do not perturb the local dynamics of the other base-pairs located at a distance greater than 1 nm away.

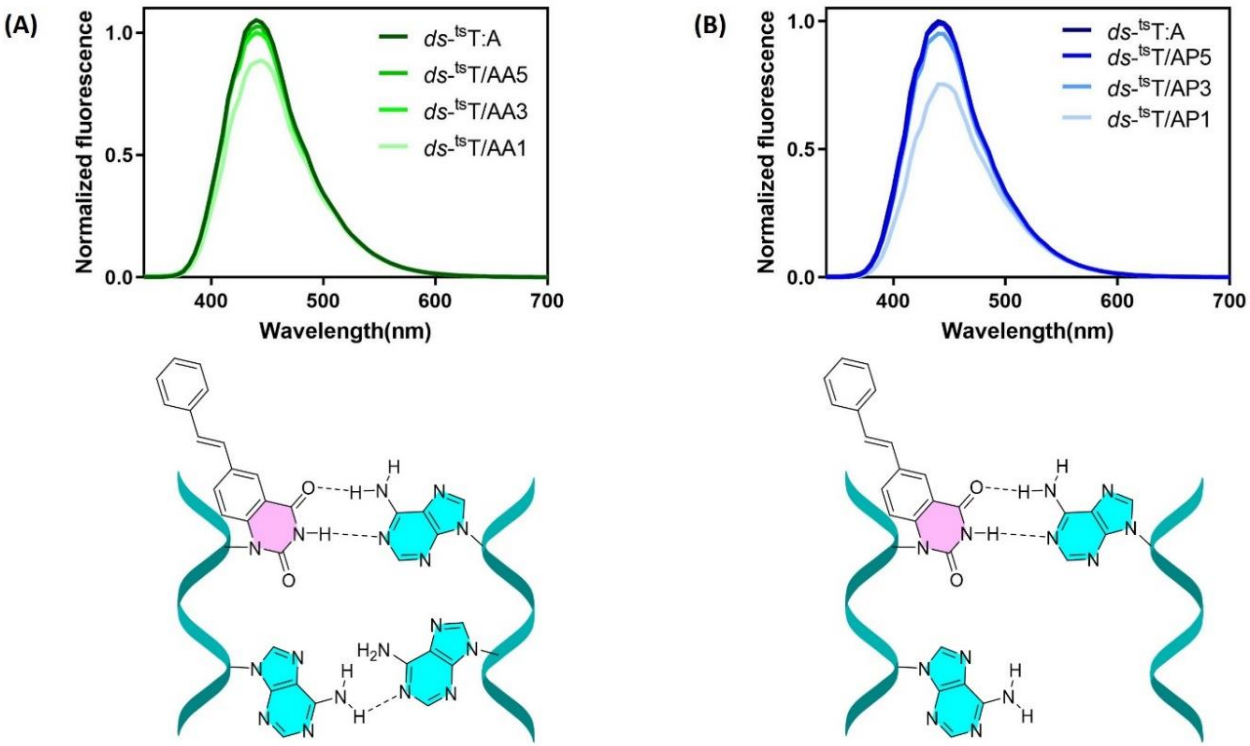

Figure 3.5. Distance-dependent detection of (A) A:A mismatch and (B) AP site by ^{ts}T fluorescence (excitation at 310 nm). Data were recorded at 22 ^{o}C in PBS buffer (pH = 7.4). DNA concentrations were kept at 2.0 µM. ODN4 sequence: 5′–GCGA **^{ts}T** ATATATATAGCG–3′. The complementary strand AA_n and AP_n represents A:A mismatch and AP site in "n" base-pairs away.

Table 3.2. Biophysical properties of duplexes containing ODN4 and its complementary strands forming A:A mismatch and AP site.[a,b]

DUP4	Sequences	φ	εφ ($cm^{-1}M^{-1}$)	TM (°C)
ds-^{ts}T	5′– GCGA **^{ts}T** ATATATATAGCG –3′ 3′– CGCT A TATATATATCGC –5′	0.135	4,130	48.0
ds-^{ts}T/AA$_1$	5′– GCGA **^{ts}T A** TATATATAGCG –3′ 3′– CGCT A **A** ATATATATCGC –5′	0.113	3,610	36.0
ds-^{ts}T/AA$_3$	5′– GCGA **^{ts}T** AT **A** TATATAGCG –3′ 3′– CGCT A TA **A** ATATATCGC –5′	0.129	3,890	36.9
ds-^{ts}T/AA$_5$	5′– GCGA **^{ts}T** ATAT **A** TATAGCG –3′ 3′– CGCT A TATA **A** ATATCGC –5′	0.132	3980	36.9
ds-^{ts}T/AP$_1$	5′– GCGA **^{ts}T A** TATATATAGCG –3′ 3′– CGCT A **(-)** ATATATATCGC –5′	0.102	3,240	37.3
ds-^{ts}T/AP$_3$	5′– GCGA **^{ts}T** AT **A** TATATAGCG –3′ 3′– CGCT A TA **(-)** ATATATCGC –5′	0.128	3,670	39.8
ds-^{ts}T/AP$_5$	5′– GCGA **^{ts}T** ATAT **A** TATAGCG –3′ 3′– CGCT A TATA **(-)** ATATCGC –5′	0.134	3,890	40.7

[a] The average extinction coefficient (Ɛ) of ^{ts}T in DNA at 310 nm is 30,600 ± 700 cm^{-1} M^{-1}.
[b] All measurements were performed at 22 °C in PBS buffer (pH = 7.4), with DNA concentrations = 2.0 μM.

3.3.2 Distance-dependent detection of a O6-methylguanine

Endogenous and exogenous methylating agents react with and modify DNA nucleobases, producing primarily N7-methylguanine and O6-methylguanine (MG).[64] MG is formed in DNA by SN1-type methylating agents,[65] such as N-nitroso compounds that are known human carcinogens.[66] Endogenous sources of methylation include S-adenosylmethionine[67] and nitrosation products.[68-69] MG, pairs to thymine rather than cytidine, causing a G:C to A:T transition in DNA. Fluorescent probes have been used to label O6 of guanines and measure the activity of O6-methylguanine-DNA methyltransferase (MGMT) in live cells.[70] In addition, external fluorescent probes were recently used to determine the activity of MGMT.[71] However, to the best of our knowledge, canonical FBAs have never been used for the detection of MG damages.

Inspired by the sensitivity of ^{ts}T to towards mismatches base-pair mismatches, we decided to use ^{ts}T to probe both MG:T and MG:C pairs. A GC-rich sequence, ODN7 (5′–GCGA**^{ts}T**CGCGCGCTAGCG–3′), as well as four sequences containing an MG at different locations (ODN7′MG$_n$, where n = 0, 1, 3, and 5) were synthesized using solid-phase DNA synthesis (ESI data are available in Table B2 and Figure

B4, Appendix B). Hybridization of ODN7 with ODN7'MG_n formed a duplex containing ^{ts}T:MG and three duplexes with a C:MG one to five bps away from the ^{ts}T:A pair (*ds*-^{ts}T/MG_n, where n = 1, 3, and 5 represents how many bps the MG is away from ^{ts}T, Table 3.3). As shown in Figure 3.6A, *ds*-^{ts}T:MG demonstrated a 17-fold lower fluorescence intensity as compared to well-matched *ds*-^{ts}T:A (94% fluorescence quenching). In comparison, the fluorescence of *ds*-^{ts}T:G was 7.1-times lower than that of the well-matched duplex (86% fluorescence quenching). Thus, ^{ts}T can selectively detect MG over G and A when base-pairing with it. The distance-dependent fluorescence data with DNA containing an MG site (Figure 3.6B) revealed that when MG:C is present one bp away from the ^{ts}T:A pair, the probe's fluorescence is quenched by 34%. This fluorescence quenching is more significant than what was determined for an AP site (24% quenching). Based on DFT calculations (Figure 3.8B and Table B3, Appendix B), we believe the higher HOMO level of MG than ^{ts}T causes PET quenching, and thus both mechanical motion and electron transfer factors are involved in fluorescence quenching. This led to the detection of MG:C even when it was three bps away (13% fluorescence quenching). However, ^{ts}T could was insensitive to MG when it was located five bps away (<5% fluorescence quenching).

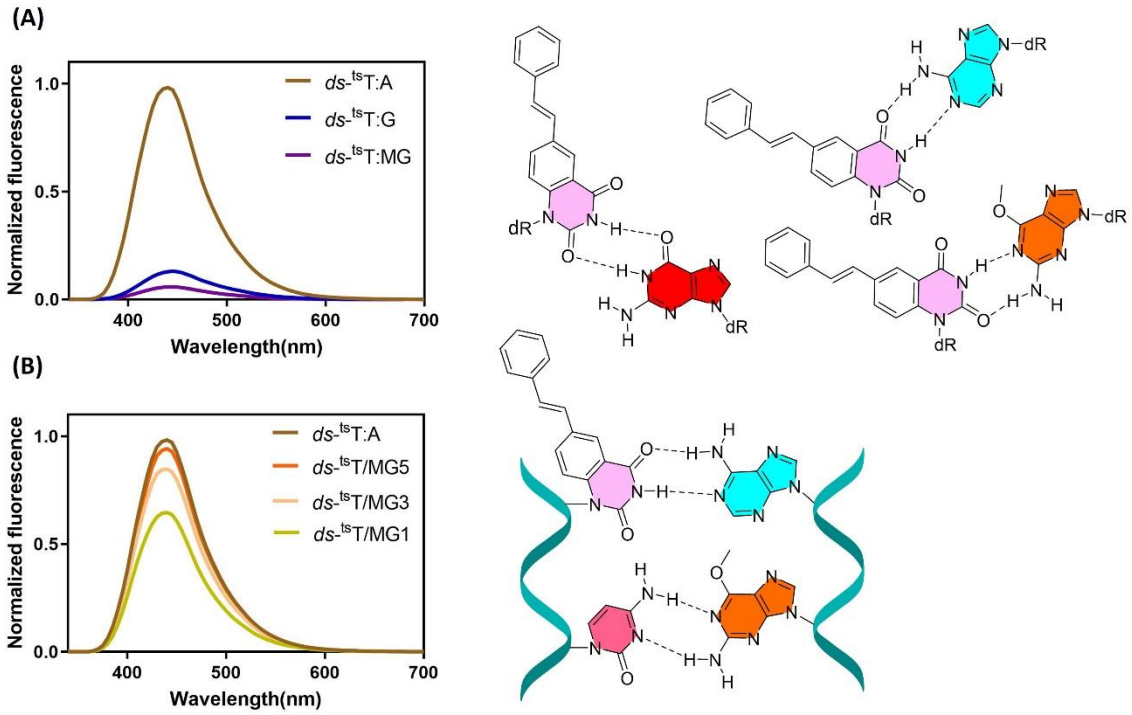

Figure 3.6. (A) fluorescence of duplex ODN7 containing ^{ts}T paired with A, G, and MG. (B) Distance-dependent detection of MG:C pair by ^{ts}T. Data were recorded at 22 ^{o}C in PBS buffer (pH = 7.4). The excitation wavelength was 310 nm. DNA concentrations were kept at 2.0 µM. ODN7 sequence: 5'– GCGA **^{ts}T** CGCGCGCTAGCG –3'.

Table 3.3. Photophysical properties of duplexes containing ODN7 and its complementary strands forming MG:C and MG:T pairs.[a,b]

DUP7	Sequences	φ	εφ ($cm^{-1}M^{-1}$)
ds-^{ts}T:A	5′– GCGA ^{ts}T CGCGCGCTAGCG –3′ 3′– CGCT A GCGCGCGATCGC –5′	0.172	5,260
ds-^{ts}T:MG	5′– GCGA ^{ts}T CGCGCGCTAGCG –3′ 3′– CGCT MG GCGCGCGATCGC –5′	0.010	310
ds-^{ts}T/MG_1	5′– GCGA ^{ts}T C GCGCGCTAGCG –3′ 3′– CGCT A MG CGCGCGATCGC –5′	0.116	3,550
ds-^{ts}T/MG_3	5′– GCGA ^{ts}T CG C GCGCTAGCG –3′ 3′– CGCT A GC MeG CGCGATCGC –5′	0.138	4,220
ds-^{ts}T/MG_5	5′– GCGA ^{ts}T CGCG C GCTAGCG –3′ 3′– CGCT A GCGC MeG CGATCGC –5′	0.165	5,050

[a] The average extinction coefficient (Ɛ) of ^{ts}T in DNA at 310 nm is 30,600 ± 700 cm^{-1} M^{-1}.
[b] All measurements were performed at 22 °C in PBS buffer (pH = 7.4), with DNA concentrations = 2.0 μM.

3.3.3 Detection of 8-oxoguanine damage over longer distances

Guanine is the most susceptible base to oxidation due to its low redox potential.[72] Therefore, 8-oxoguanine (OG) is the most abundant form of oxidative DNA damage generated by reactive oxygen species resulting from metabolism, ionizing radiation, and chemicals.[73] OG in DNA can adopt a *syn* conformation and pair with adenine during replication,[74-75] ultimately leading to G to T mutations.[76] All previously reported FBAs that have been used to probe OG could only detect it either in the adjacent position[77] or when located opposing to the FBA and pairing to it.[38, 78-81] Having identified FBAs that their fluorescence is efficiently quenched through PET, the reporter system can be employed as a spectroscopic ruler[82] to investigate site-specific DNA damage formation and repair.[83]

To further expand the applications of ^{ts}T in the detection of DNA damages, ODN4 was hybridized with different complementary strands containing OG to form duplexes with OG:A pair one to five bps away from ^{ts}T:A (*ds*-^{ts}T/OG_n, where n = 1, 3, and 5, Table 3.4). Although the fluorescence of ^{ts}T is not sensitive towards an A:A mismatch and an AP site more than one bp away, surprisingly, it was sensitive to OG:A pair even when it was five bps away from ^{ts}T (Figure 3.7).

Table 3.4. Biophysical properties of duplexes containing ODN4 or ODN6 and their complementary strands forming OG:A pairs.[a,b]

Oligonucleotides		Sequences	φ	εφ ($cm^{-1}M^{-1}$)	TM
DUP4	*ds*-^{ts}T	5′– GCGA **^{ts}T** ATATATATAGCG –3′ 3′– CGCT A TATATATATCGC –5′	0.135	4,130	48.0
	ds-^{ts}T/OG_1	5′– GCGA **^{ts}T A** TATATATAGCG –3′ 3′– CGCT A **OG** ATATATATCGC –5′	0.036	1,100	41.4
	ds-^{ts}T/OG_3	5′– GCGA **^{ts}T** AT **A** TATATAGCG –3′ 3′– CGCT A TA **OG** ATATATCGC –5′	0.058	1,770	44.9
	ds-^{ts}T/OG_5	5′– GCGA **^{ts}T** ATAT**A**TATAGCG –3′ 3′– CGCT A TATA **OG** ATATCGC –5′	0.101	3,090	45.3
DUP6	*ds*-^{ts}T	5′– GCGA **^{ts}T** ATAGATATAGCG –3′ 3′– CGCT A TATCTATATCGC –5′	0.167	5,110	52.3
	ds-^{ts}T/OG_5	5′– GCGA **^{ts}T** ATAG **A** TATAGCG –3′ 3′– CGCT A TATC **OG** ATATCGC –5′	0.115	3,520	50.1

[a] The average extinction coefficient (Ɛ) of ^{ts}T in DNA at 310 nm is 30,600 ± 700 cm^{-1} M^{-1}.
[b] All measurements were performed at 22 °C in PBS buffer (pH = 7.4), with DNA concentrations = 2.0 µM.

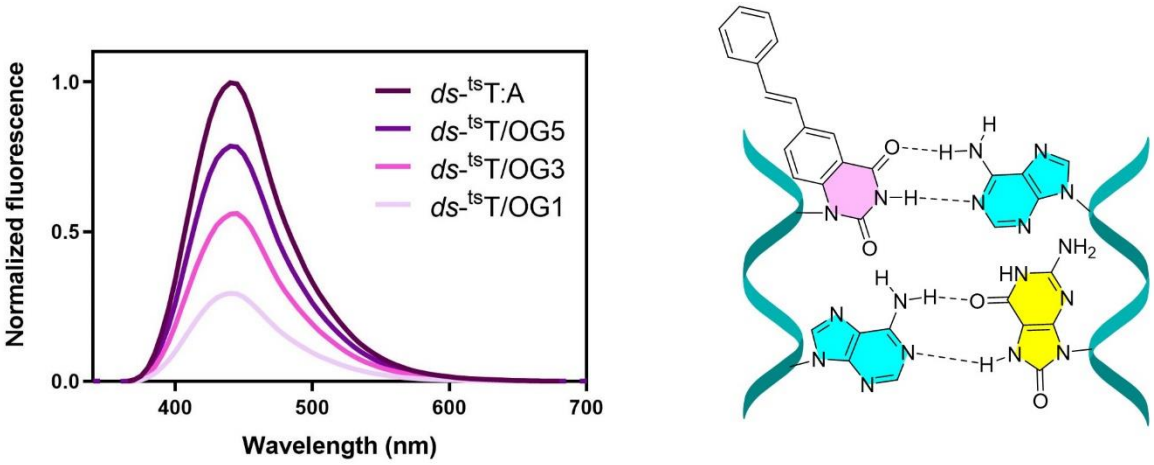

Figure 3.7. Distance-dependent detection of OG:A by ^{ts}T. Fluorescence data (excitation at 310 nm) were recorded at 22 °C in PBS buffer (pH = 7.4). DNA concentrations were kept at 2.0 µM. ODN4 sequence: 5′–GCGA **^{ts}T** ATATATATAGCG –3′. The complementary strand OG_n represents OG located n base-pairs away.

Since OG:A does not induce changes in local dynamics more than an AP site, duplex perturbation could not be responsible for this long-distance detection (Figure 3.8A). DFT studies demonstrated that the HOMO energy level of ^{ts}T fits between HOMO of G and OG (Figure 3.8B and Table B3, Appendix B). This is in agreement with experimental data confirming OG has a lower redox

potential (0.74 mV vs. NHE) than G (1.29 mV vs. NHE).[84] Therefore, although ^{ts}T does not undergo PET quenching by natural DNA bases, its fluorescence can be selectively quenched by OG located over 10 Å.

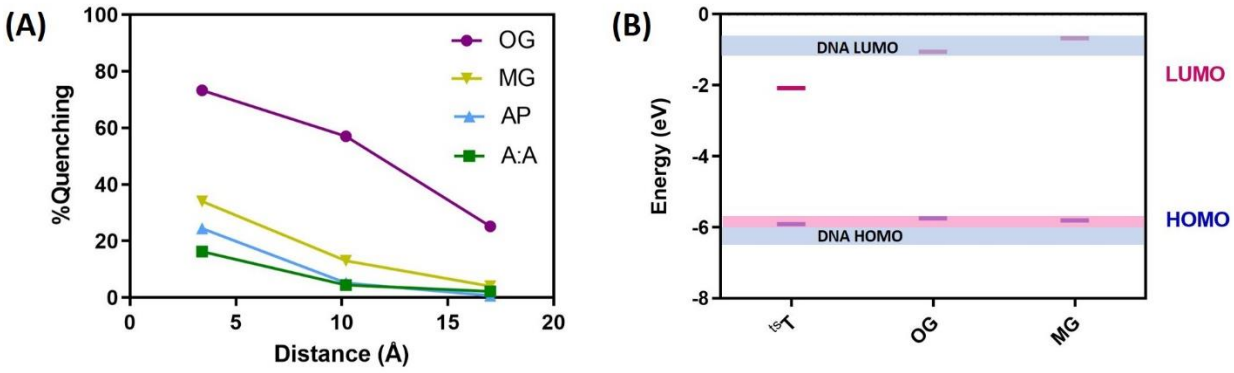

Figure 3.8. (A) Distance-dependent detection of A:A mismatch, AP site, and OG:A by ^{ts}T in ODN4, and MG:C by ^{ts}T in ODN7. Fluorescence data (excitation at 310 nm) were recorded at 22 ^{o}C in PBS buffer (pH = 7.4). DNA concentrations were kept at 2.0 µM. ODN4 sequence: 5'– GCGA **^{ts}T** ATATATATAGCG –3'. ODN7 sequence: 5'– GCGA **^{ts}T** CGCGCGCTAGCG –3'. (B) Calculated HOMO/LUMO energy levels (eV) of ^{ts}T, OG and MG. The HOMO/LUMO energy range of natural DNA bases is shown by the blue area. The HOMO of ^{ts}T fits between the HOMO of DNA and HOMO of MG and OG (pink area). DFT calculations were performed using B3LYP/6-31++G(d) in water.

DNA-mediated electron transfer happens through superexchange or hopping mechanisms, where in the latter G acts as a stepping stone for hole migration.[85-90] Since in the AT-rich duplexes (ODN4: 5'– GCGA **^{ts}T** ATATATATAGCG –3', Table 3.4) there is no G between ^{ts}T and OG, PET most likely happens through a superexchange mechanism, which is a short-range charge transfer based on overlap between the orbitals' functions. We hypothesized that it might be possible to increase the ^{ts}T sensitivity towards an OG located in the further distances by introducing some GC pairs in between. Our initial experiment with ODN6 (5'– GCGA **^{ts}T** ATAGATATAGCG –3', forming *ds*-^{ts}T/OG$_5$ similar to ODN4 but containing a G between ^{ts}T and OG, Table 3.4) demonstrated a slight increase in the ^{ts}T fluorescence quenching (31% *vs* 25%). To confirm the presence of PET between ^{ts}T and OG, 2'-deoxy-8-oxoguanosine nucleoside (0 – 2000 eq.) was added to a 2.0 µM solution of *ss*-^{ts}T (ODN4) and successfully quenched the fluorescence of ^{ts}T (Figure 3.9).

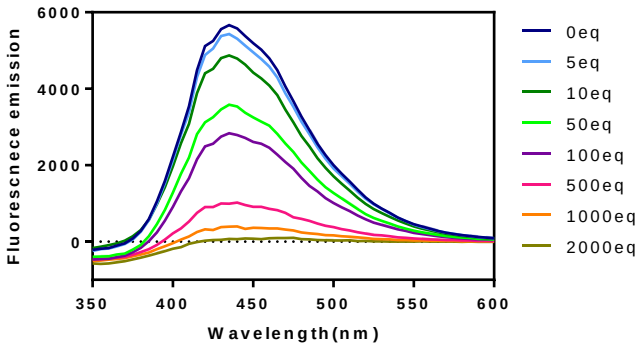

Figure 3.9. Titration of 2′-deoxy-8-oxoguanosine nucleoside to single stranded DNA (ODN4) at 22 ^{o}C in PBS buffer (pH = 7.4). DNA concentrations were kept at 2.0 µM.

3.4 FRET between ^{ts}T and tC

Förster resonance energy transfer (FRET) is a harmonic energy transfer process from a donor to an acceptor.[91] FRET efficiency depends on the distance and orientation between the donor and the acceptor.[92] In the context of FRET, "orientation" means the topology of the transition dipole moments of the donor and acceptor. In almost all FRET-based assays, orientation factors have been regarded as an average value because of the free rotation of fluorophores tethered to molecules of interest. In DNA, the orientations of FBAs are fixed and FRET efficiency reflects both distance and orientation.[93] The construction of such FRET pairs is very significant because the structures and dynamics of biomolecules can be analyzed with higher resolution as compared to conventional FRET-based assays that report only distances. The distance- and orientation-dependent FRET system not only facilitates a better understanding of biomolecular interactions and structural changes but also complements other analytical methods, such as X-ray crystallography and NMR spectrometry.

tC is one of the most commonly used and commercially available FBAs.[34, 94-96] Although it has a relatively high quantum yield (0.19), its brightness is limited by the low extinction coefficient (4,000 $M^{-1}cm^{-1}$). On the other hand, ^{ts}T has a moderate quantum yield (0.14) and owes its high brightness to the exceptionally high extinction coefficient (30,600 $M^{-1}cm^{-1}$). Considering the overlap between the absorbance of tC and emission of ^{ts}T (Figure 3.10), we decided to evaluate the FRET efficiency between ^{ts}T and tC, which pairs a high extinction coefficient of donor with a high quantum yield of the acceptor. For this purpose, GC- and AT-rich sequences containing ^{ts}T (ODN7 and ODN6, respectively) and their fully complementary strands containing tC at different positions (ODN6′tC_4

and ODN7'tC_n, where n = 2, 4, and 6) were synthesized (ESI data are available in Table B2 and Figure B2, Appendix B) and annealed together to form duplexes (*ds*-^{ts}T/tC_n, with tC being n base-pair away from ^{ts}T, Table 3.5). The distances between FRET donor and acceptor were calculated using Studio Discovery package.[97] Figure 3.11A shows the DNA model containing ^{ts}T(ODN7) and tC (ODN7'tC_6).

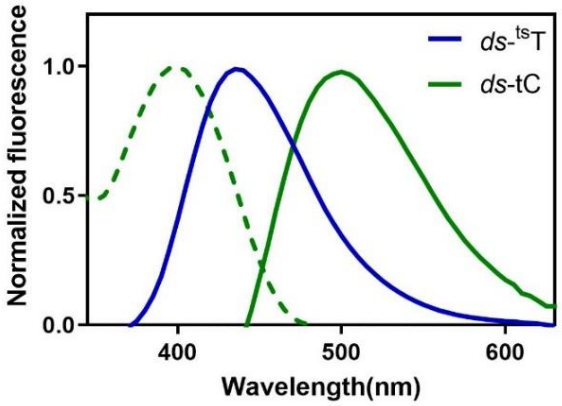

Figure 3.10. Spectral overlap between normalized fluorescence emission of *ds*-^{ts}T (a duplex containing ODN6: 5'– GCGA **^{ts}T** ATAG ATATAGCG –3'), shown by solid blue line, with the normalized absorbance (dashed green line) and normalized fluorescence (solid green line) of *ds*-tC (a duplex containing ODN6'tC_4: 5'– CGCTATAT **tC** TATATCGC –3'). Data recorded at 22 ^{o}C in PBS buffer (pH=7.4) and DNA concentrations were kept at 2.0 μM.

Because ^{ts}T and tC retain the hydrogen bonds necessary for establishing WCF base-pairs, they should be rigidly fixed in a DNA double-helix structure *via* hydrogen bonds and stacking interactions. This assumption is supported by thermal melting experiments (Table B4 and Figures B4 and B5, Appendix B). We measured the static fluorescence spectra of double-stranded DNA carrying both the donor and the acceptor at various positions (Figure 3.11B and Figure B6, Appendix). For *ds*-tC (which lacks the FRET donor) a weak fluorescence of tC was observed at ^{ts}T excitation wavelength (310 nm). However, in the presence of the donor (*ds*-^{ts}T/tC), the fluorescence of tC enhanced and the fluorescence of ^{ts}T decreased, indicating an effective energy transfer between ^{ts}T and tC (Figure 3.11B, and Figure B6, Appendix B). Comparison between GC-rich DNA (ODN7, Figure B6C, Appendix) with AT-rich DNA (ODN6, Figure B6D, Appendix) showed the nucleobases between FRET donor and acceptor have a negligible effect on FRET efficiency (Table 3.5).

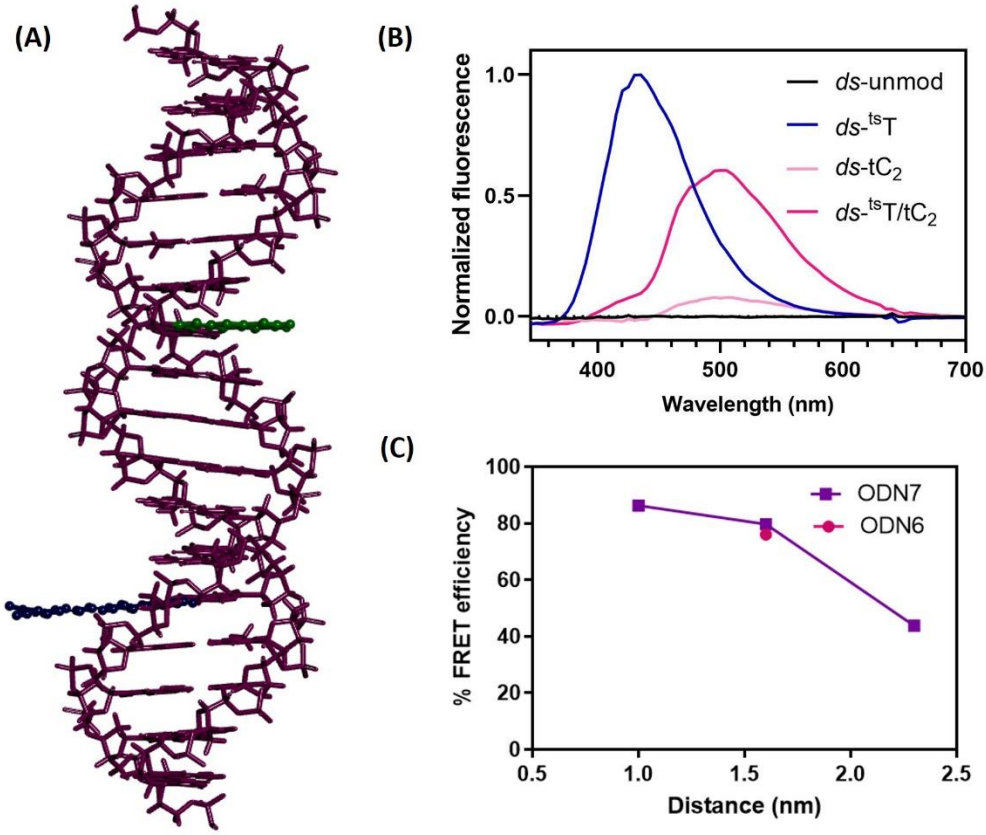

Figure 3.11. (A) DNA model (ODN7, sequence: 5'– GCGA **^{ts}T** CGCGCGCTAGCG –3') generated using the Discovery Studio package.[97] The structures of ^{ts}T (shown by blue stick) and tC (shown by green stick) were superimposed onto the native thymidine and cytosines at the desired positions with GaussView version 6.1.[98] (B) The normalized fluorescence emission of unmodified duplex (*ds*-unmod) and duplexes containing only ^{ts}T (*ds*-^{ts}T), only tC (*ds*-tC_2), and ^{ts}T/tC pair (*ds*-^{ts}T/tC_2), where tC is located two bps away from ^{ts}T. The excitation wavelength was 310 nm, and ODN7 was used in the experiment. (C) FRET efficiency in ^{ts}T/tC pair as a function of the distance between donor and acceptor, plotted for ODN7 and ODN6 duplexes (ODN6 sequence is 5'– GCGA **^{ts}T** ATAGATATAGCG –3'). Measurements were recorded at 22 ^{o}C in PBS buffer (pH = 7.4). DNA concentrations were kept at 2.0 µM.

As the distance between donor and acceptor was increased, the FRET efficiency decreased. Even though the orientation dependency of our FRET pair could not be observed, future studies using tC positioned five bps away from ^{ts}T could provide some insight. This is because in canonical right-handed B-form DNA, the helical twist angle, that is, the rotating angle of the base-pairs with respect to the helical axis, is approximately 34.3° per one base-pair.[99-100] Therefore, a valley of FRET efficiency should appear at approximately five base-pairs (180/34.3 ≈ 5.25).[101] Nevertheless, to our surprise,

the calculated Förster radius (R_0) — the distance at which 50% energy transfer occurs— for ^{ts}T/tC pair was exceptionally small (1.5–2.0 nm), compared with previously reported FRET pairs.[102-104] This suggests ^{ts}T/tC pair is highly sensitive to small distances within the angstrom range and can be employed as a spectroscopic ruler.[105] The application of FRET systems in studying the B → Z helical transition has already been demonstrated.[106] The high sensitivity of ^{ts}T/tC FRET pair towards small changes in distances may enable probing the B → A secondary structure switching and other conformational changes.

Table 3.5. FRET efficiency, quenching efficiency, Förster radius (R_0) and distance between ^{ts}T and tC in duplexes containing ODN6 or ODN7 and their complementary strands containing tC at different locations.[a]

Oligonucleotides		Sequences	FRET efficiency (%)	Quenching efficiency (%)	R_0 (nm)	d (nm)
ODN7	*ds*-^{ts}T/tC$_2$	5′– GCGA **^{ts}T** C G CGCGCTAGCG –3′ 3′– CGCT A G **tC** GCGCGATCGC –5′	86.3	90.5	1.46	1.0
	ds-^{ts}T/tC$_4$	5′– GCGA **^{ts}T** CGC G CGCTAGCG –3′ 3′– CGCT A GCG **tC** GCGATCGC –5′	79.7	80.9	2.04	1.6
	ds-^{ts}T/tC$_6$	5′– GCGA **^{ts}T** CGCGC G CTAGCG –3′ 3′– CGCT A GCGCG **tC** GATCGC –5′	43.8	31.1	2.01	2.3
ODN6	*ds*-^{ts}T/tC$_4$	5′– GCGA **^{ts}T** ATA G ATATAGCG –3′ 3′– CGCT A TAT **tC** TATATCGC –5′	76.0	73.0	1.61	1.6

[a] All measurements were performed at 22 °C, PBS buffer and pH = 7.4. DNA concentrations = 2.0 μM.

3.5 Summary

In summary, ^{ts}T is one of the brightest and most microenvironmentally sensitive FBAs reported to date ($\varepsilon \times \varphi$ = 150 – 29,700 cm^{-1} M^{-1}). The fluorescence lifetime of ^{ts}T (τ = 4 – 11 ns) is on the same time scale as local dynamic motions of base-pair mismatches (0.1 – 10 ns),[63, 107-108] yet faster than the global anisotropy decay of ^{ts}T in duplex DNA (θ = 20 ns). These properties together enable unprecedented sensitivity and specificity in the detection of an adenine residue in the complement strand. In addition to highly sensitive matched/mismatched base-pair discrimination, ^{ts}T has provided insights into the fundamental dynamic behavior of duplex and single-stranded DNA using TCSPC experiments. The exceptional brightness and sensitivity of ^{ts}T may enable other types of demanding

applications, such as tracking of single-molecule dynamics.[109] Thanks to the high sensitivity of ^{ts}T, we now know duplex perturbation by a mismatch or an abasic site does not dramatically alter the local dynamics $\geq$3 base-pairs away. Furthermore, since the HOMO energy level of ^{ts}T is higher than the HOMO of natural DNA bases but lower than the HOMO of OG, its fluorescence can selectively get quenched by this DNA oxidative damage. We have shown ^{ts}T can sense an OG even up to 2 nm distances and an MG up to 1 nm distances. In addition, ^{ts}T/tC can be used as a FRET donor/acceptor system, to probe dynamic changes over short distances and local conformational changes.[110]

3.6 Experimental

3.6.1 Theoretical computations

The molecular geometries and thermal corrections were optimized with B3LYP DFT functional theory[111] paired with the 6-31++G(d) basis set.[112] Calculations were performed in the water phase (C-PCM algorithm)[113] at 298.15 K. The first frequency was utilized to assess whether structures were in their true optimized form. Conformers distributions were executed using Spartan,[114] and Gaussian 16[115] was used to calculate orbital energies. In order to simplify calculations, deoxyribose (dR) was replaced with a methyl group.

To calculate the distance between FRET donor and acceptor, DNA models were generated using the Discovery Studio package.[97] The structures of ^{ts}T and tC were superimposed onto the native thymidine and cytosines at the desired positions with GaussView version 6.1.[98]

3.8.2 Oligomer synthesis, purification and folding

Synthesis: Unmodified oligonucleotides and those containing OG modification were purchased from Sigma-Aldrich as HPLC-purified products. Standard DNA phosphoramidites, solid supports, and all necessary reagents were purchased from LinkTech and Sigma-Aldrich. MG- and tC-modified oligonucleotides were synthesized on a 1.0 µmol scale using a Bioautomation Co. Mermade 4 DNA synthesizer according to the Trityl-off procedure. Three coupling reactions were performed for the site-specific introduction of the modified nucleoside into oligonucleotides. MG phosphoramidite (N-isobutyryl protected) and tC phosphoramidite were purchased from Glen Research and dissolved in dry acetonitrile (0.1 M) immediately prior to use. The synthesis of the oligonucleotides was monitored by DMT deprotection. Upon completion of the sequences, MG-modified oligonucleotides were cleaved from the solid support and deprotected by 1 mL of 10% DBU (1,8-Diazabicyclo[5.4.0]undec-7-ene) in anhydrous methanol in a glass vial. After keeping the solution at r.t for 5 days in the dark, the volume was reduced under vacuum and 1 mL, 10 mM aqueous sodium hydroxide solution was added. The tC-modified oligonucleotides were cleaved from the solid support and deprotected by treatment with 1.0 mL of 33 % aqueous ammonium hydroxide at 55 ^{o}C overnight in a 1.5 mL screw-top cap tube.

Purification: The obtained solutions were lyophilized to dryness and purified by HPLC column chromatography using a semi-prep C-18 reverse-phase column (YMCbasic B-22-10P 150 x 10 mm) using a Varian 140 Pro Star HPLC system. The gradient conditions were typically acetonitrile: 0.1 M triethylammonium acetate (TEAA, pH 7.4), 2:98 to 10:90 over 35 minutes and with rate of 3.00 mL/min. Elution was monitored by UV absorption at 260 nm (for MG-modified oligonucleotides) and 395 nm (for tC-modified oligonucleotides). Peaks were collected and twice lyophilized to dryness from water. The purities of MG and tC containing oligonucleotides were found to be >90% (260 nm) according to analytical, reverse-phase chromatography using a Waters XBridge C8, 5 µm 4.6 x 150 mm. A gradient of 5–40% of acetonitrile in 0.1 M triethylammonium acetate (TEAA, pH 7.4), was applied over 35 minutes at 0.4 mL/min. Oligonucleotides were analyzed by LC-MS using a Dionex Ultimate 3000 UHPLC coupled to a Bruker Maxis Impact QTOF in negative ESI mode. Samples were run through a Phenomenex Luna C18(2)-HST column (2.5 µM 120A 2.1 x 100 mm) using a gradient of 90% mobile phase A (100 mM HFIP and 5 mM TEA in H_2O) and 10% mobile phase B (MeOH) to 40% mobile phase A and 60% mobile phase B in 20 minutes. The data was processed and spectra deconvoluted using the Bruker DataAnalysis software version 4.2.

Folding: Oligonucleotide stock solutions were prepared in deionized water and their concentrations were determined by absorbance at 260 nm using the molar extinction coefficient calculated using a nearest-neighbor model.[116] The molar extinction coefficient of tC nucleotides at 260 nm was taken from the previous report (12,150 $cm^{-1}M^{-1}$)[95] and the molar extinction coefficient of MG was estimated to be the same as G.[117] Calculated extinction coefficients of ^{ts}T-modified oligonucleotides are available in Table 2.4 (Chapter 2) and the extinction coefficients of synthesized MG- and tC-modified oligonucleotides are presented in Table B5, Appendix B. Double stranded oligonucleotides were prepared by diluting the complementary sequences (1.0 : 1.2 equiv. ratio) in the PBS buffer (pH = 7.4, Na^+ concentration of ≈137 mM) and heating to 95 °C for 5 min, followed by slow cooling to room temperature over 4 h. In the FRET experiment, since both complementary strands were fluorescently labeled, a 1.0 : 1.0 ratio of single-stranded DNAs were used for annealing.

3.8.3 Biophysical experiments

Fluorescence spectroscopy: Oligonucleotide stock solutions were diluted into PBS buffer (pH = 7.4, Na+ concentration of ≈137 mM) to a final concentration of 2.0 µM using their extinction

coefficient at 260 nm. All measurements were collected on a Molecular Devices SpectraMax M5 in a 1 cm path-length quartz cuvette. Quantum yields were calculated using the most red-shifted absorbance maxima of samples. Quinine hemisulfate (φ_R = 0.546) in 0.5 M H_2SO_4 (n_R = 1.346) was used as the fluorescent standard. Quantum yields were calculated using the equation shown below[92]:

$$\Phi = \Phi_{\mathrm{R}} \frac{F}{F_{\mathrm{R}}} \frac{A_{\mathrm{R}}}{A} \frac{n^2}{{n_{\mathrm{R}}}^2}$$

where φ_R is the quantum yield of the fluorescent standard, F and F_R are the integrated emissions of the sample and reference respectively. A and A_R are the optical densities of the sample and reference respectively (both set to 0.10 ± 0.01). n and n_R are the refractive indexes of the sample and reference respectively.

Melting Temperature Analysis (T_m): UV thermal denaturation data were obtained by measuring the absorbance at 260 nm as a function of temperature in a 1 cm path length thermo-controlled strain-free quartz cuvette on a Varian CARY 100 UV-visible spectrophotometer equipped with a Peltier temperature controller. Solutions of pre-folded duplex DNA (0.2 µM) in aqueous buffer (PBS buffer, pH = 7.4) were equilibrated at 20 °C for a minimum of 10 min and slowly ramped to 90 °C with 0.2 °C steps at a rate of 12 °C h^{-1}. The melting temperatures were determined from the maximal slope of the curve (maximal first derivative). T_m values were calculated as the average from the heating and cooling curves that showed little or no hysteresis.

Fluorescence Lifetime and Dynamic Anisotropy of Oligonucleotides: TCSPC experiments employed a picosecond laser source (DD-310L, Horiba Jobin Yvon GmbH) at a repetition rate of 10 MHz in combination with a double-grating emission monochromator and a PPD-900 detection module (Fluorolog3 FL3-222, Horiba). Samples were kept at 25 °C by means of a Varian Cary PCB-150 Peltier water bath (Agilent). The fluorescence lifetime τ_F was collected with a channel width of 27 ps and retrieved from one exponential decay by iterative reconvolution with the instrument response function (IRF) using a custom-written MATLAB routine (R2019b).[118]

$$I(t) = IRF * e^{-t/\tau_F} \qquad \text{(Eq. B1)}$$

The time-resolved anisotropy was computed by sequentially recording the parallel I_{VV} and perpendicular I_{VH} polarization components with respect to the field vector of the exciting light pulse

$$r(t) = \frac{I_{VV} - GI_{VH}}{I_{VV} - 2GI_{VH}} \quad \text{(Eq. B2)}$$

where the *G*-factor is defined as $G = I_{HV}/I_{HH}$.[92] The dynamic anisotropy of the dye-labeled DNA molecules is best described by a single-rotor model

$$\mathrm{r}(t) = (r_0 - r_\infty)e^{-t/\theta} + r_\infty \quad \text{(Eq. B3)}$$

where r_0 is the fundamental anisotropy, r_∞ represents the value to which the local anisotropy decays and ϑ is the rotational decay time.[6]

Based on the rotational decay time, the hydrodynamic radius of the construct assuming a globular shape of the molecule and a strong coupling of ^{ts}T and the host-molecule can be calculated according to

$$R_H = \sqrt[3]{\frac{3k_B T \cdot \theta}{4\pi \cdot \eta}} \quad \text{(Eq. B4)}$$

and the angle between the absorption and emission dipole is calculated

$$\beta = \cos^{-1}\sqrt{\frac{5 \cdot r_0 + 1}{3}} \quad \text{(Eq. B5)}$$

The steady-state anisotropy <*r*> is calculated with

$$\langle r \rangle = r_0 / (1 + \tau_F/\theta) \quad \text{(Eq. B6)}$$

FRET analysis: FRET experiments conducted on 2.0 µM solution of DNA duplexes in PBS buffer (pH = 7.4). The following equations were used to calculate the FRET and quenching efficiencies.

FRET efficiency = $(I_{DA,\,500}) / [\,(I_{DA,\,435}) + (I_{DA,\,500})]$ (Eq. B7)

Quenching efficiency = $1 - [(I_{DA,\,435}) / (I_{D,\,435})]$ (Eq. B8)

where fluorescence intensities (I) at 435 nm and 500 nm were used for donor and acceptor emission intensity, respectively. R_0 calculated using the following equation:

FRET efficiency = $R_0^6 / (R_0^6 + d^6)$ (Eq. B8)

where d is the distance between ^{ts}T and tC.

3.9 Appendix B

3.9.1 Tables

Table B1. Photophysical properties of oligonucleotides containing ^{ts}T[a, b]

Oligonucleotides		λ_{em} max (nm)	φ	Εφ (cm^{-1} M^{-1})
ODN1	^{ts}T:A	440	0.139	4,250
	^{ts}T:G	445	0.017	520
	^{ts}T:C	440	0.005	150
	^{ts}T:T	440	0.005	150
	ss-^{ts}T	445	0.028	860
ODN2	^{ts}T:A	440	0.098	3,000
	^{ts}T:T	440	0.012	370
	ss-^{ts}T	440	0.020	610
ODN3	^{ts}T:A	440	0.134	4,100
	ss-^{ts}T	445	0.026	800

[a] The average extinction coefficient (Ɛ) of ^{ts}T in DNA at 310 nm is 30,600 ± 700 cm^{-1} M^{-1}.
[b] All measurements were performed at 22 °C in PBS buffer (pH = 7.4), with DNA concentrations = 2.0 μM.

Table B2. Synthesized oligomers with their extinction coefficient (Ɛ) at 260 nm and calculated and observed masses.

Oligonucleotides	Sequences (5′ → 3′)	$Ɛ_{260}$ ($cm^{-1}M^{-1}$)	Calc. (m/z)	Found (m/z)	δ (ppm)
ODN7′MG	CGCTAGCGCGCG **MG** TCGC	149,000	5199.8957	5200.0781	35.1
ODN7′MG1	CGCTAGCGCGC **MG** ATCGC	152,000	5183.9007	5184.0625	31.2
ODN7′MG3	CGCTAGCGC **MG** CGATCGC	152,000	5183.9007	5184.0156	22.2
ODN7′MG5	CGCTAGC **MG** CGCGATCGC	152,000	5183.9007	5184.0156	22.2
ODN7′tC_2	CGCTAGCGCG **tC** GATCGC	157,000	5275.8734	5275.8438	5.6
ODN7′tC_4	CGCTAGCG **tC** GCGATCGC	157,000	5275.8734	5275.8945	4.0
ODN7′tC_6	CGCTAG **tC** GCGCGATCGC	157,000	5275.8734	5275.8828	1.8
ODN6′tC_4	CGCTATAT **tC** TATATCGC	165,000	5223.8692	5223.8125	10.9

Table B3. Calculated [b3lyp/6-31++G(d)] HOMO and LUMO energy values (eV) in water phase.

	^{ts}T	MG	OG	G	A	C	T
LUMO	-1.99	-0.68	-1.06	-0.78	-1.08	-1.17	-1.33
HOMO	-5.85	-5.81	-5.75	-6.16	-6.38	-6.58	-6.63

Table B4. Biophysical properties of duplexes containing ODN6 or ODN7 and their complementary strands containing tC at different locations.[a, b]

Oligonucleotides		Sequences	*T*m (°C)	I_{435}	I_{500}
ODN7	*ds*-unmod	5′– GCGATCGCGCGCTAGCG –3′ 3′– CGCTAGCGCGCGATCGC –5′	58.6	0.00	0.00
	ds-^{ts}T	5′– GCGA **^{ts}T** CGCGCGCTAGCG –3′ 3′– CGCT A GCGCGCGATCGC –5′	64.1	1.00	0.30
	ds-^{ts}T/tC$_2$	5′– GCGA **^{ts}T** C G CGCGCTAGCG –3′ 3′– CGCT A G **tC** GCGCGATCGC –5′	57.4	0.10	0.60
	ds-tC$_2$	5′– GCGATC G CGCGCTAGCG –3′ 3′– CGCTAG **tC** GCGCGATCGC –5′	58.6	0.00	0.08
	ds-^{ts}T/tC$_4$	5′– GCGA **^{ts}T** CGC G CGCTAGCG –3′ 3′– CGCT A GCG **tC** GCGATCGC –5′	56.3	0.19	0.75
	ds-tC4	5′– GCGATCGC G CGCTAGCG –3′ 3′– CGCTAGCG **tC** GCGATCGC –5′	58.2	0.00	0.11
	ds-^{ts}T/tC$_6$	5′– GCGA **^{ts}T** CGCGC G CTAGCG –3′ 3′– CGCT A GCGCG **tC** GATCGC –5′	55.0	0.69	0.54
	ds-tC$_6$	5′– GCGATCGCGC G CTAGCG –3′ 3′– CGCTAGCGCG **tC** GATCGC –5′	57.6	0.02	0.09
ODN6	*ds*-unmod	5′– GCGATATAGATATAGCG –3′ 3′– CGCTATATCTATATCGC –5′	55.4	0.00	0.00
	ds-^{ts}T	5′– GCGA **^{ts}T** ATAGATATAGCG –3′ 3′– CGCT A TATCTATATCGC –5′	52.3	0.84	0.28
	ds-^{ts}T/tC$_4$	5′– GCGA **^{ts}T** ATA G ATATAGCG –3′ 3′– CGCT A TAT **tC** TATATCGC –5′	55.2	0.23	0.71
	ds-tC$_4$	5′– GCGATATA G ATATAGCG –3′ 3′– CGCTATAT **tC** TATATCGC –5′	56.9	0.00	0.10

[a] The average extinction coefficient (Ɛ) of ^{ts}T in DNA at 310 nm is 30600 ± 700 cm^{-1} M^{-1}.

[b] All measurements were performed at 22 °C in PBS buffer (pH = 7.4), with DNA concentrations = 2.0 µM.

3.9.2 Figures

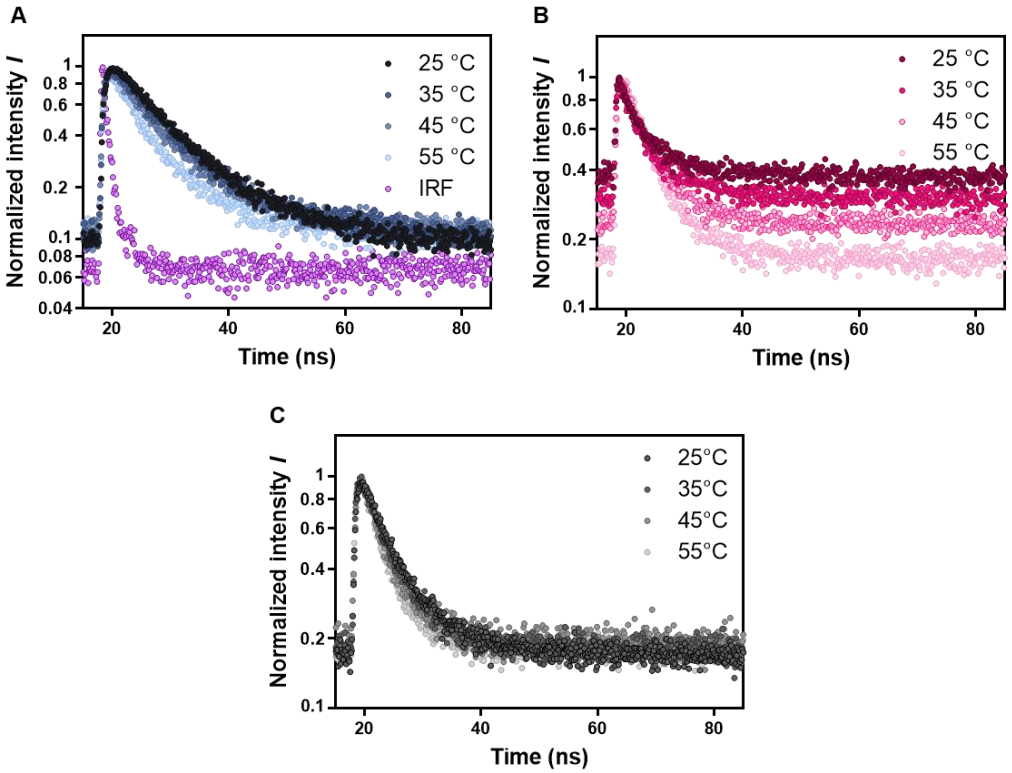

Figure B1. Fluorescence lifetime data for ODN1 constructs (A) *ds*-^{ts}T:A, (B) *ds*-^{ts}T:T and (C) *ss*-^{ts}T at different temperatures reaching the melting temperature of the *ds*-DNA at 55 °C.

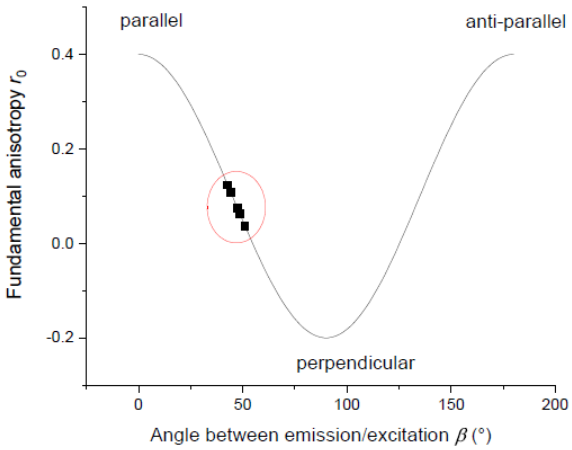

Figure B2. The dependency of fundamental anisotropy of the ODN1 samples (*ss*-^{ts}T:T and *ds*-^{ts}T:T at 25 ^{o}C and *ds*-^{ts}T:A at 25, 35 and 55 ^{o}C) to the angle between emission and excitation dipole moment.

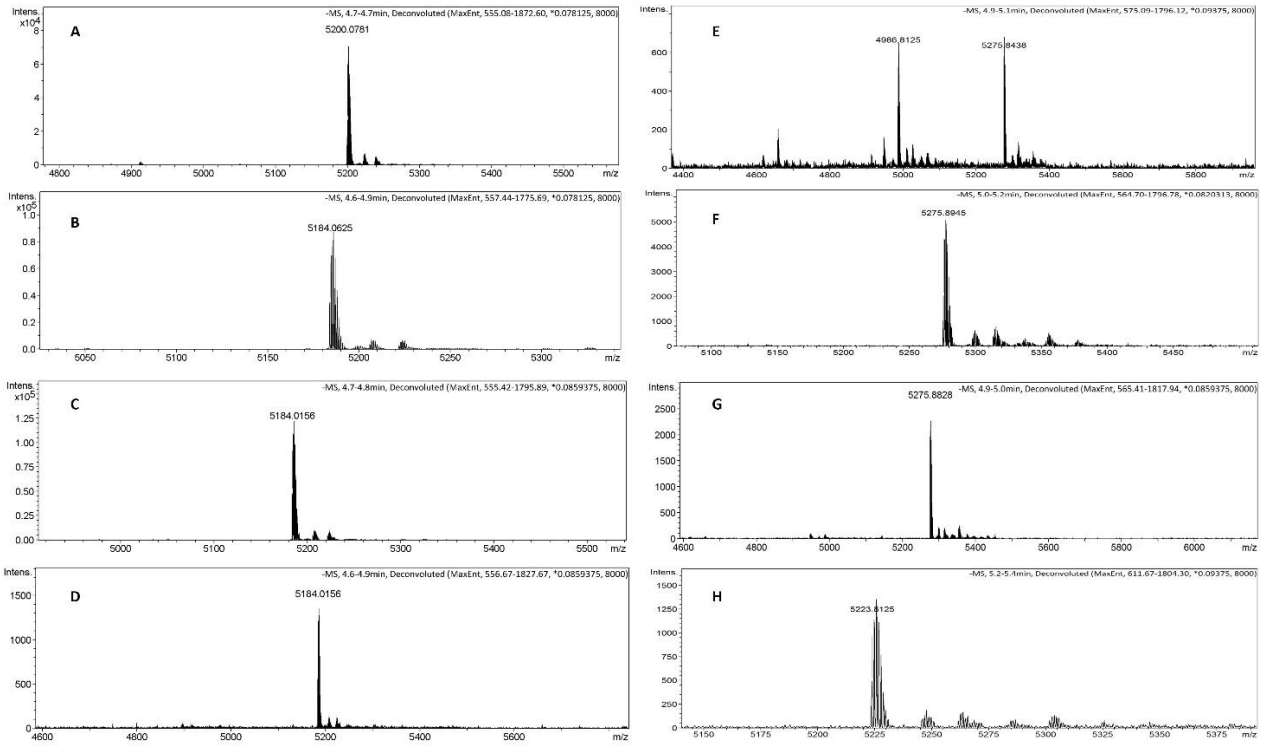

Figure B3. ESI-MS analysis of (A) ODN7'MG, (B) ODN7'MG1, (C) ODN7'MG3, (D) ODN7'MG5, (E) ODN7'tC_2, (F) ODN7'tC_4, (G) ODN7'tC_6, and (H) ODN6'tC_4.

.

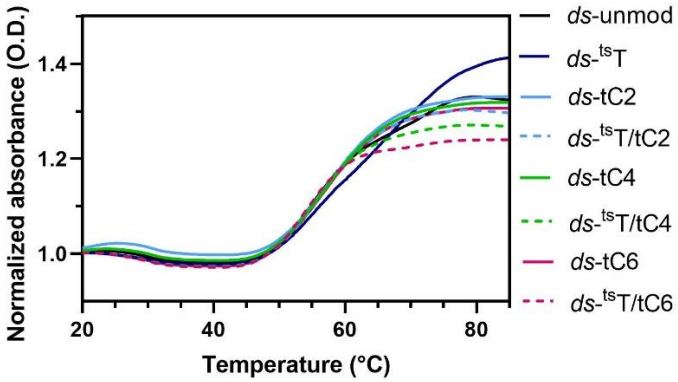

Figure B4. Normalized thermal melting data of unmodified duplex (*ds*-unmod) and duplexes containing only ^{ts}T (*ds*-^{ts}T), ^{ts}T/tC pair (*ds*-$^{ts}T/tC_n$), where tC is located n base-pairs away from ^{ts}T, and only tC (*ds*-tC_n). ODN7 was used in the experiment. Data were recorded in PBS buffer (pH = 7.4). DNA concentrations were kept at 0.2 µM.

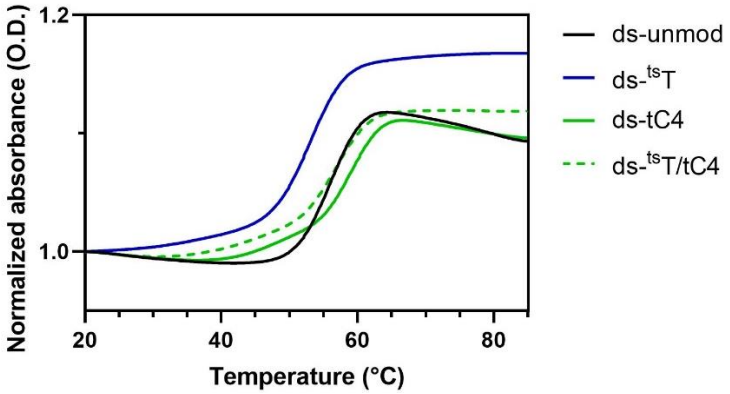

Figure B5. Normalized thermal melting data of unmodified duplex (*ds*-unmod) and duplexes containing only ^{ts}T (*ds*-^{ts}T), ^{ts}T/tC pair (*ds*-^{ts}T/tC$_4$), where tC is located four base-pairs away from ^{ts}T, and only tC (*ds*-tC$_4$). ODN6 was used in the experiment. Data were recorded in PBS buffer (pH = 7.4). DNA concentrations were kept at 0.2 µM.

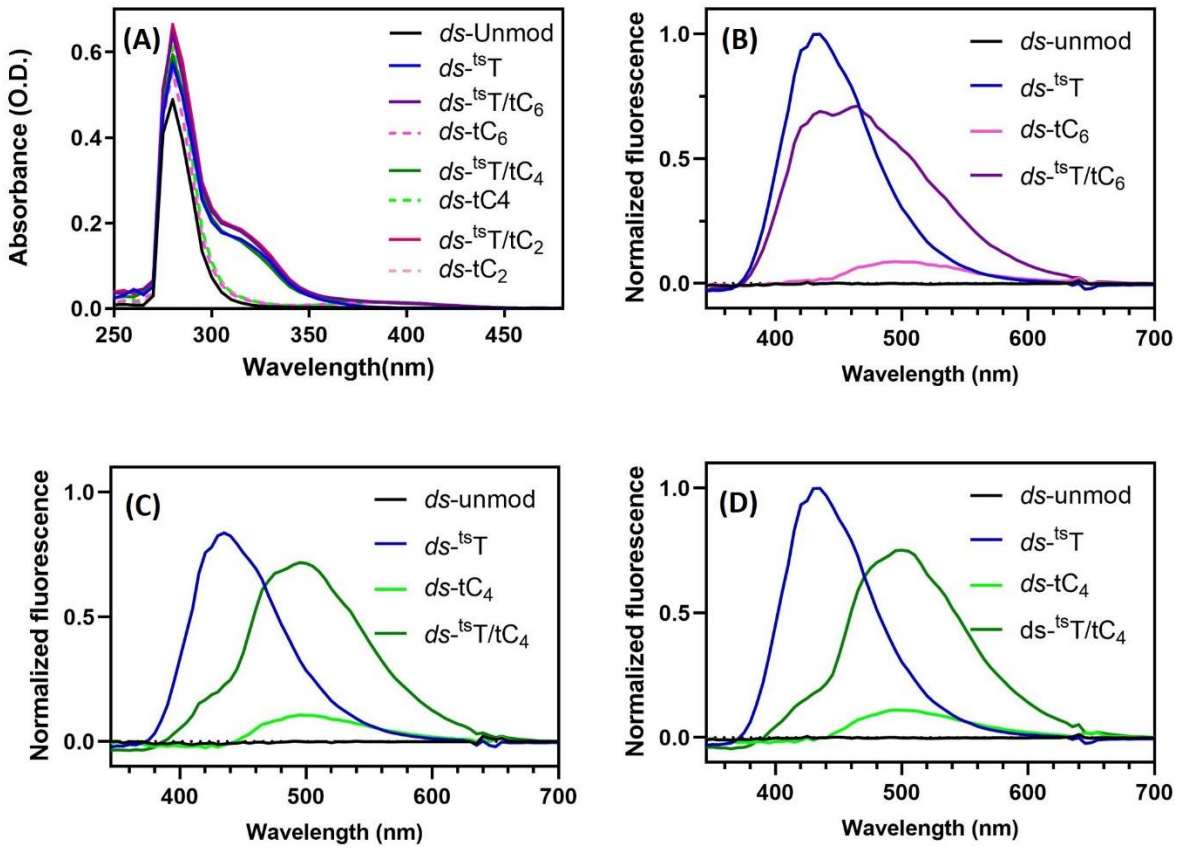

Figure B6. (A) The normalized absorbance and (B–D) normalized fluorescence emission of unmodified duplex (*ds*-unmod) and duplexes containing only ^{ts}T (*ds*-^{ts}T), only tC (*ds*-tC$_n$), and ^{ts}T/tC pair (*ds*-^{ts}T/tC$_n$), where tC is located n base-pairs away from ^{ts}T. The excitation wavelength was 310 nm. ODN7 was used in (B) and (C) and ODN6 was used (D). Data were recorded at 22 ^{o}C in PBS buffer (pH = 7.4). DNA concentrations were kept at 2.0 µM.

3.10 References

[1] Vignal, A.; Milan, D.; SanCristobal, M.; Eggen, A., A review on SNP and other types of molecular markers and their use in animal genetics. *Genet. Sel. Evol.* **2002,** *34* (3), 275-305.

[2] Sobrino, B.; Brión, M.; Carracedo, A., SNPs in forensic genetics: a review on SNP typing methodologies. *Forensic Sci. Int.* **2005,** *154* (2-3), 181-194.

[3] Venkatesan, N.; Seo, Y. J.; Kim, B. H., Quencher-free molecular beacons: a new strategy in fluorescence based nucleic acid analysis. *Chem. Soc. Rev.* **2008,** *37* (4), 648-663.

[4] Krasheninina, O. A.; Novopashina, D. S.; Apartsin, E. K.; Venyaminova, A. G., Recent advances in nucleic acid targeting probes and supramolecular constructs based on pyrene-modified oligonucleotides. *Molecules* **2017,** *22* (12).

[5] Liu, L.; Shao, Y.; Peng, J.; Liu, H.; Zhang, L., Selective recognition of ds-DNA cavities by a molecular rotor: switched fluorescence of thioflavin T. *Mol. Biosyst.* **2013,** *9* (10), 2512-2519.

[6] Fang, X.; Mi, Y.; Li, J. J.; Beck, T.; Schuster, S.; Tan, W., Molecular beacons. *Cell Biochem. Biophys.* **2002,** *37* (2), 71-81.

[7] Tan, L.; Li, Y.; Drake, T. J.; Moroz, L.; Wang, K.; Li, J.; Munteanu, A.; James Yang, C.; Martinez, K.; Tan, W., Molecular beacons for bioanalytical applications. *Analyst* **2005,** *130* (7), 1002-1005.

[8] Huang, K.; Martí, A. A., Recent trends in molecular beacon design and applications. *Anal. Bioanal. Chem.* **2012,** *402* (10), 3091-3102.

[9] Kuang, T.; Chang, L.; Peng, X.; Hu, X.; Gallego-Perez, D., Molecular beacon nano-sensors for probing living cancer cells. *Trends Biotechnol.* **2017,** *35* (4), 347-359.

[10] Tyagi, S.; Kramer, F. R., Molecular beacons: probes that fluoresce upon hybridization. *Nat. Biotechnol.* **1996,** *14* (3), 303-308.

[11] Piatek, A. S.; Tyagi, S.; Pol, A. C.; Telenti, A.; Miller, L. P.; Kramer, F. R.; Alland, D., Molecular beacon sequence analysis for detecting drug resistance in Mycobacterium tuberculosis. *Nat. Biotechnol.* **1998,** *16* (4), 359-363.

[12] Tyagi, S.; Bratu, D. P.; Kramer, F. R., Multicolor molecular beacons for allele discrimination. *Nat. Biotechnol.* **1998,** *16* (1), 49-53.

[13] Hwang, G. T., Single-labeled oligonucleotides showing fluorescence changes upon hybridization with target nucleic acids. *Molecules* **2018,** *23* (1), 124.

[14] Sinkeldam, R. W.; Wheat, A. J.; Boyaci, H.; Tor, Y., Emissive nucleosides as molecular rotors. *Chemphyschem* **2011,** *12* (3), 567-570.

[15] Seidel, C. A. M.; Schulz, A.; Sauer, M. H. M., Nucleobase-specific quenching of fluorescent dyes. 1. Nucleobase one-electron redox potentials and their correlation with static and dynamic quenching efficiencies. *J. Phys. Chem.* **1996,** *100* (13), 5541-5553.

[16] Luo, G.; Zheng, L.; Zhang, X.; Zhang, J.; Nilsson-Ehle, P.; Xu, N., Genotyping of single nucleotide polymorphisms using base-quenched probe: a method does not invariably depend on the deoxyguanosine nucleotide. *Anal. Biochem.* **2009,** *386* (2), 161-166.

[17] Crockett, A. O.; Wittwer, C. T., Fluorescein-labeled oligonucleotides for real-time pcr: using the inherent quenching of deoxyguanosine nucleotides. *Anal. Biochem.* **2001,** *290* (1), 89-97.

[18] Kurata, S.; Kanagawa, T.; Yamada, K.; Torimura, M.; Yokomaku, T.; Kamagata, Y.; Kurane, R., Fluorescent quenching-based quantitative detection of specific DNA/RNA using a BODIPY((R)) FL-labeled probe or primer. *Nucleic Acids Res.* **2001,** *29* (6), E34.

[19] Xiang, D. S.; Zhai, K.; Wang, L. Z., Multiplexed DNA detection with a composite molecular beacon based on guanine-quenching. *Analyst* **2013,** *138* (18), 5318-5324.

[20] Vaughn, C. P.; Elenitoba-Johnson, K. S. J., Hybridization-induced dequenching of fluorescein-labeled oligonucleotides: A novel strategy for PCR detection and genotyping. *Am. J. Pathol.* **2003,** *163* (1), 29-35.

[21] Asseline, U.; Chassignol, M.; Aubert, Y.; Roig, V., Detection of terminal mismatches on DNA duplexes with fluorescent oligonucleotides. *Org. Biomol. Chem.* **2006,** *4* (10), 1949-1957.

[22] Köhler, O.; Jarikote, D. V.; Seitz, O., Forced intercalation probes (FIT Probes): thiazole orange as a fluorescent base in peptide nucleic acids for homogeneous single-nucleotide-polymorphism detection. *Chembiochem* **2005,** *6* (1), 69-77.

[23] Jarikote, D. V.; Krebs, N.; Tannert, S.; Röder, B.; Seitz, O., Exploring base-pair-specific optical properties of the DNA stain thiazole orange. *Chemistry (Easton)* **2007,** *13* (1), 300-310.

[24] Bethge, L.; Singh, I.; Seitz, O., Designed thiazole orange nucleotides for the synthesis of single labelled oligonucleotides that fluoresce upon matched hybridization. *Org. Biomol. Chem.* **2010,** *8* (10), 2439-2448.

[25] Ishiguro, T.; Saitoh, J.; Yawata, H.; Otsuka, M.; Inoue, T.; Sugiura, Y., Fluorescence detection of specific sequence of nucleic acids by oxazole yellow-linked oligonucleotides. Homogeneous quantitative monitoring of in vitro transcription. *Nucleic Acids Res.* **1996,** *24* (24), 4992-4997.

[26] Ward, D. C.; Reich, E.; Stryer, L., Fluorescence studies of nucleotides and polynucleotides. I. Formycin, 2-aminopurine riboside, 2,6-diaminopurine riboside, and their derivatives. *J. Biol. Chem.* **1969,** *244* (5), 1228-1237.

[27] Dueymes, C.; Décout, J. L.; Peltié, P.; Fontecave, M., Fluorescent deazaflavin–oligonucleotide probes for selective detection of DNA. *Angew. Chem. Int. Ed.* **2002,** *41* (3), 486-489.

[28] Okamoto, A.; Tainaka, K.; Saito, I., Synthesis and properties of a novel fluorescent nucleobase, naphthopyridopyrimidine. *Tetrahedron Lett.* **2003,** *44* (36), 6871-6874.

[29] Hawkins, M. E.; Balis, F. M., Use of pteridine nucleoside analogs as hybridization probes. *Nucleic Acids Res.* **2004,** *32* (7), e62.

[30] Okamoto, A.; Tainaka, K.; Saito, I., Clear distinction of purine bases on the complementary strand by a fluorescence change of a novel fluorescent nucleoside. *J. Am. Chem. Soc.* **2003,** *125* (17), 4972-4973.

[31] Okamoto, A.; Tanaka, K.; Fukuta, T.; Saito, I., Design of base-discriminating fluorescent nucleoside and its application to t/c snp typing. *J. Am. Chem. Soc.* **2003,** *125* (31), 9296-9297.

[32] Suzuki, A.; Yanaba, T.; Saito, I.; Saito, Y., Molecular design of an environmentally sensitive fluorescent nucleoside, 3-deaza-2'-deoxyadenosine derivative: Distinguishing thymine by probing the DNA minor groove. *Chembiochem* **2014,** *15* (11), 1638-1644.

[33] Mata, G.; Luedtke, N. W., Synthesis and solvatochromic fluorescence of biaryl pyrimidine nucleosides. *Org. Lett.* **2013,** *15* (10), 2462-2465.

[34] Bielecka, P.; Dembska, A.; Juskowiak, B., Monitoring of pH using an i-motif-forming sequence containing a fluorescent cytosine analogue, tC. *Molecules* **2019,** *24* (5), 952.

[35] Greco, N. J.; Tor, Y., Simple fluorescent pyrimidine analogues detect the presence of DNA abasic sites. *J. Am. Chem. Soc.* **2005,** *127* (31), 10784-10785.

[36] Tanpure, A. A.; Srivatsan, S. G., A microenvironment-sensitive fluorescent pyrimidine ribonucleoside analogue: synthesis, enzymatic incorporation, and fluorescence detection of a DNA abasic site. *Chem. Eur. J.* **2011,** *17* (45), 12820-12827.

[37] Saito, Y.; Suzuki, A.; Okada, Y.; Yamasaka, Y.; Nemoto, N.; Saito, I., An environmentally sensitive fluorescent purine nucleoside that changes emission wavelength upon hybridization. *Chem. Commun.* **2013,** *49* (50), 5684-5686.

[38] Greco, N. J.; Sinkeldam, R. W.; Tor, Y., An emissive C analog distinguishes between G, 8-oxoG, and T. *Org. Lett.* **2009,** *11* (5), 1115-1118.

[39] Suzuki, A.; Nemoto, N.; Saito, I.; Saito, Y., Design of an environmentally sensitive fluorescent 8-aza-7-deaza-2'-deoxyadenosine derivative with dual fluorescence for the specific detection of thymine. *Org. Biomol. Chem.* **2014,** *12* (4), 660-666.

[40] Tanpure, A. A.; Srivatsan, S. G., Synthesis and photophysical characterisation of a fluorescent nucleoside analogue that signals the presence of an abasic site in RNA. *Chembiochem* **2012,** *13* (16), 2392-2399.

[41] Kashida, H.; Yamaguchi, K.; Hara, Y.; Asanuma, H., Quencher-free molecular beacon tethering 7-hydroxycoumarin detects targets through protonation/deprotonation. *Bioorg Med Chem* **2012,** *20* (14), 4310-4315.

[42] Siraiwa, S.; Suzuki, A.; Katoh, R.; Saito, Y., Design and synthesis of a novel fluorescent benzo[g]imidazo[4,5-c]quinoline nucleoside for monitoring base-pair-induced protonation with cytosine: distinguishing cytosine via changes in the intensity and wavelength of fluorescence. *Org. Biomol. Chem.* **2016,** *14* (16), 3934-3942.

[43] Johnson, A.; Karimi, A.; Luedtke, N. W., Enzymatic incorporation of a coumarin–guanine base pair. *Angew. Chem. Int. Ed.* **2019,** *58* (47), 16839-16843.

[44] Wojciechowski, F.; Hudson, R. H. E., Fluorescence and hybridization properties of peptide nucleic acid containing a substituted phenylpyrrolocytosine designed to engage guanine with an additional H-bond. *J. Am. Chem. Soc.* **2008,** *130* (38), 12574-12575.

[45] Hudson, R. H. E.; Ghorbani-Choghamarani, A., Selective fluorometric detection of guanosine-containing sequences by 6-phenylpyrrolocytidine in DNA. *Synlett* **2007,** *2007* (06), 870-873.

[46] Schmidt, O. P.; Jurt, S.; Johannsen, S.; Karimi, A.; Sigel, R. K. O.; Luedtke, N. W., Concerted dynamics of metallo-base pairs in an A/B-form helical transition. *Nat. Commun.* **2019,** *10* (1), 4818.

[47] Brunet, A.; Salomé, L.; Rousseau, P.; Destainville, N.; Manghi, M.; Tardin, C., How does temperature impact the conformation of single DNA molecules below melting temperature? *Nucleic Acids Res.* **2018,** *46* (4), 2074-2081.

[48] Torigoe, H.; Ono, A.; Kozasa, T., HgII ion specifically binds with T:T mismatched base pair in duplex DNA. *Chem. Eur. J.* **2010,** *16* (44), 13218-13225.

[49] Schmidt, O. P.; Benz, A. S.; Mata, G.; Luedtke, N. W., HgII binds to C–T mismatches with high affinity. *Nucleic Acids Res.* **2018,** *46* (13), 6470-6479.

[50] Sandin, P.; Börjesson, K.; Li, H.; Mårtensson, J.; Brown, T.; Wilhelmsson, L. M.; Albinsson, B., Characterization and use of an unprecedentedly bright and structurally non-perturbing fluorescent DNA base analogue. *Nucleic Acids Res.* **2008,** *36* (1), 157-167.

[51] Bonifacio, G. F.; Brown, T.; Conn, G. L.; Lane, A. N., Comparison of the electrophoretic and hydrodynamic properties of DNA and RNA oligonucleotide duplexes. *Biophys. J.* **1997,** *73* (3), 1532-1538.

[52] Fernandes, M. X.; Ortega, A.; Lopez Martinez, M. C.; Garcia de la Torre, J., Calculation of hydrodynamic properties of small nucleic acids from their atomic structure. *Nucleic Acids Res.* **2002,** *30* (8), 1782-1788.

[53] Roth, E.; Glick Azaria, A.; Girshevitz, O.; Bitler, A.; Garini, Y., Measuring the conformation and persistence length of single-stranded DNA using a DNA origami structure. *Nano Lett.* **2018,** *18* (11), 6703-6709.

[54] Abels, J. A.; Moreno-Herrero, F.; van der Heijden, T.; Dekker, C.; Dekker, N. H., Single-molecule measurements of the persistence length of double-stranded RNA. *Biophys. J.* **2005,** *88* (4), 2737-2744.

[55] Mariam, J.; Krishnamoorthy, G.; Anand, R., Use of 6-methylisoxanthopterin, a fluorescent guanine analog, to probe Fob1-mediated dynamics at the stalling fork barrier DNA sequences. *Chem. Asian J.* **2019,** *14* (24), 4760-4766.

[56] Datta, K.; Johnson, N. P.; Villani, G.; Marcus, A. H.; von Hippel, P. H., Characterization of the 6-methyl isoxanthopterin (6-MI) base analog dimer, a spectroscopic probe for monitoring guanine base conformations at specific sites in nucleic acids. *Nucleic Acids Res.* **2011,** *40* (3), 1191-1202.

[57] Hawkins, M. E.; Pfleiderer, W.; Balis, F. M.; Porter, D.; Knutson, J. R., Fluorescence properties of pteridine nucleoside analogs as monomers and incorporated into oligonucleotides. *Anal. Biochem.* **1997,** *244* (1), 86-95.

[58] Johnson, J.; Okyere, R.; Joseph, A.; Musier-Forsyth, K.; Kankia, B., Quadruplex formation as a molecular switch to turn on intrinsically fluorescent nucleotide analogs. *Nucleic Acids Res.* **2012,** *41* (1), 220-228.

[59] Tinland, B.; Pluen, A.; Sturm, J.; Weill, G., Persistence length of single-stranded DNA. *Macromolecules* **1997,** *30* (19), 5763-5765.

[60] Uzawa, T.; Cheng, R. R.; Cash, K. J.; Makarov, D. E.; Plaxco, K. W., The length and viscosity dependence of end-to-end collision rates in single-stranded DNA. *Biophys. J.* **2009,** *97* (1), 205-210.

[61] Doose, S.; Barsch, H.; Sauer, M., Polymer properties of polythymine as revealed by translational diffusion. *Biophys. J.* **2007,** *93* (4), 1224-1234.

[62] Sim, A. Y.; Lipfert, J.; Herschlag, D.; Doniach, S., Salt dependence of the radius of gyration and flexibility of single-stranded DNA in solution probed by small-angle x-ray scattering. *Phys. Rev. E Stat. Nonlin. Soft Matter Phys.* **2012,** *86* (2 Pt 1), 021901.

[63] Rossetti, G.; Dans, P. D.; Gomez-Pinto, I.; Ivani, I.; Gonzalez, C.; Orozco, M., The structural impact of DNA mismatches. *Nucleic Acids Res.* **2015,** *43* (8), 4309-4321.

[64] Kyrtopoulos, S. A.; Ampatzi, P.; Davaris, P.; Haritopoulos, N.; Golematis, B., Studies in gastric carcinogenesis. IV. O6-Methylguanine and its repair in normal and atrophic biopsy specimens of human gastric mucosa. Correlation of O6-alkylguanine-DNA alkyltransferase activities in gastric mucosa and circulating lymphocytes. *Carcinogenesis* **1990,** *11* (3), 431-436.

[65] Kyrtopoulos, S. A., DNA adducts in humans after exposure to methylating agents. *Mutat. Res.* **1998,** *405* (2), 135-143.

[66] Mirvish, S. S., Role of N-nitroso compounds (NOC) and N-nitrosation in etiology of gastric, esophageal, nasopharyngeal and bladder cancer and contribution to cancer of known exposures to NOC. *Cancer Lett.* **1995,** *93* (1), 17-48.

[67] Rydberg, B.; Lindahl, T., Nonenzymatic methylation of DNA by the intracellular methyl group donor S-adenosyl-L-methionine is a potentially mutagenic reaction. *EMBO J.* **1982,** *1* (2), 211-216.

[68] Harrison, K. L.; Jukes, R.; Cooper, D. P.; Shuker, D. E., Detection of concomitant formation of O6-carboxymethyl- and O6-methyl-2'-deoxyguanosine in DNA exposed to nitrosated glycine derivatives using a combined immunoaffinity/HPLC method. *Chem. Res. Toxicol.* **1999,** *12* (1), 106-111.

[69] Sedgwick, B., Nitrosated peptides and polyamines as endogenous mutagens in O6-alkylguanine-DNA alkyltransferase deficient cells. *Carcinogenesis* **1997,** *18* (8), 1561-1567.

[70] Li, X.; Qian, S.; Zheng, L.; Yang, B.; He, Q.; Hu, Y., A mechanism-based fluorescent probe for labeling O6-methylguanine-DNA methyltransferase in live cells. *Org. Biomol. Chem.* **2012,** *10* (16), 3189-3191.

[71] Le, D.-V.; Jiang, J.-H., Fluorescence determination of the activity of O6-methylguanine-DNA methyltransferase based on the activation of restriction endonuclease and the use of graphene oxide. *Microchimica Acta* **2020,** *187* (5), 300.

[72] Radak, Z.; Boldogh, I., 8-Oxo-7,8-dihydroguanine: links to gene expression, aging, and defense against oxidative stress. *Free Radic. Biol. Med.* **2010,** *49* (4), 587-596.

[73] Kasai, H.; Nishimura, S., Hydroxylation of deoxyguanosine at the C-8 position by ascorbic acid and other reducing agents. *Nucleic Acids Res.* **1984,** *12* (4), 2137-2145.

[74] Tchou, J.; Kasai, H.; Shibutani, S.; Chung, M. H.; Laval, J.; Grollman, A. P.; Nishimura, S., 8-oxoguanine (8-hydroxyguanine) DNA glycosylase and its substrate specificity. *Proc. Natl. Acad. Sci. U. S. A.* **1991,** *88* (11), 4690-4694.

[75] Ilya Dementyev, A. K., A molecular dynamical investigation of the 7,8-dihydro-8-oxoguanine mutation in dsDNA. *MSURJ* **2021,** *16* (1), 25-30.

[76] Cheng, K. C.; Cahill, D. S.; Kasai, H.; Nishimura, S.; Loeb, L. A., 8-Hydroxyguanine, an abundant form of oxidative DNA damage, causes G----T and A----C substitutions. *J. Biol. Chem.* **1992,** *267* (1), 166-172.

[77] Edwards, S. K.; Ono, T.; Wang, S.; Jiang, W.; Franzini, R. M.; Jung, J. W.; Chan, K. M.; Kool, E. T., In vitro fluorogenic real-time assay of the repair of oxidative DNA damage. *Chembiochem* **2015,** *16* (11), 1637-1646.

[78] Lee, C. Y.; Park, K. S.; Park, H. G., Pyrrolo-dC modified duplex DNA as a novel probe for the sensitive assay of base excision repair enzyme activity. *Biosens Bioelectron* **2017,** *98*, 210-214.

[79] Ono, S.; Li, Z.; Koga, Y.; Tsujimoto, A.; Nakagawa, O.; Sasaki, S., Development of a specific fluorescent probe for 8-oxoguanosine. *Nucleic Acids Symp. Ser.* **2007,** (51), 315-316.

[80] Wilson, D. L.; Kool, E. T., Fluorescent probes of DNA repair. *ACS Chem. Biol.* **2018,** *13* (7), 1721-1733.

[81] Zhu, R.-Y.; Majumdar, C.; Khuu, C.; De Rosa, M.; Opresko, P. L.; David, S. S.; Kool, E. T., Designer fluorescent adenines enable real-time monitoring of MUTYH activity. *ACS Cent. Sci.* **2020,** *6* (10), 1735-1742.

[82] Doose, S.; Neuweiler, H.; Sauer, M., Fluorescence quenching by photoinduced electron transfer: A reporter for conformational dynamics of macromolecules. *Chemphyschem* **2009,** *10* (9-10), 1389-1398.

[83] Ciccia, A.; Elledge, S. J., The DNA damage response: Making it safe to play with knives. *Mol. Cell* **2010,** *40* (2), 179-204.

[84] Steenken, S.; Jovanovic, S. V., How easily oxidizable is DNA? One-electron reduction potentials of adenosine and guanosine radicals in aqueous solution. *J. Am. Chem. Soc.* **1997,** *119* (3), 617-618.

[85] Fujitsuka, M.; Majima, T., Charge transfer dynamics in DNA revealed by time-resolved spectroscopy. *Chem. Sci.* **2017,** *8* (3), 1752-1762.

[86] Lin, S.-H.; Fujitsuka, M.; Majima, T., Sequence-dependent photocurrent generation through long-distance excess-electron transfer in DNA. *Angew. Chem. Int. Ed.* **2016,** *55* (30), 8715-8717.

[87] Narayanan, M.; Kodali, G.; Xing, Y.; Stanley, R. J., Photoinduced electron transfer occurs between 2-aminopurine and the DNA nucleic acid monophosphates: Results from cyclic voltammetry and fluorescence quenching. *J. Phys. Chem. B* **2010,** *114* (32), 10573-10580.

[88] Tanaka, M.; Elias, B.; Barton, J. K., DNA-mediated electron transfer in naphthalene-modified oligonucleotides. *J. Org. Chem.* **2010,** *75* (8), 2423-2428.

[89] Wagenknecht, H.-A., Electron transfer processes in DNA: mechanisms, biological relevance and applications in DNA analytics. *Nat. Prod. Rep.* **2006,** *23* (6), 973-1006.

[90] Wagenknecht, H.-A., Reductive electron transfer and transport of excess electrons in DNA. *Angew. Chem. Int. Ed.* **2003,** *42* (22), 2454-2460.

[91] Förster, T., Energy migration and fluorescence. 1946. *J. Biomed. Opt.* **2012,** *17* (1), 011002.

[92] Lakowicz, J. R., *Principles of fluorescence spectroscopy*. 3rd ed.; Springer: New York, 2006.

[93] Preus, S.; Wilhelmsson, L. M., Advances in quantitative FRET-based methods for studying nucleic acids. *Chembiochem* **2012,** *13* (14), 1990-2001.

[94] Zhao, Y.; Cui, X.; Ge, Z.; Meng, Q.; Zhang, C., Unusual photophysical properties of fluorescent cytosine analogues utilized in real-time detecting i-motif DNA: A theoretical study. *J. Lumin.* **2021,** *240*, 118442.

[95] Sandin, P.; Wilhelmsson, L. M.; Lincoln, P.; Powers, V. E. C.; Brown, T.; Albinsson, B., Fluorescent properties of DNA base analogue tC upon incorporation into DNA — negligible influence of neighbouring bases on fluorescence quantum yield. *Nucleic Acids Res.* **2005,** *33* (16), 5019-5025.

[96] Preus, S.; Jønck, S.; Pittelkow, M.; Dierckx, A.; Karpkird, T.; Albinsson, B.; Wilhelmsson, L. M., The photoinduced transformation of fluorescent DNA base analogue tC triggers DNA melting. *Photochem. Photobiol. Sci.* **2013,** *12* (8), 1416-1422.

[97] BIOVIA, D. S., BIOVIA Discovery Studio Visualizer, v16.1.0.15350. *San Diego: Dassault Systèmes* **2015**.

[98] Keith, T. A. M., J. M., GaussView, Version 6.1. *Roy Dennington, Semichem Inc., Shawnee Mission, KS* **2016**.

[99] Dickerson, R. E., Definitions and nomenclature of nucleic acid structure components. *Nucleic Acids Res.* **1989,** *17* (5), 1797-1803.

[100] Olson, W. K.; Bansal, M.; Burley, S. K.; Dickerson, R. E.; Gerstein, M.; Harvey, S. C.; Heinemann, U.; Lu, X. J.; Neidle, S.; Shakked, Z.; Sklenar, H.; Suzuki, M.; Tung, C. S.; Westhof, E.; Wolberger, C.; Berman, H. M., A standard reference frame for the description of nucleic acid base-pair geometry. *J. Mol. Biol.* **2001,** *313* (1), 229-237.

[101] Hirashima, S.; Sugiyama, H.; Park, S., Construction of a FRET system in a double-stranded DNA using fluorescent thymidine and cytidine analogs. *J. Phys. Chem. B* **2020,** *124* (40), 8794-8800.

[102] Massey, M.; Algar, W. R.; Krull, U. J., Fluorescence resonance energy transfer (FRET) for DNA biosensors: FRET pairs and Förster distances for various dye–DNA conjugates. *Anal. Chim. Acta* **2006,** *568* (1), 181-189.

[103] Muschielok, A.; Andrecka, J.; Jawhari, A.; Brückner, F.; Cramer, P.; Michaelis, J., A nano-positioning system for macromolecular structural analysis. *Nat. Methods* **2008,** *5* (11), 965-971.

[104] Bood, M.; Sarangamath, S.; Wranne, M. S.; Grøtli, M.; Wilhelmsson, L. M., Fluorescent nucleobase analogues for base-base FRET in nucleic acids: synthesis, photophysics and applications. *Beilstein J. Org. Chem.* **2018,** *14*, 114-129.

[105] Sahoo, H.; Roccatano, D.; Hennig, A.; Nau, W. M., A 10-Å spectroscopic ruler applied to short polyprolines. *J. Am. Chem. Soc.* **2007,** *129* (31), 9762-9772.

[106] Dumat, B.; Larsen, A. F.; Wilhelmsson, L. M., Studying Z-DNA and B- to Z-DNA transitions using a cytosine analogue FRET-pair. *Nucleic Acids Res.* **2016,** *44* (11), e101.

[107] Shweta, H.; Singh, M. K.; Yadav, K.; Verma, S. D.; Pal, N.; Sen, S., Effect of T·T mismatch on DNA dynamics probed by minor groove binders: Comparison of dynamic Stokes shifts of Hoechst and DAPI. *J. Phys. Chem. B* **2017,** *121* (48), 10735-10748.

[108] Isaacs, R. J.; Rayens, W. S.; Spielmann, H. P., Structural differences in the noe-derived structure of G–T mismatched DNA relative to normal DNA are correlated with differences in 13C relaxation-based internal dynamics. *J. Mol. Biol.* **2002,** *319* (1), 191-207.

[109] Nobis, D.; Fisher, R. S.; Simmermacher, M.; Hopkins, P. A.; Tor, Y.; Jones, A. C.; Magennis, S. W., Single-molecule detection of a fluorescent nucleobase analogue via multiphoton excitation. *J. Phys. Chem. Lett* **2019,** *10* (17), 5008-5012.

[110] Didenko, V. V., DNA probes using fluorescence resonance energy transfer (FRET): designs and applications. *Biotechniques* **2001,** *31* (5), 1106-1121.

[111] Zhao, Y.; Schultz, N. E.; Truhlar, D. G., Exchange-correlation functional with broad accuracy for metallic and nonmetallic compounds, kinetics, and noncovalent interactions. *J Chem Phys* **2005,** *123* (16), 161103.

[112] Hariharan, P. C.; Pople, J. A., The influence of polarization functions on molecular orbital hydrogenation energies. *Theor. Chim. Acta* **1973,** *28* (3), 213-222.

[113] Cossi, M.; Barone, V., Time-dependent density functional theory for molecules in liquid solutions. *J. Chem. Phys.* **2001,** *115* (10), 4708-4717.

[114] W. Hehre, J. Y., P. Klunzinger, L. Lou, Wavefunction Inc. *Irvine, CA* **2008**.

[115] Frisch, M. J., Gaussian, Inc. *Wallingford, CT* **2010**.

[116] Cantor, C. R.; Warshaw, M. M.; Shapiro, H., Oligonucleotide interactions. 3. Circular dichroism studies of the conformation of deoxyoligonucleotides. *Biopolymers* **1970,** *9* (9), 1059-1077.

[117] Abner, C. W.; Lau, A. Y.; Ellenberger, T.; Bloom, L. B., Base excision and DNA binding activities of human alkyladenine DNA glycosylase are sensitive to the base paired with a lesion. *J. Biol. Chem.* **2001,** *276* (16), 13379-13387.

[118] Enderlein, J.; Erdmann, R., Fast fitting of multi-exponential decay curves. *Opt. Commun.* **1997,** *134* (1), 371-378.

Chapter 4 | ^{ts}C probes folding of *i*-motif structures

"***Fold*** and live to fold again"

Stu Ungar

4.1 Introduction: Single-stranded secondary structures

Duplex DNA dissociates into single strands during DNA replication, transcription, and repair. This allows the kinetic access to single-stranded secondary structures, such as hairpin, triplex, G-quadruplex or *i*-motif structures (Figure 4.1).[1-2] These structures are topologically distinct, providing unique recognition sites for proteins and small molecules that mediate gene expression, recombination, and chromosome stability.[3-6] For example, it was suggested that triplex DNA might act as a regulator of DNA replication or transcription by blocking DNA or RNA polymerase and thereby initiating termination of DNA/RNA synthesis.[7-8] G-quadruplex forming sequences can be found throughout the entire human genome with a high frequency in the telomeric regions of eukaryotic chromosomes and the promoter regions of many proto-oncogenes.[9-11] Mounting evidence suggests that G-quadruplexes play roles in regulating gene expression, recombination and programmed cell death.[12]

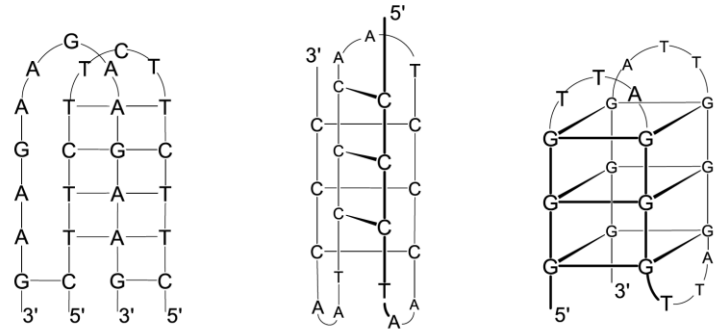

Figure 4.1 Schematic representation of selected DNA secondary structures triplex, *i*-motif, and G-quadruplex.

4.1.1 Triplex structures

Intermolecular triplex DNA formation occurs by sequence-specific binding of a triplex-forming oligonucleotide (TFO) to a duplex DNA. The TFO binds to the major groove of duplex DNA either in a parallel or *anti*-parallel fashion.[13-14] Binding of the TFO to duplex DNA occurs *via* non-canonical *Hoogsteen* hydrogen bonding without disrupting the *WCF* hydrogen bond of the duplex DNA to form base triads (Figure 4.2A). Polypyrimidine TFOs bind to polypurine tracks in duplexes *via* the formation

of C^+-GC and T-AT triads in a parallel fashion (Figure 4.2B). Polypurine TFOs bind in an *anti*-parallel fashion *via* A-AT, G-GC, and T-AT triads.[13-14]

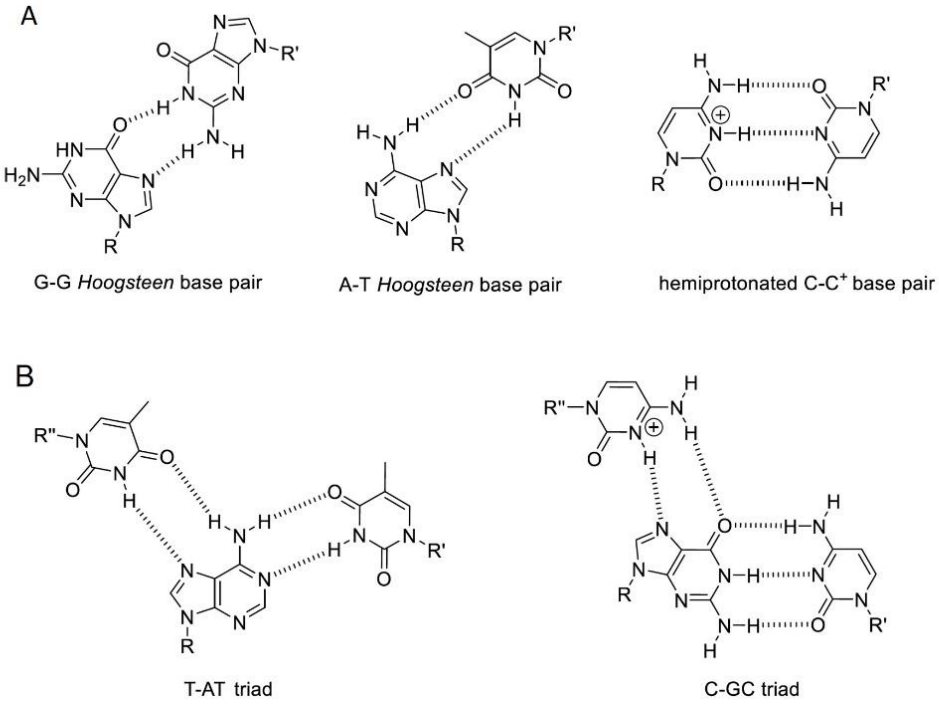

Figure 4.2. (A) Examples of non-canonical base-pairs. (B) Examples of triads formed in triplex DNA structures.

4.1.2 G-quadruplex structures

Nucleic acid sequences containing stretches of sequential guanosines can fold into four-stranded structures known as G-quadruplexes (Figure 4.1).[15-16] A G-quadruplex consists of planar G-tetrads stacked upon each other with a monovalent ion such as K^+ or Na^+ intercalated between each tetrad. Four guanosines associate *via WCF* and *Hoogsteen* base-pairing to form each tetrad (Figure 4.2A).[15-18] A wide variety of different G-quadruplex conformations have been reported. They can form in an intermolecular fashion to give tetrameric, dimeric, or monomeric G-quadruplexes, or can be assembled in an intramolecular fashion. The adjacent strands can have either a parallel or an *anti*-parallel orientation. Depending on the type of G-quadruplex, the glycosidic bonds can be *syn* or *anti*.[11, 19]

4.1.3 *i*-Motif structures

C-rich sequences can fold into *i*-motif structures at slightly acidic pH (Figure 4.1).[20] Two strands of duplex DNA containing hemiprotonated C:C$^+$ base-pairs (Figure 4.2A) can intercalate in an *anti*-parallel fashion to form a four stranded *i*-motif structure. Alternatively, a single-strand can form an *i*-motif in an intramolecular fashion. Various types of different *i*-motif structures can form depending on the number of base-pairs, loop topology, and environmental conditions.[21-23] The spatial arrangement of proton-bound dimers of cytosine results in two broad and flat major grooves and two extremely narrow minor grooves. The degree of freedom of the base-pairs in *i*-motif DNA is relatively limited. Although, propeller twist and buckling are allowed within each base-pair, *i*-motifs exclude shifts, rolls and twisting of the stacked base-pairs.[20] The helical twist between adjacent C-C$^+$ pairs (12-17°) is much smaller than B-DNA (36°) or A-DNA (32.7°). The lifetime of the proton-bound dimers are very short for the outermost pairs (≈ 1 ms) and relatively long for the innermost pairs (≈ 1 hour),[24] which suggest some dynamics from the residues adjacent to the loop region. X-ray crystallographic analyses demonstrated that *i*-motifs have high densities of nucleobases, due to compact interactions between four-stranded segments, as well as C-H$^+$-C base-pairs that exhibit an unusually close base-stacking distances (3.1 Å) as compared to B-form duplex DNA (3.4 Å).[25-26]

The stability of *i*-motif DNA strongly depends on external factors such as ionic strength, temperature, pH, and hydration.[27-28] Since the protonation of the cytosine residues is a requirement for folding; the pH plays a crucial role in the stability of the structure. Cytosine is the most intrinsically basic canonical nucleobase, with a pK_a = 4.2 for its conjugate acid in water.[29-30] The maximal stability of the *i*-motif occurs at pH values near the pK_a of cytosine, but long-range electrostatic and local hydrogen bonding interactions can raise the effective pK_a of protonated cytidine residues in folded structures.[21] The apparent pK_a values for cytosine residues in *i*-motif structures are typically in the range of 5.5–6.6 *in vitro*.[31] In addition, pK_a values of cytosines can reach values close to or even above 7, in the presence of molecular crowding conditions,[32-35] modifications,[36] small molecule binding,[37-39] metals,[40-42] minor groove tetrads,[43-45] or with certain sequences[43, 46] and strand lengths.[47]

Due to the self-complementarity nature of duplex DNA, G-quadruplex and *i*-motif structures can exist in a dynamic equilibrium with the double-stranded DNA.[48] The double helix is more stable than the corresponding single-stranded DNAs folded into intramolecular structures at physiological

conditions of pH and temperature. The combination of multiple factors such as protein binding,[49-51] molecular crowding,[34] and negative supercoiling[52] could be responsible for shifting the equilibrium toward intramolecular structures and increasing the marginal stability of *i*-motif DNA under physiological conditions. Cytosine-rich sequences are present throughout the human genome, and putative *i*-motif forming sequences have been found in more than 40% of gene promoter regions.[9] Stable *i*-motif structures were reported in several oncogenes, such as VEGF,[53] RET,[54] c-MYC[55] and Rb.[56] Finally, in 2018, the formation of *i*-motif DNA structures in the nuclei of human cells provided strong evidence that *i*-motif structures can potentially form in regulatory regions of the human genome, including promoters and telomeric regions.[57]

The biological relevance of the equilibrium between duplex DNA and *i*-motif structures *in vivo*, has strongly encouraged the development of sensitive methods for the direct detection of *i*-motif DNA structures.[58] Fluorescent labels are frequently used to modify *i*-motif DNA sequences for sensing purposes.[59] Miscellaneous fluorescence parameters are exploited, for example, quenching,[60] anisotropy change,[61] FRET signal,[62-63] or excimer emission signal.[64-65] *Pei* reported Neutral Red (Figure 4.3A), as the first light-up fluorescent probe for *i*-motif DNA.[66] In addition, a ratiometric fluorescent probe with ultra pH-sensitivity was developed based on hairpin-contained *i*-motif strand (labeled with Rhodamine Green and BHQ2 at two termini) and complementary strand (labeled with Rhodamine Red).[67] Despite the large number of FBAs that have been extensively used to probe and detect diverse DNA structures, only a few have been reported to sense *i*-motif structures. Previous challenges to making FBAs suitable for detecting *i*-motif structures include: (1) the fluorescent cytidine analogs undergo protonation under acidic conditions, and subsequently their HOMO energy level significantly decreases. Thus, their fluorescence is quenched in the protonated form *via* PET from non-protonated nucleobases; (2) in the neutral pH and within the duplex form, the complementary G-rich sequence can effectively quench the fluorescence of FBA by PET.[68] As a result, most of the FBAs remain in the dark state in both *i*-motif and duplex structures, thereby limiting their sensitivity in real-time tracking of *i*-motif → duplex transitions. Some FBAs that have been used for *i*-motif detection are presented below.

Our group reported ^{DMA}C (Figure 4.3B) as the first FBA suitable for tracking proton-coupled DNA folding. ^{DMA}C showed little-to-no perturbation of DNA structure or stability when incorporated into the telomeric repeat sequence.[60] Upon protonation of ^{DMA}C, its fluorescence decreased and red-

shifted. Thus, ^{DMA}C's fluorescence intensity could be used for real-time tracking of the conformational changes by altering the pH and/or initiating a strand-displacement reaction. Other FBAs previously incorporated into *i*-motif structures include tC, tC^{o} and pC (Figure 4.3B). The fluorescence of these probes was pH-sensitive and red-shifted upon *i*-motif formation.[69-71] However, all these FBAs have very low brightness in *i*-motif and thus limited applications. Recently, *Sugiyama*'s group reported ^{FP}C (Figure 4.3B) as a highly fluorescent probe (εφ = 1,920 $M^{-1}cm^{-1}$) for *i*-motif DNA, which also could be used in ^{19}F-NMR. However, when ^{FP}C was located in an internal position, it destabilized the *i*-motif structure.

Inspired by the brightness and high sensitivity of ^{ts}T towards DNA dynamics,[72] we synthesized cytidine analog, ^{ts}C (Figure 4.3) and incorporated it into C-rich sequences. This chapter describes the fluorescence properties of ^{ts}C and its impact on the thermal stability of folded DNA structures. In addition, the potential of ^{ts}C in probing conformational changes which involve *i*-motif structures will be discussed.

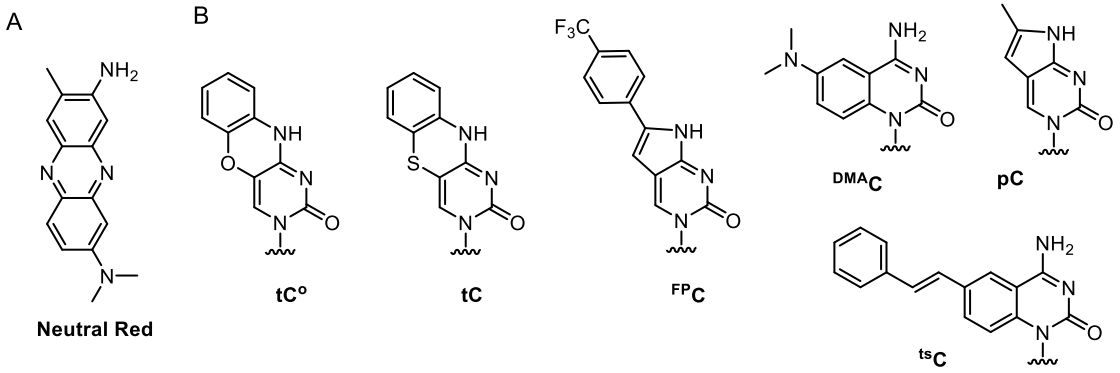

Figure 4.3. (A) An intercalating fluorescent probe that exhibits higher fluorescence intensity when it binds to *i*-motif DNA. (B) FBAs that can sense and report *i*-motif structures.

4.2 Synthesis and photophysical properties of ^{ts}C nucleoside

Synthesis commenced from the conversion of the previously prepared silyl-protected ^{ts}T (**8a**, Chapter 2), into the cytidine analog, by treating it with 2,4,6-triisopropylbenzene-sulfonyl chloride (iPr_3PhSO_2Cl) followed by aqueous ammonia (Scheme 4.1). This two-step procedure afforded silyl-

protected ^{ts}C (**12**) in a 63% yield. In the next step, benzoic anhydride was used to synthesize silyl/benzoyl-protected ^{ts}C (**13**) in an 87% yield. This protects the amino group during the solid-phase DNA synthesis in the next steps. The silyl groups were cleaved with TBAF to give the benzoyl-protected ^{ts}C nucleoside (**14**) in a 76% isolated yield.

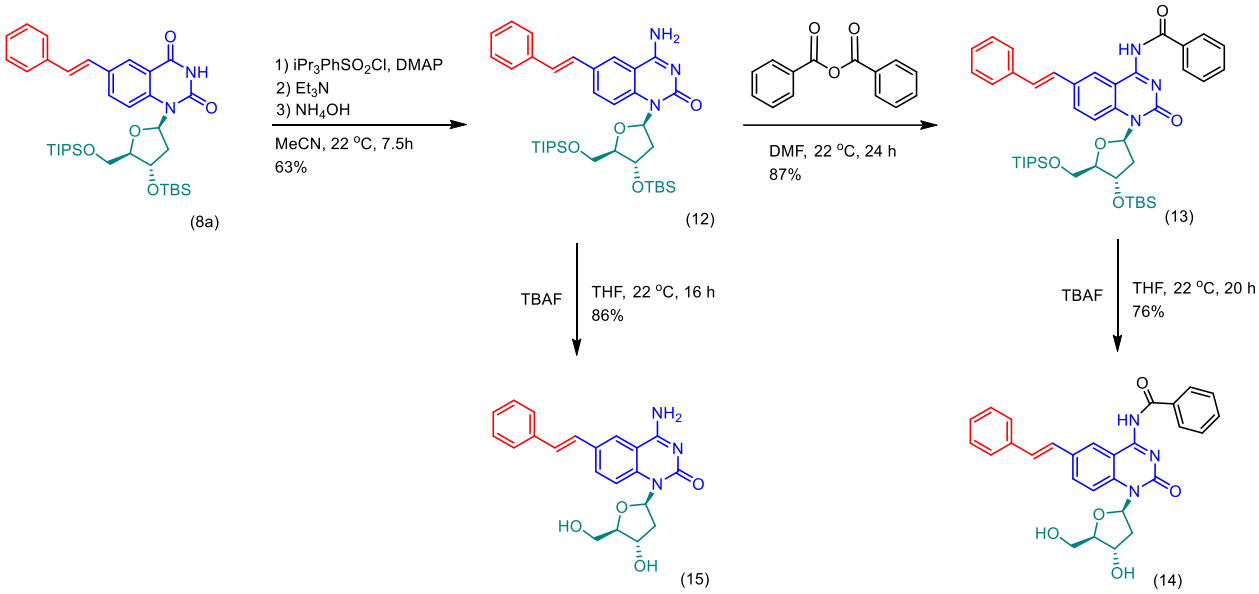

Scheme 4.1. Synthesis of the ^{ts}C nucleoside. TMSOTf = trimethylsilyl trifluoromethanesulfonate, TBS = *tert*-butyldimethylsilyl, DMAP = 4-dimethylaminopyridine, DMF = dimethylformamide, TBAF = tetra-*n*-butylammoniumfluoride, THF = tetrahydrofuran.

To conduct photophysical experiments on the deprotected free nucleoside, **12** was treated with TBAF to yield **15** with 86% isolated yield (Scheme 4.1). The maximal absorbance wavelengths of **15** (λ_{abs} = 310 – 320 nm, Table 4.1) are red-shifted enough to allow selective excitation in the context of DNA. Depending on the solvent polarity, ^{ts}C exhibits highly variable quantum yields (φ = 0.07 – 0.28) and maximal fluorescence emission wavelengths (λ_{em} = 425 – 455 nm), shown in Table 4.1.

To systematically characterize the microenvironmental sensitivity of ^{ts}C, and compare it with ^{ts}T, *Stokes* shifts of **15** were plotted against Reichardt's solvent polarity parameter (E_T^{30}), and a linear slope of 84 cm^{-1}/kcal.mol^{-1} was observed (Figure 4.4A). Although this suggests that ^{ts}C is a push-pull fluorophore and has a TICT excited state, the slope was lower than what was previously reported for ^{ts}T **9** (101 cm^{-1}/kcal.mol^{-1}, Figure 2.6A, Chapter 2). To further evaluate the potential of ^{ts}C as a fluorescent molecular rotor, the absorption and fluorescence emission properties of nucleoside **15**

were measured in various mixtures of methanol and glycerol. Consistent with rotation-induced fluorescent quenching, the quantum yield of ^{ts}C increased with increasing viscosity (Figure 4.4B). However, the slope of quantum yield against glycerol content for ^{ts}C **15** was 54,000-fold lower than that of ^{ts}T **9**. This different behavior of ^{ts}C and ^{ts}T can be explained by the stronger electron-withdrawing property of thymine than cytosine, resulting in a weaker push-pull system in ^{ts}C. Finally, the pH sensitivity of ^{ts}C free nucleoside **15** was determined in PBS buffer. As shown in Figure 4.4C, upon decreasing the pH and protonation of N3, the fluorescence intensity of ^{ts}C was decreased. The pK_a value of **15** was determined as 3.4. This value is somewhat lower than the pK_a of cytidine (4.2).[73]

Table 4.1. Photophysical properties of ^{ts}C nucleoside **15** in various solvents[a]

Solvent	ε_{max} (cm^{-1} M^{-1})	λ_{abs} max (nm)	λ_{em} max (nm)	Stokes shift (10^3 cm^{-1})	φ	E_T^{30} (kcal mol^{-1})[74]
THF	33,200	320	425	7.7	0.14	37.4
Dioxane	40,800	315	425	8.2	0.16	36
DMSO	20,200	320	430	8.0	0.28	45.1
DMF	19,800	320	425	7.7	0.25	43.2
MeCN	18,000	315	432	8.6	0.22	45.6
MeOH	33,000	310	435	9.3	0.13	55.4
Water	18,800	312	455	10.1	0.07	63.1
PBS buffer	22,600	312	455	10.1	0.07	-

[a] All data were collected at 22 °C, and the concentration of ^{ts}C nucleoside was fixed at 5.0 μM. In order to maximize the solubility, all samples had a final DMSO content of 0.04%.

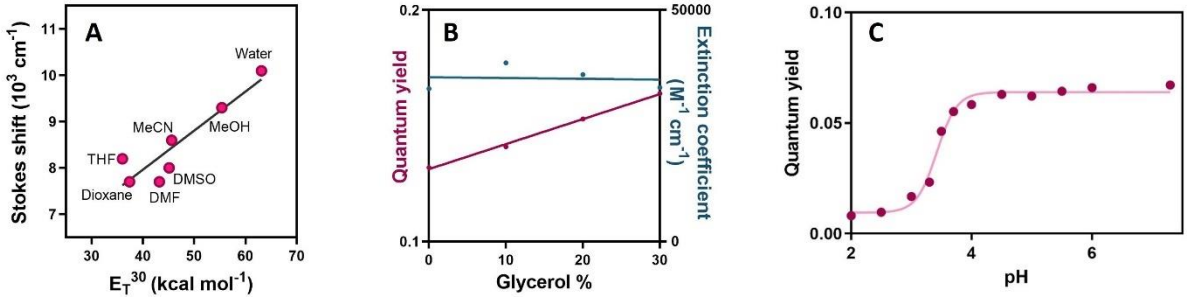

Figure 4.4. (A) Plot between *Stokes* shift of ^{ts}C nucleoside **15** (5.0 μM) and E_T^{30} values of various solvents (R^2 = 0.827). (B) Quantum yield and extinction coefficient of ^{ts}C nucleoside **15** (5.0 μM) versus glycerol content. Extinction coefficients were calculated at 315 nm, and emission spectra were collected using Ex = 310 nm. (C) The plot of fluorescence quantum yield of **15** (5.4 μM in PBS buffer) versus pH. All data were recorded at 22 °C.

4.3 Synthesis and biophysical properties of ^{ts}C-modified DNA

4.3.1 Synthesis of ^{ts}C-modified DNA and *i*-motif formation

To facilitate site-specific incorporation of ^{ts}C into DNA, synthesis of phosphoramidite **17** commenced with DMT protection of the 5′-hydroxyl group of **14** in a yield of 58%. Phosphorylation of the 3′-hydroxyl group of **16** gave **17** in an isolated yield of 75%. Phosphoramidite **17** was compatible with standard, automated DNA synthesis, and no deamination to give the corresponding thymidine analog was observed. ^{ts}C-modified oligonucleotides (ODN8–10) were then purified using HPLC and their mass was confirmed by ESI (Table C1 and Figure C1, Appendix C). ODN8 has the same sequence as ODN7 (Chapter 2), but with a ^{ts}C replacing ^{ts}T, was used to compare the photophysical properties of these two *trans*-stilbene nucleobase analogs. In addition, ^{ts}C was incorporated at two different locations of a 24-mer telomeric sequence (ODN9–10, Figure 4.5). Telomeric DNA is a region of repetitive nucleotide sequences (5'-CCCTAA-3')$_n$[75] associated with specialized proteins at the ends of chromosomes and is known to form *i*-motif structures under acidic conditions.[76-79]

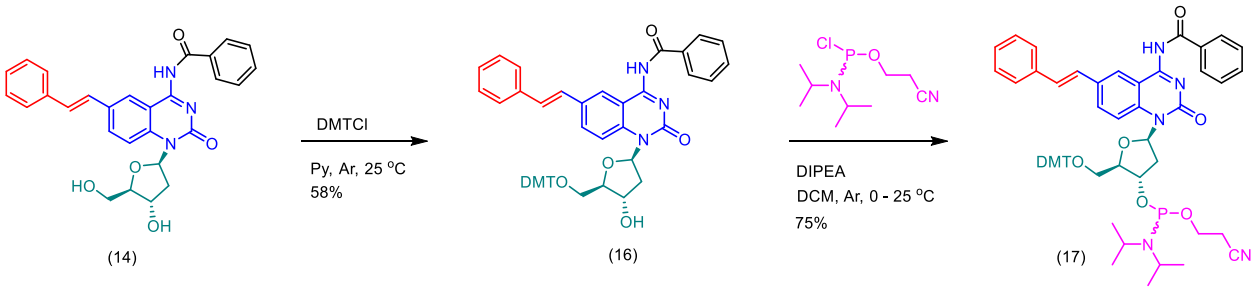

Scheme 4.2. Synthesis of the ^{ts}C phosphoramidite **17**. DMTCl = 4,4′-dimethoxytriphenylmethyl chloride, DIPEA = *N,N*-diisopropylethylamine.

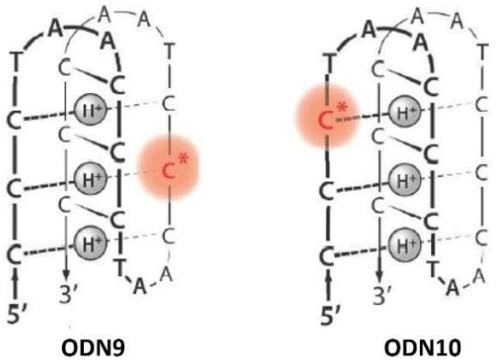

Figure 4.5. Secondary structure of a human telomeric *i*-motif containing the ^{ts}C probe at two different positions. The dominant *i*-motif conformation "5′E" is shown.[80-82]

Circular dichroism (CD) measurements were conducted to confirm the formation of *i*-motif and B-form duplex of ^{ts}C-modified DNA. Oligonucleotides were folded by heating and slowly cooling single-stranded oligonucleotides (with and without the complementary strand) in PBS buffer at different pHs. At pH = 6.0 to 8.0, the CD spectra of ODN10 exhibited maxima at λ_{max} = 274 nm, minima at λ_{min} = 248 nm (Figure 4.6A), consistent with an unfolded *ss*-DNA.[83] However, at pH = 5.0, the CD spectrum red-shifted (λ_{max} = 285 nm and λ_{min} = 252 nm), and its intensity increased, confirming the formation of an *i*-motif structure at this acidic pH (Figure 4.6A).[84] The CD spectrum showed the *i*-motif structure still exists at pH = 4.5. However, at pH = 3.0, due to the protonation of all cytidines and the subsequent unstructuring of the *i*-motif, the CD intensity was decreased (Figure 4.6A). In Figure 4.6B, the CD data of the corresponding unmodified DNA at pH = 5.0 (positive control) and ODN8 at pH = 5.0 (negative control) are shown. Further CD experiments on DUP8-10/ODN8-10, confirmed ^{ts}C has little, if any, impact on the global structure of B-form duplex and *i*-motif structures (Figure C2, Appendix C).

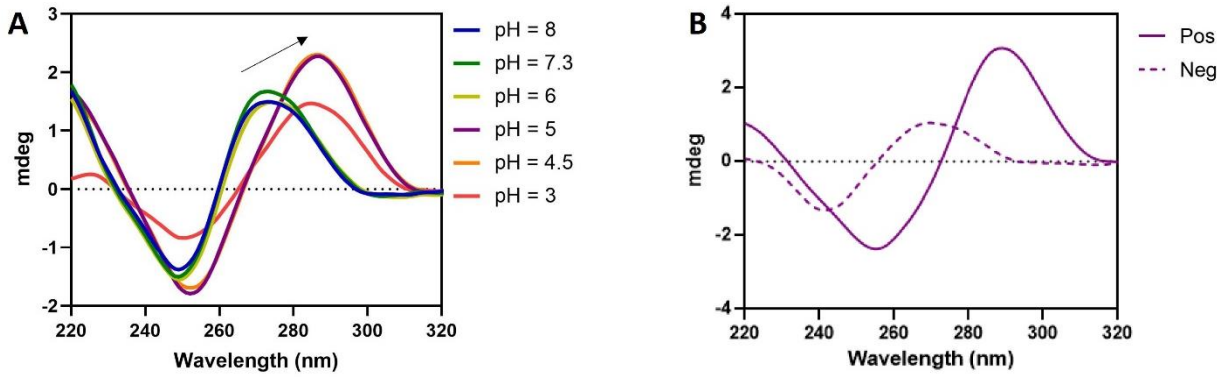

Figure 4.6. CD spectra of (A) ODN10 at pH = 3.0 to 8.0, and (B) ODN8 (as the negative control, Neg) and the unmodified DNA corresponding to ODN 10 (as the positive control, Pos) at pH = 5. Data were recorded at 22 ^{o}C in PBS buffer (variable pH). DNA concentrations were kept at 2.0 µM. ODN10 sequence is 5'- CC **^{ts}C** TAACCCTAACCCTAACCCTAA -3' and ODN8 sequence is 5'- GCGA **^{ts}C** CGCGCGCTAGCG -3'.

Thermal denaturation (T_m) studies were used to evaluate the impact of ^{ts}C on the global structure and stability of duplex and *i*-motif DNA. T_m data of ODN10 at different pHs is consistent with formation of an *i*-motif at pH = 5.0 (T_m = 40.4 ^{o}C, Table 4.2), but not at pH = 6.0 or higher. In agreement with CD results, the *i*-motif at pH = 4.0 showed a lower T_m (26.6 ^{o}C). It is worth mentioning that ^{ts}C,

slightly stabilizes *i*-motifs as compared to the wild-type sequence containing cytidine (ΔT_m = +0.7 to +1.8 °C, Table 4.2) and has little impact on the stability of duplex DNA, in particular in DUP10 (Table 4.2). T_m spectra are available in Figure C3, Appendix C.

Table 4.2. Biophysical properties of oligonucleotides containing ^{ts}C[a, b]

Oligonucleotides		ε_{260} (cm^{-1} M^{-1})	pH	T_m(°C)	ΔT_m(°C)[c]
ODN8[d]	*ds*-^{ts}C	291,000	7.3	64.9	+5.4
			5.0	N.M[e]	N.M[e]
	ss-^{ts}C	159,000	7.3	-	-
			5.0	-	-
ODN9[d]	*ds*-^{ts}C	402,000	7.3	57.2	-7.7
			5.0	49.6	N.M[e]
	ss-^{ts}C	226,000	7.3	-	-
			5.0	41.5	+1.8
ODN10[d]	*ds*-^{ts}C	402,000	7.3	65.3	+0.4
			5.0	61.2	N.M[e]
	ss-^{ts}C	226,000	7.3	-	-
			5.0	40.4	+0.7

[a] The average extinction coefficient (ε) of ^{ts}C in DNA at 310 nm is 20,800 ± 700 cm^{-1} M^{-1}. [b] All data were collected at 22 °C and in PBS buffer. [c] ΔT_m = T_m (^{ts}C-modified DNA) - T_m (corresponding unmodified DNA).
[d] ODN8 sequence: 5'–GCGA **^{ts}C** CGCGCGCTAGCG–3', ODN9 sequence: 5'–CCCTAACCCTAAC **^{ts}C** CTAACCCTAA–3', ODN10 sequence: 5'– CC **^{ts}C** TAACCCTAACCCTAACCCTAA –3'. [e] N.M: not measured.

4.3.2 Fluorescence properties of ^{ts}C-modified DNA

In the next step, fluorescence spectroscopy was used to characterize the pH-dependent folding of single stranded oligonucleotides into *i*-motif DNA. Upon decreasing the pH, the fluorescence intensity of ODN10 decreased and its spectrum shifted to red (Figure 4.7A). The fluorescence quenching also happened in ODN8 (negative control), confirming that ^{ts}C fluorescence intensity is pH-dependent regardless of *i*-motif formation (Figure 4.7B). This is in agreement with our DFT calculations which suggest protonated ^{ts}C can undergo PET quenching with neutral nucleobases (Table C2, Appendix C). However, the red-shifting of ^{ts}C emission in acidic pH was only observed for ODN10, and can be explained by the stronger π-stacking present in the more compact structure of *i*-motifs. The ½ effective pH value, pH_m, of ^{ts}C, based on fluorescence intensity of ODN10 at 450 nm,

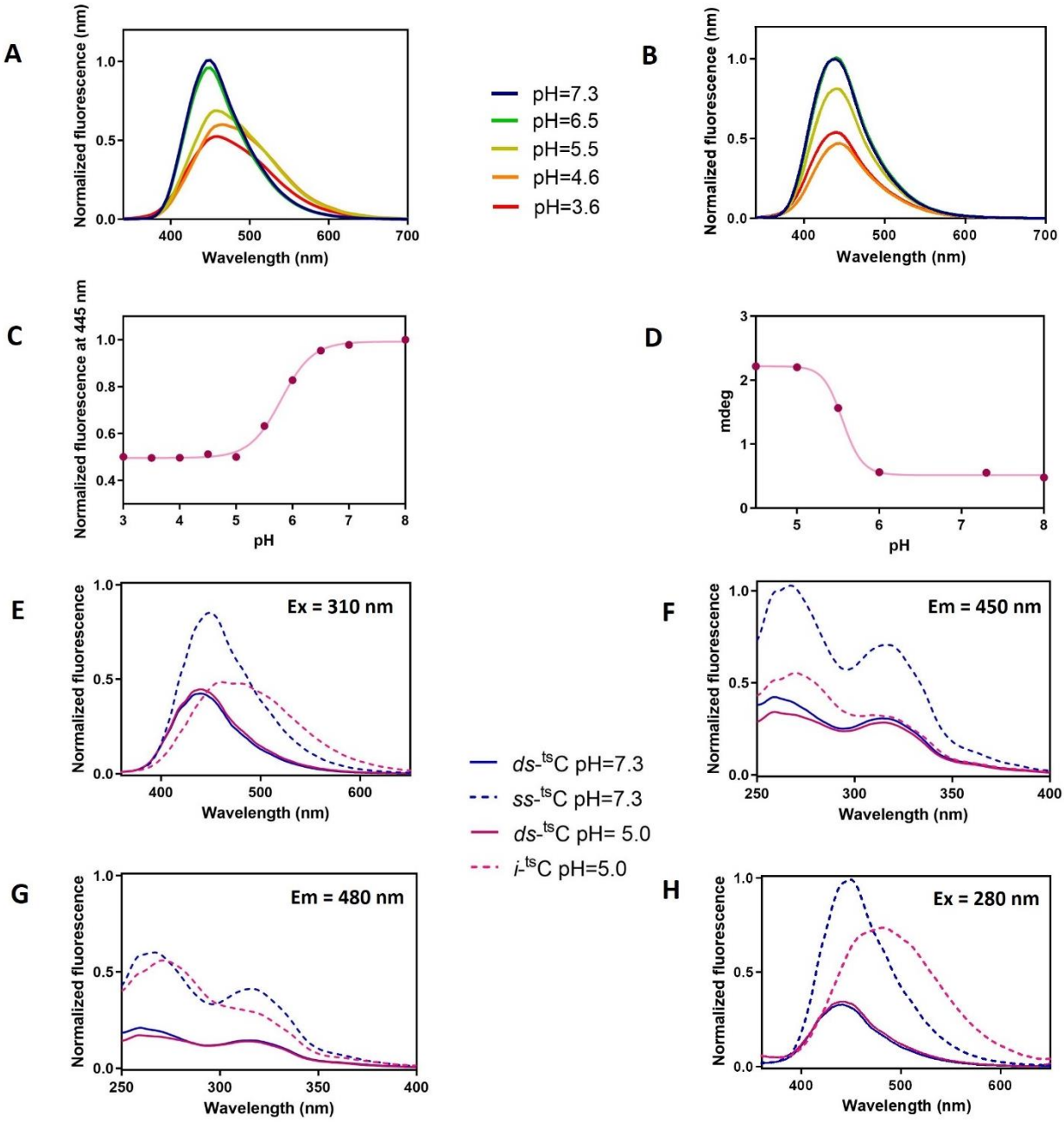

Figure 4.7. The plotted normalized fluorescence spectra (λ_{ex} = 310 nm) of (A) ODN10 and (B) ODN8 at variable pH. Normalized (C) fluorescence spectra and (D) CD intensity at 290 nm of ODN10 versus pH. (E) Fluorescence spectra (Ex = 310 nm) of ODN10 different constructs at neutral and acidic pH, normalized in respect with plot H. (F) Normalized excitation spectra (Em = 450 nm) of ODN10 different constructs at neutral and acidic pH. (G) Excitation spectra (Em = 480 nm) of ODN10 different constructs at neutral and acidic pH, normalized in respect with plot F. (H) Normalized fluorescence spectra (Ex = 280 nm) of ODN10 different constructs at neutral and acidic pH. Measurements were recorded at 22 ^{o}C in PBS buffer (variable pH). DNA concentrations were kept at 2.0 µM. ODN10 sequence is 5'-CC **^{ts}C** TAACCCTAACCCTAACCCTAA-3' and ODN8 sequence is 5'-GCGA **^{ts}C** CGCGCGCTAGCG-3'.

was calculated 5.8 (Figure 4.7C). A similar pH_m value was calculated by plotting the CD intensity at 290 nm versus pH (5.6, Figure 4.7D). These values are close to the measured pH_m for the wild-type sample of the same sequence (6.0).[60]

Figure 4.7E represents the fluorescence spectra of folded and unfolded ODN10 constructs (at pH = 5.0 and 7.3), measured by excitation at ^{ts}C maximum absorbance (310 nm). Similar to what was shown in Figure 4.7A, upon acid-mediated *i*-motif folding, a bathochromic shift was observed but the quantum yield was only quenched by 14% ($\varphi_{ss\text{-}tsC}$ = 0.051, $\varphi_{i\text{-}tsC}$ = 0.044, Table 4.3). Thereby, ^{ts}C remains bright in the *i*-motif structure (pH = 5.0) but still discriminates it from *ss*-DNA (pH = 7.3) by ~20 nm bathochromic shift. The fluorescence lifetime of *i*-^{ts}C at 440 nm emission (4.3 ns, Table 4.3) was different from the lifetime of the same sample at 545 nm emission (5.3 ns, Table 4.3). This suggests the presence of different excitons in the excited state of *ss*-^{ts}C and *i*-^{ts}C, leading to different maximum emissions and fluorescence lifetimes. The similarity between fluorescence spectra of *ds*-^{ts}C at neutral and acidic pH (Figure 4.7E) is consistent with the shielded nucleobases in the duplex structure. The lower quantum yield and shorter fluorescence lifetime of *ds*-^{ts}C than *ss*-^{ts}C and *i*-^{ts}C are explainable by PET with the G-rich complementary strand in *ds*-^{ts}C (Table 4.3). Thus, the bathochromic shift in the fluorescence emission of *i*-^{ts}C is paired with 2.4 to 2.7-fold higher quantum yield as compared with *ds*-^{ts}C (Figure 4.7E, Table 4.3).

Table 4.3. Photophysical properties of ODN10: Maximum wavelengths of absorbance (λ_{abs}), fluorescence emission (λ_{em}), fluorescence excitation (λ_{ex}), fluorescence quantum yield (φ), brightness ($\varepsilon\varphi$), fluorescence lifetime (τ) at different emissions, and the ratio between the area under the fluorescence curve upon excitation at 280 and 310 nm.[a, b]

ODN10	pH	λ_{abs} (nm)	λ_{em} (nm)	λ_{ex} (nm)	φ (%)	$\varepsilon\varphi$	τ_{440} (ns)	τ_{545} (ns)	F_{280}/F_{310}
ds-^{ts}C	7.3	260, 314	442	260, 315	1.7	350	2.9	4.0	0.80
	5.0	260, 312	441	260, 314	1.8	370	3.2	4.3	0.87
ss-^{ts}C	7.3	260, 313	444	263,315	5.1	1,060	4.5	4.6	1.14
	5.0	260, 310	465	272, 311	4.4	920	4.3	5.3	1.56

[a] The average extinction coefficient (ε) of ^{ts}C in DNA at 310 nm is 20,800 $\pm$ 700 cm^{-1} M^{-1}
[b] All data were collected at 22 ^{o}C and in PBS buffer. Inner filter effect correction was applied.

Excitation spectra of ODN10 different constructs related to emissions at 450 and 480 nm are shown in Figures 4.7F and 4.7G, respectively. All samples demonstrated an excitation peak at 310 nm, at which ^{ts}C is selectively excited, and a second excitation peak in the DNA absorbance region related to a DNA-to-probe energy transfer (Table 4.3).[60,85] Although in all different ODN10 constructs the natural DNA bases have a maximum absorbance at 260 nm, but their maximum excitation wavelengths were different (duplex and unfolded single-stranded ^{ts}C: 260–263 nm, and *i*-^{ts}C: 272 nm). This ~10 nm red-shift in the maximum excitation wavelength can be explained by the lower excitonic state present in *i*-motif structures.[86] Inspired by the distinguished excitation of DNA in *i*-^{ts}C, and to enhance the discrimination between different structures, we measured the fluorescence emissions of ODN10 different constructs by excitation at 280 nm. Data shown in Figure 4.7H, confirm that upon excitation at 280 nm, the DNA-to-probe energy transfer in duplex and unfolded *ss*-^{ts}C are minimized, while the energy transfer in *i*-^{ts}C is preserved. Thus, by excitation of samples at 280 nm, ^{ts}C, by 3.6-fold fluorescence enhancement and 20-25 nm fluorescence red-shifting, demonstrates an even higher discrimination between *i*-motif and *ds*-DNA. Similar results were obtained for ODN9 (Figure C4, Appendix C).

4.4 Probing the reversible *ds* → *i*-motif transition

Inspired by the discrimination power of ^{ts}C between *ds*-DNA, *ss*-DNA and *i*-motif structures, *i* → *ds* and ss → *ds* transitions were monitored in real-time by addition of the complementary strand (Figure 4.8A and B). At both pHs, the fluorescence of ^{ts}C decreased upon hybridization. However, the amount of decrease at 485 nm was more significant for *i* → *ds* transition because of the emission blue-shifting. The data confirm the faster *ss* → *ds* transition than the *i* → *ds* transition, consistent with the kinetic barrier of the folded *i*-motif.[87]

To monitor the *ds* → *i* transition, we first hybridized *i*-^{ts}C with 1.2 equiv. complementary strand bearing a 7-mer toehold (single-stranded overhang) at pH = 5.0 (Figure 4.8C). After formation of the duplex, an invading strand (1.44 equiv) was added to initiate a strand-displacement reaction and *ds* → *i* transition (Figure 4.8D). During this transition, a fluorescence enhancement was observed,

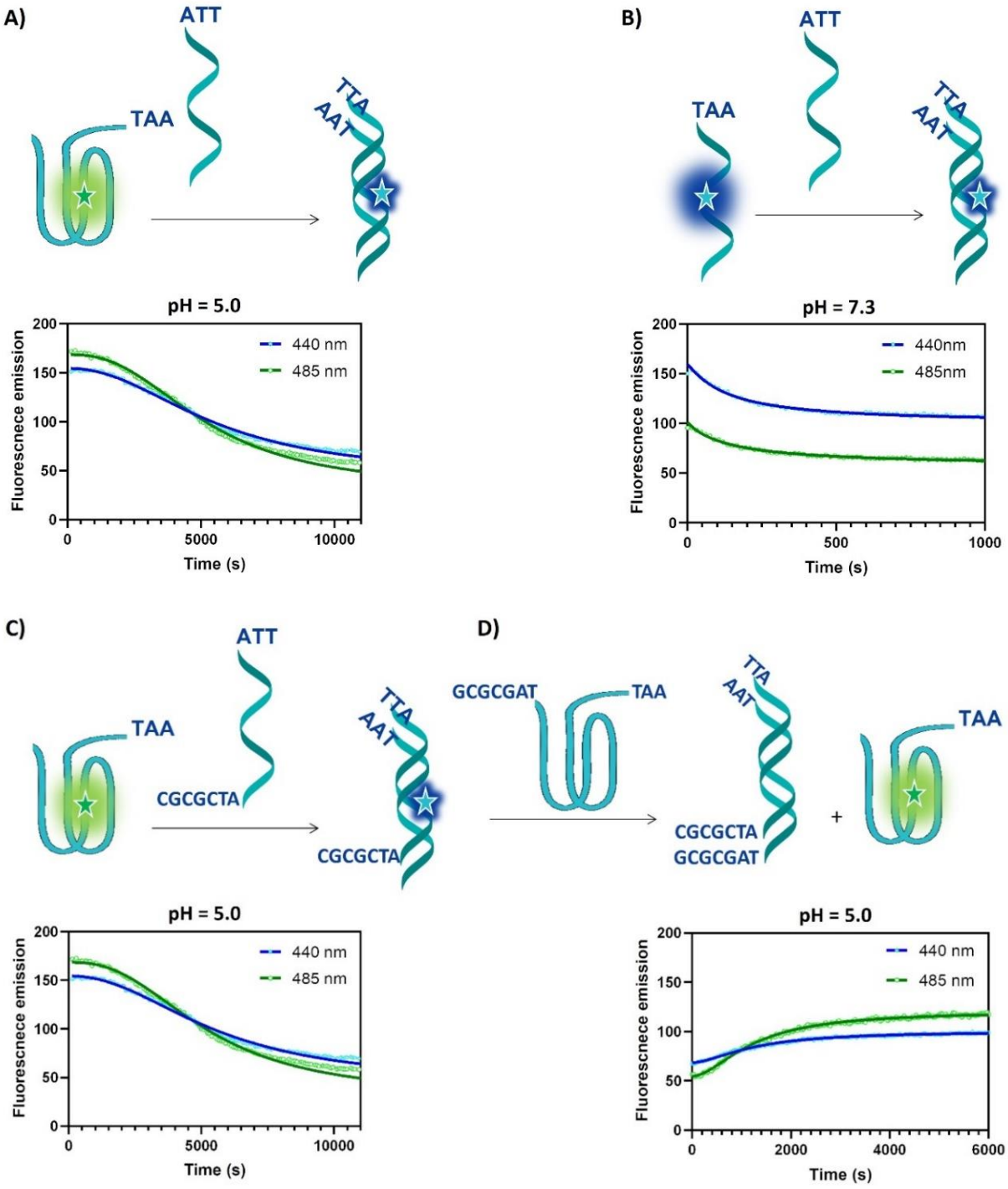

Figure 4.8. Kinetic fluorescence spectra (Ex = 280 nm) related to the hybridization of ODN10 at (A) pH = 5.0, (B) pH = 7.3, (C) pH = 5.0 with a toehold of 7 nucleotides, and (D) the strand displacement reaction at pH = 5.0 with an invading strand. Data were recorded at 22 ^{o}C in PBS buffer (variable pH). DNA concentrations were kept at 2.0 µM. ODN10 sequence is 5'-CC **^{ts}C** TAACCCTAACCCTAACCCTAA-3'.

which was more significant at 485 nm due to the red-shifted fluorescence of *i*-^{ts}C. To the best of our knowledge, this is the first example of a light-up FBA sensitive to *i*-motif. The length of the toehold played a critical role in the strand-displacement[88] and a toehold with at least seven nucleotides was required to proceed the *ds* → *i* transition. We think the reason for this relatively large toehold is folding of the invading C-rich strand into an *i*-motif structure, immediately after the addition, which poses a large kinetic barrier for unfolding and strand-displacement reaction.[89] These results indicate that *i*-motif unfolding is the rate-limiting step for duplex formation under slightly acidic conditions.

The melting experiment is another approach to study the folding and unfolding of duplex and *i*-motif structures. Figure 4.9 demonstrates the fluorescence intensity (Ex = 280 and 310 nm) and the fluorescence lifetime (laser 355 nm) of ODN10 at different wavelengths (440, 485, and 545 nm) and different temperatures. The orange area represents the melting temperature range. Figure 4.9A, related to *ss*-DNA at pH = 7.3, shows fluorescence decrease upon increasing the temperature, consistent with the enhanced dynamics of DNA. For *ds*-DNA at pH = 7.3 (Figure 4.9B), fluorescence data demonstrates three different stages: (1) pre-melting, where an increase in temperature causes a shallow decrease in the fluorescence; (2) melting, where fluorescence increases upon unfolding the duplex as the result of inhibiting PET with the G-rich complementary strand; and (3) post-melting, where fluorescence decreases due to the higher chance of internal conversion at higher temperatures.

At pH = 5.0, the fluorescence of *i*-DNA blue-shifts during melting and its intensity at 545 nm and 485 nm decreases (Figure 4.9C). In the post-melting step, the fluorescence decreases at all wavelengths with increasing the temperature. At pH = 5.0, the fluorescence of *ds*-DNA remained with little-to-no change in the pre-melting step (Figure 4.9D). This can be explained by the two opposing effects: Temperature increase, which is in favor of fluorescence decrease; and *ds* → *ss* transition, which tends to increase the fluorescence. However, once the duplex is fully melted, the temperature effect on DNA dynamics plays the leading role in the post-melting step and results in a fluorescence decrease. Taken together these results indicate the sensitivity of ^{ts}C-modified oligonucleotides towards different structures at variable pHs and temperatures.

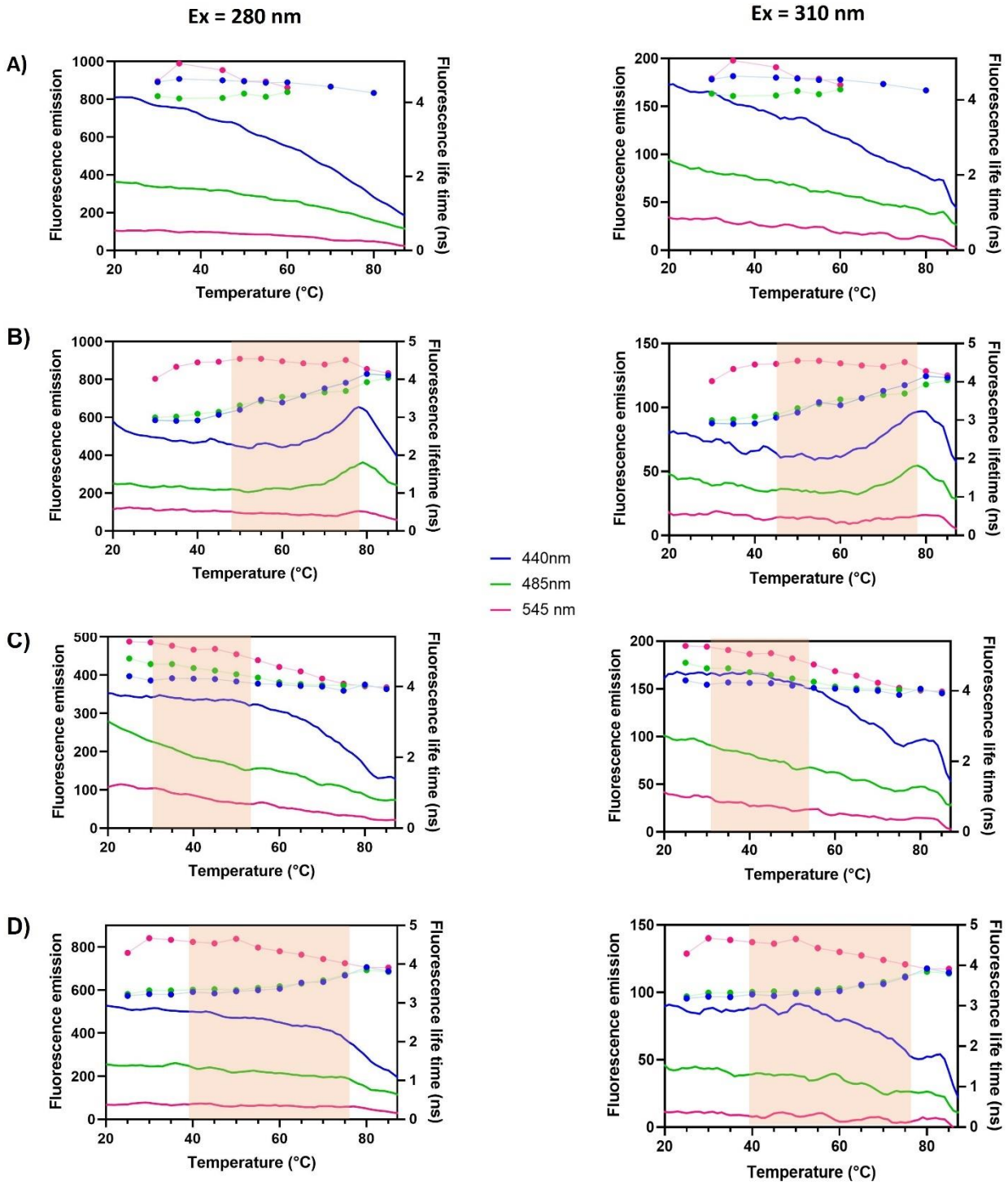

Figure 4.9. Representation of fluorescence intensity (thick sold lines), fluorescence lifetimes (thin sold lines with points), and the melting area (in orange) of (A) single-stranded, pH = 7.3, (B) double-stranded, pH = 7.3, (C) *i*-motif, pH = 5.0, (D) double-stranded, pH = 5.0. ODN10 concentrations for fluorescence intensity and melting temperature experiments were kept at 2.0 µM and for fluorescence lifetime was 10.0 µM.

4.5 Mismatch detection by ^{ts}C

Consistent with the solvent-dependent and viscosity-dependent fluorescence of ^{ts}C nucleoside, which suggested that ^{ts}C is a weaker molecular rotor than ^{ts}T, the data discussed in the previous section showed that ^{ts}C rotary property is not the dominant factor in determining fluorescence changes during DNA folding and unfolding. These observations confirmed that ^{ts}C and ^{ts}T, have different photophysical properties. Thus, we decided to compare the mismatch sensitivity of these probes. Figure 4.10A, shows the fluorescence of ODN7 (a ^{ts}T-modified DNA, previously discussed in Chapters 2 and 3) and Figure 4.10B demonstrates the fluorescence of ODN8 (a ^{ts}C-modified DNA, containing the same sequence as ODN7) with different constructs. In contrast with different base-pairing faces of ^{ts}T and ^{ts}C, which results in different T_m data (Table 4.4 and Figure C3D, Appendix C), their fluorescence intensity showed the same trend: X:A > *ss* > X:G > X:T,C (X = ^{ts}T or ^{ts}C, Figure 4.10). We suspect that both rotary and electron/energy transfer are involved in ^{ts}C mismatch discrimination. Nevertheless, the fluorescence of ^{ts}C is highly sensitive towards pairing natural nucleobases (290 – 4300 $cm^{-1}M^{-1}$). Thus, in future studies, it can be used as a probe to evaluate the effect of mismatches in altering the DNA secondary structure.

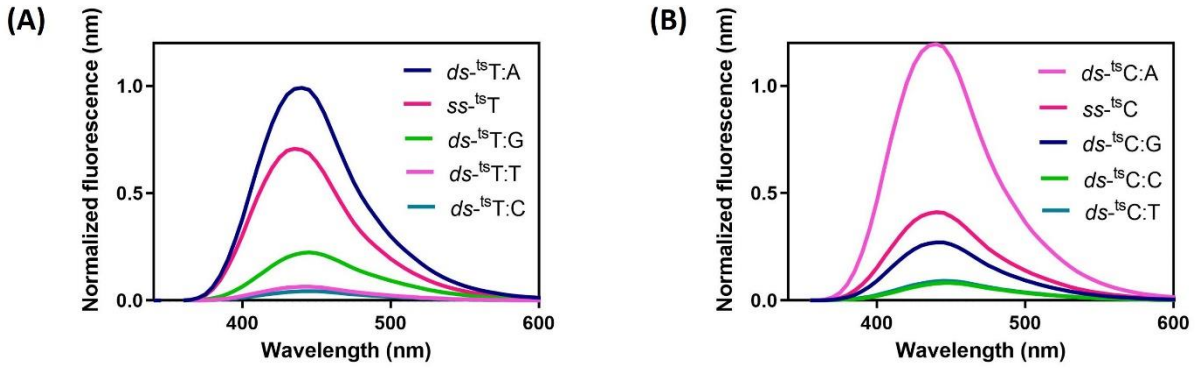

Figure 4.10. The fluorescence spectra of single-stranded and duplex of (A) ODN7 and (B) ODN8. Data were recorded at 22 ^{o}C in PBS buffer (pH = 7.3). DNA concentrations were kept at 2.0 µM. ODN7 and ODN8 sequence: 5'- GCGA **X** CGCGCGCTAGCG-3', where X = ^{ts}T in ODN7 and X=^{ts}C in ODN8.

Table 4.4. Fluorescence properties and melting temperature of oligonucleotides containing ^{ts}T and ^{ts}C[a, b]

Oligonucleotides (GCGA **X** CGCGCGCTAGCG)		λ_{abs} (nm)	λ_{em} (nm)	φ (%)	εφ (cm^{-1} M^{-1})	TM
ODN7	^{ts}T:A	310	440	17.2	5,260	64.1[c]
	^{ts}T:G	310	440	3.8	1,160	61.8
	^{ts}T:C	310	445	0.7	210	59.4
	^{ts}T:T	310	445	1.1	337	59.2
	ss-^{ts}T	315	435	12.2	3,733	-
ODN8	^{ts}C:A	310	435	20.7	4,300	59.9
	^{ts}C:G	310	440	4.7	980	64.9[d]
	^{ts}C:C	310	450	1.4	290	56.8
	^{ts}C:T	310	445	1.6	330	57.7
	ss-^{ts}C	315	435	8.3	1,730	-

[a] The average extinction coefficients (Ɛ) of ^{ts}T and ^{ts}C in DNA at 310 nm are 30,600 ± 700 cm^{-1} M^{-1} and 20,800 ± 700 cm^{-1} M^{-1}. [b] All measurements were performed at 22 °C in PBS buffer (pH = 7.4), with DNA concentrations = 2.0 µM. [c] T_m of corresponding unmodified DNA is 58.6 °C. [d] T_m of corresponding unmodified DNA is 59.5 °C.

4.6 Conclusion

We have developed the *trans*-stilbene analog of cytidine, ^{ts}C as a new FBA for the detection of *i*-motif structures. ^{ts}C phosphoramidite, synthesized in 15 steps with an 8% total yield, was incorporated into the telomeric repeat sequence $(CCCTAA)_4$, and showed negligible impact on duplex and *i*-motif stability. ^{ts}C fluorescence intensity is sensitive towards double-stranded, single-stranded and *i*-motif structures, and to the best of our knowledge, is the first light-up probe in duplex → *i*-motif transition. In addition to the change in fluorescence intensity, the emission wavelength of ^{ts}C red-shifts when it is folded into an *i*-motif. The higher nucleobase density and the shorter base-stacking distance in *i*-motif (3.1 Å) compared with duplex DNA (3.4 Å), resulted in DNA-to-probe energy transfer when the *i*-motif is excited at 280 nm. The discrimination power of ^{ts}C was used in the real-time monitoring of *i*-motif → *ds* hybridization and *ds* → *i*-motif strand-displacement. Finally, temperature-dependent fluorescence experiments revealed that ^{ts}C, like a molecular thermometer, enables monitoring of the DNA dynamics in pre-melting, melting, and post-melting steps.

4.7 Experimental

4.7.1 Theoretical computations

The molecular geometries and thermal corrections were optimized with B3LYP DFT functional theory[90] paired with the 6-31++G(d) basis set.[91] Calculations were performed in the water phase (C-PCM algorithm)[92] at 298.15 K. The first frequency was utilized to assess whether structures were in their true optimized form. Conformers distributions were executed using Spartan,[93] and Gaussian 16[94] was used to calculate orbital energies. In order to simplify calculations, deoxyribose (dR) was replaced with a methyl group.

4.7.2 Synthesis and characterization of nucleosides

All reagents were obtained from commercial sources and used without further purification. NMR data were collected on either a Bruker AVIII-400 or 500 MHz. Chemical shifts (δ) are given in parts per million (ppm) and are reported relative to residual solvent peaks: $CDCl_3$ (δH 7.26, δC 77.16 ppm), DMSO-d_6 (δH 2.50, δC 39.52 ppm), CD_2Cl_2 (δH 5.32). Coupling constants (*J*) are given in Hertz (Hz). ^{13}C-spectra were recorded broadband proton decoupled. High-resolution mass spectra were obtained on a Thermo QExactive high-resolution Orbitrap. Masses are given as m/z.

4.7.3 Biophysical experiments

Fluorescence spectroscopy: DMSO stock solutions of the ^{ts}C nucleoside **15** was prepared and diluted to an *OD* = 0.10 ± 0.01 at the most red-shifted absorbance maxima. All measurements were collected on a Molecular Devices SpectraMax M5 in a 1 cm path-length quartz cuvette. Quantum yields were calculated using the most red-shifted absorbance maxima of samples. Quinine hemisulfate (φ_R = 0.546) in 0.5 M H_2SO_4 (n_R = 1.346) was used as a fluorescent standard. Quantum yields were calculated using the equation shown below[95]:

$$\Phi = \Phi_{\mathrm{R}} \frac{F}{F_{\mathrm{R}}} \frac{A_{\mathrm{R}}}{A} \frac{n^2}{{n_{\mathrm{R}}}^2}$$

where φ_R is the quantum yield of the fluorescent standard, *F* and F_R are the integrated emissions of the sample and reference, respectively. *A* and A_R are the optical densities of the sample and reference respectively (both set to 0.10 ± 0.01). *n* and n_R are the refractive indexes of the sample and reference

respectively. The refractive indexes of solvents used in this work are: n_{PBS} = 1.335, n_{water} = 1.333, $n_{methanol}$ = 1.328, $n_{dioxane}$ = 1.422, n_{DMF} = 1.431, n_{ACN} = 1.344, n_{DMSO} = 1.479, and n_{THF} = 1.407.

Oligonucleotide stock solutions were diluted into PBS buffer (pH = 7.3, Na^+ concentration of ≈137 mM) to a final concentration of 2.0 μM using their extinction coefficient at 260 nm. All measurements were collected on a Molecular Devices SpectraMax M5 in a 1 cm path-length quartz cuvette. Quantum yields were calculated using the most red-shifted absorbance maxima of samples. Quinine hemisulfate (φ_R = 0.546) in 0.5 M H_2SO_4 (n_R = 1.346) was used as the fluorescent standard, and quantum yields were calculated using the above equation.

Fluorescence lifetime of oligonucleotides: TCSPC experiments employed a picosecond laser source (DD-310L, Horiba Jobin Yvon GmbH) at a repetition rate of 10 MHz in combination with a double-grating emission monochromator and a PPD-900 detection module (Fluorolog3 FL3-222, Horiba). Samples (10 μM) were kept at 25 °C by means of a Varian Cary PCB-150 Peltier water bath (Agilent). The fluorescence lifetime τ_F was collected with a channel width of 27 ps and retrieved from one exponential decay by iterative reconvolution with the instrument response function (IRF) using a custom-written MATLAB routine (R2019b).[96]

CD Spectroscopy: Circular dichroism spectra of DNA samples (2.0 μM) were measured from 220 nm to 350 nm at 22 °C with a 2 nm bandwidth with 0.1 nm steps at a scanning rate of 20 nm min^{-1} in 1 cm path length thermo-controlled strain-free quartz cuvette on a JASCO J-715 spectrometer.

Melting Temperature Analysis (T_m): UV thermal denaturation data were obtained by measuring the absorbance at 260 nm as a function of temperature in a 1 cm path length thermo-controlled strain-free quartz cuvette on a Varian CARY 100 UV-visible spectrophotometer equipped with a Peltier temperature controller. Solutions of pre-folded duplex DNA (0.2 μM) in aqueous buffer (PBS buffer, variable pH) were equilibrated at 20 °C for a minimum of 10 min and slowly ramped to 90 °C with 0.2 °C steps at a rate of 12 °C h^{-1}. The melting temperatures were determined from the maximal slope of the curve (maximal first derivative). T_m values were calculated as the average from the heating and cooling curves that showed little or no hysteresis.

4.7.4 Oligomer synthesis, purification and folding

Synthesis: Unmodified oligonucleotides were purchased from Sigma-Aldrich as HPLC-purified products. Standard DNA phosphoramidites, solid supports, and all necessary reagents were purchased from LinkTech and Sigma-Aldrich. Modified oligonucleotides were synthesized on a 1.0 µmol scale using a Bioautomation Co. Mermade 4 DNA synthesizer according to the Trityl-off procedure. Three coupling reactions were performed for the site-specific introduction of the modified nucleoside into oligonucleotides. The freshly made phosphoramidite **17** was dissolved in dry acetonitrile (0.1 M) immediately prior to use. The synthesis of the oligonucleotides was monitored by DMT deprotection. Upon completion of the sequences, the oligonucleotides were cleaved from the solid support and deprotected by treatment with 1.0 mL of 33 % aqueous ammonium hydroxide at 55 ^{O}C overnight in a 1.5 mL screw-top cap tube.

Purification: The obtained solutions were lyophilized to dryness and purified by HPLC column chromatography using a semi-prep C-18 reverse-phase column (YMCbasic B-22-10P 150 x 10 mm) using a Varian 140 Pro Star HPLC system. The gradient conditions were typically acetonitrile: 0.1 M triethylammonium acetate (TEAA, pH 7.4), 2:98 to 10:90 over 35 minutes, and with the rate of 3.00 mL/min. Elution was monitored by UV absorption at 260 and 310 nm. Peaks were collected and twice lyophilized to dryness from water. The purities of ^{ts}C-containing oligonucleotides ODN8–10 were found to be >90% (260 nm) according to analytical, reverse-phase chromatography using a Waters XBridge C8, 5 µm 4.6 x 150 mm. A gradient of 5–40% of acetonitrile in 0.1 M triethylammonium acetate (TEAA, pH 7.4), was applied over 35 minutes at 0.4 mL/min. ODN8-10 were analyzed by LC-MS using a Dionex Ultimate 3000 UHPLC coupled to a Bruker Maxis Impact QTOF in negative ESI mode. Samples were run through a Phenomenex Luna C18(2)-HST column (2.5 µM 120A 2.1 x 100 mm) using a gradient of 90% mobile phase A (100 mM HFIP and 5 mM TEA in H_2O) and 10% mobile phase B (MeOH) to 40% mobile phase A and 60% mobile phase B in 20 minutes. The data was processed and spectra deconvoluted using the Bruker DataAnalysis software version 4.2.

Folding: Oligonucleotide stock solutions were prepared in deionized water, and their concentrations were determined by absorbance at 260 nm using the molar extinction coefficient calculated using a nearest-neighbor model.[97] The molar extinction coefficient of ^{ts}C nucleotide at 260 nm was determined 15,400 $cm^{-1}M^{-1}$ using the absorbance of ^{ts}C nucleoside **15** at 260 nm. For

calculated extinction coefficients, see Table 4.2. Double-stranded and *i*-motif oligonucleotides were prepared by diluting the complementary sequences (1.0 : 1.2 equiv. ratio) in the PBS buffer (pH = 7.3, Na^+ concentration of ≈137 mM) and heating to 95 °C for 10 min, followed by slow cooling to room temperature over 4 h.

4.8 Appendix C

4.8.1 Tables

Table C1. Synthesized oligomers with calculated and observed masses.

Oligonucleotides	Sequences (5' → 3')	Calc. (m/z)	Found (m/z)	δ (ppm)
ODN8	GCGA ^{ts}C CGCGCGCTAGCG	5,346.3960	5,346.8906	92
ODN9	CCCTAACCCTAAC ^{ts}C CTAACCCTAA	7,279.7496	7279.1797	78
ODN10	C ^{ts}C CTAACCCTAACCCTAACCCTAA	7,279.7496	7279.1797	78

Table C2. Calculated [b3lyp/6-31^{++}G(d)] HOMO and LUMO energy values (eV) in water.

	^{ts}C	^{ts}C^{+}	G	A	C	T
LUMO	-1.90	-5.91	-0.78	-1.08	-1.17	-1.33
HOMO	-5.73	-8.54	-6.16	-6.38	-6.58	-6.63

Table C3. Photophysical properties of ODN9[a, b]

ODN9	pH	λ_{em} (nm)	φ (%)	εφ	$F_{ex=280}/F_{ex=310}$
ds-^{ts}C	7.3	443	1.6	330	0.75
	5.0	439	1.4	290	0.81
ss-^{ts}C	7.3	448	7.3	1,520	1.10
	5.0	461	3.8	790	1.73

[a] The average extinction coefficient (Ɛ) of ^{ts}C in DNA at 310 nm is 20,800 ± 700 cm^{-1} M^{-1}. [b] All data were collected at 22 ^{o}C and in PBS buffer.

4.8.2 Figures

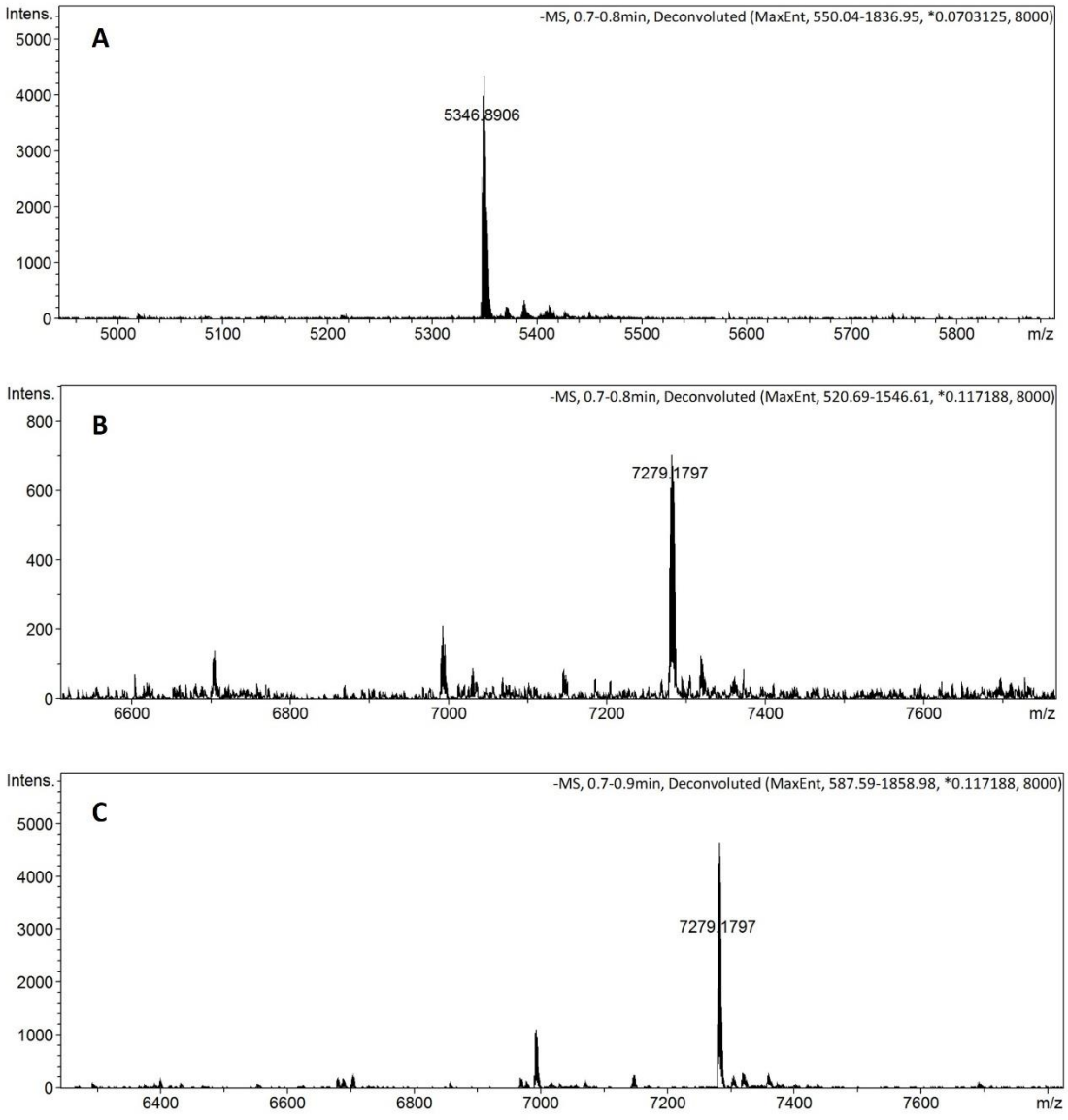

Figure C1. ESI-MS analysis of (A) ODN8, (B) ODN9, and (C) ODN10.

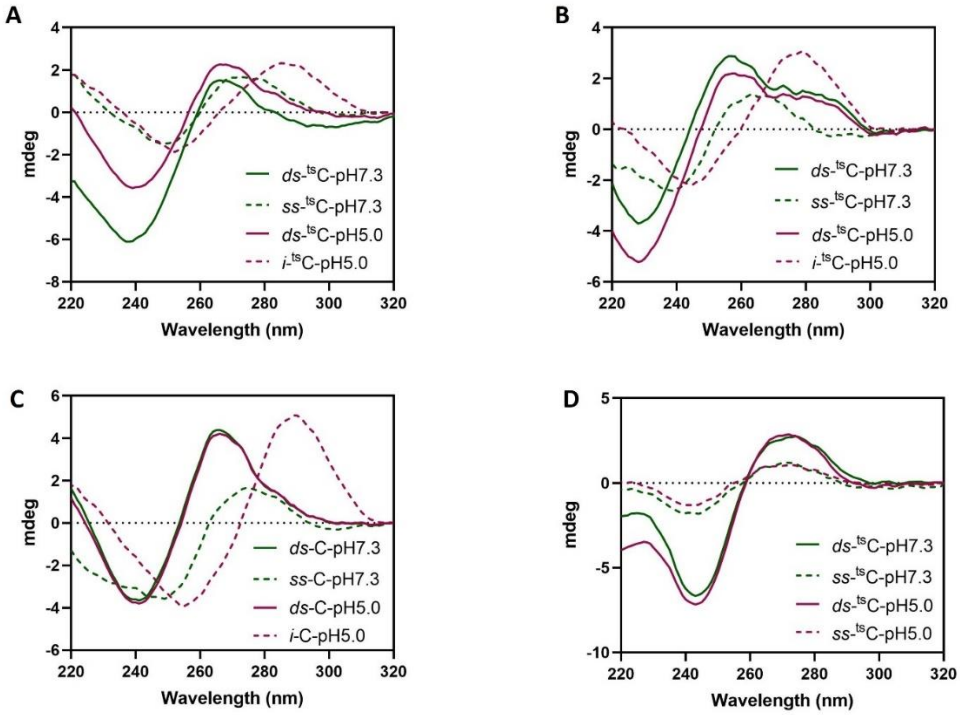

Figure C2. CD spectra of (A) ODN9, (B) ODN10, (C) the corresponding unmodified DNA, and (D) ODN8 as single-stranded, double-stranded, and *i*-motif structures at neutral and acidic pH. Measurements conducted at 22 ^{o}C and DNA concentrations were kept at 5.0 µM.

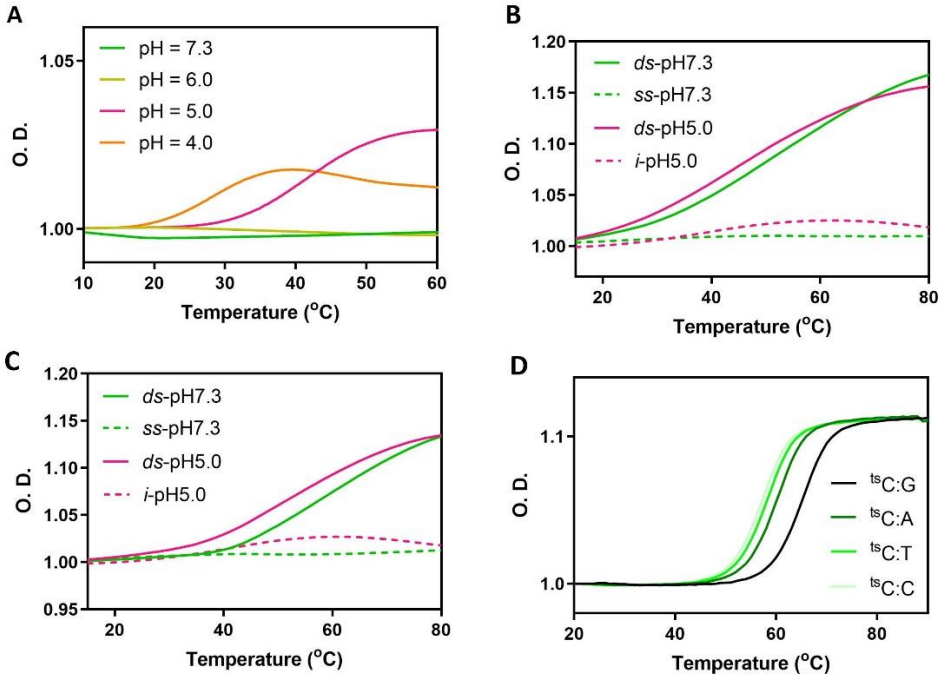

Figure C3. Normalized thermal melting data of (A) ODN10 at different pH, (B) different structures of DUP9/ODN9, (C) DUP10/ODN10 at pH = 5.0 and 7.3, and (D) matched and mismatched duplexes of ODN8. DNA concentrations were kept at 0.2 µM.

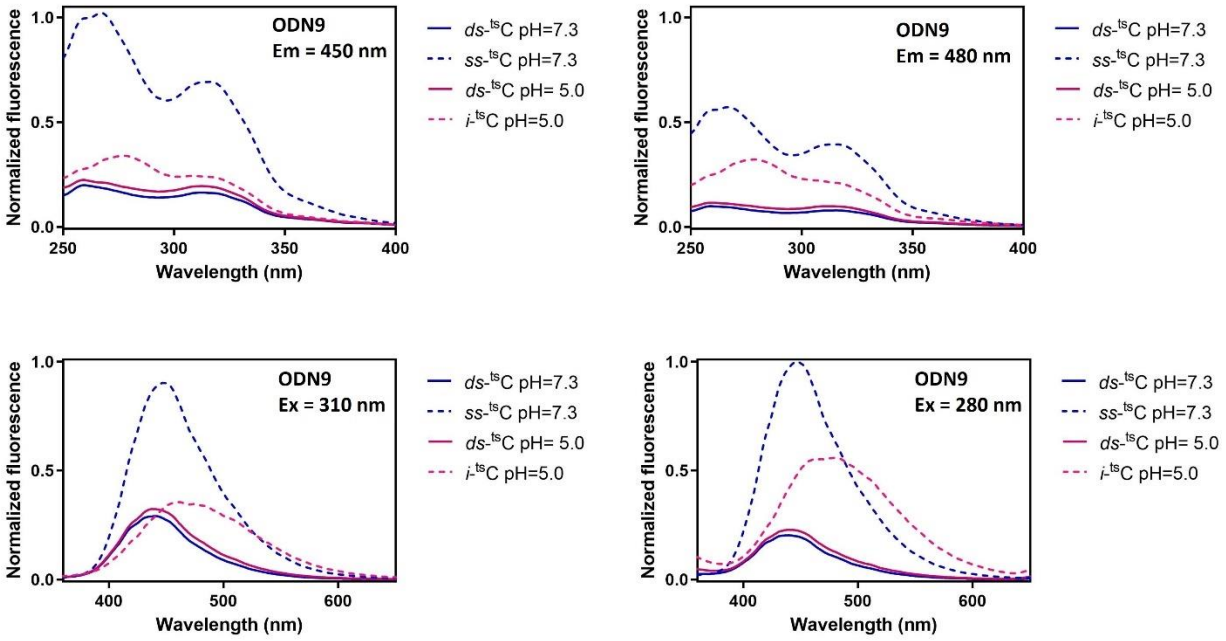

Figure C4. Normalized excitation spectra of DUP9/ODN9 related to (A) Em = 450 nm, (B) Em = 480 nm, and normalized fluorescence spectra of DUP9/ODN9 related to (C) Ex = 310 nm, and (D) Ex = 280 nm. (A) and (B) were normalized in respect together and (C) and (D) were normalized in respect together. Measurements conducted at 22 ^{o}C and DNA concentrations were kept at 2.0 µM.

4.8.3 Synthesis and characterization

1′-(3′-O-tertbutyldimethylsilyl-5′-O-triisopropylsilyl-2′-deoxy-β-D-ribofuranoside)-4-amino-6-styryl-quinazoline- 2,4-(3*H*)-dione (8a) (12)

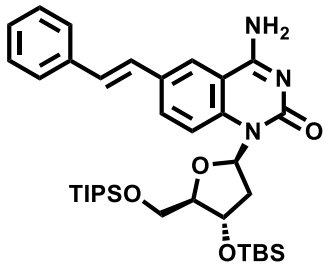

Procedure: 8a (470 mg, 0.72 mmol), 2,4,6-triisopropylbenzenesulfonyl chloride (740 mg, 4.16 mmol, 5.78 equiv) and DMAP (290 mg, 0.89 mmol, 1.24 equiv) were added to a dry round flask and dissolved in acetonitrile (20 mL). Et_3N (300 µL) was added and the reaction mixture was stirred at room temperature for 5.5 h. To the reaction solution was added sat. sol. NH_4Cl (5 mL) stirred for 2 h. Organic phase was extracted with EtOAc (3 times) and washed with brine. The organic layer was dried over $MgSO_4$, filtered and evaporated in vacuo. The crude product (1.14 g) was subjected to column chromatography on silica gel (MeOH/DCM, 0:100 → 20:100) to give **12** (290 mg, 0.45 mmol, 63% over two steps).

Characterization: R*f* (CH_2Cl_2/MeOH, 8:2): 0.80; **^{1}H NMR** (400 MHz, $CDCl_3$) δ 8.08 (s, 1H), 7.76 (d, *J* = 8.8 Hz, 1H), 7.65 (d, *J* = 8.8 Hz, 1H), 7.51 – 7.35 (m, 2H), 7.33 – 7.26 (m, 2H), 7.23 (d, *J* = 7.1 Hz, 1H), 7.10 (s, 2H), 6.96 (s, 2H), 4.73 (s, 1H), 4.04 (d, *J* = 11.2 Hz, 1H), 3.92 (d, *J* = 11.1 Hz, 1H), 3.75 (s, 1H), 2.63 (s, 1H), 2.04 (d, *J* = 1.1 Hz, 1H), 1.16 – 1.03 (m, 21H), 0.88 (s, 9H), 0.07 (s, 3H), 0.05 (s, 3H). **HRMS** (ESI): *m/z* 650.38059 ($[M+H]^+$ $C_{36}H_{56}O_4N_3Si_2^+$ requires 650.38039).

1′-(3′-O-tertbutyldimethylsilyl-5′-O-triisopropylsilyl-2′-deoxy-β-D-ribofuranoside)-4-(N-benzoyl)-amino-6-styryl-quinazoline- 2,4-(3*H*)-dione (13)

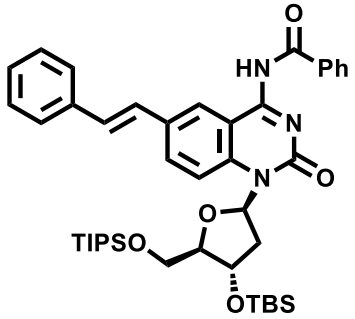

Procedure: To a stirring solution of **12** (590 mg, 0.836 mmol, 1.0 equiv.) in DMF (15 mL), was added Bz_2O (226 mg, 1.00 mmol, 1.2 equiv). The reaction mixture was stirred at room temperature for 24h. Organic phase was extracted with EtOAc (3 times) and washed with brine. The organic layer was dried over $MgSO_4$, filtered and evaporated in vacuo. The crude product was subjected to column chromatography on silica gel (Hex/EtOAc, 100:0 → 95:5) to give **13** (548 mg, 0.728 mmol, 87%).

Characterization: R*f* (Hex/EtOAc, 9:1): 0.45; **^{1}H NMR** (500 MHz, $CDCl_3$) δ 13.07 (s, 1H), 8.71 (d, *J* = 1.8 Hz, 1H), 8.45 – 8.40 (m, 2H), 7.84 – 7.78 (m, 2H), 7.58 (d, *J* = 7.2 Hz, 3H), 7.52 (t, *J* = 7.5 Hz, 2H), 7.41 (t, *J* = 7.6 Hz, 2H), 7.34 – 7.30 (m, 1H), 7.23 – 7.13 (m, 2H), 6.77 (t, *J* = 7.6 Hz, 1H), 4.78 (ddd, *J* = 8.6, 5.3, 3.9 Hz, 1H), 4.07 (dd, *J* = 11.3, 3.1 Hz, 1H), 3.95 (dd, *J* = 11.3, 3.5 Hz, 1H), 3.88 (dt, *J* = 5.3, 3.2 Hz, 1H), 2.85 (dt, *J* = 13.4, 8.0 Hz, 1H), 2.10 (ddd, *J* = 13.4, 7.5, 3.8 Hz, 1H), 1.22 – 1.09 (m, 21H), 0.92 (s, 9H), 0.12 (s, 3H), 0.11 (s, 3H). **^{13}C NMR** (126 MHz, $CDCl_3$) δ 180.0, 157.6, 147.8, 139.6, 137.1, 137.0, 133.3, 133.0, 132.6, 130.2, 130.0, 129.0, 128.4, 128.3, 126.9, 126.8, 125.9, 117.4, 117.2, 86.7, 84.5, 70.4, 62.1, 37.3, 25.9, 18.2, 18.2, 18.1, 12.1, -4.4, -4.7. **HRMS** (ESI): *m/z* 776.3807 ($[M+Na]^+$ $C_{43}H_{59}O_5NaN_3Si_2^+$ requires 776.3886).

1′-(2′-deoxy-β-D ribofuranoside)-4-(N-benzoyl)-amino-6-styryl-quinazoline- 2,4-(3*H*)-dione (14)

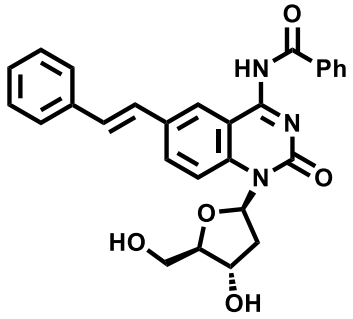

Procedure: To a stirred solution of nucleoside **13** (582 mg, 0.806 mmol, 1.0 equiv.) in THF (10 mL), was added TBAF (1M solution in THF, 4.0 mL, 5.0 equiv.). The mixture was stirred at room temperature for 20 h and then directly loaded onto a silica gel column chromatography (100% MeCN), to give deprotected nucleoside **14** (295 mg, 0.610 mmol, 76 %), as a yellow solid.

Characterization: R*f* (CH_2Cl_2/MeOH, 9:1): 0.48; **^{1}H NMR** (500 MHz, $CDCl_3$) δ 12.99 (s, 1H), 8.59 (s, 1H), 8.37 (d, *J* = 7.6 Hz, 1H), 7.81 (d, *J* = 7.3 Hz, 1H), 7.58 – 7.41 (m, 5H), 7.40 – 7.27 (m, 3H), 7.12 (s, 1H), 6.62 – 6.54 (m, 1H), 4.82 (d, *J* = 8.5 Hz, 1H), 4.12 – 3.95 (m, 2H), 3.92 – 3.81 (m, 1H), 3.77 – 3.70 (m, 1H), 3.08 (dt, *J* = 14.4, 7.2 Hz, 1H), 2.26 – 2.18 (m, 1H). **^{13}C NMR** (126 MHz, $CDCl_3$) δ 162.7, 147.7, 140.0, 136.8, 135.9, 133.0, 132.2, 130.2, 128.9, 128.8, 128.7, 128.6, 128.4, 128.3, 127.5, 126.8, 126.4, 126.0, 125.6, 116.5, 115.7, 87.2, 85.9, 71.5, 68.1, 62.5, 34.3. **HRMS** (ESI): *m/z* 506.1682 ($[M+Na]^+$ $C_{28}H_{25}O_5NaN_3^+$ requires 506.1686).

1′-(2′-deoxy-β-D ribofuranoside)-4-amino-6-styryl-quinazoline- 2,4-(3*H*)-dione (15)

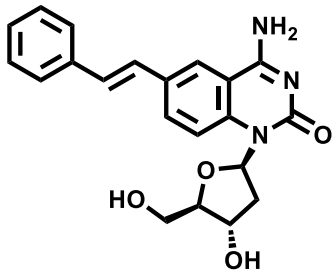

Procedure: To a stirred solution of nucleoside **12** (927 mg, 1.43 mmol, 1.0 equiv.) in THF (18 mL), was added TBAF (1M solution in THF, 7.1 mL, 5.0 equiv.). The mixture was stirred at room temperature for 18 h and then directly loaded onto a silica gel column chromatography CH_2Cl_2/MeOH/Et_3N, gradient from 100 : 0 : 0.5 to 80 : 20 : 0.5, to give deprotected nucleoside **15** (467 mg, 1.30 mmol, 86 %).

Characterization: R*f* (CH_2Cl_2/MeOH, 9:1): 0.13; **^{1}H NMR** (500 MHz, DMSO-d_6) δ 8.38 (d, *J* = 2.0 Hz, 1H), 8.10 (d, *J* = 68.2 Hz, 2H), 7.88 – 7.77 (m, 2H), 7.58 (d, *J* = 7.3 Hz, 2H), 7.40 (t, *J* = 7.7 Hz, 2H), 7.35 (d, *J* = 16.4 Hz, 1H), 7.28 (t, *J* = 7.4 Hz, 1H), 7.21 (d, *J* = 16.4 Hz, 1H), 6.77 (t, *J* = 7.8 Hz, 1H), 5.27 (d, *J* = 5.0 Hz, 1H), 5.01 (t, *J* = 5.2 Hz, 1H), 4.44 (dq, *J* = 8.6, 4.3 Hz, 1H), 3.73 (ddt, *J* = 8.0, 5.7, 2.6 Hz, 2H), 3.66 (dt, *J* = 12.2, 5.2 Hz, 1H), 2.64 (dt, *J* = 13.2, 8.3 Hz, 1H), 1.91 (ddd, *J* = 13.2, 7.4, 3.4 Hz, 1H). **^{13}C NMR** (126 MHz, DMSO-d_6) δ 163.4, 155.5, 140.8, 137.4, 132.3, 131.1, 129.3, 128.9, 128.2, 127.4, 126.8, 122.5, 117.3, 111.3, 86.9, 84.3, 70.4, 70.3, 61.4, 36.9. **HRMS** (ESI): *m/z* 402.1431 ($[M+Na]^+$ $C_{21}H_{21}O_4NaN_3^+$ requires 402.1424).

1′-[5′-*O*-(4,4-dimethoxytrityl)-2′-deoxy-β-d-ribofuranoside]-4-(N-benzoyl)-amino-6-styryl-quinazoline- 2,4-(3*H*)-dione (16)

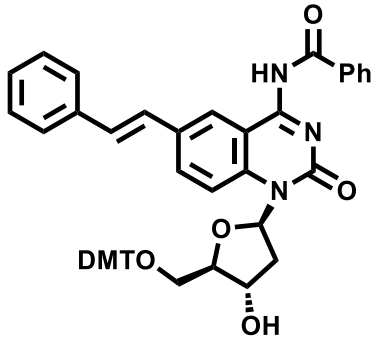

Procedure: Nucleoside **14** (290 mg, 0.600 mmol, 1.0 equiv.) was co-evaporated with pyridine (3 x 3.00 mL) and then suspended in pyridine (2.00 mL). To the stirring solution was added dropwise DMTCl (360 mg, 1.06 mmol, 1.8 equiv.) dissolved in 3.00 mL pyridine. The reaction mixture was stirred at room temperature for 4 h. The reaction was then quenched with a sat. sol. $NaHCO_3$. The resulting mixture was extracted with CH_2Cl_2 and the combined organic layer was dried over $MgSO_4$, filtered, and co-evaporated *in vacuo* with pyridine. The crude product was purified by column chromatography on silica gel (Toluene/Et_3N, 99.5 : 0.5) to obtain nucleoside **16** (273 mg, 0.347 mmol, 58 %) as a yellow foam.

Characterization: R*f* (Hex/EtOAc, 6:4): 0.58; **^{1}H NMR** (500 MHz, $CDCl_3$) δ 13.11 (s, 1H), 8.60 (d, *J* = 2.3 Hz, 1H), 8.49 – 8.35 (m, 2H), 8.08 (d, *J* = 8.9 Hz, 1H), 7.62 – 7.26 (m, 20H), 7.12 – 7.04 (m, 2H), 6.94 – 6.76 (m, 7H), 4.93 (dq, *J* = 8.3, 3.5 Hz, 1H), 4.04 (dt, *J* = 4.9, 3.0 Hz, 1H), 3.75 (s, 3H), 3.75 (s, 3H), 3.57 – 3.53 (m, 2H), 2.97 (dt, *J* = 13.6, 8.3 Hz, 1H), 2.25 (ddd, *J* = 13.6, 7.1, 3.2 Hz, 1H). **^{13}C NMR** (126 MHz, $CDCl_3$) δ 180.0, 158.7, 157.5, 147.9, 144.5, 139.0, 137.0, 136.9, 135.8, 135.6, 133.2, 132.9, 132.5, 130.5, 130.3, 130.3, 130.2, 130.2, 129.7, 128.9, 128.8, 128.7, 128.6, 128.4, 128.2, 128.1, 128.1, 128.0, 127.2, 126.7, 126.6, 126.2, 118.1, 116.9, 113.3, 113.3, 86.8, 85.2, 84.3, 71.1, 62.5, 55.3, 37.2. **HRMS** (ESI): *m/z* 808.2983 ($[M+Na]^+$ $C_{49}H_{43}O_7N_3Na^+$ requires 808.2993).

1'-[3'-*O*-[2-cyanoethoxy-(*N*,*N*-diisopropylamino)-phosphino]-(5'-*O*-(4,4-dimethoxytrityl)-2'-deoxy-β-d-ribofuranoside]-4-(N-benzoyl)-amino-6-styryl-quinazoline- 2,4-(3*H*)-dione (17)

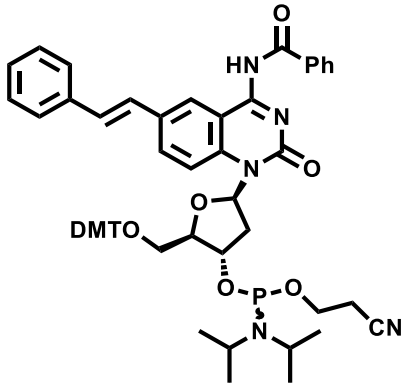

Procedure: To a stirred solution of nucleoside **16** (240 mg, 0.305 mmol, 1.0 equiv.) in CH_2Cl_2 (7.0 mL) at 0 ^oC, was added distilled diisopropylethylamine (DIPEA, 275 µL, 1.58 mmol, 5.2 equiv.) and the reaction was stirred 20 min at 0 ^oC under an atmosphere of Ar. To this solution was added 2-cyanoethyl *N*,*N*-diisopropylchlorophosphoramidite (275 µL, 1.23 mmol, 4.0 equiv) and the reaction was stirred at 22 ^oC for 180 min while it was monitored by TLC every 30 min. The reaction mixture was then loaded directly to a silica gel column, without any quenching or workup steps. The residue was purified by flash column chromatography (elution time of 10 min) on silica gel (distilled hexane/ distilled EtOAc/Et_3N, 80:20:0.5 → 60:40:0.5) to obtain nucleoside **17** (225 mg, 0.228 mmol, 75 %, diastereomeric mixture) as a yellow foam.

Characterization: R*f* (hexane/EtOAc, 6:4): 0.58; **^{1}H NMR** (500 MHz, CD_2Cl_2) δ 13.02 (s, 1H), 8.67 (d, *J* = 2.3 Hz, 1H), 8.44-8.42 (m, 2H), 8.06 (dd, *J* = 8.9, 5.2 Hz, 1H), 7.64 – 7.06 (m, 24H), 7.00 – 6.72 (m, 7H), 5.12 – 4.97 (m, 1H), 3.74 (s, 3H), 3.74 (s, 3H), 3.67 – 3.52 (m, 4H), 2.99 (dq, *J* = 13.5, 8.4 Hz, 1H), 2.60 (t, *J* = 6.3 Hz, 2H), 2.42 (t, *J* = 6.4 Hz, 1H), 1.22 (t, *J* = 7.1 Hz, 6H), 1.05 (d, *J* = 6.8 Hz, 3H). **^{31}P NMR** (203 MHz, CD_2Cl_2) δ 149.1, 140.0. **HRMS** (ESI): *m/z* 1008.4108 ($[M+Na]^+$ $C_{58}H_{60}O_8N_5NaP^+$ requires 1008.4072).

4.8.4 NMR Spectra

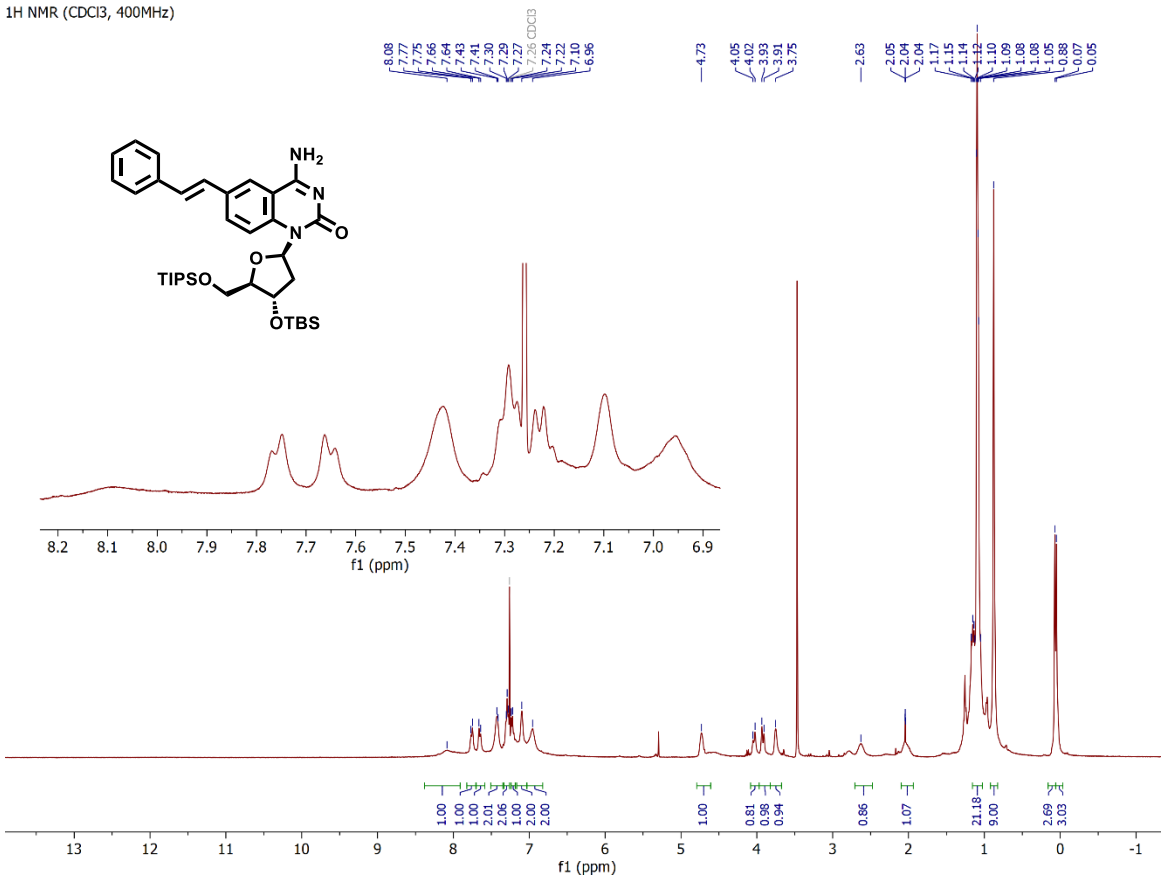

^{1}H NMR spectrum of **12**

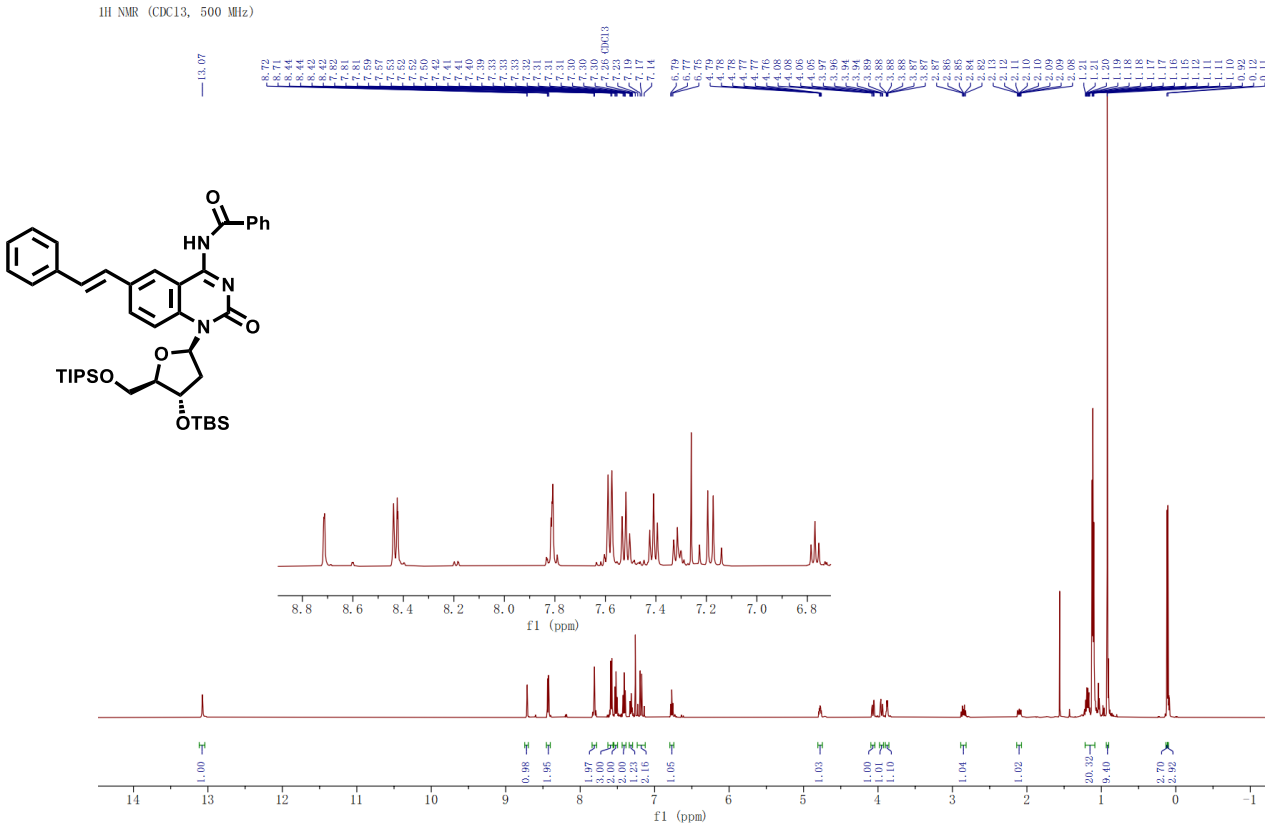

^{1}H NMR spectrum of **13**

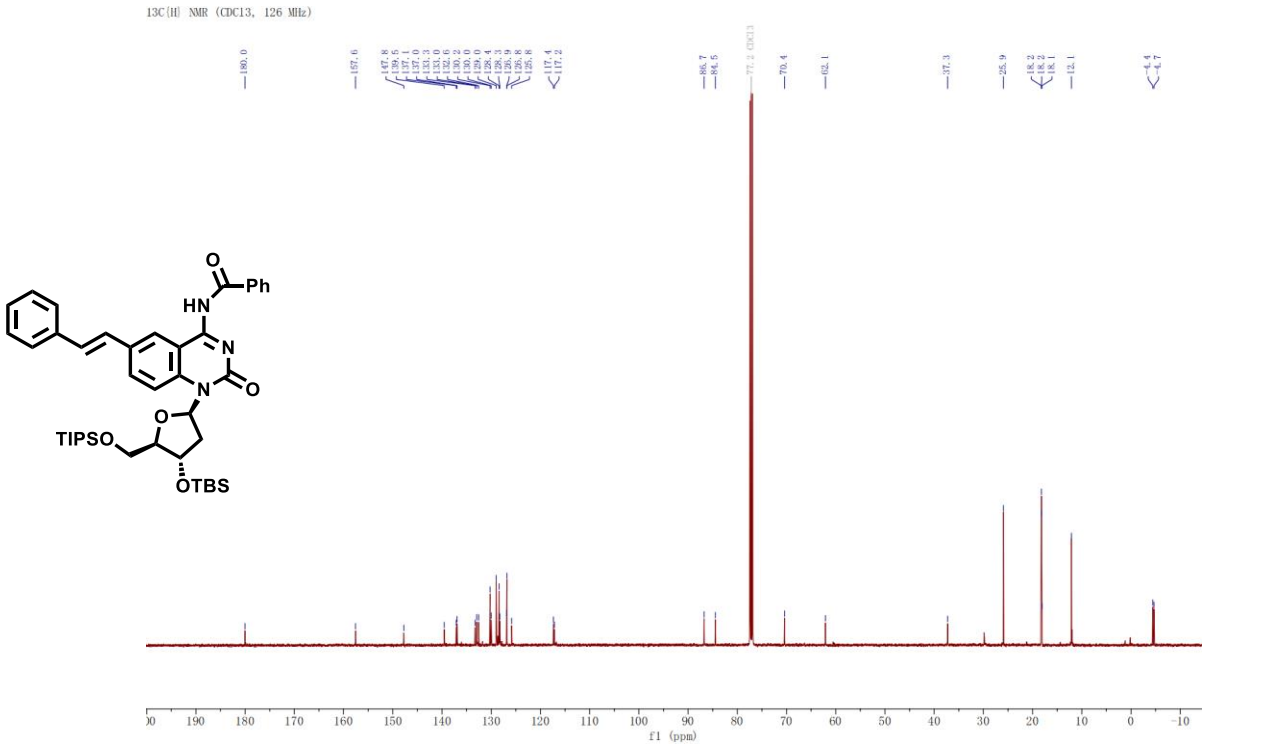

^{13}C NMR spectrum of **13**

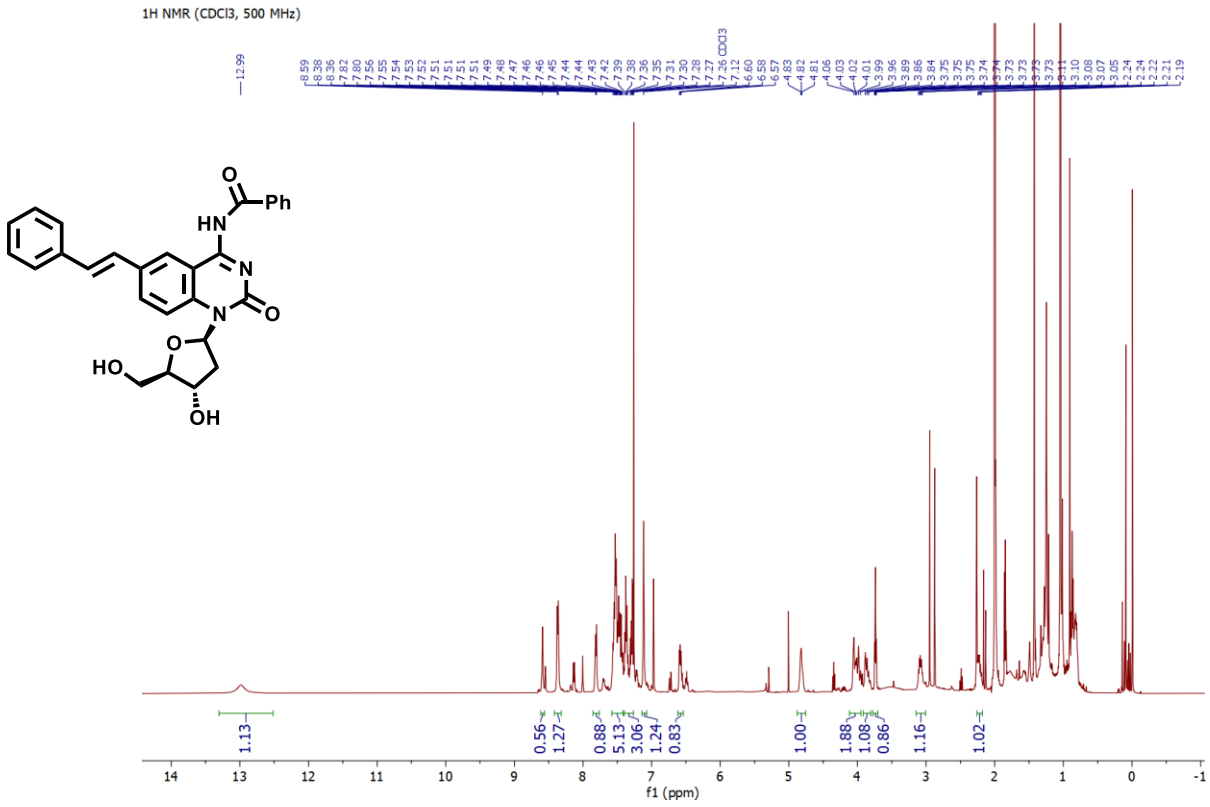

^{1}H NMR spectrum of **14**

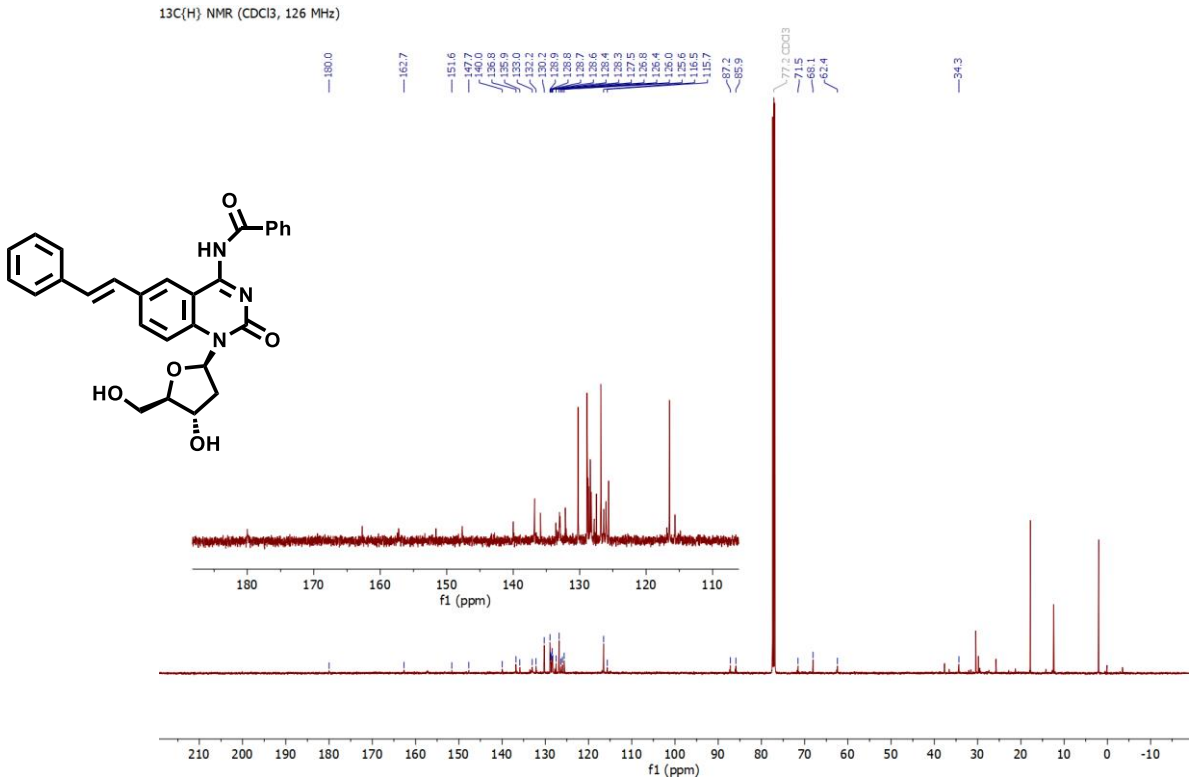

^{13}C NMR spectrum of **14**

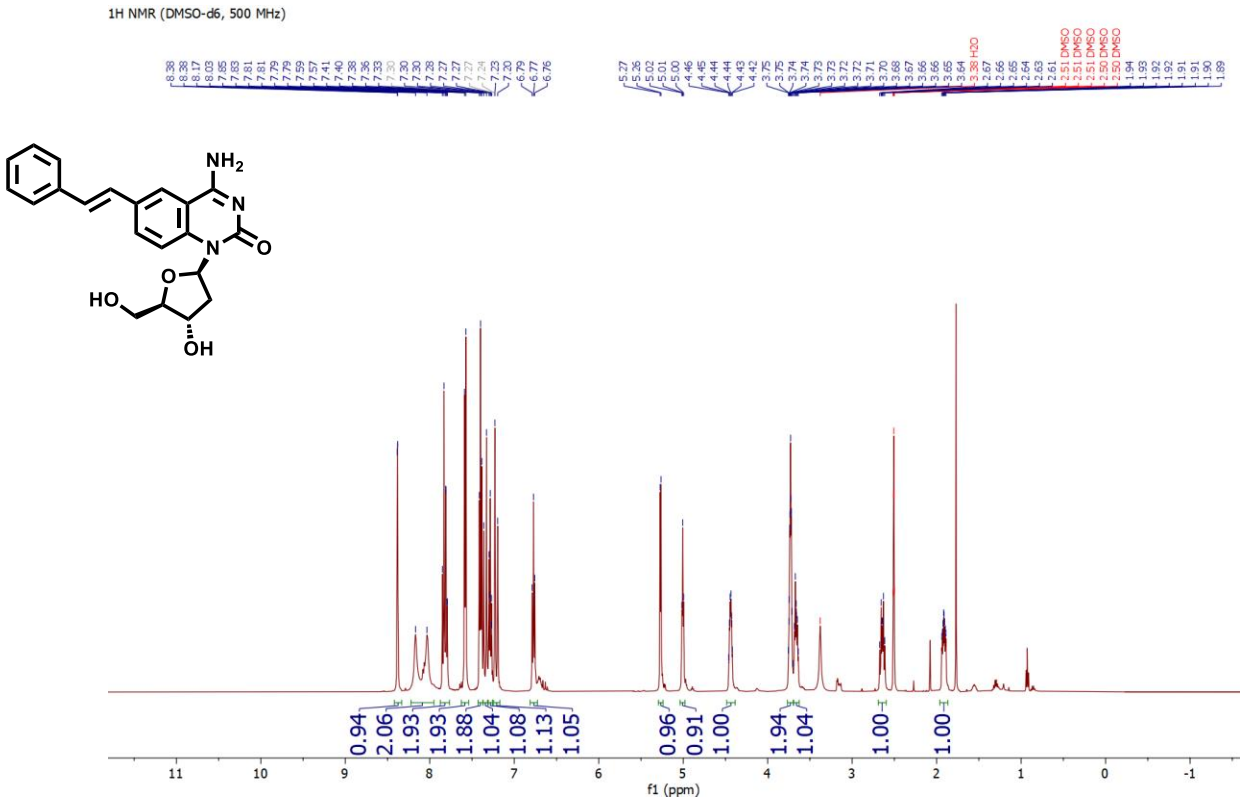

^{1}H NMR spectrum of **15**

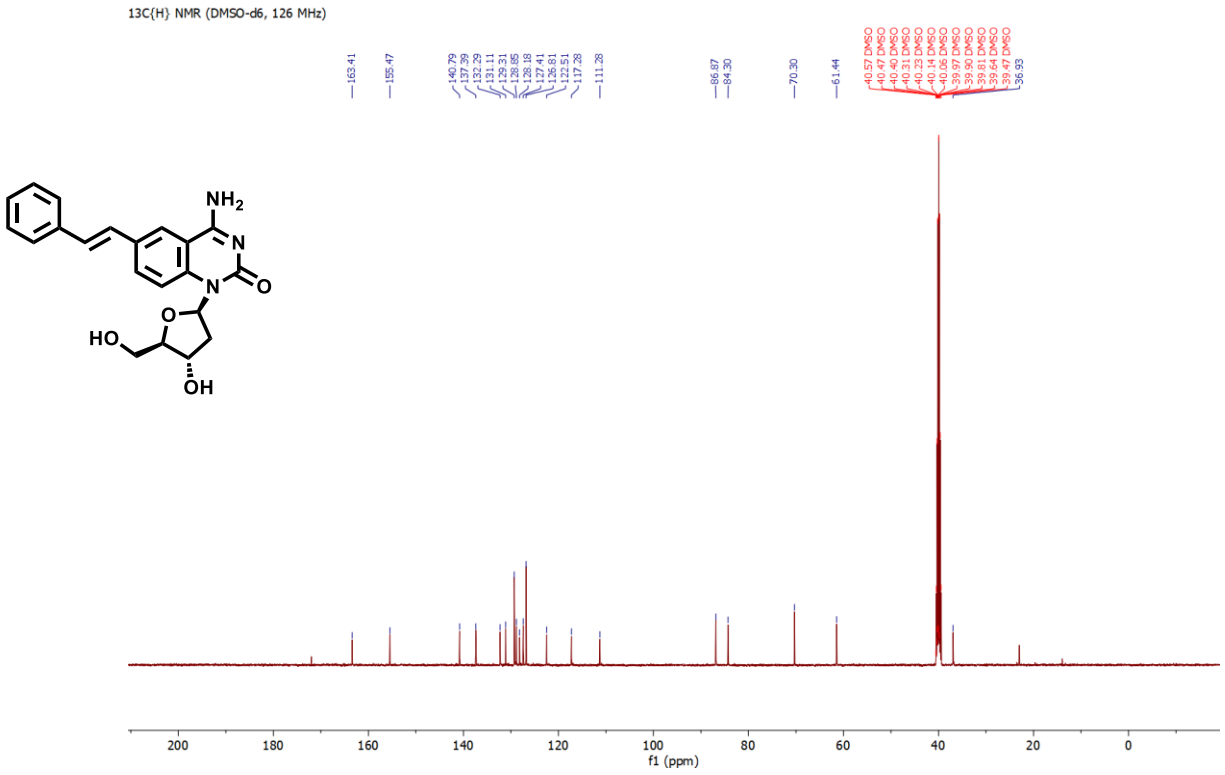

^{13}C NMR spectrum of **15**

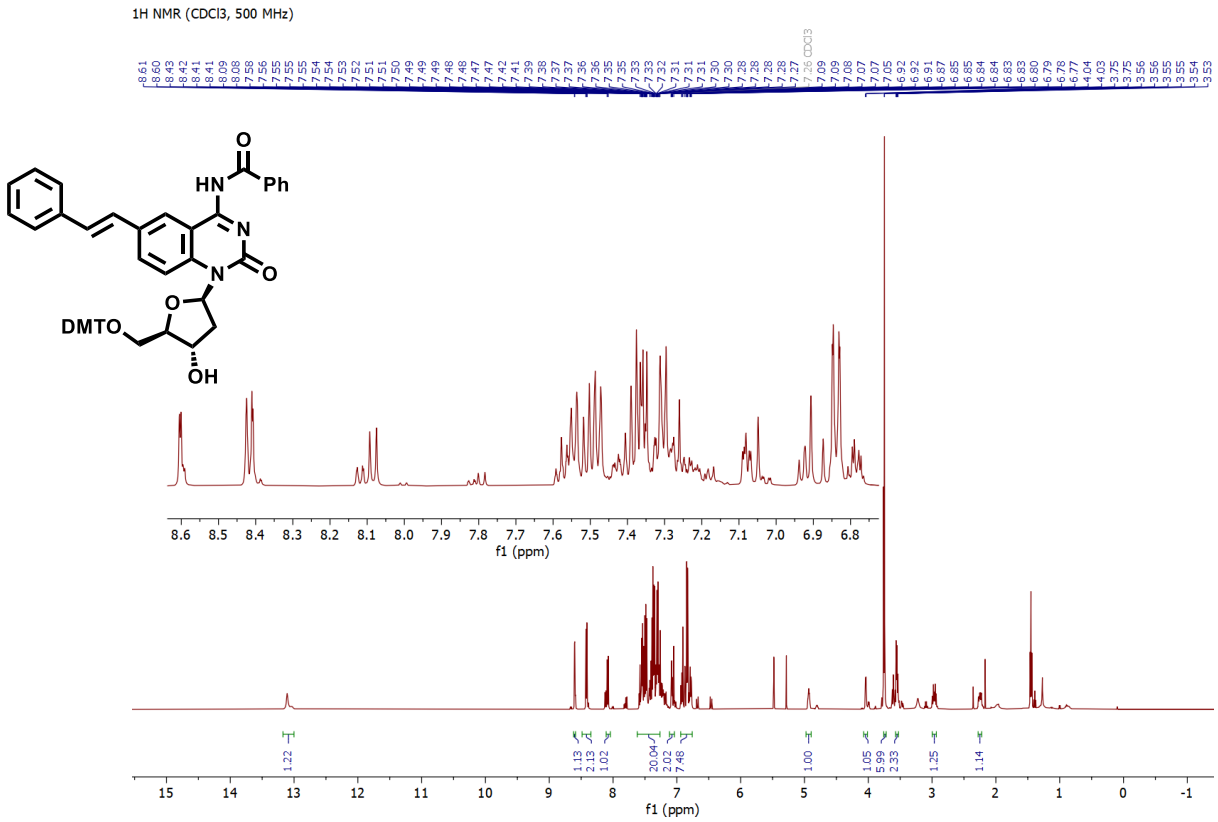

^{1}H NMR spectrum of **16**

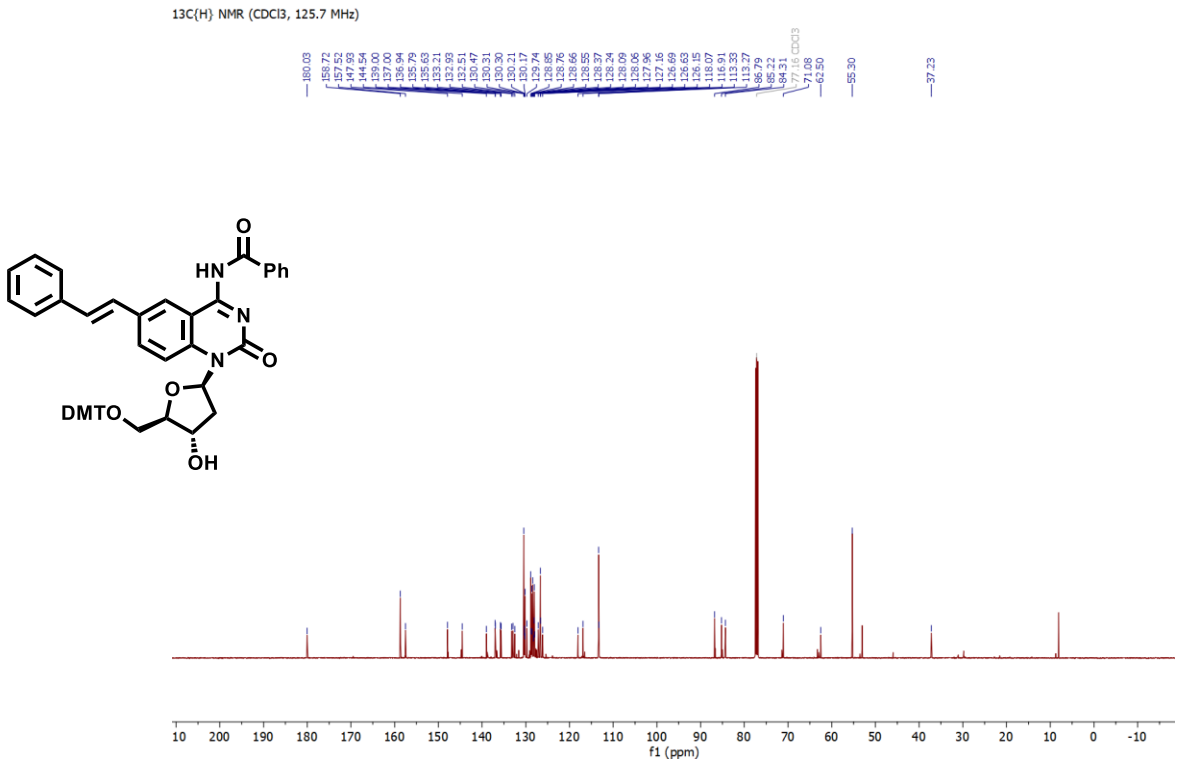

^{13}C NMR spectrum of **16**

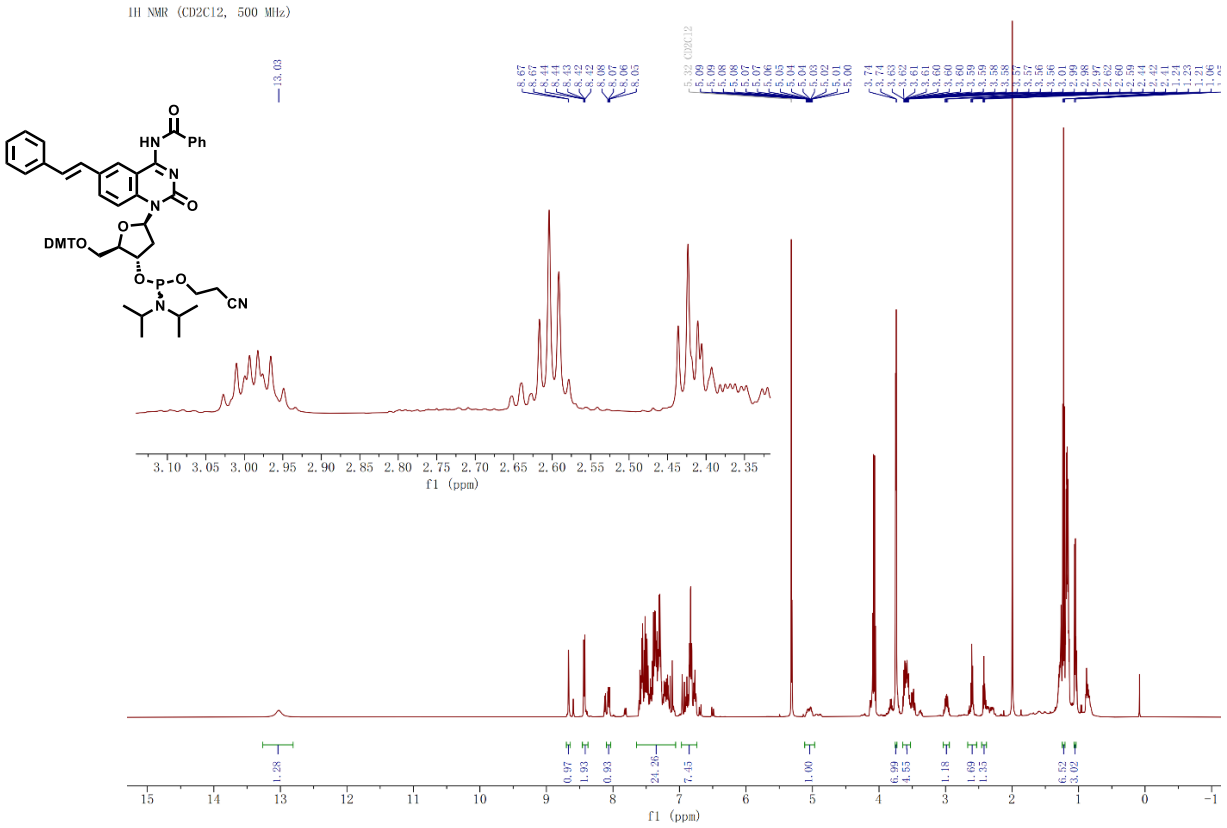

^{1}H NMR spectrum of **17**

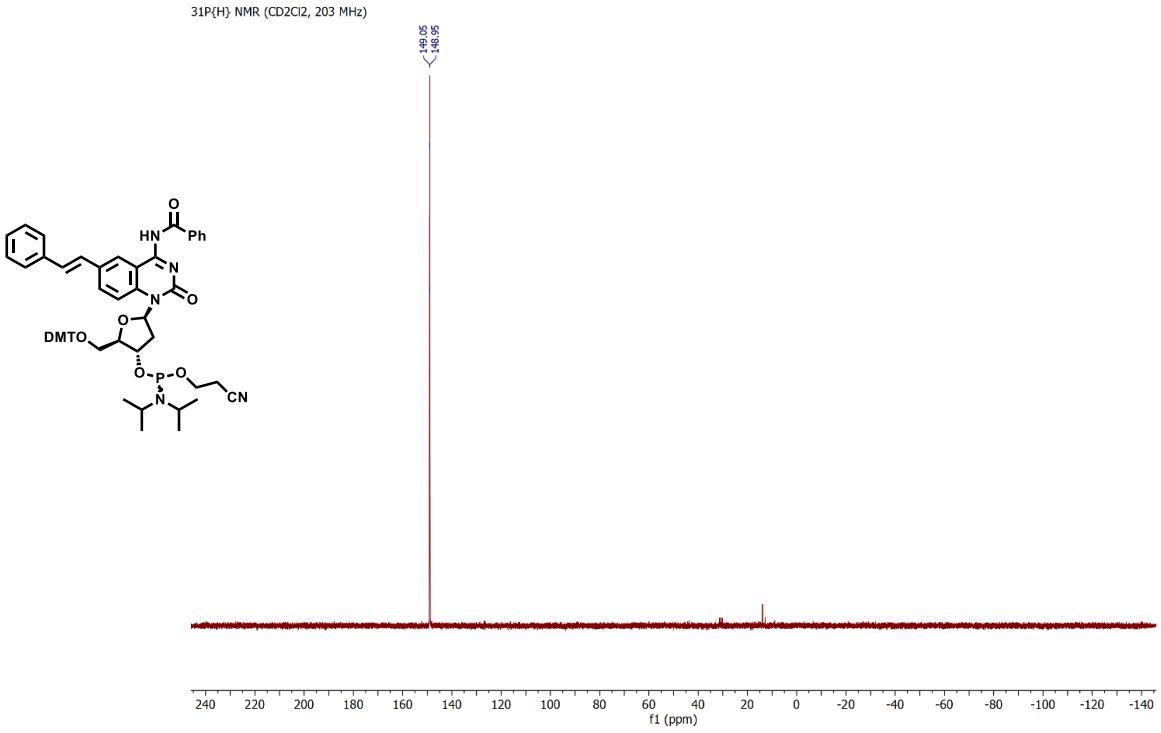

^{31}P NMR spectrum of **17**

4.9 References

[1] Choi, J.; Majima, T., Conformational changes of non-B DNA. *Chem. Soc. Rev.* **2011,** *40* (12), 5893-5909.

[2] Patel, D. J.; Phan, A. T.; Kuryavyi, V., Human telomere, oncogenic promoter and 5'-UTR G-quadruplexes: diverse higher order DNA and RNA targets for cancer therapeutics. *Nucleic Acids Res.* **2007,** *35* (22), 7429-7455.

[3] Lopes, J.; Piazza, A.; Bermejo, R.; Kriegsman, B.; Colosio, A.; Teulade-Fichou, M.-P.; Foiani, M.; Nicolas, A., G-quadruplex-induced instability during leading-strand replication. *EMBO J.* **2011,** *30* (19), 4033-4046.

[4] Bacolla, A.; Wells, R. D., Non-B DNA conformations as determinants of mutagenesis and human disease. *Mol. Carcinog.* **2009,** *48* (4), 273-285.

[5] Cahoon, L. A.; Seifert, H. S., An alternative DNA structure is necessary for pilin antigenic variation in Neisseria gonorrhoeae. *Science* **2009,** *325* (5941), 764-767.

[6] Biffi, G.; Tannahill, D.; McCafferty, J.; Balasubramanian, S., Quantitative visualization of DNA G-quadruplex structures in human cells. *Nat. Chem.* **2013,** *5* (3), 182-186.

[7] Postel, E. H.; Flint, S. J.; Kessler, D. J.; Hogan, M. E., Evidence that a triplex-forming oligodeoxyribonucleotide binds to the c-myc promoter in HeLa cells, thereby reducing c-myc mRNA levels. *Proc. Natl. Acad. Sci. U. S. A.* **1991,** *88* (18), 8227-8231.

[8] Praseuth, D.; Guieysse, A. L.; Hélène, C., Triple helix formation and the antigene strategy for sequence-specific control of gene expression. *Biochim. Biophys. Acta* **1999,** *1489* (1), 181-206.

[9] Huppert, J. L.; Balasubramanian, S., Prevalence of quadruplexes in the human genome. *Nucleic Acids Res.* **2005,** *33* (9), 2908-2916.

[10] Todd, A. K.; Johnston, M.; Neidle, S., Highly prevalent putative quadruplex sequence motifs in human DNA. *Nucleic Acids Res.* **2005,** *33* (9), 2901-2907.

[11] Bochman, M. L.; Paeschke, K.; Zakian, V. A., DNA secondary structures: stability and function of G-quadruplex structures. *Nat. Rev. Genet.* **2012,** *13* (11), 770-780.

[12] Pennarun, G.; Granotier, C.; Gauthier, L. R.; Gomez, D.; Hoffschir, F.; Mandine, E.; Riou, J. F.; Mergny, J. L.; Mailliet, P.; Boussin, F. D., Apoptosis related to telomere instability and cell cycle alterations in human glioma cells treated by new highly selective G-quadruplex ligands. *Oncogene* **2005,** *24* (18), 2917-2928.

[13] Vasquez, K. M.; Glazer, P. M., Triplex-forming oligonucleotides: principles and applications. *Q. Rev. Biophys.* **2002,** *35* (1), 89-107.

[14] Mirkin, S. M.; Frank-Kamenetskii, M. D., H-DNA and related structures. *Annu Rev Biophys Biomol Struct* **1994,** *23*, 541-576.

[15] Sen, D.; Gilbert, W., Formation of parallel four-stranded complexes by guanine-rich motifs in DNA and its implications for meiosis. *Nature* **1988,** *334* (6180), 364-366.

[16] Sundquist, W. I.; Klug, A., Telomeric DNA dimerizes by formation of guanine tetrads between hairpin loops. *Nature* **1989,** *342* (6251), 825-829.

[17] Burge, S.; Parkinson, G. N.; Hazel, P.; Todd, A. K.; Neidle, S., Quadruplex DNA: sequence, topology and structure. *Nucleic Acids Res.* **2006,** *34* (19), 5402-5415.

[18] Lane, A. N.; Chaires, J. B.; Gray, R. D.; Trent, J. O., Stability and kinetics of G-quadruplex structures. *Nucleic Acids Res.* **2008,** *36* (17), 5482-5515.

[19] Zhou, B.; Geng, Y.; Liu, C.; Miao, H.; Ren, Y.; Xu, N.; Shi, X.; You, Y.; Lee, T.; Zhu, G., Characterizations of distinct parallel and antiparallel G-quadruplexes formed by two-repeat ALS and FTD related GGGGCC sequence. *Sci. Rep.* **2018,** *8* (1), 2366.

[20] Gehring, K.; Leroy, J.-L.; Guéron, M., A tetrameric DNA structure with protonated cytosine-cytosine base pairs. *Nature* **1993,** *363* (6429), 561-565.

[21] Mergny, J.-L.; Lacroix, L.; Han, X.; Leroy, J.-L.; Helene, C., Intramolecular folding of pyrimidine oligodeoxynucleotides into an i-DNA motif. *J. Am. Chem. Soc.* **1995,** *117* (35), 8887-8898.

[22] Kendrick, S.; Akiyama, Y.; Hecht, S. M.; Hurley, L. H., The i-motif in the bcl-2 p1 promoter forms an unexpectedly stable structure with a unique 8:5:7 loop folding pattern. *J. Am. Chem. Soc.* **2009,** *131* (48), 17667-17676.

[23] Miyoshi, D.; Karimata, H.; Sugimoto, N., Hydration regulates thermodynamics of G-quadruplex formation under molecular crowding conditions. *J. Am. Chem. Soc.* **2006,** *128* (24), 7957-7963.

[24] Esmaili, N.; Leroy, J. L., i-motif solution structure and dynamics of the d(AACCCC) and d(CCCCAA) tetrahymena telomeric repeats. *Nucleic Acids Res.* **2005,** *33* (1), 213-224.

[25] Kang, C. H.; Berger, I.; Lockshin, C.; Ratliff, R.; Moyzis, R.; Rich, A., Crystal structure of intercalated four-stranded d(C3T) at 1.4 A resolution. *Proc. Natl. Acad. Sci. U.S.A.* **1994,** *91* (24), 11636-11640.

[26] Chen, L.; Cai, L.; Zhang, X.; Rich, A., Crystal structure of a four-stranded intercalated DNA: d(C4). *Biochemistry* **1994,** *33* (46), 13540-13546.

[27] Bhavsar-Jog, Y. P.; Van Dornshuld, E.; Brooks, T. A.; Tschumper, G. S.; Wadkins, R. M., Epigenetic modification, dehydration, and molecular crowding effects on the thermodynamics of i-motif structure formation from C-rich DNA. *Biochemistry* **2014,** *53* (10), 1586-1594.

[28] Abou Assi, H.; Garavís, M.; González, C.; Damha, M. J., i-Motif DNA: structural features and significance to cell biology. *Nucleic Acids Res.* **2018,** *46* (16), 8038-8056.

[29] Christensen, J. J.; Rytting, J. H.; Izatt, R. M., Thermodynamics of proton dissociation in dilute aqueous solution. 8. pK, change in heat content, and change in entropy values for proton ionization from several pyrimidines and their nucleosides at 25 degrees. *J. Phys. Chem.* **1967,** *71* (8), 2700-2705.

[30] Izatt, R. M.; Christensen, J. J.; Rytting, J. H., Sites and thermodynamic quantities associated with proton and metal ion interaction with ribonucleic acid, deoxyribonucleic acid, and their constituent bases, nucleosides, and and nucleotides. *Chem. Rev.* **1971,** *71* (5), 439-481.

[31] Brooks, T. A.; Kendrick, S.; Hurley, L., Making sense of G-quadruplex and i-motif functions in oncogene promoters. *Febs j* **2010,** *277* (17), 3459-3469.

[32] Li, X.; Peng, Y.; Ren, J.; Qu, X., Carboxyl-modified single-walled carbon nanotubes selectively induce human telomeric i-motif formation. *Proc. Natl. Acad. Sci. U.S.A.* **2006,** *103* (52), 19658-19663.

[33] Rajendran, A.; Nakano, S.-i.; Sugimoto, N., Molecular crowding of the cosolutes induces an intramolecular i-motif structure of triplet repeat DNA oligomers at neutral pH. *Chemical Communications* **2010,** *46* (8), 1299-1301.

[34] Miyoshi, D.; Matsumura, S.; Nakano, S.-i.; Sugimoto, N., Duplex dissociation of telomere dnas induced by molecular crowding. *J. Am. Chem. Soc.* **2004,** *126* (1), 165-169.

[35] Cui, J.; Waltman, P.; Le, V. H.; Lewis, E. A., The effect of molecular crowding on the stability of human c-MYC promoter sequence I-motif at neutral pH. *Molecules* **2013,** *18* (10), 12751-12767.

[36] Assi, H. A.; Harkness, R. W. t.; Martin-Pintado, N.; Wilds, C. J.; Campos-Olivas, R.; Mittermaier, A. K.; González, C.; Damha, M. J., Stabilization of i-motif structures by 2'-β-fluorination of DNA. *Nucleic Acids Res.* **2016,** *44* (11), 4998-5009.

[37] Sun, D.; Guo, K.; Rusche, J. J.; Hurley, L. H., Facilitation of a structural transition in the polypurine/polypyrimidine tract within the proximal promoter region of the human VEGF gene by the presence of potassium and G-quadruplex-interactive agents. *Nucleic Acids Res.* **2005,** *33* (18), 6070-6080.

[38] Kendrick, S.; Kang, H. J.; Alam, M. P.; Madathil, M. M.; Agrawal, P.; Gokhale, V.; Yang, D.; Hecht, S. M.; Hurley, L. H., The dynamic character of the BCL2 promoter i-motif provides a mechanism for modulation of gene expression by compounds that bind selectively to the alternative DNA hairpin structure. *J. Am. Chem. Soc.* **2014,** *136* (11), 4161-4171.

[39] Kang, H.-J.; Kendrick, S.; Hecht, S. M.; Hurley, L. H., The transcriptional complex between the BCL2 i-motif and hnRNP ll is a molecular switch for control of gene expression that can be modulated by small molecules. *J. Am. Chem. Soc.* **2014,** *136* (11), 4172-4185.

[40] Day, H. A.; Huguin, C.; Waller, Z. A. E., Silver cations fold i-motif at neutral pH. *Chemical Communications* **2013,** *49* (70), 7696-7698.

[41] Abdelhamid, M. A. S.; Fábián, L.; MacDonald, C. J.; Cheesman, M. R.; Gates, A. J.; Waller, Z. A. E., Redox-dependent control of i-motif DNA structure using copper cations. *Nucleic Acids Res.* **2018,** *46* (12), 5886-5893.

[42] Day, H. A.; Wright, E. P.; MacDonald, C. J.; Gates, A. J.; Waller, Z. A. E., Reversible DNA i-motif to hairpin switching induced by copper(ii) cations. *Chem. Commun.* **2015,** *51* (74), 14099-14102.

[43] Mir, B.; Serrano, I.; Buitrago, D.; Orozco, M.; Escaja, N.; González, C., Prevalent sequences in the human genome can form mini i-motif structures at physiological pH. *J. Am. Chem. Soc.* **2017,** *139* (40), 13985-13988.

[44] Escaja, N.; Viladoms, J.; Garavís, M.; Villasante, A.; Pedroso, E.; González, C., A minimal i-motif stabilized by minor groove G:T:G:T tetrads. *Nucleic Acids Res.* **2012,** *40* (22), 11737-11747.

[45] Serrano-Chacón, I.; Mir, B.; Escaja, N.; González, C., Structure of i-motif/duplex junctions at neutral pH. *J. Am. Chem. Soc.* **2021,** *143* (33), 12919-12923.

[46] Brazier, J. A.; Shah, A.; Brown, G. D., I-motif formation in gene promoters: unusually stable formation in sequences complementary to known G-quadruplexes. *Chem. Commun.* **2012,** *48* (87), 10739-10741.

[47] Fleming, A. M.; Ding, Y.; Rogers, R. A.; Zhu, J.; Zhu, J.; Burton, A. D.; Carlisle, C. B.; Burrows, C. J., 4n–1 is a "sweet spot" in DNA i-motif folding of 2′-deoxycytidine homopolymers. *J. Am. Chem. Soc.* **2017,** *139* (13), 4682-4689.

[48] Phan, A. T.; Mergny, J. L., Human telomeric DNA: G-quadruplex, i-motif and Watson-Crick double helix. *Nucleic Acids Res.* **2002,** *30* (21), 4618-4625.

[49] Baldrich, E.; O'Sullivan, C. K., Ability of thrombin to act as molecular chaperone, inducing formation of quadruplex structure of thrombin-binding aptamer. *Anal. Biochem.* **2005,** *341* (1), 194-197.

[50] Marsich, E.; Piccini, A.; Xodo, L. E.; Manzini, G., Evidence for a HeLa nuclear protein that binds specifically to the single-stranded d(CCCTAA)n telomeric motif. *Nucleic Acids Res.* **1996,** *24* (20), 4029-4033.

[51] Marsich, E.; Xodo, L. E.; Manzini, G., Widespread presence in mammals and high binding specificity of a nuclear protein that recognises the single-stranded telomeric motif (CCCTAA)n. *Eur. J. Biochem.* **1998,** *258* (1), 93-99.

[52] Kouzine, F.; Sanford, S.; Elisha-Feil, Z.; Levens, D., The functional response of upstream DNA to dynamic supercoiling in vivo. *Nat. Struct. Mol. Biol.* **2008,** *15* (2), 146-154.

[53] Guo, K.; Gokhale, V.; Hurley, L. H.; Sun, D., Intramolecularly folded G-quadruplex and i-motif structures in the proximal promoter of the vascular endothelial growth factor gene. *Nucleic Acids Res.* **2008,** *36* (14), 4598-4608.

[54] Guo, K.; Pourpak, A.; Beetz-Rogers, K.; Gokhale, V.; Sun, D.; Hurley, L. H., Formation of pseudosymmetrical G-quadruplex and i-motif structures in the proximal promoter region of the RET oncogene. *J. Am. Chem. Soc.* **2007,** *129* (33), 10220-10228.

[55] Sun, D.; Hurley, L. H., The importance of negative superhelicity in inducing the formation of G-quadruplex and i-motif structures in the c-Myc promoter: implications for drug targeting and control of gene expression. *J. Med. Chem.* **2009,** *52* (9), 2863-2874.

[56] Xu, Y.; Sugiyama, H., Formation of the G-quadruplex and i-motif structures in retinoblastoma susceptibility genes (Rb). *Nucleic Acids Res.* **2006,** *34* (3), 949-954.

[57] Zeraati, M.; Langley, D. B.; Schofield, P.; Moye, A. L.; Rouet, R.; Hughes, W. E.; Bryan, T. M.; Dinger, M. E.; Christ, D., I-motif DNA structures are formed in the nuclei of human cells. *Nat. Chem.* **2018,** *10* (6), 631-637.

[58] Brown, S. L.; Kendrick, S., The i-motif as a molecular target: More than a complementary DNA secondary structure. *Pharmaceuticals* **2021,** *14* (2).

[59] Dembska, A.; Bielecka, P.; Juskowiak, B., pH-Sensing fluorescence oligonucleotide probes based on an i-motif scaffold: a review. *Analytical Methods* **2017,** *9* (43), 6092-6106.

[60] Mata, G.; Luedtke, N. W., Fluorescent probe for proton-coupled DNA folding revealing slow exchange of i-motif and duplex structures. *J. Am. Chem. Soc.* **2015,** *137* (2), 699-707.

[61] Huang, H.; Hong, X.; Liu, F.; Li, N., A simple approach to study the conformational switching of i-motif DNA by fluorescence anisotropy. *Analyst* **2015,** *140* (17), 5987-5991.

[62] Mergny, J.-L., Fluorescence energy transfer as a probe for tetraplex formation: The i-motif. *Biochemistry* **1999,** *38* (5), 1573-1581.

[63] Modi, S.; M. G, S.; Goswami, D.; Gupta, G. D.; Mayor, S.; Krishnan, Y., A DNA nanomachine that maps spatial and temporal pH changes inside living cells. *Nat. Nanotechnol.* **2009,** *4* (5), 325-330.

[64] Dembska, A.; Juskowiak, B., Pyrene functionalized molecular beacon with pH-sensitive i-motif in a loop. *Spectrochim. Acta A Mol. Biomol. Spectrosc.* **2015,** *150*, 928-933.

[65] Dembska, A.; Rzepecka, P.; Juskowiak, B., Spectroscopic characterization of i-motif forming C-myc derived sequences double-labeled with pyrene. *J. Fluoresc.* **2013,** *23* (4), 807-812.

[66] Xu, L.; Wang, J.; Sun, N.; Liu, M.; Cao, Y.; Wang, Z.; Pei, R., Neutral red as a specific light-up fluorescent probe for i-motif DNA. *Chem. Commun.* **2016,** *52* (99), 14330-14333.

[67] Ma, W.; Yan, L. a.; He, X.; Qing, T.; Lei, Y.; Qiao, Z.; He, D.; Huang, K.; Wang, K., Hairpin-contained i-motif based fluorescent ratiometric probe for high-resolution and sensitive response of small pH variations. *Anal. Chem.* **2018,** *90* (3), 1889-1896.

[68] Lee, Y. A.; Durandin, A.; Dedon, P. C.; Geacintov, N. E.; Shafirovich, V., Oxidation of guanine in G, GG, and GGG sequence contexts by aromatic pyrenyl radical cations and carbonate radical anions: relationship between kinetics and distribution of alkali-labile lesions. *J Phys Chem B* **2008,** *112* (6), 1834-1844.

[69] Bielecka, P.; Dembska, A.; Juskowiak, B., Monitoring of pH using an i-motif-forming sequence containing a fluorescent cytosine analogue, tC. *Molecules* **2019,** *24* (5), 952.

[70] Bielecka, P.; Juskowiak, B., Fluorescent sensor for pH monitoring based on an i-motif- – switching aptamer containing a tricyclic cytosine analogue (tC). *Molecules* **2015,** *20* (10).

[71] Reilly, Samantha M.; Lyons, Daniel F.; Wingate, Sara E.; Wright, Robert T.; Correia, John J.; Jameson, David M.; Wadkins, Randy M., Folding and hydrodynamics of a DNA i-motif from the c-myc promoter determined by fluorescent cytidine analogs. *Biophys. J.* **2014,** *107* (7), 1703-1711.

[72] Karimi, A.; Börner, R.; Mata, G.; Luedtke, N. W., A highly fluorescent nucleobase molecular rotor. *J. Am. Chem. Soc.* **2020,** *142* (34), 14422-14426.

[73] Saenger, W., Principles of Nucleic Acid Structure. Springer. *New York, Berlin, Heidelberg* **1984**.

[74] Reichardt, C., Solvatochromic dyes as solvent polarity indicators. *Chem. Rev.* **1994,** *94* (8), 2319-2358.

[75] Cimino-Reale, G.; Pascale, E.; Alvino, E.; Starace, G.; D'Ambrosio, E., Long telomeric C-rich 5'-tails in human replicating cells. *J. Biol. Chem.* **2003,** *278* (4), 2136-2140.

[76] Stewart, S. A.; Weinberg, R. A., Senescence: does it all happen at the ends? *Oncogene* **2002,** *21* (4), 627-630.

[77] Blackburn, E. H., Switching and signaling at the telomere. *Cell* **2001,** *106* (6), 661-673.

[78] Takahashi, S.; Bhattacharjee, S.; Ghosh, S.; Sugimoto, N.; Bhowmik, S., Preferential targeting cancer-related i-motif DNAs by the plant flavonol fisetin for theranostics applications. *Sci. Rep.* **2020,** *10* (1), 2504.

[79] I-Motif DNA structures may regulate promoters and telomeres. *Cancer Discov.* **2018,** *8* (6), 674-674.

[80] Guéron, M.; Leroy, J. L., The i-motif in nucleic acids. *Curr. Opin. Struct. Biol.* **2000,** *10* (3), 326-331.

[81] Phan, A. T.; Guéron, M.; Leroy, J. L., The solution structure and internal motions of a fragment of the cytidine-rich strand of the human telomere. *J. Mol. Biol.* **2000,** *299* (1), 123-144.

[82] Du, Z.; Yu, J.; Chen, Y.; Andino, R.; James, T. L., Specific recognition of the C-rich strand of human telomeric DNA and the RNA template of human telomerase by the first KH domain of human poly(C)-binding protein-2. *J. Biol. Chem.* **2004,** *279* (46), 48126-48134.

[83] Gray, D. M.; Ratliff, R. L.; Vaughan, M. R., Circular dichroism spectroscopy of DNA. *Methods Enzymol.* **1992,** *211*, 389-406.

[84] Kypr, J.; Kejnovská, I.; Renciuk, D.; Vorlícková, M., Circular dichroism and conformational polymorphism of DNA. *Nucleic Acids Res.* **2009,** *37* (6), 1713-1725.

[85] Dumas, A.; Luedtke, N. W., Highly fluorescent guanosine mimics for folding and energy transfer studies. *Nucleic Acids Res.* **2011,** *39* (15), 6825-6834.

[86] Reveguk, Z. V.; Khoroshilov, E. V.; Sharkov, A. V.; Pomogaev, V. A.; Buglak, A. A.; Tarnovsky, A. N.; Kononov, A. I., Exciton absorption and luminescence in i-motif DNA. *Sci. Rep.* **2019,** *9* (1), 15988.

[87] Li, W.; Miyoshi, D.; Nakano, S.; Sugimoto, N., Structural competition involving G-quadruplex DNA and its complement. *Biochemistry* **2003,** *42* (40), 11736-11744.

[88] Simmel, F. C.; Yurke, B.; Singh, H. R., Principles and applications of nucleic acid strand displacement reactions. *Chem. Rev.* **2019,** *119* (10), 6326-6369.

[89] Chen, C.; Li, M.; Xing, Y.; Li, Y.; Joedecke, C.-C.; Jin, J.; Yang, Z.; Liu, D., Study of pH-induced folding and unfolding kinetics of the DNA i-motif by stopped-flow circular dichroism. *Langmuir* **2012,** *28* (51), 17743-17748.

[90] Zhao, Y.; Schultz, N. E.; Truhlar, D. G., Exchange-correlation functional with broad accuracy for metallic and nonmetallic compounds, kinetics, and noncovalent interactions. *J Chem Phys* **2005,** *123* (16), 161103.

[91] Hariharan, P. C.; Pople, J. A., The influence of polarization functions on molecular orbital hydrogenation energies. *Theor. Chim. Acta* **1973,** *28* (3), 213-222.

[92] Cossi, M.; Barone, V., Time-dependent density functional theory for molecules in liquid solutions. *J. Chem. Phys.* **2001,** *115* (10), 4708-4717.

[93] W. Hehre, J. Y., P. Klunzinger, L. Lou, Wavefunction Inc. *Irvine, CA* **2008**.

[94] Frisch, M. J., Gaussian, Inc. *Wallingford, CT* **2010**.

[95] Lakowicz, J. R., *Principles of fluorescence spectroscopy*. 3rd ed.; Springer: New York, 2006.

[96] Enderlein, J.; Erdmann, R., Fast fitting of multi-exponential decay curves. *Opt. Commun.* **1997,** *134* (1), 371-378.

[97] Cantor, C. R.; Warshaw, M. M.; Shapiro, H., Oligonucleotide interactions. 3. Circular dichroism studies of the conformation of deoxyoligonucleotides. *Biopolymers* **1970,** *9* (9), 1059-1077.

Chapter 5 | Mercury-assisted DNA helical switching

"Is this all we are? A necklace of chemicals? Where, in the ***double helix***, does the soul lie?"

Tess Gerritsen

5.1 Introduction: B, A, and Z-form duplex DNA

5.1.1 Structural features

Rather than being a static molecule, double-helical DNA structures can exhibit considerable conformational flexibility. A- and B-form helices consist of two *anti*-parallel strands that are twisted to give a right-handed double helix containing a major and minor groove (Figure 5.1). B-DNA has a helical turn of 3.6 nm (10.5 base-pairs per turn) and a diameter of 2.0 nm, whereas A-DNA has a more compact (2.9 nm helical turn, equal to 11.6 base-pairs per turn) and wider (2.6 nm diameter) structure that is usually observed under dehydrating conditions.[1] A prominent feature of the A-form helix is the displacement of the base-pairs from the center of the helix, thereby creating an axial hole. Each base-pair is displaced by ~4° towards the minor groove giving the helix a deeper major groove and a shallower minor groove (Figure 5.1).[1] In addition, the ß-D-2′-deoxyribose sugars adopt a non-planar C2′-*endo* sugar pucker in the B-form helix and a C3′-*endo* conformation in the A-form DNA (Figure 5.2A).

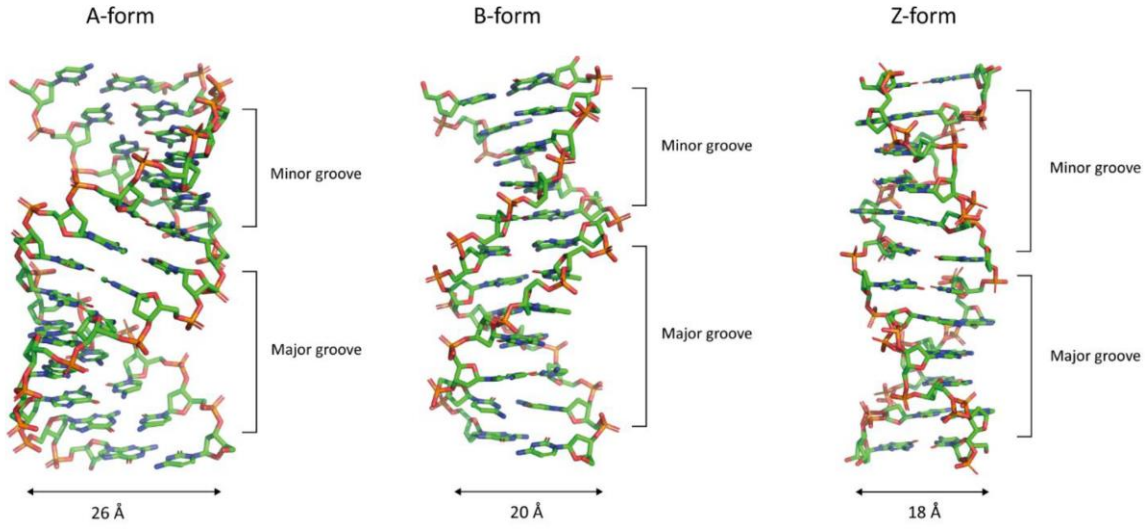

Figure 5.1. Structural variations between A, B, and Z-form duplex DNA (from left to right). Coordinates were taken from the PDB files 3V9D,[2] 2BNA,[3] and 4ocb,[4] respectively.

In contrast to B- and A-form DNA, the Z-form duplex adopts a left-handed helical structure (Figure 5.1).[5] Historically, the first high-resolution structure was determined for Z-DNA before A-DNA and B-DNA.[6] Z-DNA has 12 base-pairs per turn, a large helical twist (60°) per base-pair, and a large

helix rise (44 Å) per turn. The base-pairs are displaced in the direction of the major groove, giving rise to a helix with a deep minor groove with similar dimensions as the major groove. The Z-form duplex DNA usually forms from polynucleotides with alternating purine and pyrimidine residues such as poly d(CG) at high salt concentrations. In B- and A-DNA, both pyridine and purine residues have *anti*-glycosidic bonds, where the plane of the ribose points away from the minor groove. In the Z-form conformation, however, the purine residues rotate 180° about the glycosidic bond into the *syn* conformation, leading to a zig-zag backbone conformation where the sugars adopt a C2'-*endo* conformation for pyrimidine residues, and C3'-*endo* for purine residues (Figure 5.2).[6-8]

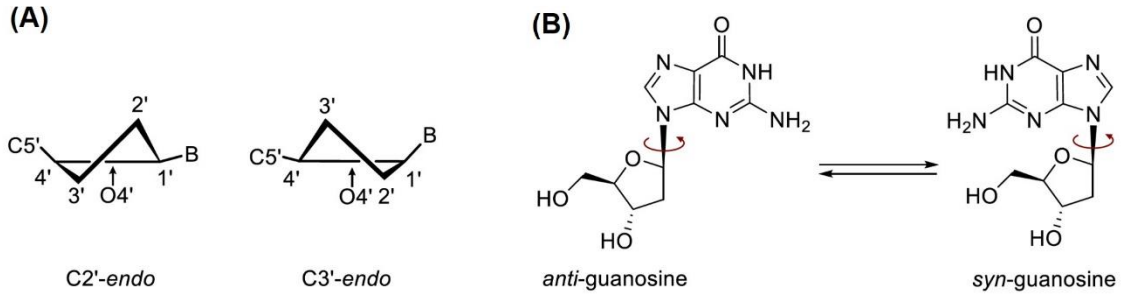

Figure 5.2. (A) Common sugar puckers, C2'-*endo* (left) and C3'-*endo* (right). (B) *Anti*- and *syn*-conformations of guanosine.

5.1.2 Biological relevance and helical transition

Despite its instability relative to B-DNA, Z-DNA might be stabilized *in vivo* by negative supercoiling.[9-10] Z-DNA has been proposed to play a role in gene expression,[5] recombination,[11] and regulation.[12-13] For example, a previous report suggests that Z-DNA sequences are required for chromatin-dependent activation of the CSF1 promoter.[14] A more recent study showed that the Z-DNA binding domain of the vaccinia virus is necessary to inhibit IFN-primed virus-induced necroptosis.[15] The amount of data that suggests the role of Z-DNA in gene regulation and several diseases, such as cancer and inflammation, continues to increase.[16-21] Meanwhile, B-DNA with alternating purine/pyrimidine sequences was found to convert to Z-DNA by many environmental factors other than high ionic strength[7, 22] (e.g., solvent addition,[23] Z-DNA-binding proteins,[24] small molecules[25] and metal complexes,[26-28] polyamines,[29] cationic polymers,[30] tension from magnetic tweezers,[31-32] and topological constraints[33]). In addition, some chemical modifications of DNA bases

were found to decrease the energy difference between B-DNA and Z-DNA.[34] For example, 8-trifluoromethyl-2'-deoxyguanosine by adopting a *syn* conformation, stabilizes the Z-DNA conformation under physiological salt concentrations.[35]

Transitions between A- and B-form duplexes were discovered by *Franklin* and *Gosling* when conducting X-ray fiber diffraction analyses under various humidity levels.[36] *In vivo*, protein binding reactions can also partially dehydrate duplex DNA, giving global A-form viral genomes,[37] as well as local A-form perturbations at specific binding sites.[38] Thus, it has been suggested that transitions between A- and B-form duplexes play important roles in biological processes.[39-43] For example, DNA-RNA hybrid duplexes that occur during transcription and initiation of DNA replication adopt A-form conformations or intermediate A- and B-form structures. Such hybrids act as regulators of gene expression, DNA replication, and DNA repair.[44-45]

Small molecules such as polyamines,[46] aminoglycosides,[47] hexaamminecobalt (III),[48] and cisplatin[49] can induce local B → A transitions *via* mechanisms independent of global changes in hydration and water activity. The binding of metal ions to discreet coordination sites in nucleic acids[50] can be coupled to the (re)folding of DNA and RNA molecules[51,52] that activate DNAzymes,[53] ribozymes,[54] riboswitches,[55] and DNA-based materials.[56] Our lab has studied several metallo nucleobase pairs,[57] where a transition metal ion is bound between mismatches.[58] For example, a former group member, *Schmidt,* reported high-affinity binding of Hg^{II} to DNA duplexes containing C:T mismatches using fluorescent techniques.[59] Conducted in parallel, by another group, crystal screening of various oligonucleotides and metal ions provided the X-ray structure of a short (8-mer) A-form DNA sequence containing two C-Hg^{II}-T base-pairs.[60] This X-ray structure revealed an unexpected metal-binding mode involving the exocyclic amine (N4) of a deprotonated cytosine residue and the imine (N3) of thymine (Figure 5.3).[60] This coordination mode was in contrast to a preliminary proposal for (N3)T-Hg^{II}-(N3)C coordination based on structural homology with T-Hg^{II}-T. The global A-form structure observed in the crystal structure was inconsistent with CD data of slightly longer, 14–21-mer duplexes containing one or two C-Hg^{II}-T base-pairs.[59] The CD spectra suggested B-form helices, and little-to-no changes in their global conformation upon adding Hg^{II}. Therefore, the metal binding mode(s) and global structural characteristics of duplex DNA containing C-Hg^{II}-T base-pairs in solution were unclear. To address this problem, *Schmidt* conducted detailed NMR studies using ^{15}N-labeled DNA and ^{199}Hg enriched mercury salts to determine the solution structures and

dynamics of C-Hg^{II}-T base-pairs in duplex DNA.[61] Unlike previous examples of metallo base-pairs, a 14-mer duplex with two C-Hg^{II}-T sites separated by six canonical base-pairs was observed as a 3:1 mixture of well-defined duplexes in dynamic equilibrium. Both structures exhibited groove and rise dimensions intermediate between ideal A- and B-form helices. The most abundant duplex contained (N3)T-Hg^{II}- (N3)C connectivity and mostly B-form helical characteristics, whereas the minor species contained (N3)T-Hg^{II}-(N4)C base-pairs and more A-form characteristics. However, the CD spectra showed a B-form signature, suggesting that local conformational changes upon the addition of Hg^{II} has not resulted in global conformational change. Inspired by these observations, we aimed to find a sequence capable of translating the local conformational changes to a global conformational change. Here we report the design and identification of small DNA duplexes containing numerous C:T mismatches that exhibits a global B → A helical transition upon adding Hg^{II}. In addition, a possible helical transition from right-handed to left-handed DNA will be discussed.

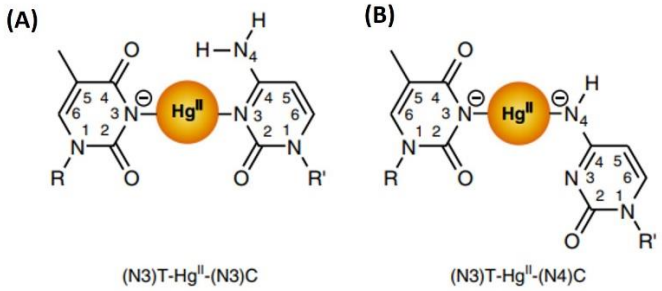

Figure 5.3. C-Hg^{II}-T binding modes. (A) (N3)T-Hg^{II}-(N3)C coordination, which in a 14-mer duplex was found as the major metallobase and demonstrated B-form characteristics. (B) (N3)T-Hg^{II}-(N4)C metal-binding mode found as the minor metallobase with local A-form characteristics.[61]

5.2 Design and screening of a hairpin library of oligonucleotides for B to A transition

In the reported 14-mer DNA by *Schmidt* (5'-CGT**C**TCATGA**T**ACG-3'), which contained two C-Hg^{II}-T sites (shown in bold), the $k_{forward}$ = 3.5 s^{-1} and $k_{reversed}$ = 7.7 s^{-1} measured using [^{15}N,^{1}H]-HSQC experiments were nearly identical to those of the global conformational exchange of duplex structures measured using [^{1}H,^{1}H]-NOESY experiments ($k_{forward}$ = 4.3 ± 0.6 s^{-1}, $k_{reversed}$ = 8.8 ± 0.9 s^{-1}).[61] These results, therefore, supported the coupling of metal-ligand isomerization reactions over long distances (> 20 Å) *via* a small, yet global conformational change of the double helix. Taken together

with the greater A-form characteristics upon metal binding, these results suggested that placing numerous C:T mismatches throughout a repetitive duplex sequence could facilitate a global B → A helical transition upon adding Hg^{II}. To test this possibility, we introduced C:T mismatches into mostly GC rich repetitive sequences that are known to have small energy differences between A- and B-forms.[60,62-67] To suppress the formation of intramolecular G-quadruplex structures that would otherwise interfere with the intermolecular duplex formation of such repetitive sequences, we designed a library of 120-mer DNA hairpins (Table D1, Appendix D) containing 7–19 mismatches and a tetraloop sequence cGCTAg that is known to stabilize both RNA and DNA hairpins.[68] To fold the hairpins, dilute solutions of DNA (1.0 μM) were heated (95 °C, 5 min) and rapidly cooled on ice at 0 °C. Samples were then incubated with 0.0 or 1.5 equiv. of Hg^{II} (relative to the number of C:T mismatches present) at 22 °C for 3 h prior to their analysis. Gel electrophoresis revealed clean, intramolecular hairpin formation for most sequences in both the presence and absence of Hg^{II}, including our primary hit ODN^5-21CT (Figure D1A, Appendix D). We used CD spectroscopy to screen for the induction of A-form structure by Hg^{II}. A summary of the effects of Hg^{II} on the CD spectra of library members is shown in Figure 5.4. Some selected CD spectra are shown in Figure 5.5 and all other CD spectra are available in Figure D2, Appendix D.

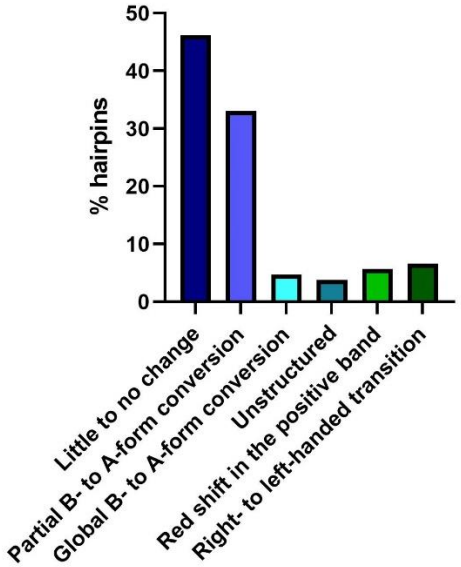

Figure 5.4. Effect of 1.5 equiv per mismatch addition of Hg^{II} in the CD spectra of 120-mer oligonucleotides.

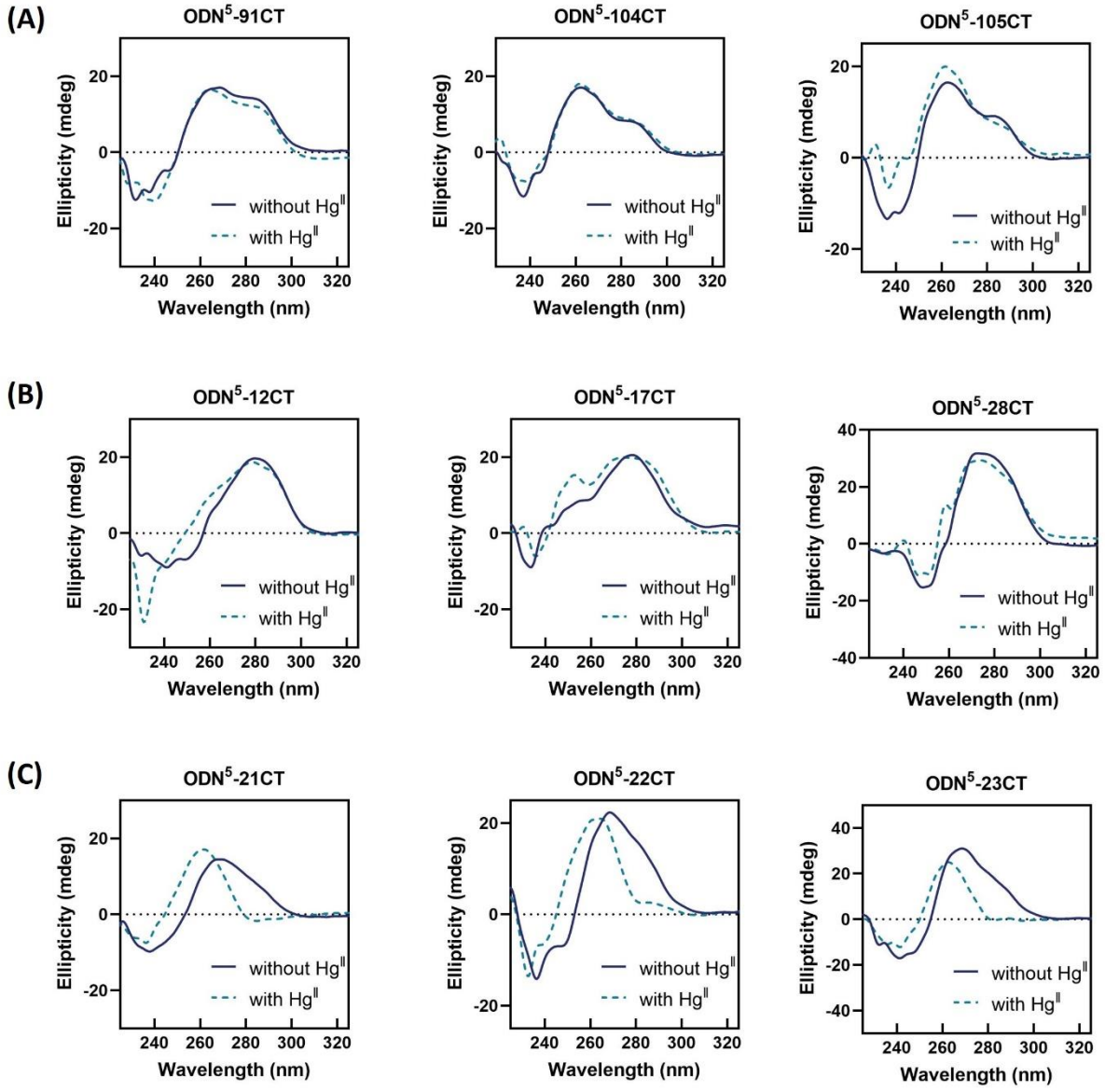

Figure 5.5. (A) CD spectra of hairpins ODN^5-91CT with the core sequence of [GGGC**C**CGGGCC**C**]$_5$, ODN^5-104CT with the core sequence of [GGGGCCCC**T**GGGCCC**C**]$_{3.5}$, and ODN^5-105CT with the core sequence of [GGGGCCC**C**]$_7$ in the presence and absence of 1.5 equiv of Hg^{II}. These three sequences contain eight, seven and seven C:T mismatches in 58-mer folded hairpin, respectively. (B) CD spectra of hairpin ODN^5-12CT with the core sequence of [GGC**C**C**T**]$_{9.5}$, ODN^5-17CT with the core sequence of [GAG**T**GG**T**]$_8$ and ODN^5-28CT with the core sequence of [GGG**C**GG**T**CGC**T**]$_5$, in the presence and absence of 1.5 equiv of Hg^{II}. These three sequences contain 17, 16 and 15 C:T mismatches in 58-mer folded hairpin, respectively. (C) CD spectra of hairpin ODN^5-21CT with the core sequence of [CCC**T**CGG**T**GG**T**]$_5$, ODN^5-22CT with the core sequence of [CCC**C**CGG**C**GG**C**]$_5$ and ODN^5-23CT with the core sequence of [CCG**C**GGG**C**CC**T**]$_5$, in the presence and absence of 1.5 equiv of Hg^{II}. These three sequences contain 15 C:T mismatches in 58-mer folded hairpin.

Among the 106 studied sequences, some sequences with high GC content, such as the $(G_3C_3)_n$-containing hairpins ODN^5-91CT and ODN^5-104CT exhibited CD spectra consistent with previous publications,[62] having a double maximum at 260 nm and 280 nm (Figure 5.5A) that are thought to reflect a mixture of A-form and B-form-like stacking of the guanine and cytosine nucleobases, respectively. 46% of studied sequences showed little-to-no change in their CD spectra upon addition of the Hg^{II} (e.g, ODN^5-91CT and ODN^5-104CT shown in Figure 5.5A). 33% of oligomer library members demonstrated a partial blue shifting in their positive and negative bands, reflecting partial conversion of B-form DNA to A-form DNA (Figure 5.5B). Finally, 5% of sequences that were in the B- form prior to metal binding demonstrated a CD consistent with a global B → A helical transition (Figure 5.5C).[63]

Among the hit sequences (ODN^5-21, 22, 23CT shown in Figure 5.5C and ODN^5-6, 9CT shown in Figure D2, Appendix D), ODN^5-21CT demonstrated the ideal A-form signature, which includes blue-shifting and increasing in the positive band intensity upon the addition of Hg^{II}. Furthermore, upon Hg^{II} addition, 4% of sequences unstructured (ODN^5-73, 88, 100, 101CT shown in Figure D2, Appendix D), and 6% demonstrated a red-shift in the CD bands (ODN^5-2, 34, 45, 87, 94, 106CT shown in Figure D2, Appendix D). The remaining 7% of oligonucleotides showed a left-handed helical signature in their CD spectra which will be discussed in Section 5.4.

Comparing the CD spectra presented in Figure D2, Appendix D with the number of mismatches in each folded hairpin, the effect of mismatch quantity on helical transition can be evaluated (Figure 5.6 and Table D2, Appendix D). All five hit sequences that show a global B- to A-form helical transition contain 15 or more mismatches. This means that in a 58-mer folded hairpin, more than 25% of the base-pairs must be mismatches to allow translation of local helical transition into the global change in the DNA secondary structure. This analysis shows that in sequences with less than 15 mismatches, there is a higher percentile of oligonucleotides that exhibit little-to-no change in their CD spectra upon the addition of Hg^{II} (Table D2, Appendix D).

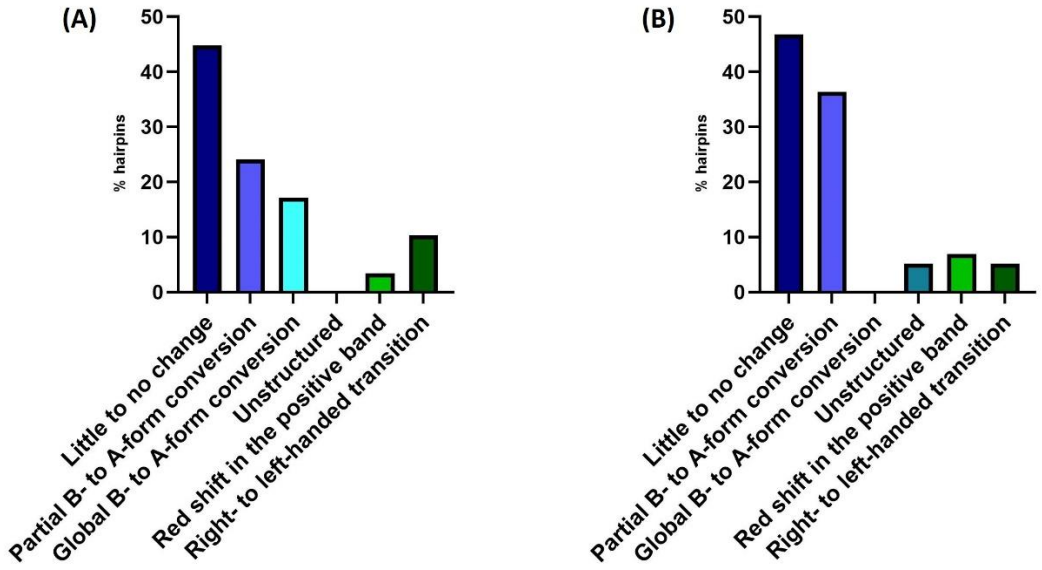

Figure 5.6. Impact of mismatch numbers in CD spectra of library sequences with (A) 15 or more mismatches (29 hairpins in total) and (B) less than 15 mismatches (77 hairpins in total) in a 58-mer folded hairpin after incubation with 1.5 equiv. per mismatch Hg^{II}.

To confirm the results obtained from CD, we used a fluorescent aminoglycoside binding assay.[64] Aminoglycoside antibiotics exhibit a general selectivity for binding A-form over B-form helices.[47] Changes in the fluorescence anisotropy of a 40 nM solution of a Neomycin-BODIPY conjugate "Neo-BODIPY"[69] were therefore measured in the presence and absence of each DNA (600 nM) pre-treated with Hg^{II} (0.0 or 1.5 equiv. per C:T mismatch). No changes in anisotropy were observed upon the addition of all hairpins in the absence of Hg^{II}, however, the pre-incubation of ODN^5-21CT with Hg^{II} caused a 3.5-fold increase in fluorescence anisotropy of Neo-BODIPY (Table 5.1 and Table D3, Appendix D). As the negative controls, the anisotropy values of the ODN^5-21TT and ODN^5-21AT were measured in the absence and presence of Hg^{II}. Both hairpins contains the same core sequence as ODN^5-21CT, but instead of C:T mismatches ODN^5-21TT includes T:T mismatches which Hg^{II} can coordinate to them and form T-Hg^{II}-T metallo base-pairs.[57] In ODN^5-21AT the C:T mismatches were replaced with A:T well-matched pairs, which Hg^{II} cannot selectively bind with. The anisotropy values of the ODN^5-21TT and ODN^5-21AT showed no change upon the addition of Hg^{II}, confirming that only C-Hg-T metallo base-pairs are capable of changing the secondary structure from B-form to A-form.

Table 5.1. DNA hairpin repeat sequences[a] and fluorescence anisotropy of Neo-BODIPY in the presence of each DNA with and without Hg^{II}.[b]

ODN[5]	DNA repeat sequence (5′ → 3′)	No Hg^{II}	+Hg^{II}
No DNA	-	0.05 ± 0.01	0.05 ± 0.01
6CT	$[GGCCCT]_{9.5}$	0.04 ± 0.02	0.06 ± 0.01
9CT	$[CGGCCC]_{9.5}$	0.05 ± 0.01	0.05 ± 0.02
21CT	**$[TGGTCCCTCGG]_5$**	**0.04 ± 0.01**	**0.14 ± 0.01**
21TT	$[TGGTCCCTCGG]_5$	0.04 ± 0.02	0.03 ± 0.01
21AT	$[TGGTCCCTCGG]_5$	0.04 ± 0.01	0.05 ± 0.01
22CT	$[CCCCCGGCGGC]_5$	0.04 ± 0.01	0.05 ± 0.01
23CT	$[CCGCGGGCCCT]_5$	0.05 ± 0.01	0.05 ± 0.01
28CT	$[TGGGCGGTCGC]_5$	0.05 ± 0.01	0.05 ± 0.01
46CT	$[GGGGCCCT]_7$	0.04 ± 0.02	0.07 ± 0.01
91CT	$[CGGGCCCGGGCC]_{4.5}$	0.05 ± 0.01	0.06 ± 0.01
104CT	$[TGGGCCCCGGGGCCCC]_{3.5}$	0.05 ± 0.01	0.06 ± 0.01

[a] Bold bases indicate C:T mismatches. Italic bases in 21AT indicate A:T base-pairs. The hit sequence (ODN[5]-21TT) is written fully in bold.

[b] All samples contained 40 nM of Neo-BODIPY, 600 nM of DNA, and 0 or 1.5 equiv of Hg^{II} per C:T mismatch in an aqueous buffer containing 200 mM $NaClO_4$ and 50 mM cacodylic acid (pH = 7.8). Averaged anisotropy values and standard deviations of three independent measurements are shown. Anisotropy values for more hairpins are reported in Table D3, Appendix D.

5.3 Reversible B → A helical transition of hairpin and duplex DNA

The Hg^{II}-induced conformational change of ODN[5]-21CT was extremely rapid (<30 s to complete) and exhibited a 1:1 stoichiometry between Hg^{II} and the number of C:T mismatches present (Figure D3, Appendix D). Titration of the ODN[5]-21CT-Hg^{II} complex into solutions of Neo-BODIPY revealed an apparent dissociation constant (K_d) of 1.4 ± 0.7 μM (Figure 5.7A). This value is similar to the values reported for neomycin binding to A-form, duplex RNA.[70] To evaluate the presence of potential artifacts from BODIPY in Neo-BODIPY, the ternary complex formed between Neo-BODIPY and ODN[5]-21CT-Hg^{II} was disrupted by adding the unlabeled neomycin B (Figure 5.7B). We observed a decrease in the fluorescence anisotropy upon adding the excess amount of unlabeled neomycin B, consistent with replacement of the Neo-BODIPY with unlabeled neomycin B in the major groove of the A-form ODN[5]-21CT-Hg^{II}. This observation suggests the lack of significant impact in the fluorescence anisotropy by the BODIPY tag.

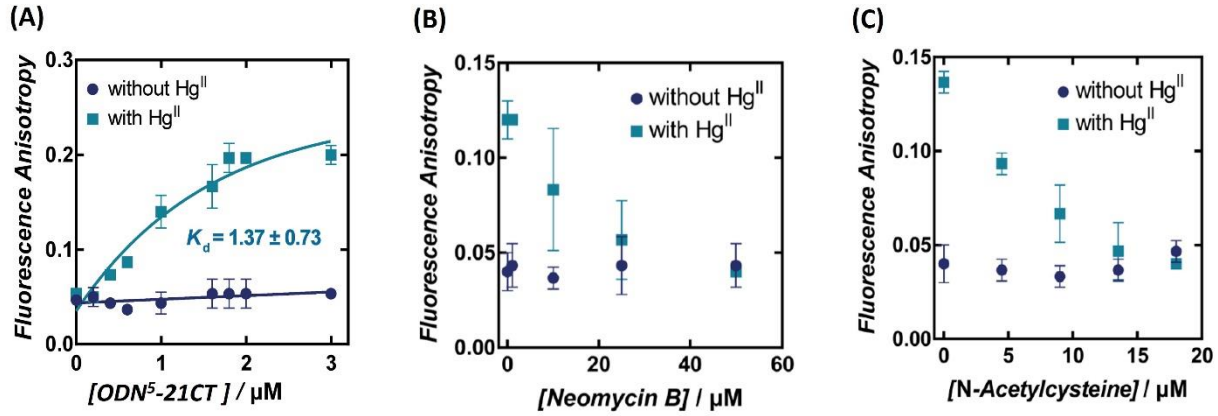

Figure 5.7. Changes in fluorescence anisotropy (λ_{ex} = 480 nm, λ_{em} = 515 nm) of Neo-BODIPY (40 nM) upon addition of (A) 0 – 3.0 µM hairpin ODN^5-21CT, (B) 0 – 50 µM unlabeled neomycin B, (C) 0 – 18 µM N-acetylcysteine. Hairpin samples were prepared in the presence (light blue) and absence (dark blue) of Hg^{II}. C-Hg^{II}-T base-pairs were formed by pre-incubation of the DNA with 1.5 equiv Hg^{II} (relative to mismatch present) for 3 h prior to addition of Neo-BODIPY. In (B) and (C) samples contained 0.6 µM ODN^5-21CT hairpin. All samples were prepared in aqueous buffer containing 200 mM $NaClO_4$ and 50 mM cacodylic acid (pH = 7.8). The data represent mean values and error bars represent standard deviation of three independent measurements.

To switch the hairpin containing Hg^{II} back to the B-form, N-acetylcysteine that sequesters Hg^{II} was added. As shown in Figure 5.7C, Neo-BODIPY binding is reversible, and by removing the Hg^{II} from C-Hg^{II}-T metallo base-pair using N-acetylcysteine, the initial B-form DNA can be regenerated. This observation was further confirmed by CD (Figure D4, Appendix D). Thus, Hg^{II} binding to ODN^5-21CT is fully reversible.

To evaluate the importance of the hairpin loop in helical switching, we prepared an analog of ODN^5-21CT as the corresponding intermolecular duplex lacking a hairpin turn (gel electrophoresis image is available in Figure D1B, Appendix D). This simple duplex "DUP^5-21CT" (sequence is available in Table D4, Appendix D) also exhibited a reversible Hg^{II}-induced switching between global B- and A-form helices (CD data are available in Figure D5, Appendix D). By alternating between the addition of Hg^{II} and N-acetylcysteine, the helical switching cycle from B- to A-form, and A-form to B-form could be repeated more than ten times on the same DNA (Figure 5.8).

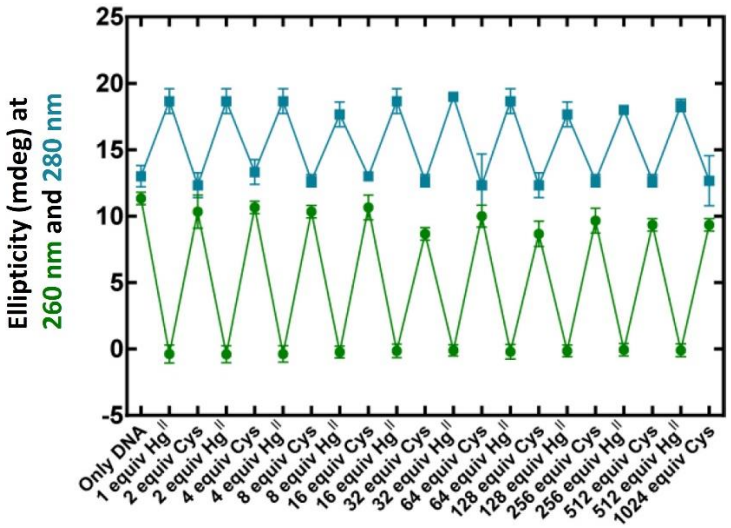

Figure 5.8. Reversible A/B-form helical switching by the addition of Hg^{II} and N-acetylcysteine in alternating order according to ellipticity at 260 nm (blue) and 280 nm (green) upon adding alternating portions of Hg^{II}. Samples contained DUP^5-21CT (1.0 µM) in aqueous buffer (200 mM $NaClO_4$ and 50 mM cacodylic acid, pH = 7.8). Samples were incubated with $Hg(ClO_4)_2$ or N-acetylcysteine for 30 sec prior to measuring CD. Equiv of Hg^{II} and N-acetylcysteine are given relative to mismatch present. The data represent mean values, and error bars represent the standard deviation of three independent measurements.

5.4 Hg^{II} switches DNA helical direction

As shown in Figure 5.4, while screening the 120-mer oligonucleotides, 7% of C:T mismatched hairpins, showed a Z-form signature on their CD spectra with a negative maximum at 280 nm and positive maximum at 255 nm (Figure 5.9A) after the addition of Hg^{II}. Even though these spectra are not entirely consistent with Z-DNA structure, which has a negative maximum at 287 nm in its CD spectra,[71-72] it suggests the DNA helical direction is changing from right-handed to left-handed. Acknowledging the relationship between the number of mismatches and helical switching from right- to left-handed (Figure 5.6 and Table D2, Appendix D), we hypothesized that mercury coordination to C:T mismatches in specific sequences is responsible for changing the helical direction. In addition, among the nine studied T:T mismatched hairpin (Figure D6, Appendix D), six of them, including ODN^5-21TT, showed a left-handed signature on their CD spectra upon the addition of Hg^{II} (Figure 5.9B). To evaluate the selective coordination of Hg^{II} to C:T or T:T mismatches, we used Ni^{II} as a negative control, which is known to coordinate to the N7 position of purines.[73] As shown in Figure 5.9, Ni^{II} had little impact on the CD spectra of the hairpins. Surprisingly when a second equiv. of Hg^{II} was added to the

ODN^5-21CT solution, the shape of CD spectrum changed suggesting conversion of the right-handed A-form DNA to left-handed DNA (Figure 5.10A). Upon the addition of N-acetylcysteine, the generated possibly left-handed structure returned to A- and then initial B-form DNA (Figure 5.10B), demonstrating a fully switchable helical transition (Figure 5.10C).

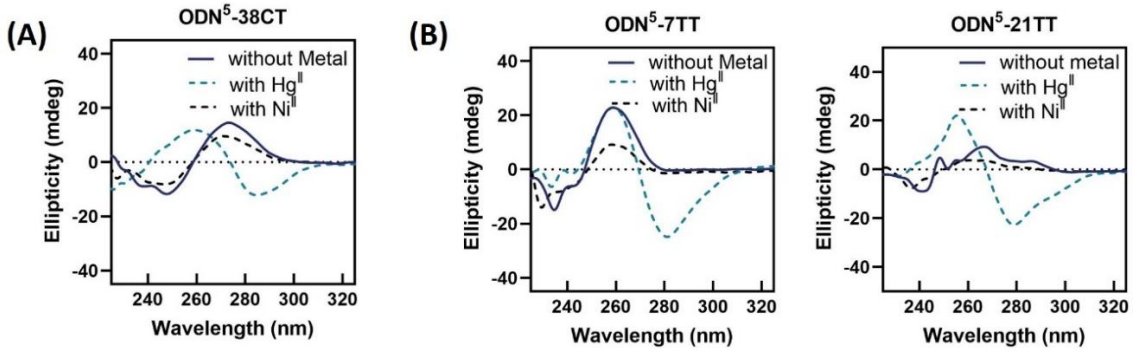

Figure 5.9. Switching the helical direction of (A) a C:T mismatched hairpin and (B) T:T mismatched hairpins, upon the addition of Hg^{II}. Ni^{II} had little impact on CD spectra and did not result in the right- to left-handed helical transition. All samples contained 1.0 µM duplex in aqueous buffer (200 mM $NaClO_4$ and 50 mM cacodylic acid, pH = 7.8). CD spectra were recorded after 10 min incubation with aliquots of $Hg(ClO_4)_2$ or $NiCl_2$.

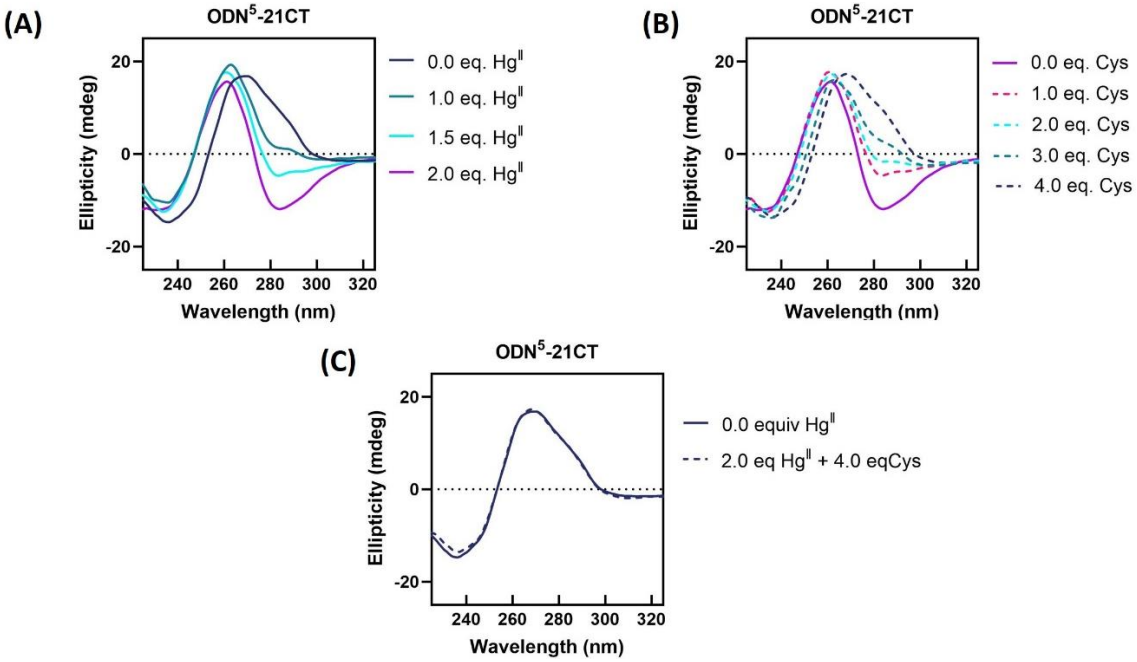

Figure 5.10. (A) B- to A-form helical transition of ODN^5-21CT upon the addition of 1.0 equiv per mismatch Hg^{II} and subsequent A-form to Z-like DNA helical switching when the second equiv. of Hg^{II} is added. (B) After addition of the 2.0 equiv. Hg^{II} (solid line), N-acetylcysteine was added (dashed lines) and regenerated the A-form and B-form DNA. (C) CD spectra of ODN^5-21CT before (solid, dark blue) and after (dashed, light blue) the addition of 2.0 equiv. Hg^{II} and subsequent addition of 4.0 equiv N-acetyl cysteine.

Inspired by these results, which suggest a B → Z helical transition in some sequences with T:T or C:T mismatches (Figure 5.9 and Figure D6, Appendix) and B → A → Z switching in ODN^{5}-21CT (Figure 5.10), we decided to conduct NMR experiments to understand how stoichiometric addition of Hg^{II} can alter the DNA helical direction. In order to reduce NMR spectral complexity, we sought the shortest possible oligonucleotide analog showing similar helical transition upon the addition of Hg^{II}. Thus, 14 DNA sequences were designed with sequences similar to ODN^{5}-7TT, ODN^{5}-21TT, ODN^{5}-21CT, ODN^{5}-38CT, and ODN^{5}-38TT (Table D4, Appendix D) and their CD spectra were recorded in the presence and absence of Hg^{II}. The data shown in Figure D7, Appendix D confirm that duplexes, as short as 10-mer that contain at least two mismatches, undergo the same type of secondary structure change upon the addition of Hg^{II}. DUP^{5}-21TT-5 (sequence: 5'- CGG **T** GG **T** CCC-3', forming eight G:C base-pairs and two T:T mismatches with the complementary strand) was chosen for NMR studies, due to its sequence similarity to ODN^{5}-21CT and simpler helical transition (i.e one step) compared to the corresponding C:T mismatched duplex.

The imino region of the 1D ^{1}H-NMR spectra of DUP^{5}-21TT-5 at 5 ^{o}C showed signals between 12 and 14 ppm (Figure 5.11) which is characteristic of the formation of WCF base-pairs. In addition, four signals are observed between 10 and 11 ppm which correspond to the four imino protons of thymines forming T:T base-pairs (Figure 5.11). The thermal stability of the duplex can be estimated by recording the disappearance of the imino signals at increasing temperatures. Most of the imino signals have disappeared at 25 ^{o}C and no imino signals are observed at 35 ^{o}C (Figure 5.11) indicating that the structure is completely unfolded between the two temperatures.

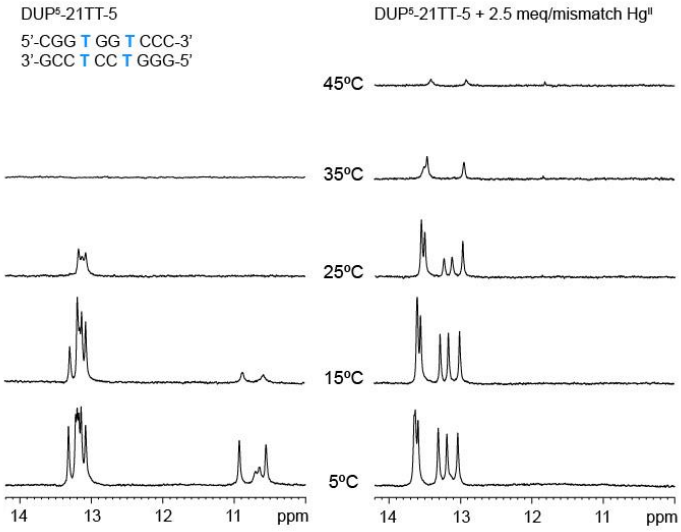

Figure 5.11. Imino region of the 1D ^{1}H-NMR spectra of DUP^{5}-21TT-5 in the absence (left) and presence (right) of 2.5 equiv. of Hg^{II} recorded at different temperatures.

The duplex DUP[5]-21TT-5 was treated with increasing amounts of Hg^{II} and the changes of the 1D-NMR spectrum were recorded at 15 ^{o}C upon each Hg^{II} addition. Figure 5.12 shows remarkable changes in the imino signals corresponding to both G:C and T:T base-pairs. The distribution of the guanine imino signals appearing between 12 and 14 ppm dramatically change as the duplex is titrated with Hg^{II}. Likewise, the imino signals corresponding to T:T base-pairs become broader in the presence of increasing amounts of Hg^{II}. Importantly, the spectrum reaches its final shape when the sample is left for several hours at room temperature indicating that the full structural conversion is relatively slow at the duplex concentration used here (0.5 mM). The spectrum of the final species does not show thymine imino protons which indicates that Hg^{II} has disrupted the T:T base-pairs and formed T-Hg-T metallo base-pairs. The Hg-containing structure is significantly more stable than the duplex as the imino signals remain visible at 45 ^{o}C (Figure 5.11). This higher thermal stability is consistent with the high stability provided by T-Hg^{II}-T metallo base-pairs.[59, 61,74] NMR results are consistent with CD experiments carried out at the same temperature (15 ^{o}C) showing the emergence of an intense negative band at 290 nm in the presence of Hg^{II} (Figure D8, Appendix D). For more details, refer to Figure D9, Appendix D.

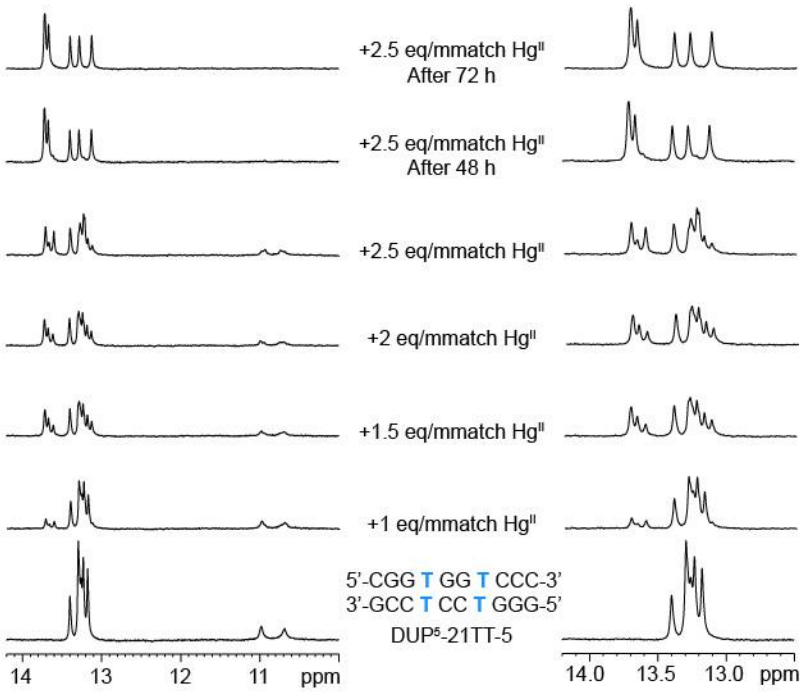

Figure 5.12. Imino region of the NMR spectra of DUP[5]-21TT-5 in the absence (bottom left) and in the presence of increasing amounts of Hg^{II}. Thymine imino signals (10 – 11 ppm) become broader in the presence of Hg^{II} and finally disappear at 2.5 eq/mismatch concentration of Hg^{II}. A detailed view of the distribution and dispersion of guanine imino protons (13 – 14 ppm) at different Hg^{II} concentrations are shown on the right.

As discussed in Section 5.1, nucleotides in Z-DNA adopt a *syn* conformation that places the aromatic proton (C8-H) very close to the H1' sugar proton.[74-77] Thus, residues adopting a *syn* conformation give a strong H1'-H8 intra-residual cross-peak in the NOESY spectrum.[78-79] The NOESY spectrum of DUP[5]-21TT-5 shows H1'-H8 cross-peaks of low to moderate intensity (Figure 5.13 A), indicating that none of the residues is in the *syn* conformation and thus eliminating the possibility that DUP[5]-21TT-5 forms a canonical Z-DNA helix in the presence of Hg^{II}. This explains CD spectra which showed its negative maximum at 280 nm, slightly shifted from the one for Z-DNA (~ 290 nm).[80-82]

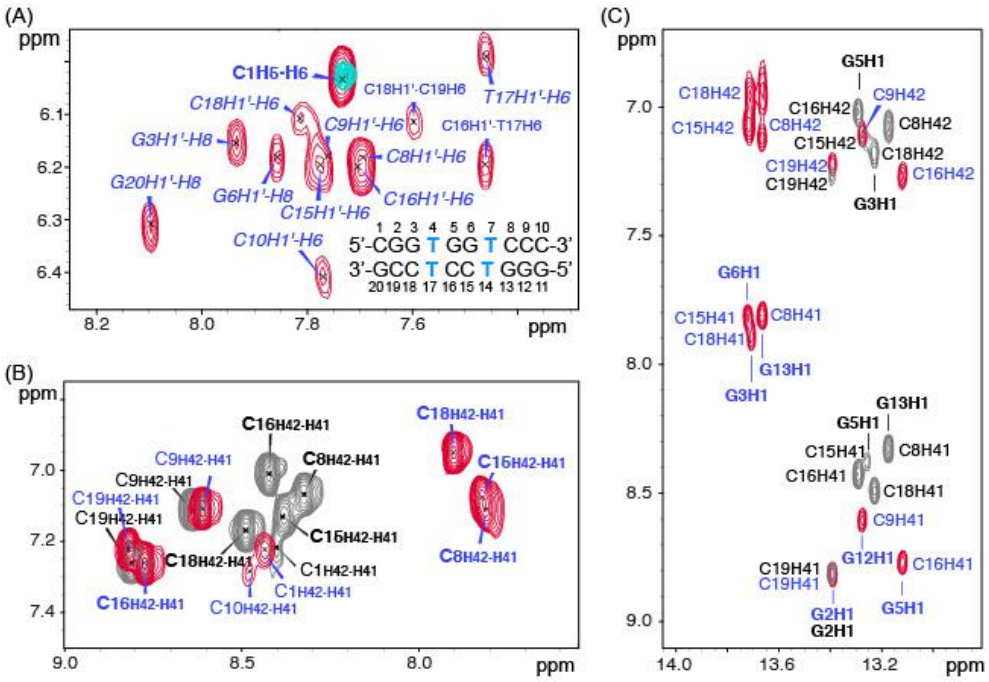

Figure 5.13. (A) Area of the aromatic region of the NOESY (red) spectrum and TOCSY (cyan) of DUP[5]-21TT in the presence of 2.5 eq/mismatch Hg^{II} showing H1'-H aromatic cross-peaks (italic labels) and the much more intense C1H5-H6 cross-peak (bold label). (B) Superposition of the NOESY spectra of DUP[5]-21TT-5 in the absence (grey) and presence (red) of Hg^{II} showing dramatic shifting of amino-amino crosspeaks of C8, C15, C16 and C18 residues. (C) Superposition of the imino regions of the NOESY spectra of DUP[5]-21TT-5 in the absence (grey) and presence (red) of Hg^{II}. Note the remarkable changes affecting residues flanking thymine residues.

NOESY spectra of DUP[5]-21TT-5 in the absence and in the presence of 2.5 eq/mismatch of Hg^{II} were acquired and signals were assigned following standard protocols. Significant differences were found for chemical shifts of protons belonging to residues flanking thymines in both strands (Figure

5.13 B and C). Such changes are indicative of a dramatic local transformation of the chemical environment as a consequence of the duplex adopting a different helicity. Apart from the very significant shifts of such cross-peaks, the features of the NOESY spectrum in the presence of Hg^{II} are similar to the one of the duplex when Hg^{II} is absent. Imino-amino cross-peaks confirm the formation of the same number and kind of WCF base-pairs. The connectivity between residues (inter-residual cross-peaks) also remains similar for both structures. Therefore, NMR data do not provide enough evidence to univocally determine the structure formed by DUP^{5}-21TT-5 in the presence of Hg^{II}. Currently, X-ray crystallography of the duplex in the presence and absence of the Hg^{II} is an ongoing part of this project.

5.5 Summary

Inspired by the long-range coupling (>20 Å) between the two metallo base-pairs *via* a global conformational exchange observed in the initial NMR results, we placed numerous C:T mismatches throughout a library of repetitive 120-mer sequences to screen for a change of global B → A helical structure upon addition of stoichiometric Hg^{II}. Indeed, we were able to identify one such sequence (ODN^{5}-21CT) exhibiting a fully-reversible switching cycle from B- to A-form, and A-form to B-form by tandem additions of Hg^{II} and N-acetylcysteine. Both transitions were complete in <30 s, and could be repeated more than ten times. While numerous examples of local A-form perturbations caused by DNA-protein and DNA-small molecule binding interactions have previously been reported,[38, 47-49, 83-85] the previous examples of global B-form → A-from helical transitions involved global dehydration of the duplex.[36-37, 86] Here, the global B- to A-form helical transition was a result of discrete, reversible metal binding. Furthermore, CD showed that upon the addition of a second equiv. of Hg^{II} to the ODN^{5}-21CT, the previously generated A-DNA reversibly converted to a left-handed structure. This observation may be explained as coordination of the second equiv. of Hg^{II} to (N3)-C while the first equiv. has been coordinated to (N4)-C. Consistent with this model, we have found that by replacing C:T mismatches in this sequence with T:T mismatches, the B-form DNA directly switches to Z-like DNA upon the addition of one equiv. Hg^{II}. To elucidate the structural details by NMR experiments, the long, 120-mer hairpin used in these studies was minimized into a much shorter (10-mer) DNA sequences that underwent these same conversions. NMR experiments demonstrated that this left-handed DNA

is not in a Z-form. Therefore, X-ray crystallography is currently being conducted to reveal the structure of this possibly left-handed DNA and the exact coordination site(s) of Hg^{II}. Future studies may involve synthesizing a 10-mer DNA containing ^{ts}T and tC modifications to enable the detailed kinetic and thermodynamic characterization of the conformational switching at the single-molecule level.[87-88] Such diverse right-handed/left-handed and A/B-form helical switching, in addition to their broad implications in structural biology and biochemistry, can potentially be utilized in the development of advanced DNA-based materials and devices.[56, 89-95]

5.6 Experimental

Hairpin and duplex folding: Oligonucleotides were purchased from Sigma-Aldrich as HPLC- and PAGE purified sequences. Oligonucleotide stock solutions were prepared in deionized water and their concentrations were determined by absorbance at 260 nm using a molar extinction coefficient (ε_{260}) calculated using a nearest-neighbor model.[96] Hairpins were prepared by diluting the sequences in aqueous buffer (200 mM $NaClO_4$, 50 mM cacodylic acid (pH = 7.8)) and heating at 95 °C for 5 min, followed by rapid cooling on ice at 0 °C. Duplex DNAs were prepared by dissolving the complementary sequences in aqueous buffer (200 mM $NaClO_4$, 50 mM cacodylic acid (pH = 7.8)) heating at 95 °C for 5 min, followed by slow cooling to room temperature over 4 h.

Gel Electrophoreses: Sucrose (40 %, 5 µl) was added to pre-annealed hairpin or duplex DNA (5 µl, 5 pmol) and the solution was loaded onto a 20 % native gel (1.6 V, 55 min). The gel was treated with SYBR gold staining and scanned on a Typhoon FLA 9500. DNA samples measured in the presence of Hg^{II} were incubated with $Hg(ClO_4)_2$ (1.5 equiv relative to mismatch present) for 3 h prior to use.

Circular Dichroism Spectroscopy: Circular dichroism spectra of pre-folded DNA hairpins (1.0 µM) were measured from 220 nm to 350 nm at 22 °C with a 2 nm band width with 0.1 nm steps at a scanning rate of 20 nm min^{-1} in 1 mm path length thermo-controlled strain-free quartz cuvette on a JASCO J-715 spectrometer. CD spectra were recorded as an average of three measurements, each with three scans. CD spectra of hairpin DNA measured in the presence of Hg^{II} (or Ni^{II}) were incubated with 1.5 equiv (relative to mismatch present) of $Hg(ClO_4)_2$ (or $NiCl_2$) for 3 h prior to use.

Neo-BODIPY Binding Assay: Pre-folded DNA hairpin (5.0 µM) in aqueous buffer (200 mM $NaClO_4$ and 50 mM cacodylic acid (pH = 7.8)) was mixed with $Hg(ClO_4)_2$ (1.5 equiv relative to mismatch present) and incubated at r.t. for 3 h. Neo-BODPIY was added to give a final concentration of 40 nM Neo-BODIPY and 0 – 3 µM DNA hairpin. The samples were incubated at r.t. for 1 h prior to measurement. Fluorescence anisotropy values were determined by measuring fluorescence polarization at λ_{em} = 515 nm (λ_{ex} = 480 nm). Fluorescence polarization was measured in three independent trials at 22 °C using a Molecular Devices Spectra spectrofluorophotometer in 384-well plates.

A → B Helical Switching by Unlabeled Neomycin B: Pre-folded DNA hairpin (1.0 μM) in aqueous buffer (200 mM $NaClO_4$ and 50 mM cacodylic acid (pH 7.8)) was mixed with $Hg(ClO_4)_2$ (22.5 μM, 1.5 equiv relative to mismatch present) and incubated at r.t. for 3 h. Neo-BODIPY (66.7 nM) was added and incubated at r.t. for 60 min. Unlabeled neomycin B trisulfate was added to the samples to give a final concentration of 40 nM Neo-BODIPY, 0.6 μM ODN5-21CT , 13.5 μM Hg^{II} and 0 – 50 μM unlabeled neomycin B and the mixture was incubated at r.t. for 60 min. Anisotropy was recorded at 22 °C using a Molecular Devices Spectra spectrofluorophotometer in a 384- well plate. Fluorescence anisotropy was recorded in triplicate by fluorescence polarization measurement (λ_{ex} = 480 nm, λ_{em} = 515 nm).

A → B Helical Switching by N-Acetylcysteine: Pre-folded DNA hairpin (1.0 μM) in aqueous buffer (200 mM $NaClO_4$ and 50 mM cacodylic acid (pH 7.8)) was mixed with $Hg(ClO_4)_2$ (22.5 μM, 1.5 equiv relative to mismatch present) and incubated at r.t. for 3 h. Neo-BODIPY (66.7 nM) was added and incubated at r.t. for 60 min. N-acetylcysteine (0 – 2 equiv relative to mismatch present) was added to the sample to give a final concentration of 40 nM Neo-BODIPY, 0.6 μM ODN5-21CT, 13.5 μM Hg^{II} and 0 – 18 μM N-acetylcysteine and the mixture was incubated at r.t. for 60 min. Anisotropy was recorded at 22 °C using a Molecular Devices Spectra spectrofluorophotometer in a 384-well plate. Fluorescence anisotropy was recorded in triplicate by fluorescence polarization measurement (λ_{ex} = 480 nm, λ_{em} = 515 nm).

Melting temperature analysis (T_m): Thermal denaturation temperatures of duplex DNA were determined by measuring the ellipticity at 280 nm as a function of temperature in a 1 mm path length thermo-controlled strain-free quartz cuvette on a JASCO J-715 spectrometer equipped with a temperature control system. Solutions of pre-folded duplex DNA in aqueous buffer (200 mM $NaClO_4$, 50 mM cacodylic acid at pH = 7.8) were equilibrated at 5 °C for a minimum of 20 min and slowly ramped to 85 °C with 0.5 °C steps at a rate of 25 °C h^{-1}. The melting temperatures were determined from the obtained maximum after differentiation of the received curves on Spectra Manager. T_m values were calculated as the average from the heating and cooling curves and were measured in triplicate.

NMR spectroscopy: Duplex DNA (0.5 mM) was prepared by dissolving 1.0 mM of the complementary sequences in aqueous buffer (150 mM $NaClO_4$, 50 mM sodium cacodylate pH 7.8 in H_2O / D_2O (9:1), heating to 95 °C for 5 min, and slowly cooling down to room temperature over 4 h. For titration experiments, Hg^{II} was added from an aqueous solution of $Hg(OAc)_2$ 14 mM and 1D NMR

spectra were recorded at 15 ^{o}C immediately after each addition. All NMR spectra were acquired on a Bruker spectrometer operating at 600 MHz and equipped with cryoprobe. NMR data was processed using TOPSPIN software. One dimensional ^{1}H-NMR were acquired using excitation sculpting for water suppression. NOESY spectra were acquired at mixing times of 150 and 250 ms. TOCSY spectra were recorded with the DIPSI-2 sequence and a mixing time of 80 ms. The software NMRFAM-Sparky[97] was used for assignment of NOESY spectra.

5.7 Appendix

5.7.1 Tables

Table D1. Names, numbers of mismatches and sequences of 120-mer DNA hairpin library[a]

Name	Mismatch numbers	Sequence
ODN^{5}-1CT	19	5′–GCGGCGGCGGCGGCGGCGGCGGCGGCGGCGGCGGCGGCGGCGGCGGCGGCGGCGGCGCGC TAGCTCCTCCTCCTCCTCCTCCTCCTCCTCCTCCTCCTCCTCCTCCTCCTCC–3′
ODN^{5}-2CT	18	5′–CCGGTCCCGGTCCCGGTCCCGGTCCCGGTCCCGGTCCCGGTCCCGGTCCCGGTCCCGGTCCCGCGCTAG CGGTCCCGGTCCCGGTCCCGGTCCCGGTCCCGGTCCCGGTCCCGGTCCCGGTCCCGG–3′
ODN^{5}-3CT	18	5′–GCCCGTGCCCGTGCCCGTGCCCGTGCCCGTGCCCGTGCCCGTGCCCGTGCCCGTGCCCGTGCCCGCTAG GGCCCGTGCCCGTGCCCGTGCCCGTGCCCGTGCCCGTGCCCGTGCCCGTGCCCGTGC–3′
ODN^{5}-4CT	18	5′–GGCCTTGGCCTTGGCCTTGGCCTTGGCCTTGGCCTTGGCCTTGGCCTTGGCCTTGGCCTTGGCCGCTAG GCCCCGGCCCCGGCCCCGGCCCCGGCCCCGGCCCCGGCCCCGGCCCCGGCCCCGGCCCCGGCC–3′
ODN^{5}-5CT	18	5′–GGCCTCGGCCTCGGCCTCGGCCTCGGCCTCGGCCTCGGCCTCGGCCTCGGCCTCGGCCTCGGCCGCTAG GCCTCGGCCTCGGCCTCGGCCTCGGCCTCGGCCTCGGCCTCGGCCTCGGCCTCGGCC–3′
ODN^{5}-6CT	18	5′–GGCCCTGGCCCTGGCCCTGGCCCTGGCCCTGGCCCTGGCCCTGGCCCTGGCCCTGGCCGCTAG GCCCTGGCCCTGGCCCTGGCCCTGGCCCTGGCCCTGGCCCTGGCCCTGGCCCTGGCC–3′
ODN^{5}-7CT	18	5′–CGGCTCCGGCTCCGGCTCCGGCTCCGGCTCCGGCTCCGGCTCCGGCTCCGGCTCCGGCTCCGGCGCTAG CCGGCTCCGGCTCCGGCTCCGGCTCCGGCTCCGGCTCCGGCTCCGGCTCCGGCTCCGGCTCCG–3′
ODN^{5}-8CT	18	5′–CGGTCTCGGTCTCGGTCTCGGTCTCGGTCTCGGTCTCGGTCTCGGTCTCGGTCTCGGTCTCGGCGCTAG CCGCGCCCGCGCCCGCGCCCGCGCCCGCGCCCGCGCCCGCGCCCGCGCCCGCGCCCGCGCCCG–3′
ODN^{5}-9CT	18	5′–CGGCCCCGGCCCCGGCCCCGGCCCCGGCCCCGGCCCCGGCCCCGGCCCCGGCCCCGGCCCCGGCGCTAG CCGTGTCCGTGTCCGTGTCCGTGTCCGTGTCCGTGTCCGTGTCCGTGTCCGTGTCCGTGTCCG–3′
ODN^{5}-10CT	18	5′–GGGCCCTCATGCTCATGCTCATGCTCATGCTCATGCTCATGCTCATGCTCATGCTTGCGCTAG CACTCATGCTCATGCTCATGCTCATGCTCATGCTCATGCTCATGCTCATGCTGGCCC–3′
ODN^{5}-11CT	18	5′–GCGTCCTGATCCTGATCCTGATCCTGATCCTGATCCTGATCCTGATCCTGATCCTGACGCTAG TCATTATCATTATCATTATCATTATCATTATCATTATCATTATCATTACGC–3′
ODN^{5}-12CT	17	5′–CCCTGGCCCTGGCCCTGGCCCTGGCCCTGGCCCTGGCCCTGGCCCTGGCCCTGGCCCCGCTAG GGGCCCGTGCCCGTGCCCGTGCCCGTGCCCGTGCCCGTGCCCGTGCCCGTGCCCGGG–3′
ODN^{5}-13CT	16	5′–GGCTCGCGGCTCGCGGCTCGCGGCTCGCGGCTCGCGGCTCGCGGCTCGCGGCTCGCGCGCTAG CTCGCGCCTCGCGCCTCGCGCCTCGCGCCTCGCGCCTCGCGCCTCGCGCCTCGCGCC–3′
ODN^{5}-14CT	16	5′–GGCCTGCGGCCTGCGGCCTGCGGCCTGCGGCCTGCGGCCTGCGGCCTGCGGCCTGCGCGCTAG CTCCGGCCTCCGGCCTCCGGCCTCCGGCCTCCGGCCTCCGGCCTCCGGCCTCCGGCC–3′

[a] Bold red bases indicate the C:T mismatches. Blue bases indicate hairpin loop regions.

Table D1 (continue). Names, numbers of mismatches and sequences of 120-mer DNA hairpin library

Name	Mismatch numbers	Sequence
ODN[5]-15CT	16	5′–GGCTCTGGGCTCTGGGCTCTGGGCTCTGGGCTCTGGGCTCTGGGCTCTGGGCTCTGGCGCTAG CCCGCGCCCCGCGCCCCGCGCCCCGCGCCCCGCGCCCCGCGCCCCGCGCCCCGCGCC–3′
ODN[5]-16CT	16	5′–GGCATTGGGCATTGGGCATTGGGCATTGGGCATTGGGCATTGGGCATTGGGCATTGGCGCTAG CCCCTGCCCCCTGCCCCCTGCCCCCTGCCCCCTGCCCCCTGCCCCCTGCCCCCTGCC–3′
ODN[5]-17CT	16	5′–GAGTGGTGAGTGGTGAGTGGTGAGTGGTGAGTGGTGAGTGGTGAGTGGTGAGTGGTGCGC TAGCCCCCCTCCCCCCTCCCCCCTCCCCCCTCCCCCCTCCCCCCTCCCCCCTCCCCCCTC–3′
ODN[5]-18CT	15	5′–GGCCCGCGGCCCGCGGCCCGCGGCCCGCGGCCCGCGGCCCGCGGCCCGCGGCCCGGGCGCTAG CCCGGTCCTCGGTCCTCGGTCCTCGGTCCTCGGTCCTCGGTCCTCGGTCCTCGGTCC–3′
ODN[5]-19CT	15	5′–GGCTCCTCGGTGGCTCCTCGGTGGCTCCTCGGTGGCTCCTCGGTGGCTCCTCGGTGGCGCTAG CCCCCGCGGCGCCCCCGCGGCGCCCCCGCGGCGCCCCCGCGGCGCCCCCGCGGCGCC–3′
ODN[5]-20CT	15	5′–GGCCTCGGGCCTCGGGCCTCGGGCCTCGGGCCTCGGGCCTCGGGCCTCGGGCCTGGGCGCTAG CCCCGGCCCCTCGGCCCCTCGGCCCCTCGGCCCCTCGGCCCCTCGGCCCCTCGGCCCCTCGGCC–3′
ODN[5]-21CT	15	5′–CGGTGGTCCCTCGGTGGTCCCTCGGTGGTCCCTCGGTGGTCCCTCGGTGGTCCCTCGCGCTAG CGCGGGCCCCCCGCGGGCCCCCCGCGGGCCCCCCGCGGGCCCCCCGCGGGCCCCCCG–3′
ODN[5]-22CT	15	5′–CGGCGGCCCCCCGGCGGCCCCCCGGCGGCCCCCCGGCGGCCCCCCGGCGGCCCCCCGCGCTAG CGTGGGTCCTCCGTGGGTCCTCCGTGGGTCCTCCGTGGGTCCTCCGTGGGTCCTCCG–3′
ODN[5]-23CT	15	5′–GGGCCCTCCGCGGGCCCTCCGCGGGCCCTCCGCGGGCCCTCCGCGGGCCCTCCGCGGCGCTAG CCTCGGCGGTCCCTCGGCGGTCCCTCGGCGGTCCCTCGGCGGTCCCTCGGCGGTCCC–3′
ODN[5]-24CT	15	5′–CGGGATTCCCGGGCATTCCCGGGCATTCCCGGGCATTCCCGGGCATTCCCGGGCCCGCGCTAG CGGTCCCTGGCATTCCCTGGCATTCCCTGGCATTCCCTGGCATTCCCTGGCATCCCG–3′
ODN[5]-25CT	15	5′–CGCTGGGTGGTCGCTGGGTGGTCGCTGGGTGGTCGCTGGGTGGTCGCTGGGTGGTCGCGCTAG CGCCCCCCCCGCGCCCCCCCCGCGCCCCCCCCGCGCCCCCCCCGCGCCCCCCCCGCG–3′
ODN[5]-26CT	15	5′–CGCCGGGCGGCCGCCGGGCGGCCGCCGGGCGGCCGCCGGGCGGCCGCCGGGCGGCCGCGC TAGCGTCCTCCCTGCGTCCTCCCTGCGTCCTCCCTGCGTCCTCCCTGCGTCCTCCCTGCG–3′
ODN[5]-27CT	15	5′–CGCCGGGTGGCCGCCGGGTGGCCGCCGGGTGGCCGCCGGGTGGCCGCCGGGTGGCCGCGCTAG CGTCCCCCCTGCGTCCCCCCTGCGTCCCCCCTGCGTCCCCCCTGCGTCCCCCCTGCG–3′
ODN[5]-28CT	15	5′–CGCTGGGCGGTCGCTGGGCGGTCGCTGGGCGGTCGCTGGGCGGTCGCTGGGCGGTCGCGCTAG CGCCCTCCCCGCGCCCTCCCCGCGCCCTCCCCGCGCCCTCCCCGCGCCCTCCCCGCG–3′
ODN[5]-29CT	15	5′–CGGTGGGCGGTGGGCGGTGGGCGGTGGGCGGTGGGCGGTGGGCGGTGGGCGGTGGCGCGC TAGCGCCCCCTCCCCCCTCCCCCCTCCCCCCTCCCCCCTCCCCCCTCCCCCCTCCCCCCG–3′
ODN[5]-30CT	14	5′–GCCCTCGGGCCCTCGGGCCCTCGGGCCCTCGGGCCCTCGGGCCCTCGGGCCCTCGGGCGCTAG CCCTCGGGCCCTCGGGCCCTCGGGCCCTCGGGCCCTCGGGCCCTCGGGCCCTCGGGC–3′

Table D1 (continue). Names, numbers of mismatches and sequences of 120-mer DNA hairpin library

Name	Mismatch numbers	Sequence
ODN[5]-31CT	14	5′–GGCCTCCGGGCCTCCGGGCCTCCGGGCCTCCGGGCCTCCGGGCCTCCGGGCCTCCGGCGCTAG CCTGCGGCCCTGCGGCCCTGCGGCCCTGCGGCCCTGCGGCCCTGCGGCCCTGCGGCC–3′
ODN[5]-32CT	14	5′–CGGTCCCGGGCTCCCGGGCTCCCGGGCTCCCGGGCTCCCGGGCTCCCGGGCTCCCGGCGCTAG CCTGGCGCCCTGGCGCCCTGGCGCCCTGGCGCCCTGGCGCCCTGGCGCCCTGGCCCG–3′
ODN[5]-33CT	14	5′–GCCTCGCGGCCTCGCGGCCTCGCGGCCTCGCGGCCTCGCGGCCTCGCGGCCTCGCGGCGCTAG CCTCGCGGCCTCGCGGCCTCGCGGCCTCGCGGCCTCGCGGCCTCGCGGCCTCGCGGC–3′
ODN[5]-34CT	14	5′–GGGCTCCCGGGCTCCCGGGCTCCCGGGCTCCCGGGCTCCCGGGCTCCCGGGCTCCCGCGCTAG CGGGCTCCCGGGCTCCCGGGCTCCCGGGCTCCCGGGCTCCCGGGCTCCCGGGCTCCC–3′
ODN[5]-35CT	14	5′–GGCTCCGCGGCTCCGCGGCTCCGCGGCTCCGCGGCTCCGCGGCTCCGCGGCTCCGCGCGCTAG CTCGGCGCCTCGGCGCCTCGGCGCCTCGGCGCCTCGGCGCCTCGGCGCCTCGGCGCC–3′
ODN[5]-36CT	14	5′–GGCTCCGGGGCTCCGGGGCTCCGGGGCTCCGGGGCTCCGGGGCTCCGGGGCTCCGGGGCTCCGGGCGCTAG CCCTGCGCCCCTGCGCCCCTGCGCCCCTGCGCCCCTGCGCCCCTGCGCCCCTGCGCCC–3′
ODN[5]-37CT	14	5′–CGGTGGTGCCCCCGGTGGTGCCCCCGGTGGTGCCCCCGGTGGTGCCCCCGGTGGTGCCGCTAG GCCCCCCCGGTGGCCCCCCCGGTGGCCCCCCCGGTGGCCCCCCCGGTGGCCCCCCCG–3′
ODN[5]-38CT	14	5′–CGGTCGGTCGGTCGGTCGGTCGGTCGGTCGGTCGGTCGGTCGGTCGGTCGGTCGGTCCGCTAG GCCCGCCCGCCCGCCCGCCCGCCCGCCCGCCCGCCCGCCCGCCCGCCCGCCCGCCCG–3′
ODN[5]-39CT	14	5′–GCGCGCGCGTGCGCGCGCGCGTGCGCGCGCGCGTGCGCGCGCGCGTGCGCGCGCGCCCGCTAG GGCTCGCTCGCCCGCTCGCTCGCCCGCTCGCTCGCCCGCTCGCTCGCCCGCTCGCTC–3′
ODN[5]-40CT	14	5′–GCGTGCGTGCGTGCGTGCGTGCGTGCGTGCGTGCGTGCGTGCGTGCGTGCGTGCGTGCGCTAG CCCGCCCGCCCGCCCGCCCGCCCGCCCGCCCGCCCGCCCGCCCGCCCGCCCGCCCGCCGC–3′
ODN[5]-41CT	14	5′–GCGGGCGGGTGGGTGGGCGGGCGGGTGGGTGGGCGGGCGGGTGGGTGGGCGGGCGGGCGC TAGCCCTCCCTCCCCCCCCCCTCCCTCCCCCCCCCCCTCCCTCCCCCCCCCCTCCCTC–3′
ODN[5]-42CT	14	5′–GGGCGTCGGGCGGTCGGGCGGTCGGGCGGTCGGGCGGTCGGGCGGTCGGGCGGTCGGCGC TAGCCTCCCGCCCTCCCGCCCTCCCGCCCTCCCGCCCTCCCGCCCTCCCGCCCTCCGCCC–3′
ODN[5]-43CT	14	5′–GCCGGTCTCATGATCTCATGATCTCATGATCTCATGATCTCATGATCTCATGATCTGCGCTAG CATCTCATGATCTCATGATCTCATGATCTCATGATCTCATGATCTCATGATCCCGGC–3′
ODN[5]-44CT	14	5′–GCCTCGGGGCCTCGGGGCCTCGGGGCCTCGGGGCCTCGGGGCCTCGGGGCCTCGGGGCGCTAG CCCCTCGGCCCCTCGGCCCCTCGGCCCCTCGGCCCCTCGGCCCCTCGGCCCCTCGGC–3′
ODN[5]-45CT	14	5′–GCCTTGGGGCCTTGGGGCCTTGGGGCCTTGGGGCCTTGGGGCCTTGGGGCCTTGGGGCGCTAG CCCCCCGGCCCCCCGGCCCCCCGGCCCCCCGGCCCCCCGGCCCCCCGGCCCCCCGGC–3′
ODN[5]-46CT	14	5′–GCCCTGGGGCCCTGGGGCCCTGGGGCCCTGGGGCCCTGGGGCCCTGGGGCCCTGGGGCGCTAG CCCCCTGGCCCCCTGGCCCCCTGGCCCCCTGGCCCCCTGGCCCCCTGGCCCCCTGGC–3′

Table D1 (continue). Names, numbers of mismatches and sequences of 120-mer DNA hairpin library

Name	Mismatch numbers	Sequence
ODN[5]-47CT	14	5′–CGGTTGGCCGGTTGGCCGGTTGGCCGGTTGGCCGGTTGGCCGGTTGGCCCGCTAG GGCCCCCCGGCCCCCCGGCCCCCCGGCCCCCCGGCCCCCCGGCCCCCCGGCCCCG–3′
ODN[5]-48CT	14	5′–CCCCGGTGCCCCGGTGCCCCGGTGCCCCGGTGCCCCGGTGCCCCGGTGCCCCGGTGCCGCTAG GCCCCTGGGCCCCTGGGCCCCTGGGCCCCTGGGCCCCTGGGCCCCTGGGCCCCTGGG–3′
ODN[5]-49CT	14	5′–GGGTATCGGGTTATCGGGTTATCGGGTTATCGGGTTATCGGGTTATCGGGTTATCGGCGCTAG CCTCTAACCCTCTAACCCTCTAACCCTCTAACCCTCTAACCCTCTAACCCTCTACCC–3′
ODN[5]-50CT	14	5′–AGAATGGTAGGATGGTAGGATGGTAGGATGGTAGGATGGTAGGATGGTAGGATGGTACGCTAG TCCCCTCCTCCCCTCCTCCCCTCCTCCCCTCCTCCCCTCCTCCCCTCCTCCCCTTCT–3′
ODN[5]-51CT	14	5′–GGGTACCGGGTTACCGGGTTACCGGGTTACCGGGTTACCGGGTTACCGGGTTACCGGCGCTAG CCTTTAACCCTTTAACCCTTTAACCCTTTAACCCTTTAACCCTTTAACCCTTTACCC–3′
ODN[5]-52CT	14	5′–CGCCAATCATCCAATCATCCAATCATCCAATCATCCAATCATCCAATCATCCAATCACGCTAG TGCTTGTATGCTTGTATGCTTGTATGCTTGTATGCTTGTATGCTTGTATGCTTGTCG–3′
ODN[5]-53CT	13	5′–GGCTCCCGGCGCTCCGGCGCTCCGGCGCTCCGGCGCTCCGGCGCTCCGGCGCTCCGGCGCTCCGGCGCTAG CCGGCGCTCCGGCGCTCCGGCGCTCCGGCGCTCCGGCGCTCCGGCGCTCCGGGCGCC–3′
ODN[5]-54CT	13	5′–CGCCCCCCCTCCCCCCCTCCCCCCCTCCCCCCCTCCCCCCCTCCCCCCCTCCCCCCCCGCTAG GGGGTGGCGGGGGTGGCGGGGGTGGCGGGGGTGGCGGGGGTGGCGGGGGTGGCGGGGGTGGCG–3′
ODN[5]-55CT	12	5′–GCGGGGCCCCGGGGCCCCGGGGCCCCGGGGCCCCGGGGCCCCGGGGCCCCGGGGCCCCGGGGCCCCGCTAG GGGCCCCGTTGCCCCGTTGCCCCGTTGCCCCGTTGCCCCGTTGCCCCGTTGCCCCGC–3′
ODN[5]-56CT	12	5′–CCGGTTGGCCCGGTTGGCCCGGTTGGCCCGGTTGGCCCGGTTGGCCCGGTTGGCCCGCGCTAG CGGGCCCCCGGGCCCCCGGGCCCCCGGGCCCCCGGGCCCCCGGGCCCCCGGGCCCCGG–3′
ODN[5]-57CT	12	5′–CCGGCCGGCCCGGCCGGCCCGGCCGGCCCGGCCGGCCCGGCCGGCCCGGCCGGCCCGCGCTAG CGGGCCTTCCGGGCCTTCCGGGCCTTCCGGGCCTTCCGGGCCTTCCGGGCCTTCCGG–3′
ODN[5]-58CT	12	5′–GGGCGCCCCGGGCGCCCCGGGCGCCCCGGGCGCCCCGGGCGCCCCGGGCGCCCCGGGCGCTAG CCCGTGGCTCCCGTGGCTCCCGTGGCTCCCGTGGCTCCCGTGGCTCCCGTGGCTCCC–3′
ODN[5]-59CT	12	5′–GGCTGGTAGGGCTGGTAGGGCTGGTAGGGCTGGTAGGGCTGGTAGGGCTGGTAGGCTCGCTAG AGCCTCCCATCCCTCCCATCCCTCCCATCCCTCCCATCCCTCCCATCCCTCCCATCC–3′
ODN[5]-60CT	12	5′–GGCTGGTAGGGCTGGTAGGGCTGGTAGGGCTGGTAGGGCTGGTAGGGCTGGTAGGCTCGCTAG AGCCTCCCCGCCCTCCCCGCCCTCCCCGCCCTCCCCGCCCTCCCCGCCCTCCCCGCC–3′
ODN[5]-61CT	11	5′–GGTCTGGATAGGTCTGGATAGGTCTGGATAGGTCTGGATAGGTCTGGATAGGTCTGGCGCTAG CCATACCTCTCCATACCTCTCCATACCTCTCCATACCTCTCCATACCTCTCCATACC–3′
ODN[5]-62CT	11	5′–GGTCTGGGTGGGTCTGGGTGGGTCTGGGTGGGTCTGGGTGGGTCTGGGTGGGTCTGGCGCTAG CCATACCCCCCCATACCCCCCCATACCCCCCCATACCCCCCCATACCCCCCCATACC–3′

Table D1 (continue). Names, numbers of mismatches and sequences of 120-mer DNA hairpin library

Name	Mismatch numbers	Sequence
ODN^{5}-63CT	11	5′–GCCCTCGCGGGCCCTCGCGGGCCCTCGCGGGCCCTCGCGGGCCCTCGCGGGCCCTCGCGCTAG CGCGGGCCCTCGCGGGCCCTCGCGGGCCCTCGCGGGCCCTCGCGGGCCCTCGCGGGC–3′
ODN^{5}-64CT	11	5′–GCCCCCGTGGGCCCCCGTGGGCCCCCGTGGGCCCCCGTGGGCCCCCGTGGGCCCCCGCGCTAG CGTGGGCCCCCGTGGGCCCCCGTGGGCCCCCGTGGGCCCCCGTGGGCCCCCGTGGGC–3′
ODN^{5}-65CT	11	5′–GCCCTCGTGGGCCCTCGTGGGCCCTCGTGGGCCCTCGTGGGCCCTCGTGGGCCCTCGCGCTAG CGCGGGCCCCCGCGGGCCCCCGCGGGCCCCCGCGGGCCCCCGCGGGCCCCCGCGGGC–3′
ODN^{5}-66CT	11	5′–TCATCTCATCTCATCTCATCTCATCTCATCTCATCTCATCTCATCTCATCTCATCTCATCTCCGCTAG GATATGATATGATATGATATGATATGATATGATATGATATGATATGATATGATATGA–3′
ODN^{5}-67CT	11	5′–GGGATATCTGGGGATATCTGGGGATATCTGGGGATATCTGGGGATATCTGGGGATATCGCTAG ATCTCCCCATATCTCCCCATATCTCCCCATATCTCCCCATATCTCCCCATATCTCCC–3′
ODN^{5}-68CT	11	5′–GGGATAATAGGGGATAATAGGGGATAATAGGGGATAATAGGGGATAATAGGGGATAACGCTAG TTCTCCCCTCTTCTCCCCTCTTCTCCCCTCTTCTCCCCTCTTCTCCCCTCTTCTCCC–3′
ODN^{5}-69CT	11	5′–GGAAATAGGGTGAAATAGGGTGAAATAGGGTGAAATAGGGTGAAATAGGGTGAAATACGCTAG TCTTTCCCCCTCTTTCCCCCTCTTTCCCCCTCTTTCCCCCTCTTTCCCCCTCTTTCC–3′
ODN^{5}-70CT	11	5′–CGGGACAAAGCGGGACAAAGCGGGACAAAGCGGGACAAAGCGGGACAAAGCGGGACACGC TAGTTTCCCTCTTTTTCCCTCTTTTTCCCTCTTTTTCCCTCTTTTTCCCTCTTTTTCCCG–3′
ODN^{5}-71CT	11	5′–CGGGAACAAGGCGGAACAAGGCGGAACAAGGCGGAACAAGGCGGAACAAGGCGGACACGC TAGTTTCCTCCTTTTTCCTCCTTTTTCCTCCTTTTTCCTCCTTTTTCCTCCTTTTTCCCG–3′
ODN^{5}-72CT	11	5′–CGGGAATAAGGTGGAATAAGGTGGAATAAGGTGGAATAAGGTGGAATAAGGTGGATACGCTAG TCTCCCCCTTCTTCCCCCTTCTTCCCCCTTCTTCCCCCTTCTTCCCCCTTCTTCCCG–3′
ODN^{5}-73CT	11	5′–AGGTAAGGTAAGGTAAGGTAAGGTAAGGTAAGGTAAGGTAAGGTAAGGTAAGGTAAGCGCTAG CTTCCCTTCCCTTCCCTTCCCTTCCCTTCCCTTCCCTTCCCTTCCCTTCCCTTCCCT–3′
ODN^{5}-74CT	11	5′–GGAATGGAATGGAATGGAATGGAATGGAATGGAATGGAATGGAATGGAATGGAATGGCGC TAGCCCTTCCCTTCCCTTCCCTTCCCTTCCCTTCCCTTCCCTTCCCTTCCCTTCCC–3′
ODN^{5}-75CT	11	5′–CCCGATTTCTCCCGATTTCTCCCGATTTCTCCCGATTTCTCCCGATTTCTCCCGATTCGCTAG ACTCGGGATAACTCGGGATAACTCGGGATAACTCGGGATAACTCGGGATAACTCGGG–3′
ODN^{5}-76CT	11	5′–GGGCATTCCCGGGCATTCCCGGGCATTCCCGGGCATTCCCGGGCATTCCCGGGCCCGCGCTAG CGGTCCCTGGAATTCCCTGGAATTCCCTGGAATTCCCTGGAATTCCCTGGAATTCCC–3′
ODN^{5}-77CT	11	5′–CGGGATAAAGTGGGATAAAGTGGGATAAAGTGGGATAAAGTGGGATAAAGTGGGATACGCTAG TCTCCCCCTTTCTCCCCCTTTCTCCCCCTTTCTCCCCCTTTCTCCCCCTTTCTCCCG–3′
ODN^{5}-78CT	10	5′–GCTGGCCCGGGCCCTGGCCCGGGCCCTGGCCCGGGCCCTGGCCCGGGCCCTGGGCCCCGCTAG GTGCCCCGGGCCCTGGCCCGGGCCCTGGCCCGGGCCCTGGCCCGGGCCCTGGCCCGC–3′

Table D1 (continue). Names, numbers of mismatches and sequences of 120-mer DNA hairpin library

Name	Mismatch numbers	Sequence
ODN[5]-79CT	10	5′–GCTGGTTATGGTTATGGTTATGGTTATGGTTATGGTTATGGTTATGGTTATGGTTACCGCTAG GTCACCCTAACCCTAACCCTAACCCTAACCCTAACCCTAACCCTAACCCTAACCCGC–3′
ODN[5]-80CT	10	5′–CCCCATGGCCCCATGGGGCCCCATGGGGCCCCATGGGGCCCCATGGGGCCCCATGGGCGCTAG CCCCTGGGTCCCCCTGGGTCCCCCTGGGTCCCCCTGGGTCCCCCTGGGTCCATGGGG–3′
ODN[5]-81CT	10	5′–GCTGGCGTGGGCGGTGGCGTGGGCGGTGGCGTGGGCGGTGGCGTGGGCGGTGGCGTCCGC TAGGCCGCCCCCGCCCCCGCCCCCGCCCCCGCCCCCGCCCCCGCCCCCGCCCCCGC–3′
ODN[5]-82CT	10	5′–GCTGGCGGTGGCGGTGGCGGTGGCGGTGGCGGTGGCGGTGGCGGTGGCGGTGGCGTCCGC TAGGCCGCCCCCGCCCCCGCCCCCGCCCCCGCCCCCGCCCCCGCCCCCGCCCCCGC–3′
ODN[5]-83CT	10	5′–GCTCATGATCATGATCATGATCATGATCATGATCATGATCATGATCATGATCATGCTCGCTAG ATCATGCTCATGCTCATGCTCATGCTCATGCTCATGCTCATGCTCATGCTCATGCGC–3′
ODN[5]-84CT	10	5′–GCTCATGATCATGATCATGATCATGATCATGATCATGATCATGATCATGATCATGCTCGCTAG ATCATTATCATTATCATTATCATTATCATTATCATTATCATTATCATTATCATGCGC–3′
ODN[5]-85CT	10	5′–GGCCCGGGGCCCCTCGGGGCCCCTCGGGGCCCCTCGGGGCCCCTCGGGGCCCCTGGGCGCTAG CCCCGGGGCCCCTCGGGGCCCCTCGGGGCCCCTCGGGGCCCCTCGGGGCCCCTGGCC–3′
ODN[5]-86CT	10	5′–TATAACAGGGGATAACAGGGGATAACAGGGGATAACAGGGGATAACAGGGGATATATCGCTAG ATATCTCCCCTTTCTCCCCTTTCTCCCCTTTCTCCCCTTTCTCCCCTTTATA–3′
ODN[5]-87CT	10	5′–GCGCTTTTCCCCACTTTTCCCCACTTTTCCCCACTTTTCCCCACTTTTCCCCACACGCGCTAG CGTTTGGGGACAATTGGGGACAATTGGGGACAATTGGGGACAATTGGGGACAAGCGC–3′
ODN[5]-88CT	10	5′–CGGGATTCCCGGGCATTCCCGGGCATTCCCGGGCATTCCCGGGCATTCCCGGGCATTCCCGGGCCCGCGCTAG CGGGCCCTGGCATGCCCTGGCATGCCCTGGCATGCCCTGGCATGCCCTGGCATCCCG–3′
ODN[5]-89CT	10	5′–CGGGATTCCCGGGCATTCCCGGGCATTCCCGGGCATTCCCGGGCATTCCCGGGCCCGCGCTAG CGGTCCCGGGCATTCCCGGGCATTCCCGGGCATTCCCGGGCATTCCCGGGCATCCCG–3′
ODN[5]-90CT	10	5′–GCTGGTTATGGTTCGGGTTATGGTTCGGGTTATGGTTCGGGTTATGGTTCGGGTTACCGCTAG GTCACCCTAACCCTAACCCTAACCCTAACCCTAACCCTAACCCTAACCCTAACCCGC–3′
ODN[5]-91CT	9	5′–GGCCCGGGCCCGGGCCCGGGCCCGGGCCCGGGCCCGGGCCCGGGCCCGGGCCCGGGCCGCTAG GCCCTGGCCCGTGCCCTGGCCCGTGCCCTGGCCCGTGCCCTGGCCCGTGCCCTGGCC–3′
ODN[5]-92CT	9	5′–GGGTCTGGGTCTGGGTCTGGGTCTGGGTCTGGGTCTGGGTCTGGGTCTGGGTCTGGGCGCTAG CCCATACCCATACCCATACCCATACCCATACCCATACCCATACCCATACCCATACCC–3′
ODN[5]-93CT	9	5′–GGGTTCGGGTTCGGGTTCGGGTTCGGGTTCGGGTTCGGGTTCGGGTTCGGGTTCGGGCGCTAG CCCTAACCCTAACCCTAACCCTAACCCTAACCCTAACCCTAACCCTAACCCTAACCC–3′
ODN[5]-94CT	8	5′–GCCCCGGGCCCTGGGCCCCGGGCCCTGGGCCCCGGGCCCTGGGCCCCGGGCCCTGGGCGCTAG CCCCGGGCCCTGGGCCCCGGGCCCTGGGCCCCGGGCCCTGGGCCCCGGGCCCTGGGC–3′

Table D1 (continue). Names, numbers of mismatches and sequences of 120-mer DNA hairpin library[a]

Name	Mismatch numbers	Sequence (5′ to 3′)
ODN^{5}-95CT	8	5′–GCGG**C**GGGCGG**T**GGGCGG**C**GGGCGG**T**GGGCGG**C**GGGCGG**T**GGGCGG**C**GGGCGG**T**GGGCGC TAGCCC**C**CGCCC**T**CCGCCC**C**CGCCC**T**CCGCCC**C**CCGCCC**T**CCGCCC**C**CCGCCC**T**CCGC–3′
ODN^{5}-96CT	8	5′–GTTA**C**GGGTTA**T**GGGTTA**C**GGGTTA**T**GGGTTA**C**GGGTTA**T**GGGTTA**C**GGGTTA**T**GGGCGCTAG CCC**C**TAACCC**T**TAACCC**C**TAACCC**T**TAACCC**C**TAACCC**T**TAACCC**C**TAACCC**T**TAAC–3′
ODN^{5}-97CT	8	5′–GTGA**C**TCATGA**T**TCATGA**C**TCATGA**T**TCATGA**C**TCATGA**T**TCATGA**C**TCATGA**T**TCACGCTAG TGA**C**TCATGA**T**TCATGA**C**TCATGA**T**TCATGA**C**TCATGA**T**TCATGA**C**TCATGA**T**TCAC–3′
ODN^{5}-98CT	8	5′–GAGATA**C**AGATA**T**AGATA**C**AGATA**T**AGATA**C**AGATA**T**AGATA**C**AGATA**T**AGATAAGACGCTAG TCTTATCT**C**TATCT**T**TATCT**C**TATCT**T**TATCT**C**TATCT**T**TATCT**C**TATCT**T**TATCTC–3′
ODN^{5}-99CT	8	5′–CGGTGTAT**C**TGCCGA**T**AT**C**TCGG**T**ATAT**C**TGCCGA**T**AT**C**TCGG**T**ATTAGAGCCTGTACGCTAG TACAGGCTCTAAT**C**CCGA**T**AT**C**TCGGCA**T**ATAT**C**CCGA**T**AT**C**TCGGCA**T**ATACACCG–3′
ODN^{5}-100CT	8	5′–GTAT**C**TATATA**C**ATATAT**C**TATATA**C**ATATAT**C**TATATA**C**ATATAT**C**TATATA**C**ATACGCTAG TAT**T**TATATA**T**ATATAT**T**TATATA**T**ATATAT**T**TATATA**T**ATATAT**T**TATATA**T**ATAC–3′
ODN^{5}-101CT	8	5′–GTAT**C**ATATAT**T**ATATAT**C**ATATAT**T**ATATAT**C**ATATAT**T**ATATAT**C**ATATAT**T**ATACGCTAG TAT**C**ATATAT**T**ATATAT**C**ATATAT**T**ATATAT**C**ATATAT**T**ATATAT**C**ATATAT**T**ATAC–3′
ODN^{5}-102CT	8	5′–CGG**T**GGGCGG**T**GGGCGG**T**GGGCGG**T**GGGCGG**T**GGGCGG**T**GGGCGG**T**GGGCGG**T**GGCGCGC TAGCGCC**C**CGCCC**C**CGCCC**C**CGCCC**C**CGCCC**C**CGCCC**C**CGCCC**C**CGCCC**C**CG–3′
ODN^{5}-103CT	8	5′–CGG**C**GGGCGG**C**GGGCGG**C**GGGCGG**C**GGGCGG**C**GGGCGG**C**GGGCGG**C**GGCGCGC TAGCGCC**T**CCGCCC**T**CCGCCC**T**CCGCCC**T**CCGCCC**T**CCGCCC**T**CCGCCC**T**CCG–3′
ODN^{5}-104CT	7	5′–CCC**C**GGGCCC**C**GGGGCCCC**T**GGGCCC**C**GGGGCCCC**T**GGGCCC**C**GGGGCCCC**T**GGGCCCGCTAG GGCCC**C**GGGGCCCC**T**GGGCCC**C**GGGGCCCC**T**GGGCCC**C**GGGGCCCC**T**GGGCCC**T**GGG–3′
ODN^{5}-105CT	7	5′–C**C**GGGGCCC**C**GGGGCCC**C**GGGGCCC**C**GGGGCCC**C**GGGGCCC**C**GGGGCCC**C**GGGGCCCCGCTAG GGGCCCC**T**GGGCCCC**T**GGGCCCC**T**GGGCCCC**T**GGGCCCC**T**GGGCCCC**T**GGGCCCC**T**G–3′
ODN^{5}-106CT	7	5′–CCC**T**GGGCCC**T**GGGGCCCC**T**GGGCCC**T**GGGGCCCC**T**GGGCCC**T**GGGGCCCC**T**GGGCCCGCTAG GGCCC**C**GGGGCCCC**C**GGGCCC**C**GGGGCCCC**C**GGGCCC**C**GGGGCCCC**C**GGGCCC**C**GGG–3′

[a] Bold red bases indicate the C:T mismatches. Bold blue bases indicate hairpin loop regions.

Table D2. Impact of mismatch numbers in CD spectra of library oligonucleotides.

CD spectra	Number of sequences	Sequences with 15 or more mismatch	Sequences with less than 15 mismatch
Little to no change	49 (46.2%)	13 **(-1.4%)**	36 **(+0.6%)**
Partial B- to A-form conversion	35 (33.0%)	7 **(-8.9%)**	28 **(+3.4%)**
Global B- to A-form conversion	5 (4.7%)	5 **(+12.5%)**	0 **(-4.7%)**
Unstructured	4 (3.8%)	0 **(-3.8 %)**	4 **(+1.4%)**
Red shift in the positive band	6 (5.7%)	1 **(-2.3 %)**	5 **(+0.8%)**
Right- to left-handed transition	7 (6.6)	3 **(+3.7%)**	4 **(-1.4%)**
Total number of oligonucleotides	106	29	77

Table D3. DNA hairpin repeat sequences[a] and fluorescence anisotropy of Neo-BODIPY in the presence of each DNA with and without Hg^{II}.[b]

ODN[5]	DNA repeat sequence (5′ → 3′)	No Hg^{II}	+Hg^{II}
No DNA	-	0.05 ± 0.01	0.05 ± 0.01
5CT	$[GGCCTC]_{9.5}$	0.04 ± 0.01	0.06 ± 0.01
6CT	$[GGCCCT]_{9.5}$	0.04 ± 0.02	0.06 ± 0.01
9CT	$[CGGCCC]_{9.5}$	0.05 ± 0.01	0.05 ± 0.02
15CT	$[TCTGGGC]_{8}$	0.04 ± 0.01	0.05 ± 0.02
19CT	$[TCCTCGGTGGC]_{5}$	0.04 ± 0.02	0.05 ± 0.01
21CT	$[TGGTCCCTCGG]_{5}$	0.04 ± 0.01	0.14 ± 0.01
21TT	$[TGGTCCCTCGG]_{5}$	0.04 ± 0.02	0.03 ± 0.01
21AT	$[TGGTCCCTCGG]_{5}$	0.04 ± 0.01	0.05 ± 0.01
22CT	$[CCCCCGGCGGC]_{5}$	0.04 ± 0.01	0.05 ± 0.01
23CT	$[CCGCGGGCCCT]_{5}$	0.05 ± 0.01	0.05 ± 0.01
25CT	$[TGGGTGGTCGC]_{5}$	0.05 ± 0.01	0.05 ± 0.01
27CT	$[CGGGTGGCCGC]_{5}$	0.04 ± 0.01	0.05 ± 0.01
28CT	$[TGGGCGGTCGC]_{5}$	0.05 ± 0.01	0.05 ± 0.01
37CT	$[TGGTGCCCCCGG]_{5}$	0.05 ± 0.01	0.04 ± 0.01
40CT	$[CGGG]_{14}$	0.05 ± 0.02	0.05 ± 0.01
44CT	$[GGGGCCTC]_{7}$	0.06 ± 0.01	0.06 ± 0.02
45CT	$[GGGGCCTT]_{7}$	0.04 ± 0.01	0.03 ± 0.01

Table D3 (continue).

ODN[5]	DNA repeat sequence (5′ → 3′)	No Hg^{II}	+Hg^{II}
46CT	$[GGGGCCCT]_7$	0.04 ± 0.02	0.07 ± 0.01
91CT	$[CGGGCCCGGGCC]_{4.5}$	0.05 ± 0.01	0.06 ± 0.01
104CT	$[TGGGCCCCGGGGCCCC]_{3.5}$	0.05 ± 0.01	0.06 ± 0.01

[a] Bold bases indicate C:T mismatches. Italic bases in ODN[5]-21AT indicate A:T base-pairs.
[b] All samples contained 40 nM of Neo-BODIPY, 600 nM of DNA, and 0 or 1.5 equiv of Hg^{II} per C:T mismatch in an aqueous buffer containing 200 mM $NaClO_4$ and 50 mM cacodylic acid (pH = 7.8). Averaged anisotropy values and standard deviations of three independent measurements are shown.

Table D4. Names, length, numbers of mismatches and sequences of hairpins and duplexes.[a]

ODN5	Length	Mismatch numbers	Sequence
ODN[5]-21CT	120	15	5′– CGGTGGTCCCTCGGTGGTCCCTCGGTGGTCCCTCGGTGGTCCCTCGGTGGTCCCTCGCGCTAG CGCGGGCCCCCCGCGGGCCCCCCGCGGGCCCCCCGCGGGCCCCCCGCGGGCCCCCCG – 3′
ODN[5]-21TT	120	15	5′– CGGTGGTCCCTCGGTGGTCCCTCGGTGGTCCCTCGGTGGTCCCTCGGTGGTCCCTCGCGCTAG CGTGGGTCCTCCGTGGGTCCTCCGTGGGTCCTCCGTGGGTCCTCCGTGGGTCCTCCG – 3′
ODN[5]-21AT	120	0	5′– CGG*T*GG*T*CCC*T*CGG*T*GG*T*CCC*T*CGG*T*GG*T*CCC*T*CGG*T*GG*T*CCC*T*CGG*T*GG*T*CCC*T*CGCGCTAG CG*A*GGG*A*CC*A*CCG*A*GGG*A*CC*A*CCG*A*GGG*A*CC*A*CCG*A*GGG*A*CC*A*CCG*A*GGG*A*CC*A*CCG – 3′
DUP[5]-21CT	58	15	5′– CGGTGGTCCCTCGGTGGTCCCTCGGTGGTCCCTCGGTGGTCCCTCGGTGGTCCCTCGC – 3′ 3′ –GCCCCCGGGCGCCCCCGGGCGCCCCCGGGCGCCCCCGGGCGCCCCCGGGCGCC– 5′
ODN[5]-7TT-1	28	8	5′–CCGGTTCCGGTTCCGGTTCCGGTTCCGG–3′
ODN[5]-7TT-2	26	8	5′–CGGTTCCGGTTCCGGTTCCGGTTCCG–3′
ODN[5]-7TT-3	22	6	5′–CCGGTTCCGGTTCCGGTTCCGG–3′
ODN[5]-21TT-1	29	7	5′–CGGTGGTCCCTCGGTCCGTGGGTCCTCCG–3′
ODN[5]-21TT-2	21	5	5′–CGGTGGTCCCTGGGTCCTCCG–3′
DUP[5]-21TT-3	14	3	5′– CGG T GG T CCC T CGG –3′ 3′– GCC T CC T GGG T GCC –5′

[a] Bold red bases indicate C:T or T:T mismatches. Bold italic bases indicate A:T match pairs. Blue bases indicate loop regions.

Table D4 (continue). Names, length, numbers of mismatches and sequences of hairpins and duplexes.[a]

ODN5	Length	Mismatch numbers	Sequence
DUP[5]-21TT-4	13	3	5′–GG **T** CCC **T** GGG **T** CC –3′ 3′–CC **T** GGG **T** CCC **T** GG –5′
DUP[5]-21TT-5	10	2	5′– CGG **T** GG **T** CCC–3′ 3′– GCC **T** CC **T** GGG–5′
DUP[5]-21TT-6	10	2	5′–GGG **T** GC **T** CCC –3′ 3′– CCC **T** CG **T** GGG –5′
DUP[5]-21CT-1	14		5′– CGG **T** GG **T** CCC **T** CGG –3′ 3′– GCC **C** CC **C** GGG **C** GCC –5′
DUP[5]-21CT-2	10		5′– CGG **T** GG **T** CCC–3′ 3′– GCC **C** CC **C** GGG–5′
ODN[5]-38TT-1	31	7	5′–CGG**T**CGG**T**CGG**T**CGG**T**CCG**T**CCG**T**CCG**T**CCG–3′
ODN[5]-38TT-2	28	6	5′–CGG**T**CGG**T**CGG**T**CCGG**T**CCG**T**CCG**T**CCG–3′
ODN[5]-38TT-3	23	5	5′–CGG**T**CGG**T**CGG**T**CCG**T**CCG**T**CCG–3′
ODN[5]-38CT-1	28	6	5′–CGG**T**CGG**C**CGG**T**CCGG**C**CCG**T**CCG**C**CCG–3′
38CT-2	28	6	5′–CGG**C**CGG**T**CGG**C**CCGG**T**CCG**C**CCG**T**CCG–3′

[a] Bold red bases indicate C:T or T:T mismatches. Bold italic bases indicate A:T match pairs. Blue bases indicate loop regions.

5.7.2 Figures

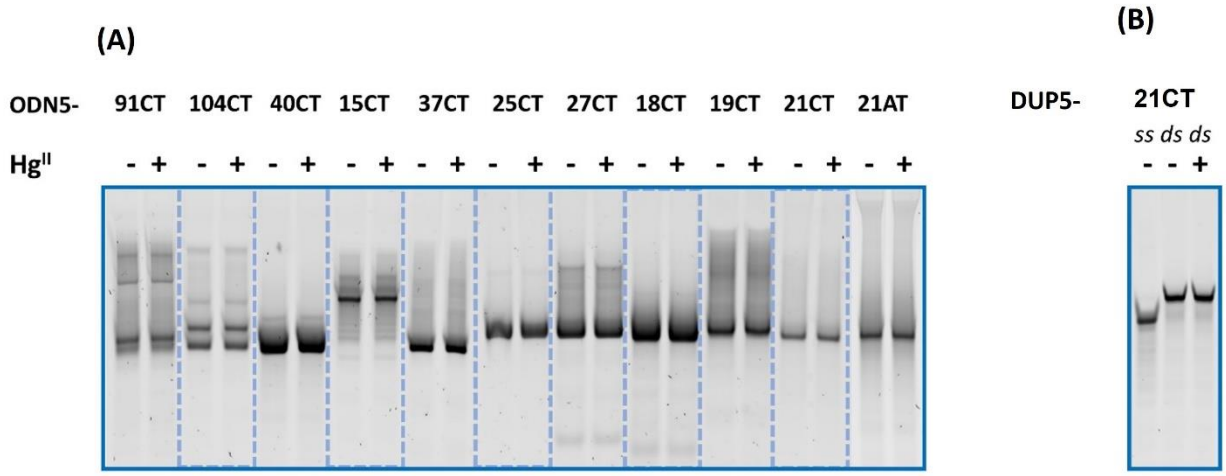

Figure D1. Native gel analysis of DNA repeat sequences in the presence and absence of Hg^{II}. (A) Intramolecular hairpin formation of some selected sequences, including the hit sequence ODN^5-21CT and its well-matched analog, ODN^5-21AT. (B) DUP^5-21CT duplex DNA formation. All samples were prepared in aqueous buffer containing 200 mM $NaClO_4$ and 50 mM cacodylic acid (pH = 7.8). Sucrose (40 %, 5 µl) was given to pre-annealed hairpin or duplex DNA (5 µl, 5 pmol) prior to loading on gel. DNA samples measured in the presence of Hg^{II} were incubated with $Hg(ClO_4)_2$ (1.5 equiv relative to mismatch present) for 3 h prior to use. For oligonucleotide sequences see Tables D1 and D4.

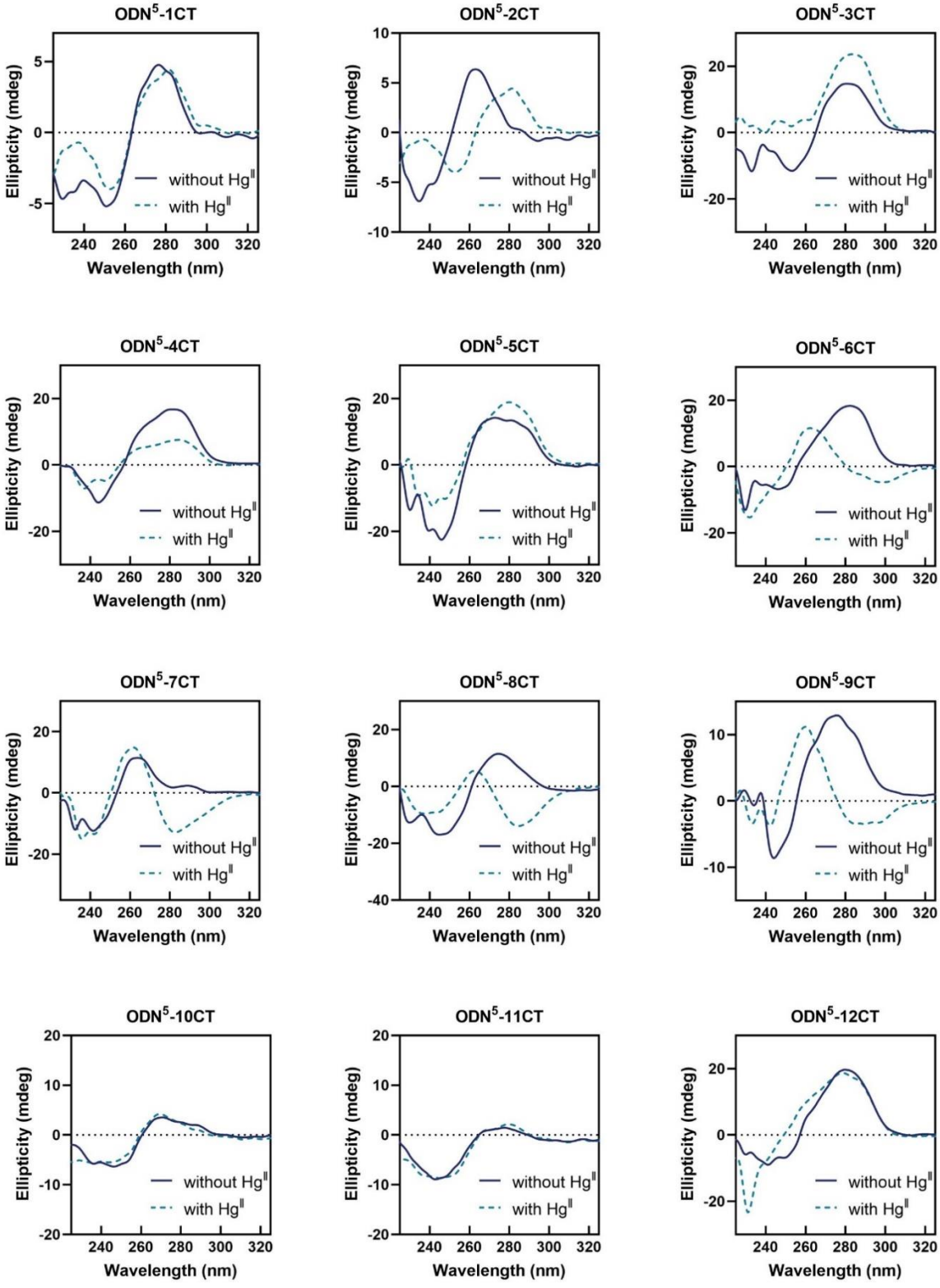

Figure D2. CD spectra of DNA hairpin repeat sequences in the presence (dashed, light blue) and absence (solid, dark blue) of 1.5 equiv Hg^{II} (equiv relative to mismatch present). All samples contained 1.0 µM hairpin in aqueous buffer 200 mM $NaClO_4$ and 50 mM cacodylic acid (pH = 7.8).

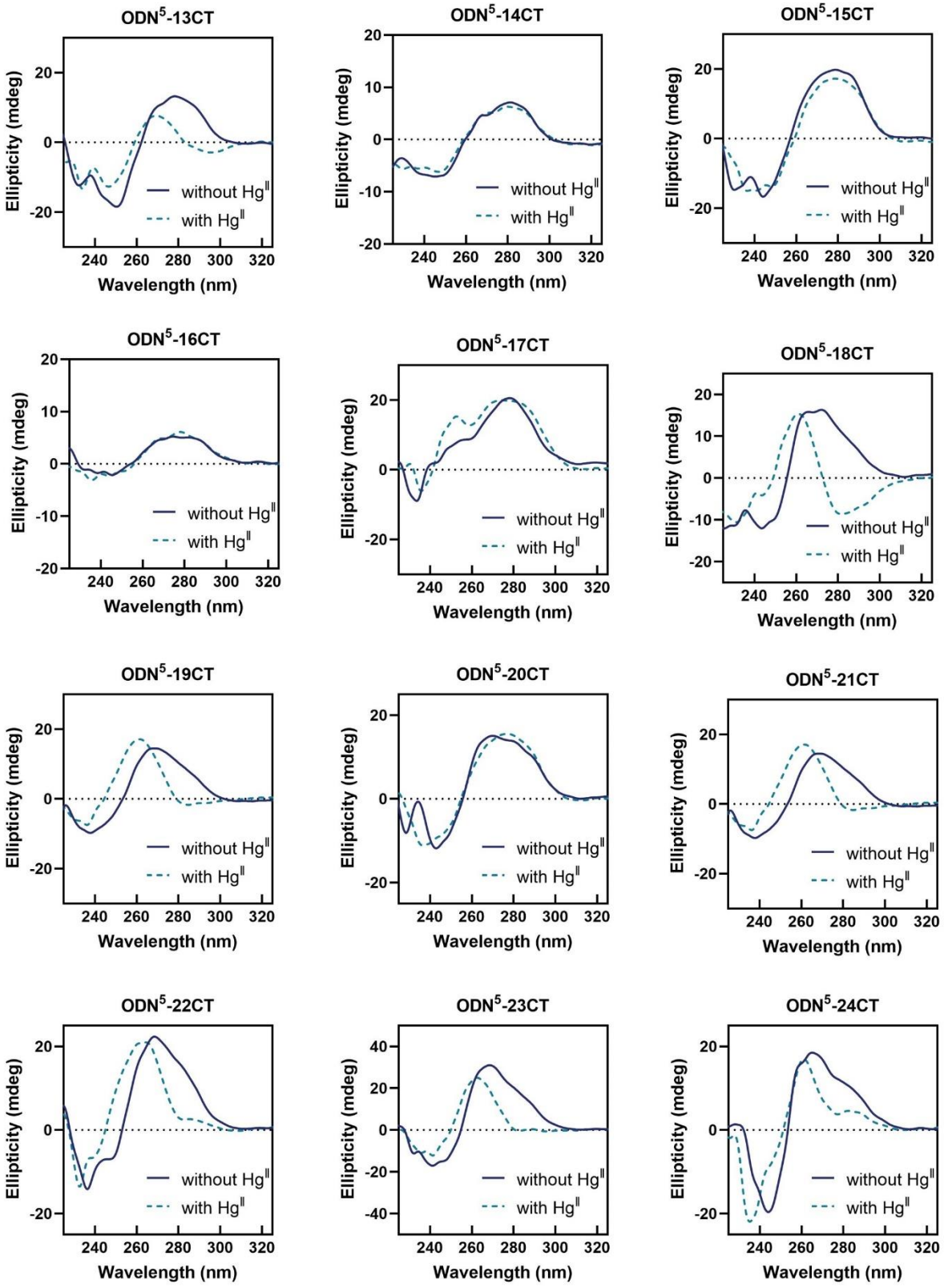

Figure D2 (continue). CD spectra of DNA hairpin repeat sequences in the presence (dashed, light blue) and absence (solid, dark blue) of 1.5 equiv Hg^{II} (equiv relative to mismatch present).

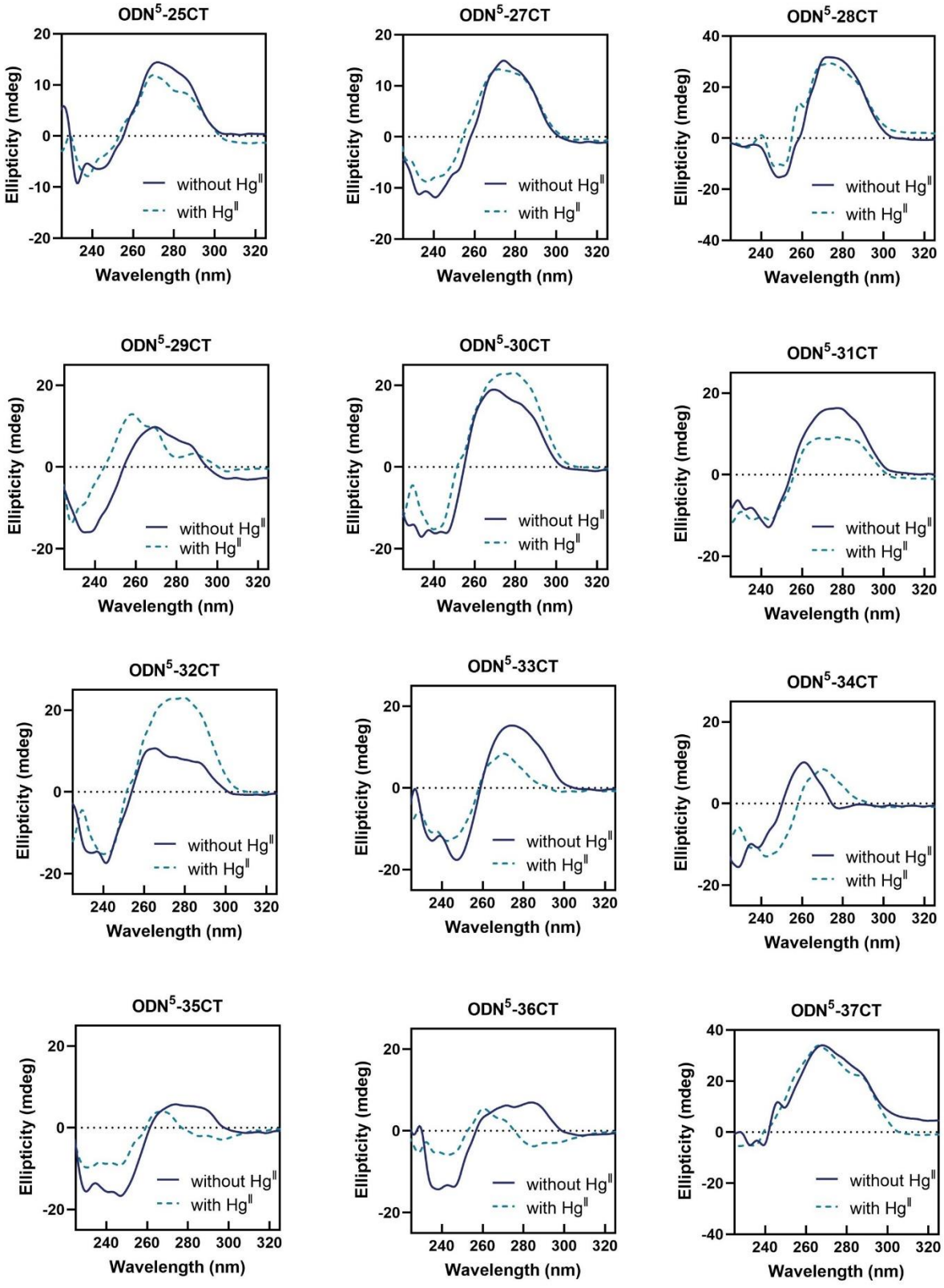

Figure D2 (continue). CD spectra of DNA hairpin repeat sequences in the presence (dashed, light blue) and absence (solid, dark blue) of 1.5 equiv Hg^{II} (equiv relative to mismatch present).

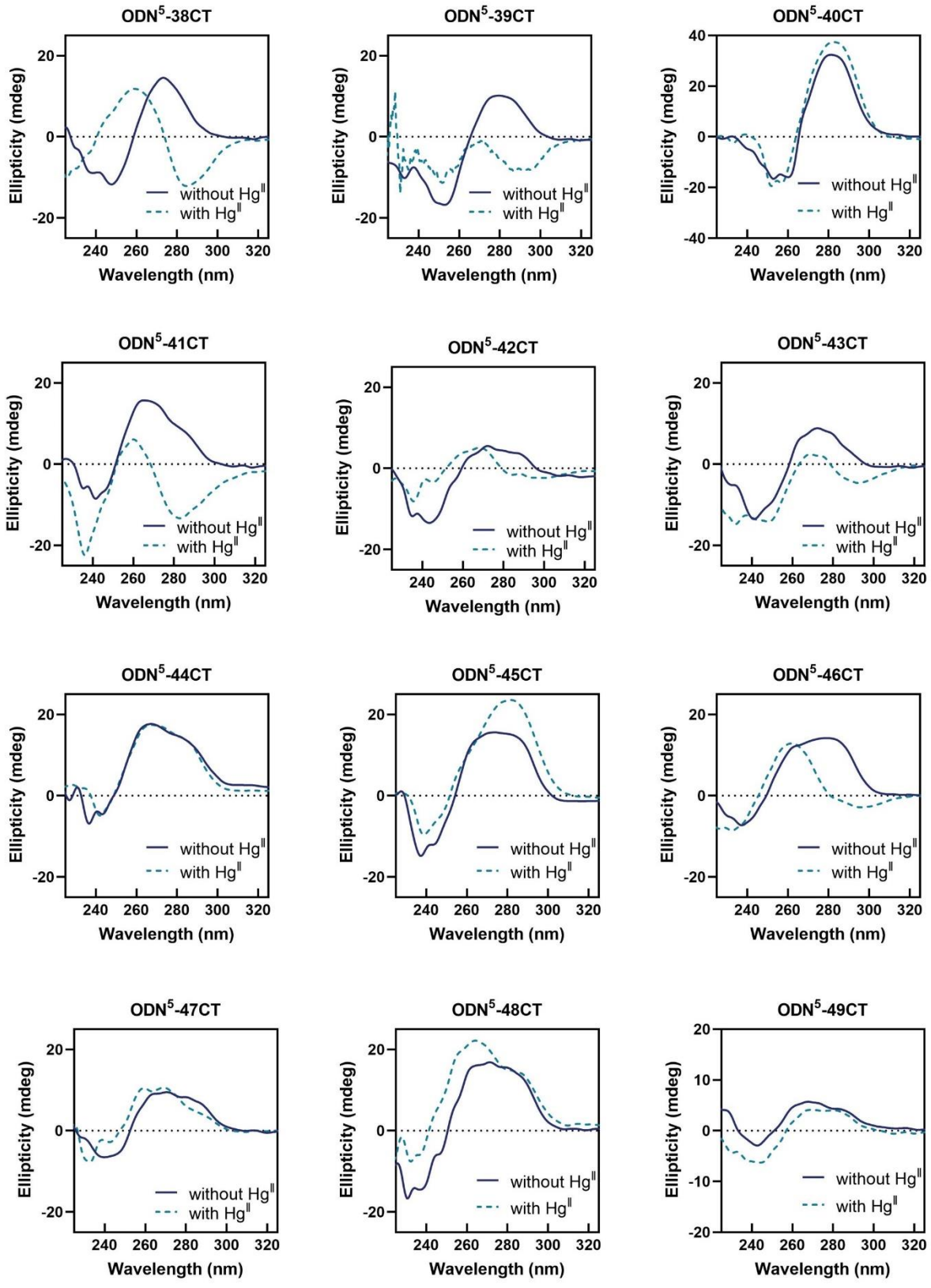

Figure D2 (continue). CD spectra of DNA hairpin repeat sequences in the presence (dashed, light blue) and absence (solid, dark blue) of 1.5 equiv Hg^{II} (equiv relative to mismatch present).

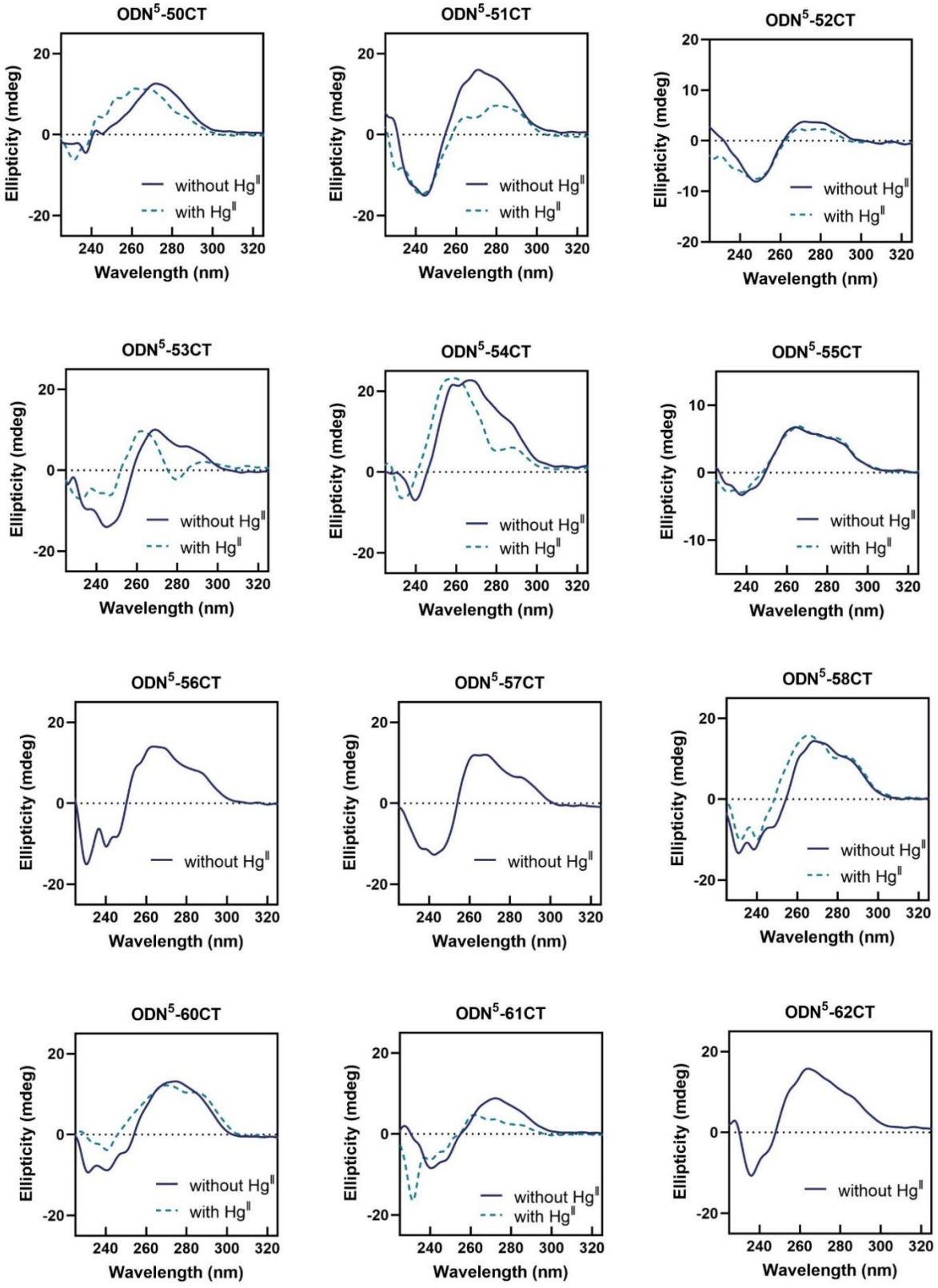

Figure D2 (continue). CD spectra of DNA hairpin repeat sequences in the presence (dashed, light blue) and absence (solid, dark blue) of 1.5 equiv Hg^{II} (equiv relative to mismatch present).

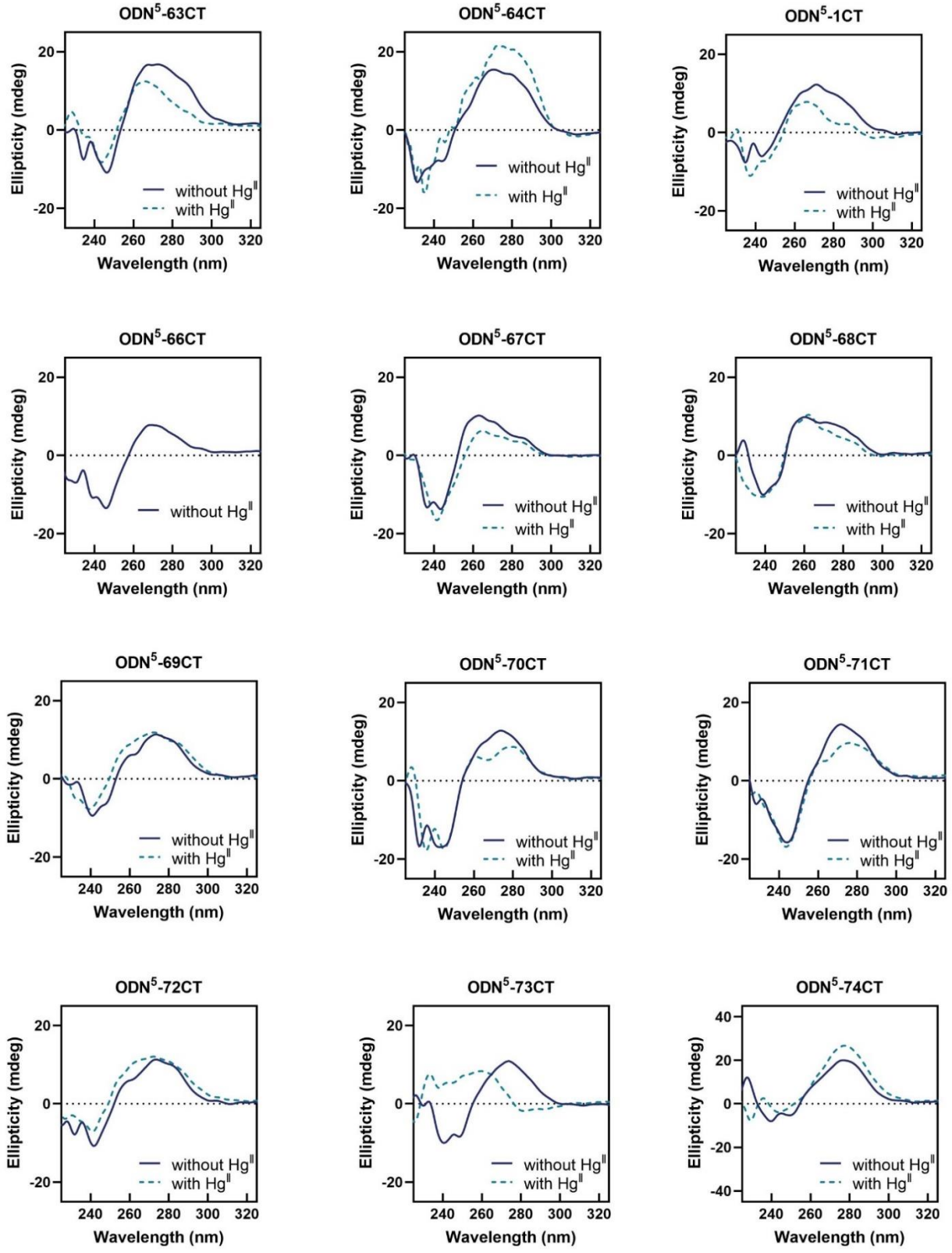

Figure D2 (continue). CD spectra of DNA hairpin repeat sequences in the presence (dashed, light blue) and absence (solid, dark blue) of 1.5 equiv Hg^{II} (equiv relative to mismatch present).

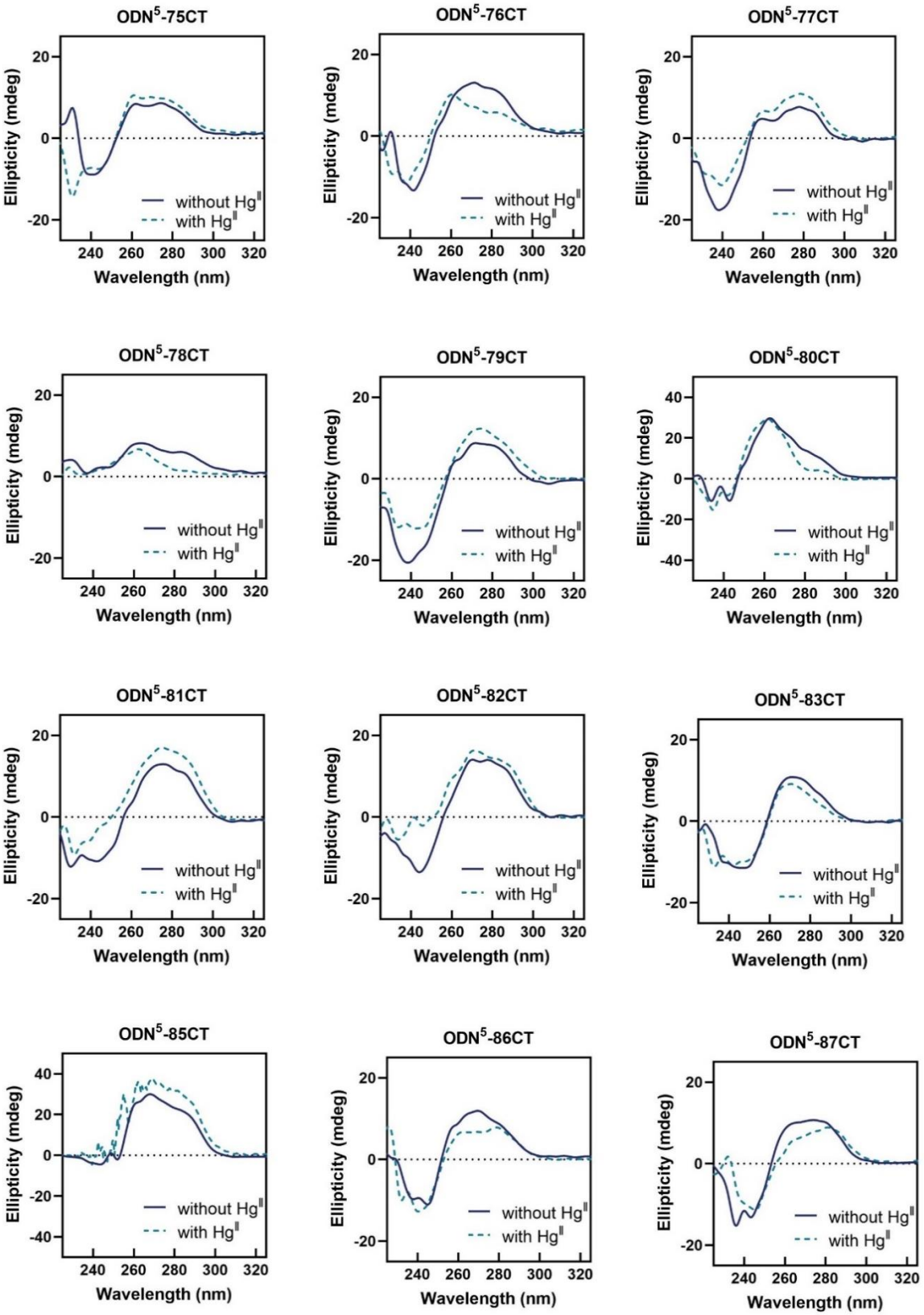

Figure D2 (continue). CD spectra of DNA hairpin repeat sequences in the presence (dashed, light blue) and absence (solid, dark blue) of 1.5 equiv Hg^{II} (equiv relative to mismatch present).

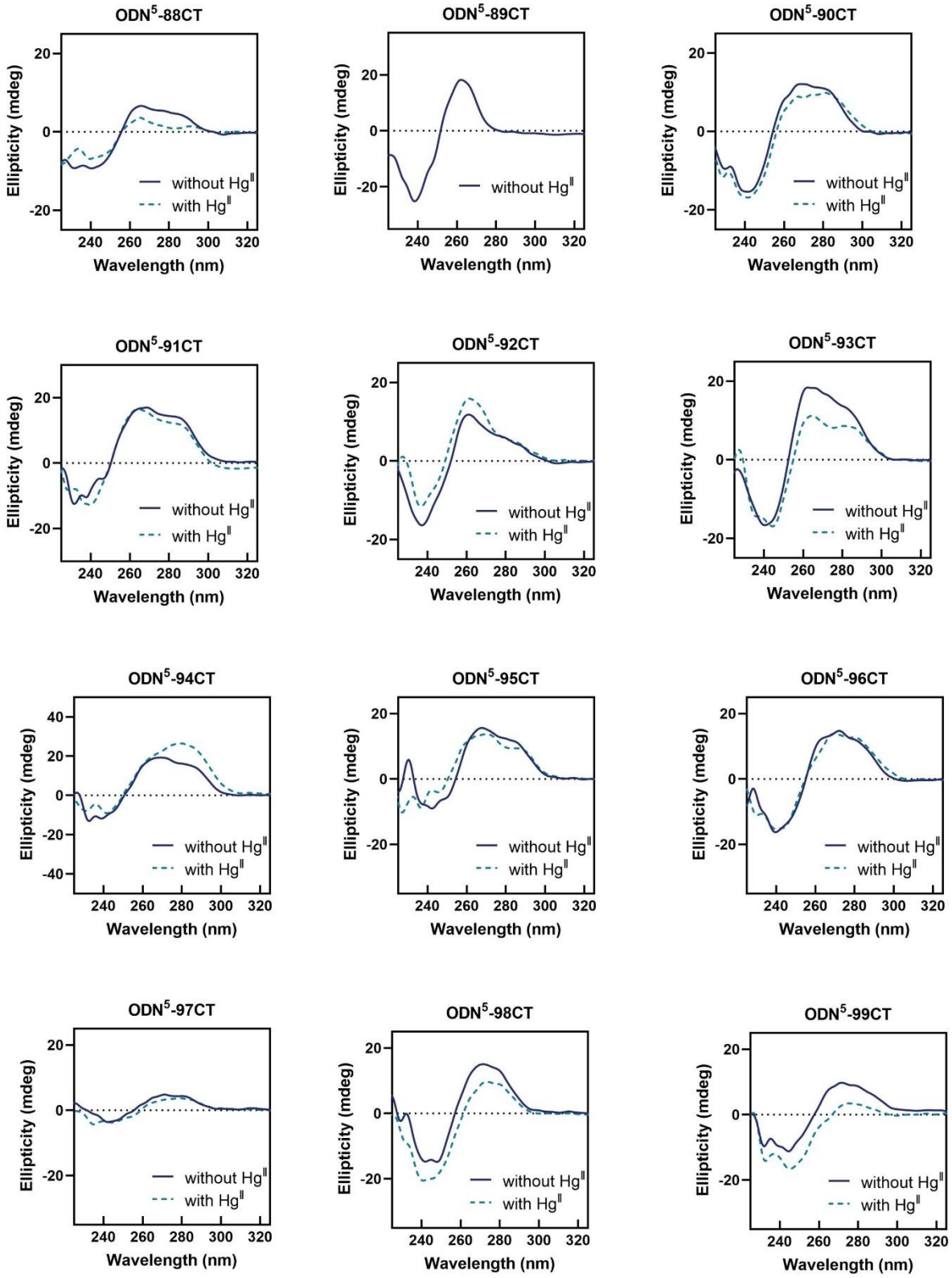

Figure D2 (continue). CD spectra of DNA hairpin repeat sequences in the presence (dashed, light blue) and absence (solid, dark blue) of 1.5 equiv Hg^{II} (equiv relative to mismatch present).

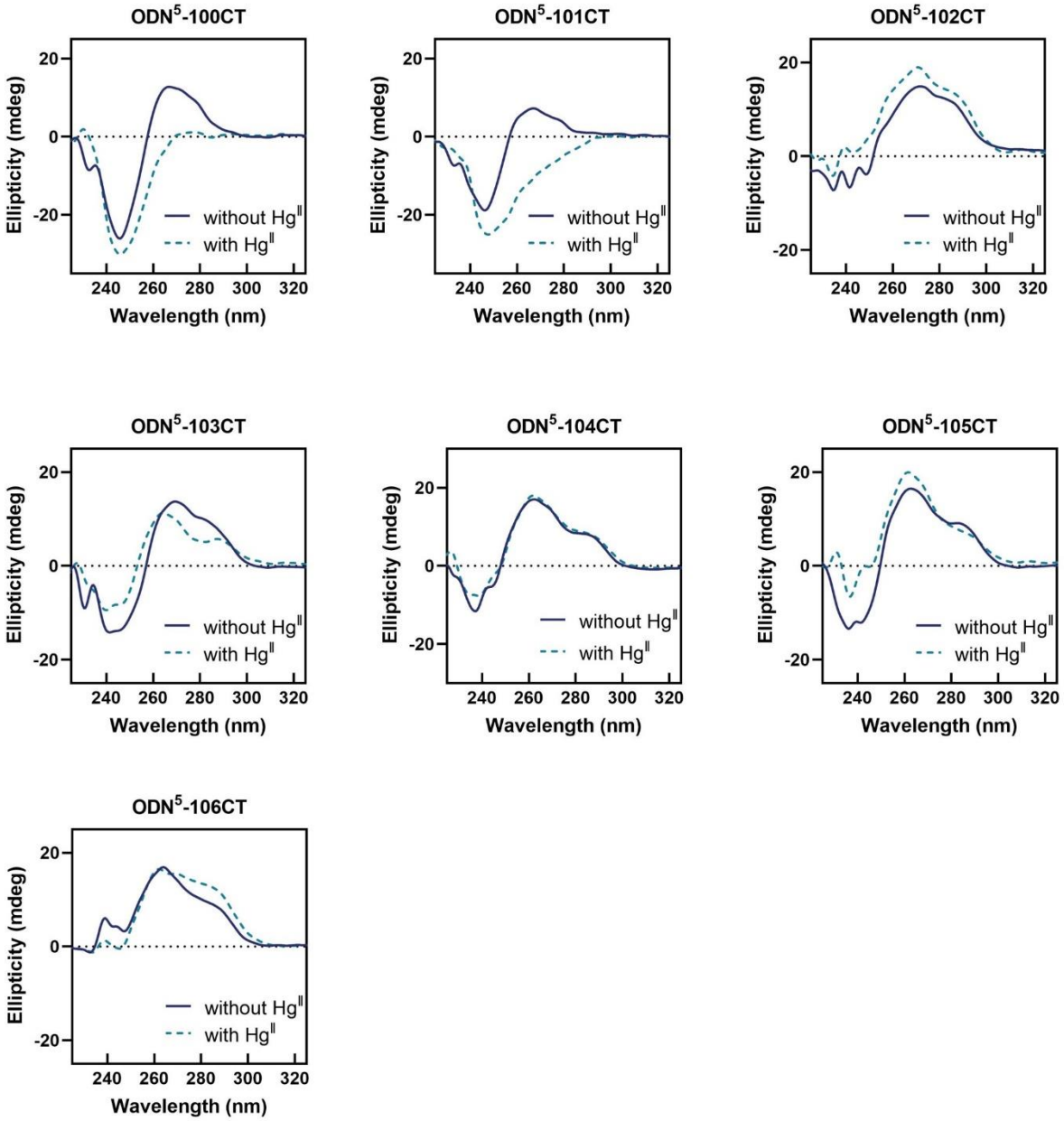

Figure D2 (continue). CD spectra of DNA hairpin repeat sequences in the presence (dashed, light blue) and absence (solid, dark blue) of 1.5 equiv Hg^{II} (equiv relative to mismatch present).

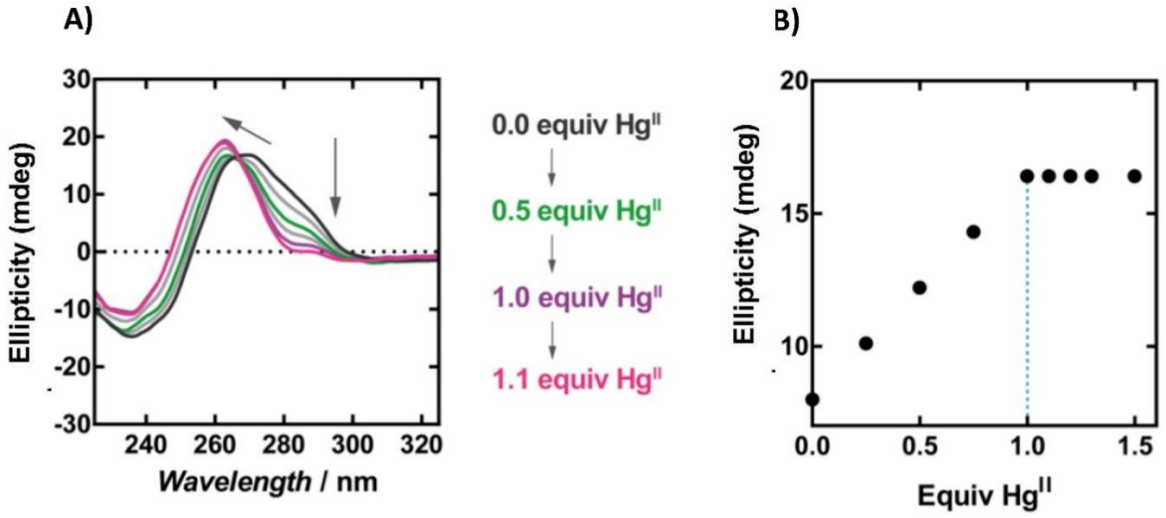

Figure D3. Stoichiometric Hg^{II} binding to ODN^5-21CT. (A) Binding of Hg^{II} to C:T mismatches induces B- to A-form helical transition of ODN^5-21CT hairpin according to changes in CD spectra. (B) 1:1 stoichiometric binding of Hg^{II} to the number of C:T mismatches present in ODN^5-21CT hairpin according to changes in ellipticity at 256 nm. Equiv of Hg^{II} are given relative to mismatch present.

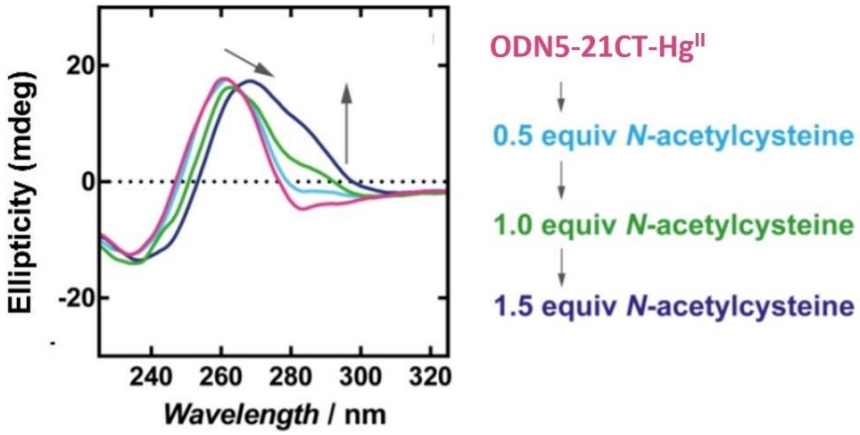

Figure D4. Reverse A- to B-form transition upon addition of N-acetylcysteine. ODN^5-21CT (1.0 µM) was preincubated with $Hg(ClO_4)_2$ (22.5 µM, 1.5 equiv relative to mismatch) for 10 min prior to addition of N-acetylcysteine. All samples contained ODN^5-21CT in aqueous buffer (200 mM $NaClO_4$ and 50 mM cacodylic acid (pH = 7.8)).

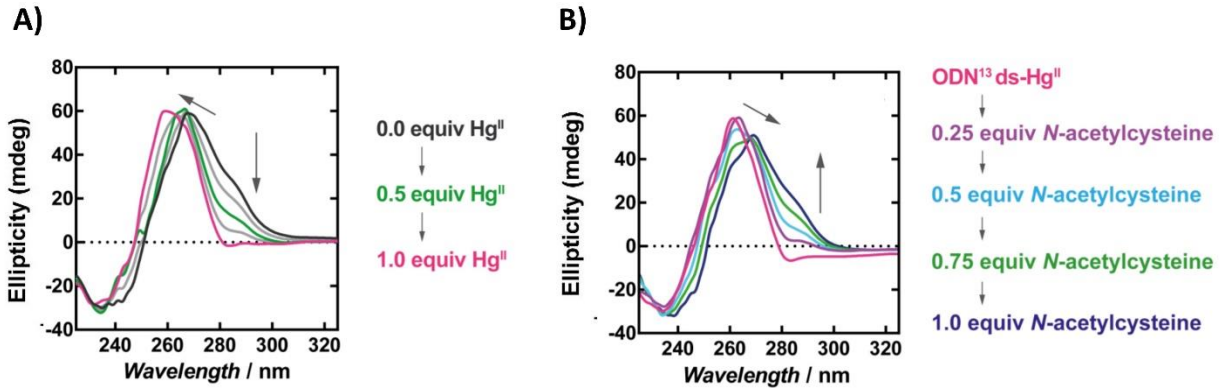

Figure D5. Stoichiometric Hg^{II} binding to ODN5-21CT(ds) and reversibility of B-A transition by N-acetylcysteine. A) Stoichiometric binding of Hg^{II} to C:T mismatches induces B- to A-form helical transition of ODN5-21CT(ds) according to changes in CD spectra. B) Reverse A- to B-form transition upon addition of N-acetylcysteine. ODN5-21CT(ds) (3.0 µM) was preincubated with $Hg(ClO_4)_2$ (45 µM, 1 equiv relative to mismatch present) for 10 min prior to addition of N-acetylcysteine. All samples contained 3.0 µM duplex in aqueous buffer (200 mM $NaClO_4$ and 50 mM cacodylic acid (pH = 7.8)). CD spectra were recorded after 10 min incubation with aliquots of $Hg(ClO_4)_2$ (A) or N-acetylcysteine (B).

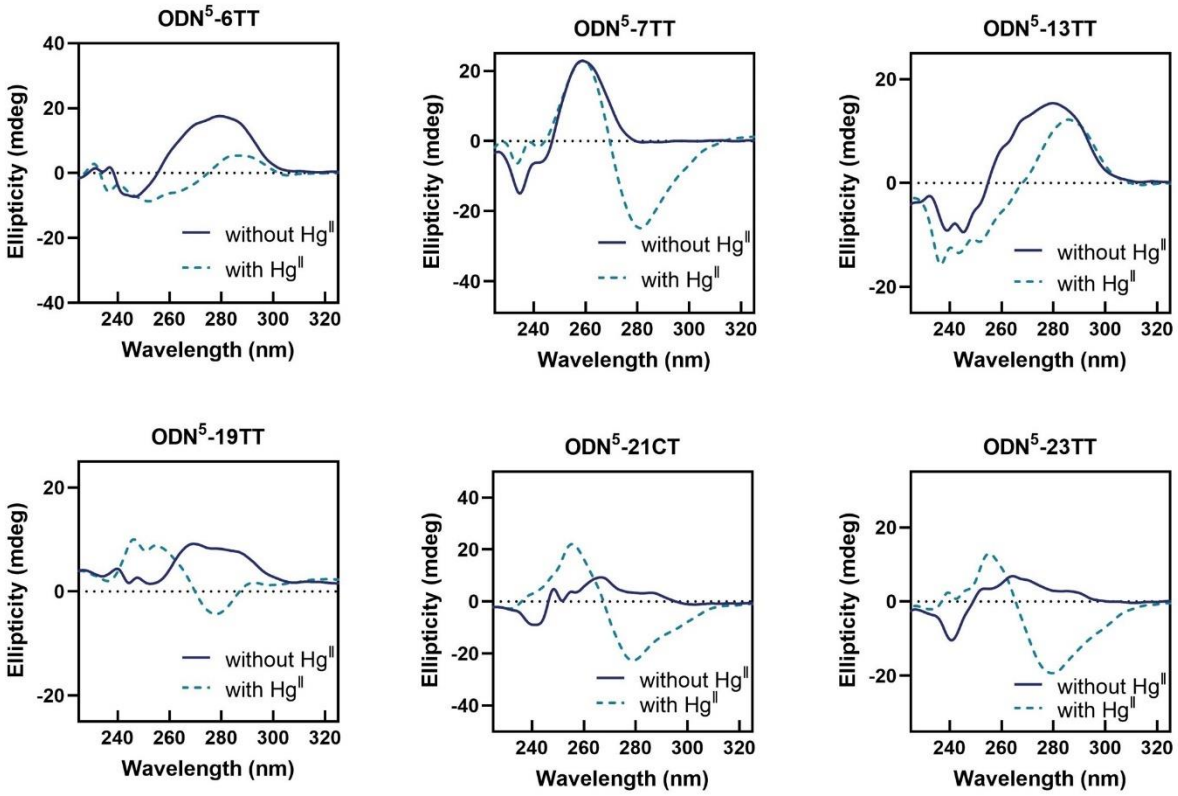

Figure D6. CD spectra of DNA hairpins containing TT mismatches in the presence (dashed, light blue) and absence (solid, dark blue) of 1.5 equiv Hg^{II} (equiv relative to mismatch present).

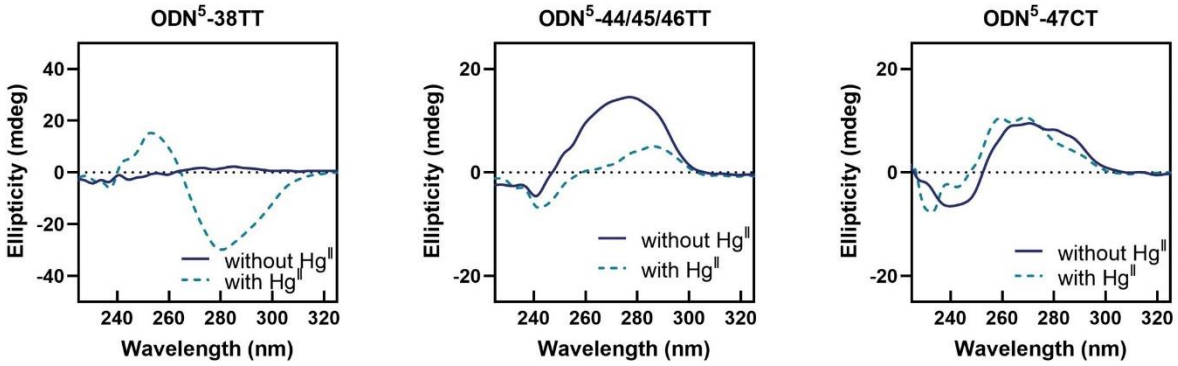

Figure D6 (continue). CD spectra of DNA hairpins containing TT mismatches in the presence (dashed, light blue) and absence (solid, dark blue) of 1.5 equiv Hg^{II} (equiv relative to mismatch present).

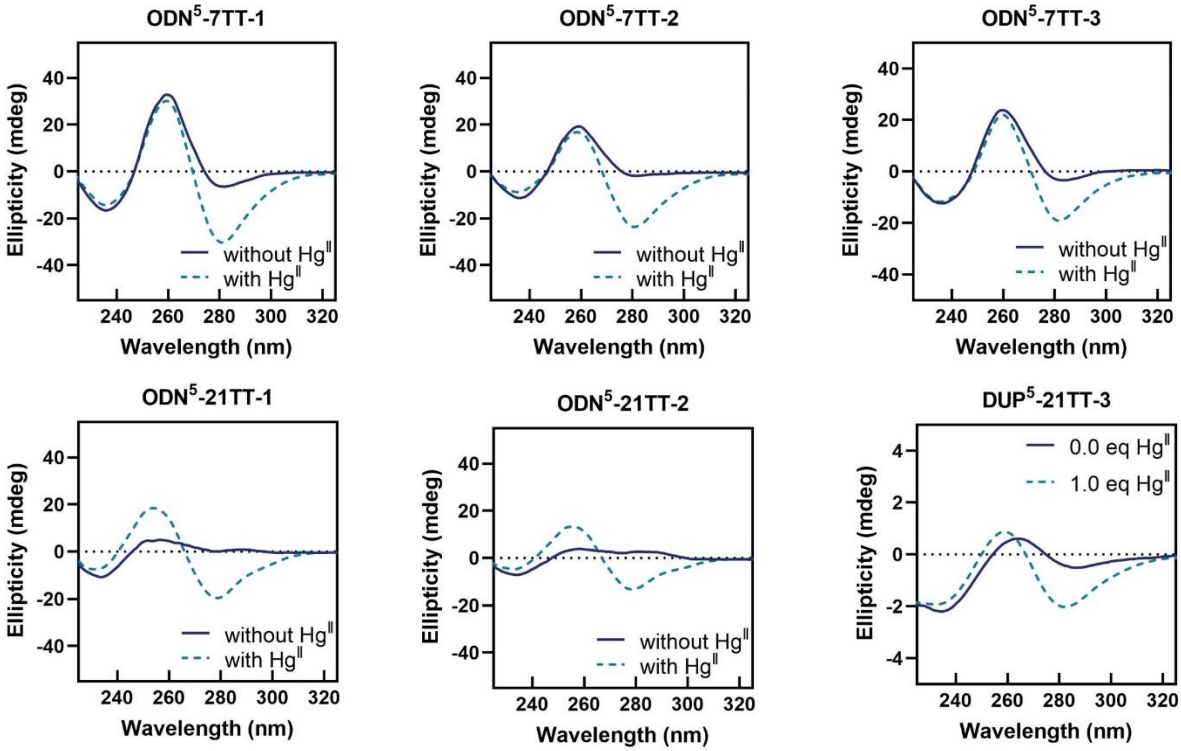

Figure D7. CD spectra of short DNA hairpins and duplexes containing CT or TT mismatches in the presence (dashed, light blue) and absence (solid, dark blue) of 1.0 or 2.0 equiv Hg^{II} (equiv relative to mismatch present).

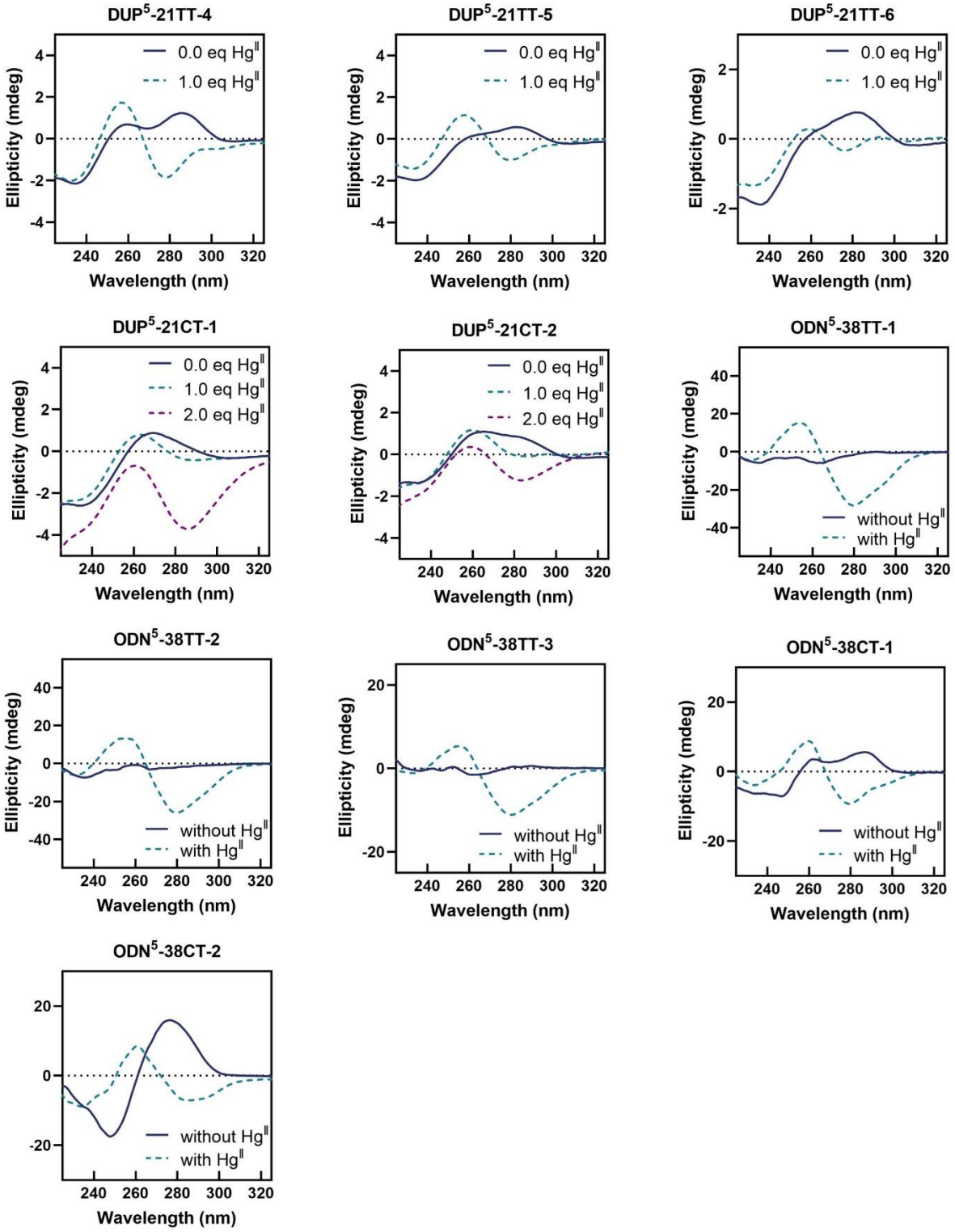

Figure D7 (continue). CD spectra of short DNA hairpins and duplexes containing CT or TT mismatches.

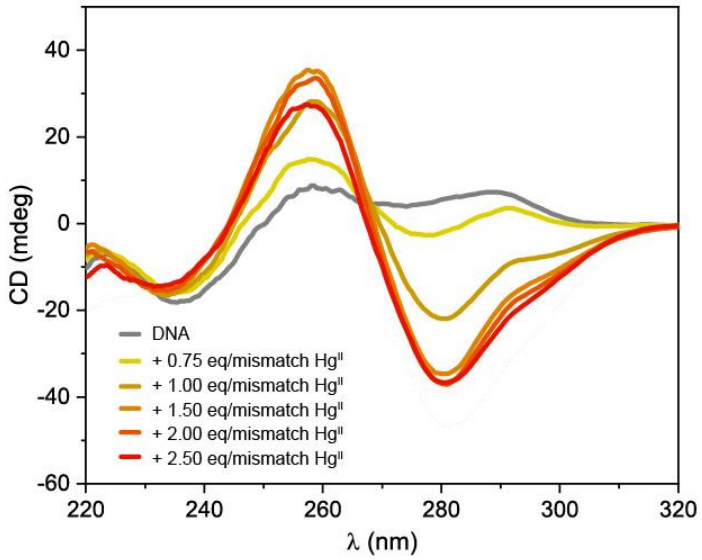

Figure D8. CD spectra of DUP^{5}-21TT-5 in the and absence (grey line) and presence of increasing concentrations of Hg^{II} 0.75-3 equiv Hg^{II} (equiv relative to mismatch present). All samples contained 100 µM duplex in aqueous buffer 200 mM $NaClO_4$ and 50 mM cacodylic acid (pH = 7.8), T 15^{o}C.

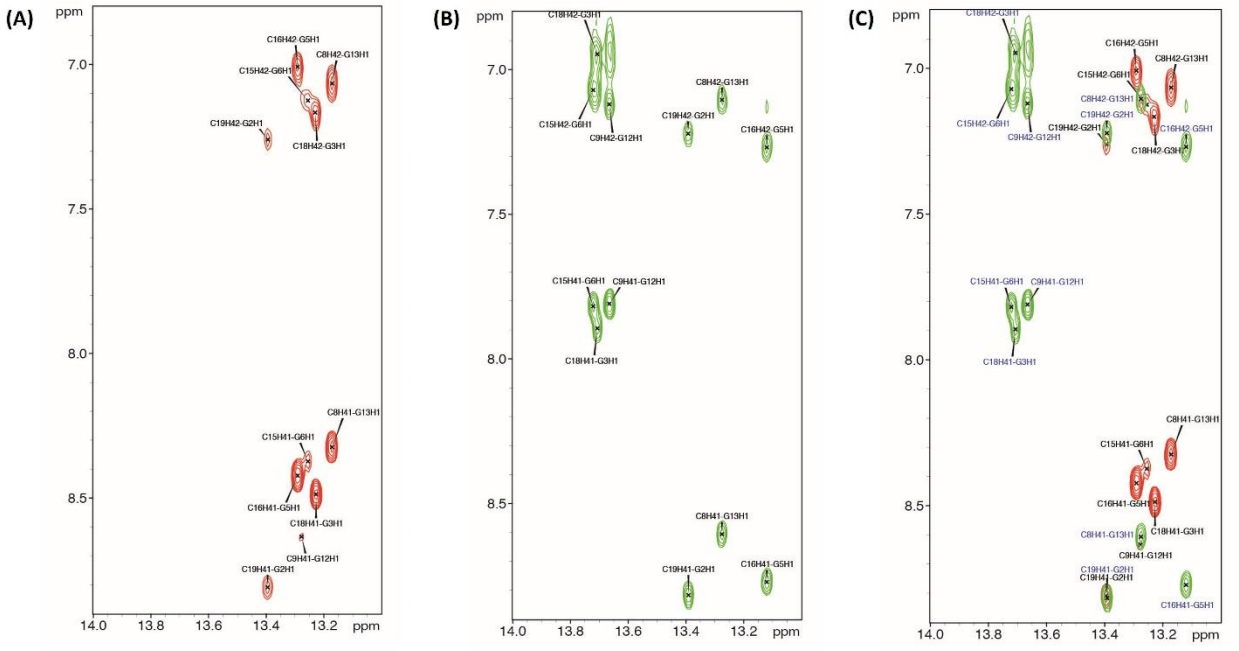

Figure D9. The purine imino regions of [^{1}H, ^{1}H]-NOESY spectra of DUP^{5}-21TT-5 (A) in the absence and (B) presence of Hg^{II} and (C) the superposition of (A) and (B). Spectra were recorded at 15 ^{o}C. The DNA sample contained 0.5 mM duplex DNA (DUP^{5}-21TT-5) and 1.25 mM of $Hg(OAc)_2$ (1.25 equiv Hg^{II} relative to mismatch) in aqueous buffer (200 mM $NaClO_4$, 50 mM cacodylic acid in H2O / D2O (9:1) at pH = 7.8).

5.7 References

[1] Ivanov, V. I.; Krylov, D. Y., [6] A-DNA in solution as studied by diverse approaches. In *Methods Enzymol.*, Academic Press: 1992; Vol. 211, pp 111-127.

[2] Weiss, M. S.; Einspahr, H.; Baker, T.; Dauter, Z., Another case of fraud in structural biology. *Acta Crystallogr. Sect. F Struct. Biol. Cryst. Commun.* **2012,** *68* (Pt 4), 365.

[3] Drew, H. R.; Samson, S.; Dickerson, R. E., Structure of a B-DNA dodecamer at 16 K. *Proc. Natl. Acad. Sci. U. S. A.* **1982,** *79* (13), 4040-4044.

[4] Luo, Z.; Dauter, M.; Dauter, Z., Phosphates in the Z-DNA dodecamer are flexible, but their P-SAD signal is sufficient for structure solution. *Acta Crystallogr. D* **2014,** *70* (Pt 7), 1790-1800.

[5] Rich, A.; Nordheim, A.; Wang, A. H., The chemistry and biology of left-handed Z-DNA. *Annu Rev Biochem* **1984,** *53*, 791-846.

[6] Ho, P. S.; Mooers, B. H., Z-DNA crystallography. *Biopolymers* **1997,** *14* (1), 65-90.

[7] Wang, A. H.; Quigley, G. J.; Kolpak, F. J.; Crawford, J. L.; van Boom, J. H.; van der Marel, G.; Rich, A., Molecular structure of a left-handed double helical DNA fragment at atomic resolution. *Nature* **1979,** *282* (5740), 680-686.

[8] Drew, H.; Takano, T.; Tanaka, S.; Itakura, K.; Dickerson, R. E., High-salt d(CpGpCpG), a left-handed Z' DNA double helix. *Nature* **1980,** *286* (5773), 567-573.

[9] Rahmouni, A. R.; Wells, R. D., Stabilization of Z DNA in vivo by localized supercoiling. *Science* **1989,** *246* (4928), 358-363.

[10] Wittig, B.; Dorbic, T.; Rich, A., The level of Z-DNA in metabolically active, permeabilized mammalian cell nuclei is regulated by torsional strain. *J. Cell Biol.* **1989,** *108* (3), 755-764.

[11] Blaho, J. A.; Wells, R. D., Left-handed Z-DNA binding by the recA protein of Escherichia coli. *J. Biol. Chem.* **1987,** *262* (13), 6082-6088.

[12] Oh, D.-B.; Kim, Y.-G.; Rich, A., Z-DNA-binding proteins can act as potent effectors of gene expression in vivo. *Proc. Natl. Acad. Sci. U.S.A.* **2002,** *99* (26), 16666.

[13] Champ, P. C.; Maurice, S.; Vargason, J. M.; Camp, T.; Ho, P. S., Distributions of Z-DNA and nuclear factor I in human chromosome 22: a model for coupled transcriptional regulation. *Nucleic Acids Res.* **2004,** *32* (22), 6501-6510.

[14] Liu, R.; Liu, H.; Chen, X.; Kirby, M.; Brown, P. O.; Zhao, K., Regulation of CSF1 promoter by the SWI/SNF-like BAF complex. *Cell* **2001,** *106* (3), 309-318.

[15] Koehler, H.; Cotsmire, S.; Langland, J.; Kibler, K. V.; Kalman, D.; Upton, J. W.; Mocarski, E. S.; Jacobs, B. L., Inhibition of DAI-dependent necroptosis by the Z-DNA binding domain of the vaccinia virus innate immune evasion protein, E3. *Proc. Natl. Acad. Sci. U. S. A.* **2017,** *114* (43), 11506-11511.

[16] Kim, S. H.; Lim, S. H.; Lee, A. R.; Kwon, D. H.; Song, H. K.; Lee, J. H.; Cho, M.; Johner, A.; Lee, N. K.; Hong, S. C., Unveiling the pathway to Z-DNA in the protein-induced B-Z transition. *Nucleic Acids Res.* **2018,** *46* (8), 4129-4137.

[17] Lee, A. R.; Park, C. J.; Cheong, H. K.; Ryu, K. S.; Park, J. W.; Kwon, M. Y.; Lee, J.; Kim, K. K.; Choi, B. S.; Lee, J. H., Solution structure of the Z-DNA binding domain of PKR-like protein kinase from Carassius auratus and quantitative analyses of the intermediate complex during B-Z transition. *Nucleic Acids Res.* **2016,** *44* (6), 2936-2948.

[18] Kim, D.; Hur, J.; Park, K.; Bae, S.; Shin, D.; Ha, S. C.; Hwang, H.-Y.; Hohng, S.; Lee, J.-H.; Lee, S.; Kim, Y.-G.; Kim, K. K., Distinct Z-DNA binding mode of a PKR-like protein kinase containing a Z-DNA binding domain (PKZ). *Nucleic Acids Res.* **2014,** *42* (9), 5937-5948.

[19] Jiao, H.; Wachsmuth, L.; Kumari, S.; Schwarzer, R.; Lin, J.; Eren, R. O.; Fisher, A.; Lane, R.; Young, G. R.; Kassiotis, G.; Kaiser, W. J.; Pasparakis, M., Z-nucleic-acid sensing triggers ZBP1-dependent necroptosis and inflammation. *Nature* **2020,** *580* (7803), 391-395.

[20] Ravichandran, S.; Subramani, V. K.; Kim, K. K., Z-DNA in the genome: from structure to disease. *Biophys. Rev.* **2019,** *11* (3), 383-387.

[21] Herbert, A., Z-DNA and Z-RNA in human disease. *Commun. Biol.* **2019,** *2* (1), 7.

[22] Pohl, F. M.; Jovin, T. M., Salt-induced co-operative conformational change of a synthetic DNA: equilibrium and kinetic studies with poly (dG-dC). *J. Mol. Biol.* **1972,** *67* (3), 375-396.

[23] Mamajanov, I.; Engelhart, A. E.; Bean, H. D.; Hud, N. V., DNA and RNA in anhydrous media: Duplex, triplex, and G-quadruplex secondary structures in a deep eutectic solvent. *Angew. Chem. Int. Ed.* **2010,** *49* (36), 6310-6314.

[24] Bae, S.; Kim, D.; Kim, K. K.; Kim, Y.-G.; Hohng, S., Intrinsic Z-DNA is stabilized by the conformational selection mechanism of Z-DNA-binding proteins. *J. Am. Chem. Soc.* **2011,** *133* (4), 668-671.

[25] Jang, Y. J.; Lee, C.; Kim, S. K., Formation of poly[d(A-T)2] specific Z-DNA by a cationic porphyrin. *Sci. Rep.* **2015,** *5*, 9943-9943.

[26] Wu, Z.; Tian, T.; Yu, J.; Weng, X.; Liu, Y.; Zhou, X., Formation of sequence-independent Z-DNA induced by a ruthenium complex at low salt concentrations. *Angew. Chem. Int. Ed.* **2011,** *50* (50), 11962-11967.

[27] Johnson, A.; Qu, Y.; Van Houten, B.; Farrell, N., B----Z DNA conformational changes induced by a family of dinuclear bis(platinum) complexes. *Nucleic Acids Res.* **1992,** *20* (7), 1697-1703.

[28] Spingler, B.; Da Pieve, C., Induction of B- to Z-DNA transition by copper and zinc complexes with C(15) substituted macrocyclic pentaaza ligands. *Dalton Trans.* **2005,** (9), 1637-1643.

[29] Thomas, T. J.; Gunnia, U. B.; Thomas, T., Polyamine-induced B-DNA to Z-DNA conformational transition of a plasmid DNA with (dG-dC)n insert. *J. Biol. Chem.* **1991,** *266* (10), 6137-6141.

[30] Shimada, N.; Kano, A.; Maruyama, A., B–Z DNA transition triggered by a cationic comb-type copolymer. *Adv. Funct. Mater.* **2009,** *19* (22), 3590-3595.

[31] Lee, M.; Kim, S. H.; Hong, S.-C., Minute negative superhelicity is sufficient to induce the B-Z transition in the presence of low tension. *Proc. Natl. Acad. Sci. U. S. A.* **2010,** *107* (11), 4985-4990.

[32] Vlijm, R.; Mashaghi, A.; Bernard, S.; Modesti, M.; Dekker, C., Experimental phase diagram of negatively supercoiled DNA measured by magnetic tweezers and fluorescence. *Nanoscale* **2015,** *7* (7), 3205-3216.

[33] Zhang, Y.; Cui, Y.; An, R.; Liang, X.; Li, Q.; Wang, H.; Wang, H.; Fan, Y.; Dong, P.; Li, J.; Cheng, K.; Wang, W.; Wang, S.; Wang, G.; Xue, C.; Komiyama, M., Topologically constrained formation of stable Z-DNA from normal sequence under physiological conditions. *J. Am. Chem. Soc.* **2019,** *141* (19), 7758-7764.

[34] Temiz, N. A.; Donohue, D. E.; Bacolla, A.; Luke, B. T.; Collins, J. R., The role of methylation in the intrinsic dynamics of B- and Z-DNA. *PLoS One* **2012,** *7* (4), e35558.

[35] Bao, H.-L.; Masuzawa, T.; Oyoshi, T.; Xu, Y., Oligonucleotides DNA containing 8-trifluoromethyl-2'-deoxyguanosine for observing Z-DNA structure. *Nucleic Acids Res.* **2020,** *48* (13), 7041-7051.

[36] Franklin, R. E.; Gosling, R. G., The structure of sodium thymonucleate fibres. I. The influence of water content. *Acta Crystallogr.* **1953,** *6* (8-9), 673-677.

[37] DiMaio, F.; Yu, X.; Rensen, E.; Krupovic, M.; Prangishvili, D.; Egelman, E. H., Virology. A virus that infects a hyperthermophile encapsidates A-form DNA. *Science* **2015,** *348* (6237), 914-917.

[38] Kulkarni, M.; Mukherjee, A., Sequence dependent free energy profiles of localized B- to A-form transition of DNA in water. *J Chem Phys* **2013,** *139* (15), 155102.

[39] Parker, S. C.; Hansen, L.; Abaan, H. O.; Tullius, T. D.; Margulies, E. H., Local DNA topography correlates with functional noncoding regions of the human genome. *Science* **2009,** *324* (5925), 389-392.

[40] Harteis, S.; Schneider, S., Making the bend: DNA tertiary structure and protein-DNA interactions. *Int. J. Mol. Sci.* **2014,** *15* (7).

[41] Guzikevich-Guerstein, G.; Shakked, Z., A novel form of the DNA double helix imposed on the TATA-box by the TATA-binding protein. *Nat Struct Biol* **1996,** *3* (1), 32-37.

[42] Rich, A.; Zhang, S., Timeline: Z-DNA: the long road to biological function. *Nat Rev Genet* **2003,** *4* (7), 566-572.

[43] Wells, R. D., Discovery of the role of non-B DNA structures in mutagenesis and human genomic disorders. *J. Biol. Chem.* **2009,** *284* (14), 8997-9009.

[44] Santos-Pereira, J. M.; Aguilera, A., R loops: new modulators of genome dynamics and function. *Nat Rev Genet* **2015,** *16* (10), 583-597.

[45] Sollier, J.; Cimprich, K. A., Breaking bad: R-loops and genome integrity. *Trends Cell Biol.* **2015,** *25* (9), 514-522.

[46] van Dam, L.; Korolev, N.; Nordenskiöld, L., Polyamine–nucleic acid interactions and the effects on structure in oriented DNA fibers. *Nucleic Acids Res.* **2002,** *30* (2), 419-428.

[47] Arya, D. P.; Xue, L.; Willis, B., Aminoglycoside (neomycin) preference is for a-form nucleic acids, not just rna: Results from a competition dialysis study. *J. Am. Chem. Soc.* **2003,** *125* (34), 10148-10149.

[48] Robinson, H.; Wang, A. H. J., Neomycin, spermine and hexaamminecobalt(III) share common structural motifs in converting B- to A-DNA. *Nucleic Acids Res.* **1996,** *24* (4), 676-682.

[49] Todd, R. C.; Lippard, S. J., Structure of duplex DNA containing the cisplatin 1,2-{Pt(NH3)2}2+d(GpG) cross-link at 1.77 A resolution. *J. Inorg. Biochem.* **2010,** *104* (9), 902-908.

[50] Lippert, B., Multiplicity of metal ion binding patterns to nucleobases. *Coord. Chem. Rev.* **2000,** *200-202*, 487-516.

[51] Šket, P.; Plavec, J., Tetramolecular DNA quadruplexes in solution: Insights into structural diversity and cation movement. *J. Am. Chem. Soc.* **2010,** *132* (36), 12724-12732.

[52] Mirihana Arachchilage, G.; Dassanayake, A. C.; Basu, S., A potassium ion-dependent RNA structural switch regulates human pre-miRNA 92b maturation. *Chem. Biol.* **2015,** *22* (2), 262-272.

[53] Liu, H.; Yu, X.; Chen, Y.; Zhang, J.; Wu, B.; Zheng, L.; Haruehanroengra, P.; Wang, R.; Li, S.; Lin, J.; Li, J.; Sheng, J.; Huang, Z.; Ma, J.; Gan, J., Crystal structure of an RNA-cleaving DNAzyme. *Nat. Commun.* **2017,** *8* (1), 2006.

[54] Zivarts, M.; Liu, Y.; Breaker, R. R., Engineered allosteric ribozymes that respond to specific divalent metal ions. *Nucleic Acids Res.* **2005,** *33* (2), 622-631.

[55] Furukawa, K.; Ramesh, A.; Zhou, Z.; Weinberg, Z.; Vallery, T.; Winkler, Wade C.; Breaker, Ronald R., Bacterial riboswitches cooperatively bind Ni2+ or Co2+ ions and control expression of heavy metal transporters. *Mol. Cell* **2015,** *57* (6), 1088-1098.

[56] Guo, X.; Seela, F., Anomeric 2'-deoxycytidines and silver ions: Hybrid base pairs with greatly enhanced stability and efficient DNA mismatch detection with α-dC. *Chemistry (Easton)* **2017,** *23* (49), 11776-11779.

[57] Schmidt, O. P.; Mata, G.; Luedtke, N. W., Fluorescent base analogue reveals T-HgII-T base pairs have high kinetic stabilities that perturb DNA metabolism. *J. Am. Chem. Soc.* **2016,** *138* (44), 14733-14739.

[58] Ono, A.; Torigoe, H.; Tanaka, Y.; Okamoto, I., Binding of metal ions by pyrimidine base pairs in DNA duplexes. *Chem. Soc. Rev.* **2011,** *40* (12), 5855-5866.

[59] Schmidt, O. P.; Benz, A. S.; Mata, G.; Luedtke, N. W., HgII binds to C–T mismatches with high affinity. *Nucleic Acids Res.* **2018,** *46* (13), 6470-6479.

[60] Liu, H.; Cai, C.; Haruehanroengra, P.; Yao, Q.; Chen, Y.; Yang, C.; Luo, Q.; Wu, B.; Li, J.; Ma, J.; Sheng, J.; Gan, J., Flexibility and stabilization of HgII-mediated C:T and T:T base pairs in DNA duplex. *Nucleic Acids Res.* **2017,** *45* (5), 2910-2918.

[61] Schmidt, O. P.; Jurt, S.; Johannsen, S.; Karimi, A.; Sigel, R. K. O.; Luedtke, N. W., Concerted dynamics of metallo-base pairs in an A/B-form helical transition. *Nat. Commun.* **2019,** *10* (1), 4818.

[62] Stefl, R.; Trantírek, L.; Vorlícková, M.; Koca, J.; Sklenár, V.; Kypr, J., A-like guanine-guanine stacking in the aqueous DNA duplex of d(GGGGCCCC). *J. Mol. Biol.* **2001,** *307* (2), 513-524.

[63] Tsai, A. G.; Engelhart, A. E.; Hatmal, M. M.; Houston, S. I.; Hud, N. V.; Haworth, I. S.; Lieber, M. R., Conformational variants of duplex DNA correlated with cytosine-rich chromosomal fragile sites. *J. Biol. Chem.* **2009,** *284* (11), 7157-7164.

[64] Watkins, D.; Gong, C.; Kellish, P.; Arya, D. P., Probing A-form DNA: A fluorescent aminosugar probe and dual recognition by anthraquinone-neomycin conjugates. *Bioorg. Med. Chem.* **2017,** *25* (4), 1309-1319.

[65] Whitley, D. C.; Runfola, V.; Cary, P.; Nazlamova, L.; Guille, M.; Scarlett, G., APTE: identification of indirect read-out A-DNA promoter elements in genomes. *BMC Bioinformatics* **2014,** *15* (1), 288.

[66] Xi, H.; Davis, E.; Ranjan, N.; Xue, L.; Hyde-Volpe, D.; Arya, D. P., Thermodynamics of nucleic acid "shape readout" by an aminosugar. *Biochemistry* **2011,** *50* (42), 9088-9113.

[67] Scarlett, G. P.; Elgar, S. J.; Cary, P. D.; Noble, A. M.; Orford, R. L.; Kneale, G. G.; Guille, M. J., Intact RNA-binding domains are necessary for structure-specific DNA binding and transcription control by CBTF122 during Xenopus development. *J. Biol. Chem.* **2004,** *279* (50), 52447-52455.

[68] Nakano, M.; Moody, E. M.; Liang, J.; Bevilacqua, P. C., Selection for thermodynamically stable DNA tetraloops using temperature gradient gel electrophoresis reveals four motifs: d(cGNNAg), d(cGNABg),d(cCNNGg), and d(gCNNGc). *Biochemistry* **2002,** *41* (48), 14281-14292.

[69] Luedtke, N. W.; Carmichael, P.; Tor, Y., Cellular uptake of aminoglycosides, guanidinoglycosides, and poly-arginine. *J. Am. Chem. Soc.* **2003,** *125* (41), 12374-12375.

[70] Luedtke, N. W.; Liu, Q.; Tor, Y., RNA–ligand interactions: Affinity and specificity of aminoglycoside dimers and acridine conjugates to the HIV-1 rev response element. *Biochemistry* **2003,** *42* (39), 11391-11403.

[71] Sutherland, J. C.; Griffin, K. P.; Keck, P. C.; Takacs, P. Z., Z-DNA: vacuum ultraviolet circular dichroism. *Proc. Natl. Acad. Sci. U. S. A.* **1981,** *78* (8), 4801-4804.

[72] Kawara, K.; Tsuji, G.; Taniguchi, Y.; Sasaki, S., Synchronized chiral induction between [5]helicene-spermine ligand and B-Z DNA transition. *Chemistry (Easton)* **2017,** *23* (8), 1763-1769.

[73] Shih, H.-C.; Tang, N.; Burrows, C. J.; Rokita, S. E., Nickel-based probes of nucleic acid structure bind to guanine N7 but do not perturb a dynamic equilibrium of extrahelical guanine residues. *J. Am. Chem. Soc.* **1998,** *120* (14), 3284-3288.

[74] Wang, A. J.; Quigley, G. J.; Kolpak, F. J.; van der Marel, G.; van Boom, J. H.; Rich, A., Left-handed double helical DNA: variations in the backbone conformation. *Science* **1981,** *211* (4478), 171-176.

[75] Gessner, R. V.; Frederick, C. A.; Quigley, G. J.; Rich, A.; Wang, A. H., The molecular structure of the left-handed Z-DNA double helix at 1.0-A atomic resolution. Geometry, conformation, and ionic interactions of d(CGCGCG). *J. Biol. Chem.* **1989,** *264* (14), 7921-7935.

[76] Fuertes, M. A.; Cepeda, V.; Alonso, C.; Pérez, J. M., Molecular mechanisms for the B-Z transition in the example of poly[d(G-C) x d(G-C)] polymers. A critical review. *Chem Rev* **2006,** *106* (6), 2045-2064.

[77] D'Ascenzo, L.; Leonarski, F.; Vicens, Q.; Auffinger, P., 'Z-DNA like' fragments in RNA: a recurring structural motif with implications for folding, RNA/protein recognition and immune response. *Nucleic Acids Res.* **2016,** *44* (12), 5944-5956.

[78] Borah, B.; Cohen, J. S.; Howard, F. B.; Miles, H. T., Poly(d2NH2A-dT): two-dimensional NMR shows a B to A conversion in high salt. *Biochemistry* **1985,** *24* (25), 7456-7462.

[79] Patel, D. J.; Kozlowski, S. A.; Hare, D. R.; Reid, B.; Ikuta, S.; Lander, N.; Itakura, K., Conformation, dynamics, and structural transitions of the TATA box region of self-complementary d[(C-G)n-T-A-T-A-(C-G)n] duplexes in solution. *Biochemistry* **1985,** *24* (4), 926-935.

[80] Kypr, J.; Kejnovská, I.; Renciuk, D.; Vorlícková, M., Circular dichroism and conformational polymorphism of DNA. *Nucleic Acids Res.* **2009,** *37* (6), 1713-1725.

[81] Ivanov, V. I.; Minyat, E. E., The transitions between left- and right-handed forms of poly(dG-dC). *Nucleic Acids Res.* **1981,** *9* (18), 4783-4798.

[82] Miyahara, T.; Nakatsuji, H.; Sugiyama, H., Similarities and differences between RNA and DNA double-helical structures in circular dichroism spectroscopy: A SAC–CI study. *J. Phys. Chem. A* **2016,** *120* (45), 9008-9018.

[83] van Dam, L.; Korolev, N.; Nordenskiöld, L., Polyamine-nucleic acid interactions and the effects on structure in oriented DNA fibers. *Nucleic Acids Res.* **2002,** *30* (2), 419-428.

[84] Barbieri, C. M.; Li, T. K.; Guo, S.; Wang, G.; Shallop, A. J.; Pan, W.; Yang, G.; Gaffney, B. L.; Jones, R. A.; Pilch, D. S., Aminoglycoside complexation with a DNA.RNA hybrid duplex: the thermodynamics of recognition and inhibition of RNA processing enzymes. *J. Am. Chem. Soc.* **2003,** *125* (21), 6469-6477.

[85] Vrána, O.; Masek, V.; Drazan, V.; Brabec, V., Raman spectroscopy of DNA modified by intrastrand cross-links of antitumor cisplatin. *J. Struct. Biol.* **2007,** *159* (1), 1-8.

[86] Vorlíčková, M.; Kejnovská, I.; Bednářová, K.; Renčiuk, D.; Kypr, J., Circular dichroism spectroscopy of DNA: from duplexes to quadruplexes. *Chirality* **2012,** *24* (9), 691-698.

[87] Füchtbauer, A. F.; Wranne, M. S.; Bood, M.; Weis, E.; Pfeiffer, P.; Nilsson, J. R.; Dahlén, A.; Grøtli, M.; Wilhelmsson, L. M., Interbase FRET in RNA: from A to Z. *Nucleic Acids Res.* **2019,** *47* (19), 9990-9997.

[88] Dumat, B.; Larsen, A. F.; Wilhelmsson, L. M., Studying Z-DNA and B- to Z-DNA transitions using a cytosine analogue FRET-pair. *Nucleic Acids Res.* **2016,** *44* (11), e101.

[89] Liu, J.; Lu, Y., Rational design of "turn-on" allosteric DNAzyme catalytic beacons for aqueous mercury ions with ultrahigh sensitivity and selectivity. *Angew. Chem. Int. Ed.* **2007,** *46* (40), 7587-7590.

[90] Park, K. S.; Jung, C.; Park, H. G., "Illusionary" polymerase activity triggered by metal ions: use for molecular logic-gate operations. *Angew Chem Int Ed* **2010,** *49* (50), 9757-9760.

[91] Thomas, J. M.; Yu, H. Z.; Sen, D., A mechano-electronic DNA switch. *J. Am. Chem. Soc.* **2012,** *134* (33), 13738-13748.

[92] Mor-Piperberg, G.; Tel-Vered, R.; Elbaz, J.; Willner, I., Nanoengineered electrically contacted enzymes on DNA scaffolds: Functional assemblies for the selective analysis of Hg2+ ions. *J. Am. Chem. Soc.* **2010,** *132* (20), 6878-6879.

[93] Wang, Z. G.; Elbaz, J.; Willner, I., DNA machines: bipedal walker and stepper. *Nano Lett.* **2011,** *11* (1), 304-309.

[94] Wen, S.; Zeng, T.; Liu, L.; Zhao, K.; Zhao, Y.; Liu, X.; Wu, H.-C., Highly sensitive and selective DNA-based detection of mercury(II) with α-hemolysin nanopore. *J. Am. Chem. Soc.* **2011,** *133* (45), 18312-18317.

[95] Hong, T.; Yuan, Y.; Wang, T.; Ma, J.; Yao, Q.; Hua, X.; Xia, Y.; Zhou, X., Selective detection of N6-methyladenine in DNA via metal ion-mediated replication and rolling circle amplification. *Chem. Sci.* **2017,** *8* (1), 200-205.

[96] Cantor, C. R.; Warshaw, M. M.; Shapiro, H., Oligonucleotide interactions. 3. Circular dichroism studies of the conformation of deoxyoligonucleotides. *Biopolymers* **1970,** *9* (9), 1059-1077.

[97] Lee, W.; Tonelli, M.; Markley, J. L., NMRFAM-SPARKY: enhanced software for biomolecular NMR spectroscopy. *Bioinformatics* **2015,** *31* (8), 1325-1327.

Chapter 6 | Other projects

6.1 Conclusions & future works

Chapter 7 | Contributions to original knowledge and future work

7.1 Conclusions & future works

7.1.1 ^{ts}T is a highly fluorescent nucleobase molecular rotor (Chapter 2)

In this work, we designed and synthesized a highly fluorescent thymidine analog that overcomes the brightness and sensitivity limitations of the previously reported FBAs. We applied DFT calculations to design a probe that does not undergo PET quenching with natural DNA bases. In addition, to increase the probe's microenvironment sensitivity, we equipped it with a rotatable conjugated linker to build a fluorescent molecular rotor. The designed probe, *trans*-stilbene analog of thymidine (^{ts}T), demonstrated molecular rotor properties as a free nucleoside (determined by viscosity experiment), stemming from its TICT excited state (confirmed by its solvatochromic properties). ^{ts}T phosphoramidite was synthesized in 12 steps with an overall yield of 26% and incorporated into DNA. This new thymidine mimic has a molar extinction coefficient (Ɛ) = 30'600 $M^{-1}cm^{-1}$ and a fluorescence quantum yield (φ) = 0.143 when incorporated into *ds*-DNA. The latter is 4.9-fold higher than the quantum yield of ^{ts}T in *ss*-DNA, confirming the lack of PET quenching, and making ^{ts}T one of the brightest reported FBAs to date. One of the current projects in our lab is synthesizing ^{ts}T triphosphate for delivering it into cells using lipid nanoparticles, which is the subject of a different line of the group's activities. Thus, this future project would, in fact, bridges two previously

unconnected research directions of Luedtke group: fluorescent base analogs and lipid nanoparticles. The high fluorescence of ^{ts}T may allow single-molecule fluorescence studies. Regarding the relatively low excitation wavelength of ^{ts}T (320 nm), one can conduct two-photon excitation experiment to expand the application of ^{ts}T *in vivo*. Another ongoing project is a collaboration with the group of Prof. Dmytro Perepichka, where the triplet excited state of ^{ts}T is under investigation. *trans*-Stilbene is known to have a very low triplet energy and was shown to be a triplet acceptor in *Dexter*-type energy transfer. Our preliminary data suggest that the rotation around the ethylenic bond in mismatched DNA does not result in an emissive triplet state. However, data suggests coordination of heavy metal Hg^{II} to the ^{ts}T:T mismatch significantly increases the chance of intersystem crossing, and an emission (with a lifetime longer than original fluorescence) appears at 540 nm. This is in agreement with the previously reported triplet energy of unmodified *trans*-stilbene (2.1 eV) and calculated triplet energy of ^{ts}T (2.0 eV). Future studies may reveal the applications of ^{ts}T as the first phosphorescent FBA or as a triplet acceptor in *Dexter* energy transfer which in the context of DNA may result in an exceptionally long-distance energy transfer.

7.1.2 Probing DNA local and global structure (Chapter 3)

This chapter focused on the sensitivity of ^{ts}T towards DNA mechanical motion. This sensitivity stems from the rotary behavior of ^{ts}T. Apart from 4.9 fold fluorescence enhancement during hybridization, ^{ts}T demonstrated 8.2-fold higher fluorescence in a well-matched duplex than in a *ds*-DNA with ^{ts}T:G mismatch and even 28-fold higher than in a *ds*-DNA with ^{ts}T:T and ^{ts}T:C mismatches. In addition, ^{ts}T showed a 17.1-fold higher fluorescence in a well-matched duplex than in a damaged duplex ^{ts}T:MG. The fluorescence lifetime and dynamic anisotropy measurements were conducted using ^{ts}T:A, *ss*-^{ts}T and ^{ts}T:T. The single-decay lifetime and single-rotor model anisotropy fit revealed ^{ts}T:A as the most rigid (with 11.1 ns lifetime) and ^{ts}T:T as the most dynamic (with 4.5 ns lifetime) base-pair. The temperature-dependent fluorescence lifetime measurements showed a decrease in the lifetime of ^{ts}T:A, with increasing temperature, due to a higher propensity to undergo rotation. ^{ts}T also acts as a FRET donor for tC, and we calculated a very low R_0 (~ 2 nm) for this FRET pair, suggesting that ^{ts}T, when paired with tC, can be utilized as a molecular ruler. In addition, we explored the distance-dependence sensitivity of ^{ts}T towards local duplex perturbation. ^{ts}T could report changes in

local dynamics induced by an A:A mismatch and an AP site introduced in one base-pair away by 16% and 24% fluorescence quenching, respectively. Surprisingly, it could detect an MG:C up to 10 Å (i.e. three base-pairs away) and an OG:A damage up to 20 Å (i.e. five base-pairs away). The dynamic motions of MG:C and OG:A is not solely responsible for this unusual sensitivity; instead, computational investigations suggested that the electron transfer between OG (or MG) and ^{ts}T is the dominant factor. Currently, we are trying to use the microenvironment sensitivity of ^{ts}T to explore the hidden details of enzymatic repair mechanisms. Regarding its discrimination between damaged DNA (OFF mode due to PET quenching), abasic sites (weak fluorescence due to mechanical motions), and well-matched duplex (strong fluorescence due to rotation restriction), we have hypothesized that ^{ts}T can separately probe glycosylase and AP lyase activity of the OGG1 enzyme. In addition, ^{ts}T will be used as the first FBA to probe MG repair by MGMT.

7.1.3 ^{ts}C probes folding of *i*-motif structures (Chapter 4)

Inspired by the unprecedented sensitivity of ^{ts}T, we described the synthesis of its cytidine analog, ^{ts}C, and its application in probing the folding of *i*-motif structures. ^{ts}C phosphoramidite was synthesized in 15 steps with 8% total yield. Upon *i*-motif formation, ^{ts}C fluorescence red-shifted, and its intensity increased due to the *i*-motif-to-probe energy transfer. Furthermore, ^{ts}C was used to evaluate the kinetic of *ss* (or *i*-motif) → *ds* transition by adding the complementary strand and *ds* → *i*-motif conversion by adding an invading strand that initiates a strand-displacement reaction. Finally, the temperature-dependent fluorescence intensities, fluorescence lifetimes, and absorbance of ^{ts}C enabled us to probe different conformational stages during the folding/unfolding of diverse DNA structures at neutral and acidic pH. Thus, ^{ts}C is a powerful tool to probe the global dynamics of DNA duplex and *i*-motif structures. In future work, a FRET acceptor may be added to the DNA structure to reveal hidden intermediates of *i*-motif folding. In addition, one can try to apply molecular crowding conditions (i.e. polyethylene glycol) or modifications (i.e. FANA) to form *i*-motif structures at the close to neutral pH. In this case the fluorescence of ^{ts}C is less likely to be quenched by protonation to provide higher sensitivity.

7.1.4 Mercury-assisted DNA helical switching (Chapter 5)

To continue our work on probing the global dynamics of DNA, this chapter focuses on rapid and reversible helical transitions of *ds*-DNA. We report a long, self-complementary DNA sequence containing numerous C:T mismatches that translate a series of local structural transitions to global switching of DNA structure. We have shown that a global B-form → A-from helical transition occurs upon the addition of one equivalent per mismatch Hg^{II}. As confirmed by CD and fluorescence anisotropy of a major groove binder, Neo-BODIPY, this transition is reversible and the initial B-form DNA can be regenerated when N-acetylcysteine is added. Both transitions were completed in <30 s and could be repeated more than 10 times. While numerous examples of local A-form perturbations caused by DNA-protein and DNA-small molecule binding interactions have previously been reported, the previous examples of global B-form → A-from helical transitions involved global dehydration of the duplex. Here the global B- to A-form helical transition was a result of discrete, reversible metal binding. Moreover, we discovered that upon addition of the second equiv. $Hg^{II,}$ the CD spectrum of the right-handed A-form DNA changes and demonstrates a left-handed DNA signature. This unexpected change in CD spectra, inspired us to build up a collaboration with Dr. Miguel Garavís, from the group of Prof. Carlos González, in an ongoing effort to resolve the structure of supposedly left-handed DNA by means of NMR and X-ray crystallography. These types of helical switchings, in addition to their broad implications in structural biology and biochemistry, can potentially be utilized in the development of advanced DNA-based materials and devices.

7.2 List of publications

7.2.1 Published research papers

[1] I. Dementyev, **A. Karimi**, A molecular dynamical investigation of the 7,8-dihydro-8-oxoguanine mutation in dsDNA, *MSURJ,* **2021**, *16*, 25.

[2] **A. Karimi**, R. Börner, G. Mata, N. W. Luedtke, A highly fluorescent nucleobase molecular rotor, *J. Am. Chem. Soc,* **2020**, *142*, 14422.

[3] O. P. Schmidt, S. Jurt, S. Johannsen, **A. Karimi**, R. K. O. Sigel, N. W. Luedtke, Concerted dynamics of metallo-base pairs in an A/B-form helical transition, *Nat. Commun*., **2019**, *10*, 4818.

[4] A. Johnson, **A. Karimi**, N. W. Luedtke, Enzymatic incorporation of a coumarin-guanine base-pair, *Angew. Chem. Int. Ed*., **2019**, *58*, 16839.

7.2.2 Manuscripts in preparation

[1] **A. Karimi**, K. Wang, K. Basran, E. Hamzehpour, D. Perepichka, N. W. Luedtke, A light-up fluorescent cytosine analog with bathochromic shift for probin i-motif DNA folding. *(in preparation)*

[2] **A. Karimi**, W. Copp, N. W. Luedtke, A fluorescent nucleobase ruler determine the location of DNA damages up to 20 Å. *(in preparation)*

[3] **A. Karimi**, W. Copp, N. W. Luedtke, Fluorescent nucleobase rotors as sensitive probes for DNA. *(in preparation)*

7.2.3 Science communication articles

[1] V. Schreier, A. Johnson, **A. Karimi**, M. O. Loehr, N. W. Luedtke, Swiss science concentrates, *CHIMIA*, **2019**, 73, 205.

[2] M. O. Loehr, **A. Karimi**, A. Johnson, N. W. Luedtke, Swiss science concentrates, *CHIMIA*, **2018**, 72, 900.

[3] M. O. Loehr, A. Johnson, **A. Karimi**, N. W. Luedtke, Swiss science concentrates, *CHIMIA*, **2018**, 72, 815.

[4] V. Schreier, A. Johnson, **A. Karimi**, N. W. Luedtke, Swiss science concentrates, *CHIMIA*, **2018**, 72, 725.

[5] **A. Karimi**, V. Schreier, A. Johnson, N. W. Luedtke, Swiss science concentrates, *CHIMIA*, **2018**, 72, 646.

[6] V. Schreier, A. Johnson, **A. Karimi**, N. W. Luedtke, Swiss science concentrates, *CHIMIA*, **2018**, 72, 546.

[7] A. Johnson, **A. Karimi**, V. Schreier, N. W. Luedtke, Swiss science concentrates, *CHIMIA*, **2018**, 72, 424.

[8] A. Johnson, **A. Karimi**, V. Schreier, N. W. Luedtke, Swiss science concentrates, *CHIMIA*, **2018**, 72, 338.

[9] A. Johnson, **A. Karimi**, C. L. Lin, V. Schreier, N. W. Luedtke, Swiss science concentrates, *CHIMIA*, **2018**, 72, 253.

[10] A. Johnson, **A. Karimi**, C. L. Lin, V. Schreier, N. W. Luedtke, Swiss science concentrates, *CHIMIA*, **2018**, 72, 151.

[11] A. Johnson, **A. Karimi**, C. L. Lin, V. Schreier, N. W. Luedtke, Swiss science concentrates, *CHIMIA*, **2018**, 72, 68.

7.3 Conference presentations

[1] **A. Karimi,** R. Börner, N. W. Luedtke, An intelligent mechanical arm in a fluorescent nucleoside mimic: DNA dynamics detection, 48th World Chemistry Congress IUPAC, Montreal, Canada, July 2021. *(Oral Presentation)*

[2] **A. Karimi**, R. Börner, N. W. Luedtke, A highly fluorescent nucleobase mimic for SNP detection and dynamic studies, 2nd Annual CRBS Symposium, Montreal, Canada, November 2020. *(Poster Presentation)*

[3] **A. Karimi**, N. W. Luedtke, A fluorescent probe for DNA-mediated Förster and Dexter energy transfer, 47th World Chemistry Congress IUPAC, Paris, France, July 2019. *(Oral Presentation)*

[4] **A. Karimi**, N. W. Luedtke, A bright fluorescent probe for detection of DNA mismatches, Universitat Zurich Doktorandentag, Zurich, Switzerland, July 2019. *(Poster Presentation)*

"O those who plunged in Seas of Knowledge deep,
And raised their wits beyond the Wisdom's Keep,
Found not the way to Day out of this Dark;
Some tale they told and went again to sleep"

Omar Khayyam